EXPERIMENTAL AND ANALYTICAL ANALYSIS OF PRE-STRESSED CONCRETE SPLICED GIRDER MODELS

Prof. Dr. Thamir K. Mahmoud
Civil Eng. Dept.
University of Baghdad

Dr. Ali H. Nasser
Civil Eng. Dept.
University of Baghdad

ABSTRACT

The present research is concerned with experimental and analytical studies of pre-stressed concrete spliced and non-spliced girder models. The test groups consisted of (16) girders of rectangular sections. Eight girders are spliced while the other eight are reference non - spliced girders. Each spliced girder is composed of three concrete segments connected by splices of ordinary reinforced concrete with hooked dowels different locations. The tested girders were of single span or continuous over intermediate supports. For single span girders two splices were used and post-tensioning was carried out for the full assembled girder. For the continuous girders pre-tensioned segments were connected by splices at quarter spans. Concentrated or uniformly distributed loads have been applied to the girders. The deflection was measured at mid-spans while the strain was measured at splice zones and at mid-spans.

Nonlinear analysis of the girders was carried out using a modified computer program. A comparison among the experimental and the analytical results for spliced and non-spliced girders was carried out to study the effects of splicing for different girders. Results have shown that at about 50% of the ultimate load which is approximately corresponds to the serviceability limit state, the deflection of the spliced girders is greater than that of the reference non-spliced girders in the range of (10%-15%) and the ultimate loads for the non-spliced girders are greater than those of the spliced girders in the range of (12%-17%).
The difference in deflection between the Finite Element and the experimental results at 50% of the ultimate load was in the range of (8%-12%). Moreover, the difference in the ultimate load between the Finite Element and the experimental results was in the range of (5%-11%).

الخلاصة

إهتم هذا البحث بالدراسة المختبرية والنظرية للروافد الخرسانية المسبقة الاجهاد (مسبقة الشد) المتكونة من قطع موصولة. تضمن البرنامج العملي عدة مجاميع شملت ستة عشر نموذجا مستطيلة المقطع. ثمانية منها ذات وصلات والثمانية المتبقية بدون وصلات لغرض المقارنة. كل رافدة من الروافد المشكلة توصيلا تتكون من ثلاث قطع خرسانية مرتبطة بوصلات ذات خرسانة اعتيادية مسلحة بقضبان معكوفة وتختلف اماكن وطريقة هذه الوصلات من رافدة الى اخرى. وتنقسم هذه الى روافد ذات فضاء واحد أي ترتكز على مسندين طرفيين واخرى مستمرة ذات اكثر من فضاء وترتكز على مساند وسطية. الروافد ذات الفضاء الواحد تحتوي على وصلتين وتم تعريضها الى عملية الإجهاد بعد التوصيل أما الروافد المستمرة فتم تشكيلها من قطع مسبقة الجهد.

الاحمال المسلطة على هذه الروافد اما ان تكون احمال مركزة في وسط كل فضاء او حمل منتظم على طول الرافدة. لقد تم قياس الهطول في منتصف طول الرافدة وكذلك تم قياس الانفعالات في المنتصف وفي منطقة الوصلات.

تم تحليل الروافد لاخطيا باستخدام برنامج تم اجراء بعض التعديلات عليه. لقد تم اجراء مقارنة بين النتائج العملية والنظرية للجسور الموصولة وغير الموصولة وقد بينت النتائج تحت تأثير 50% من الحمل الاقصى والذي يقترب من حمل حياة المنشأ الاعتيادية ان الهطول في الجسور الموصولة يزيد بنسبة (10–15%) عما هو في الجسور غير الموصولة اما الحمل الاقصى فيقل في الجسور الموصولة عما هو في غير الموصولة بنسبة (12%–17%).

لقد بينت النتائج المختبرية والنظرية تحت تأثر 50% من الحمل الاقصى ان الفرق بينهما في الهطول يتراوح بنسبة (8–12%) اما بالنسبة للحمل الاقصى فقد كان الفرق بنسبة (5–11%).

INTRODUCTION

The difficulties in the construction of long span bridges under economical aspects of time and cost have given inspiration to engineers to use segmental and/or spliced girders.

Splicing of pre-stressed precast segments can be carried out at inflection points. Usually at segment ends; dowels of ordinary rebar reinforcements are overlapped at splice zone prior to concrete casting at splice, Fig (1) .

a) Mechanically Spliced Mild Reinforcement   b) Lap Spliced Mild Reinforcement

Figure (1) Cast in- Place Splice

At each splice, a temporary support is usually used, Fig. (2). This construction procedure is useful in continuous girders of spans longer than the available lengths of pre-stressed -precast girders produced in local factories.
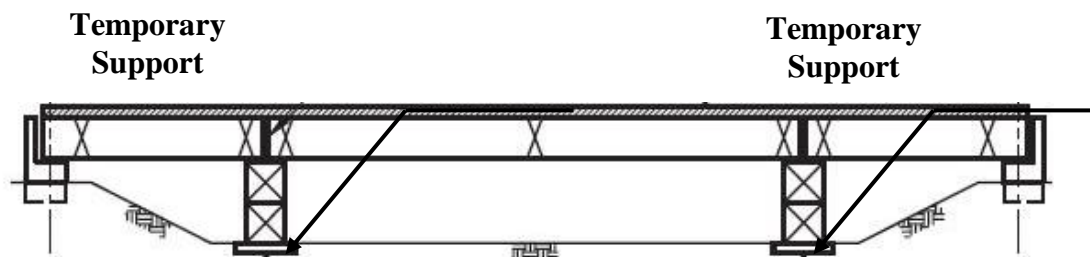
Temporary Support   **Temporary Support**

Figure (2) Temporary Support at Splice Zone.

SPLICING OF GIRDERS

The splicing of girders is used to increase the span ranges for precast pre-stressed concrete girder bridges. A spliced girder is a precast pre-stressed concrete member usually obtained by connecting pre-stressed concrete segments to obtain the required length of the bridge girder.

Splice Location

The splice for any bridge is usually located at inflection points or as determined by the requirements for bridge span. However, other considerations are also significant in determining the splice location. These other considerations include:

- Splice has lower stress limits since it generally has a lower concrete strength.
- The only pre-stressing available at the splice may be provided by the post-tensioning tendons if available.
- The use of a longer center girder segment may significantly increase the cost of transportation and increases the size of crane or cranes required for handling and erection.

Splice Width

The width of the splice depends on the duct splicing method used and on other construction requirements. However, the width of the diaphragm at the splice may also be changed if the splice width is changed, which could affect the design.

A typical splice width is 30 to 60 cm. Wider splices facilitate the placement and consolidation of concrete in the site, although the use of a diaphragm at the splice also assists in these processes. Wider splices, however, also require more field-placed concrete, and if they are cast with the deck, the placement of concrete in the larger splice and diaphragm may slow the progress of concrete placement in the deck. Wider splices also provide for more tolerance in the placement of the girders, which significantly affects the alignment and splicing of the ducts.

Splice Reinforcement

The reinforcement in the splice between girder segments is proportioned to satisfy the requirements for;

- Stress limits for the splice at the service limit state
- Shear in the splice
- The reinforcement required to satisfy shear requirements to provide a significant portion of the shear resistance. The hooked dowels or the nominal reinforcement is provided across the shear interface.

The reinforcement must be computed as part of the limiting tensile stress for the splice location. An area of reinforcement is required that resists the full tensile force in the concrete at the splice at a working stress of 0.5 fy, where fy is taken as 414 MPa, neglecting the contribution of the post-tensioning tendons crossing the splice.

The tensile force in the concrete is computed by determining the depth of tension zone at the bottom of the splice, which will be designated as x. This is accomplished using the absolute values of the computed stresses at the top and bottom of the splice. Therefore, x may be computed as (Castrodale and White 2004):

$$x = \left[f_{bot} / \left(f_{top} - f_{bot} \right) \right] h$$

…(1)

Where:

x is the depth of tension at the bottom of the splice.

f_{bot} is the absolute value of the computed stress at the bottom of the splice.

f_{top} is the absolute value of the computed stress at the top of the splice.

h is the depth of the girder.

The tensile force, T, is then computed as the product of the average stress and the width of the bottom flange as:

$$T = f_{average}(tensile\,area) = (f_{bot}/2)[b_{bot}x] \qquad ...(2)$$

Where:

T is the tensile force.

$f_{average}$ is the average stress.

b_{bot} is the width of bottom flange of girder.

The required area of reinforcement is computed by dividing this tensile force by the working stress of 0.5 fy to obtain:

$$A_s = T/0.5\,fy \qquad ...(3)$$

where As is the area of splice reinforcement.

This area of reinforcement must be provided within the tension zone. The required length to develop a hooked bar must be computed.

As required by LRPD(Castrodale and White 2004), stirrups shall be provided in the splice with a spacing not to exceed the least of the spacing in the adjacent girder segments. The same stirrup size and detailing should be used.

The reinforcement in the splice should be detailed so that access to splicing the post-tensioning ducts will not be significantly restricted.

Duct Splicing Detail

The detail for splicing of the duct should be obtained from a supplier. The length of the coupler and other duct splice details are important factors in determining the width of the splice.

The ducts should extend approximately 7.5cm into the coupler, so they must project at least 15cm from the end of the girder segment, Fig. (3).
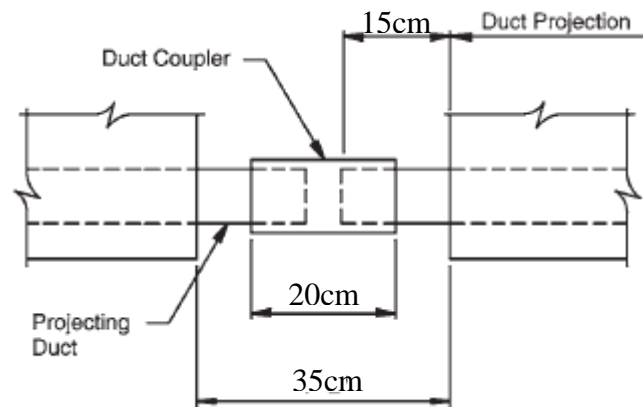

Figure (3) Schematic detail of duct splice[3]

SHEAR KEYS

Shear keys are provided in some bridges as an added factor of safety at the splice location.

TEST GIRDERS.

In this study eight spliced girders have been tested divided into three main groups. The first two groups each contains three specimens, and the third group contains two specimens.

The first group includes girders B1, B4, and B7, each having 3 pre-tensioned segments that results in a 2m length over two spans (i.e. three supports). Each is subjected to a concentrated load P at mid-span. The girder cross-sections were rectangular having dimensions of 75mm in width and depth of 160mm for B1&B7 and 140mm for B4.

The second group includes girders B2, B5, and B8 each having 3 reinforced concrete segments that results in a 4m length over one span (i.e. two supports) subjected to a uniform distributed load W over the entire span. The girder cross-section was rectangular having dimensions of (100mm) in width and total depth of (220 mm) for all girders.

The third group includes girders B3, and B6 each is of 3 pre-tensioned segments resulting in a 6m length over three spans (i.e. four supports). Each is subjected to a uniform distributed load W over the entire span. The girder cross-section was rectangular having dimensions of (100mm) in width and total depth of (220 mm) for all girders.

Figures (4, 5, and 6) shows the dimensions of the girders and reinforcement details with pre-stressing and ordinary steel. The details of cross − sectional dimensions , pre-stressing reinforcement, and ordinary reinforcement for the test girders are described in Table (1).

Eight non-spliced girders have been tested and considered as a reference to the spliced girders.

A special pre-stressing bed has been designed and fabricated for the following purposes:

(i)   pre-tensioning of segments for girders B1, B4, B7, B3, and B6.
(ii) post-tensioning of three assembled ordinary reinforced concrete segments to provide girders B2 and B8.
(iii) pre or post-tensioning of reference girders.
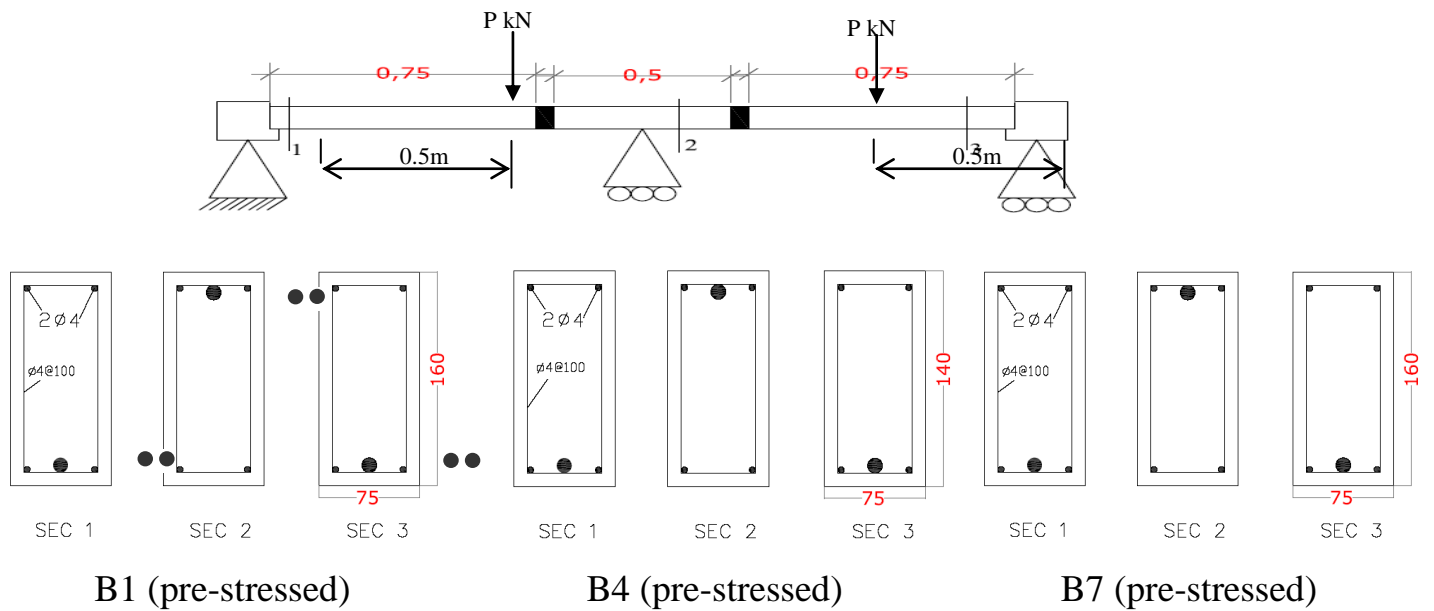
The initial wire stress was 1000 MPa for all cases.

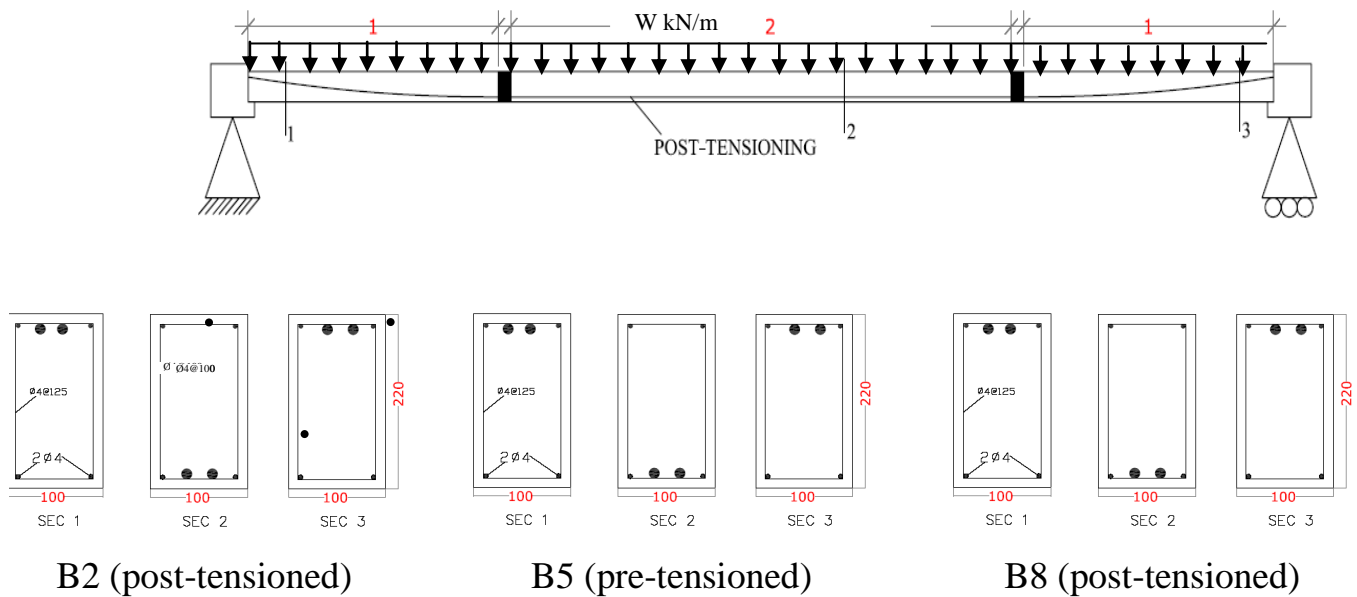**Fig. (4) Dimensions and reinforcement details of Girders (B1, B4, and B7).**

Fig. (5) Dimensions and reinforcement details of Girders (B2, B5, and B8).
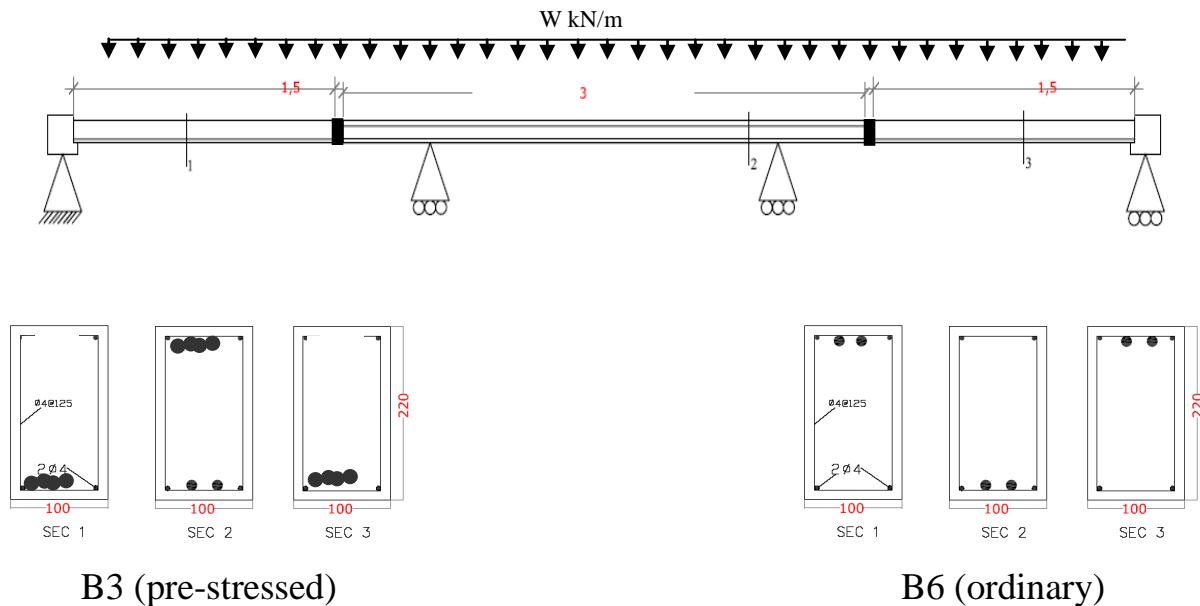
B3 (pre-stressed)   B6 (ordinary)

Fig. (6) Dimensions and reinforcement details of Girders (B3 and B6).

Table (1) Dimensions and reinforcement details for the first three groups.

Group No.	Beam section (mm)	Splicing method	Pre-stressing reinforcement				Ordinary reinforcement						Type of load
			Strand No. (wire)	Area (mm^2)	f$_{py}$ MPa	f$'_c$ (MPa)	Longitudinal reinforcement				Stirrups		
							Top		bottom				
							fy MPa	A mm^2	fy MPa	A mm^2	fy MPa	Dia mm	
G1	B1 75x160	Pre-tensioning segments spliced by ordinary R.C. splices	1	13	1570	40	480	25	480	25	480	4	Concentrated load
	B4 75x140		1	13	1570	40	480	25	480	25	480	4	
	B7 100x160		2	27	1570	40	480	25	480	25	480	4	
G2	B2 100x220	R. C. segments spliced by post-tensioning	2	27	1570	40	480	25	480	25	480	4	Uniform distributed load
	B5 100x220		2	27	1570	40	480	25	480	25	480	4	
	B8		3	40	1570	40	480	25	480	25	480	4	

	100x220													
G3	B3 100x220	Pre-tensioning segments spliced by ordinary R.C. splices	2	27	1570	40	480	25	480	25	480	4	Uniform distributed load
	B6 100x220		3	27	-	40	480	25	480	25	480	4	

f_{py} = proof yield tensile strength of pre-stressed steel

Test Results

Each spliced girder (Bi) has the same characteristics of the corresponding non-spliced girder (BiR).

The load-deflection curves of spliced girders versus that of the non-spliced girders are shown in Figures (7 to 14). Deflection of the girders was measured at mid-span for each girder by using a dial gage with travel distance of (30 mm) and accuracy of (0.01mm). Since the girder specimens are of short span the camber value of all beams was insignificant experimentally.

It is shown for different cases that the spliced girders have more deflection than that of the non-spliced girders. At about 50% of the ultimate load which corresponds to the serviceability limit state the deflection of the spliced girders is greater than that of the non-spliced girders in the range of (10%-15%). The ultimate loads for the non-spliced girders are greater than those of the spliced girders in the range of (12%-17%).
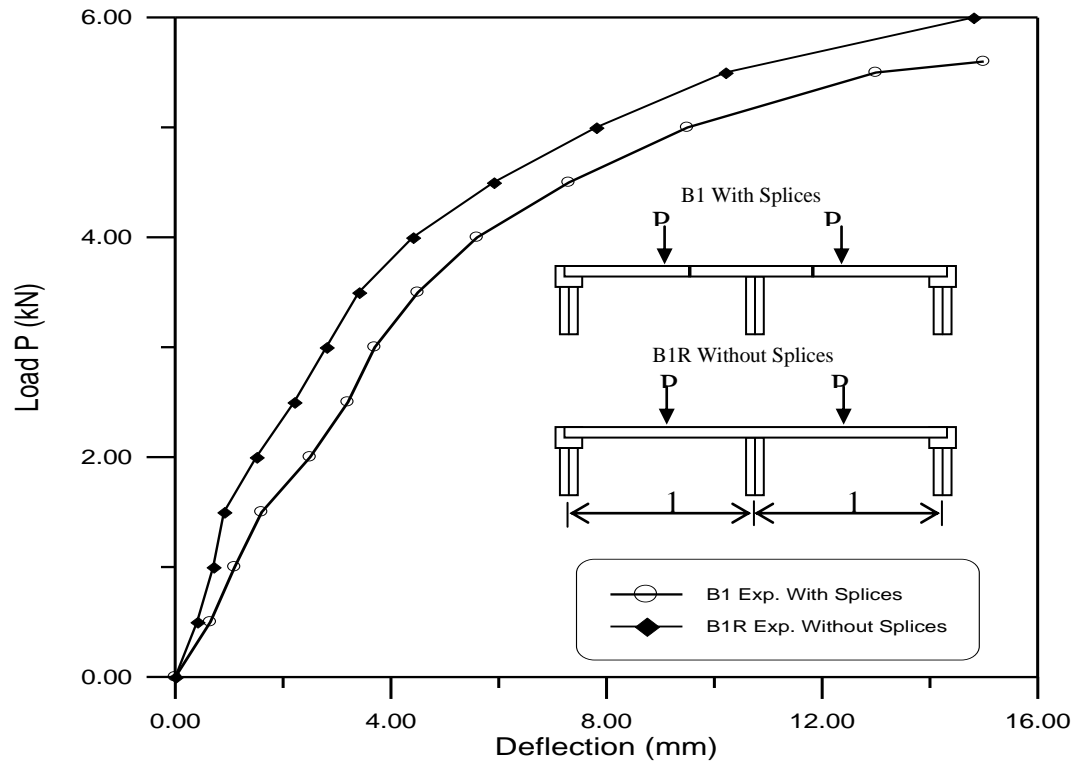
Fig.(7) Girder B1 –B1R, Load – deflection variation at mid-span considering the splicing effect.
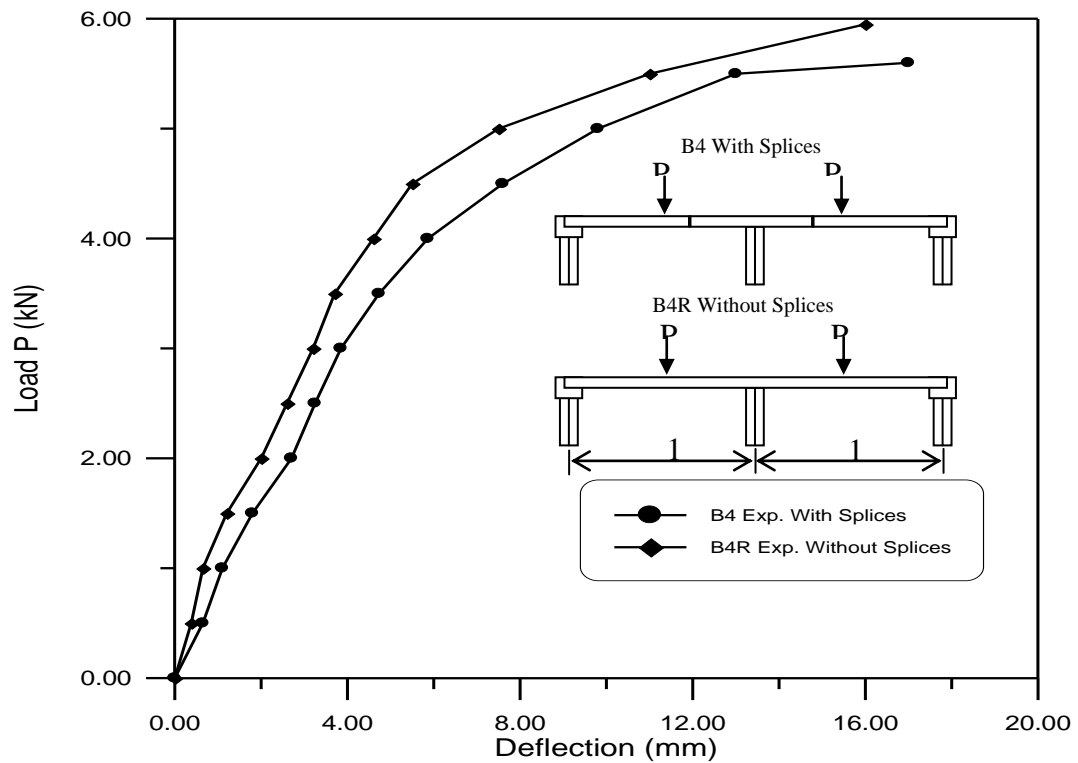

Fig.(8) Girder B4 –B4R, Load – deflection variation at mid-span considering the splicing effect.
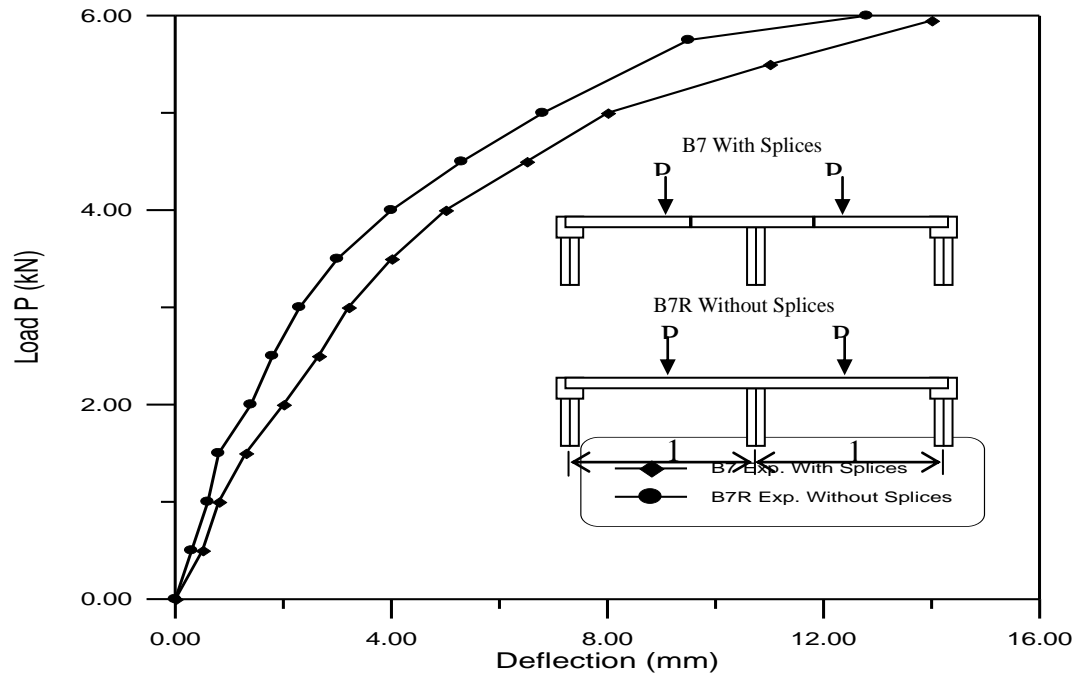
Fig.(9) Girder B7 –B7R, Load – deflection variation at mid-span considering the splicing effect.
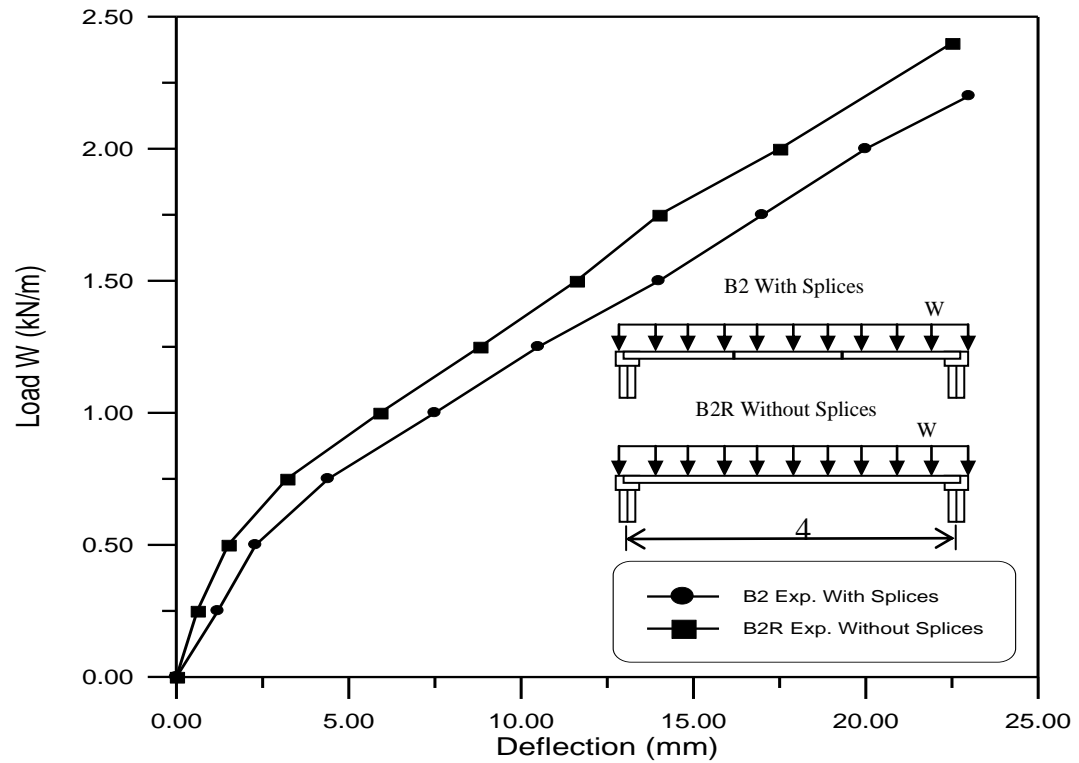

Fig.(10) Girder B2 –B2R, Load – deflection variation at mid-span considering the splicing effect.

Fig.(11) Girder B5 –B5R, Load – deflection variation at mid-span considering the splicing effect.

Fig.(12) Girder B8 –B8R, Load – deflection variation at mid-span considering the splicing effect.

4097

Fig.(13) Girder B3 –B3R, Load – deflection variation at mid-span considering the splicing effect.

Fig.(14) Girder B6 –B6R, Load – deflection variation at mid-span considering the splicing effect.
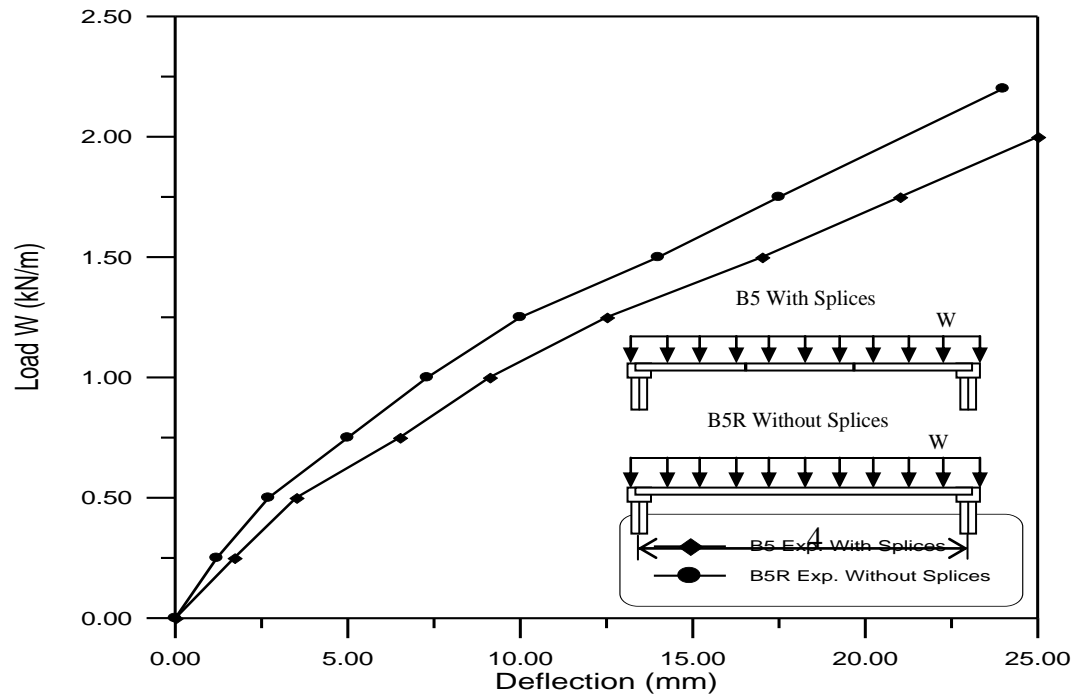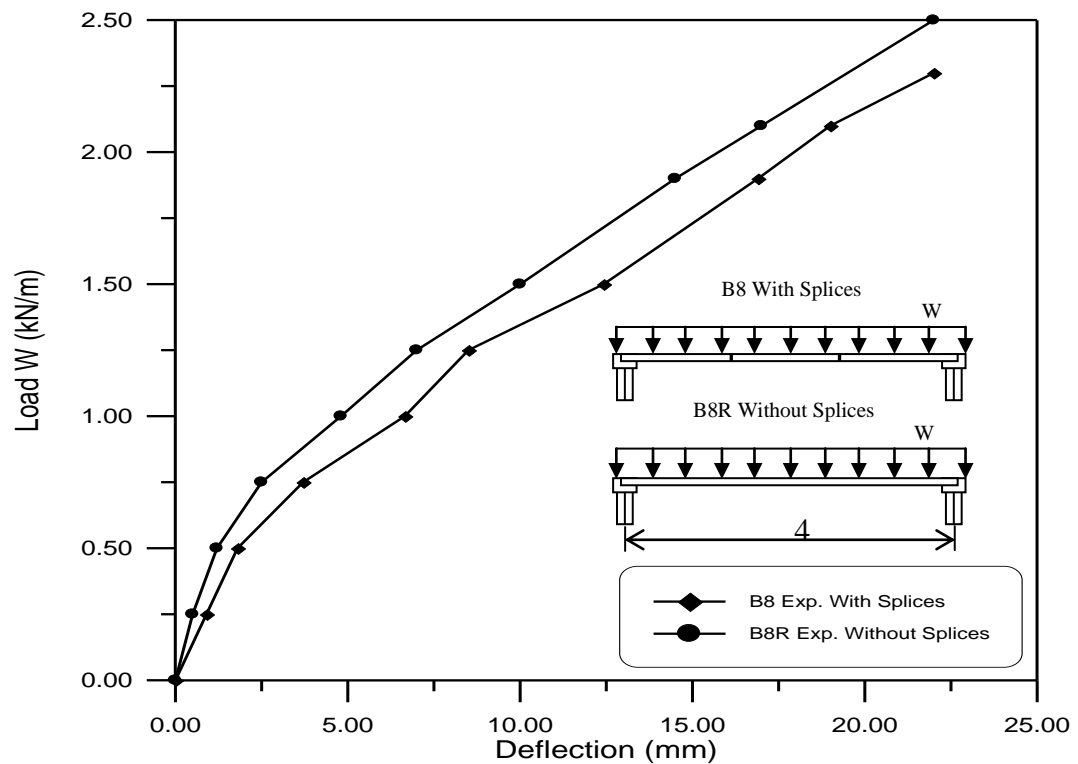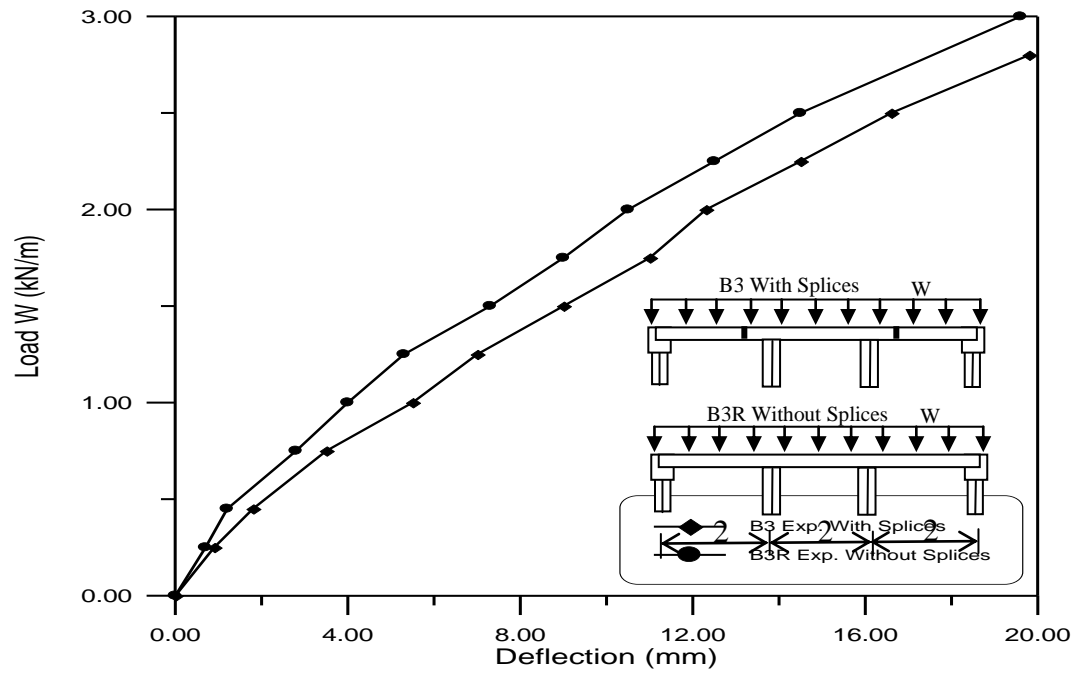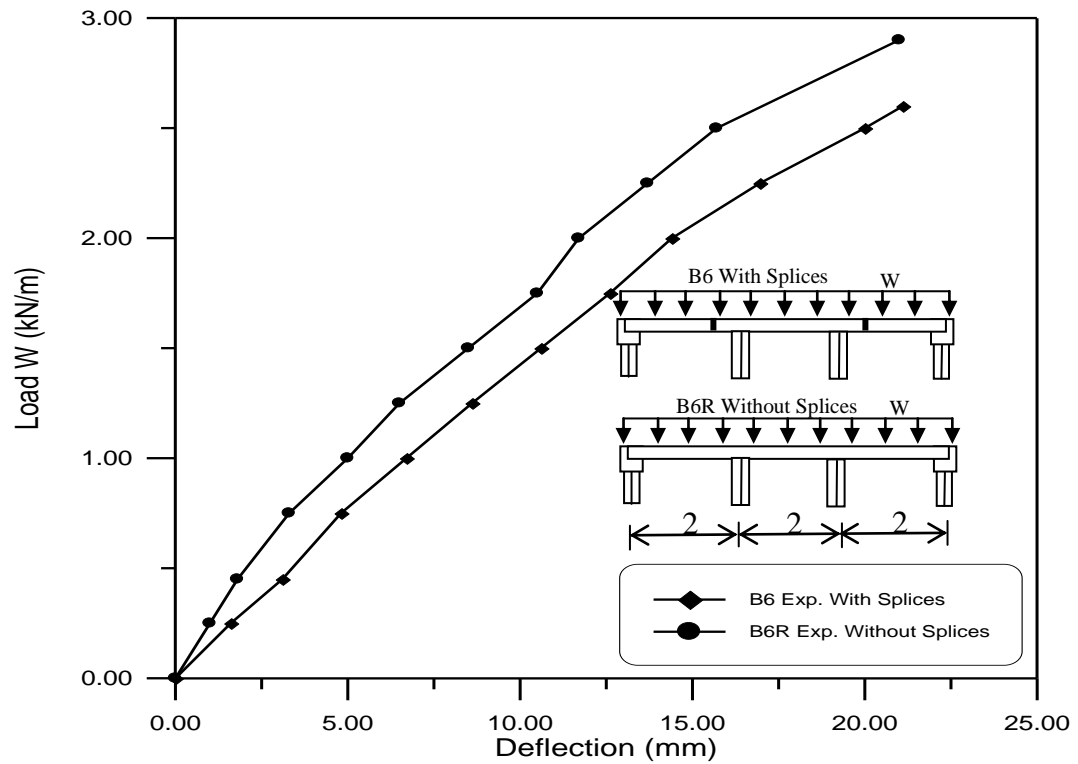
Finite Element Analysis

The finite element analysis was carried out using a modified computer program originally developed by Al-Sharabaaf (AL-Shaarbaf 1990).

The first group of girders (B1, B4, and B7) are each of two spans and 1m length for each span and have been analyzed using the finite element method for one half of the girder discretized into 56 quadratic brick elements. The second group of girders (B2R, B5R, and B8R) and the third group (B3 and B6) are analyzed by the finite element method by taking one quarter of each specimen with 32 and 48 brick elements respectively. Fine meshes were used at mid-span for each specimen.

The longitudinal reinforcement and stirrups were simulated as embedded one dimensional elements into the brick elements and the pre-stressing tendons were idealized approximately as a series of pre-stressing steel segments each of which is straight and has initial tensioning force and a constant cross-sectional area along its length.

 The finite element analysis has been carried out using the 27-point integration rule, with a force convergence tolerance of 1 %, following the modified Newton-Raphson method.

The concentrated loads for girders (B1, B4, and B7) were modeled as line loads uniformly distributed across the width of the girder and the uniformly distributed load for the other girders was modeled as groups of line loads uniformly distributed across the width of the girder (lumping procedure).

Table (2) shows the material properties, the adopted material parameters and the type of failure of these girders. The numerical load-deflection curves obtained for all girders are shown in Figs.(15 to 22). The finite element results show good agreement with the experimental results. The deflection of these girders was less than that obtained for spliced girders.

Table (2) Material properties and material parameters, and type of failure.

* Concrete	Group 1 (B1,B4, and B7)	Group 2 (B2,B5, and B8)	Group 3 (B3, and B6)
Elastic modulus, E_c (MPa)*	33460	29725	29500
Compressive strength, f'_c (MPa)*	40	40	41
Tensile strength, f_t (Mpa)*	3.3	3.9	3.8
Poisson's ratio, v	0.2	0.2	0.2
Compressive strain at f'_c *	0.0018	0.0018	0.0018
Ultimate compressive strain*	0.0039	0.004	0.0041
Cracking tensile strain*	0.002	0.002	0.0021
α_1	6	6	6
α_2	0.5	0.5	0.5

* Reinforcing steel			
Elastic modulus E_s (MPa)	200000	200000	200000
Yield stress, f_y (MPa)*	480	480	480
Ultimate strain	0.018	0.018	0.018
Yield strain	0.0018	0.0018	0.0018
* Pre-stressing steel			
Elastic modulus E_s (MPa)	195000	195000	195000
Yield point f_y*	1570	1570	1570
Ultimate strain	0.035	0.035	0.035
Yield strain	0.002	0.002	0.002
Poisson's ratio	0.3	0.3	0.3
Type of failure			
	Crushing in concrete	Crushing in concrete	Crushing in concrete

- measured by test

Fig.(15) Girder B1 –B1R: F.E.M. load – deflection variation at mid-span considering the splicing effect.

4100

Fig.(16) Girder B2 –B2R: F.E.M. load – deflection variation at mid-span considering the splicing effect.

Fig.(17) Girder B3 –B3R: F.E.M. load – deflection variation at mid-span considering the splicing effect.
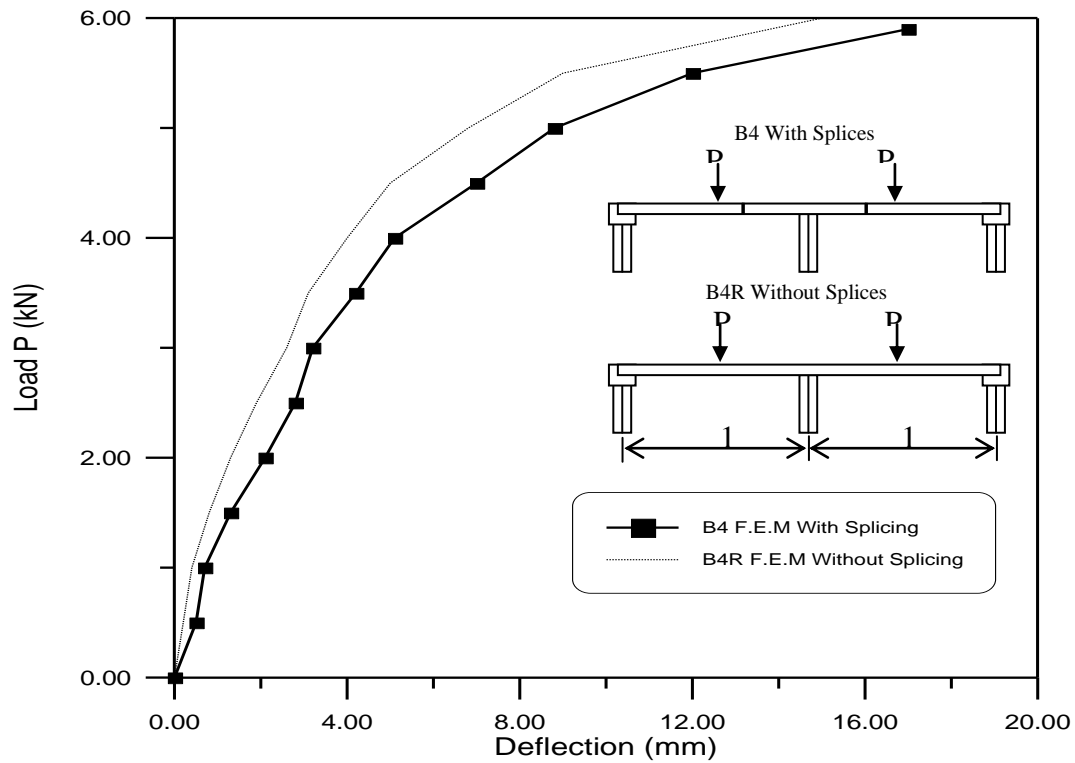
Fig.(18) Girder B4 –B4R: F.E.M. load – deflection variation at mid-span considering the splicing effect.
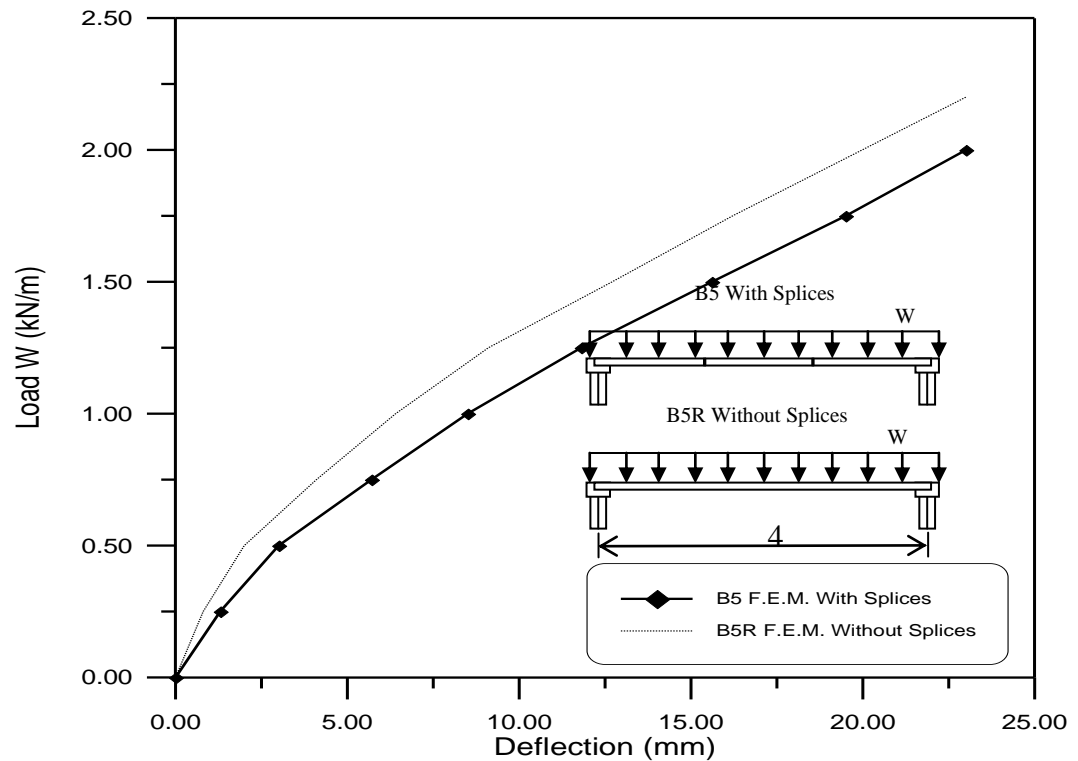
Fig.(19) Girder B5 –B5R: F.E.M. load – deflection variation at mid-span considering the splicing effect.
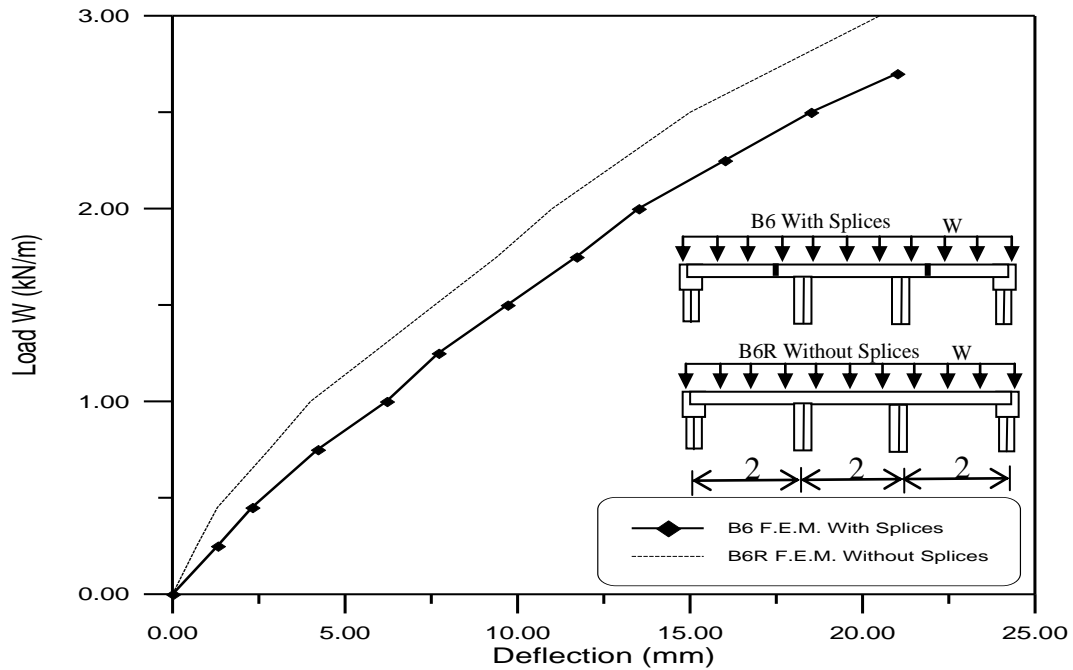
Fig.(20) Girder B6 –B6R: F.E.M. load – deflection variation at mid-span considering the splicing effect.
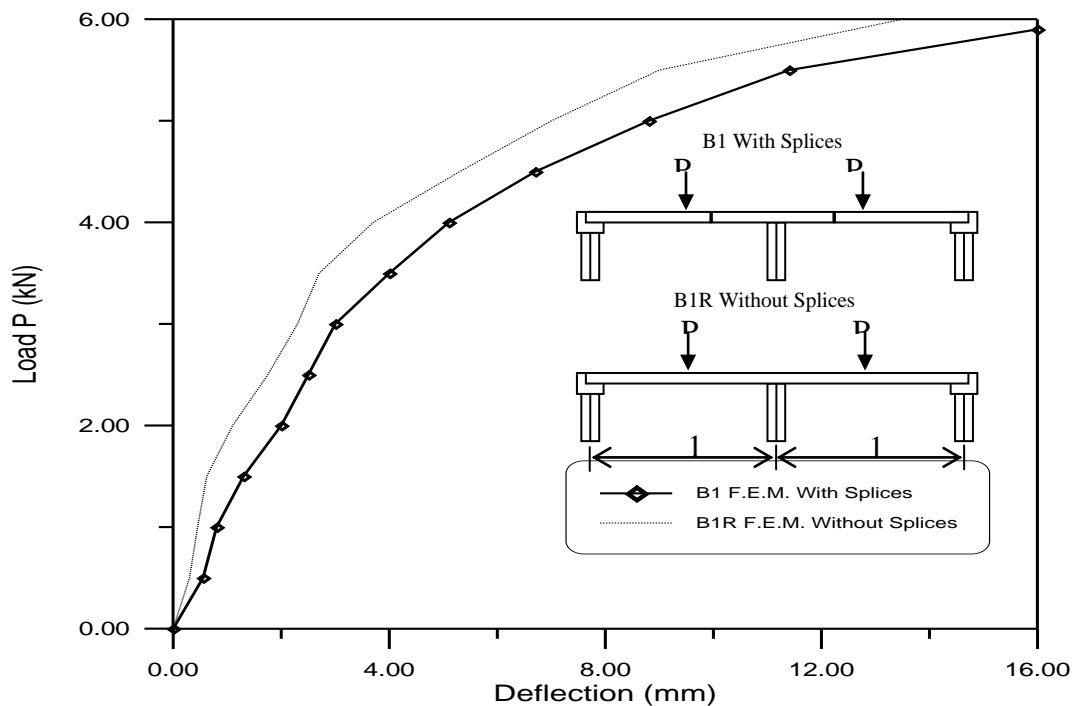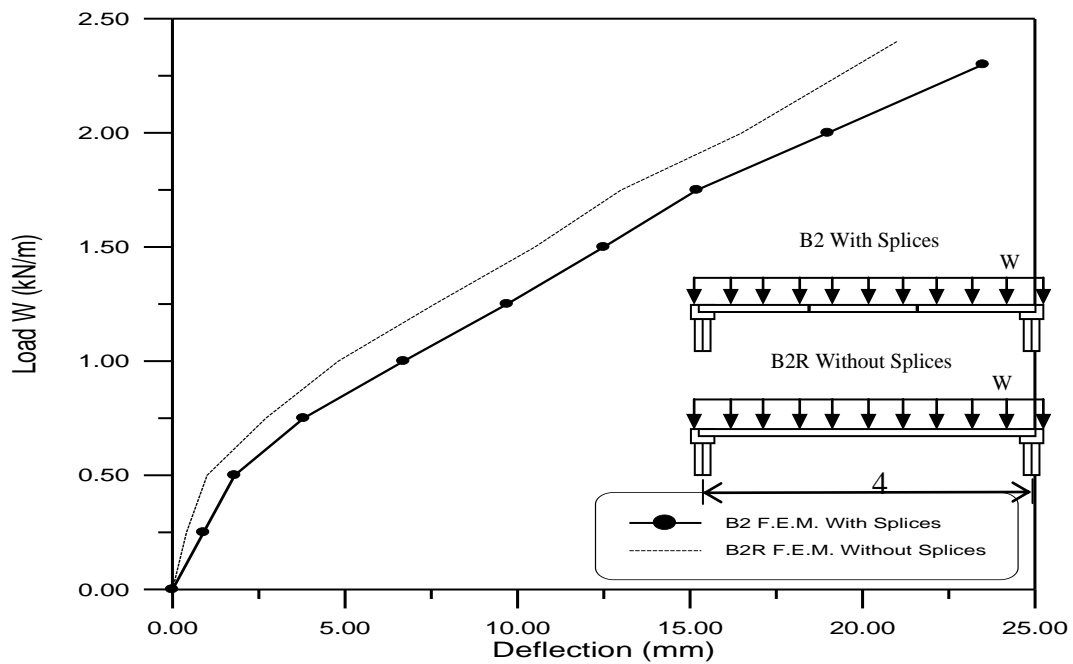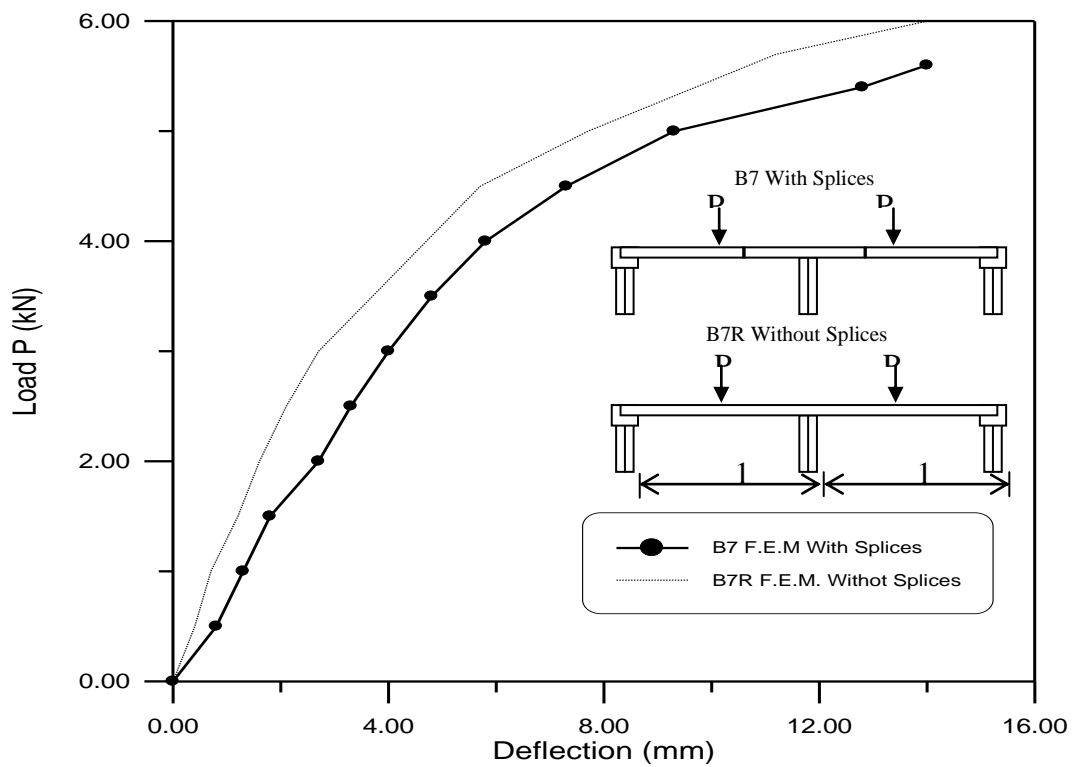

Fig.(21) Girder B7 –B7R: F.E.M. load – deflection variation at mid-span considering the splicing effect.
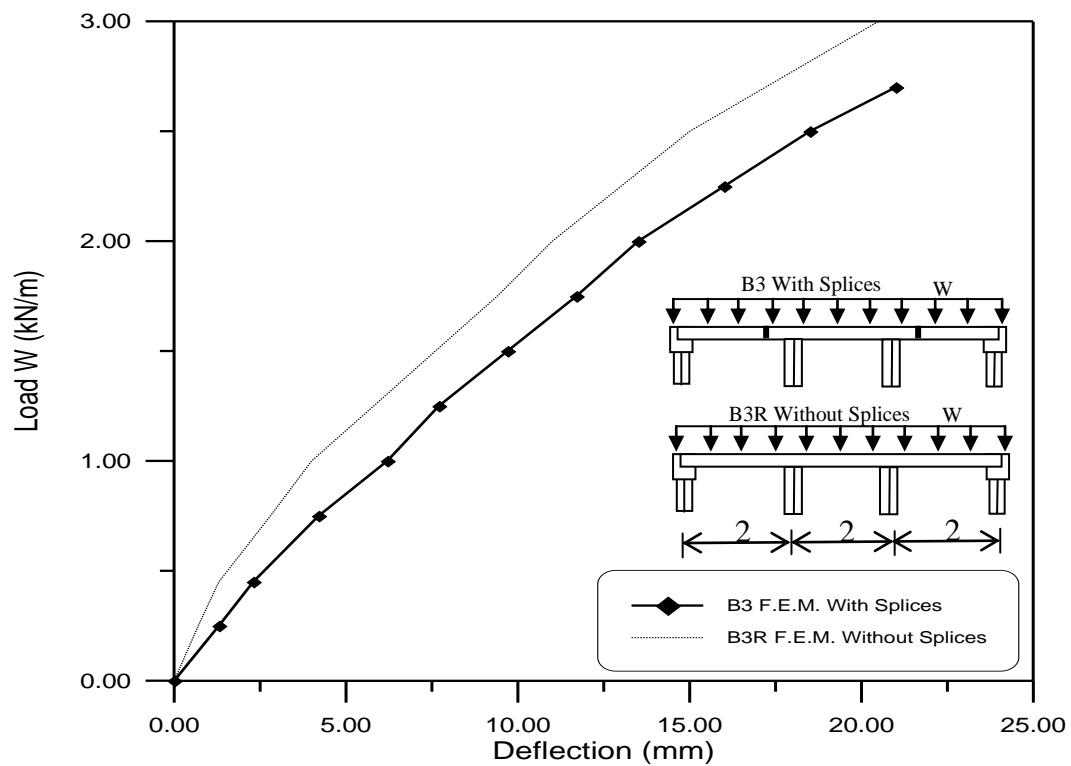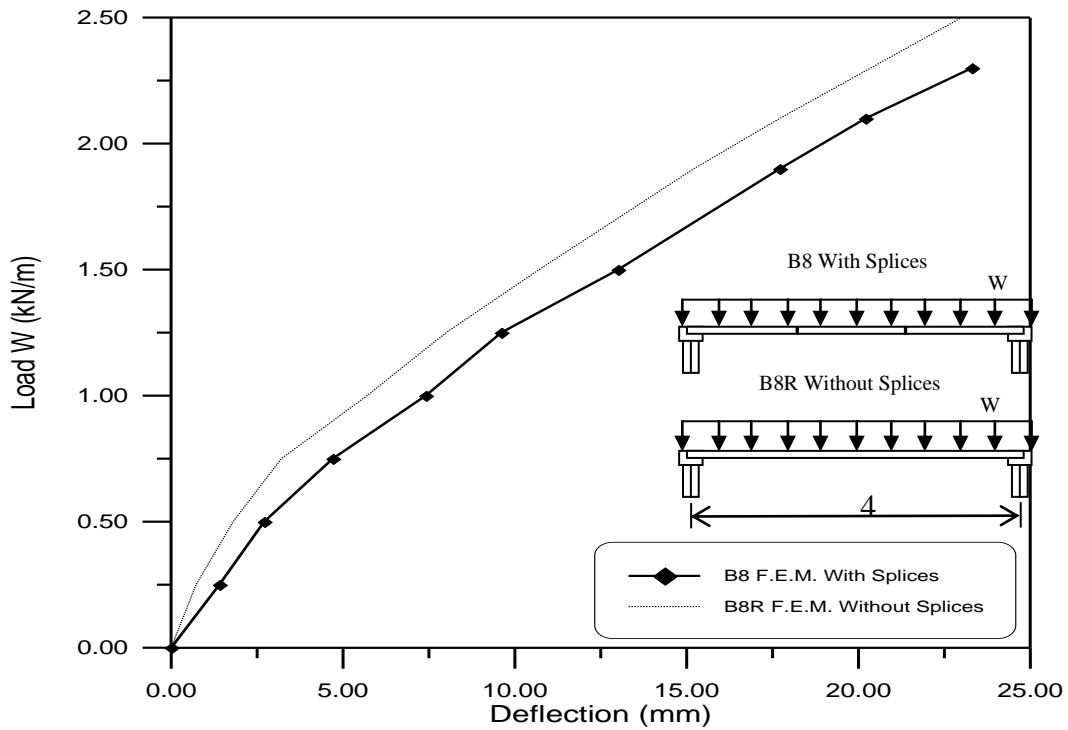
Fig.(22) Girder B8 –B8R: F.E.M. load – deflection variation at mid-span considering the splicing effect.

Discussion of Results

Table (5.6) summarizes the experimental and the finite element results for the spliced and non-spliced test girders. The table shows the deflection at 50% of the ultimate load for each girder which approximately corresponds to the serviceability limit state. Also given in the table is the ultimate load capacity for each girder.

All the differences for the above two cases results are normalized with respect to the analytical (Finite Element) results for the corresponding non-spliced case.

Table (5.6) Summary of Experimental and Analytical Results for the Test Girders

Girder No.	Mid-span Deflection at 50% of the Ultimate Load (Normalized)		Ultimate Load (Normalized)	
	Non-Spliced (F.E.M.)	Spliced* (F.E.M.)	Non-Spliced* Experimental	Spliced* Experimental
B1	1.000	1.211	0.912	0.773
B2	1.000	1.226	0.937	0.851
B3	1.000	1.292	1.090	0.832
B4	1.000	1.191	0.921	0.847
B5	1.000	1.177	0.930	0.831
B6	1.000	1.320	0.920	0.822
B7	1.000	1.223	1.150	0.767
B8	1.000	1.200	1.087	0.850

*Normalized with respect to the Finite Element Result for non-spliced corresponding case.

CONCLUSIONS

- The nonlinear finite element method presented in this study was shown to be capable of reproducing the experimental response of the spliced pre-stressed concrete girders. The isoparametric brick elements with embedded steel bars proved to be suitable for predicting the state of ultimate load and deflections with good accuracy. Generally, the differences with experimental values (in deflection or ultimate load) were in the range (8-12%) for the case of spliced and non-spliced girders.

- The experimental results showed that at about 50% of the ultimate load which corresponds to the serviceability limit state the deflection of the spliced girders is greater than that of the non-spliced girders in the range of (10%-15%) and the ultimate load for the non-spliced girders is greater than that of the spliced girders in the range of (12%-17%).

- The concept of lumping equivalent nodal forces used in the present study is capable to simulate the loads exerted by the pre-stressing tendon upon the girders. The contribution of the pre-stressing tendon stiffness to the element stiffness is found to have some effect on the analysis.

REFERENCES

- AASHTO LRFD Bridge Design Specifications, 2nd Edition with Interims, American Association of State Highway and Transportation Officials. Washington, DC. (1998– 2003).

- Volume 4 of 10: Design and Construction Inspection of Precast Concrete Spliced I-Girder Bridges." Structures Design. Office Report, Florida Department of Transportation, Tallahassee, FL. (September 2002),

- Garcia, Antonio M., "Florida's Long Span Bridges: New Forms,New Horizons." PCI Journal, Vol. 38, No. 4. (July–August 1993) pp. 34–49.

- Janssen, H. Hubert, and Spaans, Leo, "Record Span Spliced Bulb-Tee Girders Used in Highland View Bridge." PCI Journal, Vol. 39, No. 1. (Jan–Feb 1994) pp. 12–19.

- Chen, Wai- Fah and Duan, Lian, Editors, "Bridge Engineering Handbook- Chapter 11- Segmental Concrete Bridges," CRC Press, New York, 1999.

- Lwin, M., " Segmental Concrete Bridge Design and Construction Practices" Segmental Concrete Bridge Technology Virtual Team, 2000.

- American Trade Initiatives, " Performance of Concrete Segmental and Cable-Stayed Bridges in Europe." FHWA Report No. FHWA- PL- 01- 019, Washington, DC (May 2001) 104 pp.

- Castrodale Reid W. and White Christopher D., "Extending Span Ranges of Precast Prestressed Concrete Girders" NCHRP, Report 517, Washington, D.C. 2004.

- AL-Shaarbaf, I.A.S., "Three-Dimensional Nonlinear Finite Element Analysis of Reinforced Concrete Beams in Torsion", Ph.D. Thesis, University of Bradford, U.K., 1990.

THE EFFECT OF OPERATING CONDITION FOR CUMENE CRACKING ON THE PERFORMANCE OF PREPARED HX - ZEOLITE CATALYST

Prof. Dr. Abdul Halim A.K. Mohammed

Samar k. Dhidan

Maha H. Al.Hassani

ABSTRACT

The present study reports the effect of temperature and liquid hourly space velocity (LHSV) on the cumene cracking reaction rate and selectivity by using a laboratory continuous flow unit with fixed bed reactor operating at atmospheric pressure. The prepared HX zeolite was made from Iraqi kaolin with good crystallinity .The activity and selectivity of prepared HX-zeolite was compared with standard HY zeolite and HX zeolite catalysts in the temperature range of 673-823K and LHSV of 0.7-2.5 h^{-1}. It was found that the cumene conversion increases with increasing temperature and decreasing LHSV at 823K and LHSV of 0.7 h^{-1} the conversions 65.32, 42.88 and 59.42 mol% for HY, HX and prepared HX catalysts respectively and at LHSV of 2.5 h^{-1} and the same temperature the conversions decrease to 29.24, 12.53 and 22.89 mol%, respectively .It also found that the benzene yield increases with increasing temperature at 823K and LHSV of 0.7 h^{-1} the benzene yields were 58.79, 38.56 and 54.56 mol% for HY zeolite , HX zeolite and prepared HX zeolite, respectively and the selectivity to benzene is nearly constant over the studied temperatures range. The kinetics of cumene cracking (the kinetics parameters-rate constant)and activation energy are used in this study to characterize differences between various catalysts. The reaction was found to be first order with activation energy equal to 78.58 , 89.10 and 97.77 kJ/mol for HY, prepared HX and HX , respectively.

الخلاصة

تبحث الدراسـة الحاليـة تـأثير درجـة الحـرارة و السـرعة الفراغيـة علـى معدل تفاعل التكسـير للكيـومين و الانتقائية باستخدام وحدة جريان مستمر مختبرية تحتوي على مفاعل ذو حشوة ثابتة تعمل تحت الضـغط الجوي . HX zeolite المحضر صنع من الكأولين العراقي و يمتلك نسبة تبلور جيدة .تم مقارنة الفعالية و الانتقائية لـل HX zeolite المحضر مع عوامل مساعدة قياسية HY zeoilte و HX zeolite ضمن مدى درجات حرارة 673-823 ك ولسرع فراغية 0.7- 2.5 سـا⁻¹ .وقد لـوحظ زيـاده تحول الكيومين مع زيـادة درجـة الحرارة ونقصان السـرعة الفراغيـة في درجـة حرارة 823 ك وسرع فراغيـة0.7 سـا⁻¹ كـان التحـول 65.32، 42.90 و 59.42 مـول% لكـل مـن HY ، HX و Prepared HX على التوالي و بسرعة فراغيـة2.5 سـا⁻¹ و نفس درجـة الحرارة كـان التحـول 29.24 ، 12.53 و 22.89 على التوالي و كما لـوحظ ان نـواتج البنزين تـزداد بزيـاده درجـة الحرارة عند درجة 823 ك وسرعة فراغيـه 0.7 سـا⁻¹ نواتج البنزين كانت 58.79، 38.56و54.56 مـول% لكل مـن HY ، HX و Prepared HX على التوالي . وقد لـوحظ ان انتقائيه البنزين هي تقريبا ثابته على مدى درجـات الحرارة المدروسة لكافه العوامل السـاعدة المدروسة. امـا حركيـة التفاعـل لتكسـير الكيـومين وثابت معدل التفاعـل وطاقـه التنشـيط اسـتخدمت فـي هذه الدراسـة لتشخيص الاختلافات بين العوامل المساعدة المختلفه.ولقد لـوحظ بـان التفاعـل من المرتبـه الاولـى مـع طاقات تنشيط 78.58 ،89.10 و 97.77كيلو جول / مول لكل من HY، prepared HX و HX على التوالي .

A. H. A.K. Mohammed	The Effect of Operating Condition for Cumene
S.k. Dhidan	Cracking on The Performance of Prepared
M.H. Al.Hassani	HX - Zeolite Catalyst

INTRODUCTION

The cracking of pure hydrocarbon and in particularly the dealkylation of cumene can provide important method for investigation the nature of catalyst [Prater and Lago,1956]. The dealkylation of cumene has been recognized as suitable rapid method for screening catalysts as compared with the gas oil method because it is possible to analyze the reaction products with a gas chromatographic analysis rather than by distillation, effecting an appreciable saving in time [Nicholson D. E. ,1955].

Donald and Wojciechowski (1977a) studied the catalytic cracking of cumene and they observed over 60 reaction products and the selectivity behavior of the major ones has been examined. They used a fixed bed reactor charged with LaY zeolite catalyst. A total of 67 compounds have been isolated in the reaction products. Twenty-eight of these have been found to be light hydrocarbons up to a boiling point of 80°C and include most isomers of C_4, C_5, and C_6. The remaining fractions contain phenyl compounds, 29 of which have higher boiling points than dipropyl benzene and comprise less than 0.1% of the total products.

Cumene dealkylation reaction on fresh catalyst had been reported to be promoted by Brönsted acid sites [Tanabe K.,1970]. The high selectivity of the reaction over acid catalysts is related to the high proton affinity of the benzene ring and to the stability of the ejected carbonium ion [Peter A. J.,1977].

The catalytic cracking of cumene commences with chemisorption of cumene on a single active site. This is followed by splitting the molecules to propylene and benzene. The reverse reaction, the alkylation of benzene to cumene requires the adsorption of either benzene or propylene on an active site followed by a radical mechanism [Donald and Wojciechowski,1977b].

The knowledge of the kinetics of the reaction at the active sites is of primary importance in determining the nature and the difference between catalytic action in heterogeneous catalysis [Prater and Lago,1956].

Haensel V.(1951) has used cumene as a test for cracking catalyst (silica-alumina) at a reaction temperature between 350-550°C and LHSV 5 h^{-1} in fixed bed reactor. He found that the yields of benzene are ranging from 5- 39 wt%, and found that the reaction is partly reversible in the lower temperature range.

Plank and Nace (1955) studied the cumene cracking and coke formation over silica-alumina at 800-1000 F° (699.66-810.77 k) and 2-6 h^{-1} LHSV in fixed bed reactor and found that when temperature increases the conversion of cumene increases, and decreases as LHSV increases.

Schwab and Sieb (1964) studied the catalytic activity and the activation energy in the cracking of cumene, and they found that the replacement of the Na ion by divalent cations Ca or Mg decreased the activation energy of 231 kJ/mole by a factor of 2.

Pansing and Malloy (1965) reported, the cracking rates which are inferred from the rate of appearance of propylene gas are thus liable to serious error; however rates determined from benzene appearance are more reliable. The value of activation energy obtained by Pansing and Malloy was 86.52 kJ/mole.

Donald and Wojciechowski (1977b) used cumene cracking reaction to evaluate the activity of 100/140 mesh of LaY zeolite catalyst. And they studied the kinetic of cumene dealkylation over LaY at three reaction temperature 360, 430, and 500°C in tubular reactor and they assumed that the endothermic chemisorption of cumene must be in order to

construct a plausible picture of the reaction energy surface, and they were also shown that the diffusion limitations affects the rate of catalyst decay to a different extent than the rate of reaction ,and they also found the activation energy for the dealkylation of cumene to be 94.5 kJ /mole .

Corma and Wojciechowski (1980) studied the initial selectivities for primary products in the catalytic cracking of cumene on HY and LaY zeolite catalysts in an integral fixed bed glass tubular reactor . It was observed that the reaction products and their characteristics behavior have been found to be the same for both LaY and HY zeolites at 360, 430 and 500 °C, which is due to the similarity in the nature of the active sites in both catalysts. At a temperature range 360-500°C the obtained selectivity for benzene ranged from 0.16 to 0.94 and from 0.65 to 0.94 mol% over HY and LaY zeolites, respectively.

Selim et al. (1992) studied the activities of different Nd-zeolite prepared from the original NaX and NaY zeolites by ion exchange at reaction temperature between 300-420°C by using microcatalytic technique. Cumene cracking was used as a reaction model and found that NdY-zeolite was more active than NdX-zeolite, and the reaction is a first order with an activation energy of 67.2 kJ/mol. Also it was observed that the catalytic activity at the same temperature was found to be higher for Y-zeolites than that corresponding X-zeolite.

Al-Kattaf and de Lase (2001) used a riser simulator to study the kinetics of cumene cracking over two sizes of zeolite crystals (0.4 and 0.9 μm). It was shown that the kinetics follows first order reaction and the main reaction pathway of cumene cracking involves the cleavage of the isopropyl group to produce benzene and propene.

Samar, K. Dh. (2008) prepared HX-zeolite from Iraqi kaolin . The catalytic activity of catalyst prepared from local kaolin was studied by using cumene cracking as a model for catalytic cracking and compared with standard HY zeolite and HX zeolite catalysts. The activity test was carried out in a laboratory continuous flow unit with fixed bed reactor at duration time in the range 10-240 minutes, temperature 823 K , and LHSV 1 h^{-1} .

This work deal with the study of the effect of temperature and LHSV on the cumene cracking reaction rate and selectivity by using prepared and standard catalysts and the study of kinetic of dealkylation process .

MATERIALS AND CATALYSTS PREPARATION
-Cumene

Cumene supplied by BDH with 98% purity was use as a feedstock in this work. It has molecular weight 120.20 g/mol, density of 0.860 g/cm^3 and boiling point of 423K.

-HY-Zeolite

HY-Zeolite (CBV600) was supplied from Zeolyst International (UWE Ohlrogge (VF)) as a powder. This zeolite has 0.2 wt% of Na_2O, SiO_2/Al_2O_3 mole ratio of 5, unit cell of 24.3 Å, pore volume of 0.92 and surface area of 660 m^2/g. A 70 g of HY-zeolite as a powder was mixed with 30 g montmorillonite clay as binder. The chemical composition of montmorillonite is: 51.3%SiO_2, 28.73%Al_2O_3, 1.3%Na_2O, 3.4% CaO, and 3.3 % MgO. The resulting mixture was mixed with water to form a paste. The paste was placed in a cylindrical cavity of 2 cm inside diameter, and 10 cm long. Extrudates shapes were obtained when the paste was compressed manually. Very uniform spaghetti shaped paste was ejected and put in a porcelain crucible at room temperature overnight. Extrudates were dried in a programmable electrical furnace at 120°C for 2 hr. The calcination was done at

A. H. A.K. Mohammed	The Effect of Operating Condition for Cumene
S.k. Dhidan	Cracking on The Performance of Prepared
M.H. Al.Hassani	HX - Zeolite Catalyst

550°C for 2 hr. Then the calcined extrudates were cut into 4-8 mm long [Samar, K. Dh.,2008] .

NAX-ZEOLITE

Synthetic crystalline zeolite type 13X was delivered by Linde Company as a pellets (3×5) mm. This catalyst has 14 wt% of Na, SiO_2/Al_2O_3 mole ratio of 2.2, unit cell of 24.9 Å, pore volume of 0.35, and surface area of 340 of m^2/g. Hydrogen-form from standard Na-X zeolite was prepared by ion exchange method of the original Na-X catalyst with ammonium nitrite solution [Samar, K. Dh.,2008].

PREPARED HX-ZEOLITE

The prepared HX-zeolite from Iraqi kaolin was prepared by steps consisting from; a gel formation step of metakaolin in alkaline medium in presence of additional silica to crystallize the zeolite was achieved at 60 ^oC for 1 hr, and with stirring. In ageing step of the reactants at room temperature for 5 days and crystallization step at 87±2 ^oC for 24 hr. The next steps were decantation, washing, filtration and drying. A 100 g of catalyst powder was prepared by mixing 25 g of the binding material which is kaolin with 75g of catalyst powder and the paste was placed in a cylindrical cavity a extrudates shapes were obtained when the paste was compressed manually then the extrudates were dried and calcined . The hydrogen-form catalyst was prepared by ion exchange method of the original catalyst with ammonium nitrite solution .This catalyst has 0.848 % Na_2O, SiO_2/Al_2O_3 mole ratio of 2.8,pore volume 0.318 cm^3/gm and surface area 290.19 m^2/g after ion exchange [Samar, K. Dh.,2008] .

ACTIVITY TEST

The cracking activity tests were performed in a continuous laboratory unit . Figure 1 shows the process flow diagram of this unit. The unit consists of feed tank, flow meter, feed pump, evaporator, reactor, separator, collector and cooler with appropriate control system for heating. The reactor was a carbon steel tube with an outside diameter of 1.9 cm, 2 mm thickness and 80 cm length. A 30 cm^3 (17 cm height) fresh catalyst was charged to the reactor between two layers of inert materials (glass balls). The catalytic cracking reaction conditions, employed are temperature 673-823K, liquid hourly space velocity of 0.7-2.5 h^{-1} (0.35-1.25 ml/min of cumene)and the pressure kept atmospheric. The charged catalyst was replaced of each temperature. Liquid products were trapped by condenser at -5 ^oC , collected periodically and analyzed by using gas chromatography.The gas chromatography model Packard 438A was used for the analysis .This device equipped with column of 0.25mm diameter, 50 m length and FID detector.

CATALYST ACTIVITY

Cumene cracking was chosen as a model to evaluate the activity of the prepared HX-zeolite and to compare the results with the activity of the standard catalysts HY and HX Zeolite. Cumene conversions over the prepared and standard catalysts were determined after the first 10 minutes of each run.

Gaseous Product to gas chromatography analysis

Liquid Products to gas chromatography analysis

1	Feed Container	10	Mixer
2	Feed Burette	11	Reactor
3	Three Way Valve	12	Thermocouple
4	Dosing Pump	13	Condenser
5	Nitrogen Cylinder	14	Collector
6	Gas Regulator	15	Temperature Controller
7	Two Way Valve	16	Cooling Machine
8	One Way valve		
9	Evaporator/Preheater		
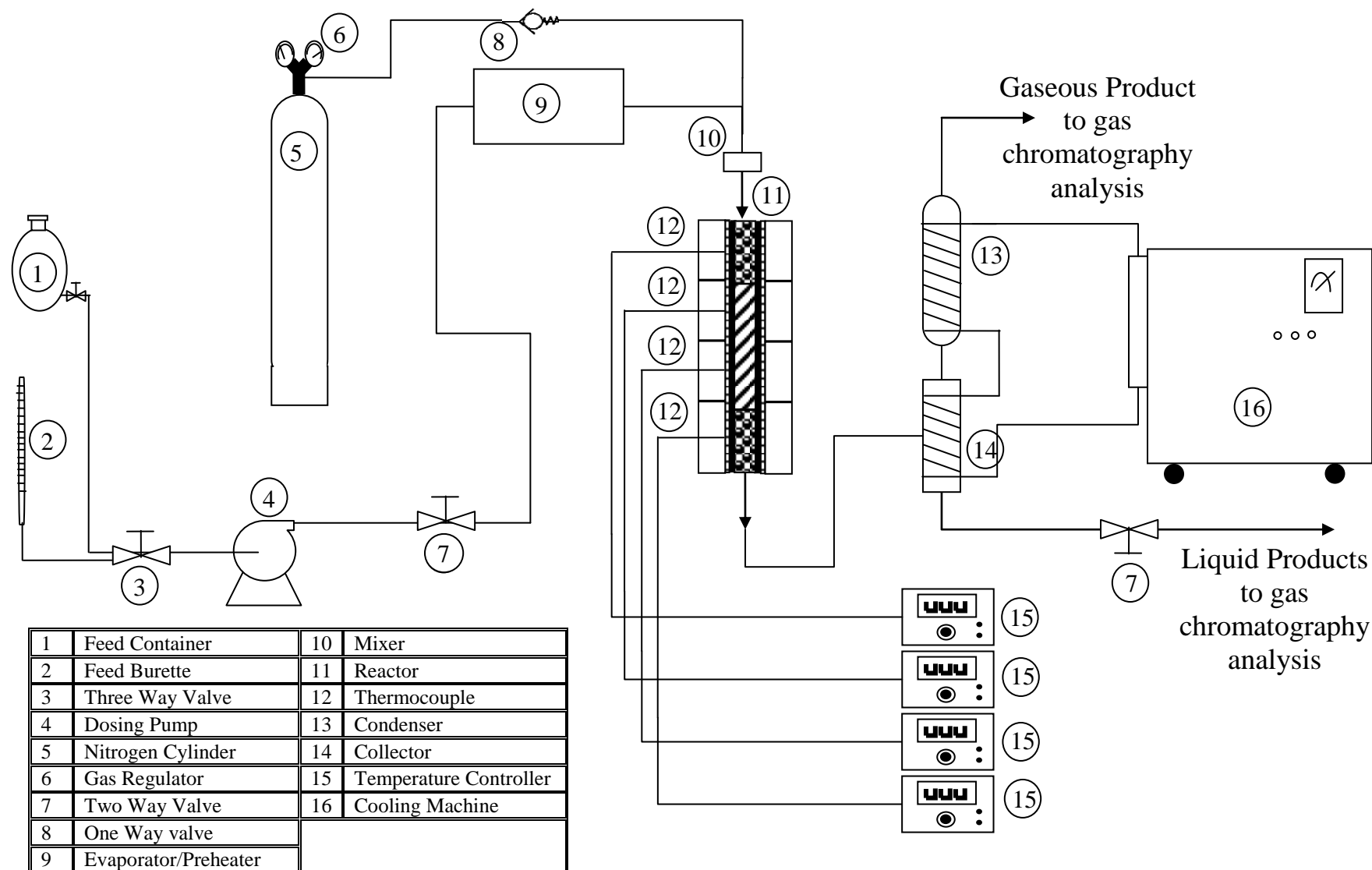
Figure 1. Flow Diagram of The Laboratory Reaction Unit.

A. H. A.K. Mohammed	The Effect of Operating Condition for Cumene
S.k. Dhidan	Cracking on The Performance of Prepared
M.H. Al.Hassani	HX - Zeolite Catalyst

RESULTS AND DISCUSSION

Effect of LHSV and Temperature

Figures 2,3 and 4 show the effect of LHSV on conversion at different temperatures using HY- zeolite , HX- zeolite and prepared HX-zeolite .

From these figures the changes of cumene conversion are function of LHSV (which is inverse of space time). At LHSV of 0.7 h^{-1} and temperature 823K, the conversions of cumene are 65.32, 42.88 and 59.42 mol% for HY, HX and prepared HX catalysts, respectively and at LHSV of 2.5 h^{-1} and the same temperature the conversions decrease to 29.24, 12.53 and 22.89 mol%, respectively.

As the LHSV increases cumene conversion decreases which means that decreasing in the residence time offers a less of contact time for cumene with catalysts.

The above mentioned figures show that the cracking rates favor low LHSV. These observations agree well with the previous investigation reported by Plank and Nace (1955) and Selim et al. (1992).

The conversion increases as the temperature increases over the studied catalysts (fig. 2-4). At 673K and LHSV of 0.7 h^{-1}, the conversions are 9.0, 1.4 and 5.9 mol% for HY, HX and prepared HX catalysts respectively, while at 823K using the same LHSV the conversions reach 65.32, 42.90 and 59.42 mole% respectively.

This is attributed to the increase of active sites that can be used for the reaction when the temperature increases. These observations are well agreed with the results reported by Plank and Nace (1955), Ahmed J. A. (1982), Emad F.M. (1985) , Selim et al.(1992) and Al-Khattaf and de Lasa (2001).
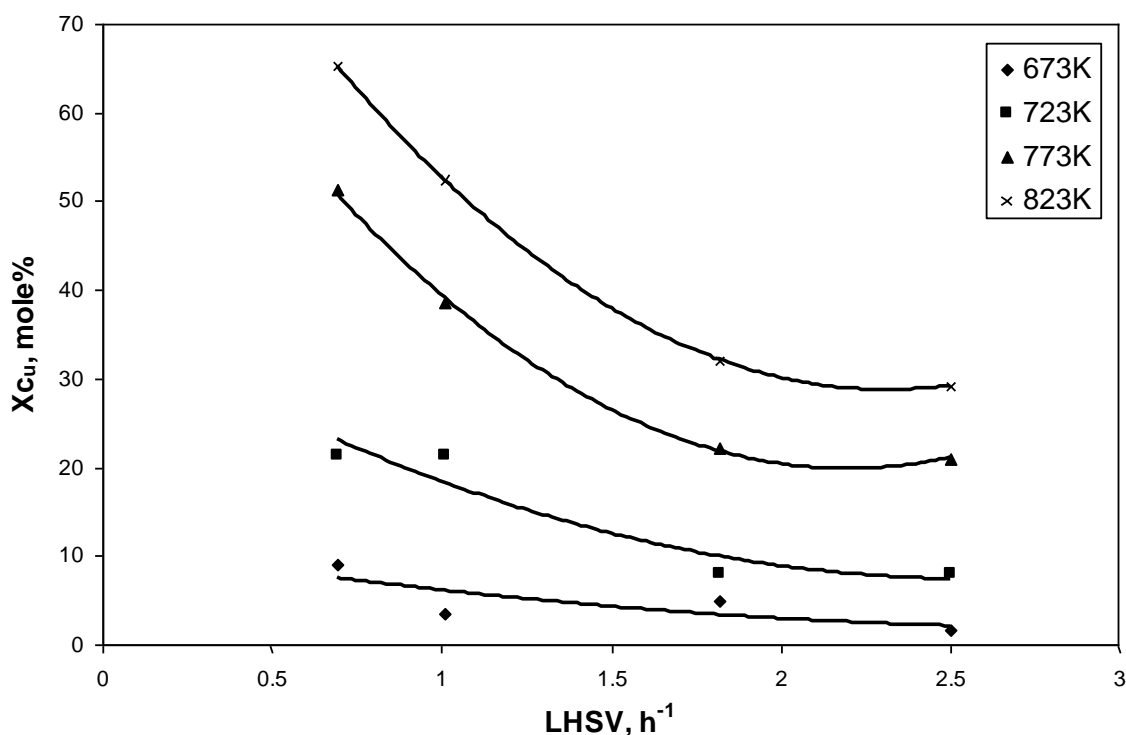

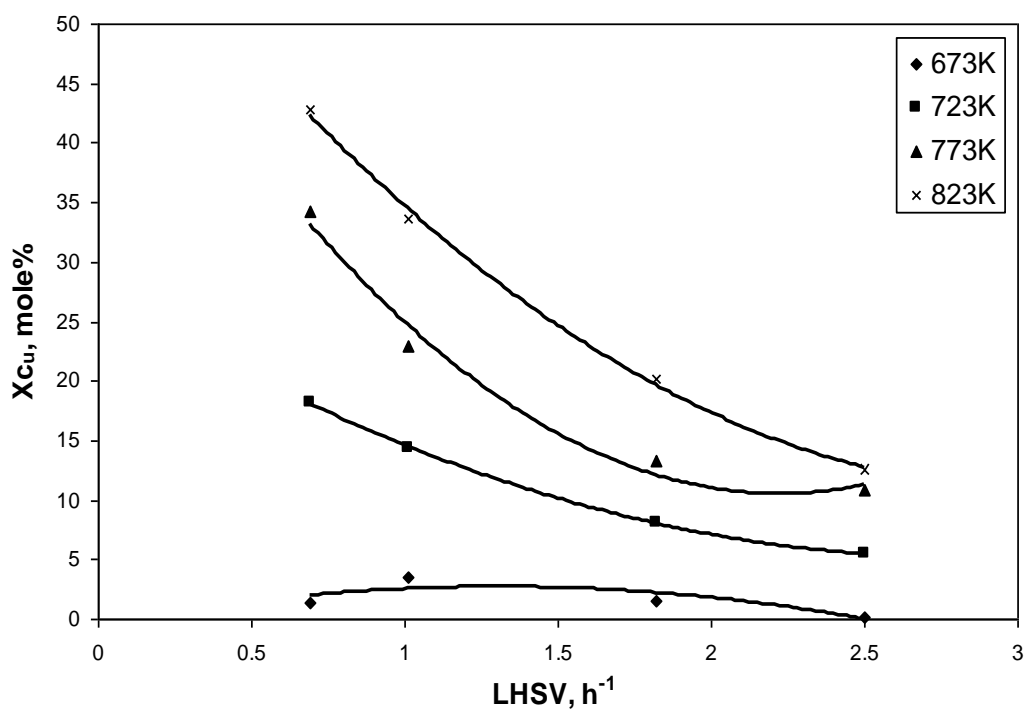**Figure 2** Effect of LHSV on Cumene Conversion at Different Temperatures Using HY Catalyst.

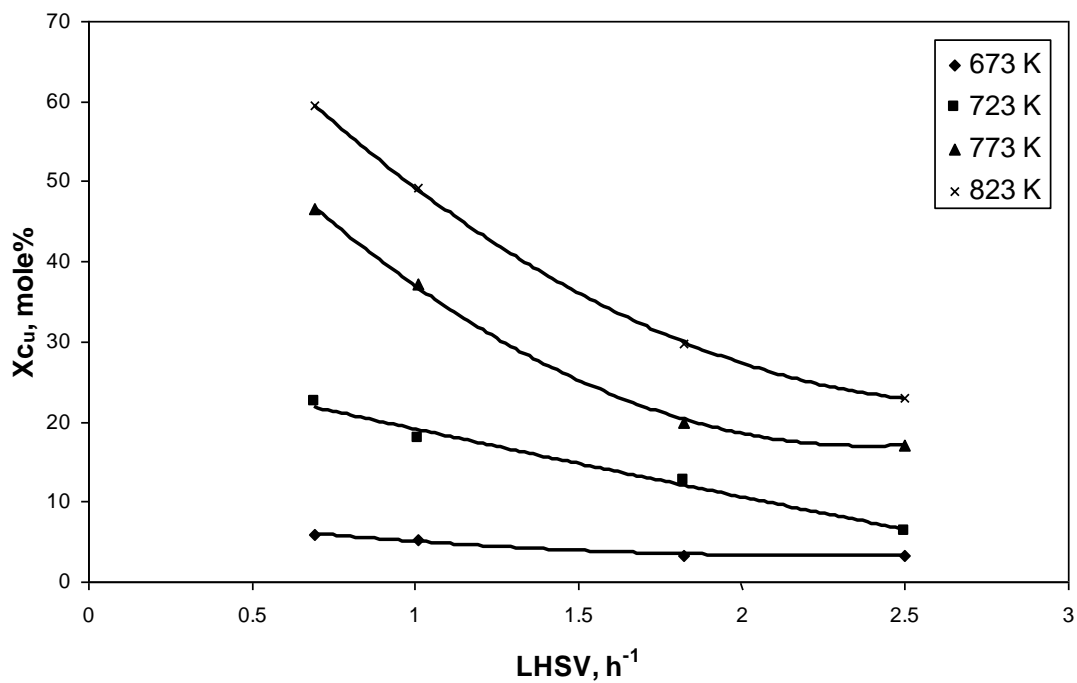**Figure 3** Effect of LHSV on Cumene Conversion at Different Temperatures Using HX Catalyst.

Figure 4 Effect of LHSV on Cumene Conversion at Different Temperatures Using Prepared HX-zeolite.

A. H. A.K. Mohammed	The Effect of Operating Condition for Cumene
S.k. Dhidan	Cracking on The Performance of Prepared
M.H. Al.Hassani	HX - Zeolite Catalyst

KINETICS OF CUMENE CRACKING

The obtained results from the laboratory reaction unit of cumene cracking were analyzed by the available kinetic models.

The results correlated with zero, first and second order kinetic equations (eq. 1,2 and 3)assuming ideal plug flow models[Prater and Lago,1956 and Levenspiel,1999].

$$X_{cu} = \frac{k}{Ccu_{in} LHSV} \qquad \ldots(1)$$

$$-\ln(1 - X_{cu}) = \frac{k}{LHSV} \qquad \ldots(2)$$

$$\frac{1}{Ccu_{in}} \frac{X_{cu}}{1 - X_{cu}} = \frac{k}{LHSV} \qquad \ldots(3)$$

The results show that cumene conversion data have a deviation from the zero and second order kinetic models and well correlated with first order kinetic model as shown in figures 5-7, and that in agreement with Prater and Lago(1956), Lyandres et al.(1969) , Corma and Wojciechowski (1982), Selim et al. (1992), Al-Khattaf and de Lase (2001) and Jennifer et al. (2006) .

Plots of conversion vs. 1/LHSV shown in figures 5-7 give straight lines with slopes equal to rate constants. The results of the rate constant at different temperatures for the three catalysts are given in table 1 .These values decreases in the following order: HY>Prepared HX > HX, which is may be due to the effect of pore volume, Si/Al mole ratio and acidity difference among the studied catalysts.

Table 1, Values of Rate Constant for 1st Order Reaction Rate.

Temperature, K	HY	HX	Prepared HX
		k, h^{-1}	
673	0.060	0.016	0.040
723	0.186	0.141	0.217
773	0.491	0.281	0.477
823	0.729	0.396	0.634
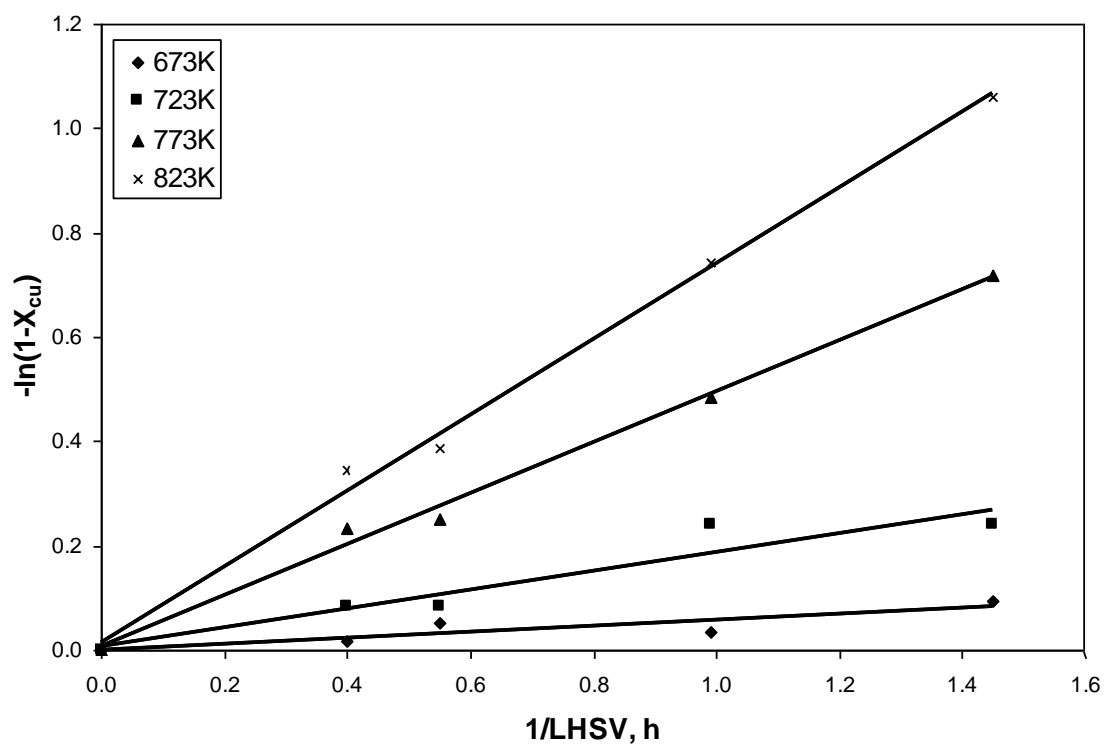
Figure 5 First Order Test of HY Catalyst.

Figure 6 First order Test of HX Catalyst.

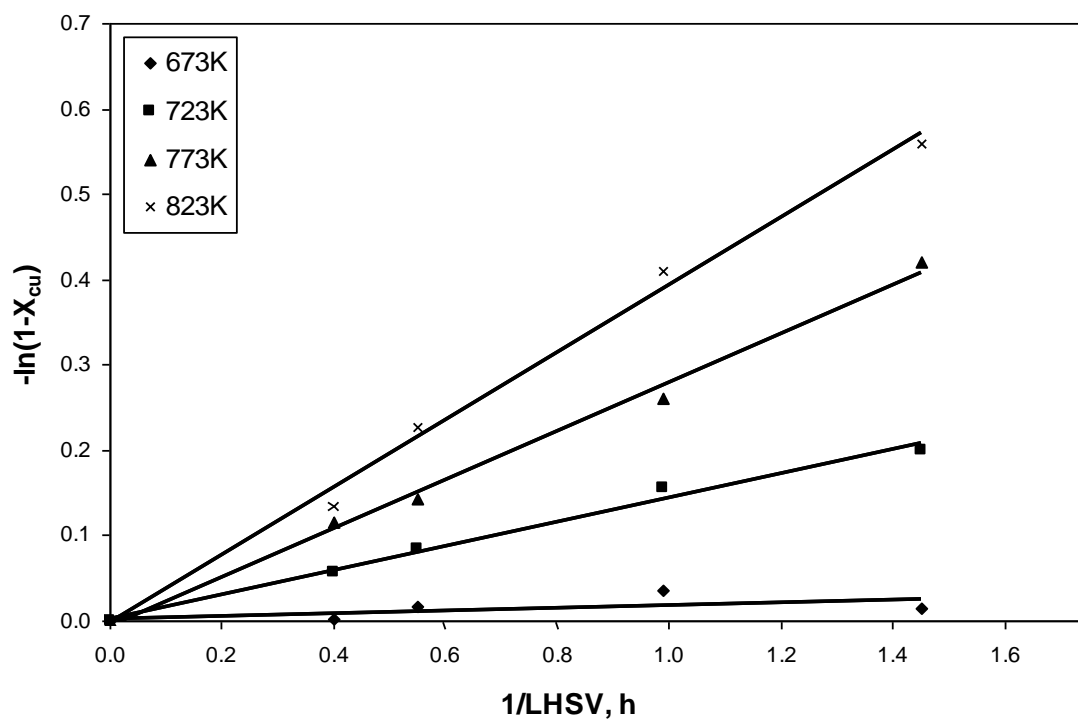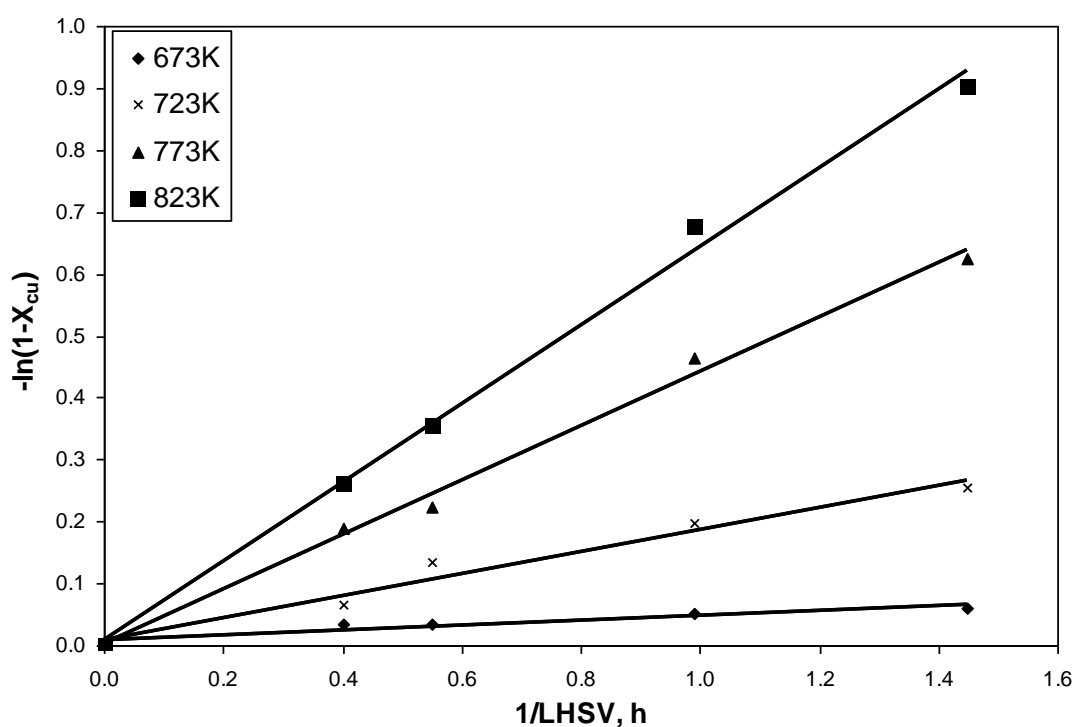| A. H. A.K. Mohammed | The Effect of Operating Condition for Cumene |
| S.k. Dhidan | Cracking on The Performance of Prepared |
| M.H. Al.Hassani | HX - Zeolite Catalyst |

Figure 7 First Order Test of Prepared HX.

THERMODYNAMICS OF CUMENE CRACKING

The apparent activation energy for the cumene cracking reactions was calculated by using the Arrhenius equation(4), which satisfies the relationship between rate constant and the reaction temperature.

$$k = k_o e^{\left(-\frac{E_a}{RT}\right)} \qquad \ldots(4)$$

The plot of ln k vs. (1/T) shown in figures 8-10 used for activation energy calculation using HY, HX and prepared HX.

The values of apparent activation energy for HY, HX and prepared HX catalysts are78.58 , 97.77 and 89.01 kJ/mol, respectively .

The role of catalyst is the reduction of the energy barrier for the reactants to reach the complex state which then decomposes to product. As the apparent activation energy decreases the reaction rate increases and catalyst activity increases.
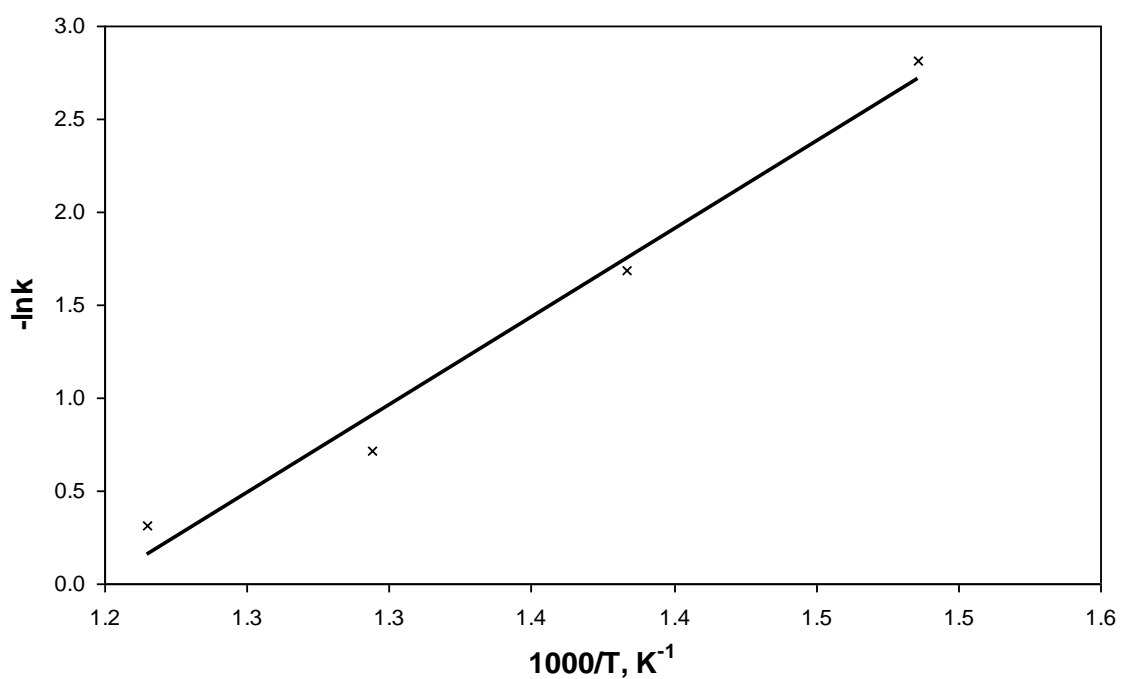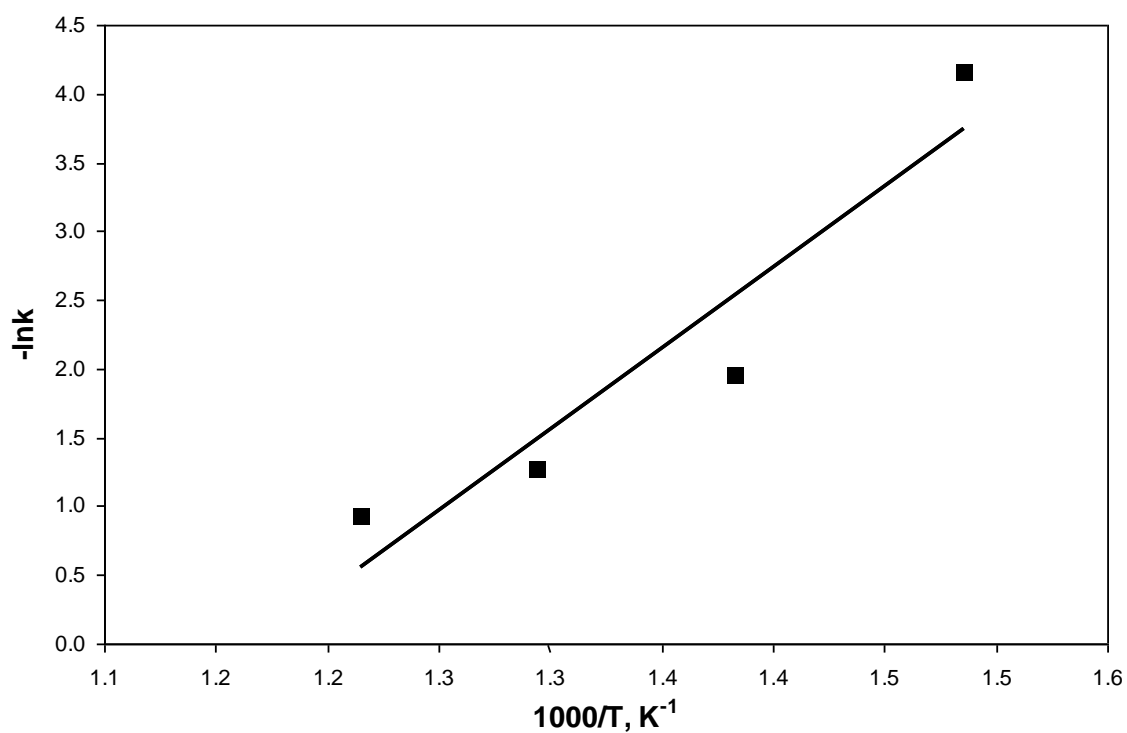
Figure 8 Plot of –lnk vs 1/T for HY Catalyst**.**

Figure 9 Plot of –lnk vs 1/T for HX Catalyst.

A. H. A.K. Mohammed	The Effect of Operating Condition for Cumene
S.k. Dhidan	Cracking on The Performance of Prepared
M.H. Al.Hassani	HX - Zeolite Catalyst
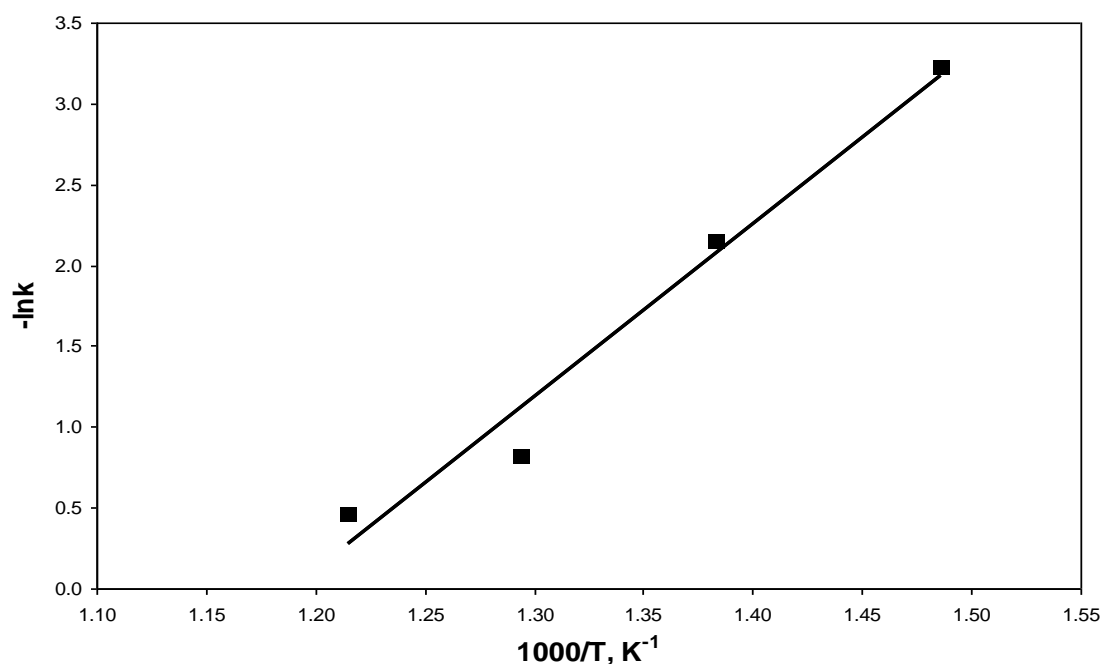
Figure 10 Plot of –lnk vs 1/T for Prepared HX Catalyst**.**

YIELD AND SELECTIVITY

By plotting cumene conversion vs. benzene yield a straight line is obtained with a slope equal to benzene selectivity and as shown in figures 11-13.

It was found that the benzene yield increases with increasing temperature. At 823K and 0.7 hr^{-1} the benzene yields were 58.79, 38.56 and 54.56 mol% for HY zeolite , HX zeolite and prepared HX zeolite, respectively. And at the same LHSV and at 673K the benzene yields were decreased to 6.53, 1.00 and 4.40 mol%, respectively.

Benzene selectivity is nearly constant over the studied temperature range for HY, HX and prepared HX . This is also observed by Peter et al. (1974) ,Donald and Wojciechowski (1977a)and Corma and Wojciechowski (1980).

4118

Figure 11 Benzene Yield as a Function of Cumene Conversion for HY Catalyst at Different Temperatures.

Figure 12 Benzene Yield as a Function of Cumene Conversion for HX Catalyst at Different Temperatures.
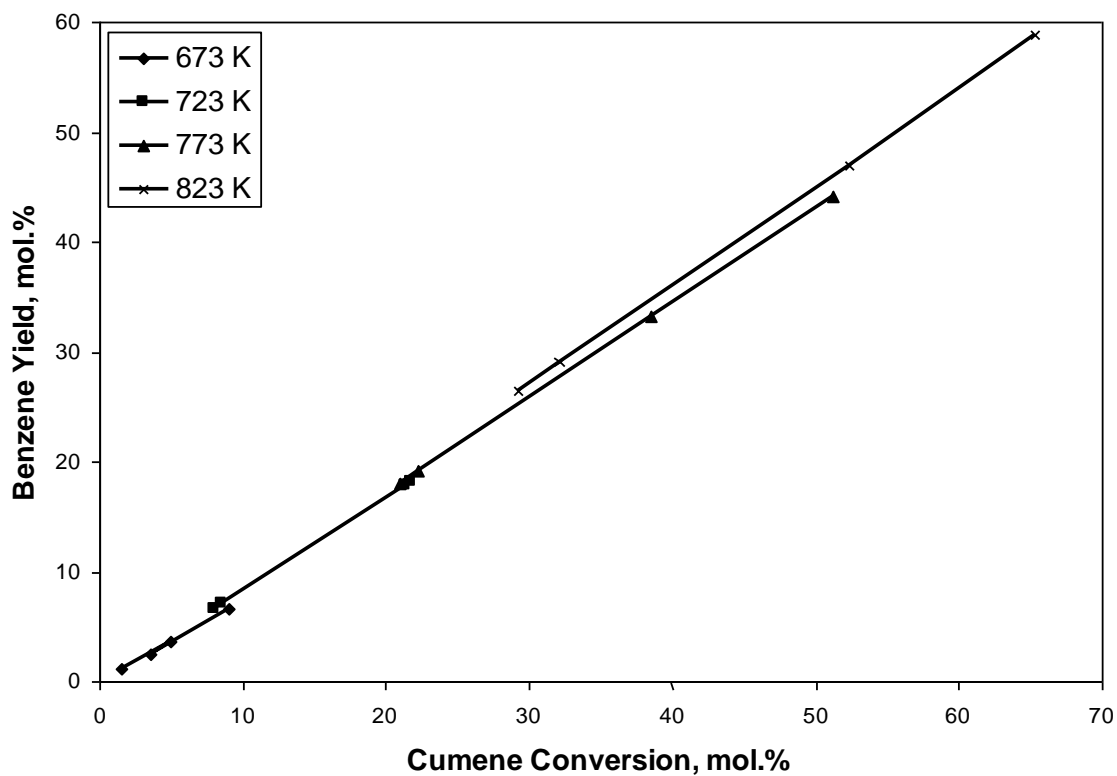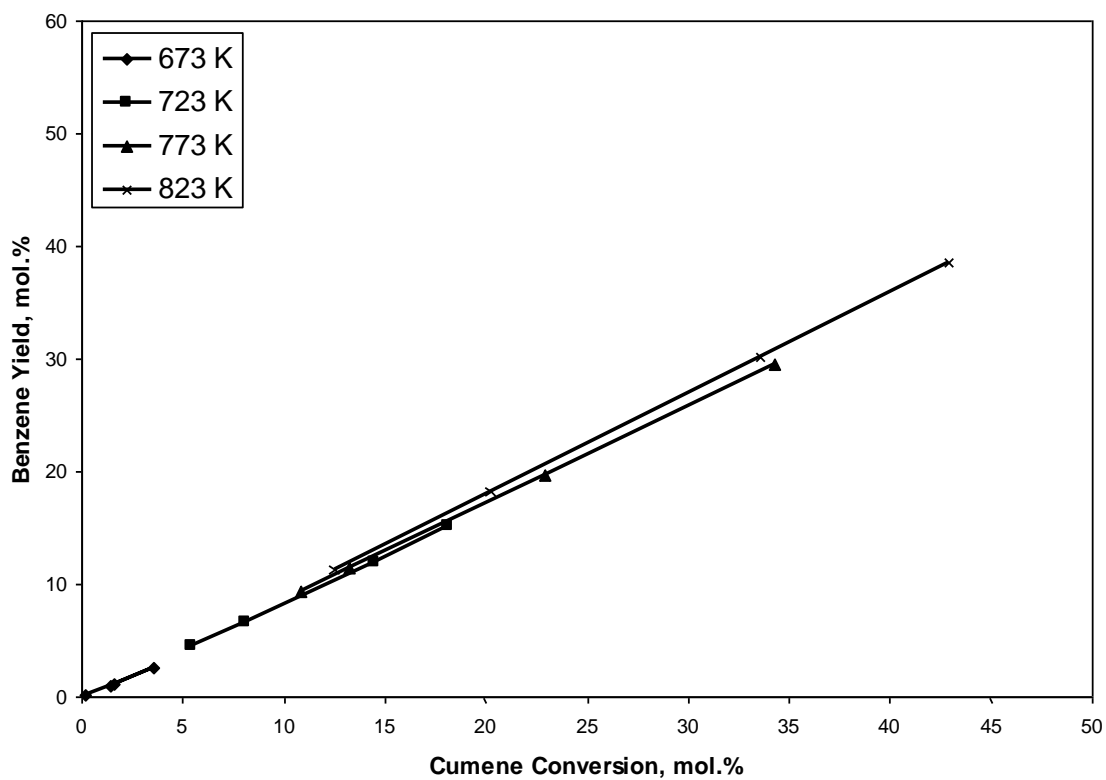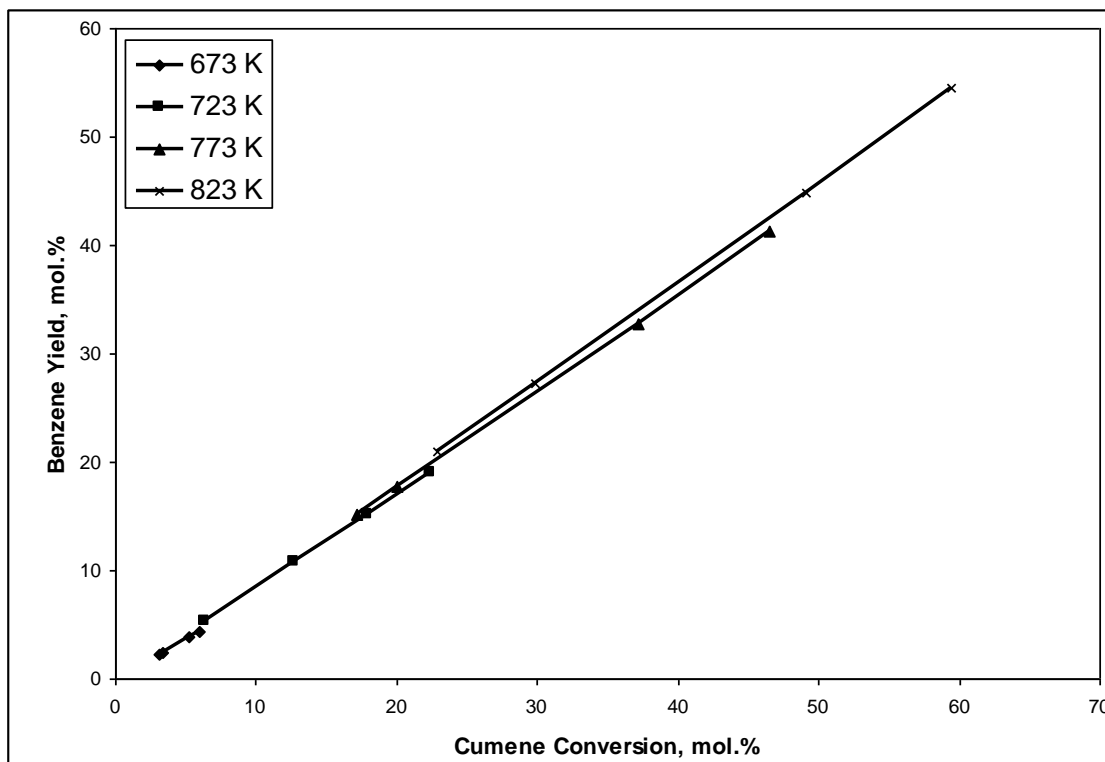
A. H. A.K. Mohammed	The Effect of Operating Condition for Cumene
S.k. Dhidan	Cracking on The Performance of Prepared
M.H. Al.Hassani	HX - Zeolite Catalyst

Figure 13 Benzene Yield as a Function of Cumene Conversion for prepared HX at Different Temperatures.

CONCLUSIONS

- Cumene conversion increases with temperature increasing from 673 to 823K and decreases with the LHSV increasing from 0.7 to 2.5 h^{-1}.

- From the kinetic study for cumene cracking over the studied catalysts, it was found that the reaction follow first order reaction model.

- It was observed that the values of activation energy(E_{act}) for catalytic cracking of cumene over the standard and prepared catalysts take the following order:

- E_{act} of HX-zeolite> E_{act} of Prepared HX-zeolite >E_{act} of HY-zeolite.

- 4. All the standard and prepared catalysts gave high benzene selectivity, and no significant change in selectivity was observed. While the yield exhibits a variation between the catalysts activity, and increases with the temperature increasing from 673 to 823K.

REFERENCES

- Samar ,K. Dh.,2008, "Catalytic Dealkylation of Cumene ", M.Sc. Thesis , University of Baghdad .
- Ahmed, J. A.,1982, " *Study of the Cracking Properties of Some Reforming Catalysts*", M.Sc. Thesis, University of Baghdad.
- Al-Khattaf , S. , and De Lase , H. ,2001, "*Catalytic Cracking of Cumene in a Riser Simulator: A Catalyst Activity Decay Model*" ,*Ind. Eng. Chem. Res.* , Vol. 40, 5398.
- Blanding, F. H.,1953, *"Reaction Rates in Catalytic Cracking of Petroleum"*,*Ind. Eng.Chem.*, Vol. 45, 1186-1197.

● Corma, A. , and Wojciechowski , B. W. ,1980, *"The Nature of The Active sites in The Reactions of Cumene on HY and LaY Catalyst*", *The Canadian Journal of Chemical Engineering* , Vol. 58.

● Corma, A., and Wojciechowski, B.W.,1982, "*The Catalytic Cracking of Cumene*", *Catal. Rev.-Sci. Eng.*,Vol. 24 , 1-65.

● Decroocq, D. , 1984,*"Catalytic Cracking of Heavy Petroleum Fractions*", Imprimerir Louis-Jean, Paris.

● Donald, B. , and Wojciechowski , B. W. ,1977 a,*"On Identifying The Primary and Secondary Products of The Catalytic Cracking of Cumene*", *J. Catal.* ,Vol. 47, 11-27.

● Donald, B. , and Wojciechowski , B. W.,1977b, *"The Catalytic Cracking of Cumene /The Kinetics of The Dealkylation Reaction*", *J. Catal.* , Vol. 47, 343-357.

Emad, f. M. ,1985," *Studies in Naphtha Reforming Processes*", M.Sc. Thesis, University of Baghdad.

● Haensel, V.,1951, " *Catalytic cracking of pure hydrocarbons*", *Advances in Catalysis* , Vol.3 ,193 , Academic Press, New York and Lodon.

● Jennifer, B., Brent, B., and Patrick, S.,2006, "*Heterogeneous Kinetics- Cumene dealkylation Over Cracking Catalyst*" , Rice University .

www.owlnet.rice.edu/~bbiseda/chbe%20390%20Lab%20Report.doc

● Levenspiel, O., 1999,"*Chemical Reaction Engineering*", 3rd Ed.,John Wiley & Sons.

● Lyandres,S. E. , Martyushin, E. I., and Akopyan , L. A. ,1969, " *How Fluidization Nonuniformity Affects a First-Order Catalytic Reaction* ", Moscow Institute of Chemical Engineering , translated from Khimiya i Tekhnlogiya Topliv i Masel, No. 12, 15-19.

● Nicholson , D. E. ,1955, *"Catalyst Activity in Cracking of Pure Hydrocarbon*" *Ind.Eng.Chem.* , Vol. 47, No. 6, 1216-1218.

● Pansing , W. F. , and Malloy J. B. , 1965,*"Characterizing Cracking Catalysts by The Kinetics of Cumene Cracking*", *Ind. Eng. Chem. Process Des.Dev.*, Vol. 4, No. 2.

● Peter A. Jacobs ,1977, "*Carboniogenic Activity of Zeolites*", Elsevier Noth-holland Inc.

● Peter,A. J.,Hugo ,E.L., and Jan, B. U.,1974,*"Active sites in Zeolites : I. Cumene Cracking Activity of NH$_4$Y Zeolites After Different Reactor Prtreatments*" , *J. Catal.* ,Vol. 33, 17-30.

● Plank, C. J. , and Nace , D. M. ,1955, *"Coke Formation and Its Relationship to Cumene Cracking*" , *Ind. Eng . Chem.* , Vol. 47, No. 11.

● Prater ,C. D., and Lago ,R. M.,1956,*"The Kkinetics of The Cracking of Cumene by Silica-Alumina Catalyst*" , *Advances in Catalysis* , Vol. 8, Academic Press, New York and London.

● Schwab, M. and Sieb, B.,1964, "*The Ion-Exchange Properties of Zeolites. I. Univalent Ion Exchange in Synthetic Faujasite* " , *Z. Naturforsch.*, Vol. 18a ,164.

● Selim, M. M., Kira , A. I. , Ali , S. A. H., and Abdel-Hamid , S. M.,1992 "*Effect of γ-Irrediation on The Crystallinity and Catalytic Activity of NdX and NdY Zeolites*", *J. Radio Anal. Nucl. Chem. Letters* , Vol. 164, No. 4, 229.

● Tanabe,K., 1970 ,"*Solid Acids and Bases*" , Academic Press, New York and London.

INTEGRATION OF MOBILE PHONES INTO LAN ENVIRONMENT

Assis. Prof. Hamid M. Ali   &   Mohammed Dhiyaa Al-Qassar
Computer Engineering Dept., College of Engineering, Baghdad University

ABSTRACT

The aim of this paper is to integrate mobile phones into LANs by connecting the two parties and providing the mobile with a transparent access to the services and resources hosted by the LAN. Quick assessment of the typical related approaches for accessing LAN (like WLAN and Bluetooth BNEP) shows that they are inappropriate for mobile phones. The paper further inspects the LAN access approach based on Bluetooth PAN Profile and marking up its potential drawbacks. A modified approach is proposed and implemented by altering the access nature or model from peer-to-peer communication to a client/server service providing, and switching from BNEP to RFCOMM protocol.

الخلاصة

يهدف البحث لتكامل الهاتف النقال مع شبكات الحاسوب المحلية LAN عن طريق ربطهما معا وتمكين الهاتف النقال من الوصول بشفافية للخدمات والموارد التي توفرها وتستضيفها الشبكة المحلية. ان التقييم السريع للطرق المتبعة في الربط مع الشبكة المحلية (مثل WLAN و Bluetooth BNEP) يظهر عدم ملائمتها للهاتف النقال. يعمد البحث الى تحليل طريقة الربط المعتمدة على Bluetooth PAN Profile ومن ثم يؤشر النقاط التي تحول دون ملائمتها للهاتف النقال. يلي ذلك طرح تعديلات مقترحة على الطريقة المذكورة وذلك من خلال استبدال نموذج ند-لند بنموذج خادم\عميل واستبدال بروتوكول BNEP ببروتوكول RFCOMM وتصميم وتطبيق نضام يعتمد هذه التعديلات.

KEYWORDS

Mobile Phone, LAN Environment, Bluetooth, PAN, Symbian OS, S60

INTRODUCTION

The objective of current telecommunication environment is the availability of all communication services anytime, anywhere, to anyone, by a single identity number (address) and a pocket-sized communication terminal. Achieving these goals means that the communication system must support mobile clients, which requires that the communication terminals (that clients hold) are mobile too. [WINCH1998]

Although originally targeted for different scopes of applications, those two environments (of mobile phones and computer networks) can be joined together to come out with new horizons, tools and approaches for the current classical applications domain. Mobile phones will gain access to enormous volume of resources (which they lack) hosted by computer networks. On the other hand, computer applications can reach out and extend to the very large market segment of mobile phones (according to International Telecommunication Union the number of mobile subscribers is 2,137,069,400 subscribers, about 32% of the world population have mobile phones). [ITU2006]

The connection (integration) of mobile phones with computer networks is not a new aspect. It had already been well established in the enterprise (WAN) and micro (PAN) scales. The integration trend has not (widely) commercially targeted the in-between local (LAN) scale yet. Due to several reasons (discussed later in the paper), the current standards and technologies used successfully to connect other types of mobile devices (like PDAs and laptops) to the LAN are usually impractical to be used with mobile phones. This problem is addressed by the paper by proposing an approach to connect mobile phones to LAN and integrating the two environments by providing the mobile phone with a proper and transparent access to the resources and services hosted by the LAN.

- **MOBILE PHONE CONNECTIVITY**

Mobile phone's connectivity to computer networks can be categorized into three models according to the scale of the geographic area covered by the connected network. Each model (or category) has its unique architecture and applications. [PAN 2003]

Wide and Metropolitan Area Network (WAN/MAN) Model

Mobile phones use data carrier services (embedded within the cellular mobile phone network and usually provided by the network operator), like GPRS and EDGE, to connect to WAN/MAN networks. Since these services are part of the mobile network, and since mobile networks are interconnected all over the world with other mobile networks and computer networks (like the Internet), then WAN/MAN networks provide virtually a global coverage.

An illustration of this model is shown in Fig. 1. Mobile phone sends/receives data packets over GPRS, EDGE or similar data carrier services. All the data is directed to/from data network gateway, which links the mobile and data networks together. The gateway translates between data carrier service format and the destined data network format.

This model is suitable for such applications as web browsing, emails and other public Internet services. It also can be used with private enterprise applications where a connection to a private computer network is required. This connection is achieved either through the Internet by using VPN approach or by making a direct connection between the private computer network and the data network gateway.
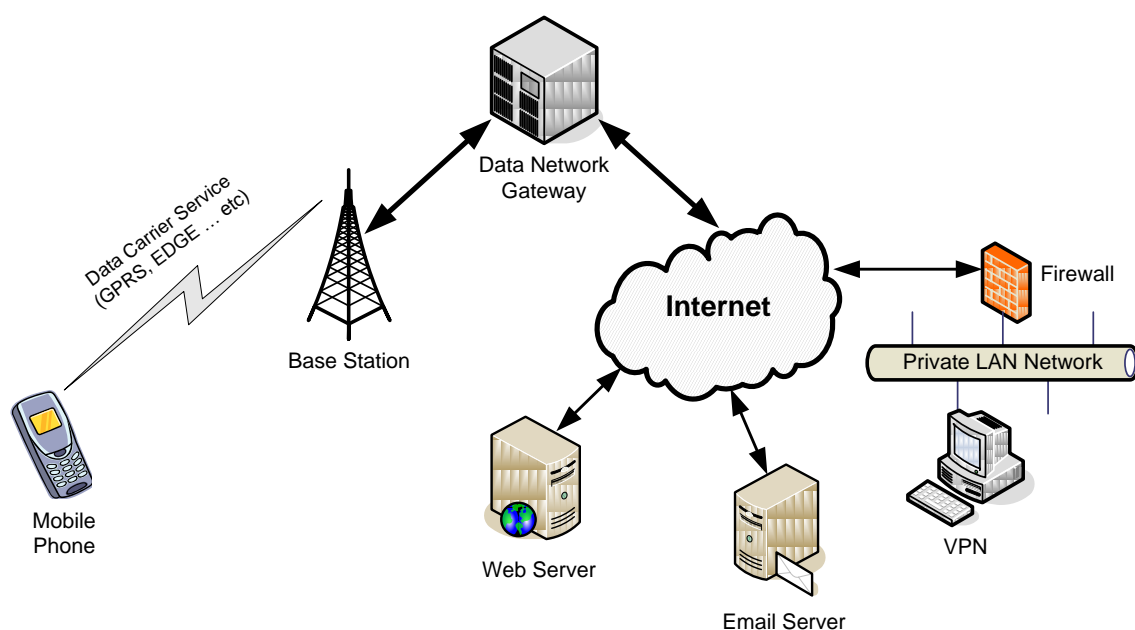

Fig. 1 – WAN/MAN Connectivity

Local Area Network (LAN) Model

Mobile phones use wireless LAN (WLAN) standards, like IEEE 802.11, to connect to wireless computer networks, or to conventional wired computer networks through a wireless access point. Such wireless networks cover a typical range of 100m (usually the whole network is located within single building).

An illustration of this model is shown in Fig. 2. This model can be used for private custom applications where a high end mobile phone with advanced specifications (large memory, fast processor, high resolution display and wireless network interface card) is used as a very light hand held smart terminal (the same function as PDA).
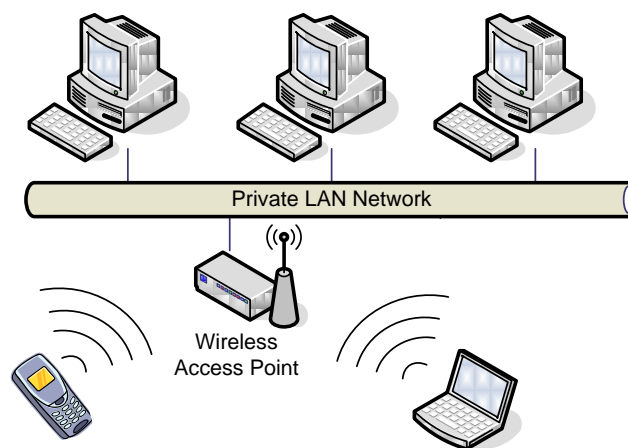
Fig. 2 – LAN Connectivity

Personal Area Network (PAN) Model

Mobile phones use short-range wireless technologies (like infrared or Bluetooth) or short distance wired standards (like RS-232 or USB) to form or to join a PAN network. Such networks cover a typical range of 10m (usually the networked devices are located in the vicinity of a single person).

An illustration of this model is shown in Fig. 3. Possible applications of this model would be connecting the mobile phone to a computer in order to transfer files (ring tones, wallpapers … etc.) between the two devices, synchronizing and backing up important data (address book, schedule, calendar … etc.) or using the mobile phone as a modem by the computer. All of these applications are based on exchanging data between the mobile phone and the computer that it is directly connected to; therefore, PAN connectivity is used as a cable replacement by mobile phones (and similar mobile devices).

Fig. 3 – PAN Connectivity

4124

• ACCESSING LAN THROUGH PAN

It is possible to use PAN to access a remote network (LAN or WAN/MAN) through a Network Access Point (NAP), Fig. 4 shows this approach. NAP is a device that is connected to both PAN and the remote network. The NAP can be a dedicated specialized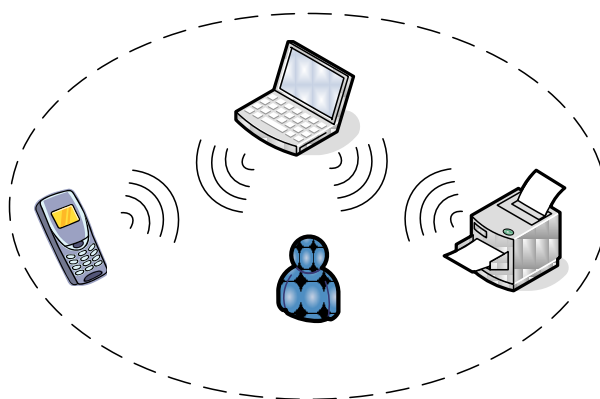 device or just a conventional networked device like desktop computer. The main job of NAP is to act as a link through which other devices in the PAN can reach the remote network. NAP may operate at different levels (bridge, router, gateway or proxy) depending on the differences between the two networks it is connected to. [PAN2003]
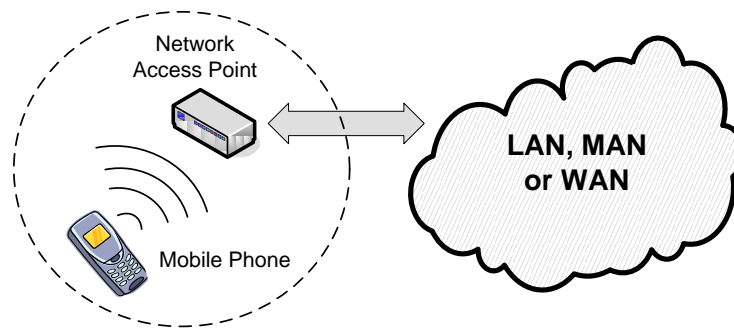

Fig. 4 – Connecting to Remote Networks via PAN

LAN-through-PAN can be important for mobile phones (as compared to using PAN to access WAN/MAN) for the following reasons:

- WLAN is hardly ever supported by mobile phones for two main reasons. First, WLAN consumes a lot of power, which means the typical mobile phone battery will be drained quickly. Second, mobile phones with WLAN are very expensive. Therefore, the number of mobile phone models, their prices and their sales volume make the LAN connectivity model virtually impractical.

- WLAN is a new aspect in the mobile phone industry as compared to PAN (infrared, USB and Bluetooth) which is a well-known feature that is offered by many models previously and most of the models currently. Hence, by using PAN to access LAN there is no need to replace the current mobile phone devices with newer ones in order to achieve LAN connectivity.

- Although private LANs can be accessed through WAN/MAN model, but this requires the approval of a third party represented usually by the mobile network operator to use the data service provided by the network. This scheme also requires either connecting the private LAN to the Internet and using VPN, or having a direct access to the mobile network data service. All these requirements will increase the cost, security risks and management complexity.

• BLUETOOTH

As mentioned before, PAN can use different communication technologies, but the most popular and suitable is Bluetooth especially regarding mobile phones. Bluetooth is a wireless communication standard for cable replacement between digital devices by using simple, low cost and low power communication modules with non-directional short range, frequency hopping and ad-hoc radio links. Therefore, it meets all the requirements imposed by the nature and purpose of PAN (in general) and limitations of mobile phones (in particular). Beside that, several older phone models and almost all current models are supplied with Bluetooth. Hence, Bluetooth will be a logical choice to implement a LAN-through-PAN solution.

Bluetooth System Architecture

Bluetooth system architecture is segmented into several layers. These layers, some of which are shown in Fig. 5, form the Bluetooth protocol stack that can be logically partitioned into the following groups: [GANGULI2002]

- **Transport protocol group**: facilitates the identification of other Bluetooth devices. It also configures and manages the physical and logical links, allowing the higher protocol layers to transmit data through these layers. The layers of the transport protocol group work together and form a virtual pipe that is used to transport data from one device to another. This group includes radio, baseband, Link Manager Protocol (LMP), Host Controller Interface (HCI) and the Logical Link Control and Adaptation Protocol (L2CAP) layers.

- **Middleware protocol group**: provides additional protocols that help new and existing applications to operate over Bluetooth links. It consists of both third party and industry standard (usually Internet related) protocols and the protocols defined by the Bluetooth Special Interest Group (SIG) for wireless communication in Bluetooth devices. The third party and industry standard protocols include protocols such as Point-to-Point Protocol (PPP), Internet Protocol (IP) and Transmission Control Protocol (TCP) while the protocols defend by the SIG include protocols such as Radio Frequency Communication (RFCOMM), Bluetooth Network Encapsulation Protocol (BNEP) and Service Discovery Protocol (SDP).

- **Application Group**. The application group includes the actual applications that use Bluetooth links. These applications are not necessarily aware of the Bluetooth wireless communication. An example of such applications is a Web browsing client.
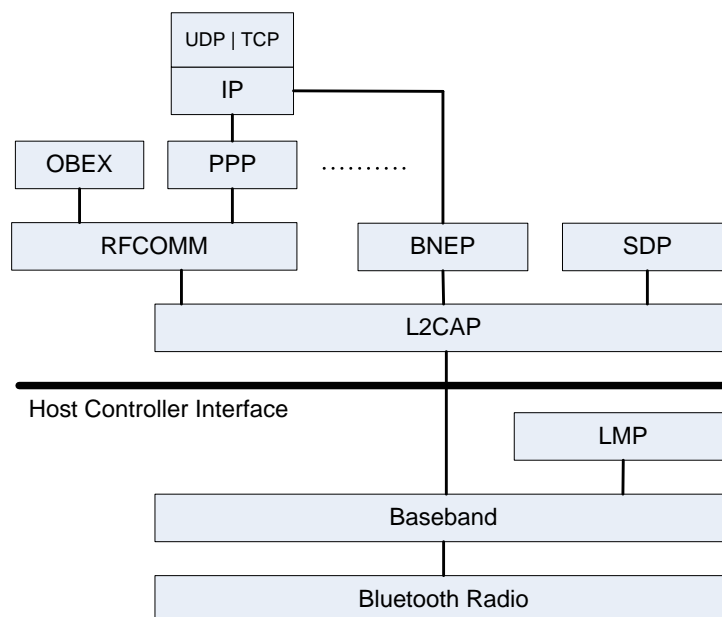

Fig. 5 – Bluetooth Protocol Stack

Bluetooth Protocols

The core Bluetooth protocols defined by the Bluetooth specification, and shown in Fig. 5 are: [GANGULI2002]

Bluetooth Radio helps to transmit and receive data over the air. The frequency band used by Bluetooth devices is the globally available unlicensed ISM band ranging from 2400 MHz to 2483.5

MHz. Within the band, Bluetooth has 79 channels spaced 1 MHz apart. The choice of this band takes into consideration the size and power limitations of most mobile devices.

Baseband is responsible for the determination and instantiation of the air interface by defining processes to identify other devices and establish connectivity between them. The key functions performed by the baseband include connection creation, selection of a frequency hopping sequence, timing hops, operations related to power control and security, packet processing and the selection of link types. The baseband layer and the radio layer can be functionally correlated to the physical layer of the Open Systems Interconnection (OSI) reference model.

LMP performs all the functions related to link management. These functions include for example link setup, link security and link configuration. In addition, LMP layer offer other management services like time management, mode control management and power management. The LMP uses the underlying services of the baseband layer to manage the links; therefore, it does not perform operations related to information delivery.

L2CAP is specifically concerned with functions such as protocol multiplexing (sharing of the air interface between multiple protocols and applications), segmentation and reassembly of data packets and negotiating an acceptable level of service.

RFCOMM provides the protocol stack with the support of serial communication similar to that in cable technology. RFCOMM provides a Protocol Data Unit (PDU) structure to emulate the RS-232 control and data signals over the baseband layer. The upper level services are thereby provided with capabilities to transport both control and data signals by using the serial line transmissions.

SDP is a simple protocol that allows devices to locate and gather information about the services of other devices. SDP involves communication between an SDP server and an SDP client. The server maintains a list of service records that describe the characteristics of services associated with the server. Each service record contains information about a single service. A client may retrieve information from a service record maintained by the SDP server by issuing an SDP request. SDP uses a request/response model where each transaction consists of one request PDU and one response PDU.

BNEP is used to transfer both control and data packets over Bluetooth to provide networking capabilities for Bluetooth devices. BNEP encapsulates packets from various networking protocols, which are transported directly over the Bluetooth L2CAP. [BNEP2003]

Bluetooth Network Topology

The connection between Bluetooth devices can be either point-to-point (between two Bluetooth devices) or point-to-multipoint (several Bluetooth devices connected to each other). Either way, a Bluetooth connection creates a network known as a Piconet. Each piconet consists of one master controlling unit and up to seven active slave units. All Bluetooth units participating in the piconet are time- and hop-synchronized to the same physical channel. The master unit's system clock and Bluetooth address determines the hopping phase and sequence of the piconet physical channel. The software and hardware specifications of a master and slave unit are the same. However, the unit that establishes a piconet becomes the master unit controlling all traffic within the piconet.

The spectrum of connectivity in a piconet is increased by formation of multiple piconets in the same area. Overlapping piconets form a Scatternet. As a result, a Bluetooth device can also participate in
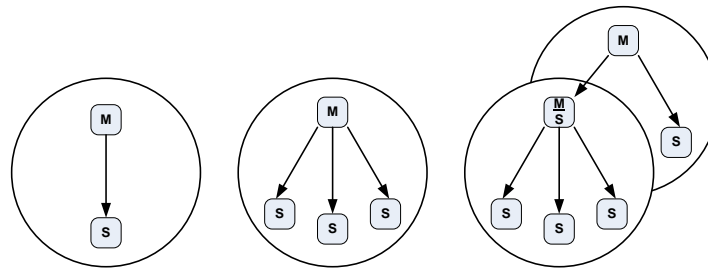
Fig. 6 – Bluetooth Piconet and Scatternet

multiple piconets at the same time (but not as a master in both of them). A piconet and scatternet are shown in Fig. 6. [GANGULI2002]

* BLUETOOTH PAN PROFILE

The Bluetooth PAN Profile describes how two or more Bluetooth enabled devices can form an ad-hoc network and how the same mechanism can be used to access a remote network through a NAP. Bluetooth PAN Profile is based on BNEP, which is used to provide networking capabilities for Bluetooth devices. Several device roles are defined by the profile to organize cooperation and interaction between PAN devices. [PAN2003]

BNEP Protocol

If two applications run on two different devices within the Bluetooth network but each application uses a different network layer protocol (for example IP and IPX over Bluetooth), then in order for the two applications to interoperate and exchange information, a common packet format needs to be defined to encapsulate network layer protocols over the Bluetooth media.

The same thing applies for the scenario when one of the devices is part of a Bluetooth network and the other is part of another type of network (like Ethernet). BNEP encapsulates packets from various networking protocols, which are transported directly over the Bluetooth L2CAP.

BNEP is implemented using connection oriented L2CAP channels. The Bluetooth is considered as a transmission media in the same OSI layer as Ethernet, Token Ring, etc. L2CAP is considered as the Bluetooth MAC layer. The Bluetooth device address space is administrated by the IEEE, and is assigned from the Ethernet address space. This means that it is possible to build a Bluetooth network access point as a bridge between Bluetooth devices and an Ethernet network.

The use of the BNEP for transporting an Ethernet packet is shown in Fig. 7. BNEP removes and replaces the Ethernet header with the BNEP header. Finally, both the BNEP header and the
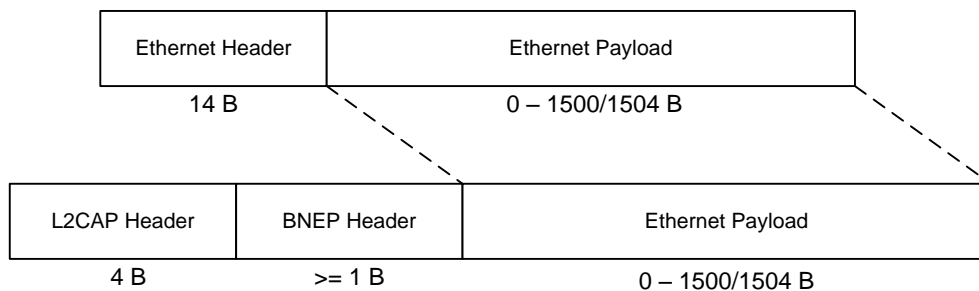

Fig. 7 – Using BNEP to Transport Ethernet Packets

Ethernet payload is encapsulated by L2CAP and sent over the Bluetooth media. [BNEP2003]

PAN Profile Device Roles

Bluetooth PAN Profile defines three roles or services:

- Network Access Point (NAP): A Bluetooth device that supports the NAP service is a Bluetooth device that provides some of the features of an Ethernet bridge. The device with the NAP service is simply referred to as NAP. The NAP and the PAN User exchange data using BNEP. NAP has an additional network connection to a different network media in which the Ethernet packets are either exchanged via Layer 2 (Data Link) bridging or Layer 3 (Network) routing mechanism.

- Group Ad-hoc Network (GN): A Bluetooth device that supports the GN service is able to forward Ethernet packets to each of the connected Bluetooth devices (PAN Users) as needed. The GN and the PAN User exchange data using BNEP. GN does not provide access to any additional networks. Instead, a GN is intended to allow a group of devices to form temporary network and exchange information.

- PAN User (PANU): This is the Bluetooth device that uses either the NAP or the GN service. PANU supports the client role for both the NAP and GN role.

The NAP/GN performs Ethernet Bridge functions to forward Ethernet packets from one PANU to another PANU or from a PANU to another network. NAP/GN regards each established Bluetooth BNEP connection as a valid Bridge Port. Thereby the NAP/GN shall perform bridging between all of the BNEP connections. In addition, NAP regards the optional Ethernet connection as a valid Bridge Port too (if the NAP is acting as a bridge and not as a router, otherwise a normal routing is performed by the NAP). Fig. 8 shows the protocols used in each of the three roles and their interaction with each other. [PAN2003]
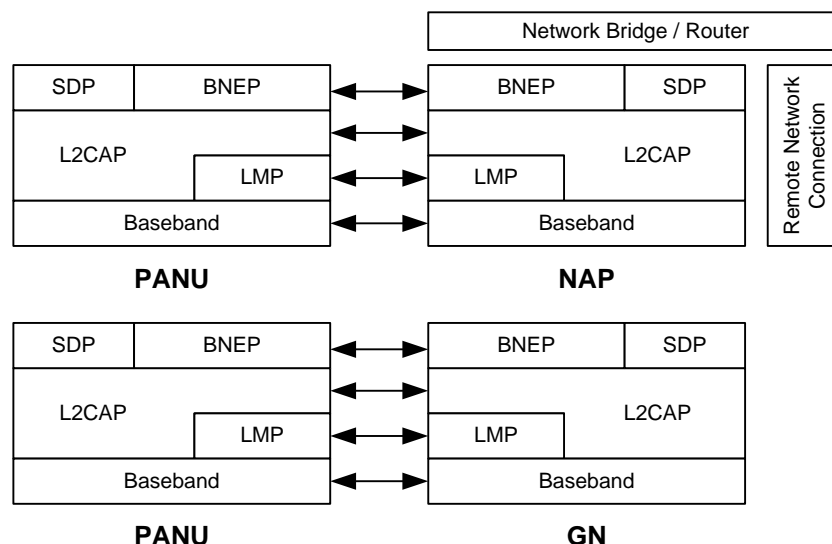
Fig. 8 – NAP, GN and PANU Device Roles

- **PROPOSED MODIFICATIONS TO BLUETOOTH'S PAN PROFILE**

Bluetooth SIG engineered the Bluetooth protocol stack from ground up to support PAN. Furthermore a specific protocol, BNEP, and device role are designed to enable a Bluetooth device act as a NAP allowing other devices in the PAN to reach for LAN or WAN/MAN through it. However, using Bluetooth PAN Profile and BNEP to implement a LAN-through-PAN solution for integrating mobile phones with computer network services has the following downsides:

- The Bluetooth PAN Profile and BNEP were designed from the beginning so that more capable computing devices like desktop or laptop computers can benefit from them. That doesn't mean that these standards will not work with the less capable devices like mobile phones, but it means that no commercial mobile phone product has supported the PAN and BNEP yet (i.e. no current mobile phone model has a built-in support for PAN or BNEP). Therefore, in order to implement a LAN-through-PAN solution, one needs first to implement a BNEP protocol and a PAN profile.

- BNEP is a Bluetooth based protocol. It will not work with different networks like infrared or future short-range wireless standards. That means if a NAP is built based upon BNEP and Bluetooth PAN Profile, the only way to connect to this PAN is through Bluetooth. Although Bluetooth is very promising and efficient but future upgrades and network standards spectrum served by such a NAP would be limited to Bluetooth technology only.

- In order to make use of the BNEP and Bluetooth PAN Profile network, transport and application layers must be available on and supported by the Bluetooth device (PANU). As mentioned before, BNEP and Bluetooth PAN Profile were designed with minds set to desktops, laptops and similar computing devices as main targeted devices. Such rich resourced devices can easily afford the complex structure of multilayered network protocol stack, especially for the upper and intermediate layers. On the other hand, mobile phones are limited in resources and a simpler networking structure is preferred.

Fig. 9 shows the proposed approach to implement a LAN-through-PAN solution. The following modifications are made to the PANU and NAP architecture, shown previously in Fig. 8:

- Bluetooth technology is still used between PANU and NAP; however RFCOMM is used instead of BNEP since, unlike BNEP, virtually every Bluetooth device supports RFCOMM.

- The NAP does not forward packets from PANU to PANU (i.e. does not perform GN role). It is unlikely that networking is required between the PANUs (mobile phones) and if it is, then they can connect to each others using separate one-to-one Bluetooth connections.

- The network bridge/router is replaced by a network services proxy at the application layer level. The proxy is loosely coupled with the lower networking layers so that the networking technologies and standards used can be upgraded and/or changed with no or minimum alteration to the proxy implementation itself. This makes the NAP more flexible and network type independent. In addition to that, the proxy acts on behalf the mobile phone to access the required network services and obtaining the results, relieving the mobile phone from carrying out network housekeeping tasks.

It is much more practical and appropriate to design mobile phones network solutions as a thin client with the minimum basic functionalities and relocate all the complex tasks to a more capable device that will act as a fat server (which in our case can be the NAP, a dedicated server or both of them).
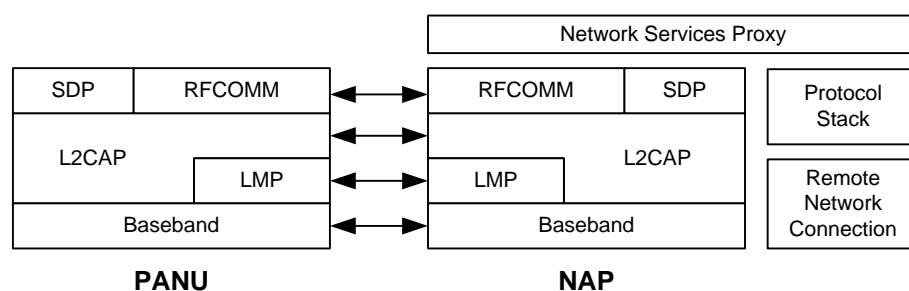
Fig. 9 – Modified NAP and PANU Architecture

* PROPOSED SYSTEM DESIGN

This section briefly demonstrates the design of a system that implements LAN-through-PAN model based on the modified Bluetooth PAN profile that is proposed by this paper.

System Components

Fig. 10 shows the (high level) components of the system. The mobile phone is hooked to the computer network by a modified network node (NAP). NAP acts like a gateway that connects to Bluetooth network at one side, and to a wired or wireless computer network at the other side. The mobile phone, then, can select a Service Access Point (SAP) to talk to. The SAP is another modified network node whose job is to act as a window for the mobile phone from which it can view the available resources and services in the network. The mobile phone issues the request for a resource or a service to the SAP and the later relays this request as if it was issued by the SAP itself. The SAP then relays the received response back to the mobile phone. Notice that the resources and services can be hosted by any node in the network including the NAP and the SAP. The functions of the NAP and SAP can be joined as a single function and hosted by a single node, but splitting them into two different identities (so that they can be hosted by two or more nodes) enhances the mobility and reduces the redundancy.

Fig. 10 – System Components

System Architecture

Fig. 11 shows the system architecture. The interaction between system components must follow a certain protocol. The proposed protocol is divided logically into three layers, the lower three layers in Fig. 11, each has a well defined function and each is independent from the others'

Fig. 11 – System Architecture

implementation. Each layer relies on and uses the service provided by the lower one.

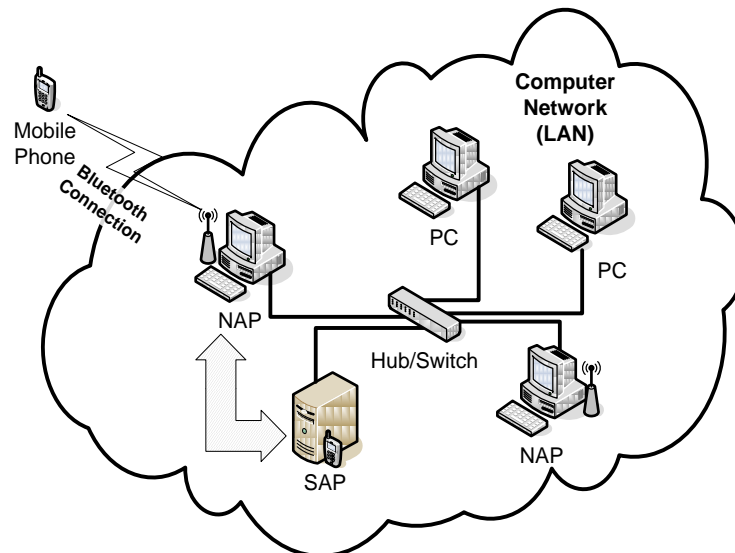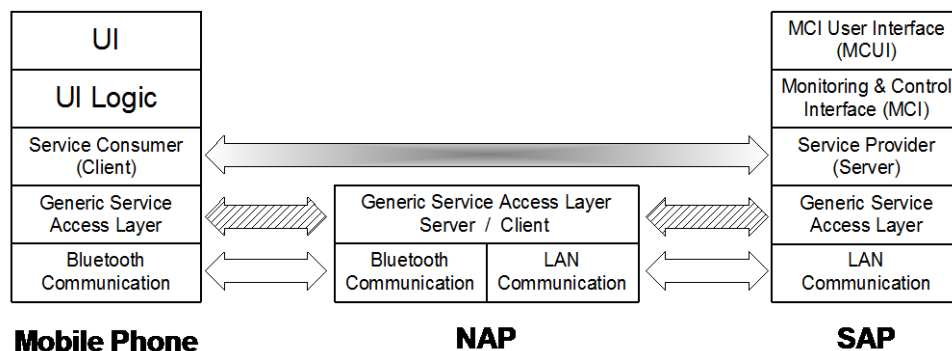**Communication Layer:** is responsible for providing the networking services for the upper layers in a high-level abstracted mode. It does that by using the more specific and detailed low level networking services offered by the OS to provide streamed network communication that appears to the upper layer as memory buffer. This layer can be thought of as an abstraction to the transport, network, data link and physical layers. According to the underlying network type, this layer can be either a Bluetooth communication layer or LAN communication layer.

Generic Service Access Layer (GSA): provides service-independent or service-neutral functions. Such functions are not limited to a certain type of services or resources; instead, it is more generic and may be needed regardless of the service or resource being accessed. For example, it maintains Access Parameters Registry (APR) at NAP. It also provides multiplexing capability so that several Service Provider layer instances can run on the same SAP.

Service Provider/Consumer layer: is responsible for providing services and consuming them. Being service dependent, there might be several versions of this layer running simultaneously above the GSA layer at both of the mobile phone (as a consumer) and the SAP (as a provider).

The remaining upper layers are not related to the interaction protocol between the system components. Instead, they perform functions local to the component on which they reside. For example, the UI and UI Logic layers on the mobile phone are responsible for managing and rendering the graphical presentation of application data, while the Monitoring and Control Interface (MCI) and MCI UI layers on the SAP are responsible for monitoring and configuring the operation of the SAP. These layers are not part of the core system but can be considered as add-ons.

PDU Formats

Exchanging of information between peer layers takes the form of PDUs, for example two separate GSA layers communicate by exchanging (virtually) GSA PDUs. Typically, a layer will take the upper layer's PDU and use it as payload, add layer's specific header to it then pass it down to the lower layer and so on till it reaches the physical layer where the actual data transmission takes place.

Fig. 12 shows the different PDU formats used by the system layers. The service request can be of any format since it is service dependent. For the system implemented as an example, where it provides a file access service similar to File Transfer Protocol (FTP), the request takes the format of a command field followed by a parameters/data field. The command field is of a fixed length (3 Bytes) and text based (although it can be used as a binary field too). The parameters / data field is of a variable length and extends to the end of the packet. This format is simple but yet very flexible and can be used for a very wide range of services.

The service provider/consumer layer uses the Request_PDU format to transfer requests from the mobile phone to the SAP. The 1 Byte m field specifies the length (maximum of 255 Bytes) of the Service Provider Address field. The Payload field contains the service request to be transferred to the addressed service provider.

The GSA layer uses the GSA_PDU format to carry requests. It is identical to the Request_PDU format, but it has GSA Address field instead. The Payload field represents a Request_PDU to be relayed to the addressed GSA layer. A special case of the GSA_PDU is when the r field has the value of 0 (zero). This format is used only for certain PDUs sent to the NAP GSA layer by the GSA layer of a mobile phone or SAP. In this case, the GSA_PDU does not carry a request or response;

instead, it represents a GSA command (GSA request) that is to be served by the NAP GSA layer. The GSA Address is removed and the rest of the PDU consists of a text based Command field (3 Bytes) followed by a parameters/data field.

When a response is transferred between any two layers, it is transferred as raw data. That means no headers are needed. Each node the request is relayed to, keeps the connection on which the request arrived open. Therefore, by the time the request reaches its final destination, the complete path is kept alive (session-oriented or connection-oriented communication). Hence, only request carrying PDUs need to have address fields.
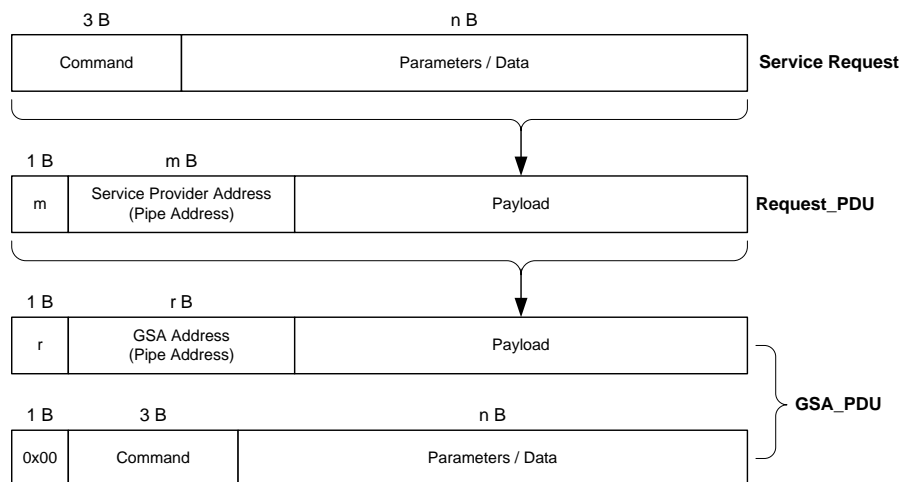
Fig. 12 – PDU Formats

Fig. 13 shows the usage of different PDU formats by system layers.
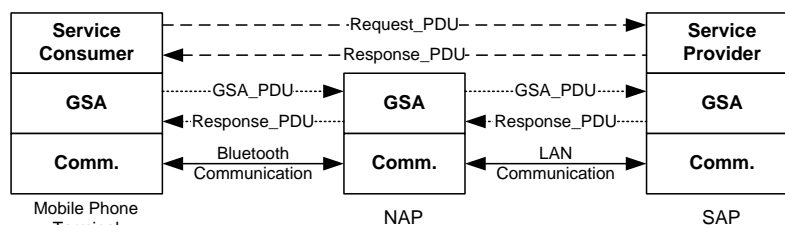
Fig. 13 – PDU Formats Usage

System Dynamic Behavior Model

The system activity diagram, Fig. 14, is a general simplified layout for the system behavior. The diagram is divided into four vertical lanes following the location the activity took place at. Again, the diagram is simplified and general; therefore not all layers and their activities are present. Instead, only the key role playing layers and abstract activities are shown by the diagram.

Fig. 14 summarizes the system layers and components into four abstract items: First is the mobile phone, which includes all the layers on the mobile terminal. Second is the NAP/GSA, which includes all the layers on the NAP with emphasizing on the GSA layer. Third is the SAP/GSA, which represents the SAP's GSA layer. Fourth is the SAP/SP, which represents the SAP's service provider layer. Notice that the vertical axis, which represents general time progress, does not flow linearly and equally in each component (lane).

The activity flow in NAP/GSA, SAP/GSA and SAP/SP is started by the administrator when he/she starts up the software on both the SAP and the NAP. After initialization, the activity flow waits for incoming requests: NAP/GSA waits for requests from mobile phones on a Bluetooth connection, SAP/GSA waits for requests relayed from a remote NAP/GSA on a LAN (pipe) connection, SAP/SP waits for requests relayed from a local SAP/GSA on Inter Process Communication (IPC) (pipe) connection.

Upon the detection of such request, the activity flow forks into two parallel paths: the first path returns to the request wait state in order to accept other requests, the second path performs further activities to serve the accepted request and provide the proper response.

In NAP/GSA, the request is examined to decide if it can be served by the NAP/GSA (labeled as GSA request in the activity diagram) or it needs to be relayed to a SAP (labeled as SP request). An example of GSA request is when a mobile phone queries the NAP for available SAPs. In both cases, when the response is valid it is relayed to the mobile terminal.

In SAP/GSA, the request is examined to determine which service provider layer instance it should be relayed to (de-multiplexing), when the response is valid it is relayed to the NAP/GSA. In SAP/SP, the request is served and the proper response is compiled and relayed to the SAP/GSA.

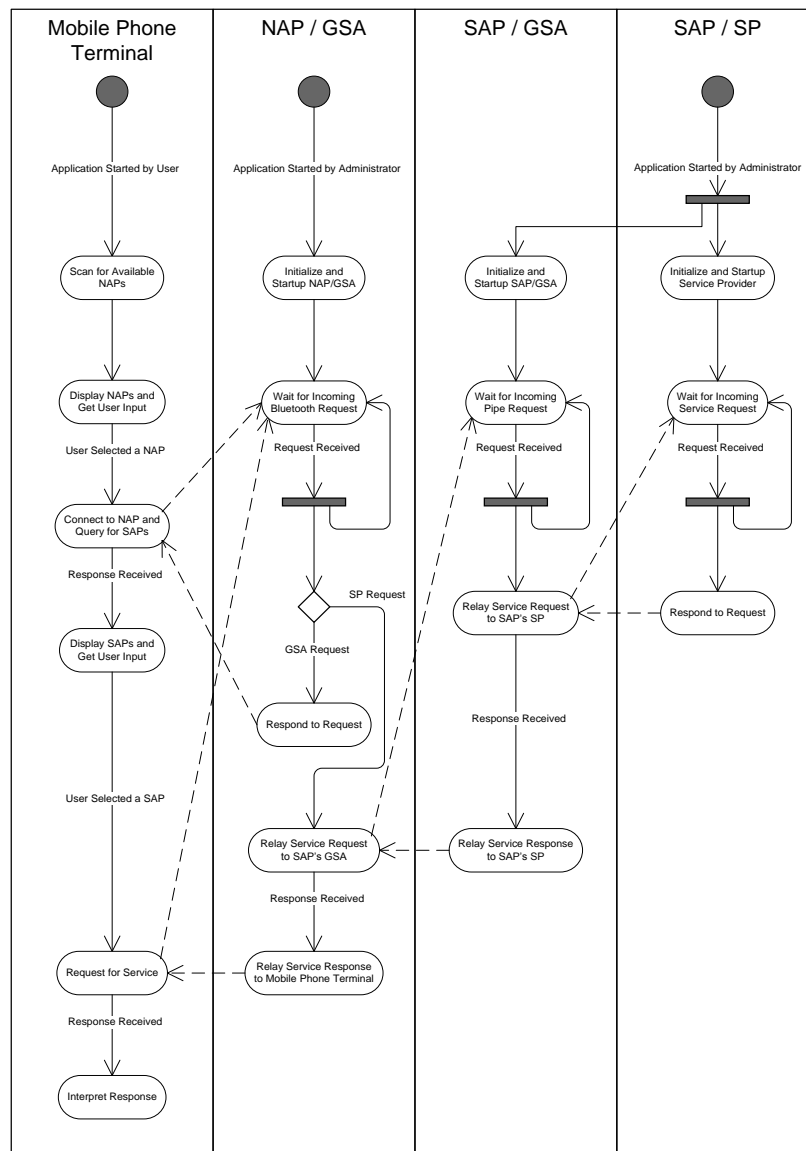On the other end of the diagram, the activity flow in mobile phone is started by the user (mobile

Fig. 14 – System Activity Diagram

4134

owner) when he/she launches the application (component) at his/her mobile. A scan process for available NAP nodes in the neighborhood is initiated. The result is presented to the user as a list of NAPs and the user can select the NAP he/she wants to connect to. A Bluetooth connection to the selected NAP is established and a request is issued to that NAP to query for available SAPs (registered with this NAP's APR). The result is presented to the user as a list of SAPs and the user can select the SAP that provides the service he/she wants to use. A request (addressed to the user selected SAP) is issued and relayed to the NAP which the mobile phone is currently connected to. The result, which is the response relayed by the NAP, is interpreted by the mobile application to produce the expected output (in our case it is a file copied to the mobile phone file system).

System Static Structure Model

Fig. 15 is a class diagram representation of the overall system components. This diagram is not a complete one, but it focuses on the major classes that define the core system components and behaviors. It also shows the relations between these classes and how they interact together.

* MOBILE PHONE SOFTWARE ENVIRONMENT

Mobile phone software environment is composed of two main elements, the Symbian OS and the Series 60 platform.

Symbian OS

Symbian OS is a 32-bit multitasking operating system, where events often happen asynchronously and applications are designed to interact with one another. For example, a phone call may interrupt a user composing an email message; a user may switch from email to a calendar application in the middle of a telephone conversation.

From the start, Symbian OS was designed for small, resource-constrained devices with wireless communications. Key design features are:

- Performance – Symbian OS is designed to make minimal demands on batteries and to have low memory footprint.

- Multitasking – All applications are designed to work seamlessly in parallel.

- Standards – The use of technologies based on agreed-upon standards is a basic principle of Symbian OS, ensuring that applications are robust, portable and interoperable.

- Object oriented software architecture.

- Memory management optimized for embedded software environment.

- Runtime memory requirements are minimized – very small executable sizes and ROM-based code that executes in place.

- Security mechanisms for enabling secure communications and safe data storage.

- Application support for international environment with built-in Unicode character sets.

- A rich and varied Application Programming Interface (API) allowing access to reusable components in developer applications. [NOKIA2004]
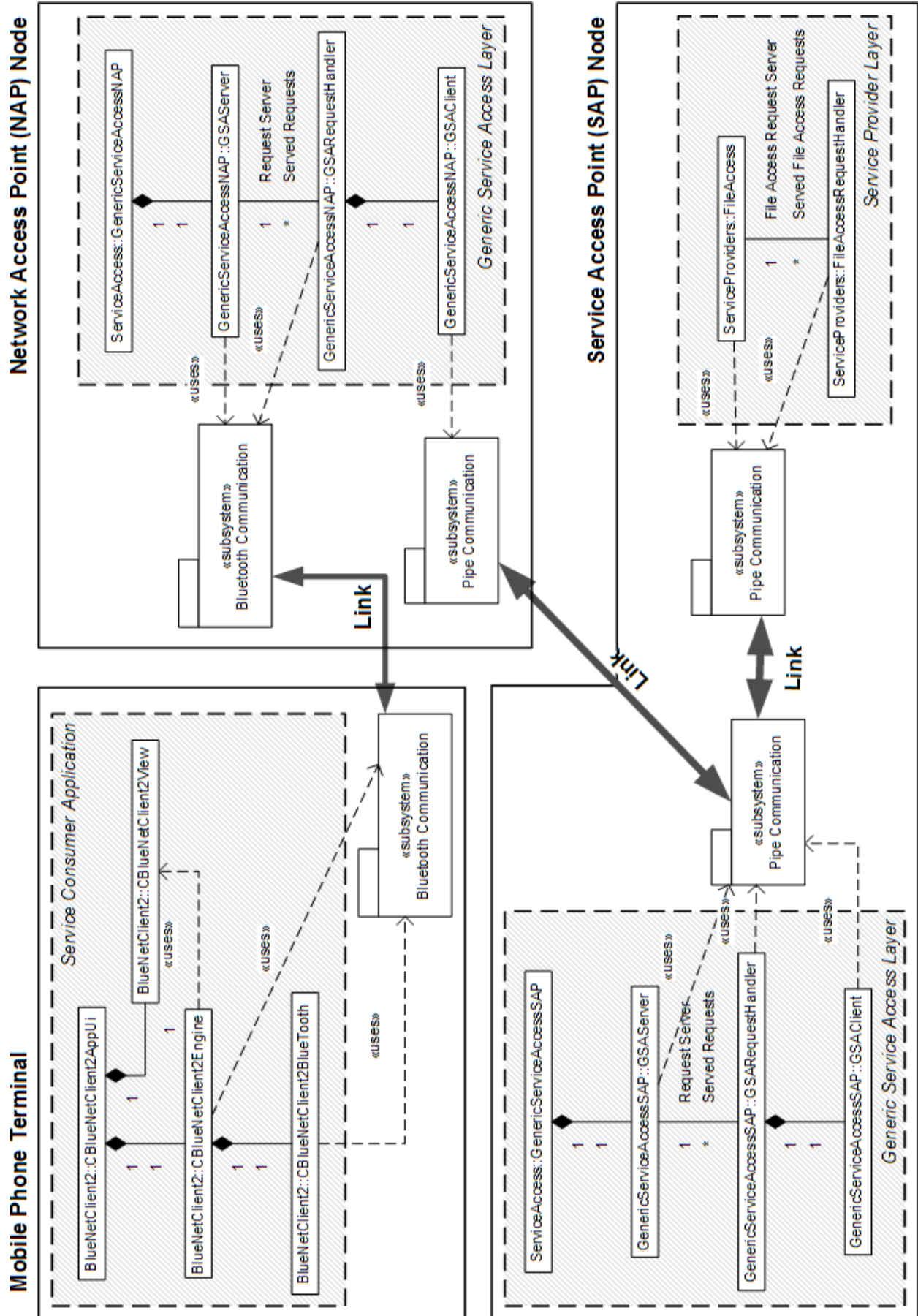
Fig. 15 – System Structure

Fig. 16 shows a representation of the Symbian OS components. The system kernel, file server and memory management are located in the Base operating system layer. The kernel manages system resources such as memory and is responsible for time slicing the applications and system tasks. Device drivers provide the control and interface to specific items of hardware – the keyboard, display, infrared port and so on. The upper layers of the system provide communication and extensive computing services such as data management, graphics, multimedia and security.
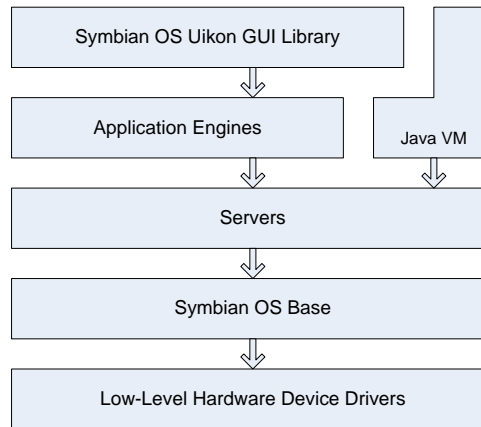
Fig. 16 – Symbian OS Architecture

Client/Server architecture is a key design feature of Symbian OS. User applications and system processes are clients that use the resources of a wide variety of system servers. Servers can be accessed only by their clients via well-defined interfaces. Virtually all servers run with a high priority, but without system privileges, to ensure a timely response to all of their clients while controlling access to the resources of the system. Some core application engines, written as servers, enable software developers to create their own user interfaces to the application data. Examples include contacts, calendar, multimedia services (decoding and rendering of image formats) and messaging. [LEIGH2004]

The kernel runs in privileged mode, it has access to the entire memory space. The process is a unit of protection in Symbian OS. Each process has its own virtual address space. The kernel assumes the existence of a Memory Management Unit (MMU), which is responsible for translating virtual addresses. The thread is a unit of execution in Symbian OS. A process has one or more threads. [NOKIA2003]

Memory intensive operations such as context switching are minimized. Symbian OS is primarily event-driven rather than multithreaded. Multithreading is possible but is avoided because it potentially creates several kilobytes of overhead per thread. Conversely, a primarily event-driven approach does not need any context switching and can have an overhead as low as a few tens of bytes. [NOKIA2004]

Event-driven (cooperative) multitasking approach is achieved via the use of Active Objects. Each active object is given a task to complete. Each thread has an Active Scheduler, which is responsible for running a waiting active object. A thread may contain one running active object and many active objects waiting to be run. Unlike multitasking with threads, once an active object has started to run, it cannot be preempted by another active object instead it is up to the running active object to give up use of the processor and join the waiting queue. The control is returned to the active scheduler to decide which waiting active object to run next. [NOKIA2003]

Series 60 Platform

The Series 60 (S60) platform, developed by Nokia, is a complete smart phone reference design that includes a host of wireless applications. The platform builds on the Symbian OS, complementing it with a configurable graphical user interface library.

The success of smart phone category devices is highly dependent on the availability of innovative applications and content from third parties – that is, the growth of the mobile services and applications businesses. Diversification between handset designs and capabilities has greatly increased. This has resulted in minimal similarity amongst competitive devices in terms of screen size, keypad, browser and other elements of the user interface. Applications, services and other content have to be adapted to these different devices.

Nokia has made the S60 platform available for licensing by other handset manufacturers enabling them to bring phones to market with equivalent and compatible functionality. Standardizing the application environment helps service creation and application interoperability. Common input methods, APIs and supported technologies allow services and applications to interoperate seamlessly, but still give licensees the freedom to innovate and design excellent smart phones. [NOKIA2004]

The core of S60 platform is Symbian OS. S60 platform adds the extensive Avkon UI layer, a full suit of applications based on the Avkon and Uikon libraries plus a number of key application engines. S60 platform contains the majority of the UI and framework APIs used by third party Graphical UI (GUI) applications. Fig. 17 shows the components of S60 platform.

 The Avkon library defines many UI components and application framework components. Avkon builds on and extends the framework and controls provided in the generic Symbian Uikon library. Each GUI application is then based on framework classes provided as part of the Avkon library and on the UI layers below that – for example in Uikon. The S60 GUI library determines the rendering of all GUI elements, so the individual applications share a common look and feel. [LEIGH2004]
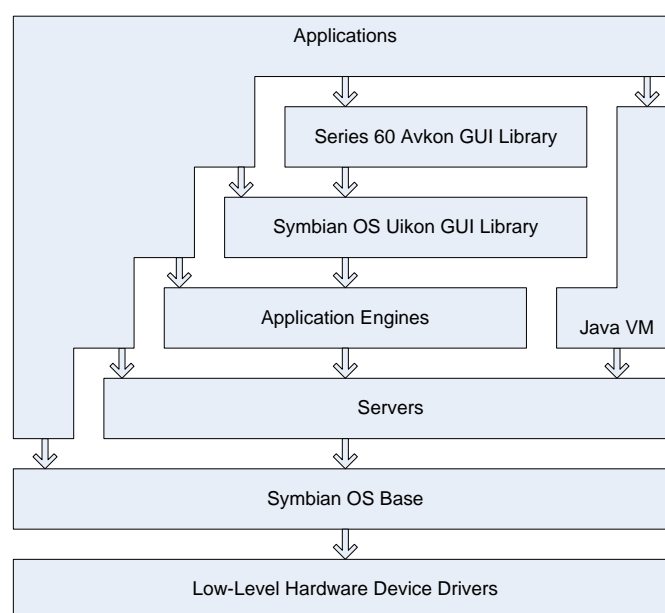
Fig. 17 – S60 Platform Architecture

* RESULTS

Fig. 18 shows screen shots for mobile phone component GUI during different user interactivities with the component. The initial screen (1) is shown when the user starts up the component application, the status pane displays the application title (**BlueNetClient2**) and icon, the main pane is empty (indicated by the **no data** string) and the control pane displays the two commands **Options** and **Back** that corresponds to the mobile terminal soft keys. **Back** is used to step back to the previous screen (and to exit the application when is used at the initial screen). **Options** command is used to display the options menu (2) at any point during the application execution.

(1)   (2)   (3)

(4)   (5)   (6)

(7)   (8)   (9)
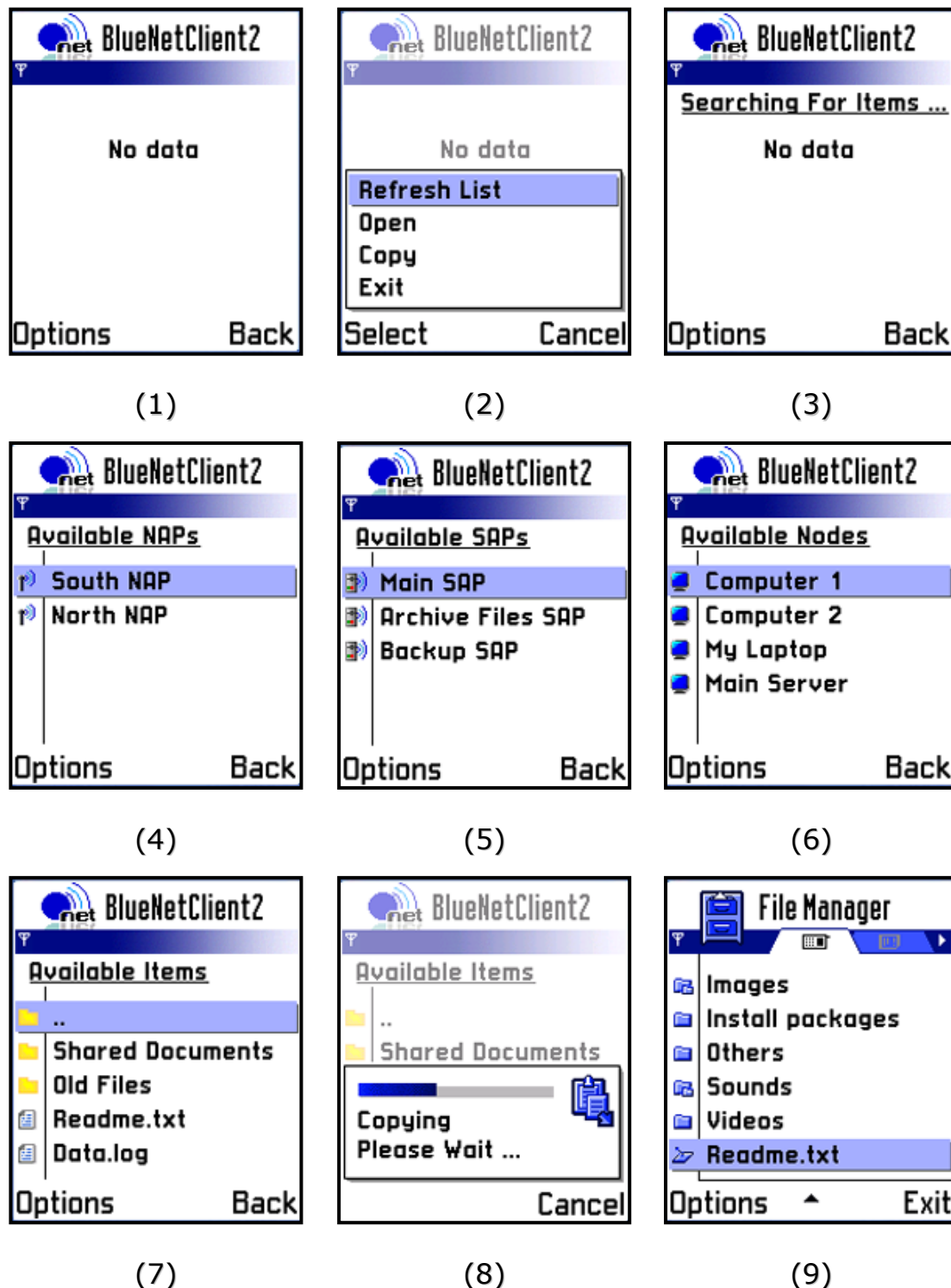
Fig. 18 – Mobile Terminal Component GUI

4139

In order to show the available NAPs in the neighborhood, the user selects **Refresh List** menu command**.** This triggers a scan operation (3) to search and find those NAPs, which are then displayed to the user (4). After selecting the desired NAP, the user selects the **Open** menu command from the options menu in order to list the available SAPs (5) that can be reached through the selected NAP (i.e. the SAPs that are registered with the selected NAP APR).

In order to access the service of a certain SAP, the user highlights the desired SAP and selects **Open** menu command again. The mobile phone component acts as a client to the service provided by the SAP. A different client is needed for each service type. In this implementation, the service that is developed as a demonstration is computer network shared files access; therefore, the client (**BlueNetClient2**) is used to browse and fetch the public contents shared by network computers. Once the user selects **Open** (as mentioned earlier), the available computers connected to the network (as seen by the selected SAP) are displayed (6). The same method is used for browsing the shared folders and files of a selected computer (7), by highlighting a folder and selecting the **Open** menu command. The user can go back to the parent folder by either using the **Back** soft key command or opening the "‥" folder.

Finally, when the user finds the required file she/he can copy it to the mobile phone by highlighting the file and selecting **Copy** menu command. A progress bar will show up indicating the file is being transferred (8). The file will be stored in the mobile phone file system and can be found by launching the **File Manager** application (9) that is built into the mobile terminal as a part of the software package provided by the mobile phone manufacturer. In this example, the file transferred is the **Readme.txt** file shown at the end of the list (9).

* CONCLUSIONS

- Mobile phones are resources limited compared to computers, but they are more available and accessible considering their cost, size and usage. An important feature in mobiles is that they combine mobility and connectivity. Summing all of this, a mobile phone can act as a lightweight personal terminal used to access remote services provided by more capable and resource rich devices like database servers, file servers … etc.

- Mobile phones support connectivity to WAN/MAN (through mobile data services like GPRS) and PAN (through infrared or Bluetooth) data networks but not to LAN because wireless LAN hardware and software standards are impractical for implementation in mobile phones. Bluetooth has built-in support to bridge a PAN and a LAN using BNEP protocol and by defining the role of NAP, although this approach's hardware (Bluetooth transmitter) can be implemented in mobile phones but the software (BNEP) is not suitable since it's designed originally for more capable devices (like PCs) communicating with each others using complex peer-to-peer model.

- By modifying the Bluetooth LAN-through-PAN scheme, its implementation becomes practical for many mobile phones. The modification, proposed by the paper, is to replace the BNEP with the RFCOMM (already supported by Bluetooth enabled mobile phones), promoting the NAP to act at the application layer and switching to client/server model instead of peer-to-peer. This simplifies and reduces resources needed for implementation by moving most of the burden from the mobile phone (the client) to the NAP (the gateway which can be considered as the "/" symbol) and the SAP (the server).

REFERENCES

- [BNEP2003] Bluetooth Network Encapsulation Protocol V1.0 Specification, Bluetooth SIG, 2003.

- [GANGULI2002] Madhushree Ganguli, Getting Started with Bluetooth, Premier Press, 2002.

- [ITU2006] World Telecommunication/ICT Indicators, International Telecommunication Union, May 2006.

- [LEIGH2004] Leigh Edwards et al, Developing Series 60 Applications – a Guide for Symbian OS C++ Developers, Addison Wesley, 2004.

- [NOKIA2003] Symbian OS: Getting Started with C++ Application Development, Nokia Corporation, 2003.

- [NOKIA2004] Series 60 Developer Platform 1.0/2.0: Basics, Nokia Corporation, 2004.

- [PAN2003] Personal Area Networking Profile V1.0, Bluetooth SIG, 2003.

- [WINCH1998] Robert G. Winch, Telecommunication Transmission Systems, McGraw-Hill, 2nd Edition 1998.

ABBREVIATIONS

API: Application Programming Interface
BNEP: Bluetooth Network Encapsulation Protocol
GSA: Generic Service Access
GUI: Graphical User Interface
IEEE: Institute of Electrical and Electronics Engineers
IP: Internet Protocol
ISM: Industrial Scientific and Medical
L2CAP: Logical Link Control and Adaptation Protocol
LAN: Local Area Network
LMP: Link Manager Protocol
MAC: Medium Access Control
MAN: Metropolitan Area Network
MHz: Mega Hertz
NAP: Network Access Point
OBEX: Object Exchange Protocol
PAN: Personal Area Network
PDU: Protocol Data Unit
RFCOMM: Radio Frequency Communication
SAP: Service Access Point
SDP: Service Discovery Protocol
SIG: Special Interest Group
TCP: Transmission Control Protocol
UDP: User Datagram Protocol
VPN: Virtual Private Network
WAN: Wide Area Network
WLAN: Wireless LAN

GENETIC ALGORITHM BASED LOAD FLOW SOLUTION PROBLEM IN ELECTRICAL POWER SYSTEMS

By

Asst. Prof. Hassan A. Kubba   Samir Sami Mahmood
Electrical Engineering Department   M.Sc. Electrical Engineering
Baghdad University   Baghdad University

ABSTRACT

In this paper, a proposed method based on real-coded genetic algorithm is presented and applied to solve multiple load flow solution problem. Genetic algorithm is a kind of stochastic search algorithm based on the mechanics of natural selection and natural genetics. They combine the concepts of survival of the fittest with genetic operators such as selection, crossover and mutation abstracted from nature to form a surprisingly robust mechanism that has been successfully applied to solve a variety of search and optimization problems. Elitist method is also used in this research, and blending models are implemented for crossover operator. In the proposed work, five busbars typical test system and 362-bus Iraqi National Grid are used to demonstrate the efficiency and performance of the proposed method. The results show that, genetic algorithm is on-line load flow solution problem for small-scale power systems, but for large-scale power systems, it is recommended that the load flow solution using genetic algorithm is for planning studies. The main important feature of the purposed method is to give high accurate solution with respect to the conventional methods.

الخلاصة

في هذه البحث، تقدم طريقة مقترحة مبنية على اساس خوارزمية جينية مشفرة بالاعداد الحقيقية لحل مسألة سريان الحمل متعددة الحلول. تعتبر الخوارزمية الجينية احدى طرق البحث العشوائية القائمة على تقنيات الانتخاب (الانتقاء) الطبيعي و الجينات الطبيعية. تجمع الخوارزمية الجينية مبادئ (بقاء الاصلح) مع عوامل جينية كالانتخاب (الانتقاء)، العبور و التغيار الاحيائي (الطفرة) المستخلصة من الطبيعة لتكوين تقنية متينة استخدمت بنجاح في حل مختلف مسائل البحث و ايجاد القيم المثلى. تم في هذا البحث استخدام طريقة انتخاب الامثل بالاضافة الى استخدام نماذج الخلط في عملية العبور. لتبيان كفاءة و مدى فعالية الخوارزمية الجينية في حل مسائل سريان الحمل متعددة الحلول، تم تطبيق الطريقة المقترحة على منظومة قدرة كهربائية قياسية. تبين النتائج كون الطريقة المقترحة ملائمة للحل اللحظي لمسائل سريان الحمل و بالتالي التطبيق العملي اثناء التشغيل لمنظومات القدرة صغيرة الحجم. أما بالنسبة لمنظومات القدرة كبيرة الحجم، فيوصي الباحث باستخدام الطريقة المقترحة لاغراض التصميم و التخطيط. اهم خواص الطريقة المقترحة هي الحصول على نتائج و حلول لمسألة سريان الحمل بقيم عالية الدقة.

KEYWORDS

 Continuous Genetic Algorithm, Chromosome Crossover, Load Flow Analysis, Newton-Raphson Method, Mutation, Multi-Objective Minimization.

INTRODUCTION

With increasing computer speeds, researchers are increasingly applying artificial and computational intelligence techniques, especially in power system problems. These methods offer several advantages over traditional numerical methods. Among these techniques is that of genetic algorithm. Genetic algorithms (GAs) are efficient stochastic search algorithms that emulate natural phenomena. They have been used successfully to solve wide range of optimization problems. Because of existence of local optima, these algorithms offer promise in solving large-scale problems. A genetic algorithm mimics Darwin's evolution process by implementing "survival of the fittest" strategy. Genetic algorithm solves linear and nonlinear problems by exploring all regions of the search space and exponentially exploiting promising areas through selection, crossover, and mutation operations. They have been proven to be an effective and flexible optimization tool that can find optimal or near-optimal solutions [Talib 2007]. In this study, an improved genetic algorithm solution of the load flow problem is presented in order to minimize the total active and reactive power mismatches of the given systems, a real-coded genetic algorithm has been implemented.

THE CONCEPTS OF LOAD FLOW ANALYSIS

The load flow studies are the backbone of the design of a power system. They are the means by which the future operation of the system is known ahead of time. The load flow problem is one of the basic problems in the power system engineering, and can be expressed as a set of non-linear simultaneous algebraic equations, and thus it is to have multiple solutions [Woon 2004]. A load flow study is the determination of voltage, current, power, and power factor or reactive power at various points in an electrical network under existing or contemplated conditions of normal operation, so power flow calculations provide power flows and voltages for a specified power system subject to the regulating capability of generators, condensers, and tap changing under load transformers as well as specified net interchange between individual operating systems. This information is essential for the continuous evaluation of the current performance of a power system and for analyzing the effectiveness of alternative plans for system expansion to meet increased load demand. The continual expansion of the demand for electrical energy due to the growth of industries, commercial centers, and residential sections requires never-ending additions to existing power systems. The systems engineer must decide what components must be added to the system many years before they are put into operation and he does this by means of power flow studies. The load flow solution usually provides additional information, e.g. losses [Kubba 1987]. The load flow is the most frequently carried out study by power utilities and is required to be performed at almost all the stages of power system planning, optimization, operation, control, and contingency analysis.

ITERATIVE NUMERICAL (LF) SOLUTION METHODS

* NEWTON-RAPHSON METHOD

At each iteration of the Newton-Raphson method, the nonlinear problem is approximated by a linear matrix equation (Jacobian matrix). The linearzing approximation can best be visualized in the case of a single-variable problem as shown in figure (1).
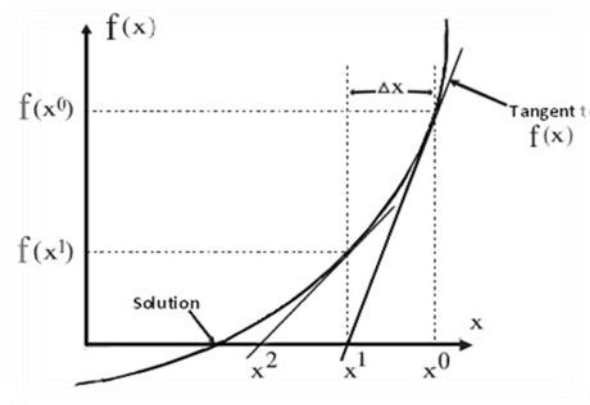
Fig. 1 Single-Variable Linear Approximation [Taylor 1967]

The Newton-Raphson load flow equation are

$$\Delta P_k = P_k^{sp} - |V_k| \sum_{m=1}^{N} |V_m| (g_{km} \cos \delta_{km} + b_{km} \sin \delta_{km})$$

$$\Delta Q_k = Q_k^{sp} - |V_k| \sum_{m=1}^{N} |V_m| (g_{km} \sin \delta_{km} - b_{km} \cos \delta_{km})$$

where $\begin{aligned} \bar{V}_k &= |V_k| e^{j\delta_k} \\ \bar{V}_m &= |V_m| e^{j\delta_m} \end{aligned}$, $\begin{aligned} \bar{I}_k &= |I_k| e^{j\alpha_k} \\ \bar{Y}_{km} &= |Y_{km}| e^{j\theta_{km}} = g_{km} + jb_{km} \end{aligned}$ and $\delta_{km} = \delta_k - \delta_m$ (Kubba 1987).

The Jacobian matrix equation can be written as:

$$\begin{bmatrix} J_1 & J_2 \\ J_3 & J_4 \end{bmatrix} \begin{bmatrix} \Delta\delta_1 \\ \Delta\delta_2 \\ \vdots \\ \Delta\delta_N \\ \Delta V_1 \\ \Delta V_2 \\ \vdots \\ \Delta V_N \end{bmatrix} = - \begin{bmatrix} \Delta P_1 \\ \Delta P_2 \\ \vdots \\ \Delta P_N \\ \Delta Q_1 \\ \Delta Q_2 \\ \vdots \\ \Delta Q_N \end{bmatrix}$$

where $\Delta\delta_k = \delta_k^{v+1} - \delta_k^{v}$ and $\Delta V_k = V_k^{v+1} - V_k^{v}$ when v is the iteration index and

$$\begin{bmatrix} J_1 & J_2 \\ J_3 & J_4 \end{bmatrix} = \begin{bmatrix} \dfrac{\partial \Delta P}{\partial \delta} & \dfrac{\partial \Delta P}{\partial V} \\ \dfrac{\partial \Delta Q}{\partial \delta} & \dfrac{\partial \Delta Q}{\partial V} \end{bmatrix}$$ Newton-Raphson load flow method may have the final formulation of

(Grisby 2007)

$$\begin{bmatrix} \Delta P \\ \Delta Q \end{bmatrix} = \begin{bmatrix} J_1 & J_2 \\ J_3 & J_4 \end{bmatrix} \begin{bmatrix} \Delta \delta \\ \Delta V \end{bmatrix}$$

Using Newton-Raphson method to solve the mismatch powers equations either in polar coordinates with (ΔV) and $(\Delta \delta)$ as variables or in rectangular coordinates with (Δe) and (Δf) as variables [Al-Shakarchi 1973].

* FAST DECOUPLED LOAD FLOW METHOD

Fast decoupled load flow method, possibly the most popular method used by utilities, is well known for its speed of solution, reduced memory, and reliable convergence (Nanda 1987). The algorithm is simpler, faster and more reliable than Newton's method and has lower storage requirements. The fast decoupled load flow method is based on Newton's load flow method with the modifications of neglecting the J_2 and J_3 Jacobian submatrices due to the weak coupling between "P-V" and "Q-δ" quantities in power transmission system. Together with other approximations, the fast decoupled load flow equations become:

$$\begin{bmatrix} \frac{\Delta P}{V} \end{bmatrix} = [B'][\Delta\delta]$$

$$\begin{bmatrix} \frac{\Delta Q}{V} \end{bmatrix} = [B''][\Delta V]$$

where $B'_{km} = -\dfrac{1}{x_{km}}$ for $m \neq k$ and $B'_{kk} = \displaystyle\sum_{m\omega k} \dfrac{1}{x_{km}}$ for $m = k$

$B''_{km} = -B_{km}$ for $m \neq k$ and $B''_{kk} = \displaystyle\sum_{m\omega k} B_{km}$ for $m = k$ (Stott and Alsac 1974)

GENETIC ALGORITHM

Genetic algorithms (GAs) are adaptive methods which may be used to solve search and optimization problems. Over many generations, natural populations evolve according to the principles of natural selection and "survival of the fittest". By mimicking this process, genetic algorithms are able to "evolve" solutions to real world problems, if they have been suitably encoded [Holland 1975]. Genetic algorithms work with a "population of individuals", each representing a possible solution to a given problem. Each individual is assigned a "fitness score" according to how good a solution to the problem it is. The highly-fit individuals are given opportunities to "reproduce", by "cross breeding" with other individuals in the population. This produces new individuals as "offspring", which share some features taken from each "parent". The least fit members of the population are less likely to get selected for reproduction, and so "die out". A whole new population of possible solutions is thus produced by selecting the best individuals from the current "generation", and mating them to produce a new set of individuals. This new generation contains a higher proportion of the characteristics possessed by the good members of the previous generation. In this way, over many generations, good characteristics are spread throughout the population. By favouring the mating of the more fit individuals, the most promising areas of the search space are explored. If the genetic algorithm has been designed well, the population will converge to an optimal solution to the problem. There are some differences between genetic algorithms and traditional searching algorithms (such as numerical techniques). They could be summarized as follows [Younes 2006]:

- The algorithms work with a population of strings, searching many peaks in parallel, as opposed to a single point.
- Genetic algorithms work directly with strings of characters representing the parameters set, not the parameters themselves.
- Genetic algorithms use probabilistic transition rules instead of deterministic rules.
- Genetic algorithms use objective function information instead of derivatives or other auxiliary knowledge (convexity, modality, continuity, differentiability).
- Genetic algorithms have the potential to find solutions in many different areas of the search space simultaneously.

GENETIC ALGORITHM IMPLEMENTATION

A simple genetic algorithm is an iterative procedure, which maintains a constant size population of candidate solutions. During each iteration step (generation), three genetic operators (reproduction, crossover, and mutation) are performing to generate new populations (offspring), and the chromosomes of the new populations are evaluated via the value of the fitness which is related to cost function. Based on these genetic operators and the evaluations, the better new populations of candidate solutions are performed [Younes 2006]. With the above description, the three steps in executing the genetic algorithm operating on fixed-length character strings are as follows:

1. Randomly create an initial population of individual fixed-length character strings.
2. Iteratively perform the following sub steps on the population of strings until the termination criterion has been satisfied:
A. Assign a fitness value to each individual in the population using the fitness measure.
B. Create a new population of strings by applying the following three genetic operations. The genetic operations are applied to individual string(s) in the population chosen with a probability based on fitness.
i. Reproduce an existing individual string by copying it into the new population.
ii. Create two new strings from two existing strings by genetically recombining substrings using the crossover operation at a randomly chosen crossover point.
iii. Create a new string from an existing string by randomly mutating the character at one randomly chosen position in the string.
3. The string that is identified by the method of result designation (e.g. the best-so-far individual) is designated as the result of the genetic algorithm for the run. This result may represent a solution (or an approximate solution) to the problem.

Now, we'll discuss briefly each step of the implementation of the genetic algorithm:

- CHROMOSOME REPRESENTATION

Genetic algorithms operate on representations of solutions to problems. Since they work with encoded parameters of the optimization problem, the choice of a representation form has a large impact on the performance. There are different ways of encoding solutions, and probably no single best way for all problems. The performance of genetic algorithms depends on the choice of a suitable representation technique. Most genetic algorithms applications use Holland's fixed-length simple binary coding. This is historically the most widely used representation. Each chromosome is comprised of zeroes and ones, with each bit representing a gene [Abdul-Haleem 2005]. A conceptually simpler technique would be the real-coded representation, in which each chromosome vector is coded as a vector of floating point numbers of the same length as the solution vector. Each element was forced to be within the desired range, and the genetic operators were carefully designed to preserve this requirement [Michalewicz 1996].

- POPULATION INITIALIZATION

In the genetic algorithm, populations of chromosomes are created randomly by generating the required number of individuals using a random number generator that uniformly distributes numbers in the desired range. The extended random initialization is a variation whereby a number of random initializations are tried for each individual and the one with the best performance is chosen for the initial population. Other users of genetic algorithms have seeded the initial population with some individuals that are known to be in the vicinity of the global optimum. This approach is only applicable if the nature of the problem is well understood beforehand or if the genetic algorithm is used in conjunction with knowledge based system [Abdul-Haleem 2005].

- OBJECTIVE FUNCTION OR FITNESS FUNCTION

The objective function is used to provide a measure of how individuals have performed in the problem domain. In the case of a minimization problem, the mostly fit individuals will have the lowest numerical value of the associated objective function. This raw measure of fitness is usually only used as an intermediate stage in determining the relative performance of individuals in a genetic algorithm. Another function is the fitness function, is normally used to transform the objective function value into a measure of relative fitness [Ibrahim 2005].

- REPRODUCTION

The selection, or competition, is a stochastic process in which the chance of an individual surviving is proportional to its adaptation level. The adaptation is measured by the phenotype (search point, solution) evolution, that is, the characteristics presented by an individual in the problem environment (search space). The genetic algorithm, through selection, determines which individuals will go to the reproduction phase. There are several selection methods, where the fittest individuals from each generation are preferentially chosen for reproduction [Zamanan 2006]. Some of these methods are:
a. ROULETTE WHEEL SELECTION METHOD.
b. TOURNAMENT SELECTION METHOD.

- RECOMBINATION

Recombination produces new individuals in combining the information contained in two or more parents (parents-mating population). This is done by combining the variable values of the parents. Depending on the representation of the variables, different methods must be used. For the recombination of binary valued variables, the name "crossover" is established. This has mainly historical reasons. During the recombination of binary variables, only parts of the individuals are exchanged between the individuals. Depending on the number of parts, the individuals are divided before the exchange of variables (the number of cross points). The number of cross points distinguishes the methods.

In single-point crossover, one crossover position **a $\in$ [1, 2 , ……… , N_{var-1}]**, where (N_{var}) is the number of variables of an individual, is selected uniformly at random and the variables exchanged between the individuals about this point, then two new offspring are produced.

In double-point crossover, two crossover positions are selected uniformly at random and the variables exchanged between the individuals between these points. Then two new offspring are produced. For multi-point crossover, (**c**) crossover positions **$a_i \in$ [1 , 2 , ……… , N_{var-1}]; i = 1: m**, where (N_{var}) is the number of variables of an individual, are chosen at random with no duplicates and sorted into ascending order. Then, the variables between successive crossover points are exchanged between the two points to produce two new offspring. The section between the first variable and the first crossover point is not changed between individuals. Uniform crossover generalizes this scheme

to make every locus a potential crossover point. A crossover mask, the same length as the individual structure is created at random and the parity of the bits in the mask indicate which parent will supply the offspring with which bits [Pohlheim 2005].

- MUTATION

By mutation, individuals are randomly altered. These variations (mutation steps) are mostly small. They will be applied to the variables of the individuals with a low probability (mutation probability or mutation rate). Normally, offspring are mutated after being created by recombination [Pohlheim 2005]. In this process, randomly selected bits of randomly selected strings are changed from (**0**) to (**1**) and vice versa. This process occurs according to pre-specified probability. Usually, less than 5% of bits are changed in this process. Mutation process is used to escape from probable local optimum [Zamanan 2006].

- TERMINATION OF THE GENETIC ALGORITHM

Termination criteria or convergence criteria for genetic process may be triggered by finding an acceptable approximate solution and bring the search to halt. The termination criteria can be one or more of the following criteria [Abdul-Haleem 2005]:

a. Using diversity measure.
b. After a specified number of generations.
c. Finding an acceptable approximate solution.
d. Repetition until no change in the solution.

LOAD FLOW SOLUTION USING GENETIC ALGORITHM

The binary genetic algorithm is conceived to solve many optimization problems that stump traditional techniques. But, what if we are attempting to solve a problem where the values of the variables are continuous and we want to define them to the full machine precision? In such a problem, each variable requires many bits to represent it. If the number of variables is large, the size of the chromosome is also large. Of course, ones and zeros are not the only way to represent a variable. One could, in principle, use any representation conceivable for encoding the variables. When the variables are naturally quantized, the binary genetic algorithm fits nicely. However, when the variables are continuous, it is more logical to represent them by floating-point numbers. In addition, since the binary genetic algorithm has its precision limited by the binary representation of variables, using floating-point numbers instead easily allows representation to the machine precision. This continuous genetic algorithm also has the advantage of requiring less storage than the binary genetic algorithm because a single floating-point number represents the variable instead of (N_{bits}) integers. The continuous genetic algorithm is inherently faster than the binary genetic algorithm, because the chromosomes do not have to be decoded prior to the evaluation of the cost function (objective function) [Haupt 2004].

COMPONENTS OF A CONTINUOUS GENETIC ALGORITHM

- THE VARIABLES AND COST FUNCTION

A cost function generates an output from a set of input variables (a chromosome). The cost function may be a mathematical function or an experiment. The objective is to modify the output in some desirable fashion by finding the appropriate values for the input variables. The goal is to solve some optimization problem where we search for an optimum (minimum) solution in terms of the variables of the problem. If the chromosome has (N_{var}) variables (an N-dimensional optimization problem) given by ($b_1, b_2, \ldots\ldots, b_{Nvar}$), then the chromosome is written as an array with ($1 \times N_{var}$) elements so that:

chromosome = [b₁, b₂, b₃, ..., b_Nvar]

In this case, the variable values are represented as floating-point numbers. Each chromosome has a cost found by evaluating the cost function (**f**) at the variables (**b₁, b₂, ..., b_Nvar**).

cost = f (chromosome) = f (b₁, b₂, ..., b_Nvar)

Equations (10) and (11) along with applicable constraints constitute the problem to be solved [Haupt 2004].

Our primary problem in this research is the continuous functions introduced below. The two cost functions are [Kubba 1987]:

$$\Delta P_k = P_k^{sp} - V_k \sum_{m=1}^{n} V_m (G_{km} \cos\delta_{km} + B_{km} \sin\delta_{km})$$

for "**PV**" and "**PQ**" busses

$$\Delta Q_k = Q_k^{sp} - V_k \sum_{m=1}^{n} V_m (G_{km} \sin\delta_{km} - B_{km} \cos\delta_{km})$$

for "**PQ**" busses only

Where $\delta_{km} = \delta_k - \delta_m$, and
(ΔP_k) is the mismatch active power at bus (**k**) and (ΔQ_k) is the mismatch reactive power at bus (**k**). (V_k, V_m, δ_k, δ_m) are the voltage magnitude and angle at busses (**k**) and (**m**) respectively, which are the variables of the two cost functions.

* VARIABLE ENCODIND, PRECISION, AND BOUNDS

Here, the difference between binary and continuous genetic algorithms is shown. It is no longer needed to consider how many bits are necessary to represent accurately a value. Instead, (**V**) and (δ) have continuous values that are limited between appropriate bounds (which are in our problem, **0.95 ≤ V ≤ 1.05** and **-5° ≤ δ ≤ 5°** for "**5 busbars**" typical test system and $0.9 \leq V \leq 1.1$, $-20^o \leq \delta \leq 20^o$ for Iraqi National Grid). Although the values are continuous, a digital computer represents numbers by a finite number of bits. When we refer to the continuous genetic algorithm, it means that the computer uses its internal precision and roundoff to define the precision of the value. Now, the algorithm is limited in precision to the roundoff error of the computer [Haupt 2004].

* INITIAL POPULATION

The genetic algorithm starts with a group of chromosomes known as the population. We define an initial population of (N_{ind}) chromosomes. A matrix represents the population with each row in the matrix being a (**1×N_var**) array (chromosome) of continuous values. Given an initial population of (N_{ind}) chromosomes, the full matrix of ($N_{ind} \times N_{var}$) random values is generated.

All variables are normalized to have values between (**0**) and (**1**), the range of a uniform random number generator. The values of a variable are "unnormalized" in the cost function. If the range of values is between (b_{lo}) and (b_{hi}), then the unnormalized values are given by:

b = (b_hi − b_lo) b_norm + b_lo

where:

b_{hi} : highest number in the variable range.

b_{lo} : lowest number in the variable range.

b_{norm} : normalized value of variable.

This society of chromosomes is not a democracy: the individual chromosomes are not all created equal. Each one's worth is assessed by the cost function. So at this point, the chromosomes are passed to the cost function for evaluation [Haupt 2004].

- NATURAL SELECTION

Survival of the fittest translates into discarding the chromosomes with the highest cost. First, the (N_{ind}) costs and associated chromosomes are ranked from lowest cost to highest cost. Then, only the best are selected to continue, while the rest are deleted. The selection rate, (X_{rate}), is the fraction of (N_{ind}) that survives for the next step of mating. The number of chromosomes that are kept each generation is:

$$N_{keep} = X_{rate} \cdot N_{ind}$$

Natural selection occurs each generation or iteration of the algorithm. Of the (N_{ind}) chromosomes, only the top (N_{keep}) survive for mating, and the bottom ($N_{ind} - N_{keep}$) are discarded to make room for the new offspring. Deciding how many chromosomes to keep is somewhat arbitrary. Letting only a few chromosomes survive to the next generation limits the available genes in the offspring. Keeping too many chromosomes allows bad performers a chance to contribute their traits to the next generation. We often keep 50% ($X_{rate}=0.5$) in the natural selection process [Haupt 2004].

- SELECTION FOR MATING

In this process, two chromosomes are selected from the mating pool of (N_{keep}) chromosomes to produce two new offspring. Pairing takes place in the mating population until ($N_{ind} - N_{keep}$) offspring are born to replace the discarded chromosomes. Pairing chromosomes in a genetic algorithm can be as interesting and varied as pairing in an animal species. We'll look at a variety of selection methods.

a. Weighted random pairing (roulette-wheel): which is divided into:

i. Rank weighting.

ii. Cost weighting.

b. Tournament selection.

Each of the parent selection schemes results in a different set of parents. As such, the composition of the next generation is different for each selection scheme. Roulette-wheel and tournament selection are standard for most genetic algorithms. It is very difficult to give advice on which selection scheme works best. In our problem, we follow the rank-weighting roulette-wheel and tournament parent selection procedures [Haupt 2004].

- RECOMBINATION

As for the binary algorithm, two parents are chosen, and the offspring are some combination of these parents. Many different approaches have been tried for crossing over in continuous genetic algorithm. The simplest methods choose one or more points in the chromosome to mark as the crossover points. Then the variables between these points are merely swapped between the two parents. The problem with real-valued crossover methods is that no new information is introduced: each continuous value that was randomly initiated in the initial population is propagated to the next generation, only in different combinations. Although this strategy works fine for binary representations, there is now a continuum of values, and in this continuum we are merely interchanging two data points. These approaches totally rely on mutation to introduce new genetic

material. The blending models remedy this problem by finding ways to combine variable values from the two parents into new variable values in the offspring.

In our problem, we want to find a way to closely mimic the advantages of the binary genetic algorithm scheme. It begins by randomly selecting a variable in the first pair of parents to be the crossover point:

c = roundup {random*N$_{var}$}

We'll let

parent 1 = [b$_{m1}$, b$_{m2}$, ..., b$_{mc}$, ..., b$_{mNvar}$]
parent 2 = [b$_{d1}$, b$_{d2}$, ..., b$_{dc}$, ..., b$_{dNvar}$]

Where (**m**) and (**d**) subscripts discriminate between the mom and dad parent. Then, the selected variables are combined to form new variables that will appear in the children:

b$_{new1}$ = b$_{mc}$ − β (b$_{mc}$ − b$_{dc}$)
b$_{new2}$ = b$_{dc}$ + β (b$_{mc}$ − b$_{dc}$)

Where **β** is a random value between **0** and **1**. The final step is to complete the crossover with the rest of the chromosome as in binary genetic algorithm:

offspring 1 = [b$_{m1}$, b$_{m2}$, ..., b$_{new1}$, ..., b$_{dNvar}$]
offspring 2 = [b$_{d1}$, b$_{d2}$, ..., b$_{new2}$, ..., b$_{mNvar}$]

If the first variable of the chromosomes is selected, then only the variables to the right of the selected variable are swapped. If the last variable of the chromosomes is selected, then only the variables to the left of the selected variable are swapped. This method does not allow offspring variables outside the bounds set by the parent unless **β > 1** [Haupt 2004].

* MUTATION

Random mutations alter a certain percentage of the genes in the list of chromosomes. We can sometimes find our method working too well. If care is not taken, the genetic algorithm can converge too quickly into one region of the cost surface. If this area is in the region of the global minimum, that is good. However, some functions, such as the one we are modeling, have many local minima. If nothing is done to solve this tendency to converge quickly, it may end up in a local rather than a global minimum. To avoid this problem of overly fast convergence (premature convergence), the routine is forced to explore other areas of the cost surface by randomly introducing changes, or mutations, in some of the variables. The basic method of mutation is not much more complicated for the continuous genetic algorithm. Do we also allow mutations on the best solutions? Generally not. They are designated as elite solutions destined to propagate unchanged. Such elitism is very common in genetic algorithms. Why throw away a perfectly good answer? The equation of mutation used here is [Haupt 2004]:

b$_{mut}$ = (b$_{hi}$ − b$_{lo}$) b$_{norm}$ + b$_{lo}$; **b$_{mut}$:** variable under mutation.

MULTIPLE OBJECTIVE OPTIMIZATION (MOO)

In many applications, the cost function has multiple, often times, conflicting objectives. The most important approach to (MOO) are: **weighted cost functions** [Haupt 2004].

$$\mathbf{cost} = \sum_{i=1}^{N} \mathbf{w_i \, f_i}$$

Where:

$\mathbf{f_i}$ is the cost function (**i**).

$\mathbf{w_i}$ is the weighting factor and $\sum_{i=1}^{N} \mathbf{w_i = 1}$.

The problem with this method is determining appropriate values of ($\mathbf{w_i}$). Different weights produce different costs for the same ($\mathbf{f_i}$). This approach requires assumptions on the relative worth of the cost functions prior to running the genetic algorithm. Implementing this multiple objective optimization approach in a genetic algorithm only requires modifying the cost function to fit the form of eq. (17) and does not require any modification to the genetic algorithm [Haupt 2004]. Thus,

$$\mathbf{cost = w \, f_1 + (1\text{-}w) \, f_2}$$

This approach is adopted in this research for its simplicity, easy of programming and gives us the required accuracy. Here, (**w**) is chosen to be (**0.5**).

```
┌─────────────────────────────────────────┐
│   Define cost function, cost variables   │
│   Select genetic algorithm parameters    │
└─────────────────────────────────────────┘
                    │
                    ▼
        ╭─────────────────────────────╮
        │  Generate initial population │
        ╰─────────────────────────────╯
                    │
                    ▼
        ╭─────────────────────────────╮
        │ Find cost for each chromosome│
        ╰─────────────────────────────╯
                    │
                    ▼
        ╭─────────────────────────────╮
  ┌────▶│        Select mates          │
  │     ╰─────────────────────────────╯
  │                 │
  │                 ▼
  │     ╭─────────────────────────────╮
  │     │     Mating and crossover     │
  │     ╰─────────────────────────────╯
  │                 │
  │                 ▼
  │     ╭─────────────────────────────╮
  │     │          Mutation            │
  │     ╰─────────────────────────────╯
  │                 │
  │                 ▼
  │     ╭─────────────────────────────╮
  │     │ Find cost for each chromosome│
  │     ╰─────────────────────────────╯
  │                 │
  │                 ▼
  │            ◇ Convergence
  │  NO       ◇   Test   ◇
  └──────────◇           ◇
              ◇         ◇
                 YES │
                     ▼
        ╭─────────────────────────────╮
        │            End               │
        ╰─────────────────────────────╯
```
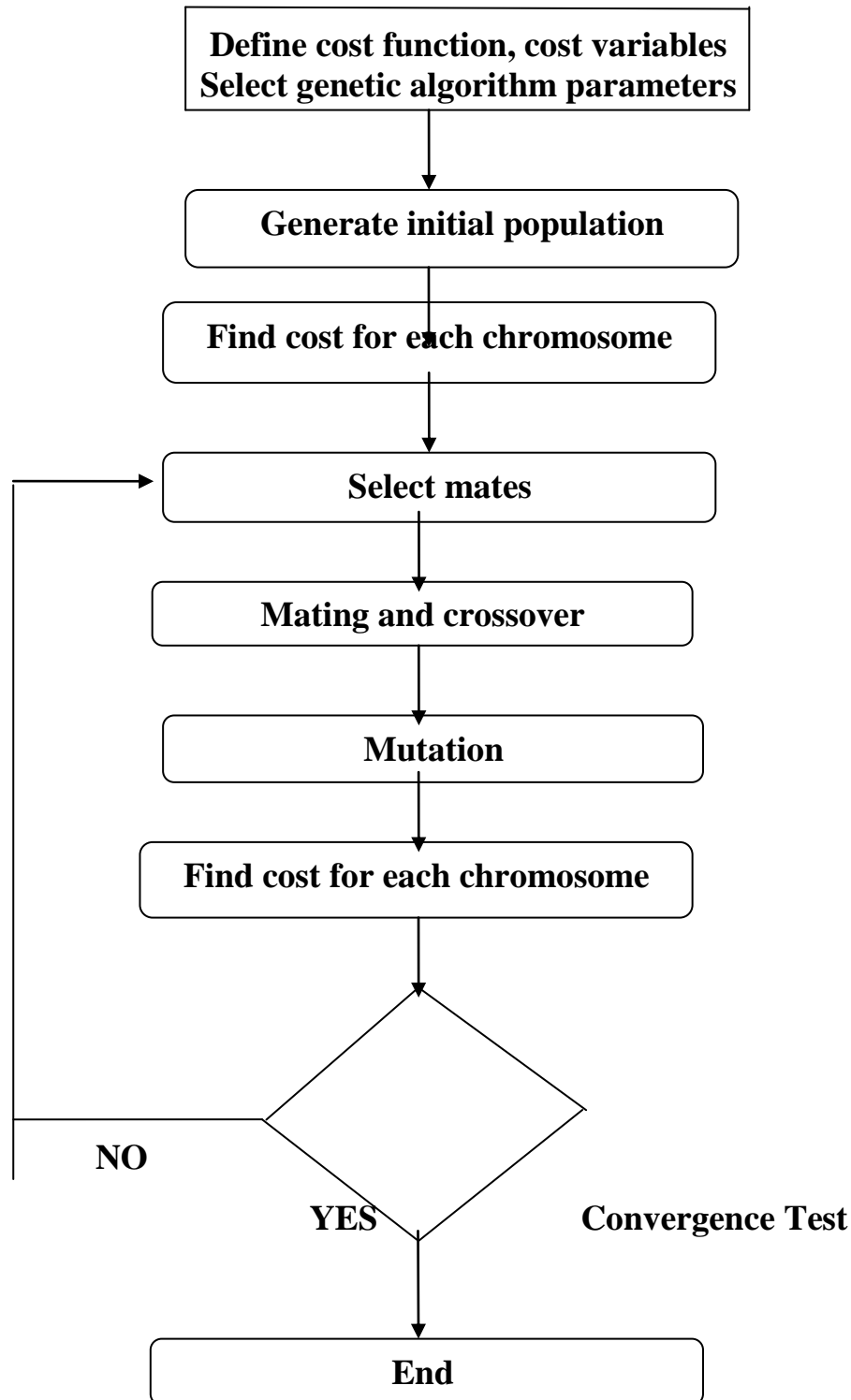
Fig. (2) Flowchart of a Continuous Genetic Algorithm

IMPLEMENTATION AND RESULTS

The proposed continuous (real-coded) genetic algorithm is demonstrated on two test systems namely, 5-buses test system [Stagg 1968] which lines data and buses data are present in appendix. The

second system is the 362-bus Iraqi National Grid (ING) with 599 branches. The software is implemented by using MATLAB version 7 with Pentium 4, 2 GHz CPU, and 2 Gbyte RAM. The input data are the nodal admittance matrix, buses data (specified values), and the slack voltage

1. Five Buses Typical Test System Results

Table (1) shows the results of the application of the genetic algorithm to "**5 bus-bars**" typical test system to find the active and reactive power mismatches described in eqs. (12) and (13) for accuracy of **0.001 p.u** (**0.1 MW/MVAR)** and the voltage magnitude and phase angle associated with each busbar. Because of the stochastic nature of the genetic algorithm process, each independent run will probably produce a different number of generations and consequently the computation time and the best amongst these should be chosen. The best of the (**10**) implementation runs are shown in this table. The base quantities are 132 KV and 100 MVA.
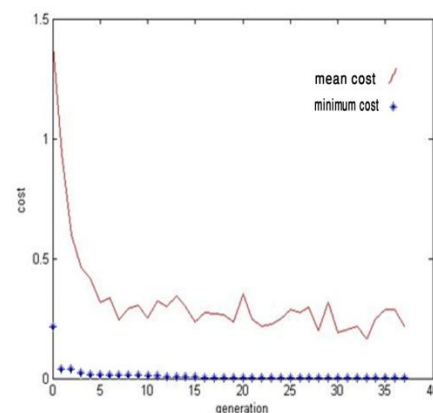
Table (2) Load Flow Solution for "5 busbars" Typical Test System with an Accuracy of (0.001)

Bus No.	Active power mismatch(p.u)	Reactive power mismatch(p.u)	Voltage magnitude(p.u)	Voltage angle(deg.)	No. of generations
1	slack	slack	1.06	0.00	—
2	0.00018139	0.00076184	1.0333	-0.2856	37
3	0.00094649	0.00028622	1.0349	-2.5267	27
4	0.00096724	0.0004207	1.0014	-1.4736	26
5	0.00091083	0.00096267	0.9786	-1.5042	35
Total	**Computational**	**Time:**			**0.516 sec.**

Figures below, the dotted curves show the evolution process of the active and reactive power mismatches (cost function) versus the number of generations and the solid curves show the mean cost of the individuals versus the number of generations at each busbar of the "**5 busbars**" typical test system with an accuracy of (**0.001**). In the figures and due to the stochastic nature of the genetic algorithm, we note that each busbar requires different number of generations to reach the required accuracy (0.001 p.u.).
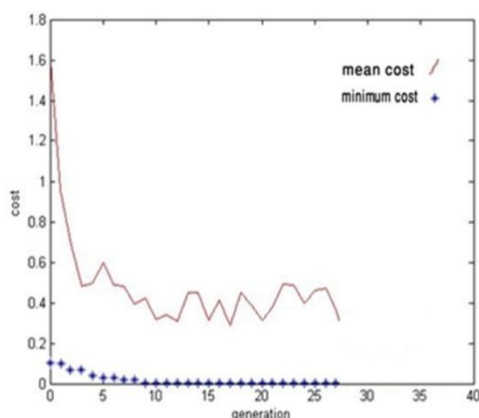
Evolution Process at Busbar 2   **Evolution Process at Busbar 3**

4154
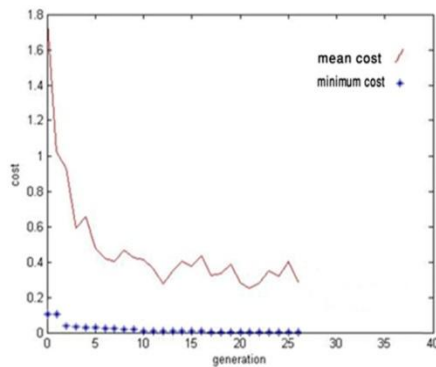
Evolution Process at Busbar 4   **Evolution Process at Busbar 5**

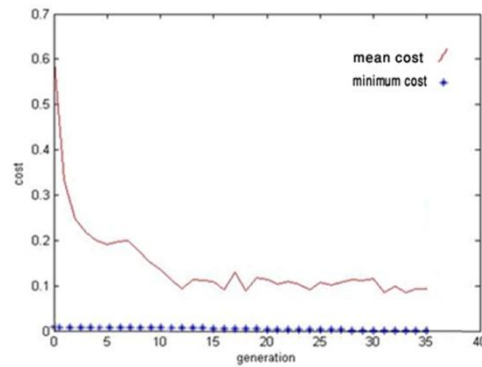In the table (2) shown, the active and reactive line flows (power flows) for the "**5 busbars**" typical test system which consists of (**7**) lines are calculated, the calculation is done for an accuracy of the active and reactive power mismatches of (**0.001**).

Table (2) Active and Reactive Power Flows for the "5 busbars" Typical Test System with an Accuracy of (0.001)

Line No.	Line Term	Active power flow (MW)	Reactive power flow (MVAR)
1	1—2	22.3473	-39.7436
2	1—3	21.5944	-4.3321
3	2—3	20.7693	7.3872
4	2—4	16.2575	-13.0168
5	2—5	17.1768	-63.7962
6	3—4	-22.2970	-123.5797
7	4—5	-3.0479	-21.5199

* Iraqi National Grid Load Flow Solution Results:
The 362-bus (ING) consists of 30-generator bus and 332-load bus with 599 branches [Al-Bakri 1994]. Table (3) illustrates the load flow solution for Iraqi National Grid using the proposed continuous (real-coded) Genetic Algorithm with a power tolerance (minimum active and reactive power mismatches) of 0.001 p.u. with base quantities of 132 KV and 100 MVA. Also, the number of iterations (generations) for each bus are tabulated. Due to the huge table, only the load flow solution results of 96 bus are tabulated in this paper.

Table (3) Load Flow Solution for "IRAQI NATIONAL GRID" with an Accuracy of (0.001)

Bus No.	Active power mismatch (p.u)	Reactive power mismatch (p.u)	Voltage magnitude (p.u)	Voltage angle (p.u)	No. of generations
1	slack	slack	1.04	0	—
2	0.0005	PV	1	18.3805	262
3	0.00021334	PV	1	2.8233	57
4	0.0008081	PV	1	-9.5400	3191
5	0.00011245	PV	1	13.6445	521
6	0.00043106	PV	1	-11.8520	34
7	0.0018487	PV	1	4.1875	5000
8	0.00066843	PV	1	7.5529	244
9	0.00023882	PV	1	12.3150	30
10	0.00016648	PV	1	4.0006	134
11	0.0003391	PV	1	-19.7704	884
12	0.00045458	PV	1	-6.3530	266
13	0.00013682	PV	1	4.5221	424
14	0.00058912	PV	1	-6.9794	76
15	0.00054176	PV	1	-8.1968	353
16	0.00021063	PV	1	13.5898	42
17	0.00078201	PV	1	4.5766	39
18	$2.4477*10^{-6}$	PV	1	11.1094	415
19	0.00090163	PV	1	7.0672	47
20	0.00089409	PV	1	-7.0275	9
21	0.00037127	PV	1	-3.2876	159
22	0.00014522	PV	1	-10.7986	24
23	0.00093387	PV	1	2.0421	216
24	0.00084462	PV	1	9.0268	472
25	0.00038532	PV	1	2.9669	17
26	0.00023586	PV	1	3.8338	527
27	$7.2047*10^{-6}$	PV	1	-6.8666	88
28	0.00011686	PV	1	0.0252	50
29	0.00026843	PV	1	7.3612	333
30	0.0005791	PV	1	9.1833	1342

Bus No.	Active power mismatch (p.u)	Reactive power mismatch (p.u)	Voltage magnitude (p.u)	Voltage angle (p.u)	No. of generations
31	0.0003	0.0002	1.02247	12.3782	36
32	0.00031048	0.00013264	1.03356	-12.5347	57
33	0.00076127	0.00088425	0.915482	-18.8922	747
34	0.00048097	$7*10^{-5}$	0.981021	-3.14901	60
35	0.00082233	0.00019414	0.909731	-7.5778	927
36	0.0007	0.0004	0.999866	0.40992	54
37	0.0009483	0.00059979	0.99142	-0.108361	3
38	0.00072258	$2.708*10^{-5}$	1.02766	2.41241	393
39	0.00010822	$3.1427*10^{-5}$	0.911085	8.90456	21
40	$7.3767*10^{-5}$	$8.2306*10^{-5}$	0.978972	7.68687	21
41	$3.9217*10^{-5}$	0.00014068	0.914069	-2.09315	30
42	0.00056231	0.00034232	0.931974	10.2677	117
43	0.00015186	0.00084486	0.916778	9.06423	69
44	0.00093275	0.00060546	0.935108	-13.2829	18
45	0.00085845	$3.9338*10^{-5}$	1.00216	-8.97243	12
46	$2.0578*10^{-5}$	0.00022034	0.935224	-7.08481	54
47	0.0005849	0.00025364	0.96548	-8.2154	120
48	0.0006	0.0009	0.96959	0.0359168	9
49	0.00046407	0.00068482	1.01733	8.11071	36
50	0.00064014	0.00040881	0.906882	16.9887	3
51	0.00081139	0.00073374	1.01725	12.1607	15
52	0.00063582	0.00036833	0.999238	0.015595	12
53	0.00064585	0.00073222	0.924709	7.0377	54
54	0.00039461	0.00031144	1.02049	4.97693	54
55	0.00050197	0.00051873	0.912678	18.5084	312
56	0.0006757	0.00066047	1.02961	13.4216	57
57	0.00048624	0.00046999	1.01989	13.0202	165
58	0.00026657	0.00078447	1.03154	-4.56727	54
59	0.00020212	0.00087574	0.998382	-0.133244	135
60	0.00099704	0.00040061	0.969316	-9.13924	336
61	0.0002	0.0005	1.09633	-3.3891	60

| 62 | 0.00062866 | 0.00048481 | 1.01166 | 3.0274 | 69 |
| 63 | $3.4536*10^{-6}$ | 0.00050729 | 1.00118 | 11.0695 | 144 |

Bus No.	Active power mismatch (p.u)	Reactive power mismatch (p.u)	Voltage magnitude (p.u)	Voltage angle (p.u)	No. of generations
64	0.00052304	$6.1774*10^{-5}$	0.926323	0.126932	30
65	0.00039148	0.00027503	0.959269	-3.93418	234
66	0.0003338	0.00048038	0.939048	5.45821	24
67	0.00045369	0.00074015	1.03691	8.05995	12
68	0.00077681	0.00053799	0.962027	-0.556099	186
69	0.00027057	0.00061177	1.0712	5.11859	144
70	0.00040663	0.00054506	0.909477	-13.4194	18
71	0.00015602	0.00084029	1.0151	4.6136	60
72	0.00085314	$4.4098*10^{-5}$	0.9505	-9.4481	54
73	0.00082757	0.00056498	0.9587	14.8084	132
74	$6.6466*10^{-5}$	0.00028761	1.0205	-0.5232	24
75	0.00045213	0.00089712	0.9106	16.254	450
76	0.00026312	0.00099152	1.0235	-0.4562	60
77	0.0003	0.0002	0.9989	-15.9269	1137
78	0.00060173	0.00081968	0.9069	9.3835	102
79	0.00097288	0.00093161	0.9115	-9.6373	399
80	0.00030775	0.00026214	1.0172	-11.3539	567
81	0.00028197	0.0003666	0.9567	10.958	72
82	0.0001	0.0007	0.9009	-9.6128	1215
83	0.00017501	0.00031678	0.9538	0.5662	36
84	0.00060463	0.00055344	0.9389	12.4227	51
85	0.00049479	0.00025939	0.9917	-17.9393	69
86	0.00074739	$6.1917*10^{-5}$	0.9976	11.2733	54
87	0.00073692	0.00062359	1.0459	3.6541	90
88	0.0002	0	0.9265	7.1323	69
89	$8.0049*10^{-5}$	0.00089968	1.0154	-0.9266	33
90	0.00051316	0.00093613	1.0007	-15.3443	189
91	$3.1397*10^{-5}$	0.00072166	1.0017	18.7953	138
92	0.00062835	0.00047428	0.9977	12.0889	27

93	$4.7755*10^{-5}$	0.00047299	1.0034	11.0409	60
94	0.00031952	0.00085516	0.9855	1.9537	135
95	0.00028333	0.00050642	1.0368	18.9362	60
96	0.0008504	0.00096063	1.0821	-15.1242	96

- CONCLUSION

The proposed method (Real-Coded Genetic Algorithm) presented in this paper can be implemented on-line for small and medium-scale power systems load flow solution and it can be used for planning study for large-scale systems. The proposed method has reliable convergence and high accuracy of solution. Whereas the traditional numerical techniques (Gauss-Seidel, Newton-Raphson, Fast decoupled,…etc.) use the characteristics of the problem to determine the next sampling point (e.g. gradient, linearity and continuity), genetic algorithm makes no such assumptions. Instead, the next sampled point is determined based on stochastic sampling or decision rules rather than on a set of deterministic decision rules. Also, whereas the traditional numerical techniques mentioned above use a single point at a time to search the problem space, genetic algorithm uses a population of candidate solutions for solving the problem. Thus, reducing the possibility of ending at a local minima.   Although binary-coded genetic algorithm has been successfully applied to a wide range of optimization problems, they suffer from disadvantage when applied to the real-world problems involving a large number of variables. Thus, we use in our problem the real-coded genetic algorithm, where all decision variables (unknowns) are expressed as real numbers. Explicit conversion to binary does not take place. A reduction of computational effort is an obvious advantage of a real-coded genetic algorithm. Another advantage is that, an absolute precision is now attainable by making it possible to overcome the crucial decision of how many bits are needed to represent potential solutions. Blending models are used in the crossover operator to remedy the problem of the crossover in the real-coded genetic algorithm which is, no new information is introduced: each continuous value that was randomly initiated in the initial population is propagated to the next generation, only in different combinations. Thus, the blending methods combine variable values from the two parents into new variable values in the offspring. At the same time, these methods do not allow offspring variables outside the bounds set by the parent unless $\beta > 1$, where β is a random number on the interval [**0**,**1**]. Finally, solving the load flow problems by genetic algorithm gives high accurate results with respect to the conventional methods, since load flow study is multiple solutions.

REFRENCES

- Abdul-Haleem G. F., 2005, "A Genetic Algorithm for Manufacturing Cell Formation", M.Sc Thesis, Mechanical Department, University of Baghdad.

- Al-Shakarchi M. R. G., 1973, "Nodal Iterative Load Flow", A dissertation submitted to the Victoria University of Manchester.

- AL-BAKRI A. A., 1994, "A Study of Some Problems on the Iraqi National Grid and Establishing a Method Algorithm for Load Flow", M.Sc. Thesis, University of Baghdad.

- Grisby Leonard L., 2007, "Power Systems", CRC Press.

- Haupt R. L. and Haupt S. E., 2004, "Practical Genetic Algorithms", A John Wiley & Sons, INC., Publication, 2nd edition.

- Holland J., 1975, "Adaptation in Natural and Artificial Systems", MIT Press.

- Ibrahim S. B. M., 2005, "The PID Controller Design Using Genetic Algorithm", A dissertation submitted to University of Southern Queensland, Faculty of engineering and surveying, Electrical and Electronics Engineering.

- Kubba H.A., 1987, "Comparative Study of Different Load Flow Solution Methods", M.Sc Thesis, University of Baghdad.

- Michalewicz Z., 1996, "Genetic Algorithms + Data Structure = Evolution Programs", AI series, Springer-Verlag, New York, 3rd edition.

- Nanda J., Kothari D. P. and Srivastava S. C., 1987, "Some Important Observations on Fast   Decoupled Load Flow Algorithm", Proceedings of the IEEE, VOL. 75, No. 5, 732-733

- Pohlheim H., 2005, "GEATBx: Genetic and Evolutionary Algorithm Toolbox for Use with   Matlab", available at http://www.geatbx.com/.

- Stott B. and Alsac O., 1974, "Fast Decoupled Load Flow", IEEE Trans. Power App. Syst., VOL. PAS-93, 859-869

- STAGG G. W. and AL-ABIAD A., 1968, "Computer Methods in Power System Analysis",   Mc-Graw Hill Publishing Company.

- Talib A., 2007, "An Optimization Approach of Robot Motion Planning Using Genetic Algorithm", M.Sc Thesis, Mechatronics Department, AL-Khwarizmi Engineering, University of Baghdad.

- Taylor D. G. and Treece J. A., 1967, "Load Flow Analysis by Gauss-Seidel Method", presented at the Symp. on power systems load flow analysis, University of Manchester Institute of Science and Technology, Manchester, U.K.

- Woon L. C., 2004, "Genetic Algorithm for Load Flow Solution Techniques", Abstract of thesis, Master of engineering (electrical), http://www.sps.utm.

- Younes M. and Rahli M., 2006, "On the Choice Genetic Parameters with Taguchi Method Applied in Economic Power Dispatch", Leonardo journal of sciences, issue 9, pp. 9-24.

- Zamanan N., Sykulski J., Al-Othman A. K., 2006, "A Digital Technique for Online Identification and Tracking of Power System Harmonics Based on Real Coded Genetic Algorithm", Proceedings of the sixth IASTED international conference, European power and energy systems, Rhodes, Greece.

LIST OF SYMBOLS AND ABBREVIATIONS

b : Any variable in the chromosome.
B : Imaginary part of admittance.
c : Crossover point.
e : Real part of bus voltage.
E : Complex bus voltage.
f : Imaginary part of bus voltage.
G : Real part of admittance.
GA : Genetic Algorithm.
LF : Load Flow.
n : Number of busses in the power system.
N : Number of objective functions.
N_{var} : Number of variables in an individual.
N_{keep} : Number of chromosomes that are kept each generation.
N_{ind} : Number of individuals in the population.
p : Iteration index.
p.u : Per unit.
PQ : Load busbars.
PV : Generator busbars.
sp : Specified value.
V : Bus voltage magnitude.
w : Weighting factor.
X_{rate} : Selection rate.
Y_{kk} : Self admittance of bus (k).
Y_{km} : Branch admittance between busses (k) and (m).
ΔP : Active power mismatch.
ΔQ : Reactive power mismatch.
δ : Bus voltage phase angle.
β : Random number on the interval [0,1].

APPENDIX I

Nodal admittance matrix elements for "**5 busbars**" typical test system, per-unit quantity = **100 MVA, and 132 KV.** The following data are all in (**p.u**), and buses data.

From Bus	To Bus	G (p.u)	B (p.u)
1	1	6.25	-18.695
1	2	-5	15
1	3	-1.25	3.75
1	4	0	0
1	5	0	0
2	2	10.83334	-23.415
2	3	-1.66667	5
2	4	-1.66667	5
2	5	-2.5	7.5
3	3	12.91667	-38.695
3	4	-10	30
3	5	0	0
4	4	12.91667	-38.695
4	5	-1.25	3.75
5	5	3.75	-11.21

Bus No.	Specified active power (p.u)	Specified reactive power (p.u)	Voltage (p.u)
1	slack	slack	1.06+j0
2	0.2	0.2	—
3	-0.45	-0.15	—
4	-0.4	-0.05	—
5	-0.6	-0.1	—

ACTIVE NETWORK SECURITY BASED RSA ALGORITHM

Ahmed Freidoon Fadhil
Civil Engineering Department
University Of Kirkuk

Wisam haitham abbood Computer and Software
Engineering Department
University Of Al- Mustansiriya

ABSTRACT

 The difficulty of building a secure network is due to the changing nature of the enterprise coupled with the increasing sophistication of the hacker threat, both from inside and outside of the network. Active networks enable individual user or groups of users to inject customized programs into the nodes of the network.

 The proposed system depends on the basic concepts (authentication and authorization) and uses RSA algorithm to add additional level of security. The proposed system also depends on active packet architecture, the packet will represented in the active node as input, and when the packet is retransmitted to another active node it carries information about each node it visits. The result of execution the packet will display in the first node where the packet started.

الخلاصة

إن الصعوبة في بناء شبكة آمنة للحاسبات ترجع إلى الطبيعة المتغيرة لمشاريع الشبكة إضافة إلى المهارة المتزايدة لقراصنة المعلومات سواء من داخل الشبكة أو من خارجها. الشبكات الفعالة (Active Network) تسمح لمستخدم واحد او مجموعة من المستخدمين ليدخل برامج مُعَدة حسب الطلب الى حاسبات الشبكة.

ان النظام المقترح يعتمد على المفاهيم الرئيسية (التوثيق، التخويل) و يستخدم خوارزمية التشفير (RSA) لزيادة امن النظام. يعتمد النظام المقترح ايضاً على معمارية الحزمة النشيطة (Active packet)، ان الحزمة (Packet) ستتمثل في الحاسبة الفعالة كمدخل, وعندما يتم نقل الحزمة الى حاسبة فعالة اخرى فانها سوف تحمل معلومات عن كل حاسبة زارتها. وان نتيجة تنفيذ الحزمة سوف يعرض في اول حاسبة كانت الحزمة بدأت فيها.

KEY WORDS

 Active network, Security, Authentication, Authorization, RSA .

INTRODUCTION

   Computer networks are becoming fundamental to the functioning of modern organizations. As the dependency on networks increases, the need to control networked resources becomes increasingly critical. At the same time, networks are becoming ever more valuable in terms of their function, the resources they offer, and the information they contain. In this way, they become not only more valuable to an organization itself but they also become an attractive target for hostile parties (both in and outside of an organization) (Gert D. L. 2005).

   In the past decade, a wide variety of security mechanisms have been developed, aimed at safeguarding the logical assets of an organization: firewall technologies, encryption and

cryptographic authentication, biometrics and the like. These measures have one common factor in that they attempt to prevent unauthorized access to resources they could be likened to the locks and secure doors used in physical security (Gert D. L. 2005).

When performing security tasks, security professionals tray to protect their environments as effectively as possible. These actions can also be described as protecting confidentiality, integrity, and availability (CIA).

CIA stands for:-

- Confidentiality:- ensure that no data is disclosed intentionally or unintentionally.
- Integrity:- make sure that no data is modified by unauthorized person, that no unauthorized changes are made by unauthorized person.
- Availability:- provide reliable and timely access to data and resources.

There is an idea (active network) that gives the user the ability to program the network (Psounis K. 1999).

ACTIVE NETWORK

The concept of active networking emerged from discussions within Defence Advanced Research Projects Agency (DARPA) research community in 1995 on the future direction of networking systems (Tennenhouse D. L. 1997).

Active Networks break with tradition by allowing the network to perform customized computations on the user data. For example, a user of an active network could send a customized compression program to a node within the network (e.g., a router) and request that the node execute that program when processing their packets. These networks are "active" in two ways:

- Routers and switches within the network actively process, i.e., perform computations on, the user data flowing through them.

- Individual authorized users and/or administrators can inject customized programs into the network, thereby tailoring the node processing to be user and/or application specific (Tennenhouse D. L. 2002).

There are three principal advantages to basing the network architecture (on the exchange of active programs, rather than static packets):

- Exchanging code provides a basis for dynamically adaptive protocols, enabling richer interactions than the exchange of fixed data formats.

- Active packet provides a means of implementing fine grained application-specific functions at strategic points within the network.

- The programming abstraction provides a powerful platform for user-driven customization of the infrastructure, allowing new services to be deployed at a faster pace than can be sustained by vendor driven standardization processes (Tennenhouse D. L. 2002).

So, active network would enable a range of applications that leveraged computation within the network, and it would accelerate the pace of innovation by decoupling services from the underlying infrastructure (Whetherall D. 1999).
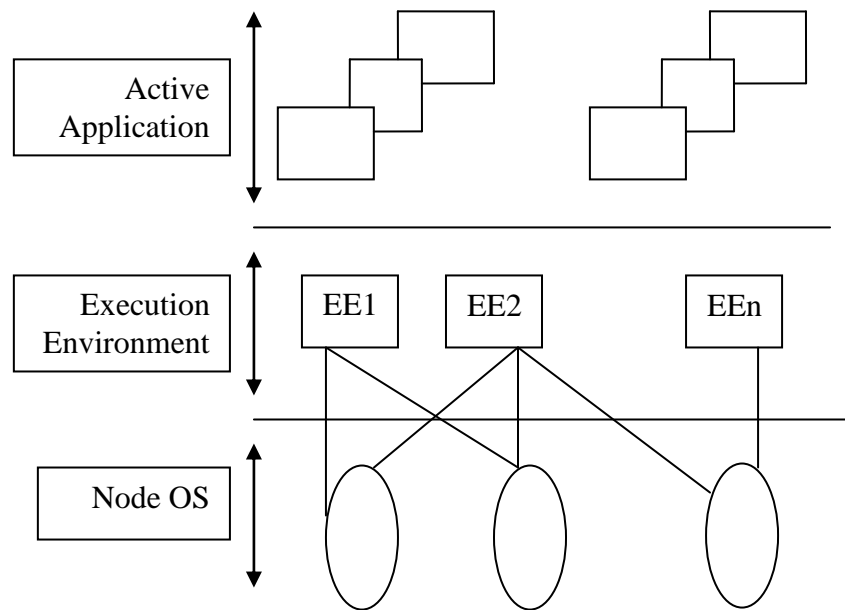
ACTIVE NETWORK ARCHITECTURES

Fig. (1): Active Network Architecture

The architectures are classified based on their approach toward the realization of active networking. **Figure 1** shows the high level AN node (Active Network Node) architecture. Each AN node runs an operating system (Node OS) and one or more execution environments (EE). When a packet arrives at a node, it will be first handled by the Node OS. Node OS verifies and identifies the content of that packet. If the packet does not require further process, it is then simply forwarded to the next node. If further process is needed, the packet is passed to the EE. The further process in the EE may include running an active application or simply store the data brought by the packet.
There are currently three architectures in implementing active network:
Active packets, active nodes and hybrid approaches. Most of the early active networks architectures follow "the active packet" approach. This scheme is fundamentally characterized by the fact that the code is carried inside the packet. The nodes are also active in a sense that they allow computation up to the application layer (Clavert K. L. 1999).

❖ **Active Packet Approach**

In active packet the code is carried by the packets. The code is either to be executed on the data of the same packet that carries the code or to be executed in order to change the state or the behavior of the node (Bhattacharjee S. 1999).

Service CODE	DATA
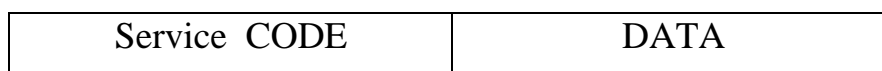
Fig. (2): Active Packet Approach Representation

❖ **Active Node Approach**

In this approach, the packets do not carry the actual code or program. Instead, the packet carries some identifiers or references to functions reside in the active nodes. The packet, nevertheless, is considered active in a sense that they decide which functions are going to be executed on their data, and they provide the parameters for these functions (Jean-Patrick G. 2003).

Service ID.	DATA

Fig. (3): Active Node Approach Representation

❖ **Hybrid Approach**

Active packets can carry code efficiently only when the code is relatively simple and restricted. On the other hand, active nodes can efficiently provide any code given that the code is predefined. In the hybrid architecture, active packets carry actual code and other more complex code resides in active nodes. Hybrid architecture makes possible to use more complex programs and be flexible enough to program command or parameters in data packets (Eva H. 2001).

SECURITY ISSUES IN ACTIVE NETWORKS

To provide security in the active network, we need two basic services: authentication and authorization.

Authentication is the core of many current security mechanisms, it encompasses the technologies used to identify and verify the authenticity of users, network components and processes. This ranges from simple password based schemes through to biometric and cryptographic mechanisms. The ultimate goal is to uniquely associate an entity external to a system with an identity stored inside the system. In most systems, this is done by requesting some identifying information from a client, for example a password, biometric reading or response to some challenge. This information is then verified against information held inside the system. When the identifier and stored information are match, the user is authenticated; otherwise the user is denied (Ravi S. 1996). **Figure 4** provides a graphical overview of the authentication method.
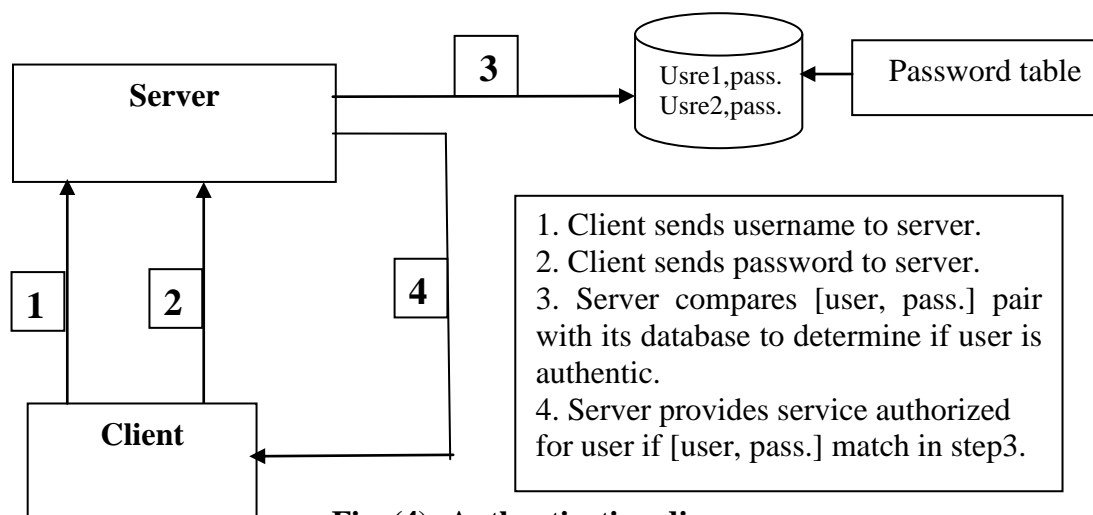

Fig. (4): Authentication diagram

In an active network, authorization to perform some requested access or action would be the overwhelming security concern. The authorization may take the form of control of access to objects or functionality, control of exposure of data, or control of resource usage. Authentication and authorization are somewhat tightly-coupled mechanisms; authorization systems depend on secure authentication systems to ensure that users are who they claim to be and thus prevent unauthorized users from gaining access to secured resources (Laat 2000).

The proposed system depends on (authentication and authorization) and used RSA (encryption-decryption) algorithm to add additional level of security.

PROPOSAL SYSTEM

The proposed system was built using the hardware architectures that show in **Fig. 5**.

Fig. (5): Hardware architecture
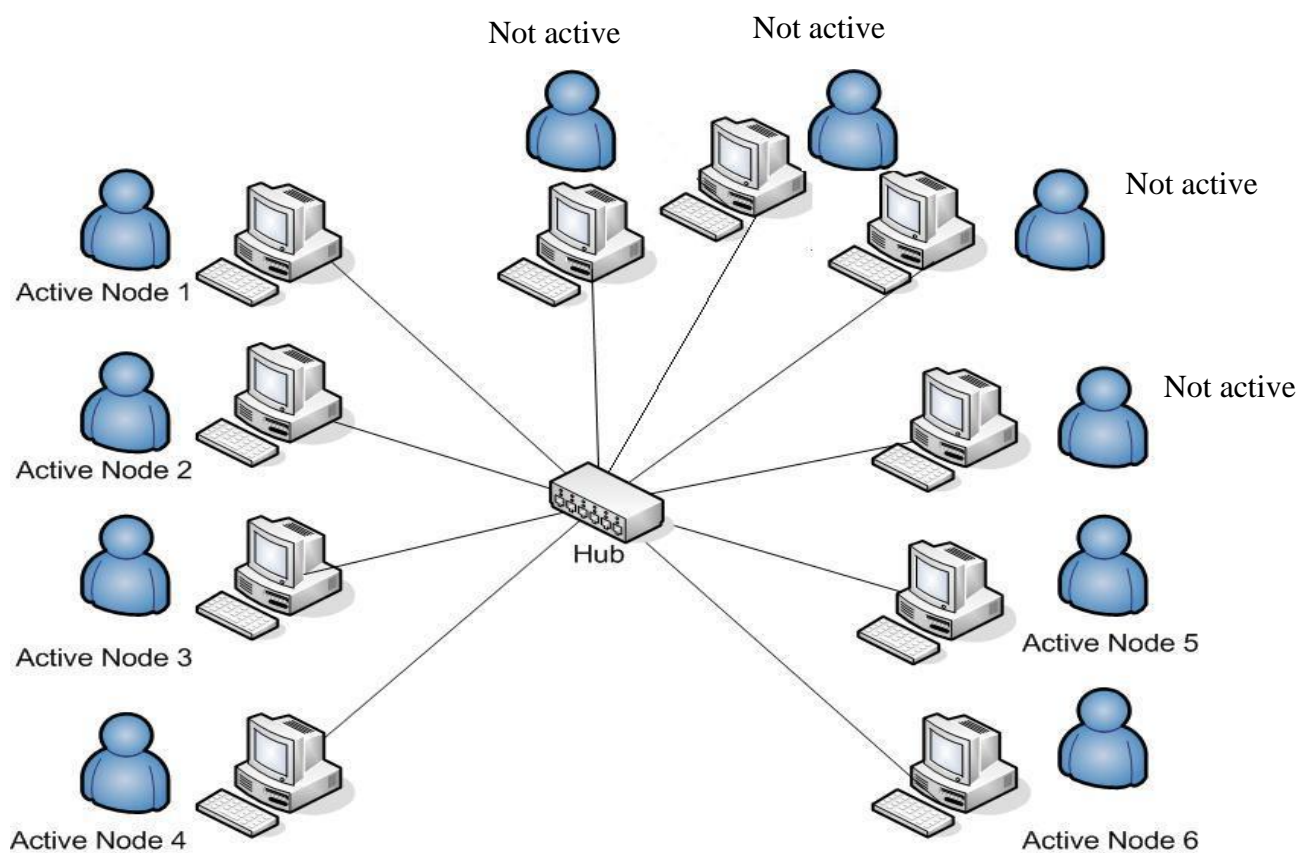
THE DESIGN PROCESS

The proposed system contains two parts, the first part is security and the second part is active network part, installed in active PC for the purpose of security by examining the received packet from inside and outside.

The proposed program installed on PCs waiting to be active (in the work the number of active PCs is 6), the active node is the PC that

- Have a program permits to make the packet passing inside it.

- The ability to make secure execution on packet.

- The authentication and authorization role are defined inside it.

- The encryption and decryption algorithm done inside it.

- When active node is busy it will search for another active node which is Idle to continue processing.

Note that all IP (Internet Protocol) addresses of active nodes are defined in packet and the active node will be busy when there is fault in PC or normal termination. The proposed system was written in Microsoft Visual Basic version 6 and uses window manner in its work. As well as it uses the database to store the information like username, password, job, and the information about authorization. And it has API (Application Program Interface) tools (An API is simply a set of functions that can be used to work with a component, application, or operating system), these functions that can be called from any application running in Windows. At run time, a function is dynamically linked into the application that calls it.

❖ **Security Part**

This part is used for securing the active node. It will exam the received packet from inside and from outside. This part is relay on the concepts authentication, authorization and encryption.

Now the first case depends on authentication and authorization rule, the authentication rule is as follows:

- o Username

- o Password

- o Job

- o E-mail

If the username and password is entered three times incorrect then the Program terminates.

The authorization rule is as follows:

- o Permit the user to use the active PC

- o Permit the user to present the result

- o Permit the user to use the active PC and present the result

The information about authentication and authorization is verified against information reside inside the system, the packet is authenticated if the identifier and stored information is match, otherwise the packet is denied. Incase of authenticated packet, active node will make a secure execution on it. When packet move from one active node to another, during processing, it carry's information about each node it visit.

Second case, this part also depends on encryption by using RSA algorithm to increase the security. The RSA algorithm is explained as follows:

1. Generate two random prime numbers p and q.
2. Multiply p and q together to generate N.
3. Choose another number e which must be relatively prime to (p-1) (q-1).
4. Calculate the value of ciphertext as $C=M^e$ (mod N).
5. Find d such that: e*d=1 (mod (p-1) (q-1)).
6. Calculate the value of plaintext message as $M= C^d$ (mod N).

Where

M: plaintext message.
C: ciphertext message.
Public key: (e, N).
Private key: (d, N).
Now if we choose p=11, q=3 then
N=33.
(p-1) (q-1) =20.
Let Z= (p-1) (q-1).
Suitable value for e =3, since 3 and 20 have no common factors.
With these choices, d can be found by solving the equation:
3d=1 (mod 20).
Which yield d = 7.
The ciphertext, C, for a plaintext message, M, is given by
$C=M^3$ (mod 33).
The ciphertext is decrypted by the receiver by making use of rule:
$M=C^7$ (mod 33).

❖ **Active Network Part**

   This part is divided into two subparts, client part and server part. After the active node receives the packet, the server part will begin working on it, in case of transmitting the packet to another active node to continue the processing, the server should changed to the client part and the server part of the new active node will receive the packet and work on it.
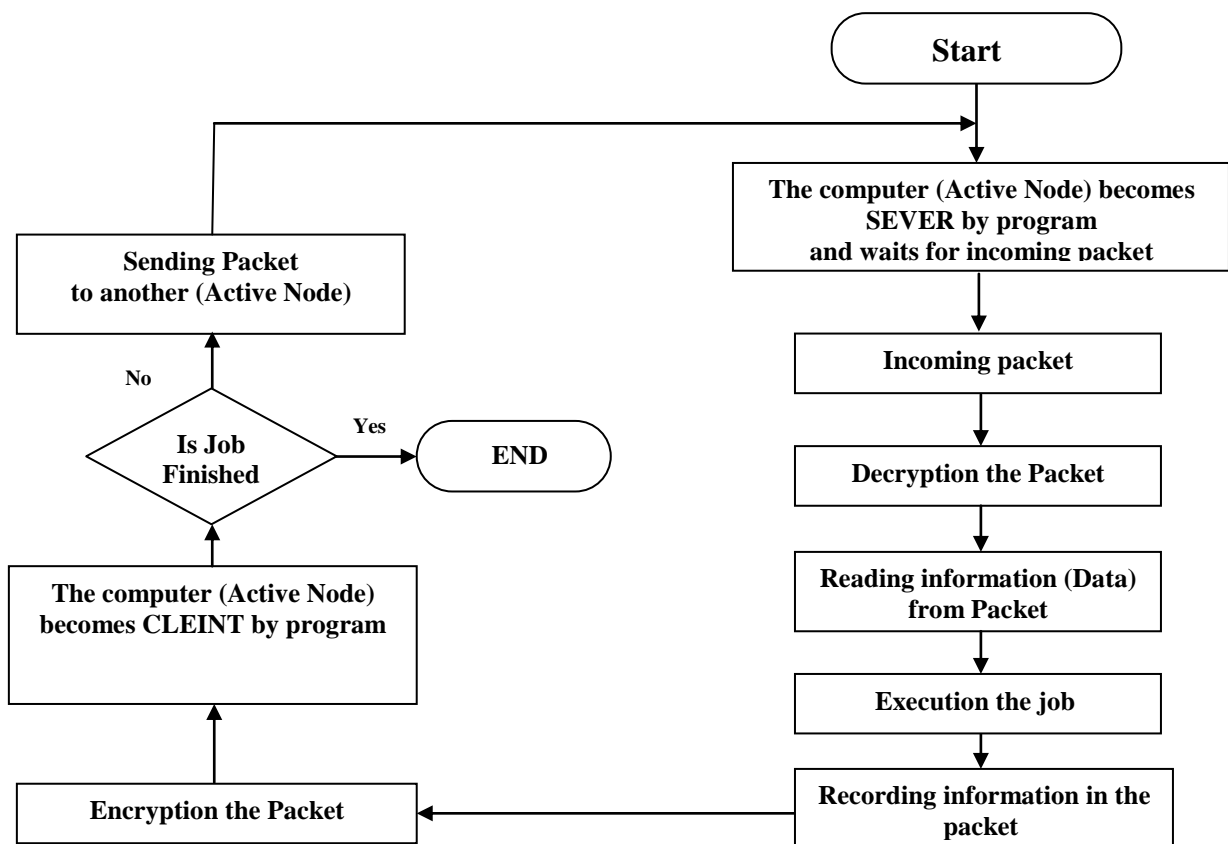
Fig. (6) : The lifecycle of Packet in active node
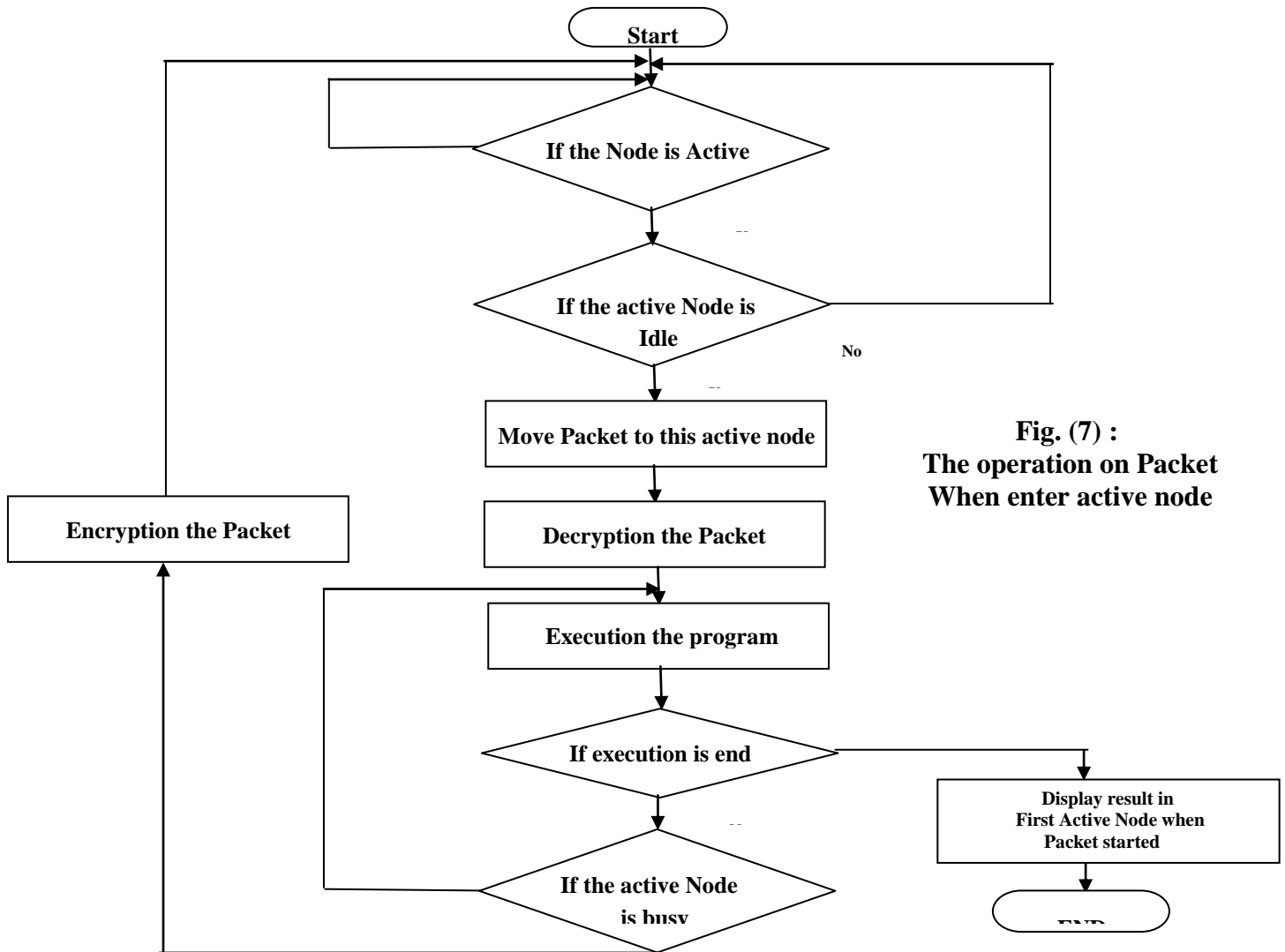
Fig. (7) :
The operation on Packet
When enter active node

* THE SOFTWARE PROCESS

The Program is performed as follows:-

Step 1:- initially install the program in computer 1.

Step 2:- the program ask about username and password.

Step 3:- input IP address for all active nodes.

Step 4:- input information and suitability for users that use active nodes.

Step 5:- then install the program on all PC's we want them to be active.

Step 6:- input the job, for our example (Loop count) as shown in **Fig. 8**.
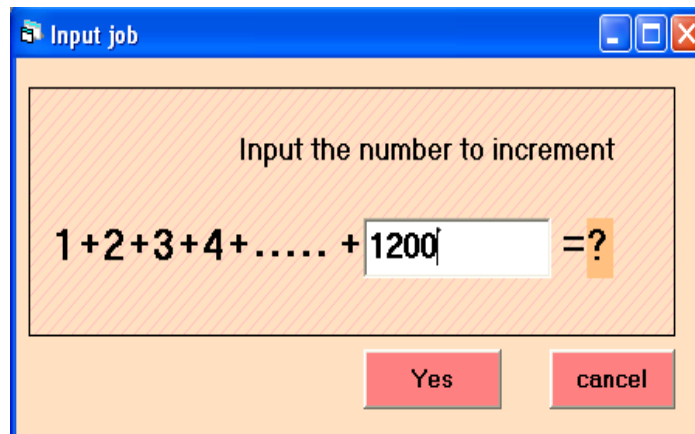
Fig. (8) Input of the job

Step 7:- run the job by entering the number we want the loop counts.

Step 8:- after 125 second, making active node 1 busy (by entering a CD in to the CD Drive which has the priority), the packet size become 15.360 and the packet travel to active node 2 and so on till the job is finish. An example is shown in **Table 2**. The active packet travels between the active nodes arbitrary by making the other nodes busy.

THE FINAL RESULT

It is clearly shown that each active node continue doing the Job as shown in **Table 1** until we make it busy (by entering a CD in to the CD Drive) and then other active node will take the Job and continue it and so on. The size of the packet increased each time the active node changed until the Job finished as shown in **Table 1**. The relationship between the time and the packet size are shown in **Fig. 9**.

Table 1: Time and size of packet lifecycle for all active nodes

Computer Name	Time lifecycle Packet in seconds	Size of Packet in KB
Computer 1	125	15.360
Computer 2	134	15.872
Computer 3	90	16.384
Computer 6	153	16.896
Computer 3	112	17.408
Computer 2	234	17.920
Computer 5	120	18.432
Computer 1	32	18.944
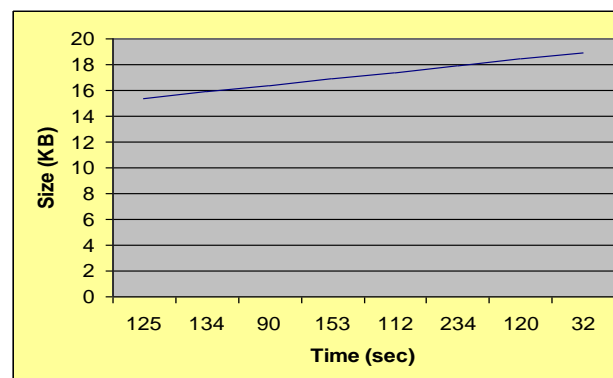
Fig. (9): The relationship between time and packet size

Table 2:

Example for the lifecycle Packet in Active Network for all Active Nodes is to travel.

	1	2	3	4	5	6	7	8
Username:	Ahmed	Wisam	Sara	Sama	Sara	Wisam	Ali	Ahmed
Computer Name:	computer 1	computer 2	computer 3	computer 6	computer 3	computer 2	computer 5	computer 1
Screen Resolution:	1024 x 768	1024 x 768	1024 x 768	1024 x 768	1024 x 768	1024 x 768	1024 x 768	1024 x 768
Windows Running time:	125 seconds.	134 seconds.	90 seconds.	153 seconds.	112 seconds.	234 seconds.	120 seconds.	32 seconds.
Program Location:	C:\both\C1	C:\both\C1	C:\both\C1	C:\both\C1	C:\both\C1	C:\both\C1	C:\both\C1	C:\both\C1
Sound Enabled:	Yes	Yes	Yes	Yes	Yes	Yes	Yes	Yes
Screensaver Enabled:	Yes	Yes	Yes	Yes	Yes	Yes	Yes	Yes
OS Platform:	Windows XP	Windows XP	Windows XP	Windows XP	Windows XP	Windows XP	Windows XP	Windows XP
OS Version:	5.01	5.01	5.01	5.01	5.01	5.01	5.01	5.01
Local IP:	187.178.128.21	187.178.128.22	187.178.128.23	187.178.128.26	187.178.128.23	187.178.128.22	187.178.128.25	187.178.128.21
Communicating with a device:	Yes	Yes	Yes	Yes	Yes	Yes	Yes	Yes
Current Power Supply:	AC Adaptor	AC Adaptor	AC Adaptor	AC Adaptor	AC Adaptor	AC Adaptor	AC Adaptor	AC Adaptor
Battery status	No Battery	No Battery	No Battery	No Battery	No Battery	No Battery	No Battery	No Battery

CONCLUSIONS

- From the results obtained from the test of the proposed system we can conclude:-

- Systems flexibility is very high, since the system can perform a variety of tasks and remain efficient.

- The security power of proposed system comes from different security tools (Authentication, Authorization and RSA algorithm), which reduce the possibility of hacking the information since the attacker has to defeat all those tools.

- The performance of proposed system is good because the throughput is displayed in the first active PC when packet started, and carries information of each node it visits.

- Cost in

   - Time (because more time spend on the cryptographic operation).

   - Packet overhead.

- The weakness of using password, which can be stolen, accidentally revealed or forgotten.

REFERENCES

- Bhattacharjee S., "Active Networks: Architectures, Composition and Applications", a PhD Thesis, Georgia Institute of Technology, 1999.

- Calvert K. L., "Architecture Framework for Active Networks", a PhD Thesis, Georgia Institute of Technology, 1999.

- Eva H., and Ludek K.,"Active networks and high speed content delivery", Proceedings of the The 7th International Conference of European University Information Systems on The Changing Universities - The Role of Technology, Vol. 13, PP. 448-456, 2001.

- Gert D. L., and Gert S., "Network Security Fundamentals", Cisco System, Inc. published by: Cisco press, 2005.
- **http:// www.ciscopress.com/bookstore/product.asp?isbn=1587051672**

- Jean-Patrick G., "Towards the design of an active network architecture supporting throughputs of gigabit networks", a PhD Thesis, University of Tennessee, December 2003.

- Laat C. de, Gross G., Gommans L., Vollbrecht J., and Spence D., "Generic AAA Architecture", IETF Network Working Group, Internet experimental RFC 2903, August 2000.

- **http://tools.ietf.org/html/rfc2903**

- Ravi S. and Pierangela S., "Authentication, Access Control, and Audit", ACM Computing Surveys, Vol. 28, No. 1, March 1996.

- Psounis K., "Active Networks: Applications, Security, Safety and Architectures", IEEE Communications Surveys and Tutorials, Vol. 2, No. 1, PP. 2-16, First Quarter 1999.

- Tennenhouse D. L., Sincoskie W. D., and Wetherall D. J., "A Survey of Active Network Research", IEEE Communication Magazine, Vol. 35, No. 1, PP. 80-86, January 1997.

- Tennenhouse D. L., and Wetherall D. J., "Towards an Active Network Architecture", DARPA Active Networks Conference and Exposition, San Francisco, CA, USA. IEEE Computer Society 2002, PP. 29-31 , May 2002.

- Wetherall D. J., "Active network vision and reality: lessons from a capsule-based system", 17th ACM Symposium on Operating Systems Principles (SOSP '99) Published as Operating Systems Review Vol. 34, No. 5, PP. 64–79, Dec. 1999 .

DETECTION OF STATIC AIR-GAP ECCENTRICITY IN THREE PHASE INDUCTION MOTOR BY USING ARTIFICIAL NEURAL NETWORK (ANN)

Prof. Dr. Qais S. Al-Sabbagh
Elect. Departement
University of Baghdad

Hayder E. Alwan

University of Baghdad

الخلاصة

تم استخدام تقنية هذا البحث يوضح تاثير اللامركزية الساكنة في الفجوة الهوائية على أداء محرك حثي ثلاثي الاطوار الشبكة العصبية الاصطناعية لكشف هذا العطل ،ان هذه التقنية تعتمد على سعة التوافقيات السالبة والموجبة للترددات. في هذا البحث تم استخدام محركين اثنين وبقدرة (2.2 كيلو واط) لتحقيق العطل بصورة حقيقية وللحصول على البيانات المطلوبة ولثلاث اختبارات (اللاحمل، نصف الحمل والحمل الكامل). تم اعتماد بصمة التيار الساكن لغرض التحليل والكشف عن وجود اللامركزية. تم اعتمادالشبكة العصبية ذات التغذية الامامية وتصحيح الاخطاء بطريقة الارجاع العكسي ، أن سعة التوافقيات السالبة والموجبة للترددات تم اعتمادها لتكون بيانات ادخال لتدريب الشبكة الاصطناعية لغرض الكشف والتمييز بين المحرك العاطل والمحرك الخالي من العطل.

ABSTRACT

This paper presents the effect of the static air-gap eccentricity on the performance of a three phase induction motor .The Artificial Neural Network (ANN) approach has been used to detect this fault .This technique depends upon the amplitude of the positive and negative harmonics of the frequency. Two motors of (2.2 kW) have been used to achieve the actual fault and desirable data at no-load, half-load and full-load conditions. Motor Current Signature analysis (MCSA) based on stator current has been used to detect eccentricity fault. Feed forward neural network and error back propagation training algorithms are used to perform the motor fault detection. The inputs of artificial neural network are the amplitudes of the positive and negative harmonics and the speed, and the output is the type of fault. The training of neural network is achieved by data through the experiments test on healthy and faulty motor and the diagnostic system can discriminate between "healthy" and "faulty" machine.

Index Terms: Static Eccentricity, Three Phase Induction Motor, Artificial Neural Network

INTRODUCTION

Rotating electrical machines play a very important role in the world's industrial life. In petrochemical and power utilities, the failure of electrical motors and generators causes a high cost. This is due to the loss of production, high emergency maintenance costs and lost revenues. Industry's response towards this problem of unexpected interruptions of work is by using "catch it before it fails" approach. The oldest technique for preventive maintenance was tearing the electrical machine down and then looking at it closely. However, taking the motor out of service is costly and time consuming. This is why today's modern industry management is more interested than ever before in adopting new condition monitoring techniques, on-line or off-line, to assess and evaluate the rotating electrical machine's performance condition[1].

The major faults of electrical machines can broadly be classified by the following [1]:
a) Stator faults resulting in the opening or shorting of one coil or more of a stator phase winding.
b) Abnormal connection of the stator windings.
c) Broken rotor bar or cracked rotor end-rings.
d) Static and /or dynamic air-gap irregularities.
e) Bent shaft (akin to dynamic eccentricity) which can result in a rub between the rotor and stator, causing serious damage to stator core and windings.
f) Bearing and gearbox failures.

The eccentricity fault and it's diagnostic techniques will be discussed briefly in this paper.

The diagnostic methods to identify the above faults may involve several types of fields of science and technology. They were described in references [1, 2] as listed below:

a) Electromagnetic field monitoring, search coils, coils wound a round motor shafts (axial flux related detection).

b) Temperature measurements.
c) Infrared recognition.
d) Radio Frequency (RF) emissions monitoring.
e) Noise and vibration monitoring.
f) Acoustic noise measurements.
g) Motor current signature analysis (MCSA).
h) Model, artificial intelligence and neural network based techniques.

There are different research works in the field of induction machine fault diagnosis include electrical, mechanical, and magnetic techniques. These techniques can be regarded as basis for developing on-line and/or off-line rotating electrical machine condition monitoring systems. Electrical and magnetic techniques include magnetic flux measurement, stator current analysis, rotor current analysis، partial discharges for evaluating stator insulation strength for high voltage motors, shaft-induced voltages, etc. Mechanical techniques include the machine bearing vibration-monitoring systems, speed fluctuation analysis of induction machines and bearing temperature measurement. MCSA for incipient fault detection has

received much attention in recent years. For most purposes current monitoring can be implemented inexpensively on any size machine [2].

R.R. Schoen et al. [3] have proposed new method for induction motor fault detection by built on line system utilizes artificial neural networks to learn the spectral characteristics of a good motor operating on line.

M. S. Arefeen et al. [4] presented a similar paper on the analysis of air-gap flux, current and vibration signals as a function of both static and dynamic air-gap eccentricity in 3-phase induction motors. They used the same approach, the air-gap permeance approach, as in [2] for calculating the flux density and unbalanced magnetic forces caused by eccentricity; except that they suggested that the dynamic and static eccentricity should both be considered simultaneously and a new theoretical analysis was presented. Also, it was suggested that in addition to monitoring the line current signature, the vibration analysis should be put forward to identify which particular form of eccentricity is dominant.

X. Huang et al. [5] propose a scheme to monitor voltage and current space vectors simultaneously in order to monitor the level of air-gap eccentricity in an induction motor. An artificial neural network is used to learn the complicated relationship and estimate corresponding signature amplitudes over a wide range of operation conditions.

F. Filippetti et al.[6] presented an induction machine rotor fault diagnosis based on a neural network approach, after the neural network was trained using data achieved through experimental tests on healthy machines and through simulation in case of faulted machines, the diagnostic system was found able to distinguish between "healthy "and "faulty "machines.

H. A. Toliyat et al. [7] have also proposed the detection of air-gap eccentricity in induction machines by measuring the harmonic content in the machine line currents. However, they proposed a new way for modeling the machine under eccentricity. The winding function approach accounting for all the space harmonics in the machine was used to calculate all the mutual and magnetizing inductance's for the induction machine with eccentric rotors between "healthy" and "faulty" machines.

- Eccentricity Related Faults

Machine eccentricity is the condition of unequal air-gap that exists between the stator and rotor [1,7]. When eccentricity becomes large, the resulting unbalanced radial forces also known as Unbalanced Magnetic Pull (UMP) can cause stator to rotor rub, and this can result in the damage of the stator and rotor. There are two types of air-gap eccentricity: the static air-gap eccentricity and the dynamic air gap eccentricity as shown in Fig. (1). In the case of the static air-gap eccentricity, the position of the minimal radial air-gap length is fixed in space. Static eccentricity may be caused by the ovality of the stator core or by the incorrect positioning of the rotor or stator at the commissioning stage. If the rotor-shaft assembly is sufficiently stiff, the level of static eccentricity does not change. In case of dynamic eccentricity, the center of the rotor is not at the center of the rotation and the position of minimum air-gap rotates with the rotor. This misalignment may be caused due to several factors such as a bent rotor shaft, bearing wear or misalignment, mechanical resonance at critical speed, etc.
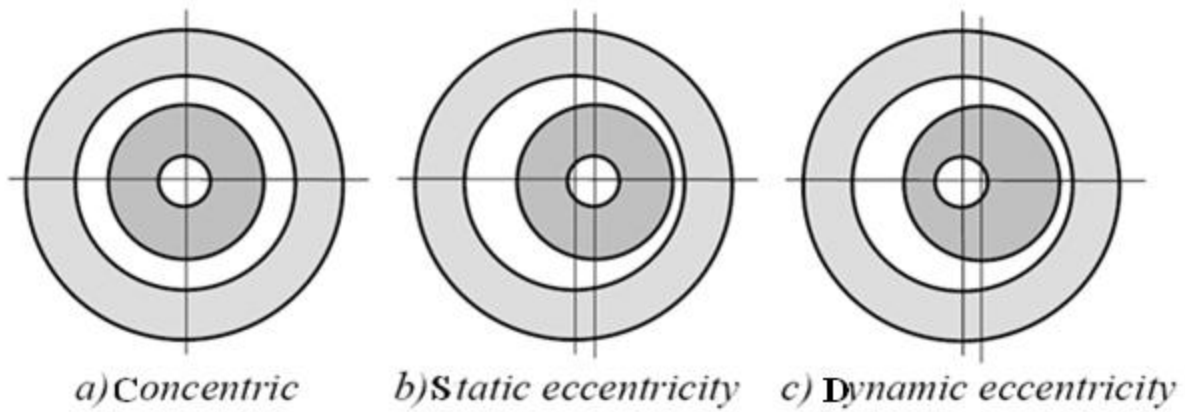
Fig. (1) Eccentricity types

In reality both static and dynamic eccentricities tend to co-exist. An inherent level of static eccentricity exists even in newly manufactured machines due to manufacturing and assembly method, as has been reported by Dorrell [8]. This causes a steady unbalanced magnetic pull (UMP) in one direction. With usage, this may lead to bent rotor shaft, bearing wear and tear etc. This might result in some degree of dynamic eccentricity. Unless detected early, these effects may snowball into stator to rotor hub causing a major breakdown of the machine [9]. The presence of static and dynamic eccentricity can be detected using MCSA.   The equation describing the frequency components of interest [1]

$$f_{ecc}= f[(k_1 R \pm n_d)(1\text{-}s)/p \pm v] \tag{1}$$

where $n_d=0$ in case of static eccentricity, and $n_d=1,2,3,\dots$ in case of dynamic eccentricity (n_d is known as eccentricity order), f is the fundamental supply frequency, R is the number of rotor slots, s is the slip, p is the number of pole pairs, k_1 is any integer, and v is the order of the stator time harmonics that are present in the power supply driving the motor. ($v=\pm1,\pm3,\pm5\dots$). In case one of these harmonics is a multiple of three, it may not exist theoretically in the line current of a balanced three phase machine. However it has been shown by Nandi [10] that only a particular combination of machine poles and rotor slot number will give rise to significant only static or only dynamic eccentricity related components. However, if both static and dynamic eccentricities exist together, low frequency components near the fundamental is [11],

$$f_1=|f \pm k_1 f_r |, \text{ where } k1 =1, 2, 3 \;\dots \tag{2}$$

can also be detected. Mixed eccentricity also gives rise to high frequency components as described by equation (1). Modeling based approaches to detect eccentricity related components in line current have been described in [11]. The simulation results obtained through the models are also well supported by permeance analysis and experimental results. Vibration signals can also be monitored to detect eccentricity-related faults. The high frequency vibration components for static or dynamic eccentricity are given by [7] using an equation similar to (1) (only the values of n_d and v are different).

THE EXPERIMENTAL SET-UP

The block diagram of the experimental set-up is shown in Fig. (2), motor specifications are shown in the Appendix, a dc generator of (3kW) rating has been used as a load for the induction motor.

The inputs to the data acquisition are from one of the motor lines as a current and from
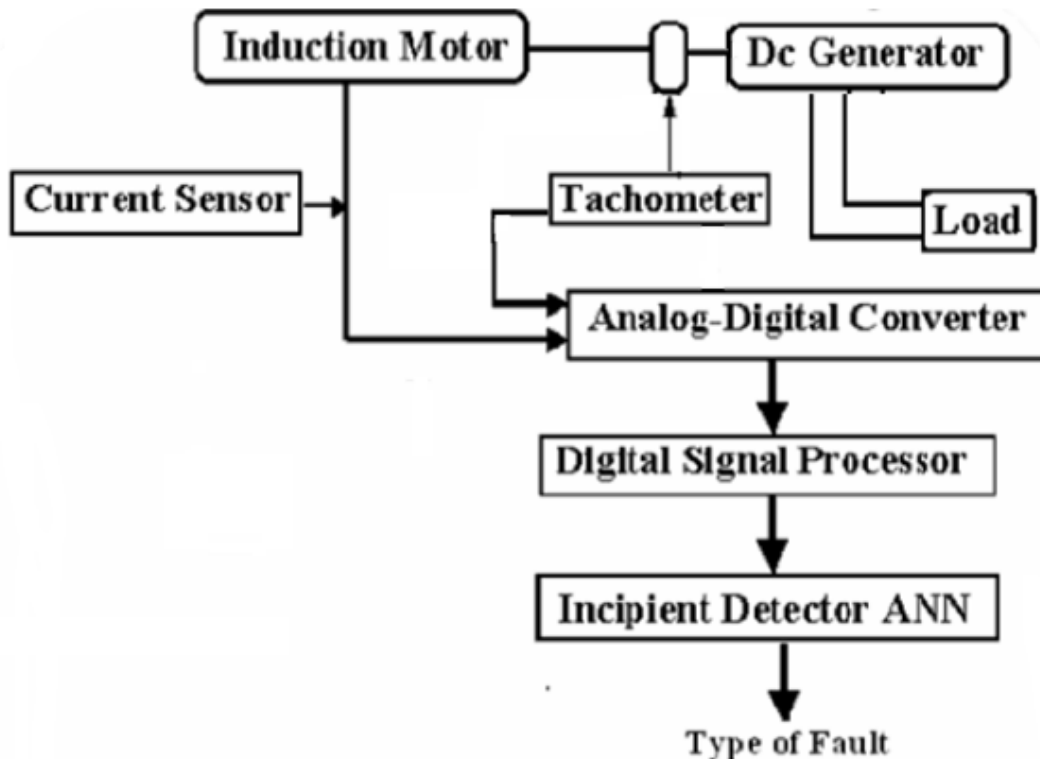
```
┌─────────────────┐                    ┌────────────────┐
│ Induction Motor │────────[  ]────────│ Dc Generator   │
└─────────────────┘           │        └────────────────┘
                              │              │      │
┌────────────────┐     ┌─────────────┐       │   ┌────────┐
│ Current Sensor │────→│ Tachometer  │       │   │ Load   │
└────────────────┘     └─────────────┘       │   └────────┘
                              │
                    ┌─────────────────────────────┐
                    │ Analog-Digital Converter     │
                    └─────────────────────────────┘
                                  │
                    ┌─────────────────────────────┐
                    │ Digital Signal Processor     │
                    └─────────────────────────────┘
                                  │
                    ┌─────────────────────────────┐
                    │ Incipient Detector ANN       │
                    └─────────────────────────────┘
                                  │
                            Type of Fault
```

Fig.(2) The Experiment Set for Fault Detection of Induction Motor

the tachometer as a speed; these two inputs signals are converted to voltage signals before using A/D converter. The data of the current and the speed given to the data acquisition circuit the line current measured by using current transformer ratio (10/4) A passing through a resistance of 1Ω which given 4 volt to the data acquisition circuit, then the line current will convert to the frequency domain by using the Fast Fourier in Matlab program package to abtain the sampling frequency and sampling time of the waveform. The speed of the motor measured by using the tachometer will be converted to the voltage value, it's found that the tachometer used in the laboratory give 0.06 volt for each rotation, then by using Equ. 1 to calculate the positive and the negative harmonics frequencies and their amplitudes will be illustrated in the tables, these amplitudes will used to train the neural network to give the incipient detection of the fault.

-EXPERIMENTAL RESULTS

The experiments included three tests (no-load, half load and full load) on both the healthy motor and the motor with eccentricity fault.

Healthy Motor Tests

The line current waveform and the Fast Fourier Transform (FFT) for no-load, half-load and full-load of healthy motor are studied in three different tests these are:

A- No-Load Test

This test involves operating the system at no-load , the values of current , speed and slip were 3.5A, 2950 rpm and 0.0166 respectively. The current waveform and it's FFT are shown in Fig. (3).
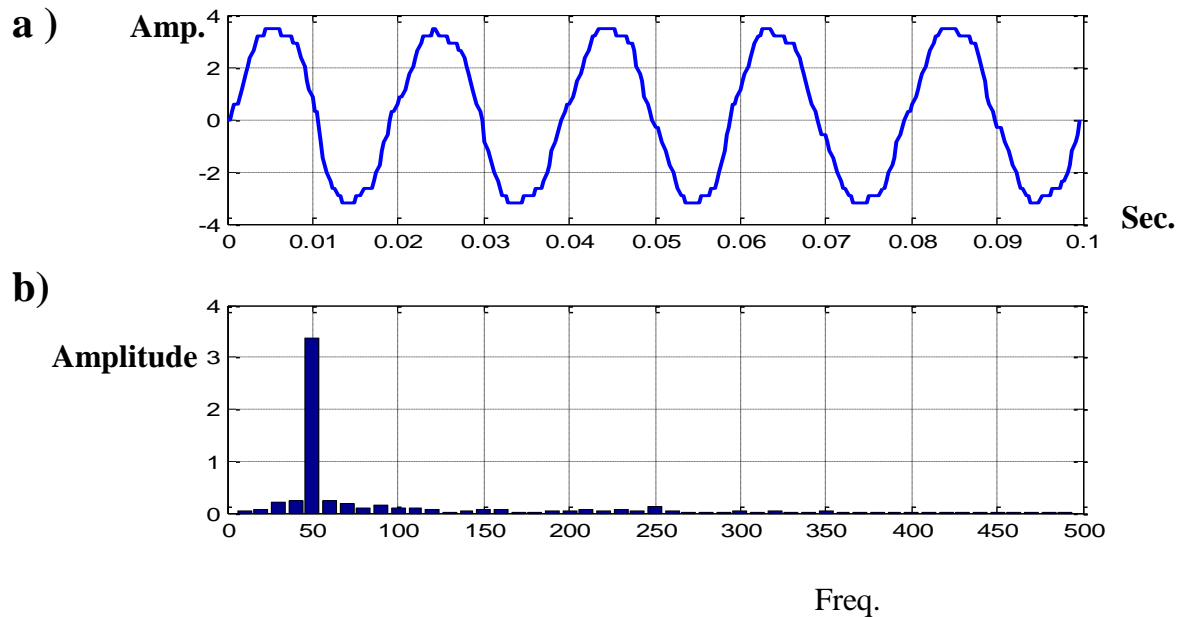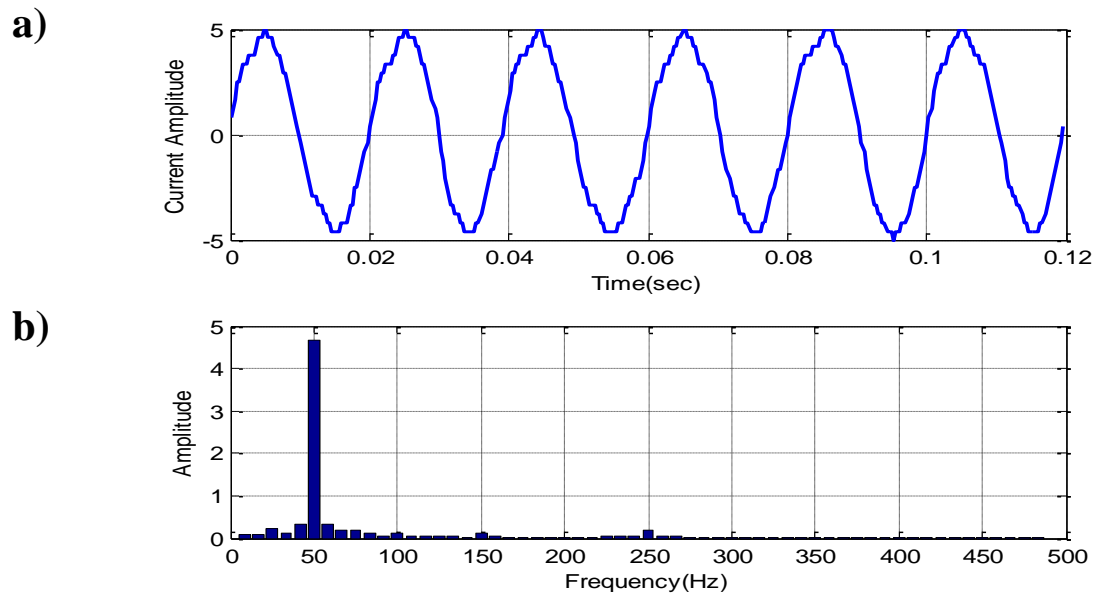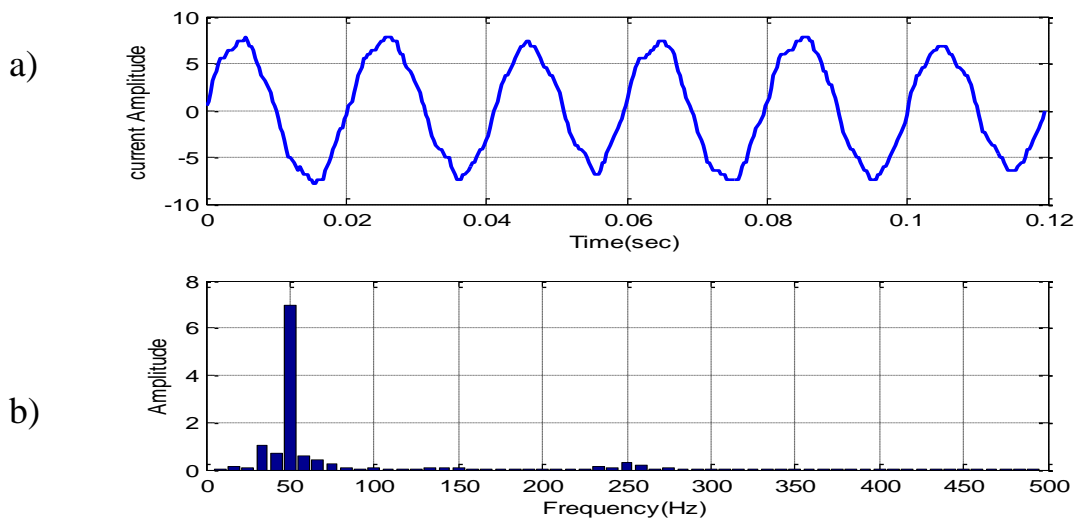

Fig. (3) Current waveform in healthy motor at no-load

a) Line current waveform   **b) Corresponding FFT**

B- Half -Load Test

This test involves operating the system at half-load, the values of current, speed, and slip are 5A, 2900 rpm and 0.033 respectively. The current waveform and it's FFT are shown in Fig. (4).

a)

b)

Fig. (4) Current waveform in healthy motor at half-load

a) Line current waveform   b) Corresponding FFT

C- Full -Load Test

This test involves operating the system at full-load , the value of current , speed and slip were 8.5A, 2850 and 0.05 respectively . The current waveform and it's FFT are shown in Fig. (5).

a)

b)

Fig. (5) Current waveform in healthy motor at half-load

a) Line current waveform   b) Corresponding FFT

Eccentricity Related Faults Test

The second experiment was eccentricity fault as mentioned before. There are two types of eccentricity dynamic and static. In this experiment the static eccentricity was tested on motor at which the centre of rotor was not at the centre of stator as shown in Fig.(6).The stator line current and it's Harmonic analyses were performed on the acquired data for three cases .Equ.1 is used to calculate side bands frequencies for three cases. All cases for n_d =0 and R=20.
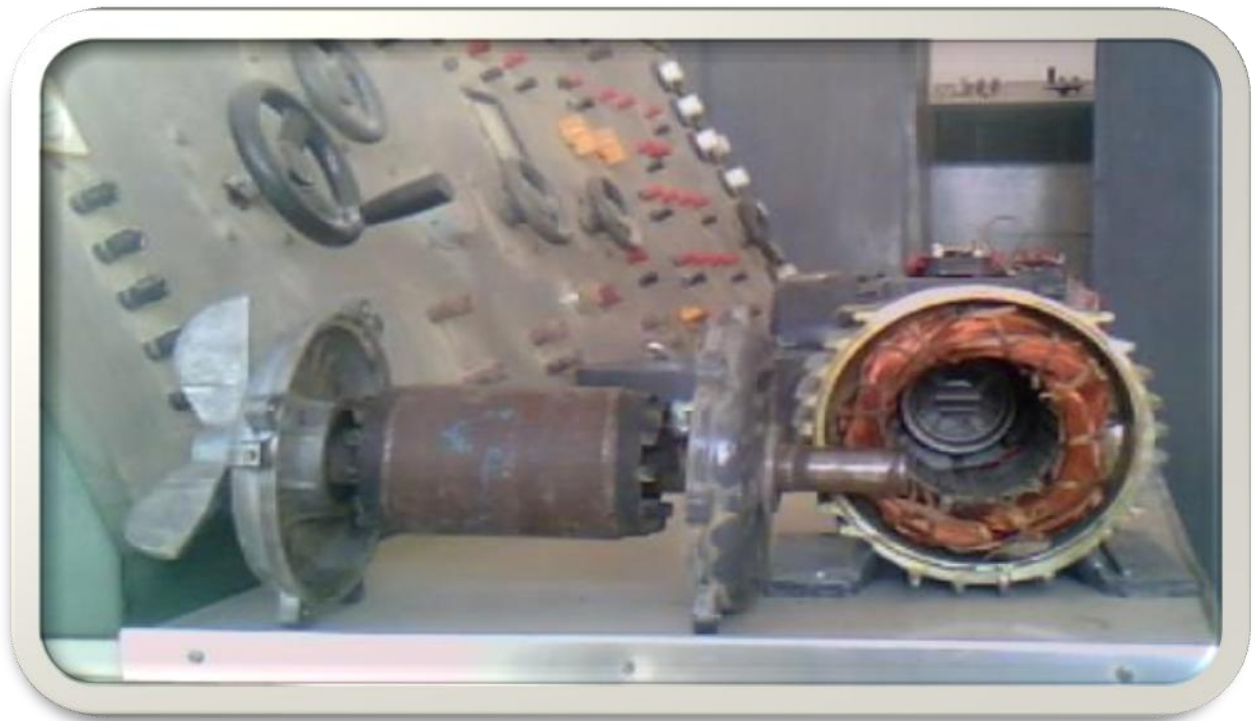
Fig. (6) Side view of rotor eccentricity motor

A- No-Load Test

This test involves operating the system at no-load ,the values of current , speed and the slip are 3.5A , 2810 rpm and 0.063 respectively. The current waveform and it's FFT are shown in Fig. (7).

a)

b)
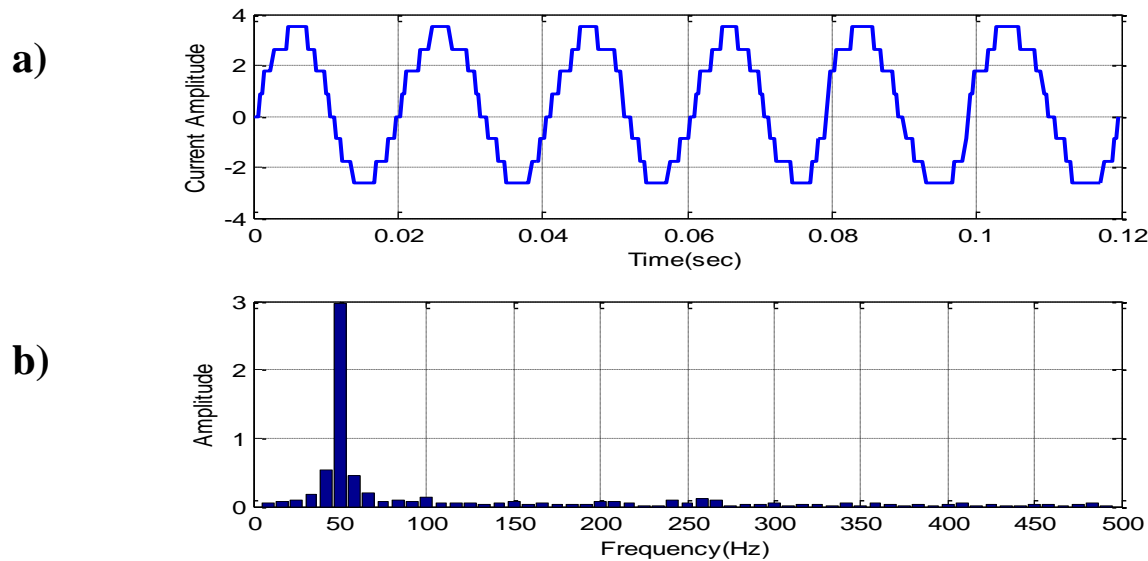
Fig. (7) Current waveform of eccentricity fault at no-load

a) Line current   **b) FFT**

Table 1 Illustrates the positive, negative harmonics and their amplitudes for different values of harmonics (v) at no-load, the data of the motor is:

Input Frequency   Motor Speed   Slip (s)   50Hz
2810 rpm   0.063

Equation (1) is used to calculate the positive and the negative harmonics and their amplitudes which are given in Table (1).

Table 1 Positive, negative harmonics at no-load (Eccentricity Fault)

v	Pos. Harmonic(Hz)	Amplitude(A)	Neg. Harmonic(Hz)	Amplitude(A)
1	987	0.03	887	0.0168
3	1087	0.0063	787	0.0129
5	1187	0.022	687	0.05
7	1287	0.02	587	0.029
9	1387	0.0177	487	0.019
11	1487	0.0387	387	0.0124
13	1587	0.024	287	0.018
15	1687	0.0234	187	0.04
17	1787	0.0167	87	0.115
19	1887	0.0166	0	0

B-Half-Load Test

This test involves operating the system at half-load, the values of current, speed and the slip are 5A, 2790 rpm and 0.07 respectively. The current waveform and it's FFT is shown in Fig. (8)
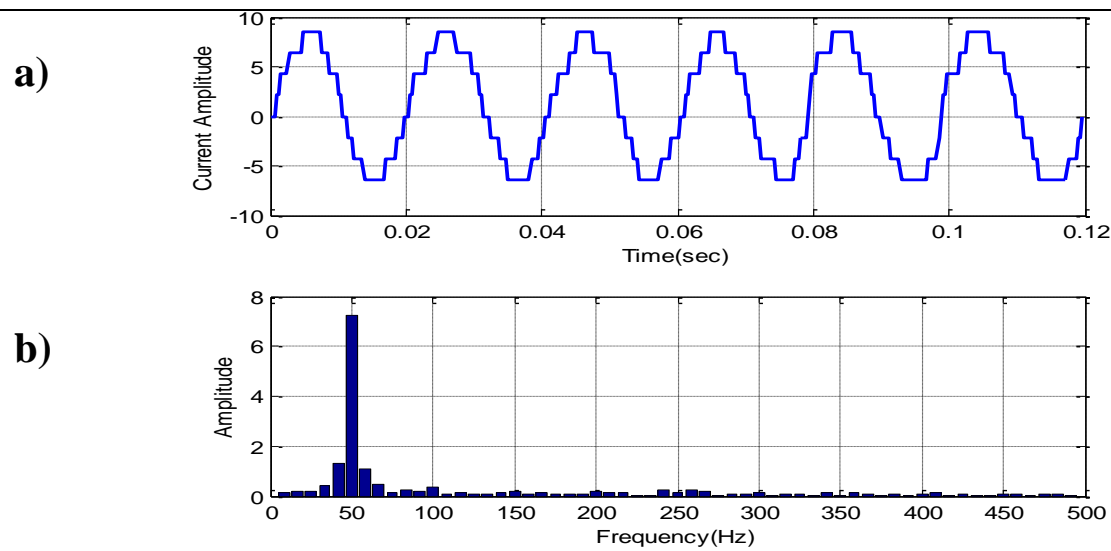
a)

b)
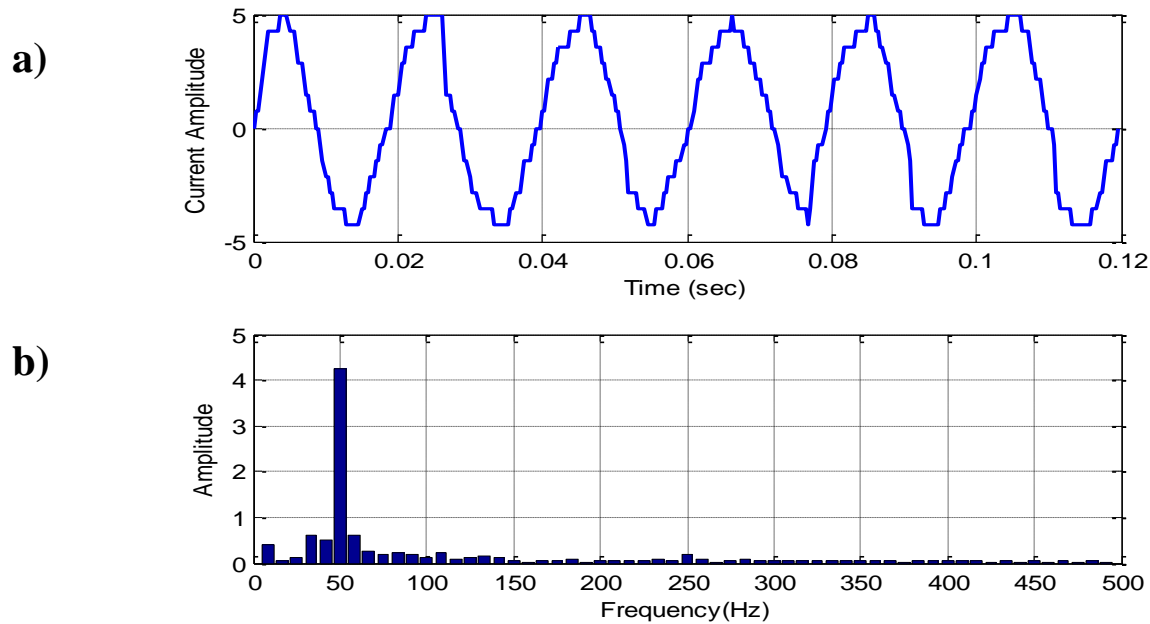
Fig(8) Current waveform of stator eccentricity fault at half-load

a) Line current waveform   b) Corresponding FFT

Table 2 illustrates the positive, negative harmonics sequence and their amplitudes for different values of **v** at half-load, the data of the motor is:

Input Frequency	Motor Speed	Slip (s)
50Hz	2790 rpm	0.07

Table 2 Positive, negative harmonics at half –load (Eccentricity Fault)

v	Pos. Harmonic(Hz)	Amplitude(A)	Neg. Harmonic(Hz)	Amplitude(A)
1	980	0.023	880	0.063
3	1080	0.0597	780	0.06
5	1180	0.047	680	0.0513
7	1280	0.0156	580	0.043
9	1380	0.01	480	0.034
11	1480	0.026	380	0.0332
13	1580	0.01	280	0.051
15	1680	0.045	180	0.089
17	1780	0.0568	80	0.364
19	1880	0.026	0	0

C-Full-Load Test

This test involves operating the system at full-load, the values of current, speed and the slip are 8.5A, 2720 rpm and 0.093 respectively. The current waveform and it's FFT is shown in Fig. (9).

Fig. (9) Current waveform of eccentricity fault at full-load

a) Line current waveform   b) FFT

Table 3 Illustrates the positive, negative harmonics sequence and their amplitudes for different values of v at full-load, the data of the motor is:

Input Frequency   Motor Speed   Slip (s)   50Hz
2720 rpm   0.093

Table 3 Positive, negative harmonics full-load (Eccentricity Fault)

v	Pos. Harmonic(Hz)	Amplitude(A)	Neg. Harmonic(Hz)	Amplitude(A)
1	957	0.0438	857	0.0323
3	1057	0.0445	757	0.027
5	1157	0.046	657	0.0334
7	1257	0.0319	557	0.082
9	1357	0.0466	457	0.0208
11	1457	0.022	357	0.066
13	1557	0.0115	257	0.157
15	1657	0.0155	157	0.086
17	1757	0.0131	57	0.673
19	1857	0.0212	0	0

*** Training of ANN for Faults Identification**

The current and speed signals acquire from a three-phase 2.2kW squirrel-cage induction motor. A software program was written using Matlab program package this program involve the fast Fourier Transform of the acquired data and the positive and negative harmonic frequency and their amplitudes. In order to make neural networks perform well, the data must be well-processed and properly-scaled before inputting them to ANN. Therefore there are two outputs corresponding to one fault and healthy condition. The number of neurons of hidden layer given to the program during the training process was two to give suitable error. The neural network being trained based on the amplitude of the side bands, a total of 120 data sets (20 data sets for the eccentricity fault condition) are used in the training. The type of network belong to supervised learning, it needs a teacher to lead it in order to achieve the determined goal. Fig. (10) illustrates the inputs and outputs of the ANN. In this research a feed-forward network is used, and it is trained with the back propagation algorithm using tan sigmoid function, pure line.
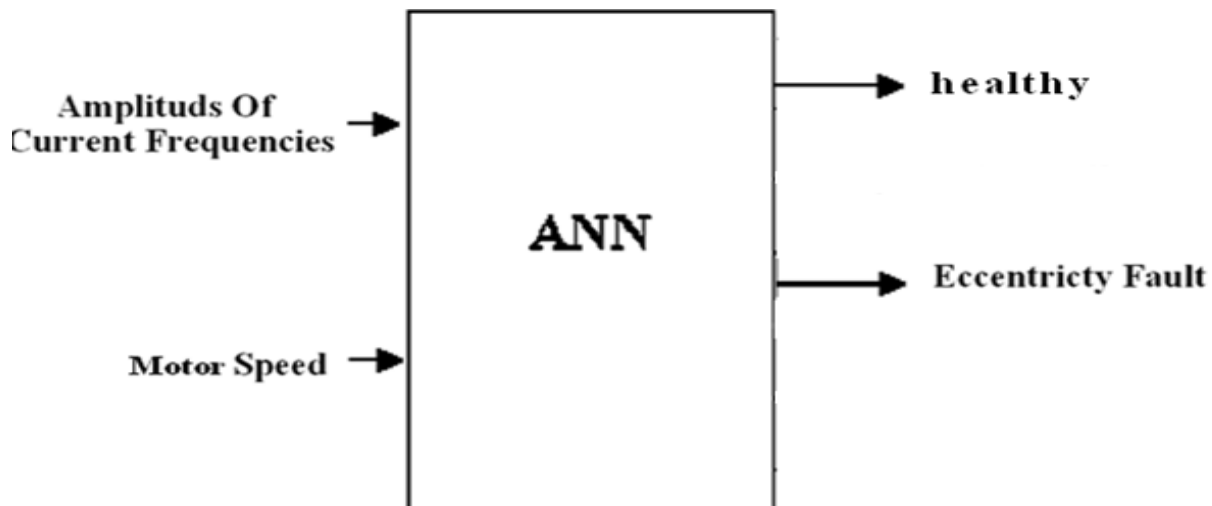
Fig. (10) Inputs and outputs of ANN
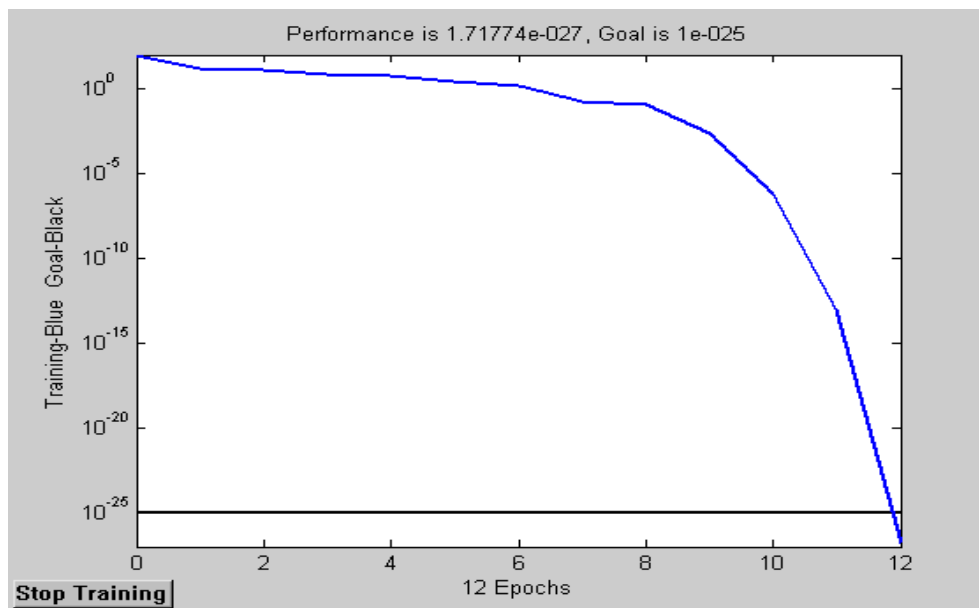
After

successful training the network, it will then used to detect the eccentricity fault. It is depicted training sum squared error related to the number of iterations in Fig. (11), the error of training parameter goal given to the program was (1e-25), but the result of the training was less than the error given to the program, as it is shown in Fig. (11).

Fig. (11) The performance of ANN Training

* CONCLUSION

The work reported in this paper has involved designing and building a motor monitoring system using an Aritificial neural network for fault detction of three phase induction motor .To accomplish this, a hardware system was designed and built to acquire three-phase stator current and speed from a (2.2kW) squirrel-cage induction motor. The ability of the phase current to detect specific fault was tested, since monitoring this parameter is the most convenient and cheapest way to sense a fault. it was clear that The sideband frequencies are function of the slip, so they are changing with the speed (that change with the load) . From the sideband frequencies calculated in the tables(1,2 and 3) it's found that the distance of the positive and negative from the fundamental increased with increasing of the load, and the same for different values of k/p and for all types of faults. From the reported work,the disadvantage of most ANN's are their   inability to respond to previously unseen conditions. Therefore , if there is an

occurance of a new fault that the network doesn't been trained to recognize ,and the fault may be misdiagnosed which produce weak output results.

REFERENCES

- N. A. Al- Nuaim, H. A. Toliyat "**A Novel Method For Modeling Dynamic Air-Gap Eccentricity in Synchronous Machines Based on Modified Winding Function Theory"** IEEE Transaction on Energy Conversion, Vol.13, 2, June 1998.

- H. A. Toliyat and M. A. Haji **"Pattern Recognition- Technique for Induction Machines Rotor Fault Detection Eccentricity and Broken Bar Fault"** Department of Electrical Engineering Texas A&M IEEE Transactions on Energy Conversion, Vol 2001.

- R. R. Schoen, T. G. Habetler **"An Unsupervised, On_Line System for Induction Motor Fault Detection Using Stator Current Monitoring"** IEEE Georgia Institute of Technology 1994.

- X**.** Huang, T. G. Habetler, R. G. Harley, 2004,**"Detection of Rotor Eccentricity Faults In closed-Loop Drive-Connected Induction Motors Using an Artificial Neural "**, IEEE 35th Annual Power Electronics Specialists Conference-PESC, Aachen, Germany, June 2004, 20-25, Vol.2, pp. 913-918.

- F**.** Filippetti, G. Franceschini, C. Tassoni **"Neural Networks Aided On-Line Diagnostics of Induction Motor Rotor Faults"**, IEEE Transaction on industry Applications, Vol.31, Issue 4, pp.892-899. 2005.
- **[7]** H. A. Toliyat and S. Nandi **"Condition Monitoring and Fault Diagnosis of Electrical Motors –A Review "** IEEE Transactions on Energy Conversion, Vol.20 NO.4, December 2005.
- D. G. Dorrell, W. T. Thomson and S. Roach, "**Analysis of Air-Gap Flux, Current, Vibration Signals as a Function of The Combination of Static and Dynamic Air-gap Eccentricity in 3-Phase Induction Motors**", IEEE Trans. Ind. Applns. n., Vol. 33, No.1, pp. 24-34, 1997.

- Barbour and W.T. Thomson**, "Finite Element Study of Rotor Slot Designs With Respect to Current Monitoring For Detecting Static Air gap Eccentricity in Squirrel-Cage Induction Motor"** IEEE-IAS annual meeting conference recordings, pp. 112-119, New Orleans, Louisiana,Oct.5-8, 1997.

- S. Nandi and H. A. Toliyat**, "Detection of Rotor Slot and Other** Eccentricity Related Harmonics In a Three Phase Induction Motor With **Different Rotor Cages"** IEEE Trans Energy Convers. Vol. 16 , no. 3 ,pp.253-260, Sep.2001.
- S. Nandi, R. M. Bharadwaj, H. A. Toliyat, A. G. Parlos " **Performance Analysis of a Three Phase Induction Motor Under Incipient Mixed Eccentricity Condition**", IEEE Trans. Energy Converse. Vol. 17. No.3. pp 392-399. Sep. 2002.

APPENDIX

(Motor Parameters):
2.2 KW (3HP), 2Pole, 50Hz, 380V

Rated Current ………. …………...........8.5A

Stator resistance (Rs)………….…..2.302 Ω

Rotor resistance(R)…………….…… 3.164 Ω

Rotor reactance (Xr)…………….…..3.587 Ω

Stator reactance (Xs)………….……..4.265 Ω

Magnetizing reactance (Xm)……........90.919 Ω

Number of slots……………………….....24

Number of rotor bars………………...……20

STUDYING OF HEATED WATER RELEASED FROM SOUTH-BAGHDAD ELECTRIC POWER STATION TO THE TIGRIS RIVER

Ass.Teacher. Tariq J.Al-Mosewi
Env. Eng. Dept.
College of Engineering
University of Baghdad
Baghdad-Iraq

Prof. Dr.Mohammed Ali I. Al-Hashimi
Building and construction Eng. Dept.
University of Technology
Baghdad-Iraq

ABSTRACT

Thermal pollution occurs when heated wastewater is discharged into rivers, lakes, oceans, or other water bodies. This will raise the temperature of the water body above its normal level and, consequently, will harm the aquatic live.

Thermal Pollution problems will intensify as electricity usage increases unless substantial changes are made in the mode of discharge of the heated water.

This paper is aimed to study the effects of heated water released from South-Baghdad Power Station on the water quality of Tigris River. Many parameters are test such as: Temperature (T), Total suspended solids (TSS), Total Dissolved Solids (TDS), Electrical Conductivity (EC), Hydrogen Ion (pH) and the dissolved oxygen (DO). Other parameters are tested to describe the heated water components such as Biochemical Oxygen Demand (BOD), Oil+Grease, and PO_4.These parameters are compared with the allowable limits of rivers according to the Iraqi standards NO.25/1967 and found that some parameters exceed the allowable limits.

الخلاصة

يحدث التلوث الحراري عندما يتم طرح مخلفات سائلة حارة الى الانهار، البحيرات، المحيطات او اي جسم مائي. حيث ان هذه المخلفات تؤدي الى زيادة درجة حرارة الجسم المائي فوق المستوى الطبيعي مما يؤدي الى اضرار في البيئة المائية.

إن التلوث الحراري تزداد حدته نتيجة لزيادة الحاجة للطاقة الكهربائية ما لم تتخذ تغييرات جوهرية في طريقة طرح المياه الحارة.

يهدف البحث إلى دراسة المياه الحارة المطروحة إلى نهر دجلة من محطة جنوب بغداد لتوليد الطاقة الكهربائية وبيان تاثيرها على نوعية مياه النهر. تم قياس عدة متغيرات مثل: درجة الحرارة،المواد الكلية العالقة،المواد الكلية الذائبة،التوصيلية الكهربائية،الرقم الهيدروجيني و الأوكسجين الذائب. وكذلك تم أجراء عدة فحوصات على المياه المطروحة مثل المتطلب الحيوي للأوكسجين، الزيوت و الشحوم والفوسفات.و قد تم مناقشة الفحوصات مع المحددات العراقية لصيانة الانهار رقم 25 لسنة 1967   حيث تبين ان بعض المتغيرات تزيد عن الحدود المسموحة خلال فترة القياس.

INTRODUCTION

The major industries produce the heated wastewater are: Steam Electric Generating Plants, petroleum refineries, steel Mills, chemical plants, etc.

Water bodies of water lose and gain heat much more slowly than do land or masses, and under most circumstance, water temperature is fairly constant and changes gradually with the season.

Thermal pollution problems will intensify as electricity usage increases unless substantial changes are made in the mode of discharge of the heated condenser cooling water. Steam generation of electrical power plant requires rejection of tremendous quantities of waste heat typically 58% - 67% of the energy input to the plant from the generation units to the surrounding (**Paily et al., 1974**). This heat is transferred in the condensers from the low-pressure steam to the cooling water, and then directly to the atmosphere by the means of a cooling tower, or directly discharge to the water body(Fig.1).

The directly discharge of heated water to the river can be more dangerous to the health of the receiving water than organic pollution. Higher temperature reduces solubility of oxygen and chemical reactions proceed at a faster pace (**Masters,1998**).

Al-Jalaby (1994) developed a two-dimensional numerical model for the simulation of the spread and mixing of thermally polluted water disposed into the river flow. This model considers the effect of density difference between the pollutant density and the river water density. Finite difference up winding scheme is used to solve partial differential equations, which include the momentum conservation, energy conservation and (K-ε) turbulence model. The results of this model are verified by integral heat balance analysis. This model is found to be sensitive to the variation in the river velocity and density. It is also insensitive to the variations in wind speed.

Li-Ren and Righetto (1998) presented unsteady state two-dimensional model to simulate the velocity and temperature fields in the estuary of the Yangtza River in Brazil. The computation is based on the advanced turbulence depth averaged two equations (k-ε) model. Variations of bottom topography and water surface elevation are included. The distribution of velocity and temperature computed by turbulence model (k-ε) is compared with experimental results and field data. It is found that the simulation by using (k-ε) model can provide more details of flow fields and temperature distribution than once by using phenomenological algebraic for models of eddy viscosity and diffusivity.

Bormans and Webster (1998) investigated the thermal stratification dynamics of the slow-flowing rivers of the Marray-Darling Basin. The net surface heat flux and the river discharge are the two most important parameters that determine the stratification status of the rivers with little effect from direct wind mixing. Excellent agreement between measured and simulated temperature profiles under a wide range of river discharge and meteorological forcing is obtained.

Cakiroglu and Yurteri (1998) presented the mathematical model to predict the long-term effects of once through cooling systems on local fish population. The fish life cycle model simulates different life stages of fish by using appropriate expressions represented by growth and mortality rates. The heart of the developed modeling approach is the prediction of plant caused reduction in total fish population by estimating recruitment to adult population with and without entertainment of ichthyoplakton and impingement of small fish. The model is applied to a local fish species, gilthead (Sparus aurata), for the cause of a proposed power plant in the Aegean region of Turkey. The simulation indicates that entertainment and impingement may lead to a population reduction of about 2% to 8% in the long run.

Joody (2001) developed one and two dimensional numerical models for the simulation of the spread and mixing of thermally polluted water disposed into the river released from the AL-Doura Power Station starting from the outfall up to 1000m downstream. The momentum and thermal –energy equations were used to describe the distribution of velocity and temperature in river. The two dimensional model also incorporates with the (k-ε) model to calculate the distribution of turbulent viscosity. The two dimensional model also discusses two cases; the first case neglects the effect of

vertical velocity distribution, while the second case include it. Comparison of observed data on Feb, 3,2001 and July, 27,2001 with data computed by two-dimensional model shows good agreement with error of 0.57% and 1.95% respectively.

Al-Suhaili and Jasim (2006) applied two dimensional numerical model for estimating temperature distribution in a river. This model was found to be sensitive to the wind speed. A laboratory physical model was built to find experimental data. The comparison of the observed results from Al-Doura Power Station and laboratory physical model with those computed by the numerical model showed a good agreement and the maximum absolute difference percentage were 16.2 %, 8.6 % respectively.

Measurements and Field Work
A river reach of 500 m Long was involved in the present work. It is started from the outfall structure of South-Baghdad station and extended to 500 m downstream. Samples were collected to predict the essential variation of the water quality after the heated water discharge.

The cooling system applied in South-Baghdad power station is once through cooling system in which the cooling water is withdrawn from the river via two pipes (1.4 m diameter), and then it is conveyed to underground rectangular channels that convey the cooling water to the six condensers with water temperature increase to about 10- 15 °C. The heated water returns to the river via an underground discharge channel and an outfall structure located in the shoreline downstream on the intake structure.

Different field measurements were performed and different data were gathered, which can be mainly classified as stream, wastewater and raw water sampling.

Stream sampling is considered to represent and give reliable measurements of water quality constituents along the stream reach. Seven parameters are involved in the present work. These parameters are temperature (T), dissolved oxygen (DO), Electrical conductivity (EC), total suspended solids (TSS), total dissolved solids (TDS) and hydrogen ion (pH).

The temperature and dissolved oxygen were measured by using portable device. While, the remaining measurements were collected every week using plastic bottle of 0.5 liter capacity and sent to laboratory of the Power Station to be tested. Collection of samples was usually conducted using a boat.

Tables from 1 to 6 show the values of TSS, TDS, EC, pH, T, BOD, Oil & grease and PO_4. While, figure from 2 to 7 show the variation of dissolved oxygen concentrations along the study reach

Table (1): The concentration of TSS, TDS, EC and pH at the upstream with time

Date	TSS (mg/l)	TDS (mg/l)	EC (micromhos/cm)	pH	T °C
14/3/2002	71	510	819	7.98	20
21/3/2002	29	595	988	7.9	21
28/3/2002	42	499	810	7.87	24
4/4/2002	45	502	816	7.9	21
11/4/2002	51	765	1015	7.88	22
20/4/2002	56	437	776	7.92	25
27/4/2002	56	437	728	7.8	27
1/5/2002	45	744	1068	7.99	26
8/5/2002	40	713	995	7.89	24.5
16/5/2002	59	752	1046	8.1	26

20/5/2002	78	723	1012	8.1	29
4/6/2002	38	345	738	8.08	27
11/6/2002	41	422	902	8.07	28
18/6/2002	25	560	949	8.19	28
25/6/2002	21	588	915	8.19	28.8
2/7/2002	33	498	822	8.1	28
9/7/2002	30	522	884	7.98	29
15/7/2002	14	494	821	7.9	31

Table (2): The concentration of TSS, TDS, EC and pH at the outfall with time.

Date	TSS (mg/l)	TDS (mg/l)	EC (micromhos/cm)	pH	T $\circ$C
14/3/2002	51	535	883	7.99	28.8
21/3/2002	20	677	989	7.98	37
28/3/2002	19	554	990	7.88	33.5
4/4/2002	19	655	1002	7.89	36
11/4/2002	22	778	1055	7.9	34
20/4/2002	41	756	1050	7.9	31
27/4/2002	40	510	913	7.88	33
1/5/2002	38	810	1226	7.91	35
8/5/2002	30	832	1150	7.83	35.5
16/5/2002	49	827	1280	8.09	37
20/5/2002	66	770	1077	8.1	35.5
4/6/2002	21	391	791	8.05	36.3
11/6/2002	12	610	975	7.88	37.5
18/6/2002	8	615	979	7.9	39
25/6/2002	10	519	988	7.91	42.3
2/7/2002	13	575	885	8.1	43.2
9/7/2002	15	603	938	7.87	44.5
15/7/2002	8	588	975	7.09	46

Table (3): The concentration of TSS, TDS, EC and pH at the downstream (50 m far from outfall) with time.

Date	TSS (mg/l)	TDS (mg/l)	EC (micromhos/cm)	pH	T $\circ$C
14/3/2002	62	530	950	7.98	26
21/3/2002	25	610	969	7.99	26
28/3/2002	22	522	950	7.89	31
4/4/2002	22	651	971	7.9	33
11/4/2002	31	772	1075	8.1	31
20/4/2002	42	580	958	8.0	29.5

27/4/2002	42	502	888	7.9	31
1/5/2002	39	785	1123	7.97	29
8/5/2002	33	809	1166	8.00	32.9
16/5/2002	55	775	1100	8.1	35
20/5/2002	68	705	1063	8.09	34
4/6/2002	25	372	690	8.1	31
11/6/2002	15	534	790	7.9	36
18/6/2002	10	512	752	7.91	36.7
25/6/2002	15	533	760	7.91	39
2/7/2002	14	511	693	8.15	41.5
9/7/2002	18	552	771	7.91	41.7
15/7/2002	12	510	753	7.14	43.5

Table (4): The concentration of TSS, TDS, EC and pH at the downstream (100 m far from outfall) with time.

Date	TSS (mg/l)	TDS (mg/l)	EC (micromhos/cm)	pH	T °C
14/3/2002	66	551	952	7.98	24
21/3/2002	25	608	961	7.89	30
28/3/2002	25	510	912	7.88	28.8
4/4/2002	29	648	966	7.9	30
11/4/2002	35	770	1027	8.1	28.5
20/4/2002	46	575	913	8.0	28
27/4/2002	47	420	835	7.9	30
1/5/2002	40	783	1100	7.97	26.7
8/5/2002	35	591	983	8.09	31
16/5/2002	56	725	1019	8.11	32.9
20/5/2002	70	751	1060	8.1	32
4/6/2002	29	341	558	8.1	28.5
11/6/2002	22	478	710	7.95	33.7
18/6/2002	16	440	703	8.01	34.5
25/6/2002	16	391	681	8.00	36
2/7/2002	19	377	605	8.16	37.4
9/7/2002	19	463	710	8.00	39.6
15/7/2002	20	400	675	8.00	41

Four parameters are involved in the present work, which are biochemical oxygen demand five day (BOD_5), Oil+grease, TSS, and (PO_4), These samples were collected once in a month (started from April and ended in July)

Table (5): The concentration of B.O.D$_5$, Oil+Grease, TSS and PO$_4$ in heated water.

	April	May	June	July
BOD$_5$ (ppm)	17	40	60	52
Oil+Grease (ppm)	112	24	45	29
TSS (ppm)	44	41	34	19
PO$_4$ (ppm)	0.75	0.7	0.44	0.38

Table (6): The concentration of BOD$_5$, Oil+Grease, TSS and PO$_4$ in raw water.

	April	May	June	July
BOD $_5$ (ppm)	10	22	48	46
Oil+Grease (ppm)	105	16	19	25
TSS (ppm)	75	76	55	70
PO$_4$ (ppm)	0.4	0.5	0.3	0.3

Results and Discussion

• The TSS concentration decreases at the outfall location in which the temperature increases. The increase of temperature will have effect on density of water (density decreases with temperature increase), therefore the suspended solids will move downward the river bottom. But in the case of washing of condensers, the concentration of TSS increases at the outfall because the washing water will be released to the river directly.

▪ The maximum TSS concentration measured at outfall location on 3/1/2002 and its equal 188-ppm, this high value may be attributed to the high concentration of TSS released from the condensers of power plant at that time, while the minimum TSS concentration measured at outfall location on 18/6/2002 and 15/7/2002 which is equal 8 ppm.

• TDS and EC concentrations increase at the outfall location due to increase in the dynamic energy of molecules, this leads to an increase in the dissolution salts in turn in (TDS) and (EC), For example the concentrations of TDS and EC on 21/3/2002 are 677 ppm and 989 micromhos/cm at outfall location, while they equal 610 ppm and 969 micromhos/cm at 50 m far from outfall location in which the temperature of water river decreases.

▪ Maximum concentration of TDS measured at outfall location on 3/1/2002, which is equal 895 ppm while the minimum concentration of TDS measured upstream on 4/6/2002,which is equal 345 ppm. On the other hand, the maximum concentration of EC measured at outfall location on 16/1/2002, which is equal 1220 micromhos/cm.while the minimum concentration measured at 100 m far from outfall location on 2/7/2002, which is 605 micromhos/cm. Moreover the concentration of EC some times exceeds the allowable limits (1000 micromhos/cm).

• The test of stream water at the study reach shows there is no effective change in pH concentration mainly at the outfall location; this can be attributed to the logarithmic equation of pH. Field observation shows, those concentration levels of pH are acceptable along the study reach and still with allowable limits of Iraqi Standards (from 7 to 8.5).

• The concentration of Dissolved Oxygen (DO) is often used as index for water quality. At least 4 (mg/l) are required to maintain a balance of desirable species in the water. On the other hand, field observation shows that the concentration of dissolved oxygen is acceptable along the study reach,

i.e greater than allowable limit of Iraqi Standards (more than 5 mg/l), but there is sudden dropping at the outfall location because of temperature increasing.

- The test of heated water released to the Tigris River shows that there are illegal concentrations of BOD_5 and Oil. The high concentration of Oil (above 10 mg/l according to the Iraqi standards, see tables 5 and 6) comes from the State Company for Vegetable Oils which disposes high concentration of oil upstream the South-Baghdad Power Station. Also the power plant itself disposes oil to the pipe of heated water. BOD_5 test shows there is illegal concentration in June and July (above 40 mg/l according to the Iraqi standards) because the difference in inlet and outlet water temperature. Also the State Company for Vegetable Oils disposes high concentrations of BOD_5 and TSS up stream Power Station at that time. PO_4 concentrations are within the permission value of Iraqi standard which is (3 ppm).

CONCLUSIONS

- The dissolved oxygen of water river does not drop under the allowable limits (5 mg/l according to the Iraqi standards) so that there is no sever effect on the organisms lived in the river.
- The concentrations of total dissolved solids are within the allowable limits (1000 mg/l according to the Iraqi Standards) along the study reach.
- The Electrical Conductivity exceeds the allowable limits (1000 micromhos/cm) along the study reach in some tests during the study period.
- The pH concentration is not affected by increase in temperature in study reach.
- The heated water samples showed that the concentration of BOD_5 are slightly rising comaired with the samples taken from the raw water.
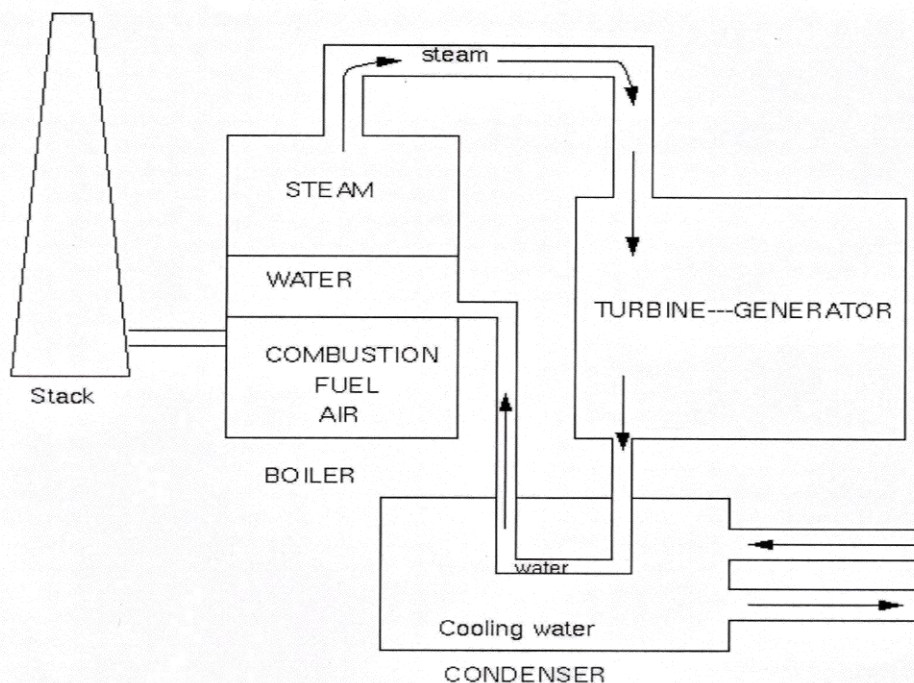
Figure (1): steam electric power plant
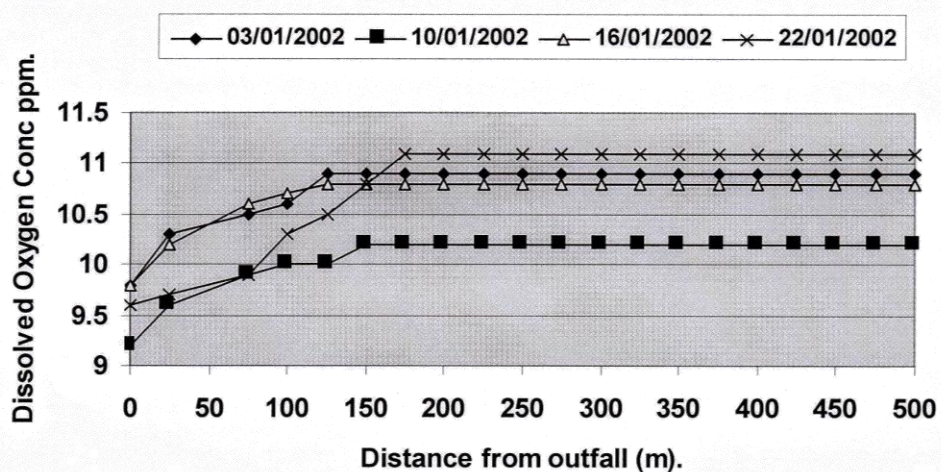
Fig (2): Concentration of Dissolved Oxygen along the study

reaches in Jan/2002.
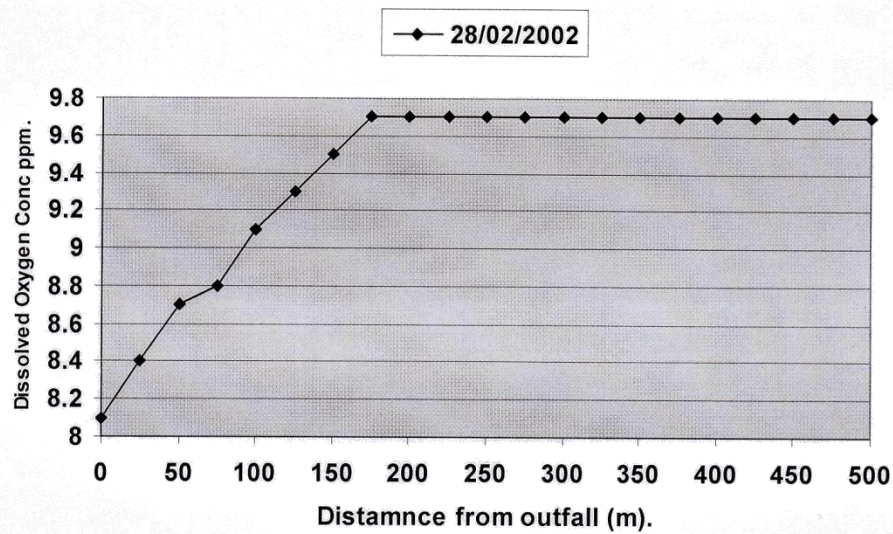
Fig (3): Concentration of Dissolved Oxygen along the study reaches in Feb/2002.
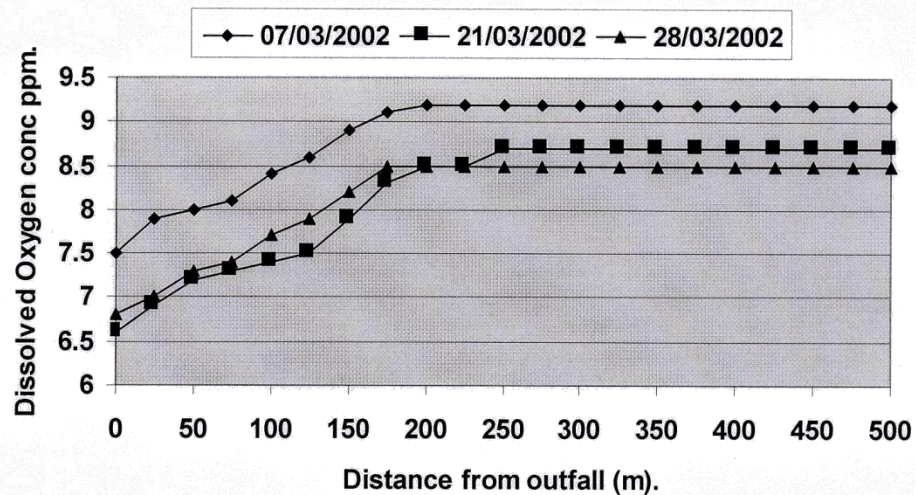
Fig (4): Concentration of Dissolved Oxygen along the study reaches in Mar/2002.
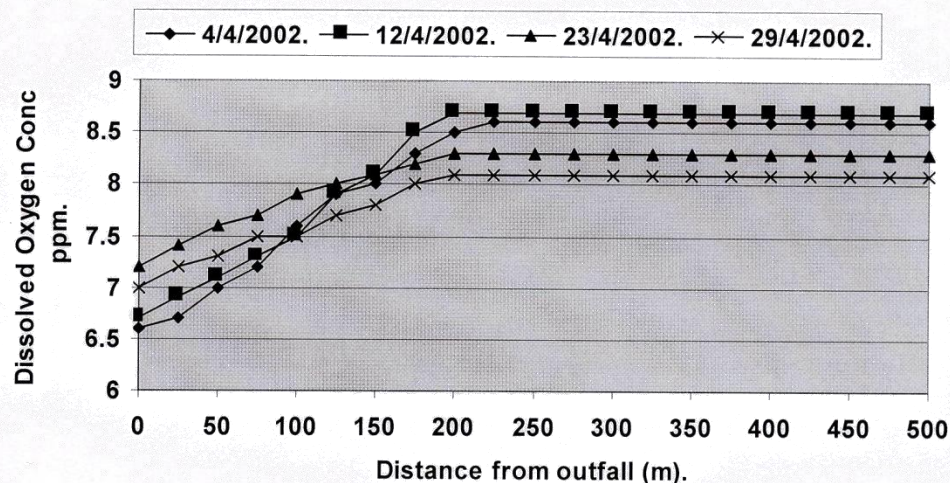
Fig (5): Concentration of Dissolved Oxygen along the study reaches in April/2002.
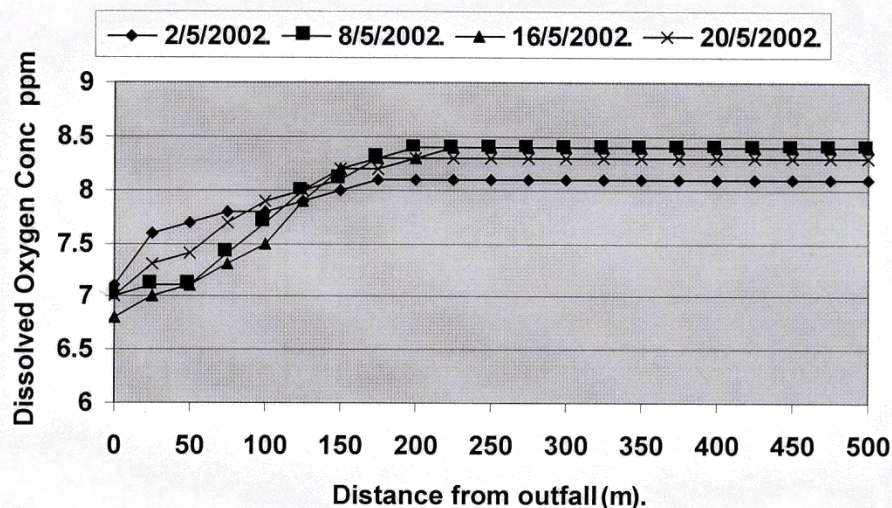
Fig (6): Concentration of Dissolved Oxygen along the study reaches in May/2002.
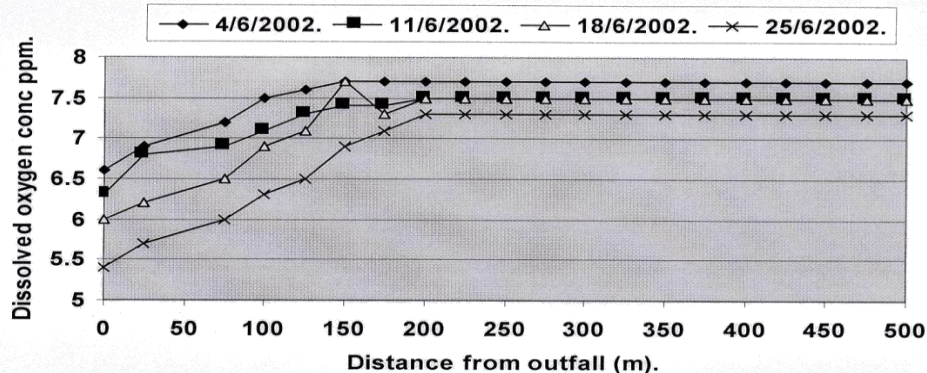
Fig (7): Concentration of Dissolved Oxygen along the study
reaches in June/2002.

REFERENCES

- **Al-Jalaby, M.A**., (1994),"Numerical model of Thermal Pollution Transport in River"M.sc.Thesis, College of Engineering University of Baghdad.

- **Al-Suhaili Rafa and Mohsin Jasim**,(2006),"Two-Dimensional Numerical model for Thermal Pollution of Single Source in River", Journal of Engineering. University of Baghdad,No.1,Vol.12.pp.25-29.

- **Bormans, M. and T.Webster Ian**, (1998),"Dynamics of temperature stratification in lowland rivers" J.Hyd.Div, Vol.124, N0.10, pp.1059-1063.

- **Cakiroglu,C., and Yurteri,C**.,(1998),"Methodology for predicting cooling water effects on fish"J .Env.Eng.,Vol.124,NO.7,PP.612-618.

- **Joody Ali.S**.,(2001)" Studying of Thermal Pollution of the Heated water Released from Al-Doura Power station" M.Sc.Thesis, College of Engineering, University of Al-Mustansiria.

- **Masters.G.M**,1998,"Intrduction to Environmental Engineering and science"2nd.ed U.S.A.

- **Paily,P.P,Macagno,E.o, and Kennedy,j**.,(1974),"Winter-regime thermal response of heated stream"J.Hyd.Div.vol.100, No.HY4,pp.531-537.

- **Rute Neves and Silvia Lourenco**,(1997),"Thermal Pollution"www.mhhe.com/physsci/physical/moor/messages/102.htm/-11k.

INTEGRATED SYSTEM FOR AIR POLLUTION AROUND REFINERIES

Prof. Dr. Rafa H. Al-Suhaili , Muna Samir Al-Khafaji , Environmental Engineering Department, College of Engineering ,University of Baghdad

ABSTRACT

A mathematical model for integrated air pollution modelling around refineries is built and named as Computerized System for Integrated Air Pollution Modelling Around Oil Refineries (CSIAPMAOR).The model based on Gaussian equation to estimate concentration of pollutants (SO2, NO2, CO, Particulates) that are emitted from a continuous air pollution elevated source. The model is designed by using Visual Basic as a main core of the system and linked with auxiliary models such as ArcMap (GIS), Surfer software, Ms-Excel and Ms-Access. The model has flexibility to select either rural, urban or stability (Smith equation) wind speed profile. It also has the option of using three types of dispersion coefficients equations for rural condition (PGT-Briggs-Martin equation) and one equation for urban condition (Briggs equation).The model has many options to display results as concentrations versus center line-downwind distance or as Three-Dimensional (3D) map. The model can compute maximum concentration with the contribution of each stack to the overall maximum concentration. Moreover the model has the ability to perform a sensitivity analysis for the effect of the most important parameters according to the Gaussian equation. AL-Doura Oil Refinery was taken as a case study using the available observed data of two sites1 and 2 for periods 15th -21st and 23rd -29th August 1997 in order to check the performance potential of the model. Results showed that Briggs equation for dispersion coefficients with rural wind speed profile has the best degree of agreement with the observed values of 0.86, 0.90 for SO2; 0.69, 0.80 for NO2; 0.73, 0.79 for CO; 0.63, 0.60 for particulates at site 1 and 2 respectively. It is found, that for AL-Doura Oil Refinery stacks number 6, 2, 7, and 3 have a large contribution on the overall maximum concentration. The model demonstrates the influence of atmospheric stability, wind speed, emission rate, exit velocity, physical height, exit temperature and rural-urban area in reducing the concentrations of pollutants. Sensitivity analysis shows that the concentrations are sensitive to stability class in comparison with other input parameters.

الخلاصة:

في هذا البحث تم بناء نظام مبرمج في الحاسوب لنمذجة متكاملة لتلوث الهواء حول المصافي وسمي ب CSIAPMAOR. النموذج مبني اساسا″على معادله گاوس لتخمين ملوثات الهواء مثل ثنائي اوكسيد الكبريت وثنائي اوكسيد النتروجين واول اوكسيد الكاربون والدقائق العالقه المنبعثة من مصادر تلوث الهواء المستمر . النموذج تم تطويرة باستخدام برنامج Visual Basic كلغة برمجيه اساسيه للنظام مع ربط النظام ببرامج مساعدة وهي: اولا″ برنامج ArcMap(GIS) تم استخدامه لاعطاء احداثيات حقيقية للخارطة الاساسية مع رسم طبقات كنتورية ذات ثلاثة ابعاد TINs . ثانيا″ برنامج Surfer وذلك لرسم خرائط كنتورية لتحليل الحساسية . ثالثا″ برنامج Ms Excel وبرنامج Ms Access وذلك لخزن كل مدخلات و نتائج البرنامج . النموذج ذو قابلية لاختياروراحدة من ثلاث حالات لحساب سرعة تغاير الرياح في المناطق الحضرية او الريفية او بالاعتماد على الاستقرارية (معادله سمث). النموذج ايضا″ له القابلية لاختيار واحدة من ثلاث معادلات للمناطق الريفية. والمعادلات هي (PGT – Briggs –

Martin equation) و معادله واحدة للمناطق الحضرية (Briggs) لحساب معاملات التشتت . بالاضافة الى امكانية النموذج لعرض نتائج تغير التراكيز مع خط منتصف الدخان المنبعث أو بشكل خارطة ثلاثية الابعاد. بالاضافة الى امكانية النموذج في حساب التركيز الاقصى للملوثات مع تحديد مساهمة كل مصدر من مصادر التلوث في قيمة هذا التركيز كما أن له امكانيه استخدام تحليل الحساسيه لتبيان تأثير تغير المعاملات المهمة على معادلة گاوس. البرنامج يتناول مصفى الدورة كموضوع دراسة باستخدام البيانات المتوفرة التي تمت ملاحظتها لموقعين عند جنوب شرق المصفى للفترتين (15-21) و(23- 29) من اب للعام 1997 . أستخدمت هذة البيانات للتحقق من كفاءة اداء البرنامج .النتائج المستحصلة من استخدام معادلة Briggs لمعاملات التشتت مع مؤشرات سرعة الرياح في المناطق الريفية أعطت توافقية عالية مع القيم المقاسة. وقيم معامل التوافق البالغة 0.86 و 0.90 لثنائي اوكسيد الكبريت و 0.69 ، 0.80 لثنائي اوكسيد النتروجين و0.73 ، 0.79 لأول اوكسيد الكربون و 0.63 ، 0.60 للدقائق العالقة في الموقعين 1 و 2 على التوالي . وايضا" وجد من خلال تحليل المساهمة بأن ثنائي اوكسيد الكبريت له التركيز الاقصى في الساعة للفترات آنفة الذكر و بذلك يفوق المعايير المسموح بها في العراق لكلا الموقعين. مداخن مصفى الدورة رقم 6 و2 و7 و3 كانت لها مساهمة كبيرة في تكوين التراكيز القصوى. و استعرض تأثير كل من استقرارية الجو و سرعة الرياح و معدل و سرعة الانبعاث و ارتفاع المداخن و حرارة الانبعاث و تأثير المناطق الحضرية و الريفية في تخفيض تراكيز الملوثات المنبعثه.

KEYWORDS
Air Pollution, Gaussian Model, GIS and Environmental Modeling, Designed Model

INTRODUCTION

Urban air pollution due to activities of the process petroleum refinery industries is one of the main problems faced by the industrial area worldwide. Many experimental analyses were carried out to determine the extent of air pollution due to the petroleum refinery industry, focusing on the concentrations of NO_2, CO, SO_2 [Abdulkareem, 2005].

The development of an air pollution model for multi-sources is no doubt useful. Integrated models using available nowadays softwares will be useful in many ways. These models can be used to predict different pollutants levels spread over the nearby area, due to different properties of multipoint sources. The integrated model can allow the variation of sources properties, such as emission rate, exit velocity, etc. Integrated models are those models that use different softwares linked in a proper way to transfer data between these softwares to achieve certain tasks. Integrated models are rather rare or expensive, while each of the softwares contributing in the developed model is available and free. For example, Visual Basic, Ms Excel, Ms Access, ArcMap (GIS), are available softwares nowadays, whereas a specialized integrated model for air pollution modelling is not freely available. Hence the development of such model is essential. The main challenge in building an integrated model for a special purpose is the proper linkage between the available softwares, i.e. the way to transfer data between these softwares.

GAUSSIAN MODEL

The Gaussian model is perhaps the oldest (Circa 1936) [Bosanquet, 1936 as cited in Wikipedia, 2008] and is the most commonly used dispersion model to estimate the concentration of a pollutant because of its simplicity [Awasthi et al., 2006]. It assumes that the air pollutant dispersion has a Gaussian distribution, meaning that the pollutant distribution has a normal probability distribution. The primary algorithm used in Gaussian model is the Generalized Dispersion Equation for a Continuous Point-Source Plume [Beychok, Milton, 2005 as cited in Wikipedia, 2008].

GIS AND ENVIRONMENTAL MODELING

Geographical Information System (GIS) is a computer based information system that enables capturing, modelling, manipulation, retrieval, analysis, and presentation of geographically referenced data [Aronoff, 1991 as cited by Rahmatizadeha et al., 2002]. The basic advantage of this science and technology is its ability to manage and integrate with the present database and for spatial analysis such as (overlay, buffering and zoning) which provides an environmental alarming system [Rahmatizadeha et al., 2002]. By doing air quality modelling in a GIS environment, the output of the pollutant records can be obtained as spatial records in the form of map layers, which

can visualize real objects by vector and raster data formats together with graphs and multimedia presentations [Matejicek et al., 2002].

THE COMPUTERIZED SYSTEM FOR INTEGRATED AIR POLLUTION MODELLING AROUND OIL REFINERIES (CSIAPMAOR):

The designed model provides options to model point source emissions from stacks present at industrial areas. The basic equation governing the phenomena is the straight-line, steady-state Gaussian plume equation for a continuous air pollution elevated source [Kiely, 1997]:

$$C(x, y, z, H_e) = \frac{Q}{2\pi\sigma_y\sigma_z U} \exp\left[-\frac{1}{2}\left(\frac{y}{\sigma_y}\right)^2\right] \left\{ \frac{\exp\left[-\frac{1}{2}\left(\frac{z - H_e}{\sigma_Z}\right)^2\right]}{+ \exp\left[-\frac{1}{2}\left(\frac{z + H_e}{\sigma_Z}\right)^2\right]} \right\} \tag{1}$$

Where: C (x, y, z) is the concentration of pollutant (g/m^3) at a receptor located at (x, y, z), x is downwind distance from the source point (m), y is crosswind distance from the plume centreline (m), z is height above ground level (m), Q is pollutant emission rate (g/s), U is mean wind speed at release height (m/s), H_e is the effective height of release of the point source (m), σy and σz are horizontal and vertical standard deviations of the emission distribution (m).

Softwares Used in the CSIAPMAOR Model

The **CSIAPMAOR** program was designed using Visual Basic (version 6.0) as the basic programming language and as a control tool for integrating the system with auxiliary models. These auxiliary softwares are Ms Access, Ms Excel for storing output results, ArcMap (GIS) (version 8.1) for Georeference of the base map, in addition for drawing TINs layers to show the spatial variation in the contaminant levels over the area under study, Surfer (version 7.0) for drawing contour maps of the sensitivity analysis.

Features and Capabilities of the Designed Model

- The model can be used to predict short-term concentrations (for periods of 24 hours or less) for pollutants SO2, NO2, CO and Particulates resulted from a point source or from multisources, instantaneously.
- The model offers three options for computing wind speed profile: rural, urban, and stability (Smith equation) wind speed profile.
- The model offers flexibility to select either rural or urban dispersion parameters, depending on the characteristics of the source location. Three options for rural dispersion coefficients: PGT, Briggs, and Martin equation, and just one option for urban condition (Briggs equation), are available.
- The model can estimate maximum hourly concentration, in addition to the location of the receptor and the hour at which it happens.
- The model can perform contribution analysis for each point source to the overall maximum concentration.
- The model has an option of drawing hourly concentration for continuous emitting from multisources as 3D TINs layer or as a contour map to show the influence of the different concentration levels extended over a base map of the area around these sources.

- The model has option for displaying hourly concentration emitting from each stack with center-line downwind distance by a bar chart.
- The model can determine the required calibration factor between the model results and a set of measured values.
- The model provides tabular printed outputs with many options
- The model has option to test sensitivity of the Gaussian model to the variation in its parameters by four options for stability class, wind speed, stack properties (exit velocity, exit temperature, physical height, emission rate) and rural versus urban area.

The model built here, has the following limitations:
- Estimate pollutants emitted from elevated point source.
- Valued for non-reactive pollutant only.
- The effect of momentum force in plume rise is neglected and only buoyancy force is considered.
- Particulates are limited for spherical shape only.
- All pollutants are totally reflected.

APPLICATION OF THE DESIGNED MODEL: CASE STUDY AL-DOURA OIL REFINERY

The model has been used first for a Cartesian receptor grid with 25 meters for a small area of (1700m × 1700m) with origin point (0 E, 0 N) in the lower left corner of the area. The (UTM) coordinates of this point are (446100.73 E, 3680688.62 N) as shown in Figure (1). This area covers all stacks of AL-Doura Oil Refinery in addition to the two sites (receptors) where measured data are available for the designed model validation; dense grid is used because these receptors are very close to AL-Doura Oil Refinery. The model is then used for a Cartesian receptor grid with 100 meters for a large area of (14000m × 11000m) as shown in Figure (1) to cover all the area surrounding the refinery in the eastern south direction. The origin point (0 E, 0 N) of this area with corresponding UTM coordinates are (443382.21 E, 3672874.80 N). The second application of the model to such an area is used to show the impact of the refinery on the large adjacent areas using contour maps which clarify the maximum concentrations and the contribution of each stack on this maximum concentration.

The model is applied using two cases, the first case with stability wind speed profile (Smith equation) using three equations for calculating the dispersion coefficients of the rural area (PGT equation, Briggs equation and Martin equation), the second case with rural wind speed profile using the same equations for the dispersion coefficients to select which case will be suitable to represent the case study.
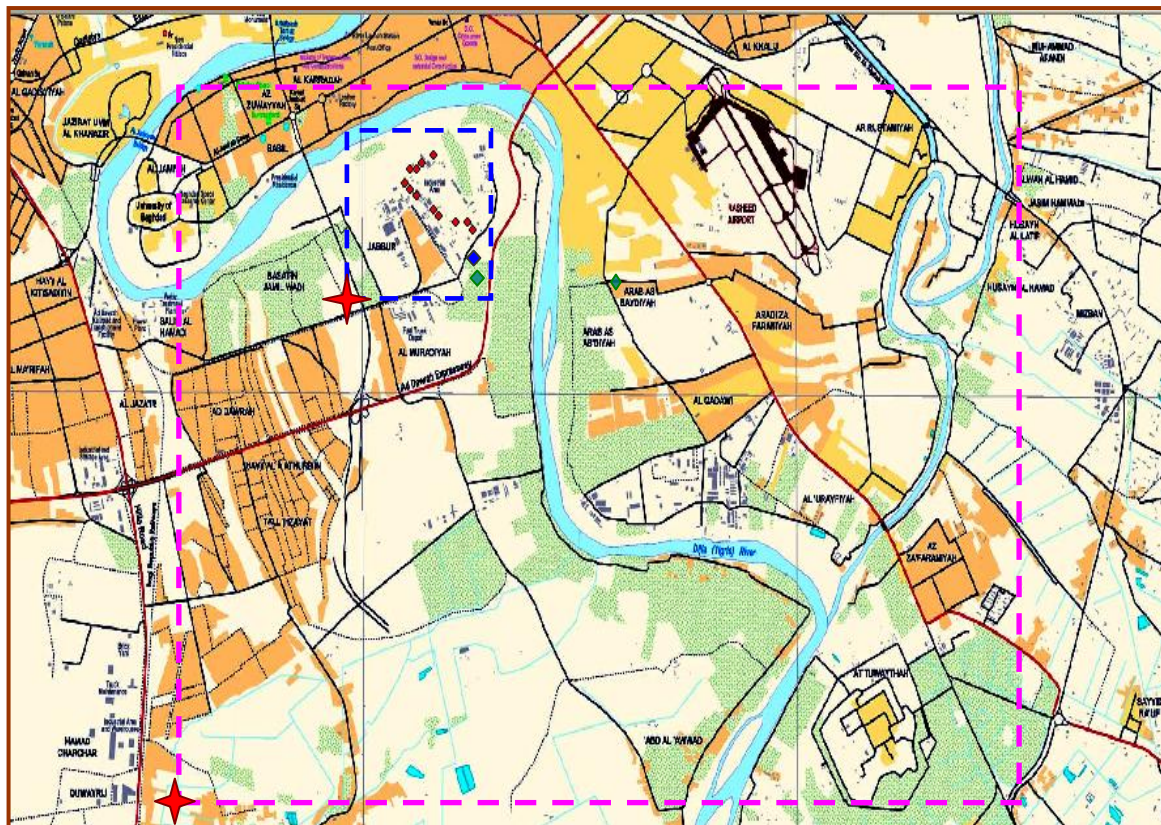
Fig (1) Boundaries of the Small and Large Area for Which the Model was Applied
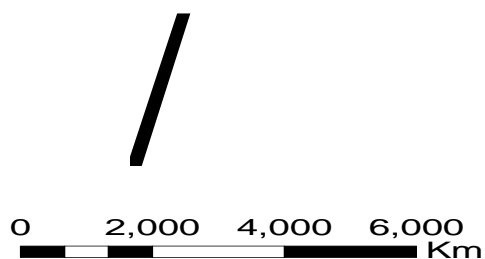
Comparison of the Model Results with the Measured Concentrations

The results obtained from the model application have been compared to the observations of the hourly concentrations measured at sites 1, and 2 for periods from (15th to 21st August 1997 at site 1) and (23rd to 29th August 1997 at site 2) as measured by AL-Rubai (1998).

Index of Agreement (IOA)

$$IOA = 1 - \frac{\sum_{i=1}^{N}(p_i - O_i)^2}{\sum_{i=1}^{N}(|P_i - O_{mean}| + |O_i - O_{mean}|)^2} \qquad (2)$$

IOA is a measure of the degree to which the observed values have been accurately estimated by the model. IOA is sensitive towards differences between observed and predicted values as well as to certain changes in proportionality, and represent more consistent measure of the performance. IOA = 0 indicates no agreement, IOA = 1 indicates perfect agreement [Willmott, 1981 as cited in Awasthi et al., 2006 and Luhar et al., 2004].

Table (1) Index of Agreement (IOA) for Sites 1, and 2, Near AL – Doura Oil Refinery

Wind speed profile	Dispersion coefficients	No. of Site	Index Of Agreement (IOA)			
			SO_2	NO_2	CO	Particulates
Stability profile (Simth equation)	PGT equation	Site 1	0.84	0.66	0.68	0.61
		Site 2	0.88	0.75	0.74	0.56
	Briggs equation	Site 1	0.87	0.69	0.72	0.64
		Site 2	0.89	0.78	0.75	0.58
	Martin equation	Site 1	0.84	0.66	0.68	0.61
		Site 2	0.88	0.75	0.74	0.56
Rural profile	P-G-T equation	Site 1	0.84	0.66	0.69	0.55
		Site 2	0.88	0.76	0.76	0.57
	Briggs equation	Site 1	0.86	0.69	0.73	0.63
		Site 2	0.90	0.80	0.79	0.60
	Martin equation	Site 1	0.85	0.69	0.69	0.57
		Site 2	0.88	0.76	0.77	0.57

Source Contribution Analysis

Contribution analysis represents the contribution of a particular source to the overall concentration in a certain location (receptor point). Recognizing the source contribution information is important to many short term modelling analyses. For the designed model, contribution of each point source (stack) of the AL-Doura oil refinery to the overall maximum concentration for each pollutant are found by applying the model for the large area (14000 m × 11000 m). The designed model uses Briggs equation for dispersion coefficients in the rural area with rural wind speed profile and meteorological data reported at (15th-21st August 1997) and (23rd-29th August 1997) from AL-Rubai, 1998, with a receptor height 1.5 m. The model finds the maximum concentration within the specified period by the user.

Table (2) Maximum Hourly Concentration of the Pollutants Emitted from Multisources of AL-Doura Oil Refinery in August, 1997

day	Max. hourly concentration for SO_2 (ppm)	Max. hourly concentration for NO_2 (ppm)	Max. hourly concentration for CO (ppm)	Max. hourly concentration for Particulate (µg/m^3) with background con.
15	0.454	0.076	1.379	45.617
16	0.474	0.089	1.751	47.682
17	0.446	0.073	1.243	45.603
18	0.474	0.079	1.391	46.319

19	0.489	0.088	1.842	47.944
20	0.473	0.076	1.589	46.312
21	0.449	0.082	1.495	46.129
23	0.482	0.083	1.586	47.479
24	0.404	0.071	1.397	44.058
25	0.433	0.073	1.375	45.084
26	0.462	0.077	1.365	46.540
27	0.474	0.085	1.556	46.953
28	0.459	0.086	1.672	46.897
29	0.481	0.085	1.627	47.924

Table (2) indicates that the maximum hourly concentration of the most pollutants had occurred in 19th August 1997. Maximum hourly concentration for SO_2 has occurred at the hour 15:00 pm, and for NO_2 has occurred at the hour 19:00 pm, and for CO has occurred at the hour 18:00 pm, and for Particulates has occurred at the hour 15:00 pm. These maximum values have resulted for the following case: meteorological data, stability class (C), north-west wind direction, and wind speed vary from (2-4) m/s.
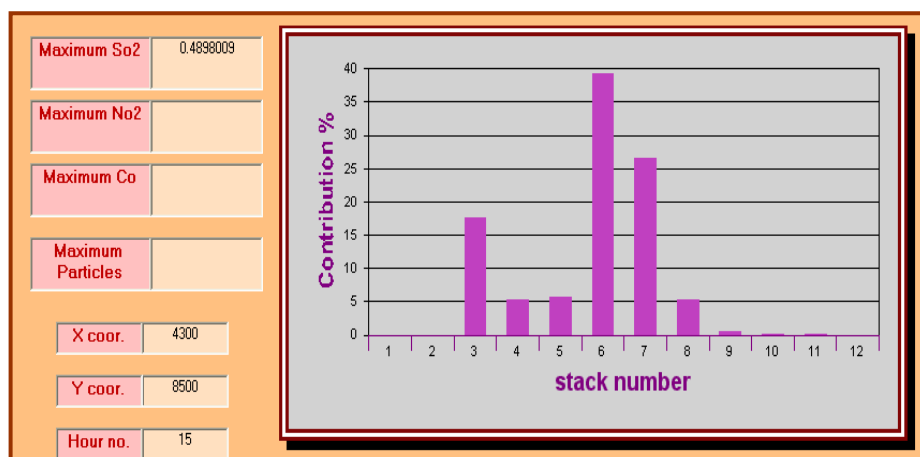
Figure (2) Contribution Analysis for SO_2 in the 19th August 1997 at a Site with Coordinates (4300, 8500) from the Origin Point
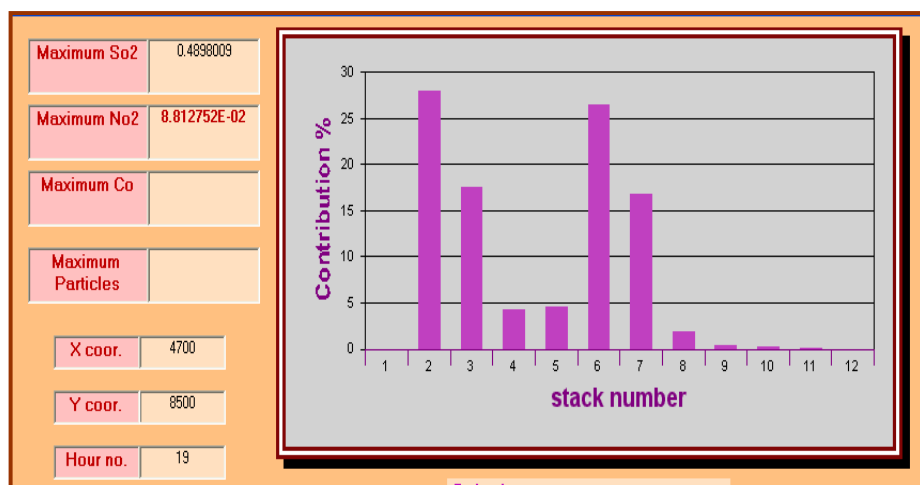
Figure (3) Contribution Analysis for NO_2 in the 19th August 1997 at a Site with Coordinates (4700, 8500) from the Origin Point

4210
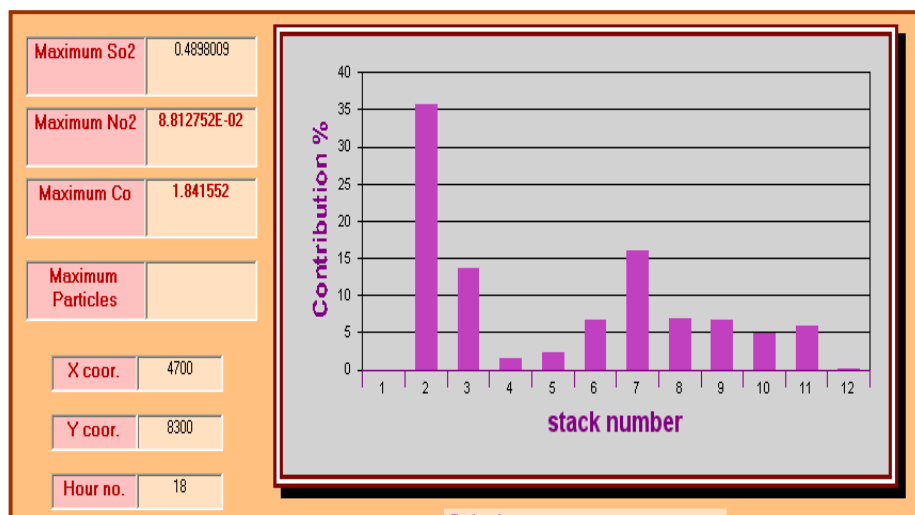
Figure (4) Contribution Analysis for CO in the 19th August 1997 at a Site
with Coordinates (4700, 8300) from the Origin Point
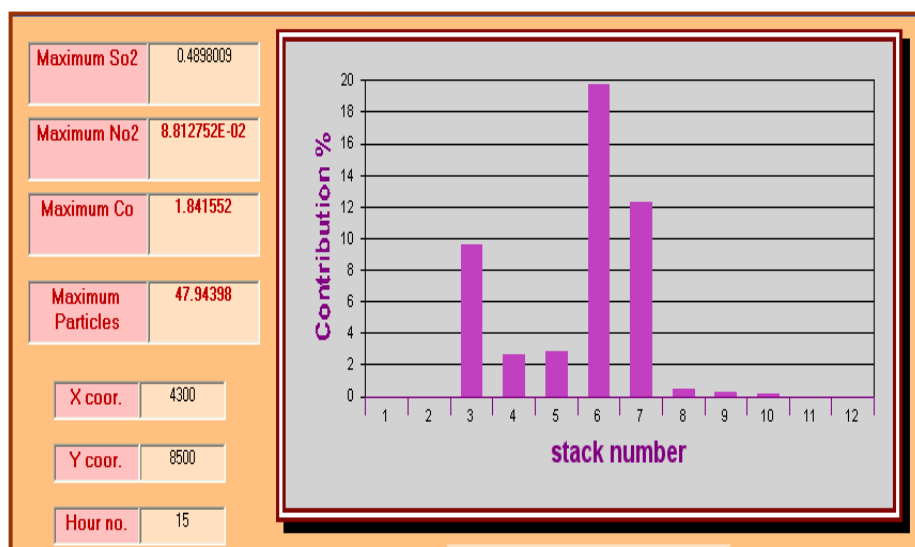
Figure (5) Contribution Analysis for Particulates with Background Concentration

in the 19th August 1997 at a Site with Coordinates (4300, 8500) from the Origin Point
TINs layer of the hourly concentrations resulted from the multisources in 19th August 1997
illustrating resulted different concentrations levels extended through the eastern south area (mostly
agricultures) surrounding AL-Doura oil refinery.

Figure (6) Contour Map for SO2 Concentration Levels, Resulting from Stacks of AL-Doura
Refinery in 19th August 1997 at 15:00 pm

Figure (7) Contour Map for NO2 Concentration Levels, Resulting from Stacks of AL-Doura
Refinery in 19[th]August 1997at 19:00 pm
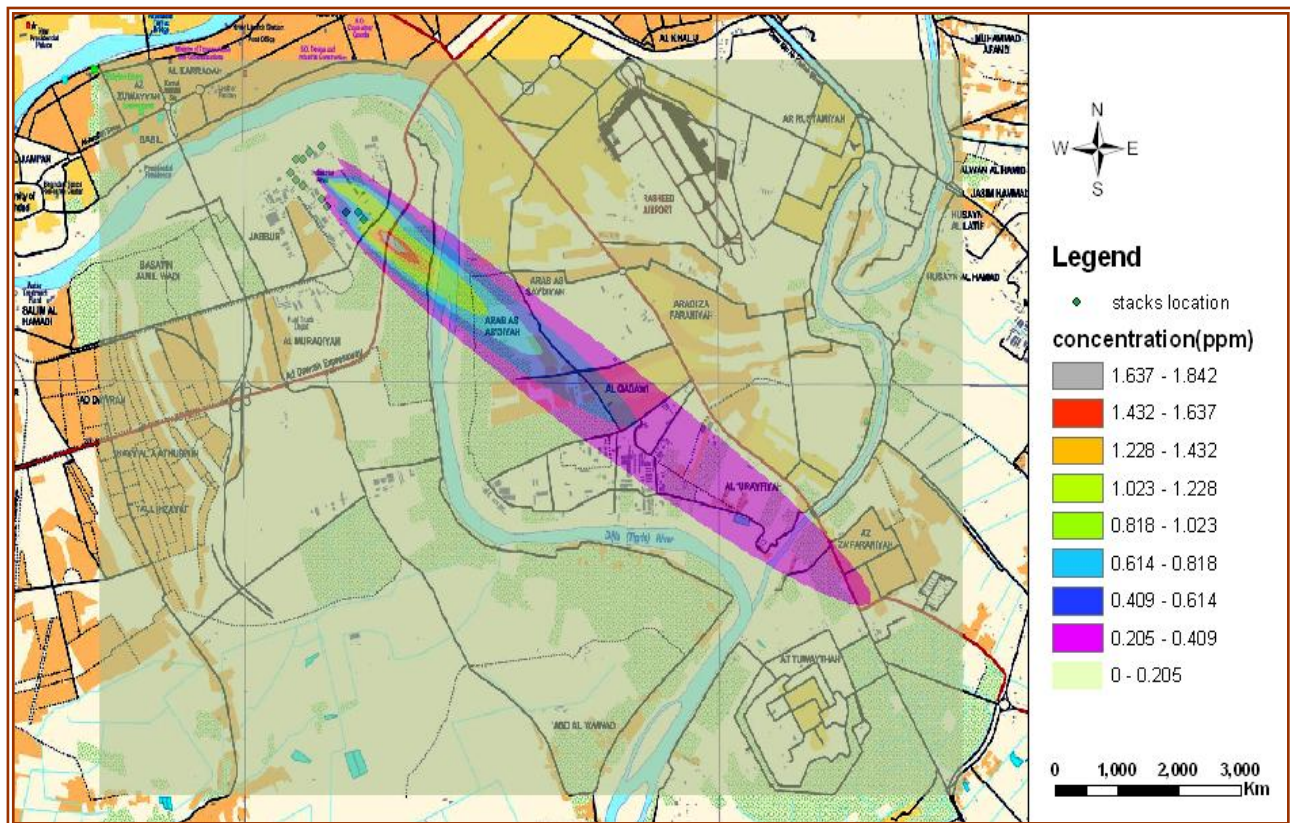
Figure (8) Contour Map for CO Concentration Levels, Resulting from Stacks of AL-Doura Oil Refinery in 19th August 1997 at 18:00 pm

Figure (9) Contour Map for Particulates Concentration Levels with Background Concentration, Resulting from Stacks of AL-Doura Refinery in 19/8/1997at 15:00 pm

* SENSITIVITY ANALYSIS

A sensitivity analysis is the process of establishing the effect of changing the value of an input variable on the model output [Carbon, 2004]. This analysis is performed using the designed model in order to find the effect of different parameters on the dispersion of the pollutants.

The Base Case

The input data of the options of Sensitivity Analysis are selected depending on the results of the contribution analysis. This analysis indicates that, stack number 6 of the AL-Doura oil refinery is responsible for the largest contribution to the maximum hourly concentrations for SO_2, NO_2, CO and Particulates. Meteorological data which cause the maximum hourly concentration for SO_2 (higher concentration than allowable) at 19th August 1997 at hour 15:00 pm is selected for sensitivity analysis.

Sensitivity Analysis for Stability Classes

The effect of atmospheric stability on the hourly concentrations with low wind speed is shown in Figure (10).
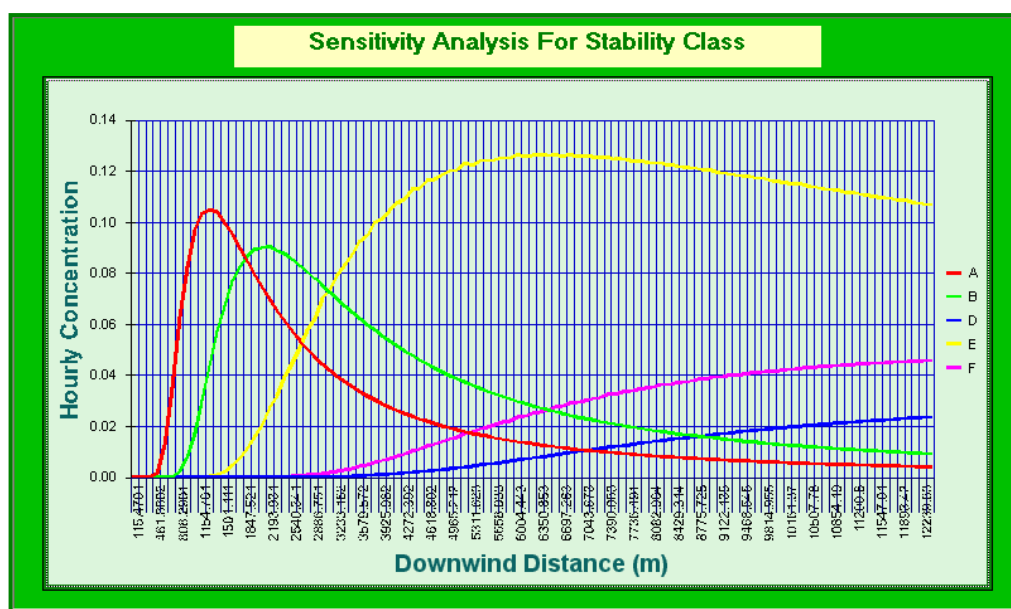
Figure (10) Sensitivity Analysis of SO_2 with Stability Classes Variation

This figure indicate that, the worst weather case condition for dispersion of pollutants with low wind speed is a winter day or an overcast night that is characterized by a slightly stable atmosphere (class E) with distance far away from the source. The other critical weather condition is sunny day (class A) with distance near from the source. Class E with wind speed equal to 0.89 m/s is considered as a critical weather case and will be named such hereafter.

Sensitivity Analysis for Wind Speed

Different values of wind speed are selected to show the influence of the wind speed with low turbulence in reducing the maximum concentration for critical weather (class E, 0.89 m/s) which represents the base case.
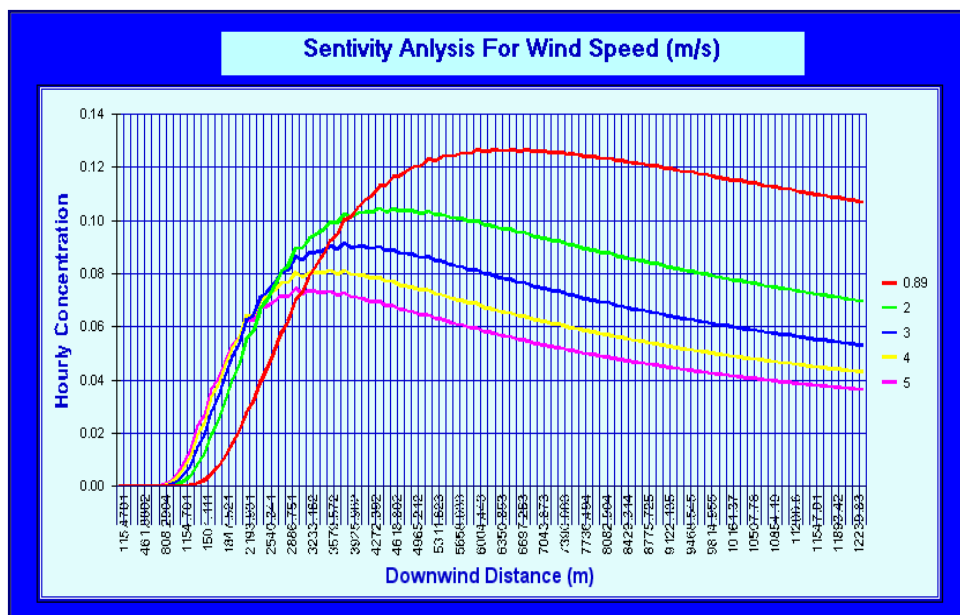
Figure (11) Sensitivity Analysis of SO$_2$ with Wind Speed Variation

The effects of wind speed work in two opposite directions are:
- Increasing wind speed will decrease plume rise, thus increases ground level concentrations; which are observed near from the source.
- increasing wind speed will increase mixing, thus decreasing ground level concentration ,this case is observed far away from the source.

Sensitivity Analysis for Stack Properties

The important parameters for the stacks represent (exit velocity (V_s), exit temperature (T_s), physical height (H_s), and emission rate (Q_s)) are selected. The sensitivity analysis is done by varying one of these properties at each run in order to examine its influence of each one in reducing the concentrations of pollutants. Three cases are selected for each parameter:
- Case 1 (influence of exit velocity on the hourly concentration)
Three cases are selected, V_{s1}=7.4 m/s which represents the base case (stack 6), V_{s2}= 11.1 m/s (1.5 V_{s1}) and V_{s3} =14.8 m/s (2 V_{s1}).
- Case 2 (influence of exit temperature on the hourly concentration)
Three cases are selected, T_{s1} =603 k which represents the base case (stack 6), T_{s1}= 904.5 k (1.5 T_{s1}) and T_{s3} =1206 k (2 T_{s1}).
- Case 3 (influence of physical height on the hourly concentration)
Three cases are selected, H_{s1} =30 m which represents the base case (stack 6), H_{s2} = 45 m (1.5 H_{s1}) and H_{s3} =60 m (2 H_{s1}).
- Case 4 (influence of emission rate on the hourly concentration)
Three cases are selected for emission rate of the SO2, Q_{s1}=198.01 g/s which represents the base case (stack 6), Q_{s2}= 132.007 g/s (Q_{s1}/1.5) and Q_{s3} =99.005 g/s (Q_{s1}/2).
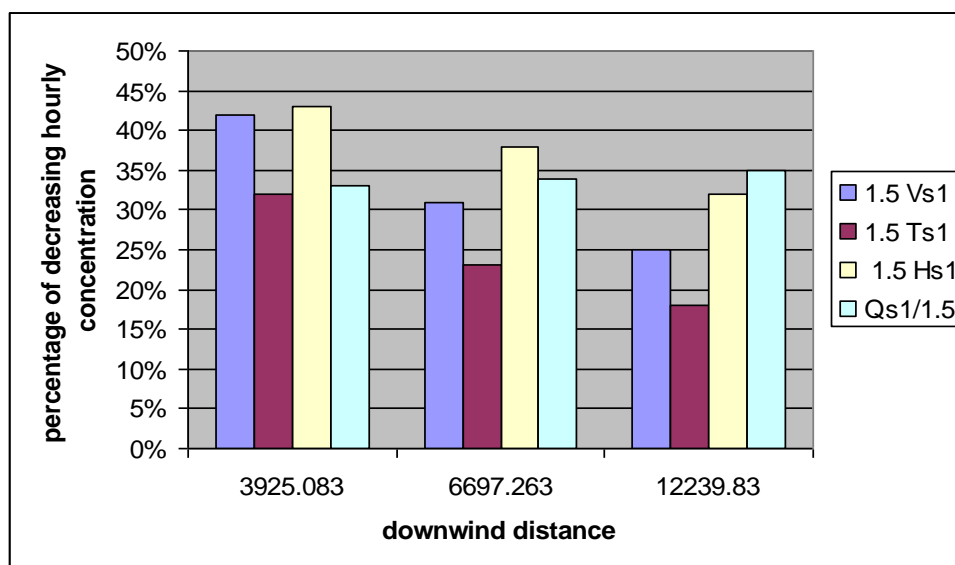
Figure (12) Sensitivity Analysis of 1.5 the Base Case for Vs1, Ts1, and Hs1 and 1/1.5 for Qs1
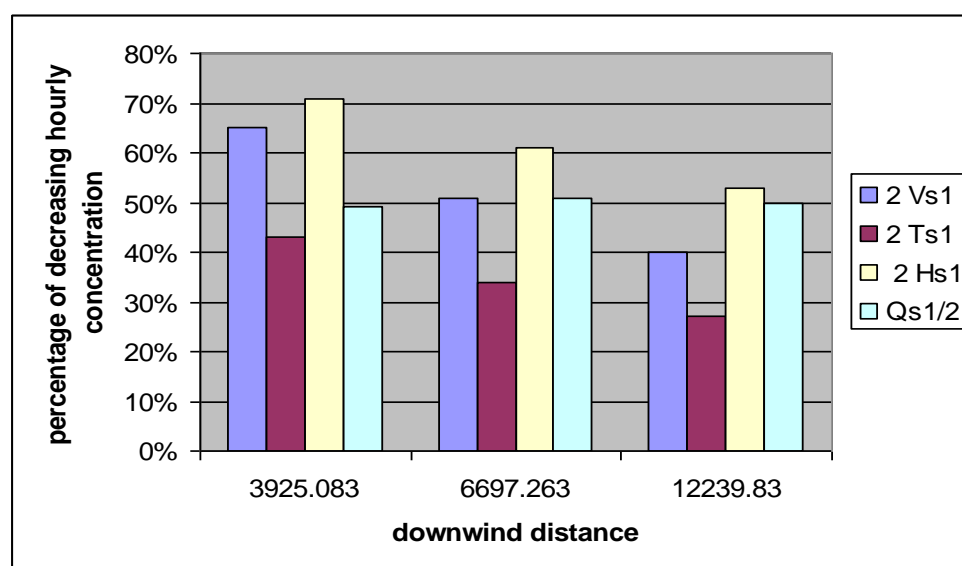

Figure (13) Sensitivity Analysis of 2 the Base Case for Vs1, Ts1, and Hs1 and 1/2 for Qs1

These Figures indicate the followings:
- Near the point source, physical height and exit velocity have higher effect on reducing hourly concentrations for the two cases of increasing these parameters by 50% and 100%.
- Far away from the source, reduction in the emission rate by a factor of 1.5 of the base case (Q/1.5) has decreased the hourly concentrations. While, if an increase in the physical height to twice of its value results in higher effect than the emission rate.

Sensitivity Analysis for Urban Area versus Rural Area
This analysis is done by taking the critical weather case (class E and wind speed is equal to 0.89 m/s) as a base case. Sensitivity analysis applies for two cases, case 1 (rural wind speed profile and Briggs dispersion coefficient for rural area) and case 2 (urban wind speed profile and Briggs dispersion coefficient for urban area).
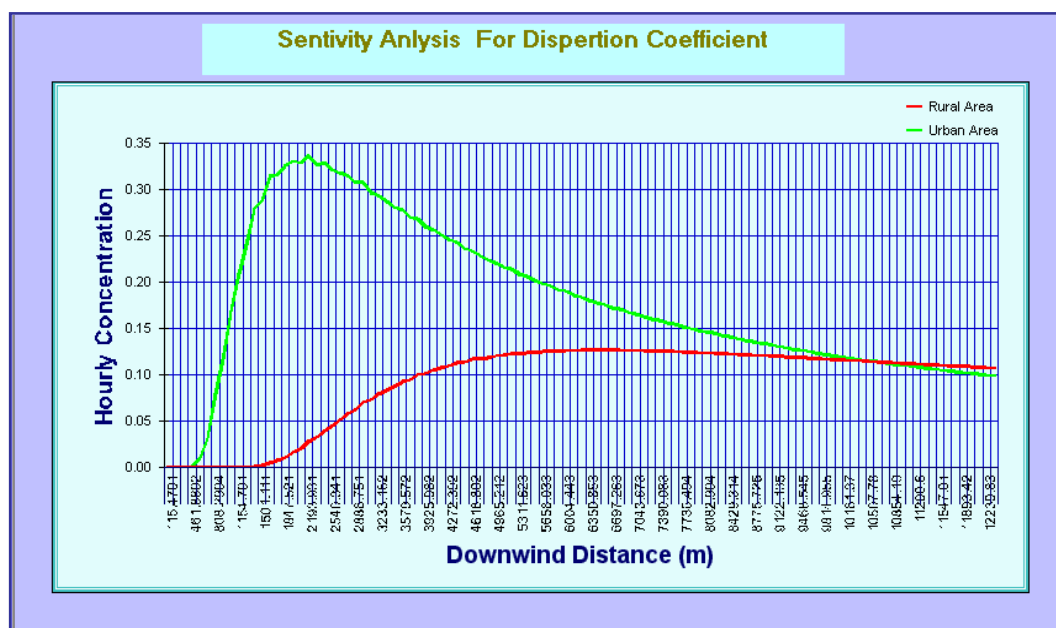
Figure (14) Sensitivity Analysis of SO_2 with Rural Versus Urban

The urban area has a large effect in increasing pollution near from source; this may be due to that, these types of area have more available sensible heat from solar surface heating and combustion sources that destabilize the surface layer of air causing mixing of the plume gases to the ground close to the source.

CONCLUSIONS

• Briggs equation for dispersion coefficients with rural wind speed profile has been found to be most suitable prediction combination for the particular sites chosen for the study; this case has yielded a large index of agreement (error- free predictions).

• The maximum hourly concentrations at the day time during period 15th -21st and 23rd -29th August 1997 for all pollutants indicate that: first maximum hourly concentrations for all pollutants happen under meteorological conditions including slightly unstable (class C) with wind speed varying from (2-10) m/s and with effects of stacks 6 and 2 of AL-Doura oil refinery. These two stacks have maximum contribution on the overall maximum concentration for the pollutant in addition to the effects of stacks 7 and 3.

• The most important observations that can be deduced from sensitivity analysis are:

▪ The effect of turbulence on the reduction of concentrations of pollutants indicated that the worst case weather condition for dispersion of pollutants is characterized by a slightly stable atmosphere (class E).

▪ The effect of point source properties with low wind speed and turbulence indicates that the physical height and emission rate has higher effect to reduce maximum hourly concentration of critical weather case (class E, 0.89 m/s) when increasing these parameters by 50% and 100% base case (stack 6).

REFERENCES:

- Abdulkareem A. S., 2005, " Urban Air Pollution by Computer Simulation: a case study of petroleum refinery company Nigeria", Leonardo Journal of Sciences, No. 6, PP. 17-28.

- AL-Rubai, H. A. G., 1998, "Mathematical Modeling for Dispersion of Air Pollutants Emitted from AL-Daura Oil Refinery Stacks", M.Sc. Thesis, University of Baghdad.

- Awasthi S, Khare M., and Gargava P., 2006, "General Plume Dispersion Model (GPDM) for Point Source Emission", Environmental Modeling and Assessment, No. 11, PP. 267-276.

- Carbon B., 2004, "Good Practice Guide for Atmospheric Dispersion Modeling", Ministry for the Environment, Wellington, New Zealand, ISBN: 0-478-18941-9.

- Kiely G., 1997, "Environmental Engineering", McGraw-Hill Publishing Company.

- Luhar A., Galbally I., and Hurley P., 2004, "Meteorological and Dispersion Modeling Using TAPM for Wagerup Phase 1: Meteorology", Report C/0810 Prepared for Alcoa World Alumina Australia P. O. Box 252, Applecross, Western Australia.

- Matejicek L. , Benesova L., and Tonika J., 2002, "Environmental Modeling in Urban Areas with GIS", Institute for Environmental Studies, Charles University, Czech Republic, Prague.

- Rahmatizadeh Sh., Delavar M. R., and Motesaddi S., 2002, "Design and Development of a Customised GIS for Air Quality Management", publishing in Geomatic, NCC. Tehran, Iran.

- Wikipedia, the free encyclopedia (2008)
http://en.wikipedia.org/wiki/Air_pollution_dispersion_terminology

AN EXPERIMENTAL STUDY OF BURR FORMATION IN DRILLING AND SLOT-END MILLING OPERATIONS

S. A. ALRABII
Department of Mechanical Engineering
University of Technology

الخلاصة

يشمل هذا البحث دراسة عملية لتأثير عوامل القطع الرئيسة على تكوين البروزات الناشئة وانواعها في عمليات التثقيب والتفريز النهائي للمجاري عند تشغيل الصلب الواطئ والصلب المقاوم للصدأ بأستخدام عدد القطع من الصلب عالي السرعات وسائل التبريد. وتم التركيز على علاقة نوع البروز الناشئ ومقاسه مع عوامل القطع. ولهذا فقد تم تطبيق مديات واسعة من سرع القطع ومعدلات التغذية وأعماق قطع لغرض الحصول على أمثل ظروف قطع. وتم قياس أرتفاع البروزات الناشئة وتحليلها عند مختلف ظروف التشغيل لأيجاد تأثير سرعة القطع، معدل التغذية، وعمق القطع على تكوين البروزات الناشئة ومقارنة النتائج التي تم الحصول عليها للصلب الواطئ الكاربوني مع تلك الخاصة بالصلب المقاوم للصدأ. وأستخدمت أقطار مختلفة من المثاقب من نوع الصلب عالي السرعات لملاحظة تأثيرها على تكوين البروزات الناشئة وأعطت القياسات الكمية لأرتفاع البروز الناشئ معلومات مفيدة بسبب تكوين بروزات ناشئة صغيرة وكبيرة منتظمة نسبيا تحت هذه الظروف.

ABSTRACT

This paper presents the results of an experimental study on the influence of the main cutting parameters on burr formation and its types in drilling and slot-end milling operations to machine low carbon and stain -less steels using HSS cutting tools and cutting fluid. Particular attention was focused on the relation between the burr type and size and cutting parameters. Therefore, a wide range of cutting speeds, feed rates, and dept of cuts were investigated to explore the optimum cutting conditions. Burr heights were measured and anal- lyzed at different machining conditions to determine the effect of the cutting speed, feed rate, and depth of cut on burr formation. The data obtained for low carbon steel were compared with those for stainless steel. Different diameters of HSS twist drills were used to observe their effects on drilling burr formation. The quantitative measurements of burrs height yield much useful information because relatively uniform small and large burrs were formed under these conditions.

KEYWORDS
 Burr Formation, Drilling and Slot-End Milling operations, Low Carbon and Stainless steels

INTRODUCTION

Burr can be produced with different machining processes like drilling and milling. It has been defined as an undesirable projection of material beyond the edge of the workpiece due to plastic deformation during machining. In machining, burrs cause several problems for product quality and functionality as they interfere with the assembly of parts, jamming of parts, misalignment, and short circuits in electrical components. It may also reduce the fatigue life and cause safety hazards.

The drilling process produces burrs on entrance and exit surfaces of the workpiece. The entrance burr forms on the entrance surface as material near the drill undergoes plastic deformation. The exit burr is apart of the material extending off the exit surface of the workpiece. Because the exit burr is larger than the entrance burr, this study has only focused on the exit burr. A drilling burr has several different shapes depending on parameters such as workpiece material property [1,2], drill geometry [2,3,4], exit surface angle [5], and process conditions [1,6]. Milling burrs are likely to form along the edges where the tool leaves the work part, namely exit burrs that must be removed by deburring processes to allow the work part to meet specified tolerances. Exit burrs formation in milling process are determined by several parameters including cutter geometry, work part geometry, and material properties, cutting conditions [7], and selected tool feed direction [8].

During metal cutting, the existence of burr not only reduces the dimension and accuracy of the workpiece., but also increases the manufacturing cost. Presently, the burr has been the most troublesome obstruction to high productivity and automation of machining process. Accordingly, for manufacturing advanced precise components, deburring operations are required to remove the burrs. However, in the machining operations the cost of deburring can reach 30% of the total machining cost. Therefore, much work has been carried out aiming to reduce the cost and time consuming of deburring. Research is still going on to improve and automate the deburring processes since fitting a deburring process into FMS with high efficiency and full automation is a difficult problem [9]. Also, understanding of burr formation and mechanism is essential in order to reduce deburring cost by reducing burr formation. In contrast, a few studies have been performed to determine the influence of cutting parameters to assist in the reduction of burrs and the production of free burr components. Thus, to avoid or minimize the burr formation during machining, it is necessary to understand and to have a deeper knowledge on the relationship between the burr formation and the parameters involved in the important machining operations like drilling and milling which are most widely used material removal processes.

Much research has been focused on macro-scale burr formation in drilling and face milling [7,10] but a few researchers have worked on burr formation in slot-end milling processes. Many studies have been conducted on the machinability of carbon steels but few of them concentrates on the problem of burr formation. This paper presents the results of an experimental study on the influence of the main cutting parameters on burr formation and its types in drilling and milling operations to machine low carbon and stainless steels using HSS cutting tools and cutting fluid. Particular attention was focused on the relation

between the burr type and size and cutting parameters. Therefore, a wide range of cutting speeds, feed rates, and depth of cuts were investigated to explore the optimum cutting conditions.

Burrs height were measured and analyzed at different machining conditions to determine the effect of the cutting speed, feed rate, and depth of cut on burr formation. The data obtained for low carbon steel were compared with those for stainless steel. Different diameters of HSS twist drills were used to observe their effects on drilling burr formation. The quantitative measurements of burrs height yield much useful information because relatively uniform small and large burrs were formed under these conditions.

EXPERIMENTAL PROCEDURE

Nomenclature of burrs studied in drilling and end milling operations

This study concentrates on the formation of burrs in drilling and milling operations. Regarding drilling operation, the entrance(minor) and exit (major) burrs positions are on the entrance and exit surfaces, respectively, as shown in **Fig,(1)**[11]. The entrance burrs are generally very small in sizes in comparison with exit burrs at different cutting conditions. While end milling operations produced burrs as shown in **Fig.(2):** burr on the top edge (burr1), exit burrs in the feed direction (burr3 and burr5) as classified and defined by Gillespie [10], and identified experimentally by Olevera and Barrow [7]. The sizes of Burr3 and burr5 were found too small to measure as compared to that size for Burr1. However, this investigation focused only on exit burr in drilling operations and on Burr1 in milling operations because these burrs are larger in sizes and quantity than others and for deburring purposes, they are considered the most important. Burr9 (a rollover burr)does not exit since it is normally formed by the side and end of the face milling cutter, as the tool exits the workpiece over the edge. This burr is actually a series of similar burrs, where each tooth produces a complete burr.

Work materials

The work materials investigated in this work are hot rolled low carbon steel (LCS), St37, and cold rolled stainless steel (SS), AISI316 and both materials are in the annealed condition. These materials were selected because they are widely used in industry for production purposes by drilling and milling operations. They are supplied with the chemical compositions and mechanical properties given in **Table (1)** and **Table (2),** respectively. Rectangular blocks 200 mm in length, 140 mm in width, and 15 mm thickness from these materials were used for studying the burr formation in drilling and milling operations.

Cutting Tools

Firstly, drilling tests were carried out using different high-speed steel (HSS) conventional twist drill diameters (5, 7, 9, 11, and 12.5 mm) in drilling the LCS block at constant medium spindle speed (500 rpm) and lower feed (0.03 mm/rev) to indicate the influence of the drill diameter on the burr formation and its size.

Secondly, other drilling tests were made using only a HSS twist drill of 12.5 mm in diameter in order to obtain burrs with larger sizes for measuring purpose at different cutting speeds and feeds.

Finally, slot-end milling tests were carried out using a HSS end mill of 10 mm in diameter in milling LCS, and SS blocks for burr formation and measuring purposes. Each test consisted of machining of a slot of 50 mm length for different cutting speeds, feeds, and depth of cuts.

Machine Tools

All drilling tests were performed on a CNC drilling machine while end milling tests were performed on a CNC vertical milling machine. A water-soluble coolant (a soluble oil, which is an oily emulsion freely miscible in water), was used as the cutting fluid during drilling and milling low carbon and stainless steels. This cutting fluid is commenly used as a coolant for lubricating and cooling purposes by reducing the harmful effects of friction and high temperatures during drilling and milling operations [12].

Cutting conditions

The cutting conditions considered in drilling and end milling tests were cutting speed, feed rate, and depth of cut. The cutting parameters ranges used in this work are listed in **Table (3)** and **Table (4)** for drilling and slot-end milling stainless steel and low carbon steel, respectively. These parameters were selected according to the prast experience of using high-speed steel (HSS) cutting tools and also to the general recommended working ranges given for speeds, feeds, and depth of cuts used for these tools in drilling and milling operations of low carbon and stainless steels[13]. During each test, only one parameter was varied at a time the one under study its effect on burr formation and its size, while the other parameters were kept unchanged.

Burr Measurements

There are several quantities for burr measurement: burr height, burr thickness, burr volume, and hardness [12]. Burr height and thickness are the most frequently and easily measured burr quantities. There are several methods [15] to measure burr height and thickness, such as contact method, optical microscope method and optical coordinate measurement machine (CMM) method. A surface profilometer, which is usually used for measuring macro-scale surface finish is normally used to measure burr height. Recently, the laser is also used to measure burr height.

For a given set of cutting conditions, the burr size obtained in drilling and end milling tests was highly variable. Then, the average heights of the exit burrs produced in drilling and milling were measured. A large number of measurements were made for each single test in order to obtain reliable results. The burr height was used as a burr size indicator in the present study to take easily a large number of measurements. The height was measured with a dial gage indicator with accuracy of +/- 0.005 mm. The results reported were the

average of 8 to 9 measurements for the height of the exit burrs formed at different positions for each hole and slot in both drilling and slot-end milling tests.

RESULTS AND DISCUSSION

Burr formation and observation in drilling tests

The exit drilling burr has different shapes and sizes depending on the cutting conditions used. From deburring cost point of view, it is important to consider both burr shape and size. **Figures (3)** and **(4)** show burr shapes observed in drilling stainless and low carbon steels, respectively. Three types of burrs formed in drilling both materials. These are uniform burr with a drill cap, uniform burr without a drill cap (transient burr), and crown (petal) burr. These types of burrs are uniform for both materials and they have a relatively small and uniform burr height and thickness around the hole periphery. Furness [16] previously proposed burr formation mechanisms for drill cap and crown burr types matched with corresponding pictures from high-speed video during drilling low carbon steel AISI 1018.

Uniform burr with a drill cap formation

The whole work of the current paper is focused on the formation of the drilling exit burrs since the entrance burrs are generally very small in sizes and difficult to measure when compared with exit burrs at different cutting conditions used for drilling low carbon and stainless steels.

A uniform burr with a drill cap is formed in the final step of drilling and can either remain attached to the workpiece [**Fig.(3)**] or be separated at drill exit [**Fig.(4)**]**.** The formation of the drill cap at the final step depends on the material ductility and process conditions. The most common burr type for ductile material is the uniform burr with a drill cap. In most cases, with reasonable combination of cutting conditions, initial fracture occurs at the outer cutting edge region, not near the drill center, creating a drill cap [1].

Kim et al [2] stated that the drill cap is first formed by plastic deformation of the work material under the chisel edge depending on the drilling thrust force. With drill advancement, the plastic deformation zone expands from the center to the edge of the drill. Finally, the drill cap is created by initial fracture occurs at the end of the cutting edges. The remaining material is then bent and pushed out ahead of the drill to form this type of burr.

Kim and Dornfeld [1] has proposed an analytical model for drilling burr formation mechanism in ductile materials to predict the final burr size of the uniform burr with a drill cap. However, this type of work is beyond the scope of this paper which only focuses on the influencing cutting parameters (cutting speed, feed, and depth of cut) in drilling and milling operations as well as effect of using different drill diameters.

Kim [6] in his preliminary experiment to investigate drilling burr formation on titanium Ti-6Al-4V has also observed a uniform burr with a drill cap during all conditions used. Typical burr shapes identified formed in most cutting conditions were rolled-back burr and leaned-burr. The level of rolling back seemed to be proportional to feed rate and spindle

speed. Crown burr that are formed in high feed rate in steel were never formed. Thermal effect caused by the friction heat is believed to have influenced the types of burrs because of low thermal conductivity of the material and no usage of coolant.

In drilling 304 stainless steel, Guo and Dornfeld [17], have proposed and divided burr formation mechanism into four stages: initiation, development, pivoting point, and deformation stages with cap formation.

Uniform burr without a drill cap (transient) burr formation

As shown in **Fig.(3),** this type of burr formed in the transient stage between uniform burr with a drill cap to a crown burr type, by early fracture, near the end of the cutting edges later than in uniform burr formation (when the material does not have moderate ductility, plastic deformation is limited), creating a larger uniform section. With further drill advancement, the strain at the chisel edge exceeds the fracture strain of the material. Continuous cutting occurs up to the final stage of drilling, creating a uniform burr without a drill cap [**Fig.(4)**]**.**

Crown (petal) burr formation

The crown burr has a large and non uniform burr height. Generally, this type of burr in both materials
has a large and irregular height distribution around the hole. A larger thrust force induces plastic deformation earlier in the process. The thicker material layer beneath the drill undergoes plastic deformation, and a larger maximum strain was induced at the center region of the exit surface leading more likely to an initial fracture, at the chisel edge, resulting in a crown burr. Also, because of inefficient cutting due to drill wear at the outer cutting edges, there is a higher possibility of initial fracture to occur at the center region and thus creating a crown burr.

Effect of drill diameter on drilling burr height

The first attempt was carried out to investigate the influence of using different conventional HSS drill diameters on drilling burr size in terms of height only since burr thickness was difficult to measure due to some technical problems. The reason for that is to ensure evidently that burr can be formed during drilling operations and to select the proper drill diameter that provides a reasonable size for suitably measuring purpose.

Figure (5) shows burr height variation with drill size in drilling low carbon steel at cutting speed of 19.6 m/min and feed of 0.03 mm/rev. It is seen that increasing the drill diameter does greatly affect the burr size. This burr size increase is believed due using higher cutting speed and lower feed and thus causing more material deformation owing to thermal effect in cutting moderate ductile material such as low carbon steel [**see Table (1)**]**.**

Therefore it was decided to choose a 12.5 mm drill diameter to use in the whole drilling tests of this paper. Also, the selection of this drill size is to form enough burr size and to be easily measured in conducting the following drilling and milling tests for low carbon and

stainless steels. However, Kim and Dornfeld [6] in their analytical model noted that increasing the drill diameter has no great influence on burr size (in terms of burr height and thickness) since they have used a smaller drill size (~ 4 mm in diameter) and lower feed (0.08 mm/rev) in cutting stainless steel AISI 304L.

Regarding the burr shape during drilling tests for low carbon steel used in this work with different drill diameters, a uniform burr with a drill cap was only observed and its size increases with increasing the drill diameter at the higher speed (19.6 m/min) and lower feed rate of 0.03 mm/min.

Effect of cutting speed on drilling burr height

Drilling test were carried out for the stainless (SS) material over a cutting speed range 4.9-13.9 m/min and at a constant feed of 0.32 mm/rev using a HSS twist drill of 12.5 mm in diameter and all results are then depicted in **Fig.(6)** which generally indicates that the increase of exit burr (major burr) height with increasing cutting speed. It can be seen that the corresponding burr heights over this speed range are higher and showed a sharp increase in comparison with those obtained for low carbon steel. The lower speed range was used for drilling stainless steel is to prevent the hardness effect of this material on the twist drill and thus avoiding the tool wear during the drilling operations. The behavior of burr height increase during cutting both materials, is attributed to the effect of cutting temperature rise with increasing cutting speed. This will result in more deformation in the workpiece near the exit surface and then more material extension, creating higher burr size.

It must be pointed that in drilling stainless steel, the steep increase in burr height with cutting speed, is related to drilling burr formation mechanism that resulted in the possibility of forming mainly two shapes of burr, namely: a uniform burr with a drill cap and a uniform burr without a drill cap (transient burr), as shown in **Fig.(3)**. A crown burr was not seen during drilling this material at different cutting speeds. Burr shape is important because the burr size, as a result, the deburring cost is greatly dependent on it. These shapes of burrs are found similar to those observed previously [1,2] in drilling stainless steel AISI 304L at low and high cutting speeds. Kim [1] stated that when feed and the cutting speed are low, the drilling burr tends to have a uniform shape along the hole periphery for most materials. The material property of workpiece makes a big difference when the feed and cutting speed increase. When the material has moderate ductility, the material tends to elongate to some extent during burr formation, resulting in a large burr height and burr volume. However, if the material is quite brittle, catastrophic fracture occurs as the feed and speed increase, resulting in irregular burrs having several large chunks, lobes, or petals as shown in drilling the aluminum alloy Al 6061 [1].

Thus, according to **Fig.(6)**, in drilling stainless steel at lower cutting speeds and in this case at higher feed (0.32 m/rev), uniform, small heights of burrs with separated drill cap first produced due to the initial fracture occurred by plastic deformation at the end of the cutting edges. These burrs have irregular shapes because some of the burr material left with the drill cap by a later fracture took place near the workpiece surface because of the drill cap bending when the drill exiting the surface. Also, another uniform burr with attached drill cap formed at medium speed and high feed owing to plastic deformation at the end of

the drill edge. Eventually, a uniform, large, thick, and sharp burr produced at high feed and cutting speed. So, the combined effect of both higher speed and higher feed (higher thrust force) caused the increase of burr height steeply and this behavior is different from that for drilling low carbon steel at various speeds since lower feed of 0.11 mm/rev (lower thrust force) was used, thus creating lower burr height.

It was proposed [14] that burr formation mechanisms for several burr shapes, matched with corresponding pictures observed by a high-speed video while drilling low alloy steel, AISI1018,. The uniform burr has a relatively small, uniform height and thickness around the hole periphery. A drill cap may or may not be formed in the final step of drilling depending on the material ductility, drill geometry, and process condition. The crown burr has large and nonuniform burr height (with irregular height distribution around the hole). Also, the transient burr is a type of burr that forms in the transient stage between the uniform burr with a drill cap and the crown burr and it has a larger burr height than uniform burr but with no cap. Kim [1] has explained the burr formation mechanisms of both uniform burrs with and without a drill cap. As the drill approaches the work exit surface, the material under the chisel edge begins to deform. The distance from the exit surface to the point at which the deformation starts depends mainly on the thrust force during drilling. As the drill advances, the plastic deformation zone expands from the center to the edge of the drill. At the final step, the remaining material is bent and pushed out ahead of the drill to form the uniform burr with a drill cap. If the material does not have moderate ductility, plastic deformation is limited, and fracture occurs early at the center region of the drill. Continuous cutting occurs up to the final stage of drilling, creating a uniform burr but with no cap.

Other tests were also performed for drilling the low carbon steel (LCS) material over a cutting speed range 3.5-27.9 m/min and at a constant feed of 0.11 mm/rev using a new HSS twist drill with 12.5 mm in diameter and all data determined are illustrated in **Fig.(6)** which also shows that the exit burr height increased with cutting speed increase. Burr heights are seen to be lower in comparison to those found for stainless steel. Also, two types of burr shapes as shown in **Fig.(4)** were mainly observed during cutting over this speed range. At lower cutting speeds, a uniform burr with separated drill cap formed while a transient burr (a uniform burr without a drill cap) produced at higher speeds. But, the uniform burr with a drill cap as shown in **Fig.(3)** during cutting stainless steel, was not observed over this speed range. The burr formation mechanisms of these shapes are the same as those described earlier [1,2] in this section and they formed at different cutting speeds except that lower feed (0.11 mm/rev) was used. And, the reason for lower burr sizes obtained in drilling low carbon steel is more likely owing to the less ductility of this material when compared with stainless steel material.

Effect of feed on drilling burr height

Regarding the feed influence on burr height in drilling tests of stainless steel (SS) over a feed range of 0.08-0.22 mm/rev and at a chosen moderate cutting speed 9.8 m/min, the results found are depicted in **Fig.(7)** which indicates clearly that burr height first increased at a feed of 0.11 mm/rev, then decreased to a minimum value at a feed of 0.16 mm/rev, and later increased sharply with increasing feed up to 0.22 mm/rev. The explanation for this

variation in burr height is thought to be due to burr shape change since at a feed range of 0.08-0.11 mm/rev, the burr formed is seen to be large and has a uniform shape with no drill cap (transient burr) as shown in and described by Kim [1]. While cutting at moderate feed of 0.18 mm/rev, a uniform burr with separated drill cap produced and it is thin with a very small height since the increase in feed as mentioned earlier [1,2], resulted in expanding the plastic deformation zone from center to the tool edge and thus initial fracture occurs at the end of the cutting edges, creating the drill cap that separated from the workpiece. In addition to that, when the drill approached the workpiece exit surface, this fracture is most probably occurred too near this surface and that is why less material left as a burr adhered to the exit surface and around the hole periphery. In order to ensure that the behavior of height to be very small at this cutting condition, the drilling test using same speed and 0.16 mm/rev, was repeated and a similar result was obtained (burr is very small and has a uniform shape with separated drill cap).

By further increase in feed up to 0.22 mm/rev, burr height raised sharply because of the formation of a large thin transient burr or uniform burr with no drill cap. This trend is attributed to higher thrust force effect induced and thus more material being removed by plastic deformation, causing a fracture in the center region of the drill and thus producing a large burr height. Also, the burr formation mechanisms of these two types of burr shapes are same as for those stated in the last section.

Other drilling tests were achieved for low carbon steel at a cutting speed of 19.6 m/min and over a feed range 0.16-0.45 mm/rev using a new HSS drill with 12.5 mm in diameter. **Fig.(7)** illustrates that burr height is lower at lower feed since the tool is fresh and new with no wear on its cutting edges but then its height increased with feed increase. This trend is believed that at a feed over 0.22 mm/rev, burr height increased owing to more plastic deformation caused by higher thrust force. During the feed range of 0.16-0.22 mm/rev, a small uniform burr with separated drill cap formed whereas a transient burr or a large uniform burr without a drill cap produced during cutting over this feed range as shown in **Fig.(4)**. And, the reason for lower burr size obtained in drilling low carbon steel is more likely due to the effect lower ductility of this material when compared with the stainless steel material.

Concerning the work of this paper, the rolled-back and leaned-back burr types observed by Kim [6], were not seen during drilling low carbon and stainless steels. This is more likely due to the effect of application of coolant which has reduced the thermal effect caused by the friction heat generation when there is no cutting but deformation as in the final stage of burr formation. Also, the higher heat conductivity of steels than titanium alloy enhances slow heat conductive dissipation to the workpiece. Therefore, the temperature rise will be lower in the region near the inner wall of the burr. This will reduce the material expansion and contribute to form a uniform burr with a drill cap instead of rolling or leaning back burr type.

Burr formation and observation in slot-end milling tests

The typical slot-end milling process is depicted in **Fig.(8)**[18]. The surface along the bottom of the slot will be scalloped. As the tool passes through the workpiece, each tooth

creates a semi-circular scratch along the bottom of the slot. Thus, the bottom surface will be scalloped. The length of each slot was 50 mm for each milling test.

All slot-end milling tests exhibited clearly formation of burr1 on the top edge of the workpiece surface. It was relatively small, uniform along the test length and their shape looks like protrusion with variable height while, burr3 and burr5 produced when the tool exits the workpiece (in the feed direction). However, burr3 and burr5 were not considered in the present work because of their measuring limitations and since they were too small in sizes when compared to burr1. Therefore, this study concentrated on burr1 formation which is considered the most important for deburring purposes since it is larger in size and presents in large quantities. In each test, a new tool was used to avoid the effect of the tool wear.

Gillespi [10] investigated the effect of cutting parameters on the size of burrs produced in end milling and explained the formation mechanisms for these burrs. He concluded that burr1 (poisson burr) is the result of lateral deformation caused when the tool enters the workpiece. The material tends to bulge at the sides when it is compressed until permanent plastic deformation occurs. Burr3 and burr5 are rollover burrs formed, however their sizes vary noticeably due to the variation of exit angle as the tool leaves the workpiece.

Wright et al [19] reported formation of three different burrs in slot-end milling : exit burr (burr5), side burr (burr3), and top burr (burr1), which occur along (1) the edge between the machined surface and the exit surface, (2) the edge between the transition surface and the exit surface, and (3) the edge between the top surface and the transition surface.

Landers et al [20] stated that, in milling, three major burr types (poisson, rollover, and tear) form due to workpicec plastic deformation. When the cutting tool edge extends over a workpiece edge, material is compressed and may flow laterally forming a poisson burr. Rollover burrs form when the cutting tool exits the workpicec and the chip tends over the edge instead of being cut. If the chip is torn from the workpiece, instead of being sheared off, some material from the chip will be left on the workpice. The material is known as a tear burr. A combination of the poisson and tear burr can end up as a so-called top burr or entrance burr along the edge of top workpiece when a tool cuts a slot or along the periphery of a hole when a tool enters a workpiece [12]. In conventional cutting process, these top or entrance type burrs are substantially smaller than exit burrs so that usually no deburring process is necessary.

In the present work, the slot-end milling test produces the following burr1 (top burr) morphologies at the machined surface: (1) knife burr type or uniform (primary burr), (2) wave-type (primary burr), and (3) secondary burrs as shown in **Fig.(9)**. Knife edge burrs are the largest burrs encountered in this type of milling. They are characterized by uniform height and thickness that is small relative to their height, gives them a laminar appearance. Wave-type burrs are believed to have the same formation mechanism as knife burrs, but are slightly smaller and do not have uniform height [**Fig.(9)**]**.** Secondary burrs are generally not periodic with respect to the feed marks on machined surface, and their size is often one order of magnitude smaller than knife or wave-type burrs (primary burrs)[21].

Hashimura and Dornfeld [22] noted, in face milling process, that uniform burrs are formed due to cumulative leaning of the transition material that is pushed by the tool flank during each successive pass. The cumulative burr (knife burr) formation mechanism under tool exit condition was presented. The exit burr forms as plastically deformed transition material is leaned down towards the machined surface as opposed to rollover of the chip. The ability of the back-up material to carry the cutting forces controls the burr and chip formation processes which are two separate processes. The cumulative deformation of the transition material explains the uniform height of the knife burr, which is approximately equal to the depth of cut.

Effect of cutting speed on slot-end milling burr height

In slot-end milling at cutting speed range of 5.1-12.2 m/min for low carbon steel (LCS) and 3.8-9.3 m/min for stainless steel (SS) at constant feed rate and depth of cut, **Fig.(10),** shows that burr1 (top burr or poisson burr) is formed in all cases, small in size, and uniform along each test length. The burr1 height increased from 0.09 to 0.15 mm for low carbon steel and from 0.08 to 0.10 mm for stainless steel with increasing speed. The burr formation for both materials is more likely a result of lateral plastic deformation due to the thermal effect that increased with increasing cutting speed. This indicates that more generated heat is dissipated and transferred by conductivity to sides of the slot at low feed rate of 14 mm/min, higher cutting speed and depth of cut of 2 mm. Also, the difference in burr1 size between these materials is owing to the difference in their mechanical properties and structures. This means that stainless steel exhibited more resistance to the cutting temperature influence than low carbon steel with speed increase.

Regarding burr1 types, similar observations to those mentioned by Avila and Dornfeld [21], are indicated in the present study. It is noted in that, at any cutting speed for each material, burr1 shape and type depend on its height. A knife edge burr (primary burr) type that only formed at the top of the round edge of the slot, is sharp look like a straight protrusion, thick, and large in size. Whereas a wave burr (primary burr) type that formed along the top edge of both sides of the slot, is curled, thin, and small in size **(see Fig. (9)).** In addition, secondary burr due feed marks at the bottom of the slot surface, is also seen with very small size but this type together with burr3 and burr5 are out of focus of the this work due to the practical difficult problems in measuring their sizes.

Effect of feed rate on slot-end milling burr height

Fig. (11) reveals that at lower feed rates, burr1 sizes are high for both materials. These burrs are only formed by lateral plastic deformation owing to the dominant thermal effect at high cutting speed. At higher feed rate, burr1 height remains unchanged for low carbon steel (LCS) but for stainless steel (SS), it is steadily decreased from 0.13 to .0.05 mm. The stability of burr1 for low carbon steel at higher feed is attributed to more cutting temperature rise at higher speeds and an accompanying increase in thrust force that pushing high amount of material being removed at high feed and depth of cut. Whereas, for stainless steel, the reduction of burr1 is more possibly due to the higher resistance of this material to shearing action than low carbon steel. Therefore, smaller chip is removed and thus creating less burr1 in size.

So, the behavior of burr1 for low carbon steel with varying feed rates is not similar to that observed in Olevra and Barrow work [7] in face milling of medium carbon steel but for stainless steel, it is found identical because they concluded that burr1 height decreased as the tool feed rate increased. This burr is formed by lateral deformation of the material when the cutting tool edge enters the workpiece. They demonstrated this trend in terms of the ploughing effect since at the beginning of the cut, the milling cutter starts with zero cut thickness and therefore no actual shearing of the material occurs. Instead, the material is plastically deformed and pushed underneath the tool. This plastic deformation facilitates the formation of burr1. Thus, at low feed rate, the tool takes longer to start cutting properly due to the small cut thickness and therefore the ploughing effect is increased. While, at high feed rate, the proper cutting action starts earlier (the cut thickness rises more rapidly) and as a consequence the ploughing effect is reduced, hence burr1 is smaller at high feed rate.

In addition, Gillespie [10] in his investigation the influence of machining variables on the size of burrs in end milling,found that feed rate and tool sharpness are the most significant variables affecting the size of burrs produced in this operation. Low feed rates and dull tools resulting in higher and thicker burrs. He also concluded that burr1 is the result of lateral deformation caused by the tool enters the workpiece (poisson burr).

As mentioned in section 3.6, similar shapes of burr1 (knife edge and wave burrs that are noted in previous work [19] at the top of the round edge and sides of the slot, respectively) are also formed over the feed range used in this work for slot-end milling each material.

Effect of depth of cut on slot-end milling burr height

Regarding the influence of depth of cut on slot-end milling burr1 height, slot-end milling tests were also conducted for both materials over a depth of cut range 0.5-2.5 mm at a constant cutting speed of 6.6 m/min and a cutting feed rate of 22 mm/min. **Fig. (12)** illustrates that for low carbon steel (LCS) and stainless steels (SS), burr1 heights are slightly increased almost with increasing the cutting depth. However, at lower cutting speed and feed rate, the depth of cut has little influence on burr1 height because of the temperature and thrust force effects on the plastic deformation of both materials.

These results are identical to ones reported previously by Olevra and Brrow [7] who determined that an increase in the axial depth of cut led to an increase in burr1 height. They interpreted these results according to the observation of Gellespie [10] for the effect of depth of cut on burr1 (poisson burr), Burr1 that forms by lateral deformation of the workpiece material under pressure of the cutting edge, will only form when the cut thickness is sufficiently large so that there is more resistance for the material ahead of the cutting edge to flow in the chip direction (parallel to the cutting edge), i.e. burr1 forms because of the material being displaced by the cutting edge is restricted to the flow mainly in the lateral direction. The foregoing helps to explain the trend shown in **Fig. (12)** for both materials in this work. When the depth of cut increases, the total amount of material being displaced by the cutting edge rises proportionally. Being restricted to flow mostly in a direction parallel to the cutting edge, this will result in larger burr1 size.

Concerning the burr1 shapes, it is found that knife edge and wave burrs, similar to those stated previously [21], are formed at the top of the round edge and sides of the slot with increasing cutting depth for both steels utilized in this experimental study.

Thus, drilling and end-slot milling operations conducted in this work revealed that the burr formation can
cnot be avoided or eliminated but it can be minimized by applying certain cutting conditions at lower and higher levels of cutting speeds, feed rates, and depth of cuts. This is attributed to the additional infuences of cutting forces and temperature during its formation causing material plastic deformation. However, the variations in burr heights obtained in this work are strongly related to its type observed at each cutting conditions. Accordingly, in order to eliminate burr formation during cutting, different strategies have been recently applied [3-5] and focused on the effect of other cutting parameters such as: tool design and angles, work part material property and geometry, tool path and feed direction. Also, much attention has been paid for complete understanding of burr mechanisms [21,22], optimizing and controlling [2,15], and modeling [17] burr formation.

CONCLUSIONS

The following conclusions were gained when conducting this experimental study on burr formation in
drilling and slot-end milling operations:

- It found that a HSS twist drill with a larger diameter provides a higher exit burr height and this is normally due to more material to be removed by plastic deformation owing to higher thermal and cutting forces effects during the drilling operation.

- Drilling tests for low carbon and stainless steels revealed formation of two types of exit burrs changing in shape (uniform burr with a drill cap and transient or uniform burr without a drill cap). Crown or petal burr was not during cutting over different levels of cutting speeds and feeds.

- In drilling tests, it was found that the exit burr height for both materials influenced greatly by the cutting speeds and feeds because relatively uniform small and large burrs with various shapes were formed.

- In slot-end milling tests, burr1 (top burr), burr3, and burr5 are formed during slot-end milling tests for low carbon and stainless steels over cutting at various levels of cutting speeds, feed rates, and depth of cuts.

- It is appeared that the shapes of burr1 were same during cutting at different speeds, feed rates, and depth of cuts and it consisted of: a knife burr type or uniform (primary burr) with a largest size over the round edge of the slot, a wave burr type (primary burr) with smaller and different heights over the whole top straight edges of the slot.

- Slot-end milling tests exhibited that the height of burr1 was generally found to be less than 0.15 mm for low carbon steel and less than 0.10 mm for stainless steel.

ACKNOWLEDGMENTS

REFERENCES

- Kim, J. and Dornfeld, D. A., " Development of an Analytical Model for Drilling Burr Formation in Ductile Materials", *Transactions of the ASME,* vol.124, 2002, pp.192-198.

- Kim, J., Min, S., and Dornfeld, D. A. ," Optimization and Control of Drilling Burr Formation of AISI 304L and AISI 4118 Based on Drilling Burr Control Chats", *Int. J. of Machine Tools & Manufacture,* 41, 2001, pp 923-936.

- Dechow. H., "Influence of Tool Geometry on Hole Quality When Drilling Ti-6Al-4V", *LMA Report,* 1998.

- Ko., S. –L and Chang, J. E., " Development of Drill Geometry for Burr Minimization in
- Drilling *", 2nd. Asia Pacific Fourm on Precision Surface Finishing and Deburring Technology*,
- 22-24,2002, pp135-150.

- Min, S., Dornfeld, D. A., and Nakao, Y., " Influence of Exit Surface Angle on drilling Burr
- Formation*", J. of Manufacturing Science and Engineering*, vol. 125, Nov. 2003, pp. 634-644.

- Kim, J., " Preliminary Experimental of Drilling Burr Formation in Titanium Alloys ", *LMA Report,* 1998.

- Olevra, O. and Barrow, G., " An experimental Study of Burr Formation in Square Shoulder Face Milling " , *Int. J. of Machine Tools & Manufacture,* vol. 36, No.9 , 1996, pp. 1005-1020.

- Chu, C. H., " Exit Burr Minimization by Selecting Tool Feed Direction " ,*LMA Report,* 1998.

- Choi, I. H. and Kim, J. D., " Electrochemical Deburring System Using Electroplated CBN Wheels ", *Int. J. of Machine Tools & Manufacture",* vol. 38, No. 1-2, 1998, pp. 29-40.

- Gillespie, L. K., " Burr produced by end-milling*", Bendix Report BDX-613-1503*, 1976.

- Donaldson, G., Lecain, G. H., and Gpoold, V.C., "Tool Design", *TATA McGraw-Hill Publishing Co., 3rd edition, 2000.*

- Lee, K. and Dornfeld, D. A*.,* " Micro-burr formation and minimization through process
- Control ", *Precision Engineering* 29 (2005) pp.246-252.

- Degarmo, E. P., "Materials And Processes In Manufacturing", *Macmillan Publishing Co*., 1988.

- Kalpakjia, S.,"Manufacturing Processes For Engineering Materials", *Addison Wesly*, 2000.

- Kim, J., " Optimization and control of drilling burr formation in metals *", Ph.D. Dissertation*,
- *Department of Mechanical Engineering, University of California at Berkeley*, 2000.

- Furness, R., High Speed Video of Drilling Burr Formation., *AMTD, Ford Motor Company*,
- 1998.

- Guo, Y. B., and Dornfeld, D. A.,**"** Finite element modeling of burr formation process in drilling 304 stainless steel", *J. of Manufacturing Science and Engineering*, vol.122, Issue 4, pp. 612-619, Nov.2000.

- Lee,K. and Dornfeld, D. A., " A study of surface roughness in the micro-end-milling process",
- *Laboratory for Manufacturing Automation, paper Kiha-03*,2004.

- Wright P. K., Dornfeld D. A., Wang, F. C., and Chu C. H., " Decision making in a multi-constraint agent-based process planning*", Trans. of NAMRI, vXXVII , 2000.*

- Landers, R. G., Ulsoy, A. G. and Furness, R. J., " Process monitoring and control of machining operations ", *Mechanical Systems Design Handbook, O: D. I. Nwokah and Hurmuzlu (eds.), CRC Press, Chapter 6, pp. 85-119*, 2002.

- Avila, M. C. and Dornfeld, D. A.," On the face milling burr formation mechanisms and minimization strategies at high tool engagement ", *Laboratory for Manufacturing Automation, paper Miguel (-2-03),* 2004.

- Hashimura, M. and Dornfeld, D. A., " Proposal of burr classification method based on the formation mechanisms in face milling*", J. Japan Society of Precision Engineering, Vol. 65, 6, pp. 872-87,1999.*

Table (1): Chemical compositions of the work materials (produced by the material manufacturers in wt% for each element).

Work material type	%C	%P	%S	%Mn	%Si	%Cr	%Ni	%N
Low carbon steel (ST37)	Max 0.17	Max 0.045	Max 0.045	Max 1.25	Max 0.045	~	~	Max 0.01
Stainless steel (AISI316)	Max 0.08	Max 0.045	Max 0.030	Max 2.00	Max 0.75	18.00 – 20.00	8.00 – 12.00	Max 0.10

Table (2): Mechanical properties of work materials.

Property / Material	Yield strength (MPa) min	Tensile strength (02%proof) (MPa) min	Elongation (% in 50 mm) min	Brinell (HB) Hardness max
Stainless Steel (AISI316)	205	515	40	217
Low Carbon Steel (ST37)	210	380	25	108

Table (3): Cutting conditions used for drilling operation.

Material	Cutting speed (m/min)	Feed (mm/rev)
Stainless Steel (AISI316)	4.9-13.9	0.08-0.32
Low carbon steel (ST37)	3.5-27.9	0.11-0.45

Table (4): Cutting conditions used for slot-end milling operation.

Material	Cutting speed (m/min)	Feed (mm/rev)	Depth of cut (mm)
Stainless Steel (AISI316)	**3.8-9.3**	**14-56**	**0.5-2.5**
Low carbon steel (ST37)	**5.1-12.2**	**14-90**	**0.5-2.5**
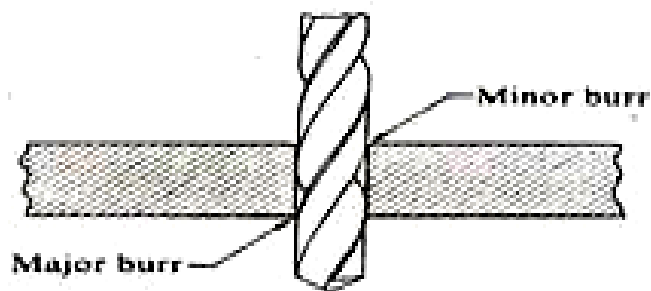
Figure 1 Minor (entrance) and major (exit) burrs positions in a drilling operation [11].
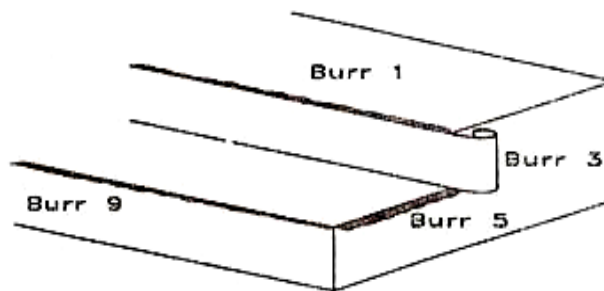
**Figure 2 Types of burrs formed in a milling operation
[10]
burr1 : top burr, burr3 and burr5 : exit burr
burr9 : rollover burr**

Uniform burr with
a drill cap

Uniform burr with
separated drill cap

Uniform burr
without a drill cup
(transient burr)
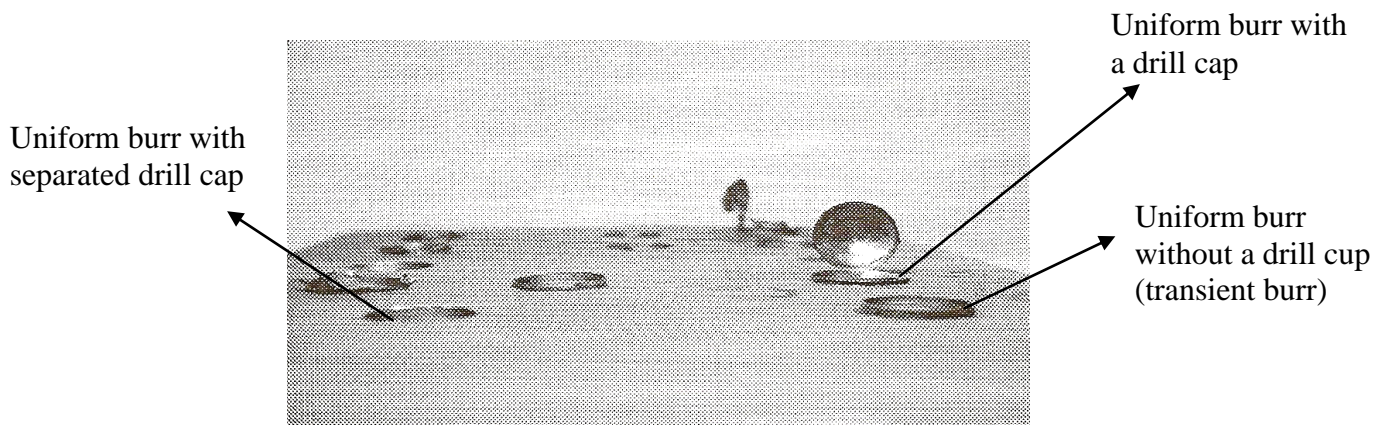
Figure 3 Photograph of the drilling stainless steel plate after machining.

Uniform burr with
separated drill cup

Uniform burr without
a drill cup (transient
burr)
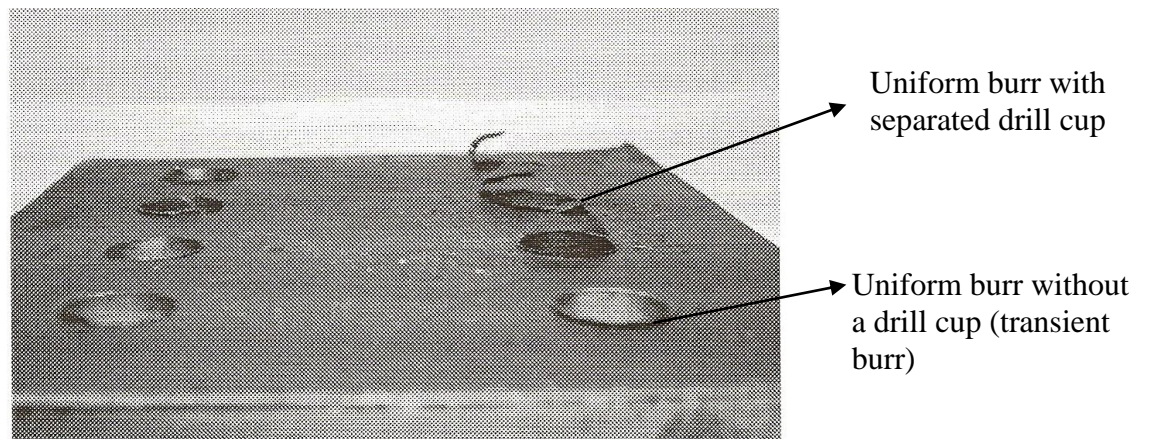
Figure 4 Photograph of drilling low carbon steel plate after machining.
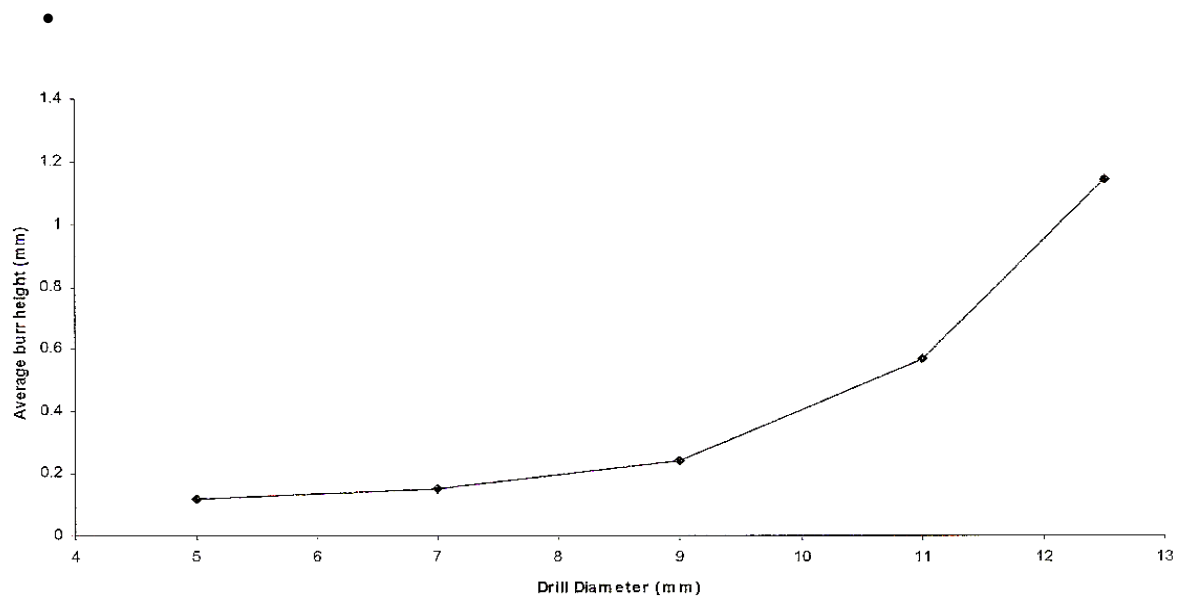
Fig.(5) Effect of using different HSS twist drill diameters on burr height in drilling low carbon steel at a cutting speed of 19.6 m/min and a feed rate of 0.03 mm/rev.
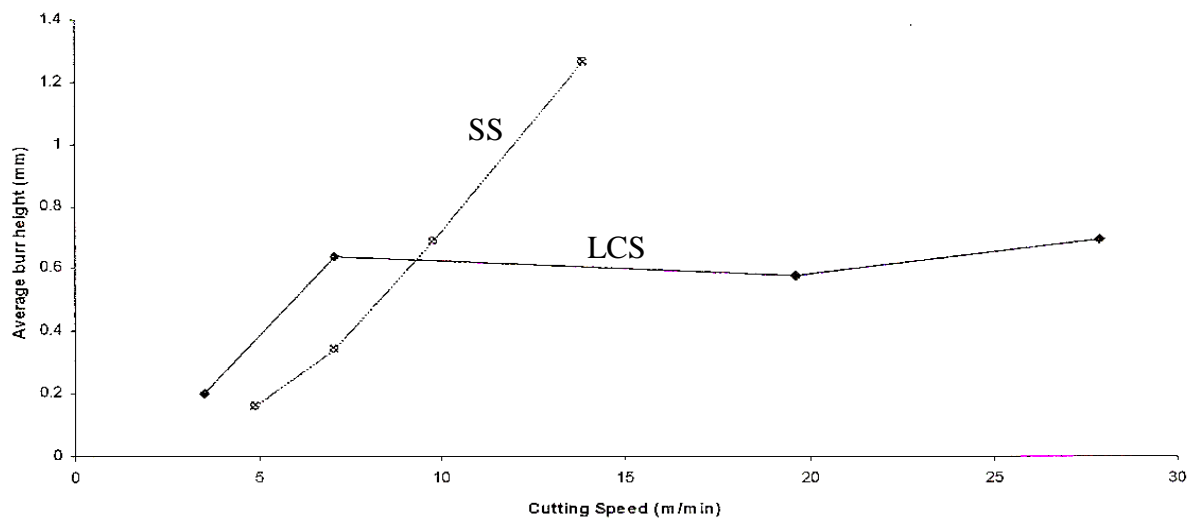
Fig.(6) Effect of cutting speed on burr height in drilling low carbon steel (at a cutting feed of 0.1 mm/rev) and steels (at a cutting feed 0.32mm/rev) with 12.5 mm drill dia.
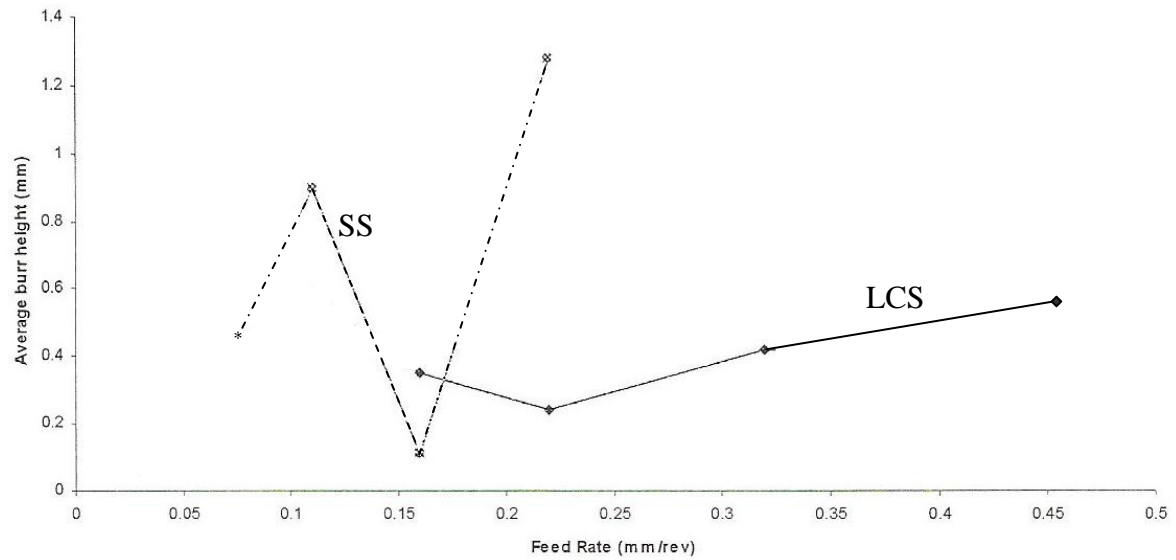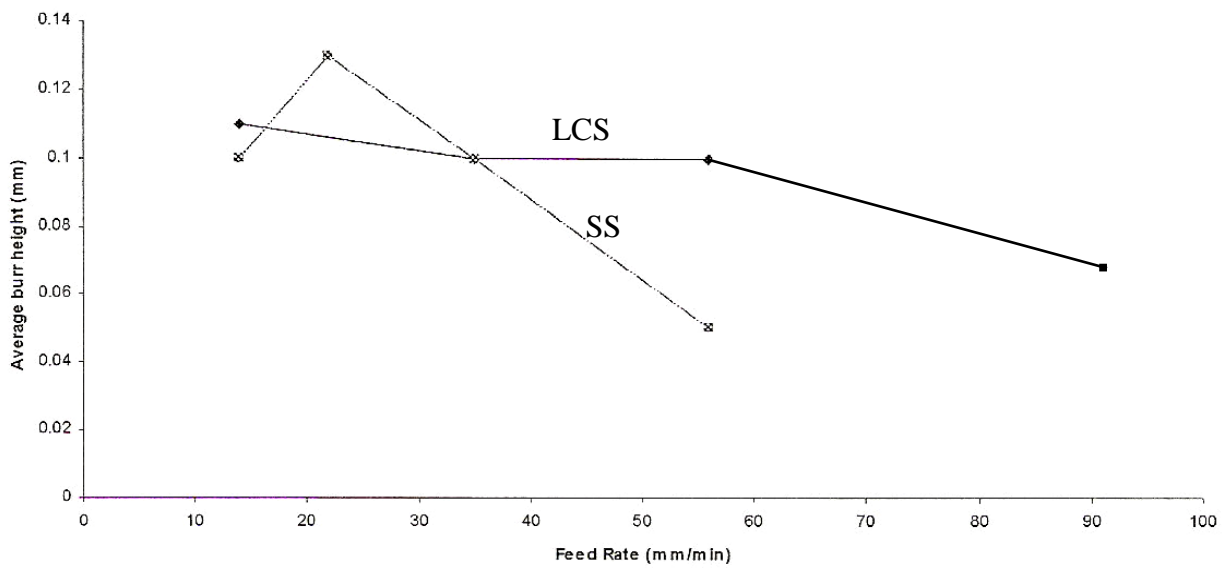
Fig.(7) Effect of cutting feed on burr height in drilling low carbon steel (at a cutting speed of 19.6 m/min) and stainless steel (at a cutting speed of 9.8 m/min) with 12.5 mm drill diameter.
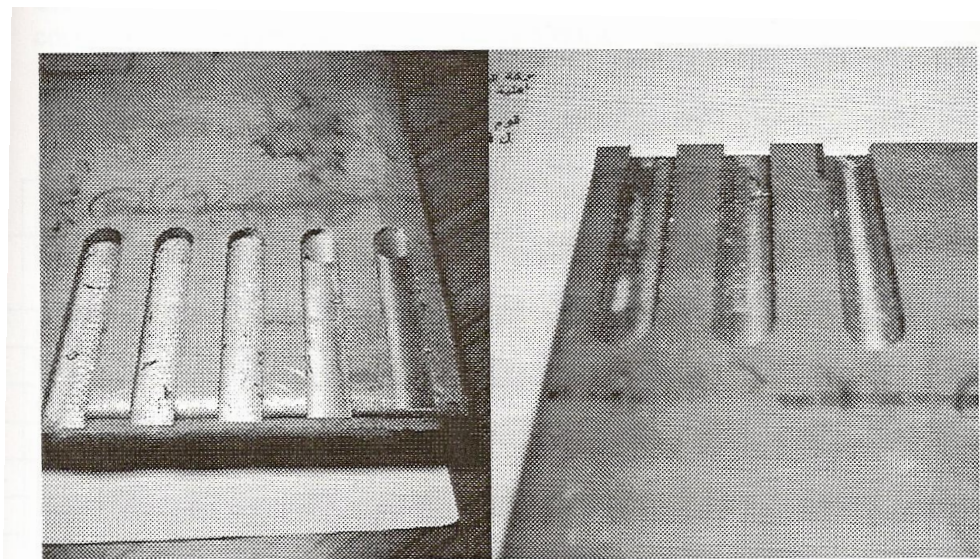

Figure 8 Photograph of milling stainless steel plate after machining.

→ Knife edge burr

→ Secondary burr

→ Wave type burr
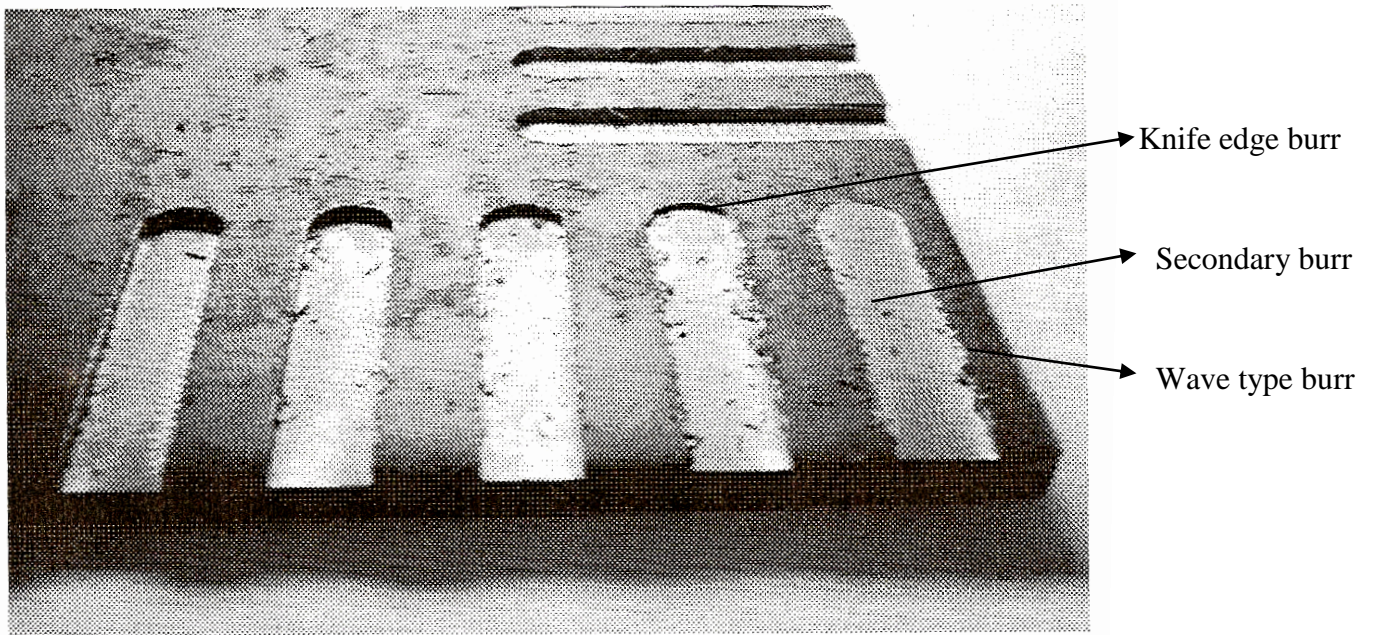
Figure 9 Photograph of milling low carbon steel plate after machining.
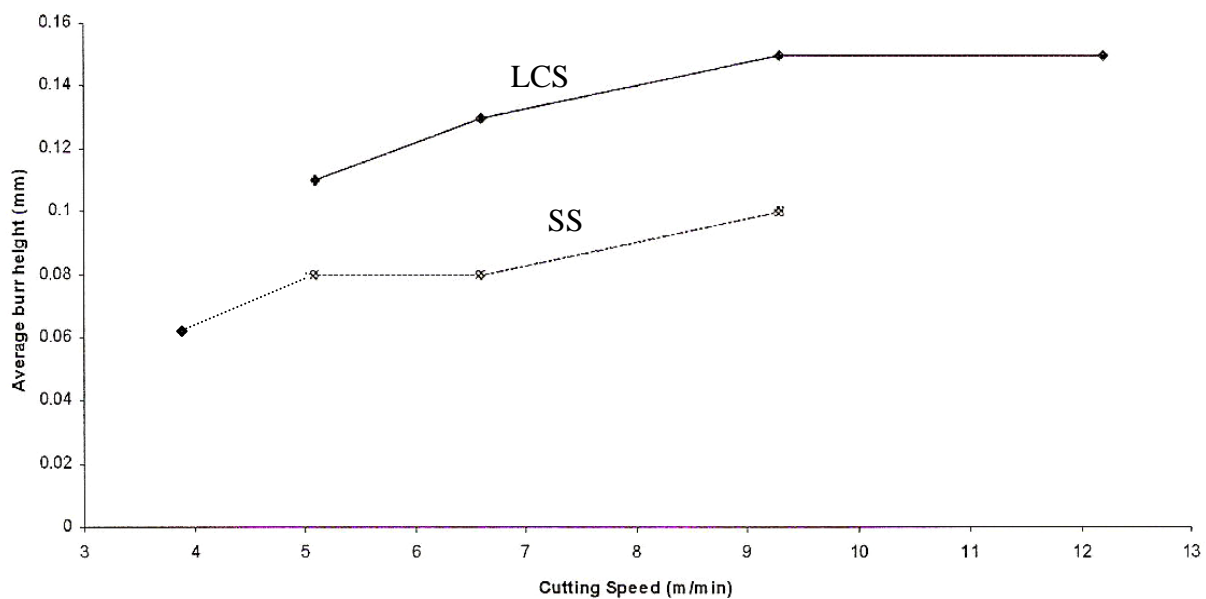
Figure 10 Effect of cutting speed on burr height in slot-end milling of low carbon steel (at a feed rate of 22 mm/min) and stainless steel (at a feed rate of 14 mm/min) with 2 mm cutting depth.

**Figure 11 Effect of feed rate on burr height in slot-end milling of low carbon steel
(at a cutting speed of 12.2 m/min) and stainless steel (at a cutting speed
of 9.3 m/min) with 2 mm cutting depth.**
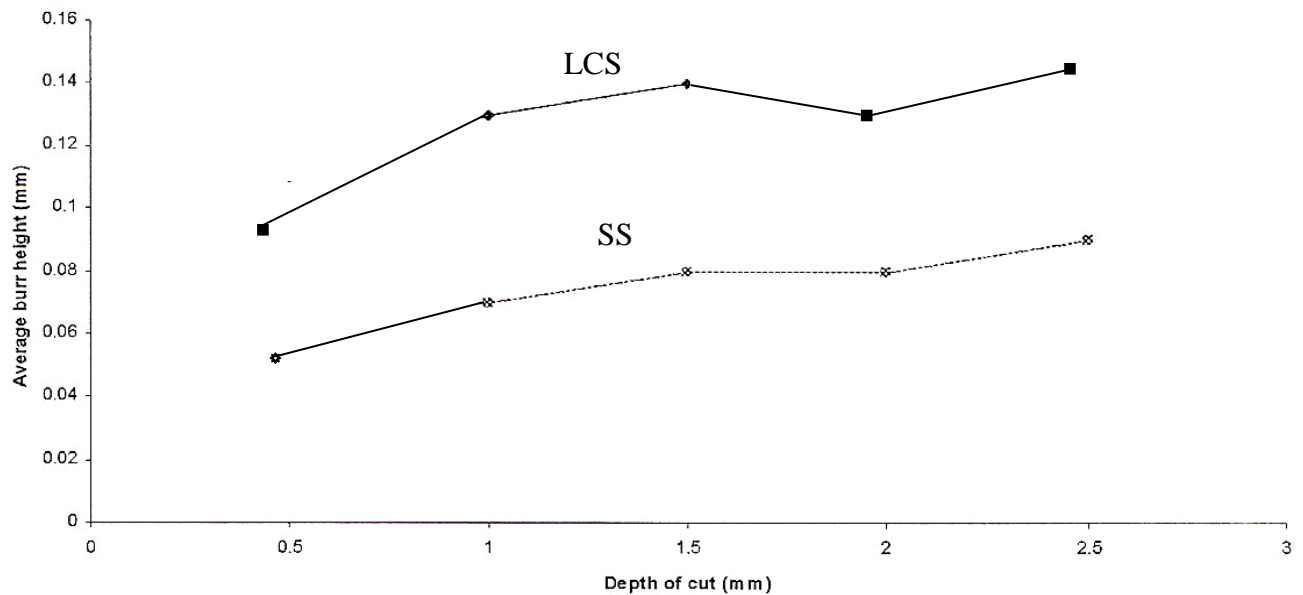
**Figure 12 Effect of depth of cut on burr height in slot-end milling low carbon steel and
stainless steel at a cutting speed of 6.6 m/min and a feed rate of 22 mm/min.**

INVESTIGATION OF PARAMETERS AFFECTING
LOST FOAM CASTING

Prof. Dr. Qasim M. Doos   Ihsan K. A. Al-Naimi

University of Baghdad / Mechanical department

ABSTRACT

The lost-foam casting process using expanded polystyrene foam pattern allows more complex and detailed passages to be cast directly into the part. The advantages of the lost-foam casting process involve, forms complex internal and external shapes without cores, reduces part mass with near net-shape capability, eliminates parting lines, and reduces machining operation and costs, Complex shapes with various sizes castings were produced in this technique in the foundry of the State Company for Electrical Industrials to evaluate the process. Successful complete castings were made. Many experimental works were done to further complements about fluidity parameter dealing with lost-foam casting process. Empirical linear and non-linear formulas were obtained from those experimental works to find the minimum temperature for pouring molten metal. Aluminum alloys were the material of choice for this work, due to the best combination of mechanical properties and castability, but the performance requirements and manufacturability issues will drive the choice of a specific aluminum that was aluminum-silicon alloy, which were used in this work.

The macroscopic properties of the alloy depend strongly on the microstructure. Therefore, photomicrographs of microstructures of various castings with different foam pattern densities were done and made comparisons with common sand castings. Mechanical tests were conducted on the castings which produced by the common sand casting and the lost-foam casting processes. These tests include tensile, hardness, and impact. Because of using the expandable polystyrene as a pattern that gave, more gasses in the cavity of the mold during casting, so the mechanical tests show some differences between the two processes.

الخلاصه:

السباكه بطريقة الرغوه المفقوده باستخدام نماذج رغوة البولستيرين المتبخر تسمح اكثر بانتاج مسبوكات ذات تفاصيل وقنوات واشكال معقده مبنيه في نفس المسبوكه. ميزات طريقة السباكه بالرغوه المفقوده هي: تكوين أشكال بسطوح خارجيه و داخليه معقده دون الحاجه الى استخدام القلوب، تقليل عدد القطع وامكانية انتاج الشكل المطلوب المقارب للشكل النهائي، عدم الحاجه لخطوط فاصله، تقليل عمليات التشغيل الاضافيه بعد انتاج المسبوكات وبالتالي تقليل الكلف. تم سباكة نماذج ناجحه معقده وباحجام مختلفه. تم اجراء تجارب عمليه عديده في مسبك الشركة العامه للصناعات الكهربائيه لغرض اضافة المعلومات المهمه لمتغير السيوبه ذات العلاقه بطريقة السباكه بالرغوه المفقوده. تم استنتاج صيغ عمليه بعلاقه خطيه وغير خطيه استنتجت من التجارب العمليه لايجاد أقل درجة حراره ممكنه لصب منصهر المعدن.

تم اختيار سبيكة كثيرة الاستخدام في مجالات مختلفه من سبائك الالمنيوم كونها تمتلك افضل جمع بين الخواص الميكانيكية المرغوبه وقابلية السباكه الجيده. ولكن متطلبات الاداء وقابلية التصنيع ادت الى اختيار سبيكه معينه (Al-Si) التي استخدمت في هذا العمل.

ان الخواص العامه تعتمد بقوه على التركيب المجهري للسبيكه. لقد تم أخذ صور ميلوغرافيه للتراكيب الداخليه للمسبوكات التي تم انتاجها في هذا العمل لنماذج مقطوعه من قطع البولستيرين المختلف الكثافة. تم اخذ صورمكبره للتراكيب الداخليه لمختلف المسبوكات باختلاف كثافة الرغوه للنماذج وعمل مقارنه مع مسبوكات تم انتاجها بالطريقه التقليديه. تم اجراء فحوصات ميكانيكيه مختلفه للمسبوكات المنتجه بطريقة الرغوه المفقوده ولكثافات مختلفه وكذلك بالطريقه التقليديه لغرض المقارنه فيما بينهم ، تشمل هذه الفحوصات فحص الشّد ، الصلاده والمتانه. بسبب استخدام نماذج مصنوعه من مادة البولستيرين التي تنتج غازات اكثر في تجويف القالب بسبب تحللها اثناء عملية السباكه، لهذا الفحوصات الميكانيكيه اعطت بعض الفروقات بين الطريقتين.

KEY WARDS

Lost-Foam Casting, Expanded Polystyrene, Fluidity, Aluminum-Silicon Alloy, Microstructure, Mechanical Tests.

INTRODUCTION

Casting processes are among the oldest methods of manufacturing date back to around 6000 B.C. (Groover 2002) when copper arrowheads and other tools were made. Shape casting involves the production of more complex geometries and almost all materials can be cast in, or nearly in the final shape. Varieties of shape-casting methods are available, thus making it one of the most versatile of all manufacturing processes. The production of a desired shape by a sand casting process first involves molding foundry sand around a suitable pattern which is made of wood or other materials in such a way that the pattern can be with- drawn to leave a cavity of the required shape in the sand. To facilitate this procedure the sand mold is split into two or more parts.

This procedure may cause some defects in the products such as fins, misalignment of mold parts and cores in spite of mold distortion. Thus, the lost-foam casting (LFC) is a method of sand casting to eliminate the above defects; moreover, it simplifies and expedites the mold making. The process uses a mold of sand packed around a polystyrene foam pattern complete with necessary system, and it may contain internal cores **Fig. 1** (Higgins 1978)**.**
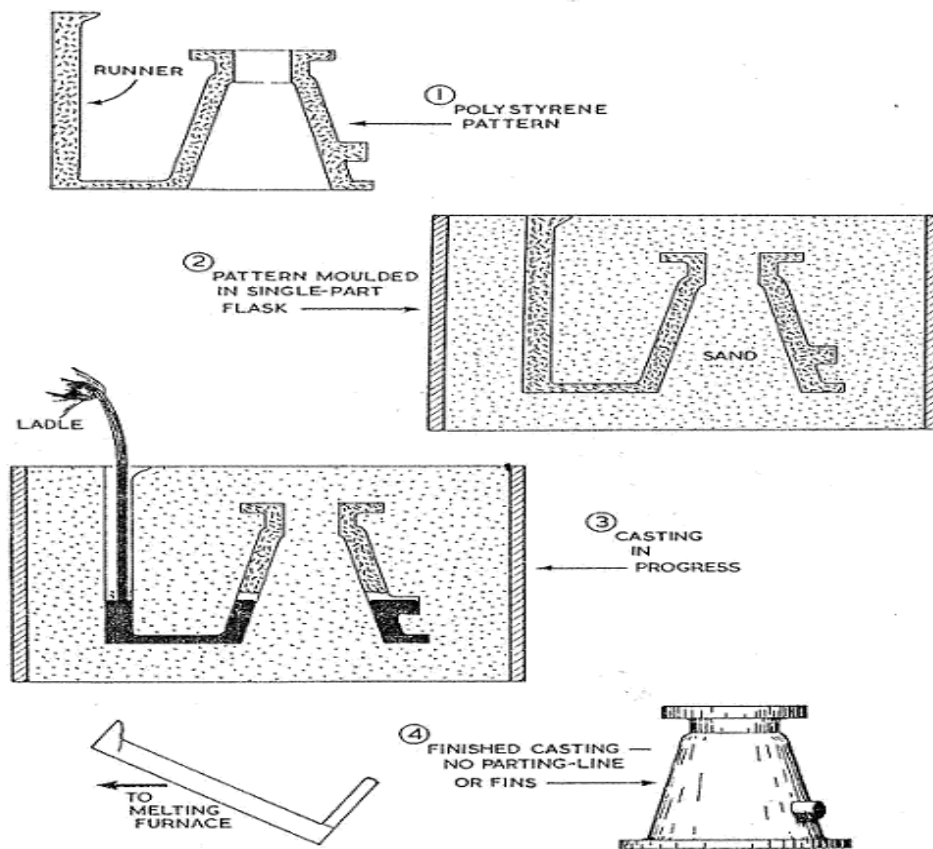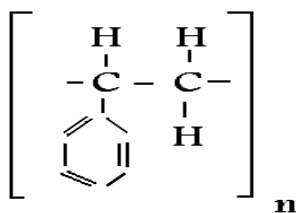
Fig. 1 Lost-foam casting process using EPS pattern (Higgins 1978).

Polystyrene is a polymer material with the formula: **(C$_8$ H$_8$) n**

Where (n) is "between 1000 to 2000". Polystyrene is a material derived from benzene and ethylene and, in its expanded form, contains only 2% of actual solid polystyrene, which extremely low relative density. **Table 1** indicates the properties of the polystyrene material. Various methods for making the pattern can be used depending on the quantities of casting to be produced. For one of kind castings, the foam is manually cut with a sharp knives and heated stainless-steel wire from large strip. For large production runs, an automated molding operation can be set up to mold the patterns (Groover 2002).

Complex internal features are produced by assembling and gluing multiple foam sections together to form a single complex foam pattern, **Fig. 2** The pattern is normally coated with a refractory compound to provide a smoother surface on the pattern and to improve its high temperature resistance (Genske 2004).

Table 1 Polystyrene properties and other data.

Polymer	Polystyrene $(C_8H_8)_n$
Symbol	PS
Polymerization Method	Addition
Degree of Crystallization	None (amorphous)
Modulus of Elasticity	3200 MPa
Tensile Strength	50 MPa
Elongation	1%
Specific Gravity	1.05
Glass Transition Temp.	100ºC
Melting Temp.	240ºC
Approximate Market share	About 10%

Four Foam Sections

Assembled Foam Pattern
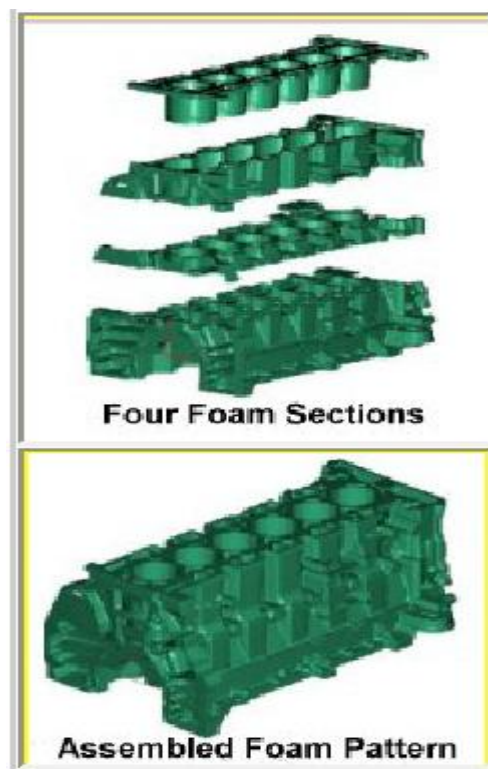
Fig. 2 Assembling and gluing multiple foam sections together to form single complex foam pattern (Genske 2004)**.**

FLUIDITY

Fluidity can be defined as the capability of the molten metal to flow into the cavities of the mold and to fill all internal details of the mold before freezing in the casting process. Fluidity is a commonly used term that combines fluid flow and heat flow characteristics (Serope 1989). Fluidity is related to viscosity, but it is not a single property as viscosity or density but a complex characteristics. So, empirical tests have been devised to measure the overall characteristics. Factors affecting fluidity include pouring temperature, metal composition, viscosity of molten metal, casting geometry, and heat transfer to the surroundings, moreover in LFC process another factors affects fluidity such as foam material, glue lines and coating. The unit of fluidity is expressed as a distance in the length unit such as (cm, mm). Fluidity is a function of producing successful complete castings.

EXPERIMENTAL WORK

Many experiments were done to measure the fluidity of aluminum-silicon alloys using the LFC process. The tests of the fluidity measurement were done by forming standardized strip fluidity test. They were done with different variables. Three commercial expanded polystyrene foam densities – 12, 15, and 20 kg/m³ were examined in these experiments along with four average thickness fingers – 4, 6, 8, and 12 mm – and six pouring temperature. The final strip fluidity pattern and finished casting are shown in **Fig. 3**

(b)

Fig. 3 Strip fluidity model   (a) EPS pattern   (b) finished casting.

It was designed as a general factorial with two replicates per condition. The factors and their associated values are given in **Table 2**.

4245

Table 2 Factors and levels for Al-Si alloy fluidity test.

Factor	Levels					
Foam Density (kg/m³)	12		15		20	
Thickness Pattern (mm)	4	6	8		12	
Pouring temperature (°C)	690	700	720	740	750	800

The results of the fluidity measurement castings, which were done in the foundry of the State Company for Electrical Industries, were summarized in the **Table 3**.

Table 3 Experimental values of fluidity measurement tests.

Pouring Temperature •C	Thickness Channel Pattern (mm)											
	ρ=12 kg/m³				ρ=15 kg/m³				ρ=20 kg/m³			
	4	6	8	12	4	6	8	12	4	6	8	12
690	28	37	45	72	25	30	41	51	21	30	33	48
700	33	40	46	85	32	38	44	81	30	34	42	78
720	36	56	71	101	33	49	70	98	32	35	44	88
740	37	62	76	125	37	60	71	109	32	52	61	94
750	63	87	124	137	53	76	113	132	47	73	105	124
800	128	138	143	159	125	135	140	155	122	134	139	148

The relationship between pouring temperature, thickness of channels, and the fluidity amount for each relative foam density are shown in **Figures 4, 5, 6** as a 3-D bar chart. **Fig. 7** shows the effect of foam density on the fluidity measurement.
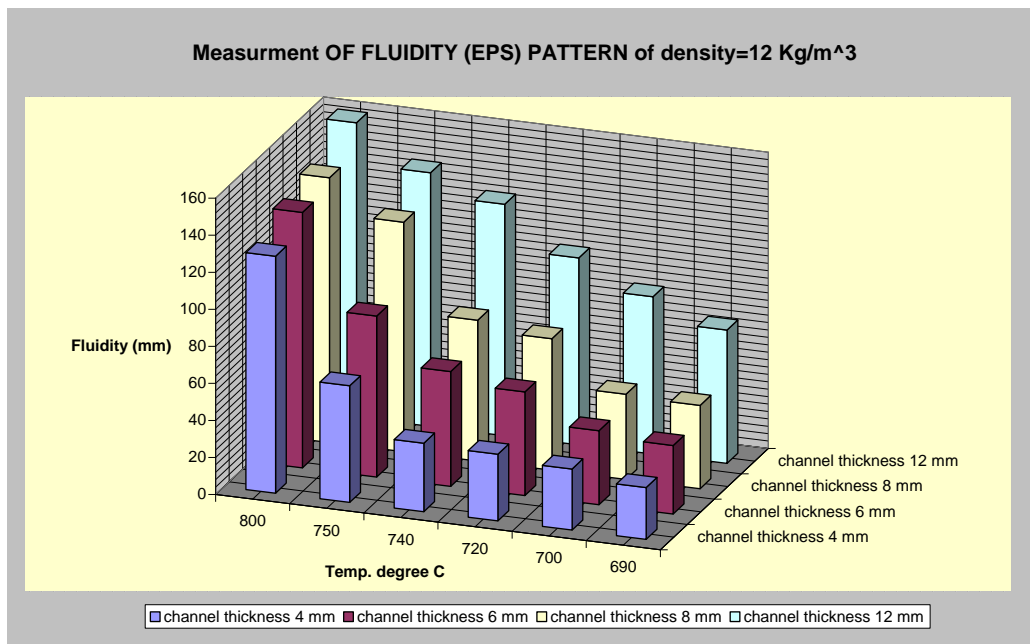
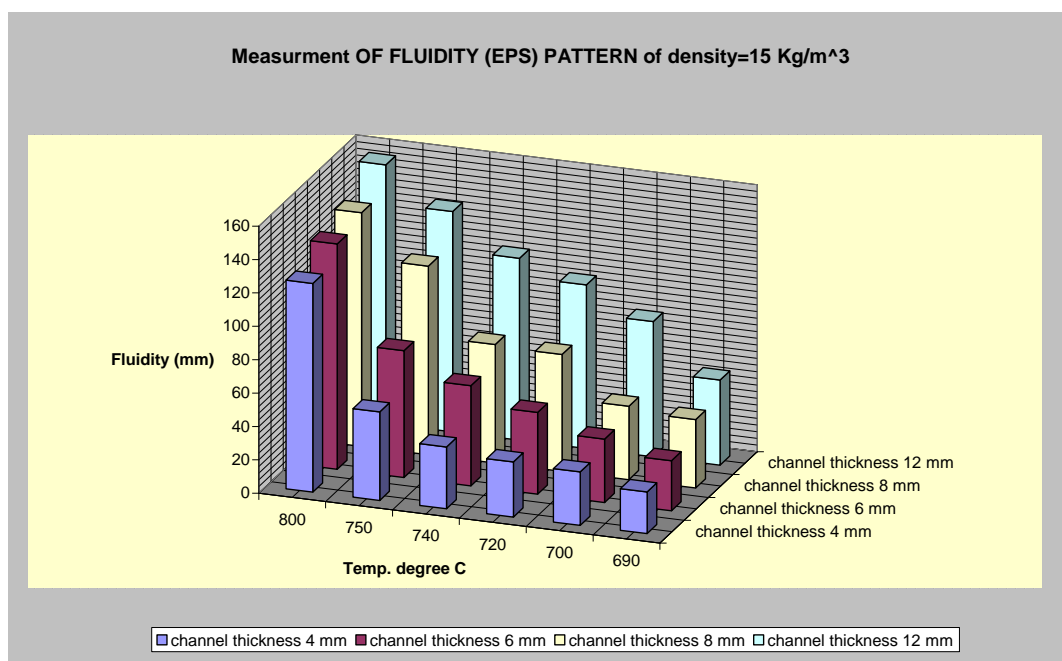**Fig. 4 Bar chart for fluidity measurement test using EPS (Density 12 kg/m³)**

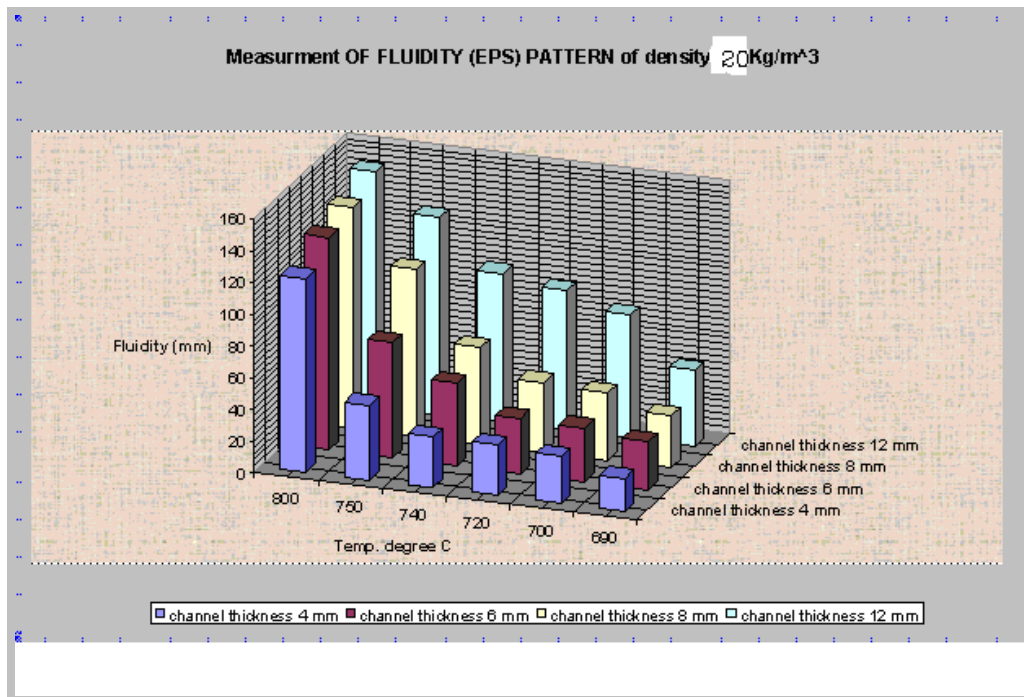**Fig. 5 Bar chart for fluidity measurement test using EPS (Density 15 kg/m³)**

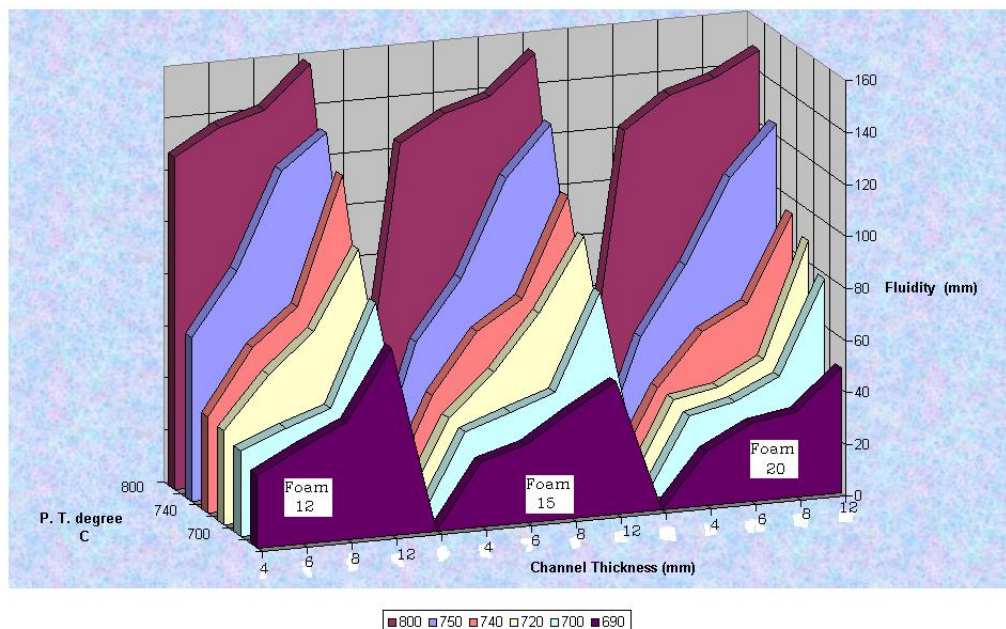**Fig. 6 Bar chart for fluidity measurement test using EPS (Density 20 kg/m³)**

Fig. 7 Effects of foam density on fluidity measurement.

EMPIRICAL EQUATIONS

It was suggested to construct an empirical equations from the data obtained of the fluidity test. They demonstrate the relationship between the associated variables that affecting the LFC process, which examined in this work. There are two group equations, one for linear relation, and the other for non-linear relation. The pouring temperature is the depended variable that required to be calculated for pre-design samples (minimum channel thickness and the related length). The minimum pouring temperature is the desired parameter in the foundries to minimize the consumption of the power required to melt the metal and oxidation of the molten metal.

Therefore, that, multiple linear regressions for some variables associated with fluidity parameter of experimental test:

$$f (T, t, L, \rho) = 0 \qquad\qquad \text{eq. (1)}$$

Where:
T: minimum pouring temperature (ºC)
t: the smallest thickness in the sample section (mm)
L: the length of the smallest section (mm)
ρ: The foam density (Kg/m^3)

$$T = f (t, L, \rho) \qquad\qquad \text{eq. (2)}$$

Linear relation with the effect of foam density

The last equation (2) modified for linear relationship between the related variables. Therefore:

$$T = a_0 + a_1 t + a_2 L + a_3 \rho \qquad\qquad \text{eq. (3)}$$

Alternatively, as a matrix form:

$$T = a_0 + \sum a_i x_i \qquad\qquad \text{eq. (4)}$$

Where, "i" is the repeated of the experimental tests.
The best values of (a_0, a_1, a_2, a_3) are determined by setting up the sum of squares of residual error (S_r).

$$S_r = \sum (T_i - a_0 - a_1 t_i - a_2 L_i - a_3 \rho i)^2 = min. \qquad\qquad \text{eq. (5)}$$

$$\delta S_r / \delta a_0 = - 2 \sum (T_i - a_0 - a_1 t_i - a_2 L_i - a_3 \rho i) = 0 \qquad\qquad \text{eq. (6)}$$

$$\delta Sr / \delta a_1 = - 2 \sum ((T_i - a_0 - a_1 t_i - a_2 L_i - a_3 \rho i) \times t_i) = 0 \qquad\qquad \text{eq. (7)}$$

$$\delta S_r / \delta a_2 = - 2 \sum ((T_i - a_0 - a_1 t_i - a_2 L_i - a_3 \rho i) \times Li) = 0 \qquad\qquad \text{eq. (8)}$$

$$\delta S_r / \delta a_3 = - 2 \sum ((T_i - a_0 - a_1 t_i - a_2 L_i - a_3 \rho i) \times \rho i) = 0 \qquad\qquad \text{eq. (9)}$$

Alternatively:

$$n\, a_0 + \sum a_1\, t_i + \sum a_2 L_i + \sum a_3\, \rho_i = \sum T_i \qquad \text{eq. (10)}$$

$$\sum a_0\, t_i + \sum a_1\, t^2_i + \sum a2\, L_i\, t_i + \sum a_3\, \rho_i\, t_i = \sum T_i\, t_i \qquad \text{eq. (11)}$$

$$\sum a_0\, Li + \sum a_1\, t_i\, Li + \sum a_2 L^2_i + \sum a_3\, \rho_i\, L_i = \sum T_i\, Li \qquad \text{eq. (12)}$$

$$\sum a_0\, \rho_i + \sum a_1\, t_i\, \rho_i + \sum a_2 L_i\, \rho_i + \sum a_3 \rho^2_{i} = \sum T_i\, \rho_i \qquad \text{eq. (13)}$$

In matrix form:

$$[A]\,\underline{a} = \underline{b} \qquad \text{eq. (14)}$$

Where:

$$[A] = \begin{pmatrix} n & \sum t_i & \sum L_i & \sum \rho_i \\ \sum t_i & \sum t^2_i & \sum t_i\, L_i & \sum t_i\, \rho_i \\ \sum L_i & \sum L_i t_i & \sum L^2_i & \sum L_i\, \rho_i \\ \sum \rho_i & \sum \rho_i\, t_i & \sum \rho_i\, L_i & \sum \rho^2_i \end{pmatrix}$$

$$\underline{a} = \begin{bmatrix} a_0 \\ a_1 \\ a_2 \\ a_3 \end{bmatrix} \qquad\qquad \underline{b} = \begin{pmatrix} \sum T_i \\ \sum T_i\, t_i \\ \sum T_i\, L_i \\ \sum T_i\, \rho_i \end{pmatrix}$$

And n is the number of repeated tests.

To solve the matrix to find (a'$_s$) values …………multiple $[A]^{-1}$

$$[A]^{-1}[A]\,\underline{a} = [A]^{-1}\underline{b} \qquad \text{eq. (15)}$$

Therefore:

$$\underline{a} = [A]^{-1}\underline{b} \qquad \text{eq. (16)}$$

From **Table 3,** substitute the data in the matrix;
The matrix [A] and <u>b</u> will be:

$$
[A] = \begin{pmatrix} 72 & 540 & 5409 & 1128 \\ 540 & 4680 & 44680 & 8460 \\ 5409 & 44680 & 522247 & 83470 \\ 1128 & 8460 & 83470 & 18456 \end{pmatrix} \quad , \quad \underline{b} = \begin{pmatrix} 52800 \\ 396000 \\ 4053330 \\ 827200 \end{pmatrix}
$$

By using eq. (16) the constant will be:

$$a_0 = 682, \ a_1 = -6.51, \ a_2 = 1.0, \ a_3 = 1.62$$

Substitute (a'_s) values in eq. (3) therefore the linear relationship of the related variables will be;

$T = 682 - 6.51 \, t + F + 1.62 \, \rho$ eq. (17)

<u>Linear relation without the effect of foam density</u>

In this case the foam density will be fixed, therefore the eq. (3) modified to:

$T = a_0 + a_1 \, t + a_2 \, L$ eq. (18)

Moreover, this equation will be repeated for three-foam density.
1. while the foam density is ($12 \ Kg/m^3$), by the same procedure the matrix [A] and <u>b</u> will be;

$$
[A] = \begin{pmatrix} 24 & 180 & 1965 \\ 180 & 1560 & 16152 \\ 1965 & 16152 & 198481 \end{pmatrix} \quad , \quad \underline{b} = \begin{pmatrix} 17600 \\ 132000 \\ 1469750 \end{pmatrix}
$$

$$a_0 = 701 \qquad a_1 = -6.9 \qquad a_2 = 1.0$$

Therefore eq. (18) will be;

$T = 701 - 6.9 \, t + F$ eq. (19)

2. The foam density equal to ($15 \ Kg/m^3$) and ($20 \ Kg/m^3$); by the same procedure respectively eq. (18) will be;

$T = 709 - 6.7 \, t + F$ eq. (20)

$T = 712 - 6 \, t + F$ eq. (21)

Non-linear relation with the effect of foam density

It was suggested the relation between the variables associated with LFC process as shown below;

$$T = a_0 + a_1 F^3 + a_2 F^2 + a_3 F + a_4 t^2 + a_5 t + a_6 \rho \qquad \text{eq. (22)}$$

By the same procedure, the dimension of the matrix is (7×7).

$$[A] = \begin{pmatrix} 72 & 5.9 \times 10^7 & 5.2 \times 10^5 & 5409 & 4680 & 540 & 1128 \\ 5.9 \times 10^7 & 1.2 \times 10^{14} & 9.5 \times 10^{11} & 7.3 \times 10^9 & 5.3 \times 10^9 & 5.3 \times 10^8 & 9 \times 10^8 \\ 5.2 \times 10^5 & 9.5 \times 10^{11} & 7.3 \times 10^9 & 5.9 \times 10^7 & 4.4 \times 10^7 & 4.5 \times 10^6 & 8 \times 10^6 \\ 5409 & 7.3 \times 10^9 & 5.9 \times 10^7 & 5.2 \times 10^5 & 4.2 \times 10^5 & 44680 & 83470 \\ 4680 & 5.3 \times 10^9 & 4.4 \times 10^7 & 4.2 \times 10^5 & 4.7 \times 10^5 & 45360 & 73320 \\ 540 & 5.3 \times 10^8 & 4.5 \times 10^6 & 44680 & 45360 & 4680 & 8460 \\ 1128 & 9 \times 10^8 & 8 \times 10^6 & 83470 & 73320 & 8460 & 18456 \end{pmatrix}$$

$$\underline{b} = \begin{pmatrix} 52800 \\ 4.5 \times 10^{10} \\ 4 \times 10^8 \\ 4 \times 10^6 \\ 3.4 \times 10^6 \\ 396000 \\ 827200 \end{pmatrix}$$

It was used Gauss-Seidle Method to solve the matrix for finding **a**'s.
Therefore the constant **a**'s are:

$a_0 = 776, \quad a_1 = 1.2 \times 10^{-4}, \quad a_2 = -0.002, \quad a_3 = -0.25, \quad a_4 = 1.87 a_5 = -85.6, \quad a_6 = 25.3$

The empirical equation for this case is:

$$\mathbf{T = 776 + 1.2 \times 10^{-4\ F3} - 0.002\ F^2 - 0.25\ F + 1.87\ t^2 - 85.6\ t + 25.3\ \rho} \qquad \text{eq. (23)}$$

CHEMICAL COMPOSITION

Many samples were taken from the castings that produced with LFC process to analyze the chemical composition. These samples were cut from the castings that were produced at the foundry of the State Company for Electrical Industries during the fluidity measurement tests. The chemical composition analysis was done in the Central Quality Control Office at Nasser State Company for Mechanical Industries. The average results of tests are shown in **Table 4.**

Table 4 Chemical composition of the alloy is used in this work.

Chemical Composition of the Alloy in w_t %										
	Si	**Fe**	**Cu**	**Mn**	**Mg**	**Zn**	**Ti**	**Ni**	**Sn**	**Al**	**Others**
Elements	**8.59**	**1.29**	**1.59**	**0.12**	**.066**	**.737**	**.026**	**.07**	**.01**	**87.48**	**0.02**

MECHANICAL PROPERTIES TESTS

Tensile tests

The tension specimens cast with pouring temperature (**720**°C) to size in sand casting without chills, the dimensions of specimens used in this test prepared according to the ASTM B 26/B 26M – 88. There were four groups of samples used in this test, one of them cast in common sand casting, and the others in LFC process the difference between them were in the foam density. Each group had two sets the difference between them was in thickness only; these thicknesses were (4.1, 2.2 mm), although of the same material and process there are variation in the results between two thicknesses for each group because of the residual stresses due to the machining of cutting the samples. The velocity test was (**0.5** mm/min.).

From this test, ultimate tensile stress, yield stress (proof stress), and elongation were obtained. The results are shown in the **Table 5**.

Table 5 Mechanical properties obtained from tensile tests.

process	*UTS (MPa)* Thickness (mm)		*Y.P (MPa)* Thickness (mm)		*Elongation %* Thickness (mm)	
	2.2	**4.1**	**2.2**	**4.1**	**2.2**	**4.1**
Common Casting	145	152	92	97	1.2	1.4
LFC 12kg/m³	125	142	86	93	1.5	1.7
LFC 15kg/m³	118	139	80	91	1.6	1.9
LFC 20kg/m³	112	137	74	86	1.6	1.9
STM (328 alloy)	170		95		1.0	

Hardness tests

Hardness is being a macroscopic property and a measure of the resistance to indentation. This test was done by using (**Vickers Hardness**).

The magnitude of the load was exerted to the specimen (0.5 kg); the results were calculated by this equation: $VHN = 1.854 \, P / L^2$

Where; P= applied load,   L =the average diagonals of the diamond indentation.

Two reading in each specimen were taken one (20×20 mm) and the second (10×10 mm) apart from the edge. The comparison results are recorded in **Table 6**

Table 6 Hardness tests

Process		Common Sand Casting	LFC Process with 12kg/m³	LFC Process with 15kg/m³	LFC Process with 20kg/m³	ASTM (328 alloy)
HV No.	M	74	63	53	51	60
	E	75	64	54	52	
HB No.	M	67	58	49	48	55
	E	68	59	50	48	

Where (HB) is equivalent to Brinell number, (10mm) ball and 500 kg load.
(M) 20×20 mm apart from the edge, and (E) 10×10 mm apart from the edge of specimen.

Impact tests

The Charpy V-notch test (simply supported beam test) was used to measure the impact strength test. The samples were prepared as the standardization of (ASTM-E 23). The results of the test are shown in **Table 7**.

Table 7 Charpy impact test

process	*Energy (kg.m)*
Common Sand Casting	**4.2**
LFC Process with 12kg/m³ Foam density	**3.7**
LFC Process with 15kg/m³ Foam density	**3.6**
LFC Process with 20kg/m³ Foam density	**3.5**

MICROSTRUCTURES

The structure of a casting is in the first instance a function of alloy composition and casting geometry. It is also sensitive to measure of variation in cooling rate within the mold. This test had done using available equipments in Production and Metallurgy Engineering Department at the University of Technology. The samples were cut from the strip. The strip dimension is (2, 5, 20 cm) that cast with three different foam density as a pattern in LFC process and one another cast by common sand casting. The samples had prepared by grinded, polished, and etched with (HF) 2% and (H$_2$O) 98% before the photomicrographs were taken. The photomicrographs of microstructure are shown in **Fiq. 8**

(a)

(b)

©

(d)

(e)

(f)
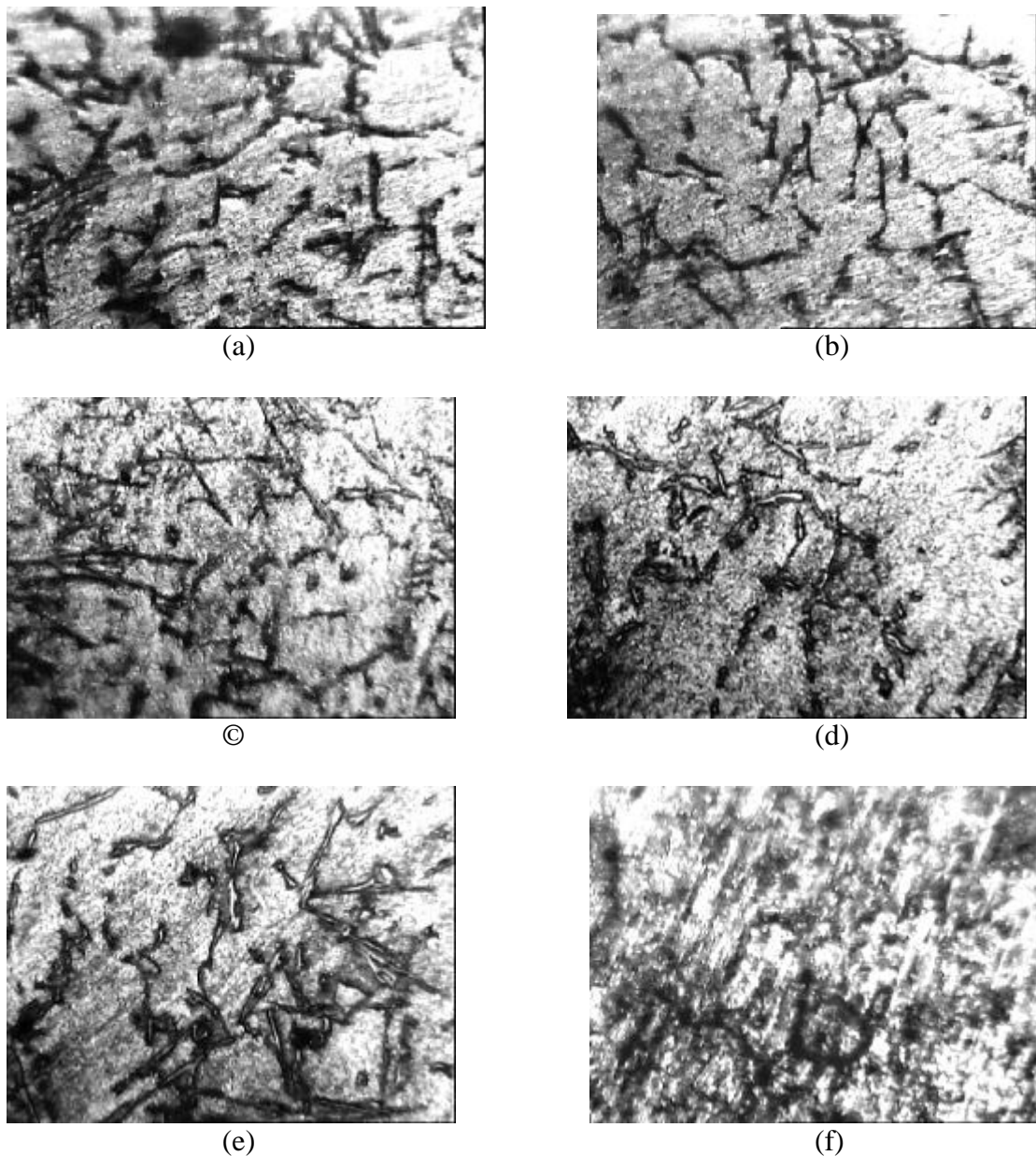
Fig. 8 Photomicrographs showing the microstructures of Al-Si alloy
(a), (b) common sand casting. (c), (d), (e), (f) LFC process x500

In **figures (8-a, and 8- b)** are showing the specimen for common sand casting. It shows regular structure of Al-Si alloy.

In **figure (8-a)** shows clear observation of the segregation of the eutectic silicon in the portion near the edge due to the high cooling rate.

Figures (8- c, d, e, f) show the microstructures of the castings that produced by LFC process. The darker area of the micrograph of these figures contains more silicon particles, indicating the high silicon content.

Figures (8 – c and d) show the microstructures of the casting used LFC process with foam density of (**12** kg/m³); the **figure (8- c)** is for the edge portion and **figure (8- d)** of the middle portion specimen of LFC process. These two figures show less segregation and less microporosity as was expected than **figures (8- e and f)** which were used foam densities (**15, 20** kg/m³) respectively because of more Pyrolysis products.

CONCLUSIONS

Based on the experimental investigation of the mechanism of the LFC process, the following conclusions can be drawn from this work:

- Fluidity is affected by foam density, increasing foam density decreasing fluidity because of the combined result of molten metal front energy loss and an increase in backpressure from decomposition products.
- Empirical formulas were obtained to calculate minimum pouring temperature for a specific thickness section and its length with using specified pattern foam density. The first formula based on linearity relation between variables and the second as a power relation. The first formula gives good results while checking some data obtained from this experimental works.

$$T = 682 - 6.51t + F + 1.62\rho$$

$$T = 776 + 1.2 \times 10^{-4}\ F^3 - 0.002\ F^2 - 0.25\ F + 1.87\ t^2 - 85.6\ t + 25.3\ \rho$$

- In this work, examination was done on the feasibility of using Al-Si alloys in the LFC process, and the experimental tests indicated that this alloys have similar castability with traditional sand casting.
- The microstructures of the final castings were examined, and the photomicrographs show little different between the castings produced by the traditional sand casting and LFC process.
- The grain size particles of microstructures are fluctuated between large and small size related with the location of it, if it is near the edge or in the middle of the casting. Fine grain sizes locate near the mold wall due to the high cooling rate.
- The mechanical properties tests were done on the castings produced with LFC process and that with the common sand casting. The tests gave good results and agreements with standardization of the nearest alloy. The effect of the foam density is relatively little in some cases on the mechanical properties, increasing foam density decreasing the mechanical properties. The percentage differences between the two processes range from (4% to 31%).

REFERENCES

- Durbin, T. L. (2005), "Modeling Dissolution in Aluminum Alloys" Ph.D. thesis, Georgia Institute of Technology.

- Genske, E. (2004), "Aluminum Cylinder Block for General Motor Track", SUV Engines, AFS,   GM Power Train Casting Development. www.gm.com/automotve/gmpowertrain.

- Groover, M. P. (2002), "Fundamental of Modern Manufacturing". John Willey and Sons, Inc.

- Hess, D. R (2004),"Comparison of Aluminum Alloys and EPS Foams for Use in the Lost Foam Casting Process", General Motors Power train, Casting Development and Validation Center, Saginaw, Michigan, American Foundry Society

- Higgins, R. A. (1978), "Engineering Metallurgy". Second edition part II

- Serope, K. (1989),   "Manufacturing Engineering and Technology". Addison Wesley Publishing   Company.

- Tschopp, M. A. (2002), "Mechanisms of Misrun Formation Aluminum Lost Foam Castings" American Foundry Society.

- Tschopp, M.A., Ramasay, C.W., Askeland, D.R. (2001), "Mechanisms of Formations of Pyrolysis Defects in Aluminum Lost Foam Castings" AFS Transactions, vol. 108.

SYMBOLS

EPS: Expanded Polystyrene
HB: Brinell number
L: The length of the smallest section (mm)
LFC: Lost-Foam Casting
T: Minimum pouring temperature (°C)
t: The smallest thickness in the sample(mm)
UTS: Ultimate Tensile Stress
VHN: Vickers Hardness number
Y.P: Yield Point
ρ :   The foam density (Kg/m^3)

EVALUATION OF SPECIFIC METHODS TO DETECT CRACK AND DAMAGE OF MECHANICAL BEAM STRUCTURES USING FREE VIBRATION ANALYSIS

Dr.Nabil H. H   **Iqbal A. R.**

University of Baghdad
College of Eng.

ABSTRACT

The importance of the beam in the service of our life and how the damaged beam costly influence the economy and even endanger the human life itself, draws our attention to study the specific methods to detect crack and damage by using free vibration analysis of mechanical beam structures. In the present research, three kinds of beam structures have been investigated namely (simply supported beam, portal frame and crane frame) by using finite element method. Six cases of damage are modeled for simply supported beam and portal frame and with seven cases for crane frame. The damage is simulated by reducing the stiffness of assumed elements with ratios (25% and 50 %) in mid- span of the simply supported beam and by introducing cracked elements at different locations with ratio of depth of crack to the height of the beam (a/h) 0.1, 0.25 for simply supported beam and 0.1 and 0.2 for portal and crane frames. A program coded in Matlab 6.5 was used to model the numerical simulation of the damage scenarios. The results showed a decreasing in the five natural frequencies with shifting in the damaged mode shape associated with their frequencies from undamaged beam which means the indication of presence of the damage. The direct comparison gives an indication of the damage but the location of the damage, is not detected. Four structural damage identification methods based on changes in the dynamics characteristics of the beam structures are examined and evaluated for damage scenarios for the three structures considered. The results of the analysis indicate that the curvature energy damage index method performs well in detecting, locating and quantifying damage in single and multiple damage scenarios for the three structures.

الخلاصة

نظرا لأهمية العتبة beam في خدمة حياتنا ، فان العتبة المتضررة تؤثرسلبا عاى الاقتصاد بل وتهدد حياة الانسان نفسها مما جذب اهتمامنا نحو دراسة طرق معينة لتحديد الشق و الضرر باستخدام الاهتزاز الحر لتراكيب العتبة الميكانيكية المتضرره. في هذا البحث تم دراسة ثلاثة انواع من تراكيب العتبه والمسماة (العتبة البسيطة المدعمة beam simple supported والهيكل البابي portal frame و الهيكل الرافعة crane frame) . تم تمثيل الضرر بستة حالات في العتبة البسيطة المدعمة والهيكل البابي وسبعة حالات في الهيكل الرافعة. إنّ الضرر (Damage) يتمثّل بتخفيض متانه العناصر المفترضة بنسبة 25 % و50 % في وسط العتبة البسيطه وكذلك يتمثل عن طريق شق عمودي في العناصر المفترضة في المواقع المختلفة بنسبة عمق الشقّ إلى إرتفاع العتبه

(a/h) 0.25, 0.1 للعتبة البسيطه و0.2,0.1 في الهيكل البابي والهيكل الرافعة. تم استخدام برنامج Matlab لتمثيل المحاكاة العددية لسينوهات الضرر. اظهرت النتائج نقص في الترددات الطبيعية الخمسة وبوجود زحف في شكل النمط المتضرّر damage mode shape نسبه للعتبه السليمه و الذي هو إشارة لوجود الضرر. تعطي المقارنة المباشرة إشارة الى وجود الضرر لكن موقع الضرر غير محدد. الطرق المحدده لايجاد الضرر التي تم استخدامها هي اربعه طرق مستندة على التغييرات في خصائص ديناميكة تراكيب العتبة و الطرق المحدده فحصت وقيّمت حالات الضرر للتراكيب الثلاثة. نتائج التحليل تشير إلى ان طريقة دليل ضرر طاقة النقوس curvature- energy damage index هي الافضل في إكتشاف وتحديد مكان الضرر في سيناريوهات الضرر damage scenarios الوحيدة الموقع والمتعدّد المواقع للتراكيب الثلاثة.

KEYWORDS
Damage, Crack, Damage location, Curvature, Frame, Frequencies.

INTRODUCTION

The ability to monitor a structure and detect damage at the earliest possible stage is of outmost importance in mechanical, civil and aerospace engineering communities. Structural damage is considered as a weakening of the structure that negatively affects its performance. Damage may be also defined as any deviation in the structural original geometric or material properties that may cause undesirable stresses, displacements, or vibrations on the structure. These weakenings and deviation may be due to cracks, loose bolts, broken welds, corrosion, fatigue, etc. **(Ren, 2002)**. Many structural components are now decaying because of age, deterioration, and lack of maintenance or repair.

Current nondestructive damage detection (NDD) technique are either visual or are based on experimental methods. Visual inspection has always been the most common method used in detecting damage in a structure, but the size and degree of complexity of today's structures being built provide less scope for visual inspections. The experimental methods such as acoustic or ultrasonic techniques, magnetic field procedure, radiography, eddy current, etc. All of these experimental methods require that the damaged region be identified a priori, and that the segment of the structure being examined must be easily accessible, subjected to these limitations, these methods can detect on or near the surface of the structure. The methods are obviously "local" inspection approaches **(Dewen, 2004)**.

One way to overcome the previously mentioned limitations is by using global damage detection methods. Structural damage identification based on changes in dynamic characteristics provides a global way to evaluate the structural condition. These methods are based on the idea that modal parameters (i.e., natural frequencies, mode shapes and modal damping ratio) are a function of the physical properties of the structure stiffness, damping, mass and boundary conditions **(Herrera, 2005)**. Therefore, changes in the physical properties will cause detectable changes for the changes in the modal parameters.

MODELING THE STIFFNESS MATRIX OF THE CRACKED ELEMENT

It is assumed that the damage in the beam structure will affect only the stiffness matrix and not to the mass matrix. This assumption is consistent with those used by **(Yuen 1985, Qian 1990** and **Kisa 2000)**.

The beam is divided into elements and the behavior of the elements located to the right of the cracked element regarded as external forces applied to the cracked element, while the behavior of elements situated to its left as constraints, see **Fig.1**. Thus the flexibility matrix of a cracked element with constraints can be calculated. The strain energy of undamaged element in case of bending **(Singor, 1951)**, is:

$$W^{(0)} = \int_0^L \frac{M_1^2 \, dx}{2EI} \qquad (1)$$

As shown in **Fig. 1**,

$$M_1 = (px + M) \qquad (2)$$

Substitute Eq. (2) in (1) to get

$$W^{(0)} = \int_0^L \frac{(px + M)^2}{2EI} \, dx \qquad (3)$$

$$W^{(0)} = \frac{1}{2EI} \left[\frac{p^2 L^3}{3} + pML^2 + M^2 L \right] \qquad (4)$$

Where:

$W^{(0)}$: The strain energy of undamaged element.

E : Elastic modulus.

I : Moment of inertia of undamaged element.

L : Length of the finite element.

p : Internal shear force at the right end of beam.

M : Internal bending moment at the right end of beam.

And by using the relation below, **(Thomson 1988).**

$$\{u\} = [C]\{P\} \qquad (5)$$

$[C]$, $\{u\}$, $\{P\}$ are the influence coefficient flexibility matrix, displacement and force vectors, respectively.

The component of flexibility matrix $[C]$ can be written as**, (Thomson 1988).**

$$c_{ij} = \frac{\partial u_i}{\partial P_j} \qquad (6)$$

And the displacement u_i computed by using Castigliano's theorem **(Singor, 1951).** As

$$u_i = \frac{\partial W^{(0)}}{\partial P_i} \qquad (7)$$

Substitute Eq. (7) into (6), the flexibility coefficient of undamaged element evaluated as

$$C_{ij}^{(0)} = \frac{\partial^2 W^{(0)}}{\partial p_i \partial p_j} \qquad (8)$$

where:

$p_1 = p$, $p_2 = M$ $i, j = 1, 2$

And using Eq. (4) in Eq. (8) gives:

$$C_{11} = \frac{\partial^2 W^{(0)}}{\partial p_1 \partial p_1} = \frac{\partial^2 W^{(0)}}{\partial p \partial p} = \frac{1}{2EI} \frac{\partial^2}{\partial p^2}\left[M^2 L + MpL^2 + \frac{p^2 L^3}{3} \right]$$

$$C_{11} = \frac{L^3}{3EI}$$

The flexibility matrix of the uncracked element can be expressed as

$$\left[C^{(0)} \right] = \frac{1}{EI} \begin{bmatrix} \dfrac{L^3}{3} & \dfrac{L^2}{2} \\ \dfrac{L^2}{2} & L \end{bmatrix} \tag{9}$$

From the equilibrium conditions shown in Fig (2), the following relationships hold:

$$\sum Fy = 0 \tag{10}$$

$$P_i + P_{i+1} = 0 \qquad or \quad P_i = -P_{i+1} \tag{11}$$

$$\sum M_A = 0 \tag{12}$$

$$M_{i+1} + P_{i+1}L + M_i = 0 \tag{13}$$

$$M_i = -P_{i+1}L - M_{i+1} \tag{14}$$

From Eq. (11) and (14) we get in matrix form

$$\begin{Bmatrix} P_i \\ M_i \end{Bmatrix} = \begin{bmatrix} -1 & 0 \\ -L & -1 \end{bmatrix} \begin{Bmatrix} P_{i+1} \\ M_{i+1} \end{Bmatrix}$$

$$\begin{Bmatrix} P_i \\ M_i \\ P_{i+1} \\ M_{i+1} \end{Bmatrix} = \begin{bmatrix} -1 & 0 \\ -L & -1 \\ 1 & 0 \\ 0 & 1 \end{bmatrix} \begin{Bmatrix} P_{i+1} \\ M_{i+1} \end{Bmatrix}$$

$$\left\{ P_i \quad M_i \quad P_{i+1} \quad M_{i+1} \right\}^T = \left[T \right]\left\{ P_{i+1} \quad M_{i+1} \right\}^T \tag{15}$$

Where

$$\left[T \right] = \begin{bmatrix} -1 & -L & 1 & 0 \\ 0 & -1 & 0 & 1 \end{bmatrix}^T \tag{16}$$

The element stiffness matrix in base system is obtained by the inversion of the flexibility matrix as

$$[K] = [C]^{-1} \tag{17}$$

The stiffness matrix of undamaged element can be written as

$$[K_u] = [T] \left[C^{(0)} \right]^{-1} [T]^T \tag{18}$$

$$[K_u] = \frac{E\,I}{L^3} \begin{bmatrix} 12 & 6L & -12 & 6L \\ & 4L^2 & -6L & 2L^2 \\ & & 12 & -6L \\ sym & & & 4L^2 \end{bmatrix} \begin{matrix} u_i \\ \theta_i \\ u_{i+1} \\ \theta_{i+1} \end{matrix} \tag{19}$$

(with column labels $u_i \quad \theta_i \quad u_{i+1} \quad \theta_{i+1}$)

The stiffness matrix of undamaged element $[K_u]$ is the same that developed by (**Merovitch 1975**), for undamaged beam element with rectangular cross-section given by Bernoulli-Eular theory have two nodes with two degree of freedoms (2 d. o.f.s), $\{u, \theta\}$ at each node, as seen in **Fig. 2**, the mass matrix for an element without crack is

$$[M_u] = \frac{\bar{m}\,L}{420} \begin{bmatrix} 156 & 22L & 54 & -13L \\ & 4L^2 & 13L & -3L^2 \\ & & 156 & -22L \\ sym & & & 4L^2 \end{bmatrix} \tag{20}$$

Where $\bar{m}$ is the mass per unit length.

According to the principle of Saint-Venant, the stress field is affected only in the region adjacent to crack. However, the calculation of the additional stress energy of a crack has been studied in fracture mechanics and the flexibility coefficient expressed by a stress intensity factor can be derived by applying the Castigliano's theorem in linear-elastic range.

From the condition of equilibrium, the stiffness matrix of the cracked element in the free-free state can be derived. For a rectangular beam having width b and height h the additional strain energy $W^{(1)}$ due to the crack, (**Dewen 2004**) can be written as

$$W^{(1)} = \int_0^{Ac} \frac{\partial W^{(1)}}{\partial A}\, dA = \int_0^{Ac} J\, dA \tag{21}$$

Where Ac is the area of the crack surface. The idea of relating J, strain energy release rate to the stress intensity factor K was proposed by (**Hellan 1984**) for the three modes, who gave the general formula of J as a function of stress intensity factor K as:

$$J = \frac{\beta}{E} K_I^2 + \frac{\beta}{E} K_{II}^2 + \frac{1+\nu}{E} K_{III}^2 \; , \qquad \beta = \begin{cases} 1 & \text{for plane stress} \\ 1-\nu^2 & \text{for plane strain} \end{cases} \qquad (22)$$

Where K_I, K_{II}, K_{III} is the stresses intensity factors for fracture mode of I, II, III which are opening, sliding and tearing types respectively, and ν is the Poisson's ratio. The stress intensity factor K_i from **(Hellan 1984)** is:

$$K_i = \sigma_i \sqrt{\pi a} \; F(a/h) \qquad (23)$$

Where σ_i is the stress for the corresponding fracture mode, a is the depth of the crack, $F(a/h)$ is the correction factor for the finite specimen.

Substituting Eq. (22) into Eq. (21) gives the additional strain energy due to the crack $W^{(1)}$

$$W^{(1)} = b \int_0^a \left(\frac{(K_I^2 + K_{II}^2)}{E_p} + \frac{(1+\nu)K_{III}^2}{E} \right) da \qquad \text{where} \quad dA = b \times da \qquad (24)$$

$E_p = E$ For plane stress, $E_p = E/(1-\nu^2)$ for plane strain and b is the width of the beam.

The case of plane stress or plane strain, it depends on the dimensions of the beam, and this study take into account the plane stress since the beam is thin (slender) when the length is more than (10) times its least lateral dimensions **(Singor 1951)**.

Taking into account only bending including the opening (I) and sliding (II) modes, the Eq. (24) becomes;

$$\boldsymbol{W^{(1)} = b \int_0^a \left\{ \left[(K_{IM} + K_{IP})^2 + K_{IIP}^2 \right] / E_P \right\} da} \qquad (25)$$

Where K_{IM}, K_{IP}, K_{IIP} are stress intensity factors for opening-type and sliding mode cracks due to M and P, respectively and by using Eq. (23)

$$K_{IM} = (6M/bh^2) \sqrt{\pi a} \; F_I(s) \quad \text{where} \quad \sigma = \frac{M y}{I} = \frac{M h/2}{bh^3/12} \qquad (26)$$

$$K_{IP} = (3PL/bh^2) \sqrt{\pi a} \; F_I(s) \quad \text{where} \quad \sigma = \frac{M y}{I} = \frac{PL/2 \quad h/2}{bh^3/12} \qquad (27)$$

$$K_{IIP} = (P/bh) \sqrt{\pi a} \; F_{II}(s) \quad \text{where} \quad \sigma = \frac{P}{A} = \frac{P}{bh} \qquad (28)$$

Where $F_I(s)$ and $F_{II}(s)$ are the correction factors for crack mode I and mode II , $(s = a/h)$ is defined as the ratio between the crack depth a and the height of the element h , the correction factor from **(Kisa 2000)** as

$$F_1(s) = \sqrt{(2/\pi s)\tan(\pi s/2)}\ \frac{0.923 + 0.199[1 - \sin(\pi s/2)]^4}{\cos(\pi s/2)} \tag{29}$$

$$F_{II}(s) = (3s - 2s^2)\frac{1.122 - 0.561s + 0.085s^2 + 0.18s^3}{\sqrt{1-s}} \tag{30}$$

And the additional flexibility coefficients due to the presence of the crack $C_{ij}^{(1)}$ are

$$C_{ij}^{(1)} = \frac{\partial^2 W^{(1)}}{\partial P_i \partial P_j} \tag{31}$$

$$P_1 = P, \quad P_2 = M, \quad i,j = 1,2$$

Substituting Eq. (33) into Eq. (39) and integrate over the crack height, we get the coefficients $C_{ij}^{(1)}$ which can be expressed in matrix form as

$$[C^{(1)}] = \frac{b\pi a^2}{E_p}\begin{bmatrix} 9\beta_1^2 L^2 + \beta_2^2 & 18\beta_1^2 L \\ 18\beta_1^2 L & 36\beta_1^2 \end{bmatrix} \tag{32}$$

Where $\beta_1 = F_1(s)/bh^2$ and $\beta_2 = F_{II}(s)/bh$
The total flexibility coefficients C_{ij} for the element with an open crack are

$$C_{ij} = C_{ij}^{(0)} + C_{ij}^{(1)} \tag{33}$$

The total flexibility matrix $[C]$ for the element with an open crack can be expressed as

$$[C] = [C^{(0)}] + [C^{(1)}] \tag{34}$$

The stiffness matrix of the cracked element $[K_c]$ can be written as

$$[K_c] = [T][C]^{-1}[T]^T \tag{35}$$

With program coded in Maple **7**, the coefficients of the stiffness matrix $[K_c]$ are calculated as :

$$[K_c] = \begin{bmatrix} k_{11} & k_{12} & k_{13} & k_{14} \\ k_{21} & k_{22} & k_{23} & k_{24} \\ k_{31} & k_{32} & k_{33} & k_{34} \\ k_{41} & k_{42} & k_{43} & k_{44} \end{bmatrix} \tag{36}$$

$$k_{11} = 12 \frac{E I E_P}{L^3 E_P + 12 b \pi a^2 E I \beta_2^2}$$

$$k_{12} = 6 \frac{E_P E I L}{L^3 E_P + 12 b \pi a^2 E I \beta_2^2}$$

$$k_{13} = -12 \frac{E I E_P}{L^3 E_P + 12 b \pi a^2 E I \beta_2^2} = -k_{11}$$

$$k_{14} = 6 \frac{E_P E I L}{L^3 E_P + 12 b \pi a^2 E I \beta_2^2}$$

$$k_{21} = k_{12}$$

$$k_{22} = 4 \frac{(L^3 E_P + 27 b \pi a^2 EI \beta_1^2 L^2 + 3 b \pi a^2 E I \beta_2^2) EI E_P}{(L E_P + 36 b \pi \beta_1^2 a^2 E I)(L^3 E_P + 12 b \pi a^2 E I \beta_2^2)}$$

$$k_{23} = -6 \frac{E_P E I L}{L^3 E_P + 12 b \pi a^2 E I \beta_2^2}$$

$$k_{24} = 2 \frac{(L^3 E_P + 54 b \pi a^2 EI \beta_1^2 L^2 - 6 b \pi a^2 E I \beta_2^2) EI E_P}{(L E_P + 36 b \pi \beta_1^2 a^2 E I)(L^3 E_P + 12 b \pi a^2 E I \beta_2^2)}$$

$$k_{31} = k_{13} = -k_{12}$$

$$k_{32} = k_{23}$$

$$k_{33} = k_{11} = 12 \frac{E I E_P}{L^3 E_P + 12 b \pi a^2 E I \beta_2^2}$$

$$k_{34} = -6 \frac{E_P E I L}{L^3 E_P + 12 b \pi a^2 E I \beta_2^2} = -k_{14}$$

$$k_{41} = k_{14}$$

$$k_{42} = k_{24}$$

$$k_{43} = k_{34} = -k_{14}$$

$$k_{44} = 4 \frac{(L^3 E_P + 27 b \pi a^2 EI \beta_1^2 L^2 + 3 b \pi a^2 E I \beta_2^2) EI E_P}{(L E_P + 36 b \pi \beta_1^2 a^2 E I)(L^3 E_P + 12 b \pi a^2 E I \beta_2^2)} = k_{22}$$

Therefore:

$$[K_C] = \begin{bmatrix} k_{11} & k_{12} & -k_{11} & k_{14} \\ k_{12} & k_{22} & -k_{12} & k_{24} \\ -k_{11} & -k_{12} & k_{11} & -k_{14} \\ -k_{14} & k_{24} & -k_{14} & k_{22} \end{bmatrix} \quad (37)$$
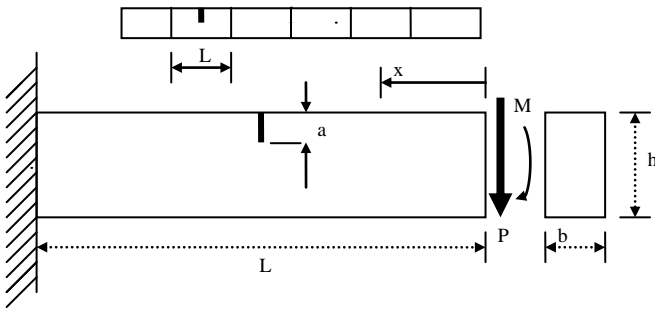
Fig.1: Diagram of a generic element   **Fig. 2:** Equilibrium condition of a generic element
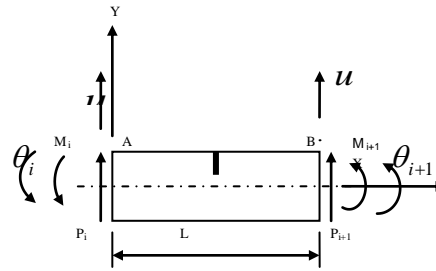
FREE VIBRATION ANALYSIS AND DAMAGE DETECTION METHODS

EIGENVALUES AND EIGENVECTORS

For free vibration with undamped system, the equation of motion expressed by matrix form is

$$[M]\{\ddot{x}\} + [K]\{x\} = \{0\} \tag{38}$$

Where:
  K : Stiffness matrix of the system.
  M : Mass matrix of the system.
  $\{x\}$: Mode shape vector.

$$M\,\ddot{X} + KX = 0 \tag{39}$$

By using Eigen Value Problem algorithm EVP , the natural frequencies and mode shapes are obtained.

DAMAGE EFFECT ON MODAL PARAMETERS

Three structures of beam (simply supported and two plane frames: portal and crane frames) had been used to study the damage effect on modal parameters (frequencies and mode shapes).

- Simply Supported Beam

The free vibration of a simply supported beam with and without damage is performed. Modal responses of the beam are generated using finite element models before and after damaging episode cases. The dimensions and material properties of the simply supported steel beam are listed in **Table 1** and **Fig .3** illustrates the model of the simply supported beam.

For Finite Element Analysis purposes, the beam is divided into 40 elements. Here, six damage scenarios are investigated, as summarized in **Table 2**. In the first two cases (1, 2), the damage is simulated by reducing the stiffness of assumed elements. In cases (3 to 6), damage is simulated in the form of cracks. The finite element model of the beam uses the stiffness matrix of the cracked element described **Eq. (37)**.
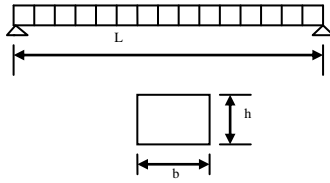
Fig.3: Simply supported beam

Table 1: Dimensions and material properties for beam

Length of the beam	$L = 254$ cm.
Height of the cross section	$h = 10.16$ cm.
Mass density	$\rho = 7808$ kg/m^3
Width of the cross section	$b = 5.08$ cm.
Elastic modulus	$E = 199.95$ GPa.

Table 2: Damage scenario for simply supported beam

Damage scenario	Damaged Position	Stiffness Reduction (%)	Crack depth ratio a/h
D1	21~ (0.5L)	25	
D2	21~ (0.5L)	50	
C1	21~ (0.5L)		0.1
C2	21~ (0.5L)		0.25
C3	9~ (0.2 L), 21~ (0.5L)		0.1
C4	9~ (0.2 L), 21~ (0.5L)		0.25

- Portal Frame

The free vibration analysis of a portal frame with and without damage was performed. The modal quantities of the portal frame were numerically generated using finite element without and with damage episodes. The dimensions of the portal frame are listed in **Table 3**; **Fig 4** illustrates the model of the frame. For modal analysis purpose, the beam and the columns were divided into 40 elements. As in the case of the simply supported beam, the dynamic characteristic (frequencies and mode shapes) before and after the damage were calculated for each damage scenario in **Table 4**.

Table 3: Dimensions and material properties for portal frame

Length of the beam in the frame	L = 243.84 cm
Column height	Hc = 243.84 cm
Cross section width	b = 5.08 cm
Cross section Height	h = 12.7 cm
Mass density	$\rho = 7808$ kg / m^3
Elastic modulus	E = 199.95 GPa
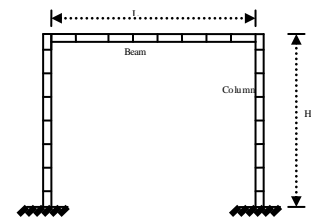
Fig.4: Portal frame

Table 4: Damage scenarios for portal frame.

Damage scenario	Damage member	Damaged position	a/h
PC1	Right column	4 (from col. base) ~ (0.1 L)	0.1
PC2	Right column	4 (from col. base) ~ (0.1 L)	0.2
PC3	Beam	21~ (0.5L)	0.1
PC4	Beam	21~ (0.5L)	0.2
PC5	Beam	21, 36 ~ (0.5L, 0.9L)	0.1
PC6	Beam	21, 36 ~ (0.5L, 0.9L)	0.2

- Crane Frame

     The modal quantities of the crane frame were numerically generated using finite element without and with damage episodes. The dimensions and material properties of the crane frame are listed in **Table 5**, **Fig. 5** illustrates the model of the crane frame. For modal analysis purpose, the vertical column was divided into 40 elements while the horizontal column divided into 20 elements. Seven damage scenarios were investigated and are summarized in **Table 6**.
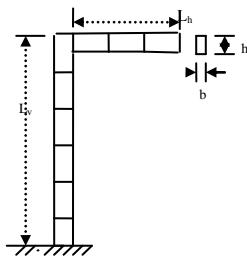
Table 5: Dimensions and material properties for crane frame

Vertical column	$L_v = 254$ cm
Horizontal column	$L_h = 127$ cm
Cross section width	$b = 5.08$ cm
Cross section Height	$h = 12.7$ cm
Elastic modulus	$E = 199.95$ GPa
Mass density	$\rho = 7808$ kg / m^3

Fig.5: Crane frame model

Table 6: Damage scenarios for crane frame

Damage scenarios	Damaged element	Damaged element	Damage severity a/h
C1	Vertical column	8 (from col.base)~ 0.2L	0.1
C2	Vertical column	8 (from col.base)~ 0.2L	0.2
C3	Vertical column	8,30~ (0.2L,0.75L)	0.1
C4	Vertical column	8,30~ (0.2L,0.75L)	0.2
C5	Horizontal column	10 ~ (0.5L)	0.1
C6	Horizontal column	10 ~ (0.5L)	0.2
C7	Horizontal column	10 ~ (0.5L)	0.5

DAMAGE DETECTION METHODS FOR BEAM STRUCTURES

In this research a different methods have been monitored here to detect damage in the beam structures which can be classified into two categories:

- Methods based on changes in mode shapes and frequencies.
    - **Eigenparameter method.**
    - **Mode shape relative difference method.**
- Methods based on the mode shape curvature.
- **A. Absolute difference curvature mode shape method.**
- **B. Curvature-energy damage index method.**

1. Methods Based on Changes in Mode Shapes and Frequencies

A. Eigenparameter Method

The eigenparameter method was proposed by **(Yuen 1985)** and **(Salawe 1993)** to detect the presence and location of damage in a cantilever beam. It is based on the premise that the mode displacements associated with each of the dynamic degrees of freedom would be affected differently by presence of damage and the changes in the mode shapes should reflect the location and extent of the damage.

$$([K] - \lambda_i [M]) \{\phi\}_i = 0 \tag{40}$$

$$([K^*] - \lambda_i^* [M]) \{\phi^*\}_i = 0 \tag{41}$$

A parameter that accounts for the changes in the frequencies and mode shapes of the structure is proposed to be used for damage detection. For the $i-th$ mode shape, the eigenparameter is defined by

$$\{U\}_i = \frac{\{\phi^*\}_i}{\omega_i^{*2}} - \frac{\{\phi\}_i}{\omega_i^2} \tag{42}$$

λ_i : The eigenvalue, $\lambda_i = \omega_i^2$.

$\{U\}_i$: Eigenparameter vector.

$\{\phi\}_i$: Undamaged mode shape vector.

$\{\phi^*\}_i$: Damaged mode shape vector.

ω_i^2 : Undamaged eigenvalue.

ω_i^{*2} : Damaged eigenvalue.

B. Mode Shape Relative Difference Method.

In this formulation, a comparison of the displacement mode shapes is used as an indicator of the damage location. The parameter used is the relative difference (RD) between the mode shapes for the

undamaged and damaged structure. For the i-th mode shape the parameter is a vector defined as (**Fox 1992**):

$$\{RD\}_i = \frac{\{\phi\}_i - \{\phi^*\}_i}{\{\phi\}_i} \tag{43}$$

Where:

$\{\phi\}_i$: Normalized undamaged mode shape vector.

$\{\phi^*\}_i$: Normalized damaged mode shape vector.

In theory a plot of the vector $\{RD\}$ as a function of the measurement locations should show a definite trend with distinct discontinuity at the damage locations.

- Methods based on the mode shape curvature

A. Absolute Difference Curvature Mode Shape.

It has been evaluated by (**Pandy 1991**) and (**Shakkar 2006**). Curvature mode shape is related to the flexural stiffness of the beam cross-sections. By definition, (**Black 1966**), the curvature at a point of an element with bending deformation, is given by:

$$\upsilon^{"} = \frac{M}{EI} \tag{44}$$

In which $\upsilon^{"}$ is the curvature at a section, M is the bending moment at a section, E is the modulus of elasticity and I is the second moment of the cross-sectional area.

If crack or other damage is introduced in a structure, it reduces the flexural stiffness EI of the structure at the cracked section in the damaged region. This in turn increases the magnitude of curvature at that section of the structure. The change in the curvature increases with the reduction in the value of the flexural stiffness EI.

Starting with the displacement mode shapes obtained from the finite element analysis, the curvature mode shapes for the undamaged structure can be obtained numerically using a central difference approximation as

$$\phi_i^{"} = \frac{\phi_{i-1} - 2\phi_i + \phi_{i+1}}{H^2} \tag{45}$$

Where:

H : Distance between the measurement points (i) and $(i+1)$.

ϕ_i : Mass normalized mode shape of the undamaged structure associated with a given frequency.

Similarly, the curvature mode shape for the damaged structure can be obtained as

$$\phi_{*,i}^{"} = \frac{\phi_{i-1}^* - 2\phi_i^* + \phi_{i+1}^*}{H^2} \tag{46}$$

Where,

ϕ_i^*: Mass normalized mode shape of the damaged structure corresponding to specific natural frequency.

For mode j the absolute difference between the curvatures of the damaged and undamaged structure is calculated as

$$\{\Delta\phi''\}_j = \left| \{\phi_*''\}_j - \{\phi''\}_j \right| \tag{47}$$

B. Curvature-Energy Damage Index Method

The presence of the damage in a beam structure increases the magnitude of the curvature at that section of the structure. In this section a damage index based on the modal curvature is proposed by **(Herrera 2005)**. It is based on the concept of the pseudo flexibility matrix. The proposed modal curvature-energy based matrix can be defined by

$$[X]_{n\times n} = [\Phi'']_{n\times m} \quad [\Lambda]^{-1}_{m\times m} \quad [\Phi'']^T_{m\times n} \tag{48}$$

Where n the number of points for mode is shape measurement and m is the number of measured modes. $[\Phi'']$ Is the modal curvature matrix formed by the curvature mode shapes $\{\phi_i''\}$:

$$[\Phi''] = [\{\phi_1''\} \quad \{\phi_2''\} \quad \cdots \quad \{\phi_m''\}] \tag{49}$$

$[\Lambda]$: Matrix contains diagonal Eigenvalues.

For the damaged structure, the proposed curvature-energy matrix can be expressed as

$$[X^*]_{n\times n} = [\Phi_*'']_{n\times m} \quad [\Lambda]^{-1}_{m\times m} \quad [\Phi_*'']^T_{m\times n} \tag{50}$$

For the undamaged structure, the corresponding curvature-energy matrix is given by Eq. (48). In terms of these curvature-energy matrices, the relationship between damaged and undamaged states, is defined by

$$\{x\} = \{x_*\}./\{x_u\} \tag{51}$$

Where the symbol $\cdot/$ is used to indicate that the division of the vectors is done by element.

$\{x_u\}$: Diagonal of matrix $[X]$.

$\{x_*\}$: Diagonal of matrix $[X^*]$.

It is proposed to define the damage index for the j th location as

$$k_j = |x_j - 1| \tag{52}$$

RESULTS AND DISCUSSION

The Results and Discussion for Simply Supported Beam

The results for the first five frequencies are listed in **Table 7** for the damage scenarios considered in **Table 2** for simply supported beam.

Table 7: Natural frequencies of the simply supported beam

Damage	Natural Frequency (rad/sec)				
Scenario	Mode 1	Mode 2	Mode 3	Mode 4	Mode 5
Exact undamaged	227.0616	908.7063	$2.0452*10^3$	$3.6329*10^3$	$5.6764*10^3$
Present undamaged	227.0525	908.2102	$2.0435*10^3$	$3.6329*10^3$	$5.6764*10^3$
D1	225.1870	908.1489	$2.0272*10^3$	$3.6319*10^3$	$5.6331*10^3$
D2	221.5876	908.0297	$1.9969*10^3$	$3.6301*10^3$	$5.5558*10^3$
C1	226.3955	908.198	$2.0377*10^3$	$3.6328*10^3$	$5.6609*10^3$
C2	222.2865	894.2703	$2.0027*10^3$	$3.6177*10^3$	$5.5702*10^3$
C3	225.9728	905.0045	$2.0286*10^3$	$3.6300*10^3$	$5.6540*10^3$
C4	211.5363	875.7897	$1.9674*10^3$	$3.5918*10^3$	$5.5540*10^3$

The Results and Discussion for Portal Frame and Crane Frame

The results for the first five natural frequencies are listed in **Table 8** for the damage scenarios considered in **Table 4** for portal frame. It can be noted that the highest variation for the first modal frequency caused by simulated damage (crack) scenario was 0.46% and the highest decreasing for mode 2, 3, 4 and 5 were 0.99, 0.26, 1.1 and 0.18 %, respectively. It can be noted that the highest variation for the damage scenarios from C1 to C6 for the first modal frequency cased by simulated damage scenario was 2 % and the highest decreasing for mode 2, 3, 4 and 5 were 1.44, 0.33, 6.3 and 9.4 %, respectively for crane frame as in **Table 9**.

Table 8: Natural frequencies for portal frame

Damage	Natural Frequency (rad/sec)				
Scenario	Mode 1	Mode 2	Mode 3	Mode 4	Mode5
Undamaged	101.9480	394.4309	653.5440	699.6075	1.3341×10^3
PC1	101.8173	393.7627	653.4660	698.1770	1.3269×10^3
PC2	101.4750	392.7021	653.4069	695.7772	1.3218×10^3
PC3	101.9471	393.4324	653.3958	698.2410	1.3339×10^3
PC4	101.9456	390.5907	653.0997	696.3602	1.3338×10^3
PC5	101.8433	393.3805	653.0262	696.3385	1.3334×10^3
PC6	101.5538	390.4968	651.8200	691.6682	1.3317×10^3

Table 9: Natural frequencies for Crane frame

Damage Scenarios	Natural Frequency (rad/sec)				
	Mode 1	Mode 2	Mode 3	Mode 4	Mode 5
Undamaged	54.6114	221.3366	644.4290	$1.5358*10^3$	$1.7672*10^3$
C1	54.3582	221.0727	644.0045	$1.4969*10^3$	$1.6594*10^3$
C2	53.6443	220.6903	643.6281	$1.4762*10^3$	$1.6363*10^3$
C3	54.2939	220.3281	643.4483	$1.4710*10^3$	$1.6362*10^3$
C4	53.5103	218.1355	642.2623	$1.4376*10^3$	$1.6010*10^3$
C5	54.5648	221.1289	643.7407	$1.5301*10^3$	$1.7644*10^3$
C6	54.5630	220.7885	642.3609	$1.5150*10^3$	$1.7596*10^3$
C7	54.5612	215.3734	621.4992	$1.3088*10^3$	$1.7232*10^3$

The Results and Discussion of Damage Detection Method

The Results and Discussion of Eigenparameter

The eignparameter was calculated for the first two mode shapes. The parameter for the first mode shows the largest change at this location of the damage, i.e. the peak value occurs in the damaged region. Also at the location the slope changes sign. The damage scenarios D1, D2, C1 and C2 correspond to a single crack at the mid-span for simple beam. It can be observed that the absolute value of the parameter increases with an increase in the severity of the damage. The peak observed in **Fig .6** for single damage as in (a) and (b). For multiple damage, the peak is clear for one location of damage for portal frame and crane frame in **Fig .6,** for (c) and (d) for cases PC5, PC6 for portal frame and C3, C4 for crane frame respectively.

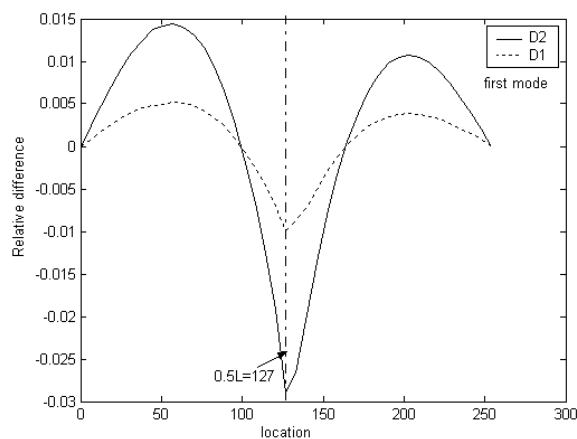**(a)**   **(b)**

(c)　　　　　　　　　　　　　　　　(d)
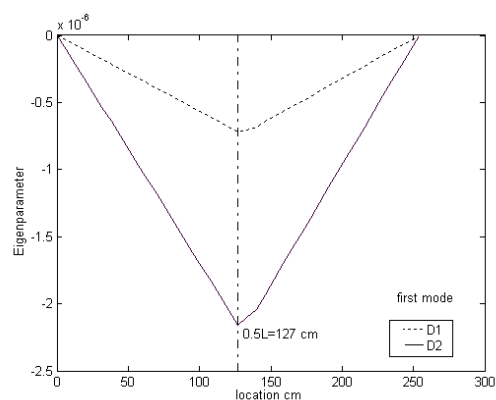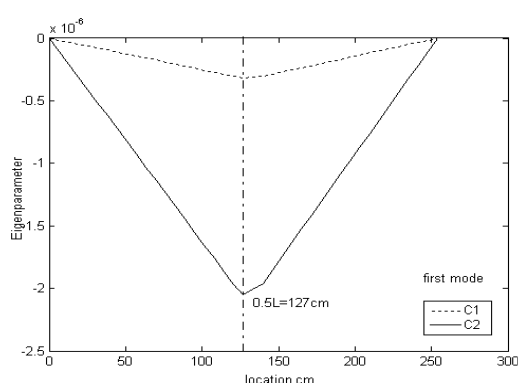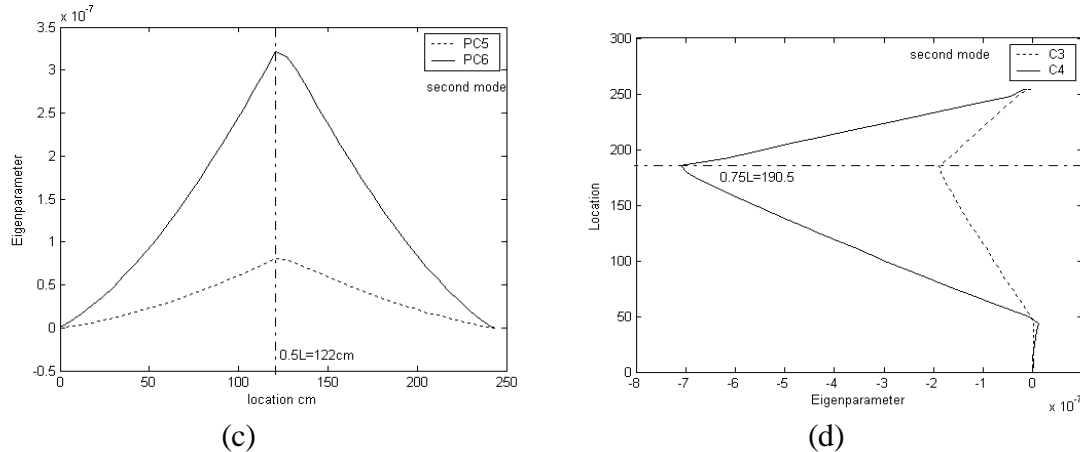
**Fig. 6:** Eigenparameter for 1st and 2nd modes of the simply supported beam (a, b), portal (c) and crane frames (d).

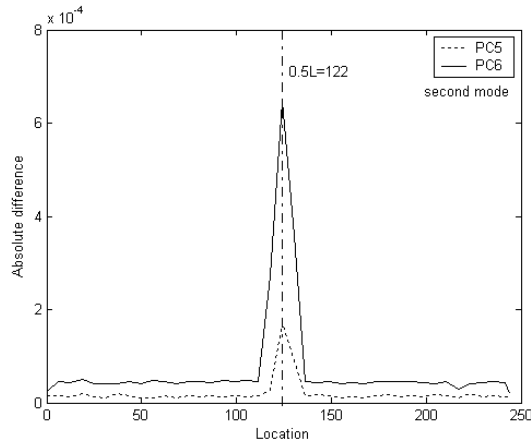## The Results and Discussion of Relative Difference Method

The peaks occur at damage location in **Fig. 7** for simply supported in (a) for single damage and (b) for multiple damage. The peak observed for one location for portal frame as in (c) and it's observed in (d). In Figures illustrated the mode difference was normalized with respect to the maximum absolute value of the mode shape of the undamaged system as in previous sections in simply supported, portal frame and crane frame. As expected, the differences are larger for case damage C2, since this correspond to a larger crack depth for the same cross section.

(a)　　　　　　　　　　　　　　　　(b)
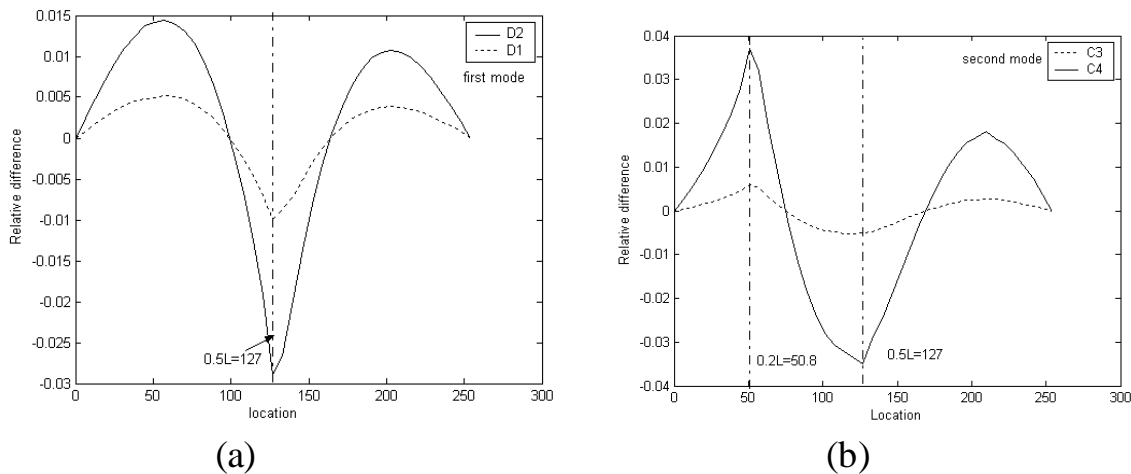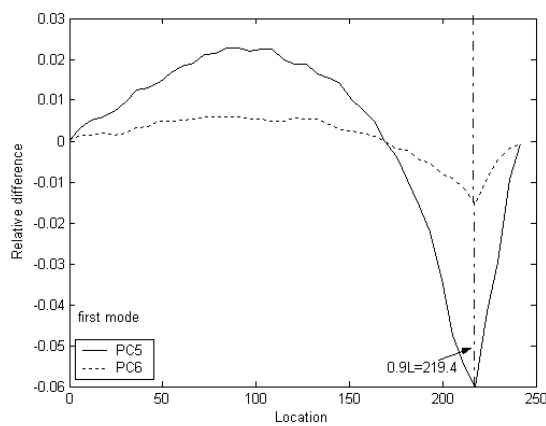
(C)
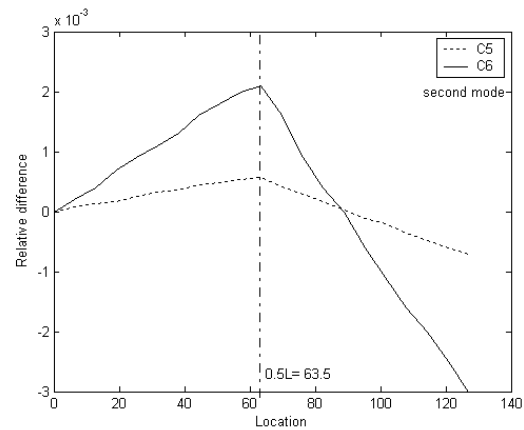
(d)

Fig. 7: Relative difference for first and second modes of the simply supported beam (a, b), portal (c) and crane frames (d).

The Results and Discussion for Absolute Difference Curvature Mode Shape

Fig. 8 Shows the results for damage scenarios D1, D2, C1, C2 for simple beam, PC5, PC6 for portal frame and C5, C6 for crane frame. As it can be seen in **Fig. 8**, the maximum difference for each curvature mode shape occurs in the damaged region, which is at location 0.5L for these damage scenarios. In the multiple damage scenarios (C3 and C4), the presence of two cracks at the vertical column is simulated. The defects are at position (0.2L=50.8cm and 0.75L=190.5cm) measured from the fixed end of the column. It is evident from the graphs displayed that the peak observed in the damage location as in (a), (b), (c) and (d).

(a)
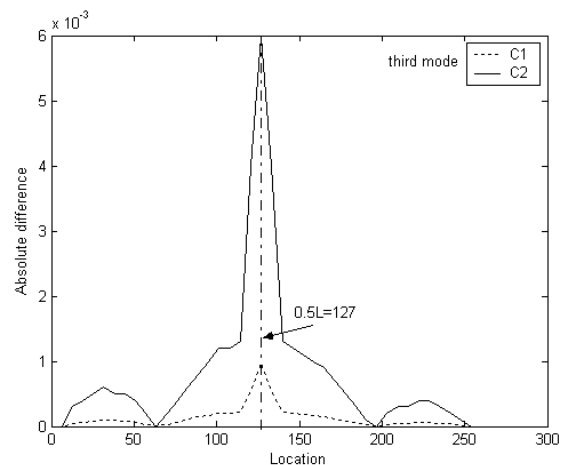
(b)
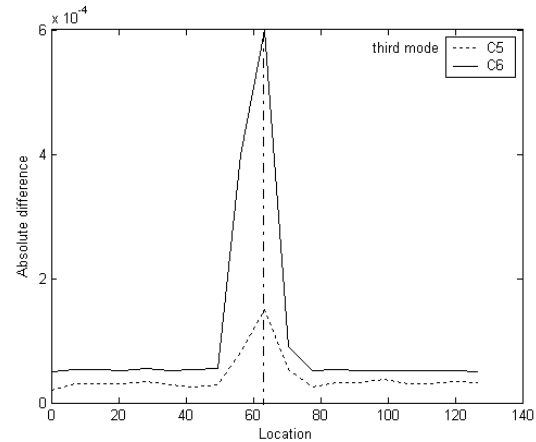
(c)   (d)

Fig. 8: Absolute difference curvatures for the three modes of the simply supported beam (a, b), portal frame (c) and crane frame (d).

### The Results and Discussion of Curvature-Energy Damage Index Method

The results of the proposed damage index for the damage scenarios D1 to C4 are shown in **Fig. 9** is calculated using only two curvature mode shapes. When two cracks are induced in the beam (damage scenarios C3 and C4), the proposed method is capable of detecting the location of the two cracks, as evidenced by the peaks in the index k_j in **Fig 9**.
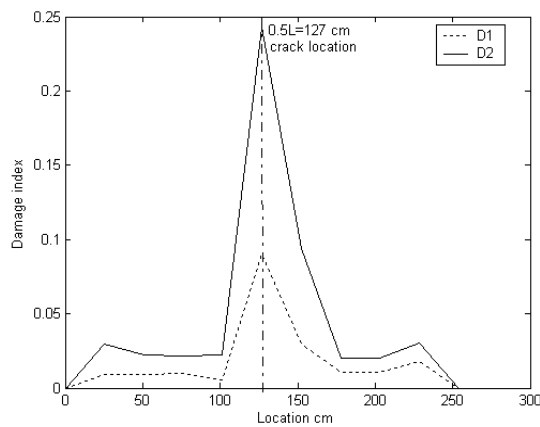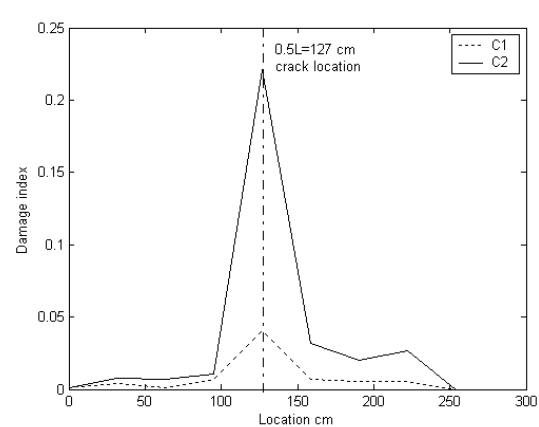
(a)   (b)
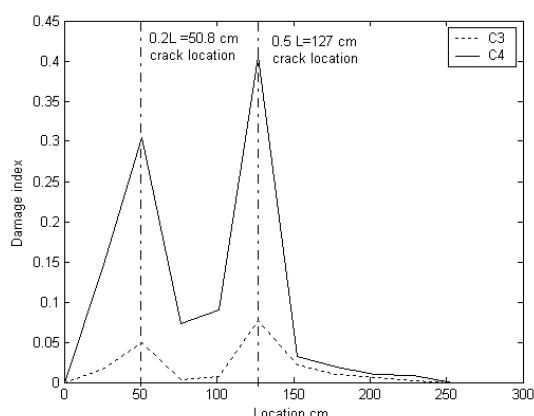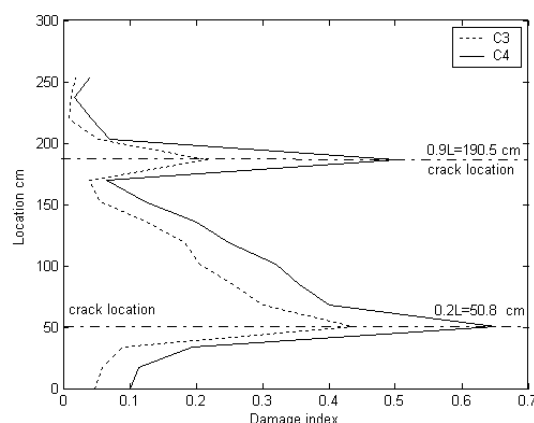
(c)   (d)

Fig. 9: Curvature-Energy damage index method for the three modes of the simply supported beam (a, b), portal frame (c) and crane frame (d).

CONCLUSION

The main conclusions from the present work according to the adopted data may be stated as follows:

- Based on assumption that the damage will change the stiffness reduction only and the mass of the beam be consistent, the increased severity of the damage will decrease the frequencies of the damaged beam.

- It's observed that, the damage representation as stiffness reduction 25% is not equal to the damage represented by crack ratio 25%, accordingly it's obvious that the crack is more sensitive than stiffness reduction in representing the damage.

- Changes on mode shape are much more sensitive to local damage when compared with changes in natural frequencies. However, using mode shapes also has some limitations, as the damage is a local phenomenon, it may not significantly influence the mode shapes of the lower modes, that are usually those measured from vibration tests, and it's obvious in large structures, as in portal frame.

- The structural damage identification technique based on changes in the displacement mode shapes, referred to eigenparameter was able to indicate the location of damage with only one crack in the three structures. For multiple damage scenarios, the eigenparameter was not locating the damage zones.

- The methodologies based on the modal curvatures energy exhibited superior performance in detecting and locating the damage. The curvature- energy damage index method is the best method used since; it does detect and locate the single or multiple damage in the three structures which considered in this study.

REFERENCES

- Black, P., (1966). "Strength of materials" /first edition.

- Dewen, B. E, M.E. (2004). "Damage detection in mechanical structures through coupled response measurements". A thesis submitted in partial fulfillment of the requirements for the degree of Doctor of Philosophy in Mechanical Engineering /University of Queensland, Brisbane, Australia.

- Fox, C. H.J. (1992). "The location of defects in structures: A comparison of the use of natural frequency and mode shape data". Proceeding of the 10th international modal analysis conference, San Diego, USA, P.522-528.

- Hellan, K., (1984). "Introduction to fracture mechanics", (Book). University of Trondheim /Norway. Printed in USA.

- Herrera, J. C., (2005). "Evaluation of structural damage identification methods based on dynamic characteristics". A thesis submitted in partial fulfillment of the requirements for the degree of Doctor of Philosophy in civil engineering / University of Puerto Rico.

- Kisa, M. and Brandon, J., (2000). "The effect of cracks on the dynamics of a cracked cantilever beam". Available online at http:// www.idealibrary.com on **IDEAL**, Cardiff, England. Academic pressRen, W. X. and De Roeck, G. (2002). "Structural damage identification using modal data. I.: Simulation verification". *ASCE*. Journal of structural engineering, Vol. 128, No. 1 January, 87-95.

- Merovitch L., (1975). "Elements of vibrations analysis", (Book)   International student edition.
- Pandy, A.K., Biswas, M. and Samman, M.M., (1991). "Damage detection from changes in curvature mode shapes ".

- Qian, G.L. and Jiang, J.S., (1990) "The dynamic behavior and crack detection of a beam with a crack". Journal of sound and vibration, Vol.138, No. 2, 233-243.

- Singor L., F., (1951). "Strength of materials". Second edition   (book).

- Thakkar, S. K., Ghoh, G. and Singh Y., (2006). "Structural damage identification and helth monitoring and damage identification of bridges". Journal. Advance in bridge engineering, March 24-25.

- Thomson, W.T, (1988). "Theory of vibration with applications". Book / third edition. University of California, USA, printed in London.

- Yuen, M., (1985). "A numerical study of the eigenparameters of a damaged cantilever". Journal of sound and vibration, Vol. 103, No.3, 301-310.

- Salawe, O.S. and Williams, C. (1993). "Structural damage detection using experimental model analysis". Proceeding of the 11th international modal analysis conference, Kissimmee, Florida, 254-260.

BOUNDING SURFACE COUPLED FINITE ELEMENT CONSOLIDATION ANALYSIS OF NORMALLY AND OVERCONSOLIDATED CLAYS

By

Omar Al-Farouk S. Al-Damluji and Ayad N. Al-Ebady

ABSTRACT

The radial mapping version of the bounding surface plasticity model is implemented in a computer program to predict the response of cohesive soils. The eight-noded isoparametric element and Biot's theory are used in this study for analyzing soil consolidation problems. The model has been used in the analysis for two classes of problems. The first involves the comparison of model predictions with the results of laboratory tests in compression and extension for normally and overconsolidated clays. The second class involves using the model to predict the results of one- and two-dimensional finite element problems of soil consolidation. The comparisons with experiments demonstrate that the model, through its simplicity, can describe realistically the soil response under different monotonic loading conditions at any overconsolidation ratio. The comparison between the bounding surface plasticity model with the classical modified Cam clay model shows considerably different rates and magnitudes of settlement, and different pore pressure behavior during the consolidation process.

الخلاصة

لقد تم تطبيق نسخة المرتسم الشعاعي على نموذج لدونة السطح المحيط في برنامج حاسوبي لتوقع استجابة الترب المتماسكة. لقد استخدمت عناصر محددة ذات ثمانية عقد مع نظرية بيو في هذه الدراسة لتحليل مسائل الانضمام في التربة. لقد تم استخدام النموذج لتحليل صنفين من المسائل. يتطرق الصنف الاول الى مقارنة توقعات النموذج مع نتائج فحوص مختبرية تحت الانضغاط و الاستطالة لاطيان منضمة اعتياديا و اخرى منضمة بزيادة. يبحث الصنف الثاني باستخدام النموذج لتوقع نتائج مسائل انضمام التربة بمعية عناصر ببعد واحد و ببعدين. تظهر المقارنات مع التجارب قدرة النموذج البسيط على توقع استجابة التربة الحقيقية تحت ظروف تحميل رتيبة مختلفة و باية نسبة من الانضمام الزائد. تظهر مقارنة بين نموذج السطح المحيط مع نموذج طين كام المعدل التقليدي معدلات و قيم مختلفة من الانضمام اضافة الى اختلاف في تصرف الضغط المسامي اثناء عملية الانضمام.

KEYWORDS
Clays, consolidation, bounding surface, constitutive relations, numerical modeling and analysis.

INTRODUCTION
Consolidation plays an important role in many soil mechanics problems. This is evident by the vast amount of literature devoted to the solution of this problem since the pioneering work of Terzaghi. Probably the most difficult problems that a soil engineer is asked to solve, is the accurate prediction of the settlement of a finite loaded foundation on a thick compressible stratum.

A major problem in applying any solution procedure to geotechnical engineering problems is to provide a realistic representation of the stress- strain characteristics for the porous medium. The

choice of appropriate constitutive or stress-strain laws or models may have a significant influence on the numerical results obtained. Their importance has been enhanced significantly with the great increase in development and application of many modern computer-based techniques such as the finite element, finite difference, and boundary integral equation methods. It has been realized that the advances and sophistication in the solution techniques have far exceeded our knowledge of the behavior of materials defined by constitutive laws. As a consequence, very often, results from a numerical procedure that may have used less appropriate constitutive laws can be of limited or doubtful validity.

The objective of this study is to implement one of the several relatively new and very promising plasticity models for soils (the bounding surface plasticity model) in a general nonlinear analysis program to establish the accuracy and limitations of the model formulation. The model has been used in the analysis of two classes of problems. The first involves the comparison of model predictions to the results of laboratory tests. The second class involves using the model to predict the results of one- and two-dimensional finite element problems of soil consolidation.

THE GOVERNING EQUATIONS FOR SINGLE FLOW IN A DEFORMING POROUS MEDIUM

In this section, the governing equations for single flow in a deforming porous medium are developed. The governing equations are developed in line of Biot's self consistent theory *(Biot, 1941; Biot, 1955; Biot, 1956)*. The solid phase is assumed to be comprised of a porous skeleton of particles surrounded by one fluid. The small strain theory is considered to be applicable, and so Darcy's law is assumed valid in terms of absolute fluid velocity.

It is assumed that a pure fluid pressure p causes only a uniform, volumetric strain by compressing the grains and that the major deformation of the porous skeleton is governed by the effective stress σ'. This is defined as follows, with the sign convention that tension is positive:

$$\sigma = \sigma' - mp \qquad (1)$$

where σ is the total stress and m is equal to unity for the normal stress components and zero for the shear stress components.

The constitutive equation relating effective stress σ' to the strains of the skeleton is now independent of the pore pressure p, and for a general non-linear material can be written in a tangential form, thus allowing plasticity to be incorporated. If creep strain is present, the expression is written in a general form as *(Lewis and Schrefler, 1987)*:

$$d\sigma' = D_T (d\varepsilon - d\varepsilon_c - d\varepsilon_p - d\varepsilon_o) \qquad (2a)$$

where $d\varepsilon$ represents the total strain of the skeleton,

$$d\varepsilon_c = c.dt \qquad (2b)$$

is the creep strain,

$$d\varepsilon_p = -m(dp/3K_s) \qquad (2c)$$

represents the overall volumetric strains caused by uniform compression of the particles by the pressure of the pore fluid, with K_s being the bulk modulus of the solid phase.

Finally, ε_o represents all other strains not directly associated with stress changes (swelling, thermal, chemical, etc.). These types of strains are defined as "autogeneous" strains *(Zienkiewicz et. al., 1977)*.

The matrix D_T and the creep function c are dependent on the level of effective stress σ' and also, if strain effects are considered, on the total strain of the skeleton ε *(Lewis and Schrefler, 1987)*.

The equilibrium equation relating the total stress σ to the body forces b and the boundary traction $\hat{t}$ specified at the boundary Γ of the domain Ω is formulated in terms of the unknown displacement vector u. Using the principle of virtual work *(Zienkiewicz, 1977)*, the general equilibrium statement can be written as:

$$\int_\Omega \delta\varepsilon^T \sigma \, d\Omega - \int_\Omega \delta u^T b \, d\Omega - \int_\Gamma \delta u^T \hat{t} \, d\Gamma = 0 \tag{3}$$

for virtual displacement δu such that on the boundary part Γ_u, where displacements are prescribed, these are not varied. Equation 3 is already a weak statement of the equilibrium relationship which also incorporates the boundary conditions.

The equilibrium statement (Eq. 3) is also valid in incremental form:

$$\int_\Omega \delta\varepsilon^T d\sigma d\Omega - \int_\Omega \delta u^T dbd\Omega - \int_\Gamma \delta u^T d\hat{t}d\Gamma = 0 \tag{4}$$

The effective stress relationship given by the equation 1 is now incorporated into this equation and the following expression is obtained:

$$\int_\Omega d\varepsilon^T d\sigma' d\Omega - \int_\Omega \delta\varepsilon^T m dp d\Omega - d\hat{f} = 0 \tag{5}$$

where

$$d\hat{f} = \int_\Omega \delta u^T dbd\Omega + \int_\Gamma \delta u^T d\hat{t}d\Gamma$$
(6)

$d\hat{f}$ represents the change in external force due to boundary and body force loadings.

Further, on taking into account the constitutive relationship given by equation 2 and dividing by dt, the following equation is obtained:

$$\int_\Omega \delta\varepsilon^T D_T \frac{\partial\varepsilon}{\partial t} d\Omega - \int_\Omega \delta\varepsilon^T m \frac{\partial p}{\partial t} d\Omega + \int_\Omega \delta\varepsilon^T D_T m \frac{\partial p}{\partial t} \frac{1}{3K_s} d\Omega$$

$$-\int_\Omega \delta\varepsilon^T D_T c d\Omega - \int_\Omega \delta\varepsilon^T D_T \frac{\partial\varepsilon_o}{\partial t} d\Omega - \frac{\partial\hat{f}}{\partial t} = 0 \tag{7}$$

The geometrical complexity of a porous medium renders impossible a strict analytical treatment of the fluid velocity within the porous space. To overcome this obstacle, the fictitious seepage

velocity (also known as bulk or Darcy's velocity) is defined as *(Bear, 1972)*:

$$q = -\frac{1}{\mu} k \nabla (p + \rho gh) \tag{8}$$

where k is the absolute permeability matrix of the medium, μ the dynamic viscosity of the fluid, p the fluid pressure, ρ the density, g the gravity, and h is the head above some arbitrary datum.

The continuity of flow requires that the following expression is valid *(Crichlow, 1977)*:

$$(\text{rate of fluid accumulation}) + \nabla . (\rho q) = 0 \tag{9}$$

which, on combining with Darcy's law given by the equation 8, results in:

$$(\text{rate of fluid accumulation}) + \nabla . \left\{ -\frac{k\rho}{\mu} \nabla (p + \rho gh) \right\} = 0 \tag{10}$$

There are many factors which contribute to the rate of fluid accumulation and these are enumerated as follows *(Lewis et. al., 1976)*:

a. Rate of change of total strain

$$\frac{\partial \varepsilon_v}{\partial t} = m^T \frac{\partial \varepsilon}{\partial t} \tag{11a}$$

b. Rate of change of the grain volume due to pressure changes

$$\frac{1-n}{K_s} \frac{\partial p}{\partial t} \tag{11b}$$

where n is the porosity.

c. Rate of change of saturation

$$n\rho \frac{\partial s}{\partial t} \tag{11c}$$

where s is the degree of saturation.

d. Rate of change of fluid density

$$ns \frac{\partial \rho}{\partial t} \tag{11d}$$

e. Finally, the change of grain size due to effective stress changes $\partial \sigma'/\partial t$

$$-\frac{1}{3K_s} m^T \frac{\partial \sigma'}{\partial t} \tag{11e}$$

Substituting for $\partial \sigma'/\partial t$ from equation 2a into 11e yields the following expression:

$$-\frac{1}{3K_s} m^T D_T \left(\frac{\partial \varepsilon}{\partial t} + \frac{m}{3K_s} \frac{\partial p}{\partial t} - c \right) \tag{11f}$$

The continuity equation for water (with no source term) therefore becomes:

$$-\nabla^T \cdot \left\{ k \frac{\rho}{\mu} \nabla(p+\rho gh) \right\} + n\rho \frac{\partial s}{\partial t} + ns \frac{\partial p}{\partial t} + \rho s \left\{ \left(m^T - \frac{m^T D_T}{3K_s} \right) \frac{\partial \varepsilon}{\partial t} + \right.$$

$$\left. \frac{m^T D_T c}{3K_s} + \left[\frac{1-n}{K_s} - \frac{1}{(3K_s)^2} m^T D_T m \right] \frac{\partial p}{\partial t} \right\} = 0 \tag{12}$$

Equation 12 can be simplified by assuming water flowing at saturated conditions and dividing by ρ results in equation 11d for water being written as:

$$n \frac{1}{\rho} \frac{\partial \rho}{\partial t} = n \frac{1}{\rho} \frac{\partial \rho}{\partial p} \frac{\partial p}{\partial t} = \frac{n}{K_w} \frac{\partial p}{\partial t} \tag{13}$$

where K_w is the bulk modulus of water.

Equation 12 then becomes:

$$-\nabla^T \cdot \left\{ \frac{k}{\mu} \nabla(p+\rho gh) \right\} + \left(m^T - \frac{m^T D_T}{3K_s} \right) \frac{\partial \varepsilon}{\partial t} + \frac{m^T D_T c}{3K_s} +$$

$$\left[\frac{1-n}{K_s} + \frac{n}{K_w} - \frac{1}{(3K_s)^2} m^T D_T m \right] \frac{\partial p}{\partial t} = 0 \tag{14}$$

FINITE ELEMENT APPLICATION IN SOIL CONSOLIDATION

The fully coupled solution of the one-phase flow equation in an elastoplastic porous medium will now be discussed in this section. The particular form of the continuity equation 14, together with the equilibrium equation 7, form the governing equations for soil mechanics problems within the line of Biot's self consistent theory.

The consolidation problem is a boundary value problem, and this type of problems requires that the governing equations are satisfied within all points of a continuum (domain Ω) and that the boundary conditions are satisfied on the boundary Γ of the domain.

The equilibrium equation 7 has the boundary condition already incorporated. Attention is therefore focused on the continuity equation. In this case the boundary conditions satisfy:

a.   The continuity of flow across the boundary,

$$\overline{B} \equiv -n^T \frac{k}{\mu} \nabla(p+\rho gh) - q = 0 \tag{15}$$

where n is the unit normal vector and q is the outflow rate per unit area of the boundary surface.

b.   Prescribed pore pressure.

The condition that the continuity equation 14 applies throughout the continuum and that equation 15 applies on the boundary requires that:

$$\int_\Omega a^T \overline{A} d\Omega + \int_\Gamma b^T \overline{B} d\Gamma = 0 \tag{16}$$

where a and b are a set of arbitrary functions since $\overline{A}$ and $\overline{B}$ are identically satisfied throughout their respective domains.

Conversely, if equation 16 is valid for any arbitrary values a and b, then the differential equations 14 and 15 must be satisfied at all points within and on the boundary of the continuum.

The finite element method will be applied to equations 7 and 16 in terms of displacements and pore pressures. In equation 14 the appearance of second derivatives for $(p+\rho gh)$ necessitates a smooth distribution in space due to the integration of these variables. In order to overcome this limitation, a weak form of equation 14 is obtained by means of Green's theorem.

Upon substitution of equation 14 and equation 15, equation 16 becomes:

$$\int_\Omega \left\{ (\nabla a)^T \frac{k}{\mu} \nabla(p+\rho gh) + a^T \left[\left(m^T - \frac{m^T D_T}{3K_s} \right) \frac{\partial \varepsilon}{\partial t} + \frac{m^T D_T c}{3K_s} \right. \right.$$

$$\left. \left. + \left(\frac{1-n}{K_s} + \frac{n}{K_w} - \frac{1}{(3K_s)^2} m^T D_T m \right) \frac{\partial p}{\partial t} \right] \right\} d\Omega$$

$$- \int_\Gamma \left\{ a^T n^T \frac{k}{\mu} \nabla(p+\rho gh) + b^T n^T \frac{k}{\mu} \nabla(p+\rho gh) + b^T q \right\} d\Gamma = 0 \tag{17}$$

Since the values of a and b are arbitrary, it can be made:
$$b = -a$$
and thus eliminate some of the terms of the boundary integrals. Equation 17 therefore reduces to:

$$\int_\Omega \left\{ (\nabla a)^T \frac{k}{\mu} \nabla(p+\rho gh) + a^T \left[\left(m^T - \frac{m^T D_T}{3K_s} \right) \frac{\partial \varepsilon}{\partial t} + \frac{m^T D_T c}{3K_s} \right. \right.$$

$$\left. \left. + \left(\frac{1-n}{K_s} + \frac{n}{K_w} - \frac{1}{(3K_s)^2} m^T D_T m \right) \frac{\partial p}{\partial t} \right] \right\} d\Omega + \int_\Gamma a^T q d\Gamma = 0 \tag{18}$$

The finite element approximation is now applied to equations 7 and 18. The displacements and pore pressures are expressed in terms of their values $\bar{u}$ and $\bar{p}$ at a finite number of points in space.

The expressions for u, p, and ε take the form:

$$u = N\bar{u} \tag{19a}$$

$$p = \bar{N}\bar{p} \tag{19b}$$

$$\varepsilon = B\bar{u} \tag{19c}$$

in which N, $\bar{N}$ are the shape functions of displacement and pore pressure, respectively and B is the strain-displacement transformation matrix. Substituting equations 19 into equations 7 and 18, the finite element discretization gives the result:

$$\delta u^T \left\{ \int_\Omega B^T D_T B d\Omega \frac{d\bar{u}}{dt} - \int_\Omega B^T m\bar{N}d\Omega \frac{d\bar{p}}{dt} \right.$$

$$+ \int_\Omega B^T D_T \frac{m}{3K_s} \bar{N}d\Omega \frac{d\bar{p}}{dt} - \int_\Omega B^T D_T c d\Omega$$

$$\left. - \frac{1}{dt} \int_\Omega B^T D_T d\varepsilon_o d\Omega \right\} - \delta u^T \left\{ \int_\Omega N^T \frac{db}{dt} d\Omega + \int_\Gamma N^T \frac{d\hat{t}}{dt} d\Gamma \right\} = 0 \tag{20}$$

$$\int_{\Omega} (\nabla a)^{T} \frac{k}{\mu} \nabla \overline{N} d\Omega \overline{p} + \int_{\Omega} a^{T} \left(m^{T} - \frac{m^{T} D_{T}}{3K_{s}} \right) B d\Omega \frac{d\overline{u}}{dt}$$

$$+ \int_{\Omega} a^{T} \frac{m^{T} D_{T} c}{3K_{s}} d\Omega + \int_{\Omega} a^{T} \left(\frac{1-n}{K_{s}} + \frac{n}{K_{w}} - \frac{1}{(3K_{s})^{2}} m^{T} D_{T} m \right) \overline{N} d\Omega \frac{d\overline{p}}{dt}$$

$$+ \int_{\Gamma} a^{T} q d\Gamma + \int_{\Omega} a^{T} \nabla^{T} \frac{k}{\mu} \rho g h d\Omega = 0 \tag{21}$$

Equation 20 is valid for any value of the virtual displacement δu and can hence be written as:

$$K \frac{d\overline{u}}{dt} + L \frac{d\overline{p}}{dt} - C - \frac{df}{dt} = 0 \tag{22}$$

where

$$K = -\int_{\Omega} B^{T} D_{T} B d\Omega \tag{23a}$$

$$L = \int_{\Omega} B^{T} m \overline{N} d\Omega - \int_{\Omega} B^{T} D_{T} \frac{m}{3K_{s}} \overline{N} d\Omega \tag{23b}$$

$$C = -\int B^{T} D_{T} c d\Omega \tag{23c}$$

$$df = -\int_{\Omega} N^{T} db d\Omega - \int_{\Gamma} N^{T} d\hat{t} d\Gamma - \int_{\Omega} B^{T} D_{T} d\varepsilon_{o} d\Omega \tag{23d}$$

in which K= the tangential spatial stiffness matrix; L = the coupling matrix representing the influence of pore pressure in force equilibrium; C = the creep matrix and df = load vector equivalent to the body force, surface traction and autogeneous strain, respectively.

The form of the function a in equation 21 is still quite arbitrary and must be specified before equation 21 can be solved. It is desirable to choose a form which will increase the accuracy of the approximation used. For this purpose, the method of weighted residuals procedure has been applied, using the Galerkin method *(Zienkiewicz, 1977)*.

The function a is replaced by a finite number of functions within each element, which is in the Galerkin method are identical to the shape functions $\overline{N}$. Equation 21 now becomes:

$$H\overline{p} + S \frac{d\overline{p}}{dt} + L^{T} \frac{d\overline{u}}{dt} - \overline{f} = 0 \tag{24}$$

where:

$$H = \int_{\Omega} \left(\nabla \overline{N} \right)^{T} \frac{k}{\mu} \nabla \overline{N} d\Omega \tag{25a}$$

$$S = \int_{\Omega} \overline{N}^{T} S \overline{N} \quad \text{with} \quad S = \frac{1-n}{K_{s}} + \frac{n}{K_{w}} - \frac{1}{(3K_{s})^{2}} m^{T} D_{T} m \tag{25b}$$

$$L^T = \int_\Omega \overline{N}^T \left(m^T - \frac{m^T D_T}{3K_s} \right) B d\Omega \tag{25c}$$

$$\overline{f} = -\int_\Gamma \overline{N}^T q d\Gamma - \int_\Omega \frac{\overline{N}^T}{3K_s} m^T D_T c d\Omega - \int_\Omega (\nabla \overline{N})^T \frac{k}{\mu} \rho g h d\Omega \tag{25d}$$

in which H = is the spatial flow (or seepage) matrix; S = the compressibility matrix and $\overline{f}$ = the load vector equivalent to fluid flow of source elements, creep function and gravity load, respectively.

It can be easily verified that the complete set of equations is symmetric if the matrix D_T is symmetric.

The integration of these equations usually requires the use of numerical techniques, and a standard method is that of Gaussian quadrature *(Zienkiewicz, 1977)*, where the integrands are evaluated at specific points of the element and boundary surface and then weighted and assumed. The procedure is carried out in terms of a set of local coordinates ξ and η having values of ± 1 on the element boundaries.

Since the discretization in space has been carried out, equations 22 and 24 now represent a set of ordinary differential equations in time. For convenience, the equations are written in the following form:

$$\begin{bmatrix} 0 & 0 \\ 0 & H \end{bmatrix} \begin{Bmatrix} \overline{u} \\ \overline{p} \end{Bmatrix} + \begin{bmatrix} K & L \\ L^T & S \end{bmatrix} \frac{d}{dt} \begin{Bmatrix} \overline{u} \\ \overline{p} \end{Bmatrix} = \begin{Bmatrix} \dfrac{df}{dt} + C \\ \overline{f} \end{Bmatrix} \tag{26}$$

The values of $\overline{u}$ and $\overline{p}$ at different values in time may now be obtained by means of appropriate time-stepping algorithms.

The method used for the time discretization may be regarded as a one- dimensional finite element scheme as distinct from the spatial discretization, Kantorovich type approach, *(Zienkiewicz, 1977)*.

The time domain is divided into a number of elements or steps and integration is carried out for each step to obtain the change of the parameters $\overline{u}$ and $\overline{p}$. The step-by-step integrations may then be summed to determine the total change of the parameters. The integration takes the same form as used for the spatial integration, i.e.,

if $F = 0$ then $\int \overline{g} F dt = 0$

where $\overline{g}$ is an arbitrary function of time.

When applying this method to equation 26, yields the following equations:

$$\int_{t_k}^{t_k + \Delta t_k} \overline{g} \begin{bmatrix} 0 & 0 \\ 0 & H \end{bmatrix} \begin{Bmatrix} \overline{u} \\ \overline{p} \end{Bmatrix} dt + \int_{t_k}^{t_k + \Delta t_k} \overline{g} \begin{bmatrix} K & L \\ L^T & S \end{bmatrix} \frac{d}{dt} \begin{Bmatrix} \overline{u} \\ \overline{p} \end{Bmatrix}$$

$$= \int_{t_k}^{t_k + \Delta t_k} \overline{g} \begin{Bmatrix} \dfrac{df}{dt} + C \\ \overline{f} \end{Bmatrix} dt \tag{27}$$

where Δt_k is the length of the k-th time step.

The first order-time derivatives of $\overline{u}$ and $\overline{p}$ may be approximated by assuming a linear variation of $\overline{u}$ and $\overline{p}$ within each step.

$$[\bar{u} \quad \bar{p}] = [N_1^t \quad N_2^t] \begin{bmatrix} \bar{u}^t & \bar{p}^t \\ \bar{u}^{t+\Delta t} & \bar{p}^{t+\Delta t} \end{bmatrix} \tag{28}$$

where $N_1 = 1 - \alpha$, $N_2 = \alpha$ and $\alpha = (t - t_k)/\Delta t_k$.

The derivatives with respect to time of N_1 and N_2 are given as:

$$\frac{d}{dt}[N_1^t \quad N_2^t] = \left[-\frac{1}{\Delta t_k} \quad \frac{1}{\Delta t_k} \right] \tag{29}$$

By substituting equations 28 and 29, equations 27 take the form:

$$\int_{t_k}^{t_k+\Delta t_k} \bar{g} \begin{bmatrix} 0 & 0 \\ 0 & H \end{bmatrix} \left[(1-\alpha) \left\{ \begin{matrix} \bar{u} \\ \bar{p} \end{matrix} \right\}_{t_k} + \alpha \left\{ \begin{matrix} \bar{u} \\ \bar{p} \end{matrix} \right\}_{t_k+\Delta t_k} \right] dt$$

$$+ \int_{t_k}^{t_k+\Delta t_k} \bar{g} \begin{bmatrix} K & L \\ L^T & S \end{bmatrix} \left[-\frac{1}{\Delta t_k} \left\{ \begin{matrix} \bar{u} \\ \bar{p} \end{matrix} \right\}_{t_k} + \frac{1}{\Delta t_k} \left\{ \begin{matrix} \bar{u} \\ \bar{p} \end{matrix} \right\}_{t_k+\Delta t_k} \right] dt$$

$$= \int_{t_k}^{t_k+\Delta t_k} \bar{g} \left\{ \begin{matrix} \dfrac{df}{dt} + C \\ \bar{f} \end{matrix} \right\} dt \tag{30}$$

Equation 30 may now be integrated, using the point collocation method, then divided by $\bar{g}$, and finally rearranged in the form:

$$\begin{bmatrix} K & L \\ L^T & S + \alpha H \Delta t_k \end{bmatrix}_{k,\alpha} \left\{ \begin{matrix} \bar{u} \\ \bar{p} \end{matrix} \right\}_{t_k+\Delta t_k} = \begin{bmatrix} K & L \\ L^T & S - (1-\alpha)H\Delta t_k \end{bmatrix}_{k,\alpha} \left\{ \begin{matrix} \bar{u} \\ \bar{p} \end{matrix} \right\}_{t_k}$$

$$+ \left\{ \begin{matrix} \dfrac{df}{dt} + C \\ \bar{f} \end{matrix} \right\}_{k,\alpha} \Delta t_k \tag{31}$$

Equations 31 are formed for all internal nodes of the domain and those boundary nodes where pore pressure value and/or displacement are not prescribed. The number of equations is thus equal to the number of unknown variables.

The complete set of equations may be used in the time-stepping procedure outlined above to determine the values of $\bar{u}$ and $\bar{p}$ at any point in time relative to their initial values.

The eight-noded isoparametric element is used in this study. The nodes in the elements used represent both displacements and pore fluid pressures, which vary quadratically over the element, as field variables on the same mesh. In other words, the nodes represent displacements and pore pressures at the same time as if there are two concurrent meshes.

NUMERICAL IMPLEMENTATION OF THE BOUNDING SURFACE PLASTICITY MODEL

Soil plasticity problems are nonlinear and history-dependent and thus require more elaborate solution schemes for boundary value problems than simple linear elasticity problems. All the techniques for nonlinear analysis can, with certain qualifications, be applied irrespective of the constitutive law, although some techniques are better suited to particular laws than others *(Naylor and Pande, 1981)*.

The bounding surface plasticity model can be used to supply properties for most numerical solution schemes applicable to soil stress analysis problems. In general, the use of a history dependent constitutive model (such as the bounding surface plasticity) in a stress analysis program requires some form of an incremental solution procedure. In addition, in order to be able to employ reasonably sized solution steps (for implicit implementation), iteration within each step is also usually necessary.

The constitutive relation in inverse form is given by the following equation:

$$\dot{\sigma}_{ij} = D_{ijkl}\dot{\varepsilon}_{kl} \tag{32}$$

The determination of the explicit form of the D_{ijkl} tensor, equation 6 of reference *(Dafalias, 1986)* involves the use of equations 1, 7-10, 22, 28, 29, 35a, and 35b of reference. *(Dafalias and Herrmann, 1986)*. Because the associated flow rule has been adopted, the R_{ij} is equal to L_{ij} and the $U_{\bar{I}}$ is equal to $F_{\bar{I}}$, etc. Combining these expressions gives:

$$D_{ijkl} = G\left(\delta_{ki}\delta_{lj} + \delta_{kj}\delta_{li}\right) + \left(K - \frac{2}{3}G\right)\delta_{ij}\delta_{kl}$$

$$-\frac{\bar{h}(L)}{B}\left[3KF_{\bar{I}}\delta_{ij} + \frac{G}{J}F_{\bar{J}}s_{ij} + \frac{\sqrt{3}G}{\cos(3\alpha)}\frac{F_{\alpha}}{bJ}\left(\frac{s_{in}s_{nj}}{J^2} - \frac{3S^3s_{ij}}{2J^4} - \frac{2\delta_{ij}}{3}\right)\right]$$

$$\left[3KF_{\bar{I}}\delta_{kl} + \frac{G}{J}F_{\bar{J}}s_{kl} + \frac{\sqrt{3}G}{\cos(3\alpha)}\frac{F_{\alpha}}{bJ}\left(\frac{s_{kn}s_{nl}}{J^2} - \frac{3S^3s_{kl}}{2J^4} - \frac{2\delta_{kl}}{3}\right)\right] \tag{33}$$

in which

$$L = \frac{1}{B}\left\{3KF_{\bar{I}}\dot{\varepsilon}_{kk} + \frac{G}{J}F_{\bar{J}}s_{ij}\dot{\varepsilon}_{ij}\right.$$

$$\left. + \frac{\sqrt{3}G}{\cos(3\alpha)}\frac{F_{\alpha}}{bJ}\left[\left(\frac{s_{ik}s_{kj}}{J^2} - \frac{3S^3s_{ij}}{2J^4}\right)\dot{\varepsilon}_{ij} - \frac{2\dot{\varepsilon}_{kk}}{3}\right]\right\} \tag{34}$$

$$B = K_p + 9K\left(F_{\bar{I}}\right)^2 + G\left(F_{\bar{J}}\right)^2 + G\left(\frac{F_{\alpha}}{bJ}\right)^2 \tag{35}$$

In the above expressions, the elastic bulk modulus K is given by equation 29 of reference (*Dafalias and Herrmann, 1986)*. The elastic shear modulus G is either defined independently or is computed from K and a specified value of Poisson's ratio. The plastic modulus K_p is obtained from equation 30 of reference *(Dafalias, 1986)* in which the hardening function $\hat{H}$ and the bounding plastic modulus are defined by equations 30 of reference *(Dafalias, 1986)* and 28 of reference *(Dafalis and Herrmann, 1986)*, respectively. $\bar{h}(\ )$ is the heavy-side step function. The quantities related to the bounding surface such as b, $F_{\bar{I}}$, etc., are given in Appendix I of reference *(Dafalias and Herrmann, 1986)*. The stress invariants are defined in equation 2 of reference *(Dafalias and Herrmann, 1986)*.

The size of the bounding surface is controlled by the measure of the preconsolidation history I_o. The evolutionary law for I_o is given by the second equation of 27b in reference *(Dafalias and Herrmann, 1986)*, i.e.:

$$\frac{dI_o}{de^p} = -\frac{\langle I_o - I_1 \rangle + I_1}{\lambda - \kappa} \tag{36}$$

The parameters λ, κ and I_1 are described in reference *(Dafalias and Herrmann, 1986)*. Using equation 26 of reference *(Dafalias and Herrmann, 1986)* and expressing the elastic volume change in terms of the bulk modulus K and the change in I gives:

$$dI_o = \frac{1 + e_{in}}{\lambda - \kappa} \left(\langle I_o - I_1 \rangle + I_1 \right) \left(d\varepsilon_{kk} - \frac{1}{3K} dI \right) \tag{37}$$

Two cases must be considered in integrating equation 37.
If $I_o > I_1$, equation 37 becomes:

$$dI_o = (1 + e_o) \frac{I_o}{\lambda - \kappa} \left(d\varepsilon_{kk} - \frac{1}{3K} dI \right) \tag{38}$$

Dividing by I_o and integrating over substep m gives:

$$\int_{I_{o_{m-1}}}^{I_{o_m}} \frac{dI_o}{I_o} = \frac{(1 + e_{in})}{\lambda - \kappa} \left[\int_{\varepsilon_{kk_{m-1}}}^{\varepsilon_{kk_m}} d\varepsilon_{kk} - \int_{I_{m-1}}^{I_m} \frac{1}{3K} dI \right] \tag{39}$$

The first two integrals may be evaluated exactly, while the third is approximated by the trapezoidal rule (K is given by equation 29 of reference *(Dafalias and Herrmann, 1986)*). Integrating and solving for I_{o_m} yields:

$$I_{o_m} = I_{o_{m-1}} \exp\left\{ \frac{(1 + e_{in})}{\lambda - \kappa} \left[\Delta\varepsilon_{kk_m} - \frac{1}{6} \left(\frac{1}{K_{m-1}} + \frac{1}{K_m} \right) \Delta I_m \right] \right\} \tag{40}$$

If $I_o \leq I_1$, equation 37 becomes:

$$dI_o = (1 + e_{in}) \frac{I_1}{\lambda - \kappa} \left(d\varepsilon_{kk} - \frac{1}{3K} dI \right) \tag{41}$$

Integrating this expression yields:

$$I_{o_m} = I_{o_{m-1}} + \frac{(1 + e_{in})}{\lambda - \kappa} I_1 \left[\Delta\varepsilon_{kk_m} - \frac{1}{6} \left(\frac{1}{K_{m-1}} + \frac{1}{K_m} \right) \Delta I_m \right] \tag{42}$$

EXAMPLES

In this section, in order to check the validity of the numerical implementation of the bounding surface plasticity model, a comparison is made with the experimental results of soft clay response under undrained monotonic deviatoric loading in compression and extension for normally and overconsolidated clays published by *Banerjee and Stipho (1978; 1979)*.

The solutions for one- and two-dimensional plane strain consolidation problems are shown in this section. In this case, a comparison has been made between the settlement predictions obtained

by *Siriwardane and Desai (1981)* and those obtained by using the bounding surface plasticity model that is used in this study. The conventional modified Cam clay model was used by Siriwardane and Desai for the elastoplastic analysis.

Model Response and Comparison with Experiments

The predictions of the bounding surface plasticity model at the constitutive matrix level (Eq. 33) and comparisons with experimental data for different overconsolidation ratios in compression and extension tests are now presented.

A series of comparisons between the experimental observations of the stress-strain in addition to pore water pressure and those predicted by the theoretical model are presented in **Figs.** 1, 2, 3, 4, and 5. These figures show by discrete symbols the experimental data for a triaxial undrained loading at overconsolidation ratios OCR = 2, 5, and 12 in compression tests and at OCR = 2 and 10 in extension tests and by continuous lines for the model simulation. All the theoretical results have been obtained by using the values of the input material parameters listed in **Table 1**.

The experimental data are taken as reported by *Banerjee and Stipho (1978; 1979)* where samples of kaolin (LL = 52, PL = 26) were tested under undrained conditions. The method of preparation of these samples and details of the testing procedure are given by *Banerjee and Stipho (1978).*

Comparison with experiments demonstrates that the predicted response by using the bounding surface plasticity model is in good agreement with experimental data and that the model can describe realistically the soil response under different loading conditions at any overconsolidation ratio.

Table 1: The Input Parameters Used to Predict the Response of the Bounding Surface Plasticity Model

Parameter	Value
λ	0.14
κ	0.05
ν	0.20
M_c	1.05
M_e	0.85
R_c	2.68
R_e	2.25
A_c	0.06
A_e	0.05
T	-0.10
C	0
s	1.0
h_c	2.0
h_e	1.5
h_o	1.75
$I_1 \left(= 3P_1\right)$	101.4 kN/m^2
m	0.02

One-Dimensional Consolidation

In this section, the solution for a one-dimensional plane strain consolidation problem is shown. The results obtained from the bounding surface plasticity model are compared with those of *Siriwardane and Desai (1981)*. Isoparametric eight-noded elements have been used instead of triangular elements that were used by Siriwardane and Desai.

The finite element mesh is shown in **Fig. 6**. The width of loading B is assumed to be equal to 0.102 m. An external surface load ($p_o = 47.9$ kN/m^2) is applied at the top surface of the model. The input material parameters used in this problem are shown in **Table 2**. Some of these parameters are the classical material parameters within the critical-state soil mechanics context. So these material parameters are taken as reported by *Siriwardane and Desai (1981)*. The others are the new material parameters related to the bounding surface plasticity model. The typical values of these parameters in the more limited ranges for practical applications are used in the analysis of this problem.
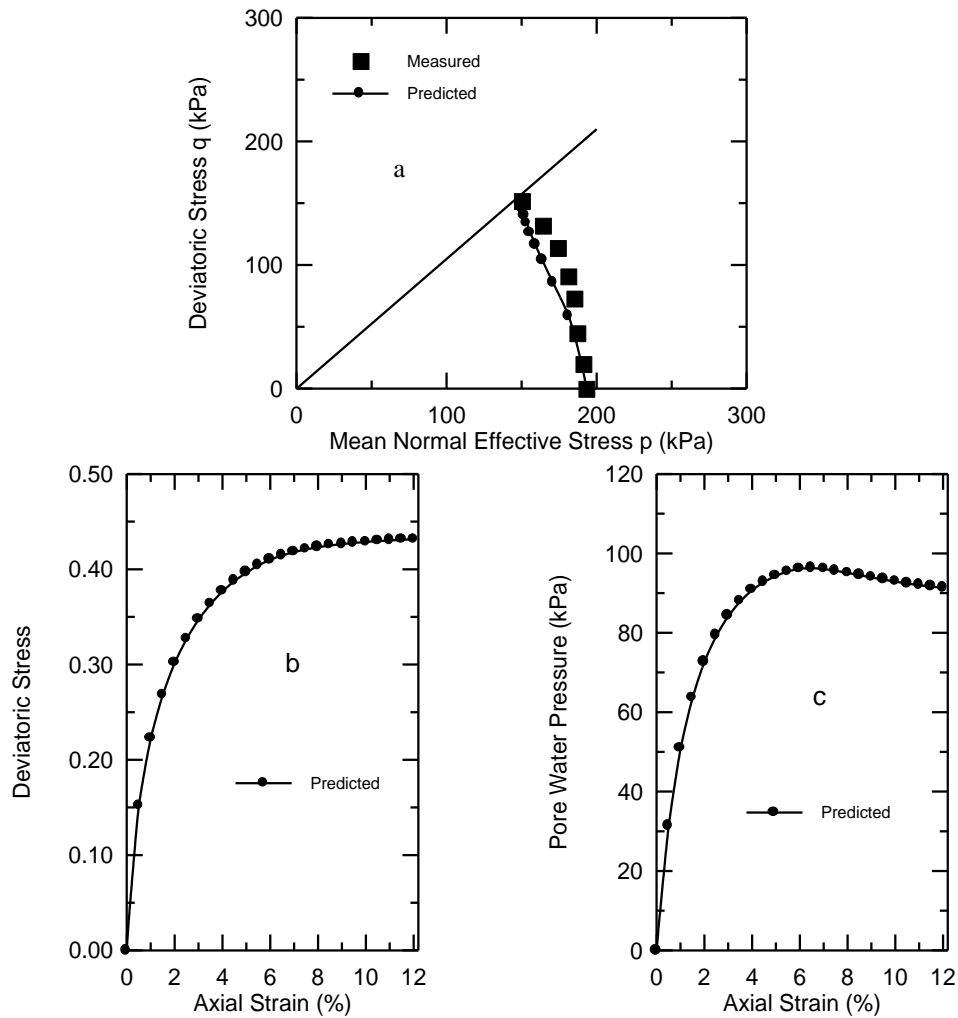
Fig. 1: Predictions of the Bounding Surface Plasticity Model for Lightly Overconsolidated Clay (OCR = 2) in Compression Test
a.   Undrained Stress Path
b.   Stress-Strain Behavior
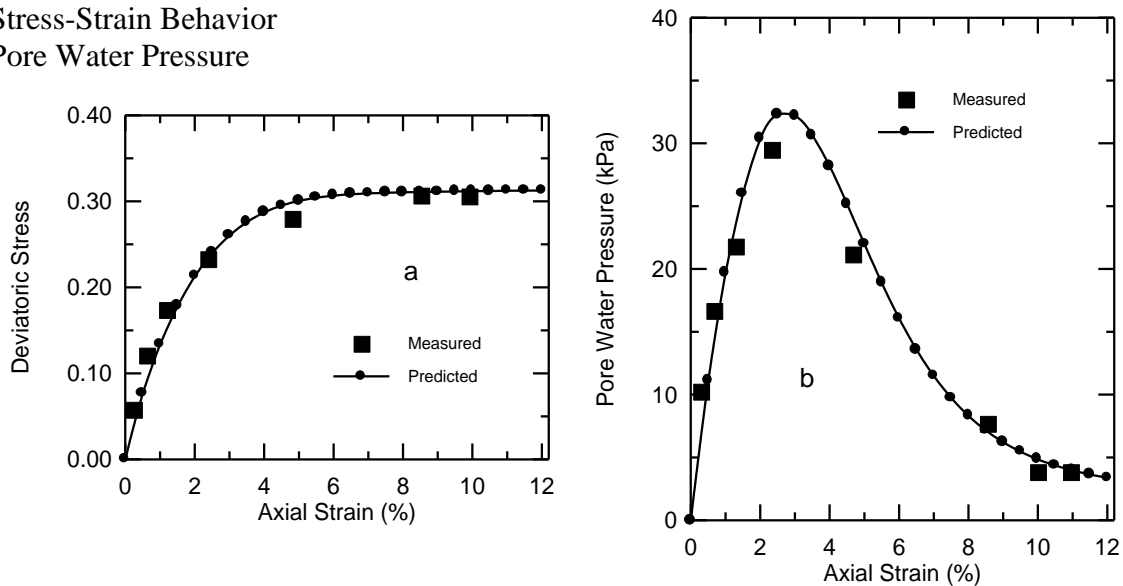c.   Pore Water Pressure

Fig. 2: Predictions of the Bounding Surface Plasticity Model for Heavily Overconsolidated Clay (OCR = 5) in Compression Test
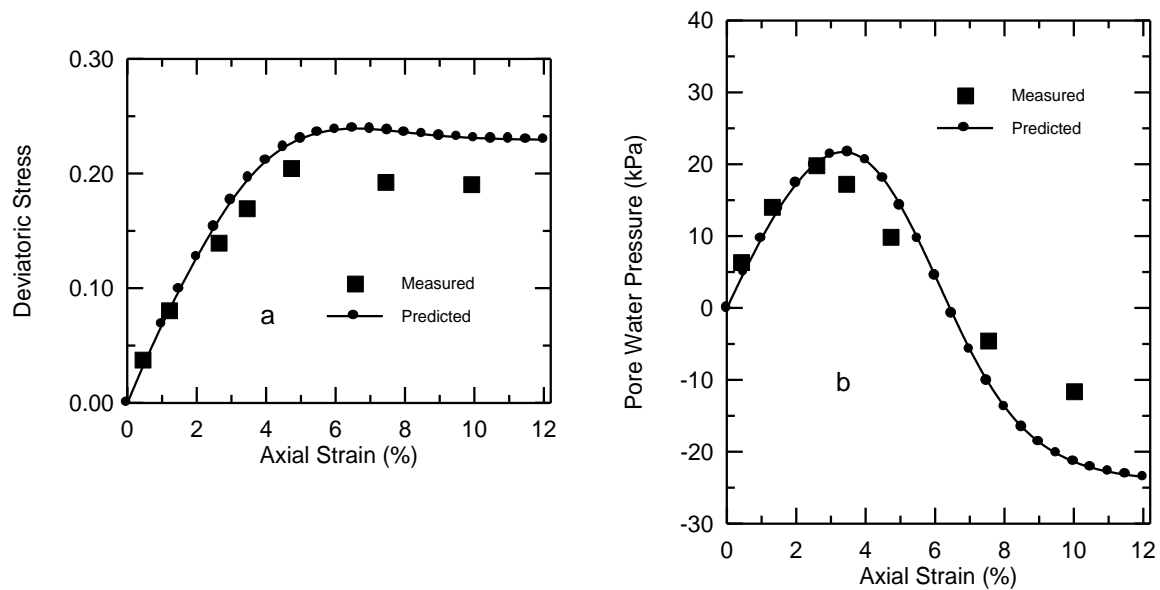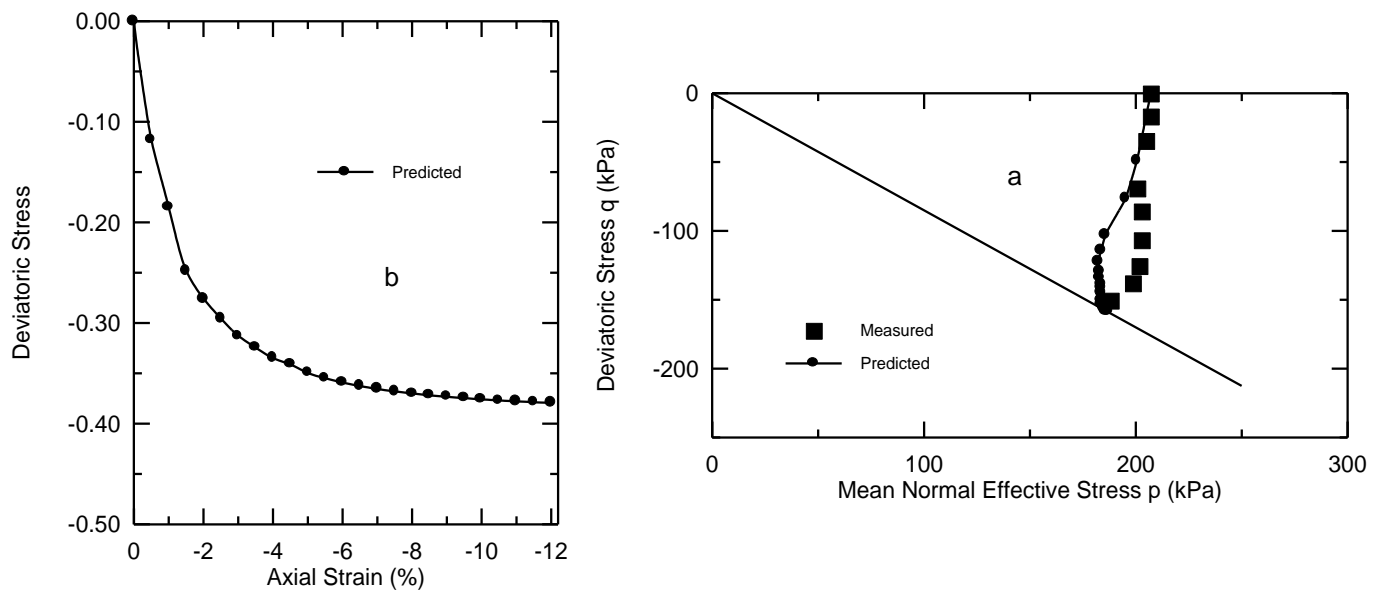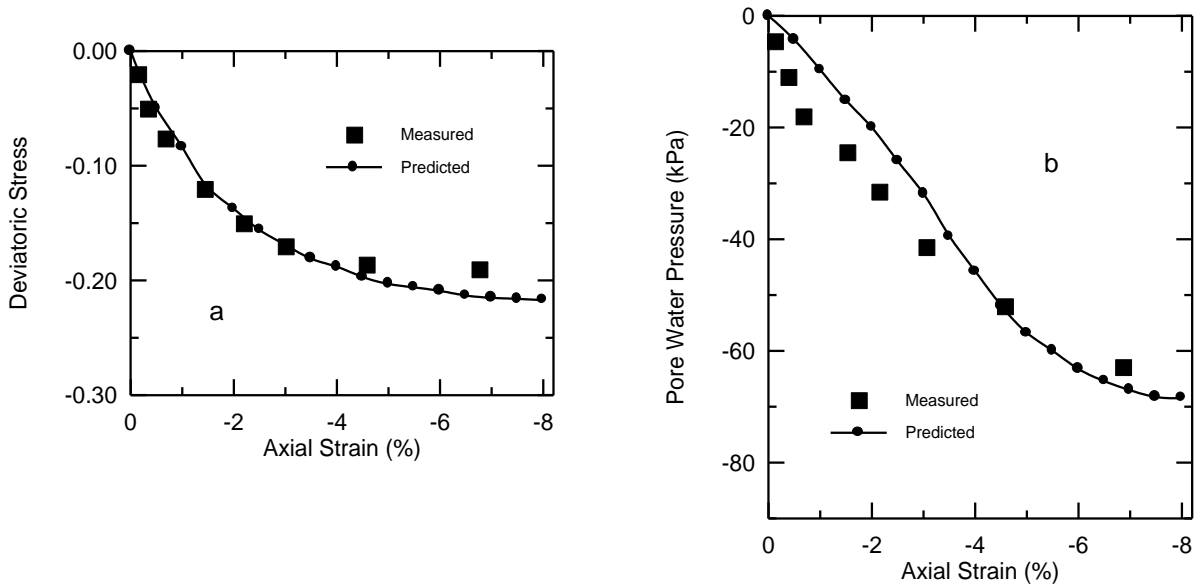a.   Stress-Strain Behavior
b.   Pore Water Pressure

Fig. 3: Predictions of the Bounding Surface Plasticity Model for Heavily Overconsolidated Clay (OCR = 12) in Compression Test
a.   Stress-Strain Behavior
b.   Pore Water Pressure

Fig. 4: Predictions of the Bounding Surface Plasticity Model for Lightly Overconsolidated Clay (OCR = 2) in Extension Test
a.   Undrained Stress Path
b.   Stress-Strain Behavior
c.

Fig. 5: Predictions of the Bounding Surface Plasticity Model for Heavily Overconsolidated Clay (OCR = 10) in Extension Test

a.   Stress-Strain Behavior
b.   Pore Water Pressure

Fig. 7 shows the comparison between the calculated settlement at a typical node (107) using the bounding surface plasticity model with that from the problem that was solved by Siriwardane and Desai. The settlements are non-dimensionalized with respect to ultimate settlement predicted by Terzaghi's theory of consolidation. The non-dimensionalized time factor ($T_v = c_v t / H^2$) is used as an abscissa and E_o is used to calculate c_v.

The dissipation of pore water pressure at a typical node (31) and the vertical section (A-A) as shown in **Fig. 6**, are shown in **Figs. 8** and **9**, respectively. Here, the pore water pressures are non-dimensionalized with respect to p_o, which is the externally applied surface loading.

Comparison between the results from the bounding surface plasticity model with those of conventional modified Cam clay model by Siriwardane and Desai (1981) shows that the use of the first leads to higher settlements at initial time levels and smaller final settlements. Also, it can be seen that the use of the bounding surface plasticity model increases the magnitude of dissipation of pore water pressure especially in the final consolidation zone. Therefore, the predicted pore pressures are less than those from the conventional modified Cam clay model.

Two-Dimensional Consolidation

The solution for a two-dimensional plane strain consolidation problem is shown in this section. The same problem was solved by *Siriwardane and Desai (1981)*. In this case, a comparison is made between the settlement predictions obtained by the bounding surface plasticity model and the results obtained by them. The critical state model was used by Siriwardane and Desai as the constitutive relationship. Triangular elements were also used to solve this problem while isoparameteric eight-noded elements are employed in this study.

The problem to be solved and the finite element mesh are shown in **Fig. 10**. The width of the loaded area B is assumed to be equal to 3.05 m. An external surface load (p_o = 47.9 kN/m^2) is applied at the top surface as shown in the Figure. The problem is solved using the input material parameters shown in **Table 3**.

Again, it is worthy to notice that the classical material parameters, which have been used by Siriwardane and Desai, are taken as the same as reported by them. The other parameters are taken as typical values in the more limited ranges for practical applications.
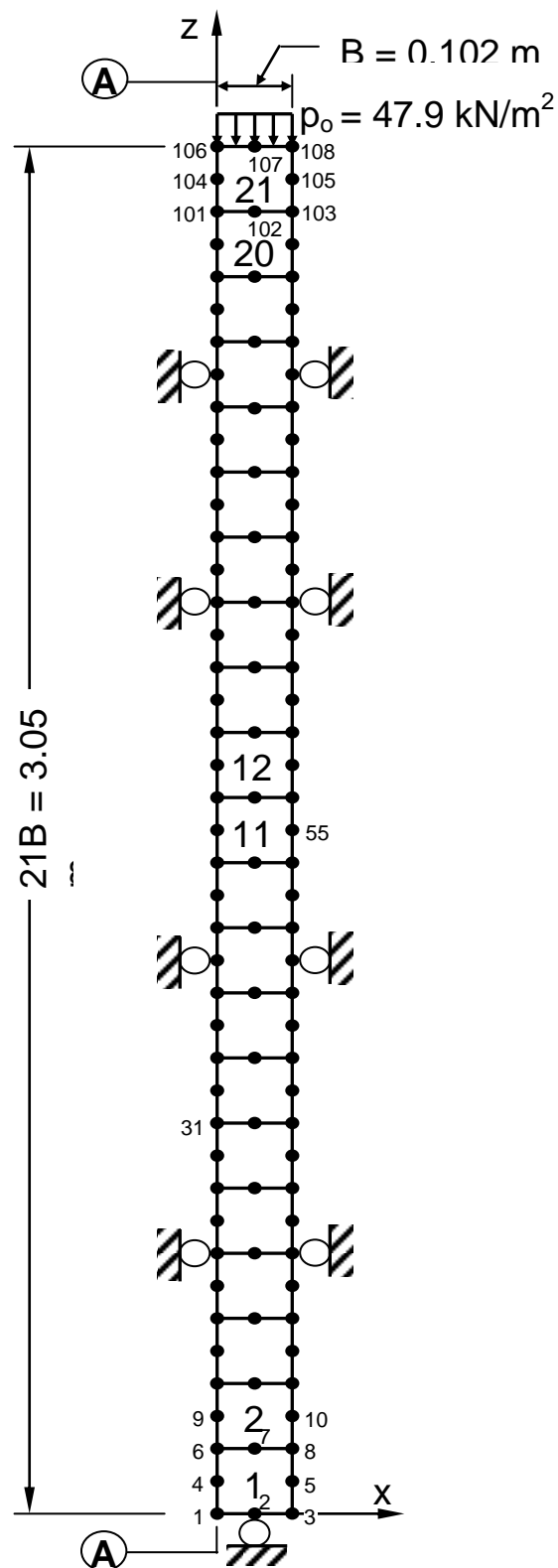

Fig. 6: Finite Element Mesh for the One-Dimensional Consolidation Problem

Table 2: Input Material Parameters for the One-Dimensional Consolidation Problem

Parameter	Value
λ	0.14
κ	0.05
ν	0.4
M_c	1.05
M_e	0.89
R_c	2.72
R_e	2.18
A_c	0.1
A_e	0.08
T	-0.10
C	0.4
s	1.0
h_c	4.0
h_e	4.0
h_o	4.0
$I_1\left(=3P_1\right)$	101.4 kN/m^2
m	0.02
K_h	1.22 x 10^{-6} m/day
K_v	1.22 x 10^{-6} m/day
e_{in}	0.9
E_o	287.3 kN/m^2

The predicted pore pressures are non-dimensionalized with respect to p_o, where p_o is the externally applied surface loading. The initial modulus E_o is used to compute the coefficient of consolidation c_v value for use in the non-dimensional time factor T_v. The predicted settlements are non-dimensionalized with respect to width of loading B.

Fig. 11 shows a comparison of timewise variation of surface settlement from the bounding surface plasticity model with those from a problem that was solved by Siriwardane and Desai (1981) using the conventional modified Cam clay model. It can be seen that the settlements from the two models do not differ significantly at initial time levels. However, at higher times the bounding surface plasticity model shows higher settlements but a smaller final settlement.

Dissipations of pore water pressure at section (B-B) in **Fig. 10** are compared in **Fig. 12**. The bounding surface plasticity model shows higher dissipation of pore water pressures at earlier times, while, at higher time levels, the two results tend to be similar.
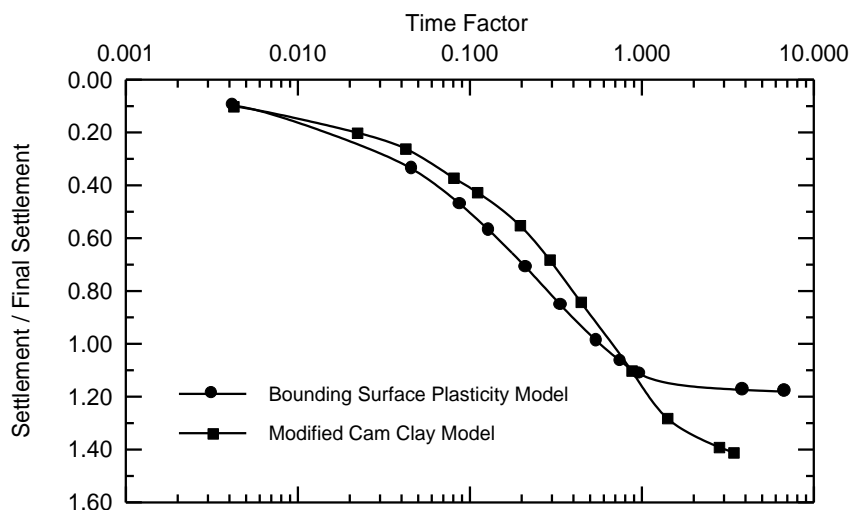

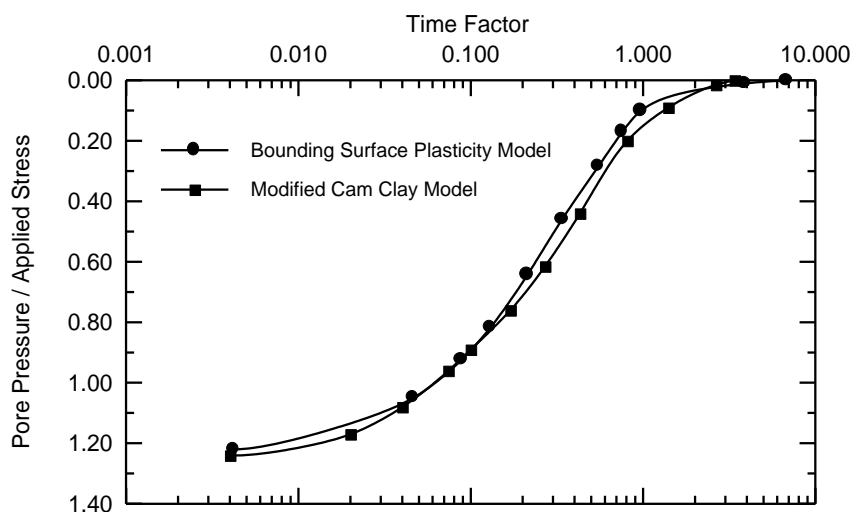**Fig. 7:** Surface Settlement versus Time

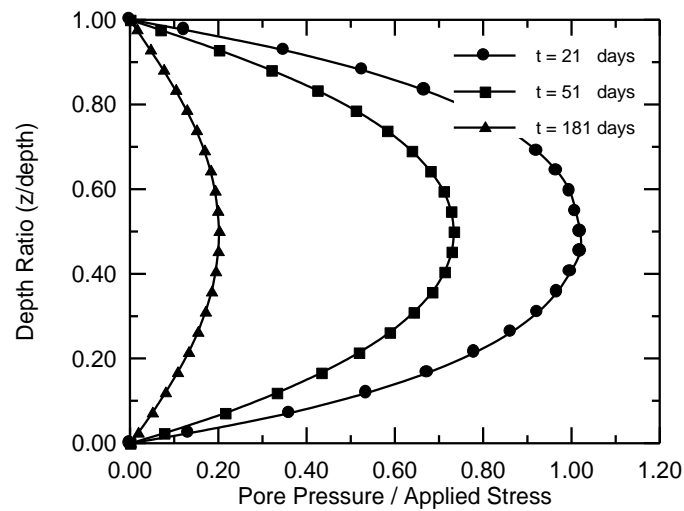**Fig. 8**: Pore Pressure versus Time at a Typical Node (Node 31)

Fig. 9: Pore Pressure versus Depth along Section A-A at Three Different Time Values Using the Bounding Surface Plasticity Model
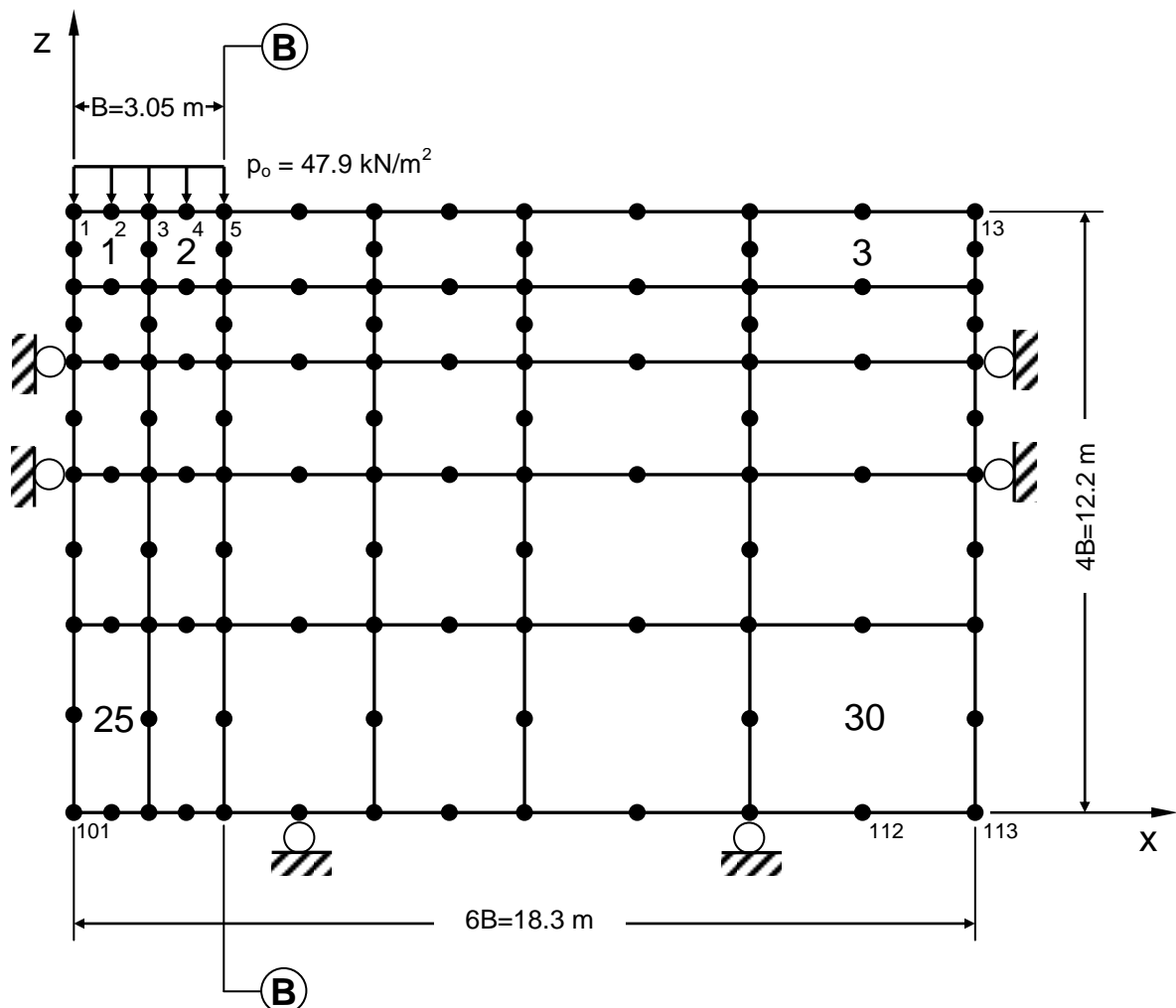

Fig. 10: Finite Element Mesh for the Two-Dimensional Consolidation Problem

CONCLUSIONS

The main conclusions that can be drawn from the present study are:

- The bounding surface plasticity model shows very good agreement with experimental results (published by Banerjee and Stipho) of soft clay response in compression and extension for any overconsolidation ratio.
- The study shows that if the medium follows the bounding surface plasticity model as a constitutive law, the soil response would show considerably different rates and magnitude of settlement, and different pore pressure behavior during the consolidation process. This appears to be an important useful result; perhaps the comparison with the actual reliable observations can provide further verification of its validity.
- The ranges of overconsolidation ratio used in this study show the capability of the model to describe realistically the soil response under monotonic loading conditions at different overconsolidation ratios which cannot be properly predicted by classical isotropic yield surface models. This aspect distinguishes this model from other isotropic yield surface formulations.

Table 3: Input Material Parameters for the Two-Dimensional Consolidation Problem

Parameter	Value
λ	0.14
κ	0.05
ν	0.4
M_c	1.05
M_e	0.89
R_c	2.72
R_e	2.18
A_c	0.1
A_e	0.08
T	-0.10
C	0.4
S	1.0
h_c	4.0
h_e	4.0
h_o	4.0
$I_1 (= 3P_1)$	101.4 kN/m^2
M	0.02
K_h	1.22 x 10^{-5} m/day

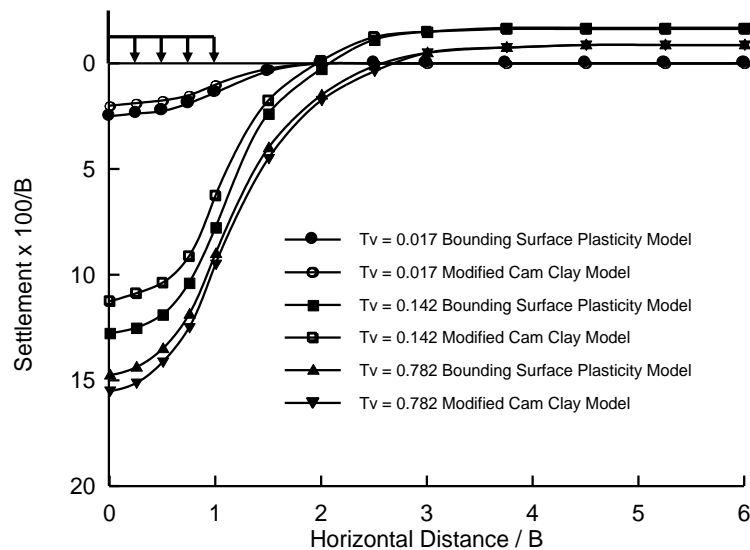| K_v	1.22×10^{-5} m/day
e_{in}	0.9
E_o	622.7 kN/m^2

Fig. 11: Surface Settlements versus Horizontal Distance at Three Different Time Values
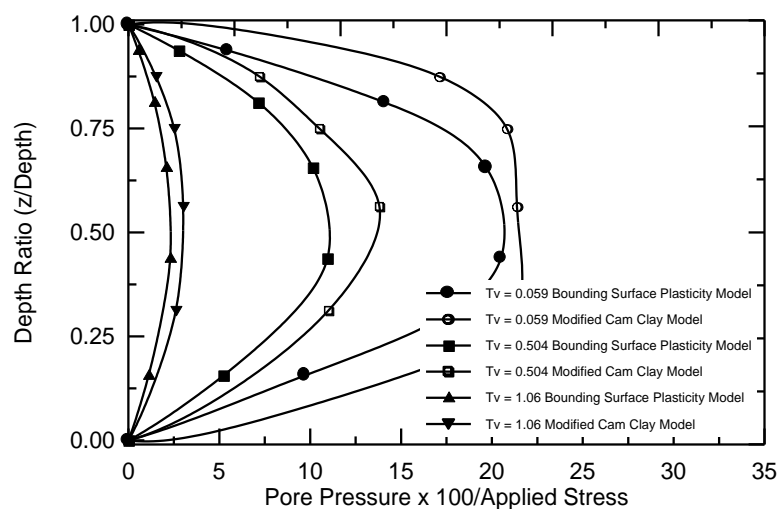

Fig. 12: Pore Water Pressures versus Depth along Section B-B at Three Different Time Values

REFERENCES

- Banerjee, P. K., and Stipho, A. S., (1978), "Associated and Non-Associated Constitutive Relations for Undrained Behavior of Isotropic Soft Clays", International Journal for Numerical and Analytical Methods in Geomechanics, Vol. 2, pp. 35-56.

- Banerjee, P. K., and Stipho, A. S., (1979), "An Elastoplastic Model for Undrained Behavior of Heavily Overconsolidated Clay", International Journal for Numerical and Analytical Methods in Geomechanics, Vol. 3, pp. 97-103.

- Bear, J., (1972), "Dynamics of Fluid in Porous Media", American Elsevier Publishing Company, Inc.

- Biot, M. A., (1941), "General Theory of Three-Dimensional Consolidation", Journal of Applied Physics, Vol. 12, pp. 155-164.

- Biot, M. A., (1955), "Theory of Elasticity and Consolidation for a Porous Anisotropic Solid", Journal of Applied Physics, Vol.26, pp. 182-185.

- Biot, M. A., (1956), "Theory of Deformation of a Porous Viscoelastic Anisotropic Solid", Journal of Applied Physics, Vol. 27, pp. 452-469.

- Crichlow, H. B., (1977), "Modern Reservoir Engineering-a Simulation Approach", Prentice-Hall, Englewood Cliffs.

- Dafalias, Y. F., (1986), "Bounding Surface Plasticity. I: Mathematical Foundation and Hypoplasticity", Journal of Engineering Mechanics, ASCE, Vol. 112, No. 9, September, pp. 966-987.

- Dafalias, Y. F., and Herrmann, L. R., (1986), "Bounding Surface Plasticity. II: Application to Isotropic Cohesive Soils", Journal of Engineering Mechanics, Vol. 112, No. 12, December, pp. 1263-1291.

- Lewis, R. W., Robert, G. K., and Zienkiewicz, O. C., (1976), "A Non-Linear Flow and Deformation Analysis of Consolidation Problems", Proceedings, Second International Conference on Numerical Methods in Geomechanics, ASCE, pp. 1106-1118.

- Lewis, R. W., and Schrefler, B. A., (1987), "The Finite Element Method in the Deformation and Consolidation of Porous Media", John Wiley and Sons Ltd., London.

- Naylor D. J., and Pande, G. N., (1981), "Finite Elements in Geotechnical Engineering", Pineridge Press Limited.

- Siriwardane, H. J., and Desai, C. S., (1981), "Two Numerical Schemes for Nonlinear Consolidation", International Journal for Numerical Methods in Engineering, Vol. 17, pp. 405-426.

- Zienkiewicz, O. C., (1977), "The Finite Element Method", McGraw-Hill, London.

- Zienkiewicz, O. C., Humpheson, C., and Lewis, R. W., (1977), "A Unified Approach to Soil Mechanics", Chapter 4 in Finite Elements in Geomechanics, Ed., Gudehus, G., John Wiley and Sons, Ltd., London.

LIST OF SYMBOLS:

B	is the strain-displacement transformation matrix.
b	body forces
C	the creep matrix
D_T	the creep function
df	load vector equivalent to the body force, surface traction and autogeneous strain, respectively.
$d\hat{f}$	represents the change in external force due to boundary and body force loadings.
$d\varepsilon$	represents the total strain of the skeleton,
$d\varepsilon_c = c.dt$	is the creep strain
$d\varepsilon_p = -m(dp/3K_s)$	the overall volumetric strains caused by uniform compression of the particles by the pressure of the pore fluid

$\bar{f}$	the load vector equivalent to fluid flow of source elements, creep function and gravity load
g	the gravity
$\bar{g}$	is an arbitrary function of time
H	is the spatial flow (or seepage) matrix
h	is the head above some arbitrary datum.
$\bar{h}(\ )$	is the heavy-side step function
K	bulk modulus of the solid phase.
k	is the absolute permeability matrix of the medium
K_w	is the bulk modulus of water
K	the tangential spatial stiffness matrix
L	the coupling matrix representing the influence of pore pressure in force equilibrium;
$N, \overline{N}$	are the shape functions of displacement and pore pressure, respectively
n	is the porosity
n	is the unit normal vector
p	Pressure
p	the fluid pressure
q	is the outflow rate per unit area of the boundary surface
S	the compressibility matrix
s	is the degree of saturation
$\hat{t}$	and the boundary traction
u	the unknown displacement vector
Δt_k	is the length of the k-th time step
ε_o	all other strains not directly associated with stress changes
μ	the dynamic viscosity of the fluid
ρ	the density
σ'	effective stress
Ω	domain

AXISYMMETRIC DYNAMIC BEHAVIOUR
OF THIN OBLATE SHELLS

By

Ahmed A. Al – Rajihy ; Ala M. Hussein Al – Jessany
Nawal H. Al – Raheimy
College of Engineering,
Babylon University

ABSTRACT

This paper presents a theoretical investigation of the axisymmetric free vibrations of an isotropic thin oblate spheroid shell. The analysis depends on the Rayliegh – Ritz's method. The non – shallow shell theory is used for the analysis. The analysis based on considering the oblate spheroid as a continuous system constructed from two spherical shell elements matched at the continuous boundaries.

Throughout the results, it is shown that when the eccentricity reaches zero, an exact thin sphere solution is emerged and when the eccentricity equals one an exact thin circular plate solution is emerged. Therefore, the eccentricity of an oblate shell at medium value lies between these two values.

It was found that the Rayleigh – Ritz's method is suitable for all eccentricities, while the literature showed that the Rayleigh's method is suitable for eccentricities less than 0.6.

الخلاصة

يتناول هذا البحث دراسة نظرية للاهتزازات الحرة للقشريات نحيفة الجدران شبه البيضوية الشكل المتناظرة المحور والمتشابهة الخواص في جميع الاتجاهات. التحليل النظري يعتمد على طريقة (Rayliegh – Ritz) وقد تم استخدام (نظرية القشريات العميقة) في التحليل. هذه التقنيه مبنية على أساس القشرية الشبه بيظويه كمنظومة مستمرة مركبه من قشريتين نصف كرويتين متناظرتين على طول حدودها المستمرة.

من خلال النتائج، تبين بأنه عندما تصل اللامركزية إلى الصفر يكون ظاهر للعيان بالضبط حل لقشرية نحيفة كروية الشكل وعندما تكون اللامركزية مساوية إلى الواحد يكون ظاهر للعيان بالضبط حل لصفيحة نحيفة دائرية الشكل، وبناءً عليه فان اللامركزية للشكل شبه البيضوي يقع عند قيمة متوسطة ما بين تلك القيمتين.

وجد إنّ طريقة (Ritz – Rayliegh) ملائمة لكل قيم اللامركزية، بينما أظهرت البحوث السابقة إن طريقة (Rayliegh) تكون ملائمة لقيم من اللامركزية اقل من (0.6).

KEY WORDS

Oblate, Spheroid, Thin shells, Axisymmetric spheroid

LIST OF SYMBOLS

a   Major semi – axis of an oblate spheroid shell.

b   Minor semi – axis of an oblate spheroid shell.

E   Young's modulus of elasticity (GN / m^2).

e   Eccentricity ratio.

h   Shell thickness (mm).

$P_n(x)$ Legendre function of the first kind.

$P'_n(x)$ First derivative of the Legendre function of the first kind.

$P''_n(x)$ Second derivative of the Legendre function of the first kind.

R_r Effective radius.

R_Φ , R_θ Principal radii of curvatures of an oblate spheroid.

U_Φ Tangential displacement mode.

u_Φ Tangential displacement of points on shell middle surface.

W   Transverse displacement mode.

w   Transverse displacement of points on shell middle surface.

$\text{C}_\Phi, \text{C}_\theta, \text{C}_r$ Strains

Φ' Inclination angle of an oblate spheroid.

Φ Inclination angle of a spherical shell model.

Φ_o Opening angle of the approximate spherical shell.

λ Non – dimensional frequency parameter ((ρ / E)$^{1/2}$ $\omega.a$).
                           (used for oblate spheroid shells)

θ Angle of rotation in the meridian direction.

ρ Density (kg / m^3).

Ω Non – dimensional frequency parameter ((ρ / E)$^{1/2}$ $\omega.R$).
                           (used for spherical shells)

ω Circular frequency (rad / sec).

INTRODUCTION

        Oblate spheroid shell is defined as the locus surface resulting by rotating an ellipse around its minor axis. This type of shells has many practical applications such as; the tanks of liquid oxygen used in space vehicles, the housing of the early – warning scanner of the airborne warning and control system aircraft (AWACS) and others. These applications may cause dynamic problems to these shells. One of the very important dynamic problems is the resonance. Therefore the free vibration of such shells may be studied to present the resonant problem.

        The dynamics of oblate spheroid shells, like other types of shells and structures, has received a considerable attention in the literature, partly because of the necessity during the

design stage of such shells, and partly because it is an interesting fundamental problem in applied mechanics.

Baker, 1969 presented a detailed study of the theory of free, axisymmetric vibration of thin elastic spherical shell and demonstrate by experiments that the normal modes of vibration predicted do exist. The theory predicts the existence of two infinite sets of normal modes, one of which is bounded in frequency and the other unbounded. The first four modes in each set are identified by experiments on a small steel shell.

As for the oblate spheroid shells, **Penzes** and **Burgin, 1965** were the first to solve the problem of the free vibrations of thin isotropic oblate spheroid shells by Galerkin's method using membrane theory and harmonic axisymmetric motion. It was shown that Galerkin's method of solution for the oblate spheroid shell yields the exact solution for the closed spherical shell as the eccentricity of the oblate spheroid shell approaches zero.

Penzes, 1969 extended the solution of the above reference to include thin orthotropic oblate spheroid shells. He used the same assumptions and equations of motion in the above reference except that the principal direction of the elastic compliances was assumed to be along parallel of latitude and along meridian. Both of the spheroid and spherical shells were investigated with various orthotropic constants. The discussion was restricted to the axially symmetric torsionless motion of shells.

Tavakoli and **Singh, 1989** used a substructure synthesis method based on state space mathematics for the eigen – solution of axisymmetric joined / hermitic thin shell structures. The authors applied the state space method to the cylindrical, conical, spherical, and toroidal shells. They compared their results with results obtained previously for the same shells by applying the theoretical analysis and the finite element method. The state space method has strengths lies primarily in its ability to join substructures and match the boundary variables comprehensively.

Fawaz, 1990 in his M.Sc. thesis the Rayliegh variation method was used to obtain natural frequencies and mode shapes of axisymmetric vibrations of thin elastic oblate spheroidal shells and presents the results theoretically and experimentally. He showed that the Rayliegh's method was found to be suitable only for oblate shells with eccentricities less than 0.6.

Chang and **Demkowicz, 1998** studied the stability analysis of multilayered vibrating viscoelastic spheres, both in vacuo and in an acoustical fluid. The analysis was done by investigating the effect of viscoelastic damping on the (continuous) Ladyzenskaya – Babuska – Brezzi (LBB) constants for the related boundary – value problems. The sphere is modeled using both 3–D viscoelasticity and the Kirchho – Love shell theory.

In the paper presented by **Antoine Chaign et. al. 2002,** linear and nonlinear vibrations of shallow spherical shells with free edge are investigated experimentally and numerically and compared to previous studies on percussion instruments such as gongs. The preliminary bases of a suitable analytical model are given. Identification of excited modes is achieved through systematic comparisons between spatial numerical results obtained from a finite element modeling, and spectral information's derived from experiments.

In this paper the free vibration characteristics of a thin elastic oblate spheroid shell will be examined using Raylrigh – Ritz's method to examine its validity for this type of shells.

THEORETICAL ANALYSIS

The review of literature reveals that even though the differential equations of motion for general shell of revolution are well spelt out, nevertheless, the formulation of these equations for oblate spheroidal shells are not available. Hence, an approximate energy approach will be presented in section (2.1) of this paper.

The Rayleigh – Ritz's Energy Method

The Rayliegh – Ritz's method is an extension of Rayliegh's quotient which can be used for more complex elastic bodies and helps to determine the natural frequencies and their associated mode shapes with general boundary conditions in an approximate form. This method is essentially statements on the ratio of potential energy to the kinetic energy. Physically, it makes sense that this ratio is related to the frequency of oscillation [Hayam]. At the natural frequency (ω), and assuming separation of variables, the shell displacements may be written in the following forms [**Penzes, 1969**] :-

$$w(\Phi', t) = W(\Phi') \cdot e^{i\omega t}$$

and

$$u_\Phi(\Phi', t) = U_\Phi(\Phi') \cdot e^{i\omega t}$$

$$\ldots (1)$$

Substituting these in the strain energy expression gives :

$$U = \int_{-h/2}^{h/2} \int_{0}^{2\pi} \int_{0}^{2\pi} \frac{1}{2} [\text{б}_{\Phi'} \ \text{Є}'_{\Phi'} + \text{б}_\theta \text{Є}'_\theta] R_\Phi \ R_\theta \sin \Phi' \ d\Phi \ d\theta \ dz \qquad \ldots (2)$$

where,

$$\text{б}_{\Phi'} = \frac{E}{(1-v^2)} [\text{Є}'_{\Phi'} + \upsilon \ \text{Є}'_\theta] \ , \quad \text{б}_\theta = \frac{E}{(1-v^2)} [\text{Є}'_\theta + \upsilon \ \text{Є}'_{\Phi'}]$$

and

$$\text{Є}'_{\Phi'} = \text{Є}^\circ_\Phi + Z \ K_\Phi \qquad , \quad \text{Є}'_\theta = \text{Є}^\circ_\theta + Z \ K_\theta$$

$$\ldots (3)$$

An expression for the maximum potential energy [U_{max}] may be obtained upon taking $e^{i\omega t}$ to be unity and applying the appropriate expressions for 6_Φ, 6_θ, ε'_θ and ε'_θ, gives;

$$U_{max} = \frac{Eh}{2(1-\upsilon^2)} \int_0^{2\pi} \int_0^{2\pi} \{ \frac{h^2}{12} \left[\frac{1}{R_\Phi^2} \left[\frac{\partial}{\partial \Phi'} \left[\frac{U_\Phi}{R_\Phi} - \frac{\partial W}{R_\Phi \partial \Phi'} \right] \right] \right]^2$$

$$+ \frac{\cos^2 \Phi'}{R_\Phi^2 R_\theta^2 \sin^2 \Phi'} \left[U_\Phi - \frac{\partial W}{\partial \Phi'} \right]^2 + 2\upsilon \frac{\cos \Phi'}{R_\theta R_\Phi^2 \sin \Phi'} \left[U_\Phi - \frac{\partial W}{\partial \Phi'} \right].$$

$$. \frac{\partial}{\partial \Phi'} \left[\frac{U_\Phi}{R_\Phi} - \frac{\partial W}{R_\Phi \partial \Phi'} \right] \right] + \frac{1}{R_\Phi^2} \left[\frac{\partial U_\Phi}{\partial \Phi'} + W \right]^2$$

$$+ \frac{1}{(R_\theta \sin \Phi')^2} (U_\Phi \cos \Phi' + W \sin \Phi')^2$$

$$+ \frac{2\upsilon}{R_\theta R_\Phi \sin \Phi'} \left[\frac{\partial U_\Phi}{\partial \Phi'} + W \right].(U_\Phi \cos \Phi' + W \sin \Phi') \}.$$

$$R_\Phi R \sin \Phi' d\Phi' d\theta \qquad \qquad \ldots (4)$$

The kinetic energy expression is :

$$K = \int_{-h/2}^{h/2} \int_0^{2\pi} \int_0^{2\pi} \frac{1}{2} \rho \left[\left[\frac{\partial U_\Phi}{\partial t} \right]^2 + \left[\frac{\partial W}{\partial t} \right]^2 \right] R_\Phi R_\theta \sin \Phi' d\Phi' d\theta \, dz \qquad \ldots (5)$$

After integrating with respect to (z) and substituting for the appropriate expressions, the maximum kinetic energy will take the form:

$$K_{max} = \frac{\omega^2 \rho h}{2} \int_0^{2\pi} \int_0^{2\pi} (U_\Phi^2 + W^2) R_\Phi R_\theta \sin \Phi' d\Phi' d\theta \qquad \ldots (6)$$

The kinetic energy for $\omega=1$ rad/sec is customarily define as K*max and therefore,

$K_{max} = \omega$ K*max

For a system with no dissipation losses, as those due to friction or damping, the maximum potential energy equals the maximum kinetic energy, i. e.

$U_{max} = \omega$ K*max

   Equating the maximum kinetic energy to the maximum potential energy, an expression for the natural frequency may be written as :

$U_{max} = K_{max}$

or;

$$\omega_r^2 = \frac{U_{max}}{K_{max}} = \frac{N}{D} \qquad\qquad r = 1, 2, 3, \ldots, n \qquad\qquad \ldots (7)$$

where N and D represent the equations in the numerator and denominator, respectively. Following the procedure of Rayleigh – Ritz's method, the radial (or transverse) and tangential displacements can be written in power series form as :

$$w(\Phi') = \sum_{i=1}^{n} a_i . W_i(\Phi') \qquad , \qquad u_\Phi(\Phi') = \sum_{i=1}^{n} b_i . U_{\Phi i}(\Phi') \qquad\qquad \ldots (8)$$

where a_i and b_i are coefficients to be determined. The functions $w(\Phi')$, $u_\Phi(\Phi')$ satisfy all the geometry boundary conditions of the system, i.e. along the matching region between the halves of the spheroid shells. Equation (7) is an exact expression for the frequency according to Rayleigh quotient. In order to use the procedure of Rayleigh – Ritz's method, equation (8) is substituted into equation (4) and (6), then the results is used in equation (7).

   Now substituting equation   (8) into equations (4) and (6), and after some mathematical manipulations, the following equation will result;

$$\omega_r^2 = \frac{\alpha}{\Psi} = \frac{N}{D} \qquad\qquad r = 1, 2, 3, \ldots, n \qquad\qquad \ldots (9)$$

where,

$$\alpha = \sum_{i=1}^{n} \sum_{j=1}^{n} c_i c_j \frac{Eh\pi}{(1-\upsilon^2)} \int_0^{2\pi} \{ \frac{h^2}{12 R_\Phi^4} \left[U'_{\Phi i} U_{\Phi j}' - 2U_{\Phi i}' W_i'' + W_i'' W_j'' \right] \sin\Phi'$$

$$+ \frac{\upsilon h^2}{6 R_\theta R_\Phi^3} \left[U_{\Phi i} U_{\Phi i}' - U_{\Phi i} W_i'' - U_{\Phi i}' W_i' + W_i' W_i'' \right] \cos\Phi'$$

$$+ \frac{h^2}{12 R_\Phi^2 R_\theta^2} \left[U_{\Phi i} U_{\Phi j} - 2U_{\Phi i} W_i' + W_i' W_j' \right] \frac{\cos^2\Phi'}{\sin\Phi'}$$

$$+ \frac{1}{R_\Phi^2} \left[U_{\Phi i}' U_{\Phi j}' + 2U_{\Phi i}' W_i + W_i W_j \right] \sin\Phi'$$

$$+ \frac{1}{R_\theta^2} \left[U_{\Phi i} U_{\Phi j} \frac{\cos^2\Phi'}{\sin\Phi'} + 2U_{\Phi i} W_i \cos\Phi' + W_i W_j \sin\Phi' \right]$$

$$+ \frac{2\upsilon}{R_\Phi R_\theta} \left[U_{\Phi i} U_{\Phi i}' \cos\Phi' + U_{\Phi i}' W_i \sin\Phi' + U_{\Phi i} W_i \cos\Phi' + W_i W_i \sin\Phi' \right] \}.$$

$$. R_\Phi R_\theta \, d\Phi' \qquad\qquad \ldots (9a)$$

$$\Psi = \sum_{i=1}^{n} \sum_{j=1}^{n} c_i c_j \int_0^{2\pi} \rho h\pi \left[U_i U_j + W_i W_j \right] R_\Phi R_\theta \sin\Phi' \, d\Phi' \qquad \ldots (9b) \qquad \text{whe}$$

re, c_i's , c_j's are equiponderate a_i , b_i , a_j , and b_j after mathematical processes and some

simplified and arrangement [**Nawal, 2005**].

where, $\sum_{i=1}^{n} \sum_{j=1}^{n} c_i c_j = \sum_{i=1}^{n} \sum_{j=1}^{n} \left(a_i a_j + b_i b_j + a_i a_i + b_i b_j - a_i b_i \right)$

An n – term finite sum leads to the estimation of the first frequencies.   Equations (9a) and (9b) give the physical properties of the shell from the stiffness and mass distribution point of view. The stiffness and mass of the shell are given by the following two equations respectively:

$$
k_{ij} = \frac{E\,h\,\pi}{(1-\upsilon^2)} \int_0^{2\pi} \frac{h^2}{12\,R_\Phi^4} \{\ \left[U_{\Phi i}{}'\ U_{\Phi j}{}'\ -2U_{\Phi i}{}'\,W_i{}''+W_i{}''\,W_j{}'' \right]\sin\Phi'
$$

$$
+\frac{\upsilon\,h^2}{6\,R_\theta\,R_\Phi^3}\left[U_{\Phi i}\,U_{\Phi i}{}'-U_{\Phi i}\,W_i{}''-U_{\Phi i}{}'\,W_i{}'+W_i{}'\,W_i{}''\right]\cos\Phi'
$$

$$
+\frac{h^2}{12\,R_\Phi^2\,R_\theta^2}\left[U_{\Phi i}\,U_{\Phi j}-2U_{\Phi i}\,W_i{}'+W_i{}'W_j{}'\right]\frac{\cos^2\Phi'}{\sin\Phi'}
$$

$$
+\frac{1}{R_\Phi^2}\left[U_{\Phi i}{}'U_{\Phi j}{}'+2U_{\Phi i}{}'\,W_j+W_i\ W_j\right]\sin\Phi'
$$

$$
+\frac{1}{R_\theta^2}\left[\ U_{\Phi i}\,U_{\Phi j}\ \frac{\cos^2\Phi'}{\sin\Phi'}+2U_{\Phi i}\ W_i\cos\Phi'\ +W_i\,W_j\sin\Phi'\ \right]
$$

$$
+\frac{2\upsilon}{R_\Phi\,R_\theta}\left[U_{\Phi i}\,U_{\Phi i}{}'\cos\Phi'\ +U_{\Phi i}{}'\,W_i\sin\Phi'\ +U_{\Phi i}\,W_i\cos\Phi'\ +W_i\,W_i\sin\Phi'\ \right]\ \}.
$$

$$
.\ R_\Phi\,R_\theta\,d\Phi' \qquad\qquad\qquad\qquad\qquad\qquad \ldots(10)
$$

where primes denote differentiation with respect to Φ'.

and

$$
m_{ij} = \int_0^{2\pi} \rho\,h\,\pi\left[U_i\,U_j\ +W_i\,W_j\ \right]R_\Phi\,R_\theta\ \sin\Phi'd\Phi' \qquad\qquad \ldots(11)
$$

Then

$$
\omega_r{}^2 = \frac{N}{D} = \frac{\displaystyle\sum_{i=1}^{n}\ \sum_{j=1}^{n}\ c_i\,c_j\ k_{ij}}{\displaystyle\sum_{i=1}^{n}\ \sum_{j=1}^{n}\ c_i\,c_j m_{ij}} \qquad\qquad\qquad \ldots(12)
$$

In order to minimize the approximate value, which is given by equation (12), it should be differentiation with respect to c_i and equating the resulting expression to zero, that is :

$$
\frac{\partial}{\partial c_i}\left(\frac{N}{D}\right) = \frac{D\ \partial N/\partial c_i - N\ \partial D/\partial c_i}{D^2} = 0 \qquad i = 1, 2, 3, \ldots., n \qquad\qquad \ldots(13)
$$

The conversional way in which this equation can equal zero is if the numerator equals zero, since D is never equal to zero. The numerator can be written in a more useful form as :

$$\frac{\partial N}{\partial c_i} - \frac{N}{D}\frac{\partial D}{\partial c_i} = 0, \qquad\qquad i = 1, 2, \ldots, n \qquad\qquad \ldots (14)$$

It is as given by equation (7) $\omega_r^2 = N / D$, and n is the number of terms in the approximate solution. The infinite degrees of freedom system has been replaced by an n degrees of freedom system. Therefore, Equation (14) can be written in general matrix notation as :

$$\left[\{K\} - \omega^2 \{M\} \right]\{c\} = \{0\} \qquad\qquad\qquad . \qquad\qquad .. (15)$$

Since i can be taken as 1, 2,3,… the evaluation of this determinant provides the estimation of the first two natural frequencies ω_1^2 and ω_2^2. Since we have used a two–term approximate solution, it results in a two degrees of freedom approximated system.

In the present work, and adopting the same argument of [**Penzes and Burgin,1965**] that the mode shapes of a spherical shell satisfies the boundary conditions of an oblate spheroid shell, the assumed mode shapes were chosen to represent the first two modes of a closed spherical shell.

Engineering Model By Non – Shallow Shell Theory :

The problem of vibration of oblate spheroid shells will be treated by an engineering modeling approach where the oblate spheroid shell is modeled as a structure composed of two spherical shells joined rigidly at their ends. Centers of curvature of the two spherical shell elements fall along the minor axis of the proposed oblate spheroid [see Fig. (1) for details].

Such approximation is not far from reality, as the oblate spheroidal tanks are produced by joining, either by welding or riveting, two spherical shell elements through a toroidal shell element.

The effective radius (R_r) of the spherical shell model represents the radius of curvature at the apex of the shell. This radius can be obtained from the geometrical relation [**Penzes, 1965**].

$$R_\Phi = \frac{a(1-e^2)}{(1-e^2\cos^2\Phi')^{3/2}} \qquad\qquad \ldots (16)$$

Setting (Φ') to zero results the radius of the shell at the apex as:

$$R_r = \frac{a}{(1-e^2)^{1/2}} \qquad\qquad \ldots (17)$$

where,

$e = \left[1 - \frac{b^2}{a^2} \right]^{\frac{1}{2}}$, a and b represent the major axis and minor axis respectively.

e = 0 for sphere   ,   e = 1 for plate.

An approximate opening angle (Φ_0) may be obtained by using the following formula:

$$\Phi_o = \cos^{-1} \frac{R_r - b}{R_r} \qquad \qquad \ldots (18)$$

Figures (2) and (3) show the values of the effective radius and opening angle versus the eccentricity respectively.
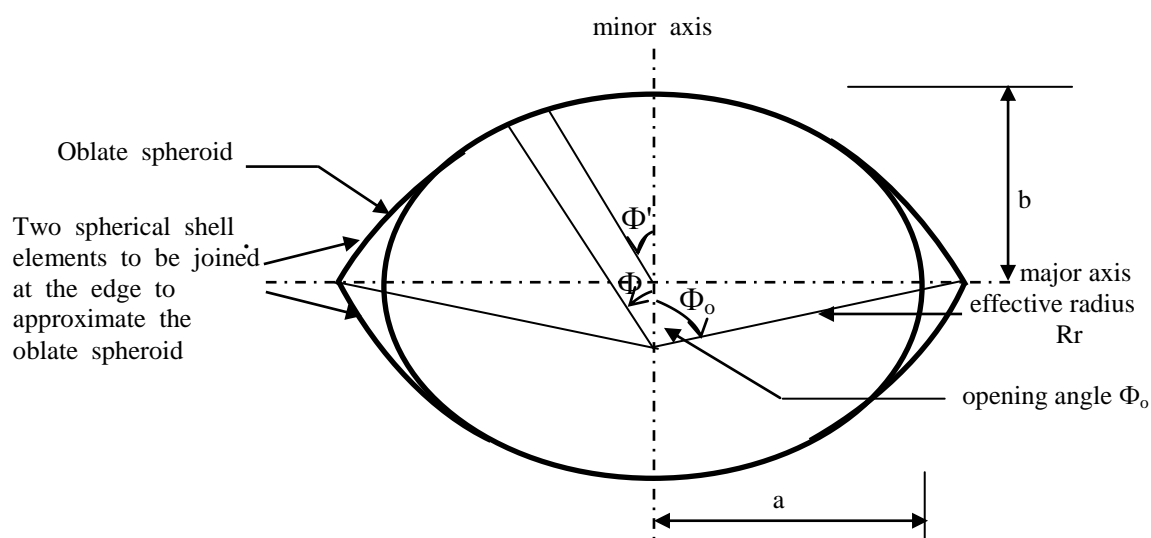

Fig. (1): An oblate spheroid and its approximate of two spherical shell elements joined at the edge.

RESULTS AND DISCUSSION:

The theoretical results and the available experiments are compared and thoroughly discussed. The lack of numerical results in the literature and the complexity of obtaining a closed form solution for the free vibrational characteristics of an oblate spheroid oblige us to seek alternative approaches for justifying the feasibility of the theoretical methods used in this paper. Eventually, these methods are general and may be used for any physical and geometrical parameters of the oblate spheroid. Therefore, the natural frequency for a thin sphere which is considered as an ultimate shape of the oblate spheroid may be determined by using these methods and the results are compared with the literature.

Table (1) shows the natural frequency of the three first axisymmetric modes of a full thin sphere. These frequencies were obtained from applying the direct analytical solution (DAS) [**Tavakoli, 1989**], the state space method (SSM) [**Tavakoli, 1989**], the finite element method (FEM) [**Tavakoli, 1989**] where a forty elements axisymmetrical model was used, Rayliegh method (RM) [**Fawaz**, **1990**], and the method derived in this paper, namely the Rayleigh – Ritz method (RRM). The results of the latter method was obtained by setting the

eccentricity ratio to zero in equation (7). Also it can be seen that the Rayleigh–Ritz's method predicts frequencies higher than the other methods given in the table. This fact is inherited to this method for its higher bounds prediction. However, it may be stated from this table that the two methods of solution presented in this work are dependable and may be used for other shell geometrical and physical parameter.

The experimental and theoretical frequencies for oblate shell are presented in table (2), this table indicates that the theoretical results by the Rayliegh and Rayleigh – Ritz's method predict frequencies higher than of the experimental. This is inherited to this particular method.

Figures (4) and (5) show the non–dimensional natural frequencies $\left(\lambda = \sqrt{\rho / E}\, \omega \cdot a\right)$ of the first two modes of vibration as functions of the eccentricity ratio (which is one of the main indices of an oblate spheroid) obtained by the Rayleigh Ritz's method and the Rayleigh's method using the non – shallow shell theory. These figures show clearly the tendency of the natural frequencies towards lower values as the eccentricity increases. Also it is indicated that the curve obtained by the Rayleigh's method, adjoin to that obtained by the Rayleigh's – Ritz's method, although with slightly higher value, until the eccentricity reaches (0.6) where the Rayleigh's method curve start to diverge. Larger divergence occure at eccentricities higher than (0.9).

This behavior could be explained by the fact that the mode shapes of a closed spherical shell would resemble those of an oblate spheroid up to certain eccentricity. As the eccentricity increases, the oblate spheroid tends to flatten up. Such "flattening" causes the uncoupling of the radial (or transverse motion) and the tangential motion where the latter is minimized and the radial or transverse motion mode shape approaches that of a circular plate. Another reason is that the spherical shape is stiffer than the oblate spheroid due to the flattening in the geometry.

However, the sudden deviation in the curve predicted by (RM) for eccentricity larger than (0.6) may be considered due to additional constraints resulting from the deviation from the true mode shape. This causes higher values for the potential energy in Eq. (7) and thus the values of the natural frequencies diverge abruptly at higher values of eccentricity. This mean that the value predicted by the (RM) for eccentricities larger than (0.6) are in tremendous error and cannot be used.

Figure (6) gives the first few natural frequencies as function of the thickness ratio for an oblate spheroid with (e = 0) obtained by RRM. However, Fig. (7) shows the same results as given by [Kraus], for complete sphere. The two figures are in good agreement and justify very well the validity of the method used in this paper.

Figure (8) show the first few frequencies as functions of thickness ratio with (e = 0.6). All these figures are for (υ = 0.3) and they show the bending as well as the membrane modes using the non – shallow shell theory. It can be noted that the variation of the natural frequency of the bending modes increases with thickness and with the mode number. This phenomenon can be elaborated due to the fact that the strain energy increased with increasing the thickness ratio. Also, for larger eccentricity ratio, the variations are more pronounced than for smaller eccentricity.

For further illustration of the effect of thickness on the bending modes, Figure (9) shows the first two bending modes of an oblate spheroid with an eccentricity of (0.3) for several thickness ratios, obtained by applying the RM and RRM. It is well indicated that the figures obey the previous observation of the effect of thickness on bending modes.

Figures (10) and (11) illustrate the boundaries of the first three bending modes and the first membrane mode respectively with increasing the eccentricity (e). It may be observed from figure (10) that as the eccentricity increased, the natural frequency slowly decrease until reaching close to (0.5) where steeper variation occurs and the three curves

converge to very close values. On the other hand, Fig. (11) shows other features concerning the behavior of the first membrane mode with increasing eccentricity ratios.

From Fig. (12) it is concluded that the main features of the mode shapes associated with the first three natural frequencies rest in the number of the nodal lines in the upper and the lower shell parts. The number of these nodal lines is related to the order of the associated natural frequency.

CONCLUSIONS:

From the results obtained, the following conclusions may be drawn;

- The Rayliegh – Ritz method predict fairly well the natural frequencies of an oblate spheroidal shell for all values of eccentricities.
- Bending modes natural frequencies tend to decrease with increasing eccentricity ratio.
- Membrane modes natural frequencies tend to increase with increasing eccentricity ratio.

REFERENCES:

- Antoine Chaigne, Mathieu Fontaine, Oliver Thomas, Michel Ferre, Cyril Tou., "Vibrations of Shallow Spherical Shells and Gongs", J. of Sound and Vibration, 2002.

- Chang Y. C. and Demkowicz L., "A stability Analysis Vibrating Viscoelastic Spherical Shells", J. Appl. Math., Vol. 2(2), PP. 213 – 242, 1998.

- Fawaz Abbas Najim, "An Investigation into the Free axisymmetric vibration characteristics of isotropic thin oblate spheroidal shells", M. Sc. Thesis, Mechanical Engineering/ University of Baghdad, 1990.

- Haym Benaroya, "Mechanical Vibration", Prentice – Hill, Inc., U.S.A., 1998.

- Kalnins A., "Effect of bending on vibrations of spherical shells", J. Acoust. Soc. Amer., Vol.
- 36 (1), PP. 74 – 81, 1964.

- Kraus H., "Thin elastic shells", John Wiley and Sons, New York 1967.

- Nawal H. A. , " Theoretical Investigation of the Axisymmetric Free Vibration of An Oblate Spheroid Shells", M. Sc. Thesis, Mechanical Engineering/ University of Babylon, 2005.

- Penzes L. and Burgin G.," Free vibrations of thin isotropic oblate spheroidal shells", General Dynamic Report No. GD/C–BTD 65 – 113, 1965

- Penzes L., " Free vibrations of thin orthotropic oblate spheroidal shells", J. Acoust. Soc. Amer., Vol. 45, pp. 500 – 505, 1969.

- Tavakoli M. S. and Singh R., "Eigensolutions of joined / hermetic shell structures using the state space method", J. Sound and Vibration Vol. 100, PP. 97 – 123, 1989.

- Wilfred E. Baker " Axisymmetric modes of vibration of thin spherical shell", J. Acoust. Soc. Amer., Vol. 33, PP. 1749 – 1758, 1961.

Table (1) : Natural frequencies of the first three axisymmetric modes of thin sphere, Hz.

$r = 0.1143$ m , $h = 0.0057$ m , $E = 207$ Gpa , $\rho = 7800$ Kg/m^3 , $\upsilon = 0.3$

| | | | | | | Differences with respect to DAS. % | | | |
n	m	DAS.[1]	SSM.[2]	FEM.[3]	R.M.[4]	RRM.[5]	δ_1%	δ_2%	δ_3%	δ_4%
0	2	5281	5291	5383	5335	5315	- 0.2	≈ 0.0	-1.0	-0.6
0	3	6321	6330	6319	6510	6513	- 0.1	≈ 0.0	-3.0	-3.0
0	4	6883	6894	6875	--------	6950	- 0.1	0.1	-----	-1.0

(1) Direct Analytical Solution [4] δ_1 % = (DAS – SSM) / DAS * 100

(2) State Space Method [4] δ_2 % = (DAS – FEM) / DAS * 100

(3) Finite Element Method [4] δ_3 % = (DAS – R M) / DAS * 100

(4) Rayleigh Method [5] δ_4 % = (DAS – RRM) / DAS * 100

(5) Rayleigh – Ritz Method [*present work*]

Table (2) : Theoretical and experimental natural frequencies
of thin oblate shell (e=0.683)
Hz.
a=0.185m , b=0.135m , h= 0.0015m , , E = 68 Gpa , ρ = 2720Kg/m^3 , υ = 0.3

	Theoretical			Differences with respect to Expt. ⁒	
	RRM	RM[5]	Expt. [5]	δ_1⁒	δ_2⁒
ω_1	2517	3110	2400	-4.87	-29.58
ω_2	2973	3378	2600	-14.34	-29.92
ω_3	3086	....	2900	-6.41	....
ω_4	3180	....	3100	-2.58	....

δ_1⁒= (Expt. – RRM) / Expt. * 100

δ_2⁒= (Expt. – R M) / Expt. * 100
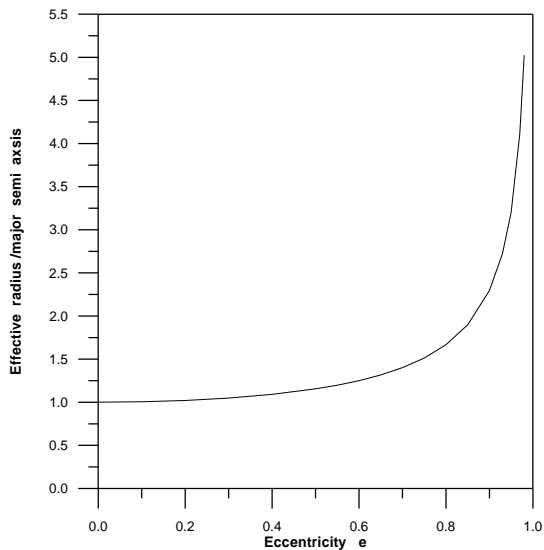
Fig. (2) The effective radius / major semi
Φ_o) of the – axis vs. eccentricity vs.
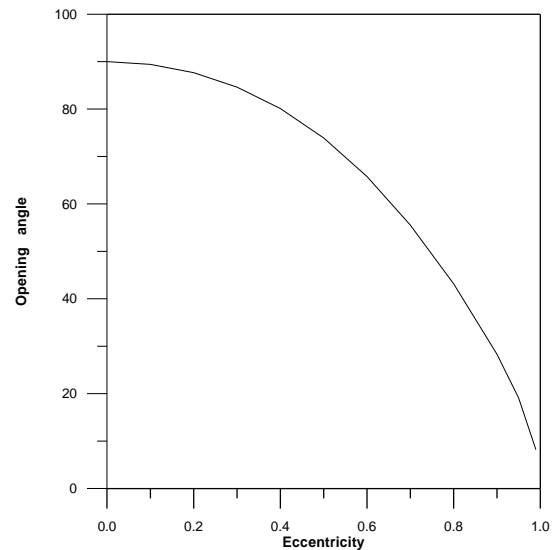
Fig. (3) : The opening angle (
approximate spherical shells
eccentricity.

4317
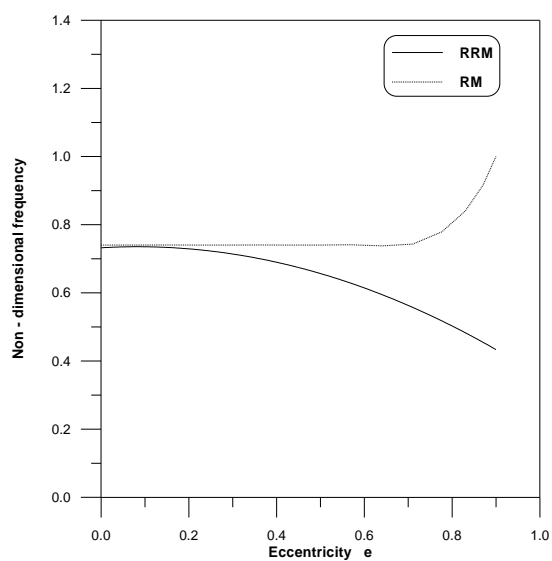
Fig. (4): A comparison between RM and RRM results
            showing the effect of eccentricity on the first
            bending mode of vibration
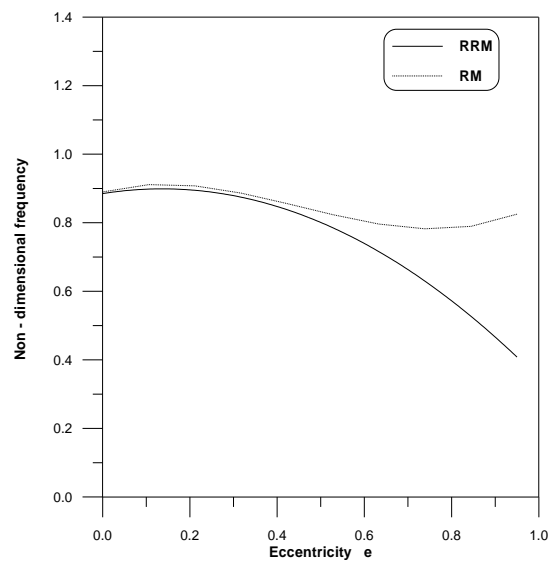
Fig. (5) :A comparison between RM and RRM results
            showing the effect of eccentricity on the second
            bending mode of vibration
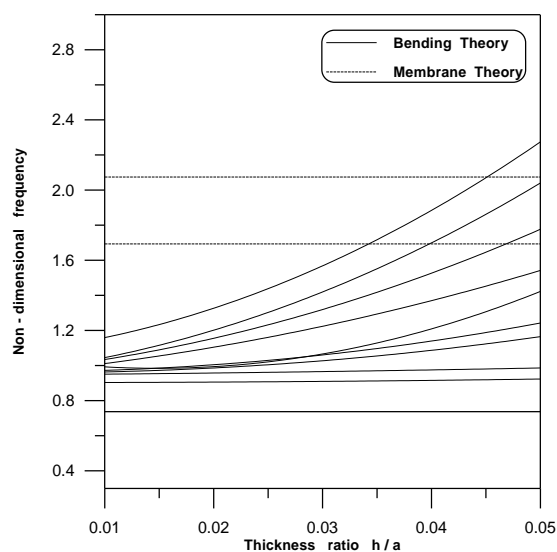
Fig. (6): Effect of the thickness ratio on the natural
            frequencies of a full sphere or an oblate
            spheroidal shell (e = 0) obtained by RRM
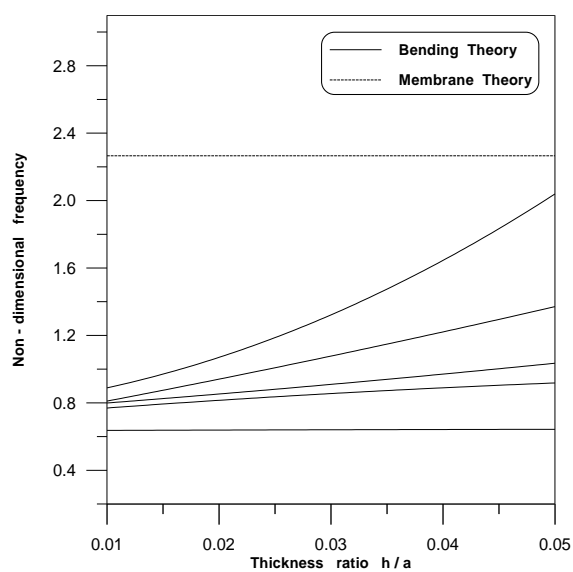
Fig. (7): Effect of the thickness ratio on the natural frequency of an oblate spheroidal   shell (e = 0.6) obtained by RRM
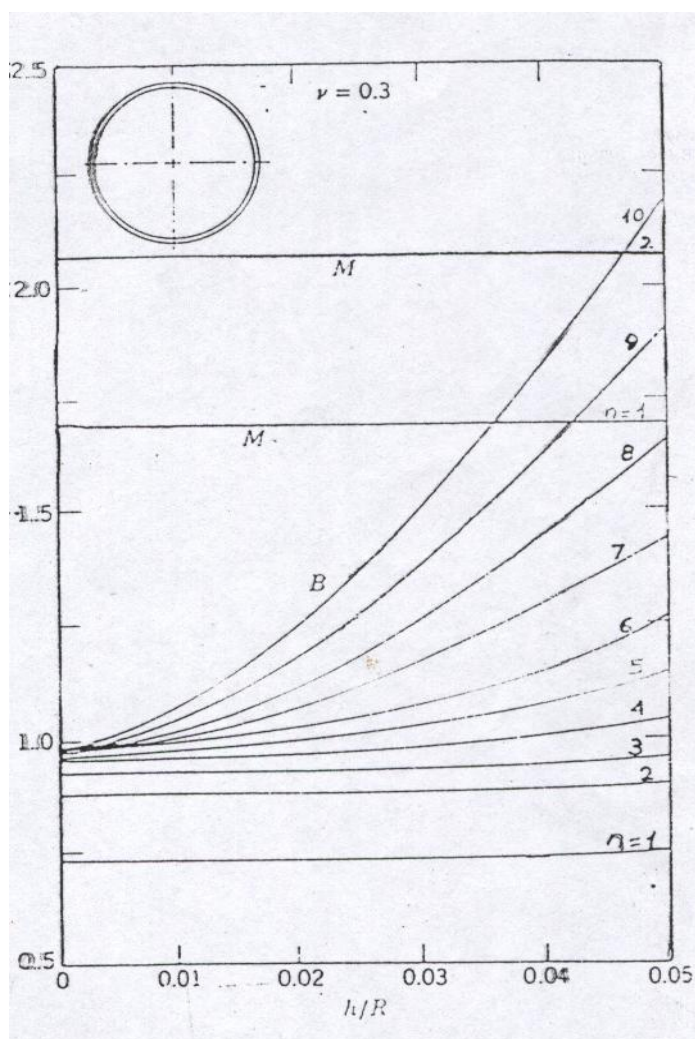
Fig. (8): Effect of the thickness ratio on the natural frequencies of a full sphere extracted from [11]
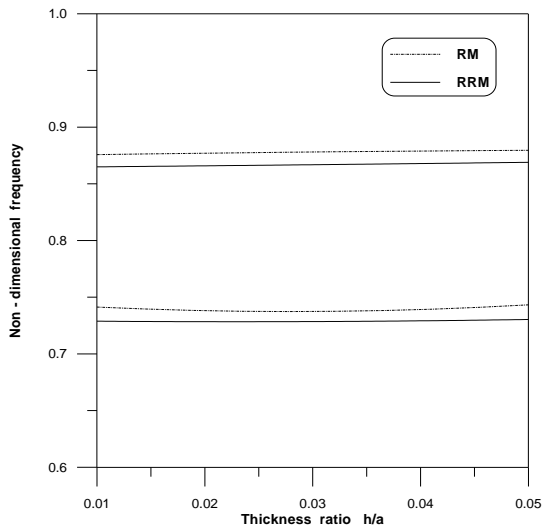
Fig. (9): Effect of thickness ratio on the first and second bending modes of an oblate spheroidal shell (e = 0.3)
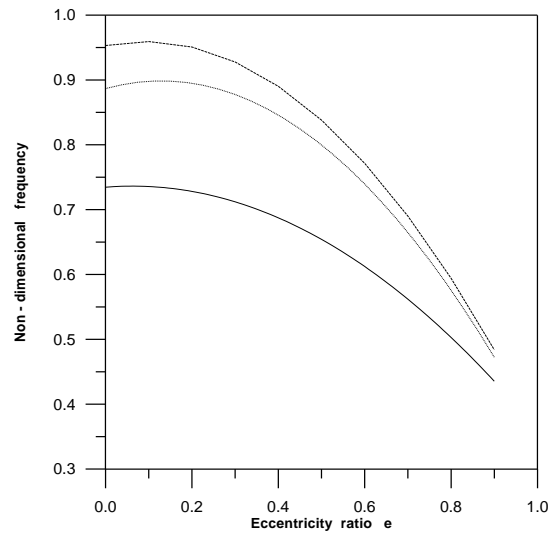
Fig. (10): Effect of eccentricity on the three first bending modes obtained by RRM
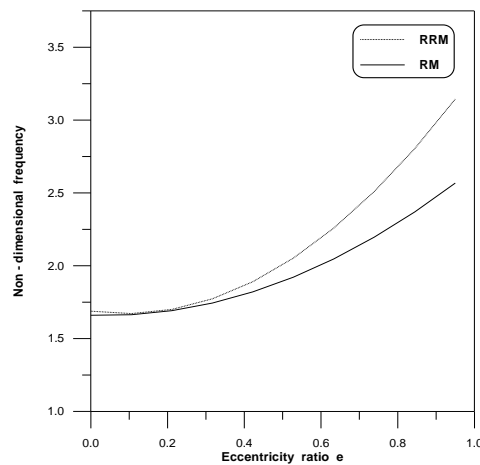
Fig. (11): Effect of eccentricity on the first membrane modes
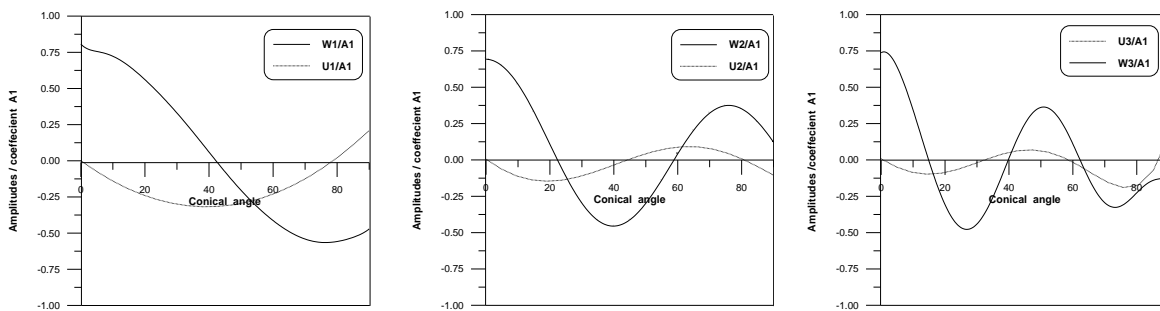
Fig. (12): Normalized mode shape associated with the first three natural frequency of non – shallow spheroidal shell (e = 0.683) obtained by RRM

MODELING OF INDUCTION HEATING PROCESS OF A CONDUCTING FERROMAGNETIC MATERIALS

Akram F. Batti, PhD.; Fadhil A. Abood, PhD.; Adil H. Ahmad, PhD.;
Essam M. Abdul-Baki, MSc.
UOT/ Baghdad / Iraq

ABSTRACT

This research deals with a modeling of the heating process of an induction furnace with a conducting ferromagnetic core. This is done by performing a sequential coupling between two types of analysis; the harmonic electromagnetic analysis and the transient thermal analysis in order to furnish a complete numerical simulation of this device. The time elapsed to apply this procedure will be too long and unreasonable because of the consideration of the nonlinearity of the magnetic circuit. This problem is solved by the idea of the "Effective Relative Permeability", which is a constant relative permeability equivalent to the nonlinear one in calculating the eddy current losses.

The Finite Element Method (FEM) is considered in order to solve this problem using the "ANSYS "computer package. An efficient coupling program deals with heat treatment procedure for any axi-symmetrical non-linear work piece has been built. The obtained results show a good agreement with the published practical measurements. This algorithm is a computer aided design for a nonlinear induction furnace with rotational symmetry, hence it can be used to design such devices instead of the traditional trial and error, experience dependant, design methods which lead to a costly and time wasting design.

خلاصة

يعنى هذا البحث بنمذجة عملية التسخين في فرن حثي ذو قلب مكون من مـادة فيرومغناطيسية. لقد تم ذلك بتنفيذ تعشيق متعاقب لنوعين من التحليلات هما: التحليل الكهرومغناطيسي التوآفقي و التحليل الحراري العابر بغية الحصول على تمثيل رقمي متكامل لهذا الجهاز. أن الوقت المستغرق لتنفيذ هذه الخطوات سيكون طويل جدا وغير منطقي بسبب أخذ لاخطية الدائرة المغناطيسية بنظر الأعتبار. عليه فقد تم حل هذه المعضلة بأعتماد فكرة "السماحية النسبية المكافأة"، والتي هي عبارة عن سماحية نسبية ثابتة القيمة ومكافئة لتلك اللاخطية عند أحتساب خسائر التيارات الدوامة.

لقد أعتمـدت طريقـة العنصـر المحـدد (FEM) لغـرض حـل هـذه المشـكلة بأسـتخدام بـرامجيـات الحاسـبة (ANSYS)، حيث تم بناء برنـامج كفوء للتعشيق يعنـى بسياقات ألمعـاملات الحـراريـة المختلفـة للعينـات اللاخطيـه المتناضرة محوريا. أن النتائج المستحصلة أظهرت أنسجاما جيدا مع القياسات العملية المنشورة. لذا فأن هذا النظـام يعتبر بمثابة تصميم بمساعدة الحاسبة للافران الحثيـة اللاخطيـة المتناضـرة دورانيـا، لذا يمكن استخدامه كبديل عن الطرق التقليدية التي تستخدم الخبرة و أعتمـاد أسلوب ألتجربـة و ألخطـأ ممـايؤدي الـى تصـاميم مكلفـة وتستغرق وقتـا طويلا.

F.A. Abood
A. F. Batti
 A.H. Ahmad
E. M. Abdul-Baki

INTRODUCTION

It is already known that the induced eddy currents inside the induction furnace core (the work piece or the specimen) is not uniform, and it depends on many factors like, the frequency of the excitation current, the shapes of the furnace and the specimen to be heated, and on the electrical conductivity and the permeability of the core material due to the equation [1]

$$\delta = \sqrt{2\rho_e / \mu f} \qquad \ldots\ldots\ldots\ldots\ldots\ldots\ldots\ldots\ldots\ldots\ldots \text{(1)}$$

The mathematical simulation of a non-linear induction furnace is a complicated problem due to the following factors:

1. The induced eddy currents will heat the specimen gradually, and since the physical properties of the core material vary with temperature, then each part inside the core will have its different properties due to its temperature which will lead to change its behavior during the heating period, so the electromagnetic analysis should be followed by a transient thermal analysis to calculate the temperature inside the core for small period of time. This procedure abbreviated in the flow chart shown in Fig. 1

2. The non uniform distribution of the induced eddy currents inside the core leading to a non uniform heat distribution inside it, this fact leads to divide the core into small parts and evaluate the parameters of each part due to its temperature.

3. The permeability is a function of three variables, the flux density B, the magnetic intensity H, and the temperature T simultaneously in a non-linear way. This factor affects the analysis as follows:
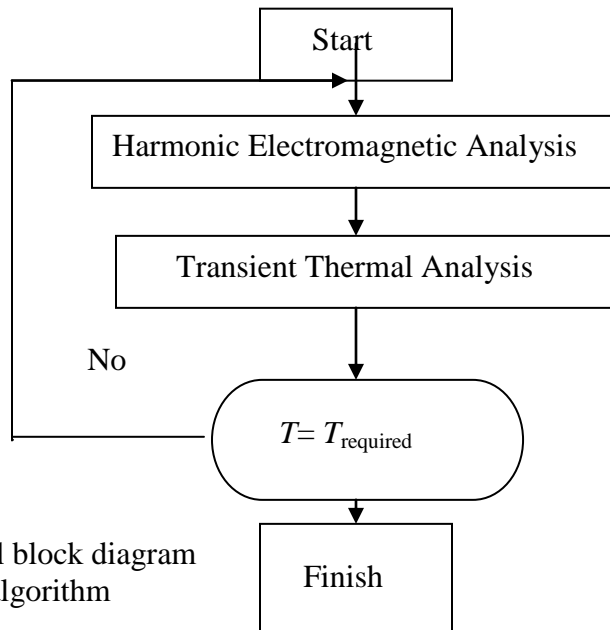

Fig. 1 General block diagram of the algorithm

a. Considering the (*B-H*) nonlinearity as it is manifested in the relationship will make the electromagnetic solution very slow. Because it is necessary to march through time with a time step much smaller than the period of the driving magnetic field.

b. The numerical analysis deals with sinusoidal functions only, but due to the nonlinear (*B-H*) relation of the ferromagnetic materials, if *B* is considered sinusoidal, then *H* will be non-sinusoidal and if *H* considered sinusoidal *B* will be not. So this conflict should be arranged for.

c. The measurement of the *(B-H)* relation of the ferromagnetic material in high temperatures is a difficult task, so the researches often use an approximated formula to overcome this problem. Such calculations should be done separately in order to prepare the *(B-H)* relations of other temperatures

d. To solve the problems in (a) and (b) above, the idea of the *"Relative Effective Permeability"* $\mu_{r,eff}$, which is a constant relative permeability effectively provides the same energy deposition that is produced when the true permeability is used. The quantity $\mu_{r,eff}$ will be a function of *H* and *T* simultaneously, as will be shown later on. So, this will lead to make the electromagnetic analysis itself an iterative process in order to update the value of the relative permeability with each temperature reached and for the right value of *H* consequently.

Then the real behavior of the core can be achieved during the heating period by dividing the core into a very small parts and a harmonic electromagnetic analysis is done taking into consideration the material parameters for each part alone to determine its induced eddy current losses, then these values considered as input data to a transient thermal analysis step to study the heat transfer for the core for a short period of time and determine the temperature distribution inside the core at the end of that period. Hence to calculate the temperature distribution for the next short period of time the above procedure must be repeated after updating the properties due to the new temperature of each part and so on until the heating period is finished by reaching the required temperature distribution inside the core.

This problem solved numerically by digital computer using the Finite Element Method (FEM). A macro program is written in (APDL) (ANSYS Programming Design Language) to satisfy all the non-linear electromagnetic and thermal analysis. This algorithm is done to model this process for any furnace with rotational symmetry. The algorithm can tell the following information about this process for a certain specimen in shape and type of material to be treated thermally in a certain way for certain purpose:

    (1) The excitation current required.
    (2) The frequency of that current.
    (3) The thermal distribution inside the specimen.
    (4) The thermal response of any point during the heating period.

Theoretical Background:
i. Electromagnetic Analysis

    It is already known that the complex electromagnetic equations can be greatly simplified based on magnetic vector potential *A* . All quantities related to the induction Joule heat can be achieved, based on the ac current, *I,* input to the induction coil. *A* can be expressed with Biot-Savart's law [1]

$$A = \frac{\mu_o I}{4\pi} \int_s \frac{dl}{|r|} \qquad \ldots\ldots\ldots\ldots\ldots\ldots\ldots\ldots \; (2)$$

The magnetic flux density B is defined as

$$B = \nabla \times A \; \ldots\ldots\ldots\ldots\ldots\ldots\ldots\ldots\ldots\ldots\ldots\ldots. \; (3)$$

From Faraday's law, the electric field intensity E and magnetic field intensity H are related by the following equations:

$$\nabla \times E = -\frac{\partial B}{\partial t} \; \ldots\ldots\ldots \qquad \ldots\ldots\ldots\ldots\ldots\ldots\ldots \; (4)$$

$$H = B / \mu \; \ldots\ldots\ldots\ldots\ldots\ldots\ldots\ldots\ldots\ldots. \; (5)$$

Based on Ampere's circuital law, the current density, J, induced in work piece is

$$J = \nabla \times H - \frac{\partial(\varepsilon \cdot E)}{\partial t} \; \ldots\ldots\ldots\ldots\ldots\ldots\ldots\ldots.. \; (6)$$

After a mathematical manipulations of above formulas, the relationship between the magnetic vector potential, A, and the induced current density, J, becomes

$$J = \nabla \times (\frac{1}{\mu} \nabla \times A) + \sigma_e \frac{\partial A}{\partial t} \; \ldots\ldots\ldots\ldots\ldots\ldots.... \; (7)$$

Finally, Joule heat generated from eddy currents is

$$Q_{induction} = \frac{J^2}{\sigma_e} \; \ldots\ldots\ldots\ldots\ldots\ldots\ldots\ldots\ldots..\ldots.. \; (8)$$

Where, $\mu, \varepsilon, \sigma,$ are the magnetic permeability, permitivity, and electrical conductivity of the medium respectively. These properties are all temperature dependent, and this classifies the electromagnetic analysis as a highly non-linear problem.

ii. Effective Relative Permeability

The calculation of $\mu_{r,eff}(H,T)$, must be started from the standard B-H Curve at the ambient temperature. To do so, a function used by Vasiliev[2] for determination of the incremental relative permeability as a function of both T and H used as follows:

$$\mu_{ri}(H,T) = 1 + (\mu_{ri}(H)_{T=0} - 1) \cdot \left[1 - (T/T_{curie})^2\right] \quad \text{when} \quad T \langle 750^o C$$

$$\ldots.. \; (9)$$

$$\mu_{ri}(H,T) = 1 \qquad\qquad\qquad\qquad when \quad T \geq 750^o C$$

Where: $\mu_{ri}(H,T)$: Is the incremental relative permeability for each H as a function of temperature T and field intensity H.

$\mu_{ri}(H)_{T=0}$: Is the incremental relative permeability for each H as a function of H when $T = 0^o C$.

Razzaq[3], provides the *B-H* curve at room temperature for Steel C45 (SAE 1045) as a curve for *B* (in Tesla) Versus *H* (in Oeresteds). A transformation in units of *H* is done to be in MKS system (Where 1 Oe= 79.577 A/m) then the magnetization curve drawn to be as shown in Fig. (2). Curie temperature for steel C45 is 750°C.
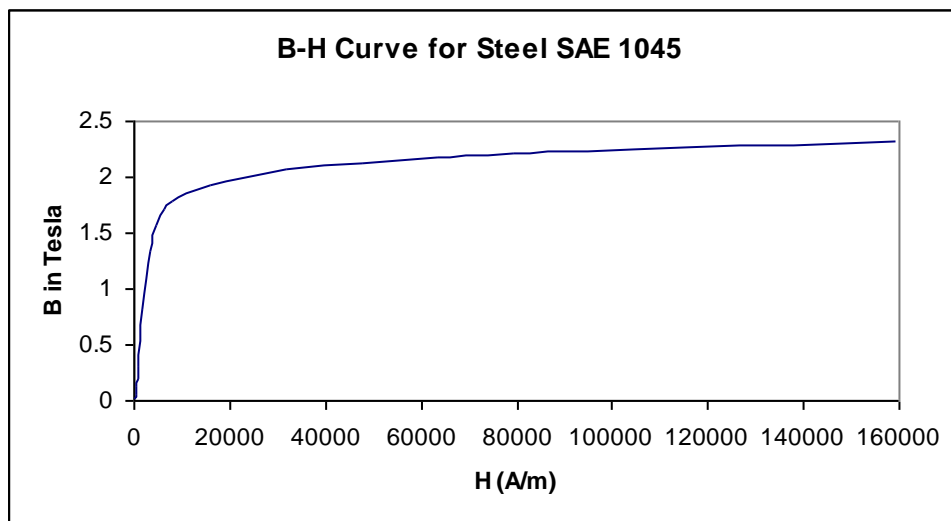
Fig. (2) The magnetization Characteristics of steel C45 at room temperature

The incremental relative permeability μ_{ri} calculated from the given *B-H* data at $T=25^oC$ for certain value of *H* as $\mu_{ri}(H)_{T=0} = \left[(\Delta B/\Delta H)/\mu_o \right]$ and substituted in (9) for the required value of *T* the result will be $\mu_{ri}(T,H)$ for that value of *H* for the required temperature. Then ΔB for the required value of *T* can be determined since, $\Delta B_T = \mu_o * \mu_{ri}(H,T) * \Delta H$. Then, by dividing the main *B-H* curve to many steps and the incremental relative permeability calculated for each step as shown in Fig. (3), then a new *B-H* curve for any value of *T* can be achieved sequentially. Fig. (4) shows group of curves for different temperatures for the carbon steel C45.

F.A. Abood
A. F. Batti
A.H. Ahmad
E. M. Abdul-Baki

Modeling of Induction Heating Process of
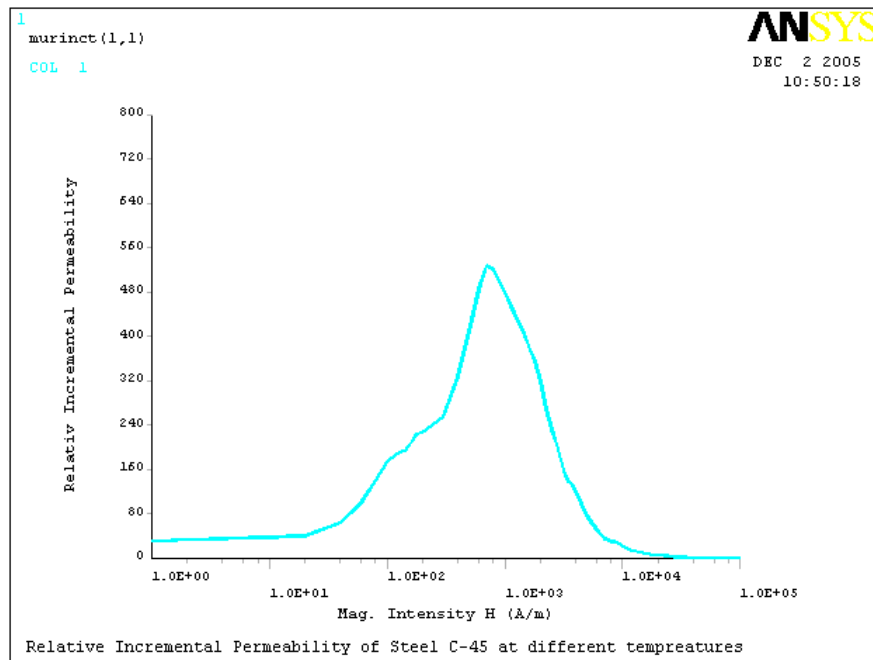A Conducting Ferromagnetic Materials

Fig. (3). Incremental relative permeability for steel C45

Fadhil [4] presents the idea of average permeability to achieve the effective relative permeability because neither *B* nor *H* is sinusoidal. Hence, for the case of considering *B* is sinusoidal only, while *H* will have a distorted shape due to *B-H* non linearity the average permeability will be

$$\mu_{ef1} = \frac{1}{T_c} \int_0^T \frac{B_{max} \, Sin\, \varpi t}{H_B(t)} dt \quad \dots\dots\dots\dots\dots\dots\dots\dots\dots (10)$$

Where $H_B(t)$: represents the distorted time variation of the field intensity.

T_c : represents the time period of one cycle.
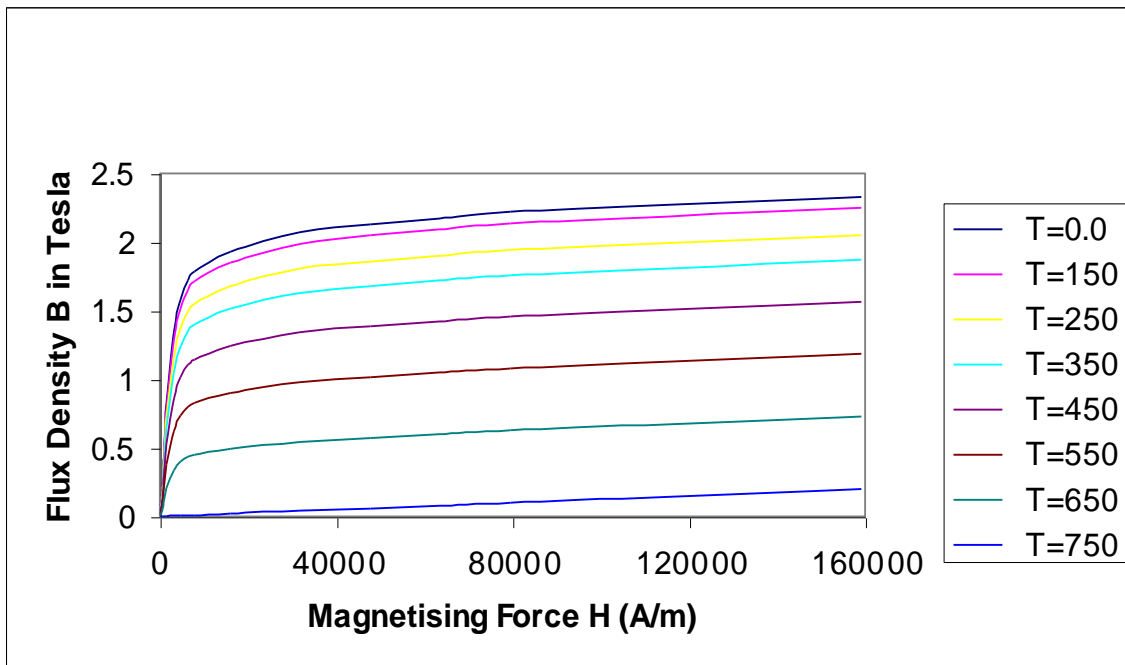
Fig. (4) The Magnetic Characteristics (*B-H* curves) for Steel C45 at different temperatures

For the case of considering *H* is sinusoidal only, while *B* will have a distorted shape due to *B-H* non linearity the average permeability will be

$$\mu_{eff\,2} = \frac{1}{T_c} \int_0^T \frac{B_H(t)}{H_{max}\sin\varpi t}\,dt \quad \text{...........................} (11)$$

Where $B_H(t)$: Is the distorted time variation of the flux density.

Since, in the real case *B* and *H* are non sinusoidal, therefore averaging both permeability would be a reasonable approximation to the effective permeability, then

$$\mu_{eff} = (\mu_{eff\,1} + \mu_{eff\,2})/2 \quad \text{.......................} (12)$$

Using equation (12) the effective relative permeability as a function of *H* and *T* can be determined as shown in Fig. (5). It is clear that Fadhil's method deals carefully with low intensity region.
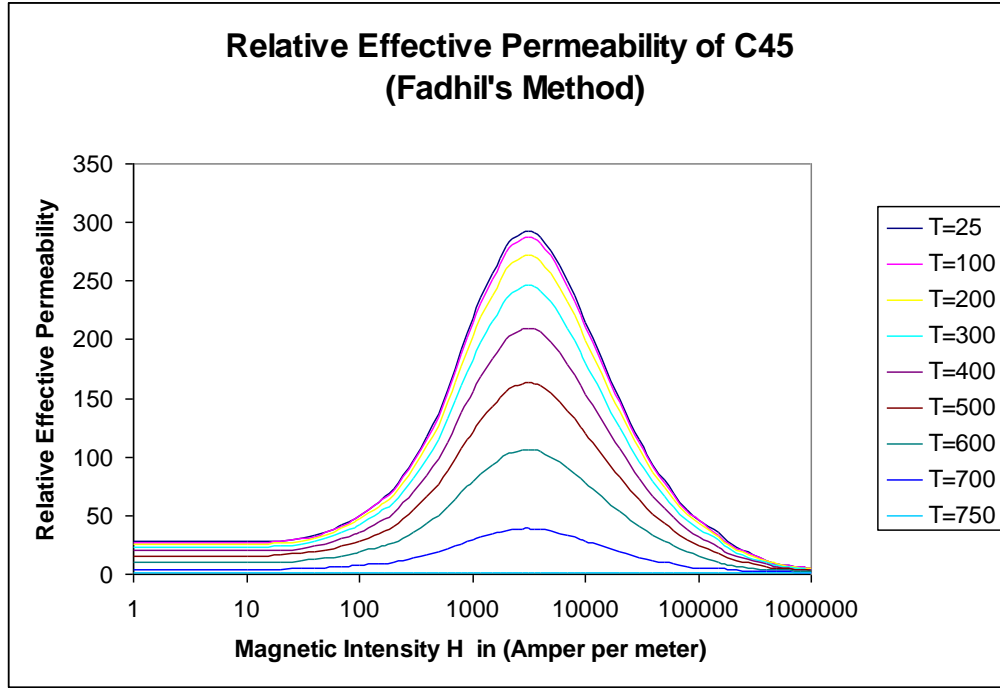
Fig. 5 The relative effective permeability of steel C45

iii. Thermal Analysis

Thermal analysis includes conduction, convection and radiation. The heating process is coupled with the electromagnetic conversion process. In the heating process, the heat conduction effect is the main issue to be considered because the heating cycle is generally very short as several seconds. The conduction equation is [2],

$$\rho_m \cdot C_p \cdot \frac{\partial T}{\partial t} = k \cdot \nabla^2 T + Q_{induction} \quad \ldots\ldots\ldots\ldots\ldots\ldots\ldots \ldots\ldots\ldots (13)$$

On surfaces of work piece, the heat conduction, radiation and free convection effects are all needed. The governing equation is,

$$\rho_m \cdot C_p \cdot \frac{\partial T}{\partial t} = k \cdot \nabla^2 T + Q_{induction} - \xi \cdot \sigma_s \cdot (T^4 - T_{air}^4) - \alpha \cdot (T - T_{air}) \ldots \quad \ldots (14)$$

Where: T_{air} Is the ambient temperature

The Model:

Jorg Cstroeski [5], published a practical measurements on a ferromagnetic material. These measurements considered as a verification of this modeling. Hence the exact furnace used by Jorg is studied in this analysis.

The furnace under study in this case is no more than a "cylindrical shape core surrounded by an inductor with the shape of torus" [5], as shown in Fig. (6). "The cylinder was made of steel C45, it had a radius of 2cm, and it was 10cm long. The torus

was made of copper, it had an interior radius of 2.5cm, an exterior radius of 3.5cm, and its height was 1cm. Three currents were used for the excitation: 10500A, 7875A, and 5250A. The frequency was 10 kHz. In the first 0.2 seconds of the heating phase, only 50% of the exciting current is used, due to the heating regulation of the heating machine. The maximum surface temperature of the cylinder during the heating phase was measured with the aid of a thermo graphical camera. Of course, the maximum surface temperature is located at the center of the cylinder, close to the inductor."[5]
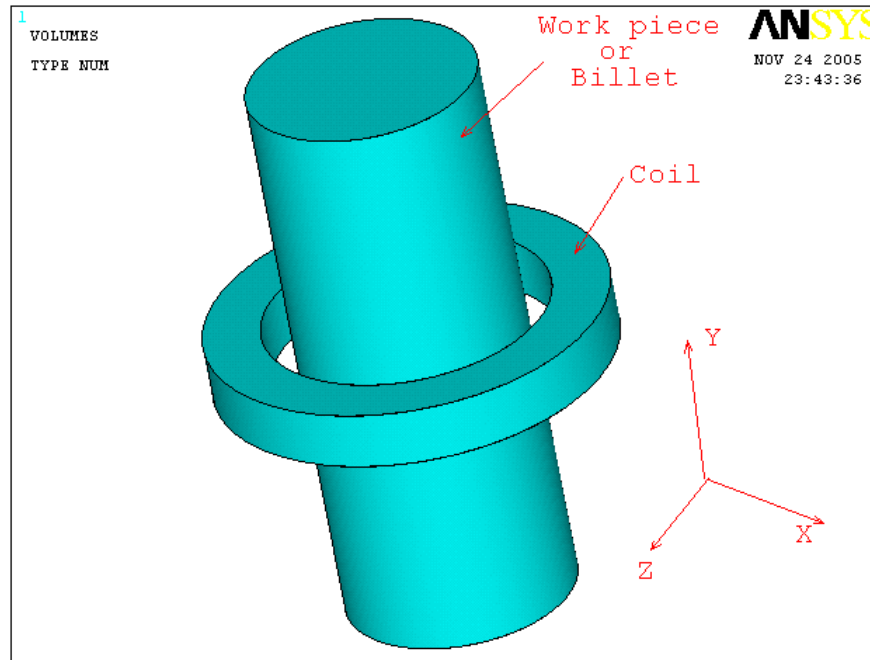
Fig. (6) Setting experiment

The electrical resistivity $\rho(T)$ [5] of steel C45 is shown in Fig. 7, The thermal properties, like the thermal conductivity and the enthalpy [5] are shown in Fig.(8) and Fig.(9).
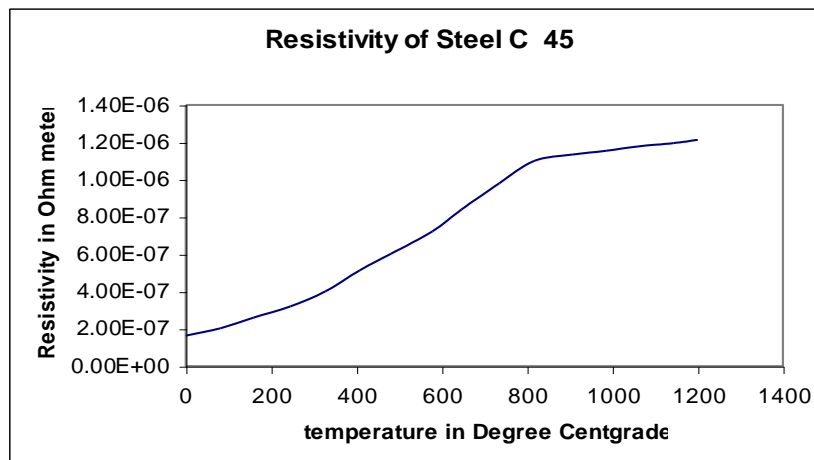
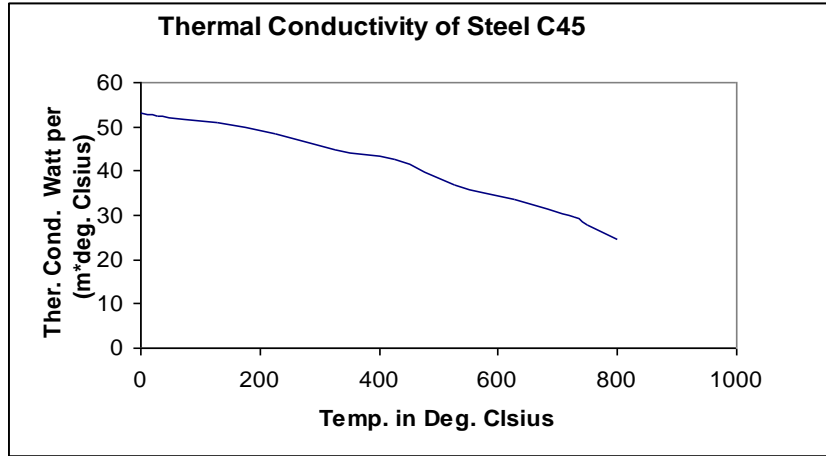**Fig. (7)** The electrical resistivity of steel C45 as a function of temperature

Thermal Conductivity of Steel C45

Fig. (8) Thermal Conductivity of Steel C45
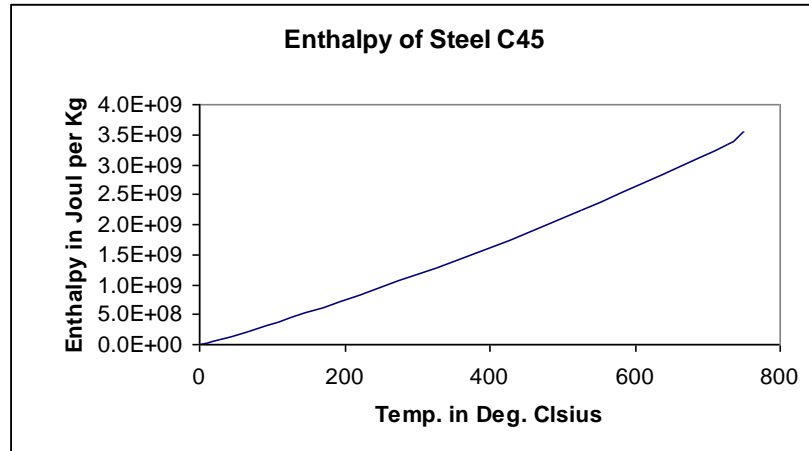
Enthalpy of Steel C45

Fig. (9) Enthalpy of Steel C45 as a function of temperature

The Furnace Simulation using FEM

To simulate this furnace, A procedure of many steps should be followed. The first step is the determination of the system geometry and the boundary region, then meshing the different areas of the model and external surfaces of the billet in order to consider the dissipation of heat due to radiation. The model of furnace is an axi-symmetric one, so a quarter of its section is considered as shown in Fig.(10), which represent the areas of the Finite Element Model. The mesh used for this model is shown in Fig.(11), in which the surface element mesh used in the thermal analysis is cleared also. This part of the procedure is represented as step 1 in Fig. 12 which shows the detailed flow chart of the algorithm

In step 2 the program scans the main four tables of data $\rho_e(T)$, $\mu_{r,eff}(H,T)$, $\lambda(T)$, $Enth(T)$ for the core material. The initial temperature for the whole elements in the core is the ambient temperature. Step 3 is very important in using the $\mu_{r,eff}(H,T)$ three dimensional table of data in that the value of H is zero at any point at time zero before

applying the current, hence the determination of the $\mu_{r,eff}$ in this step will gives a wrong results of *H* distribution
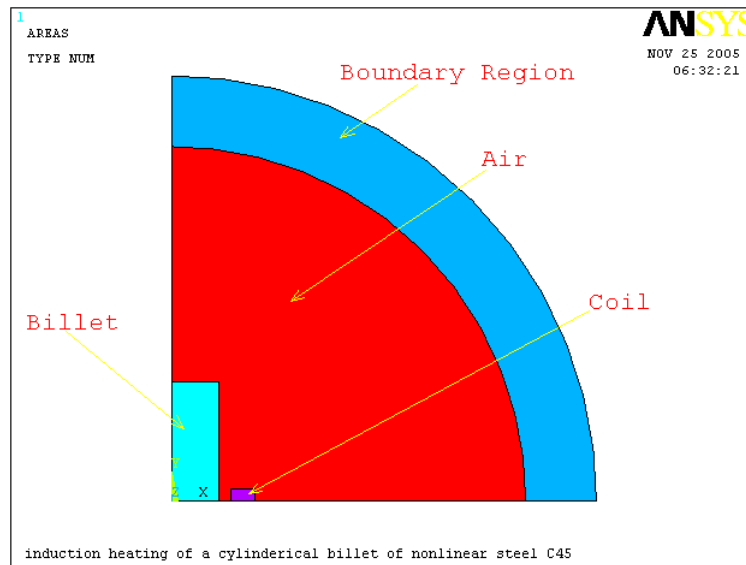

Fig. (10) The areas forming a quarter of the FE Model of the furnace
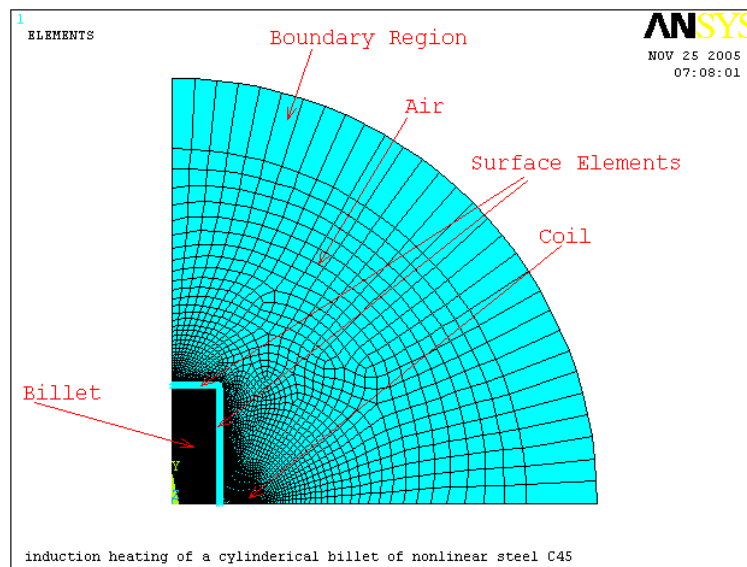

Fig. (11) The mesh of the whole system.

. Then this step is repeated assuming *H* for each element to be that determined in the previous step, then the resulted values of *H* is compared with that of the previous step and so on. If the difference is negligible then the updating step is finished. Step 4 is the determination of the values of heat generation at each element as results of applying the harmonic analysis, and feed them as input to the transient thermal analysis step. Steps 5&6 are the thermal steps in which the temperature of each node and element are determined after a specified period of time.

If the required temperature for the specified point is not reached, the steps (from 3 up to 6) are repeated for the new H and T of each element. This iteration continuous until the required temperature achieved,
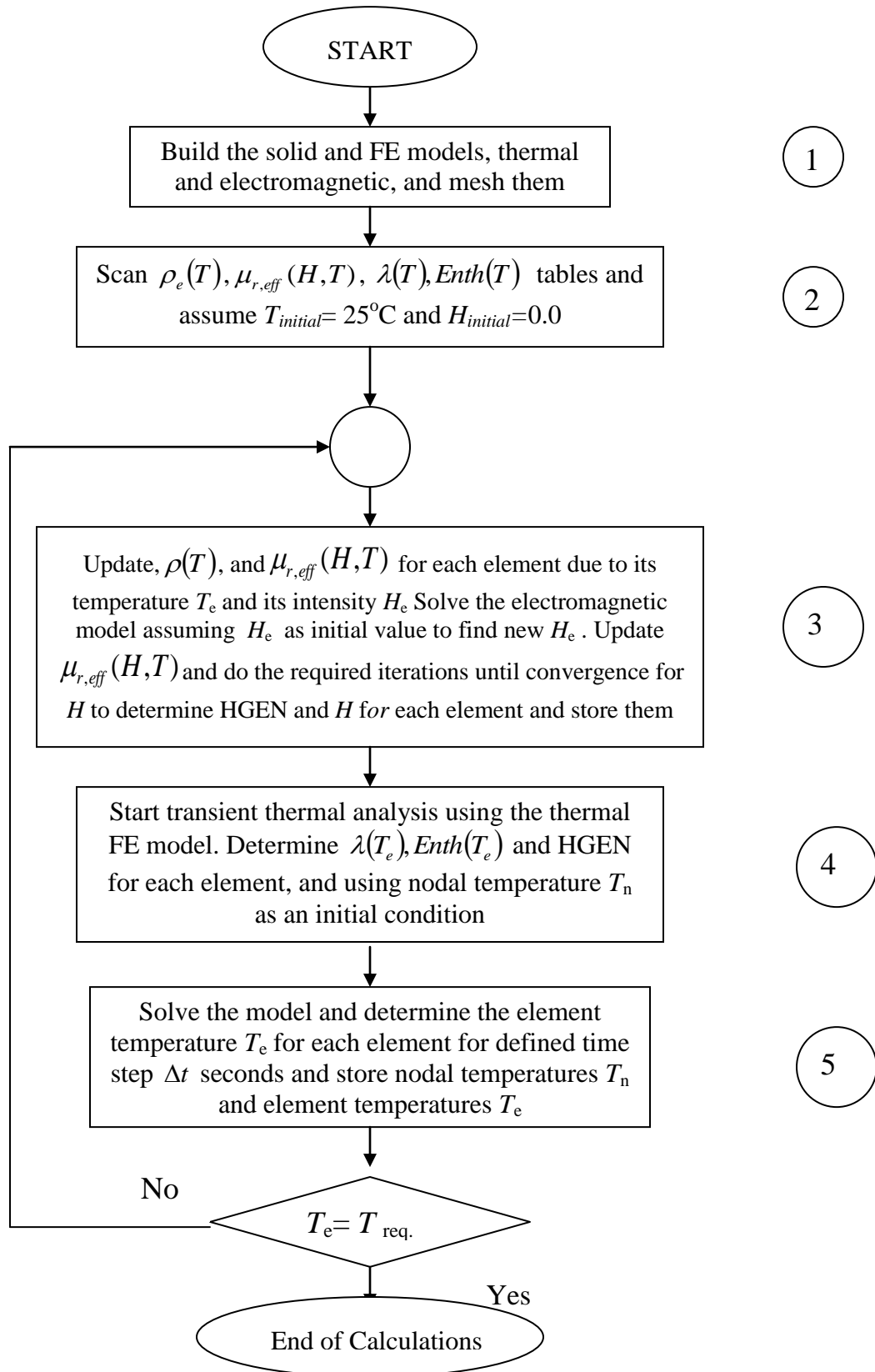
F.A. Abood
A. F. Batti
 A.H. Ahmad
E. M. Abdul-Baki

Modeling of Induction Heating Process of
A Conducting Ferromagnetic Materials

START

Build the solid and FE models, thermal and electromagnetic, and mesh them ⟶ 1

Scan $\rho_e(T), \mu_{r,eff}(H,T), \lambda(T), Enth(T)$ tables and assume $T_{initial}= 25^oC$ and $H_{initial}=0.0$ ⟶ 2

Update, $\rho(T)$, and $\mu_{r,eff}(H,T)$ for each element due to its temperature T_e and its intensity H_e Solve the electromagnetic model assuming H_e as initial value to find new H_e. Update $\mu_{r,eff}(H,T)$ and do the required iterations until convergence for H to determine HGEN and H for each element and store them ⟶ 3

Start transient thermal analysis using the thermal FE model. Determine $\lambda(T_e), Enth(T_e)$ and HGEN for each element, and using nodal temperature T_n as an initial condition ⟶ 4

Solve the model and determine the element temperature T_e for each element for defined time step Δt seconds and store nodal temperatures T_n and element temperatures T_e ⟶ 5

No

$T_e = T_{req.}$

Yes

End of Calculations

Fig. (12) Flow chart of the heating process

The obtained results

Results in Fig. (13) show the temperature response versus time for the central node at the surface close to the inductor for the three different excitation currents (10500A, 7875A, and 5250A). The curves for each case will be drawn separately.
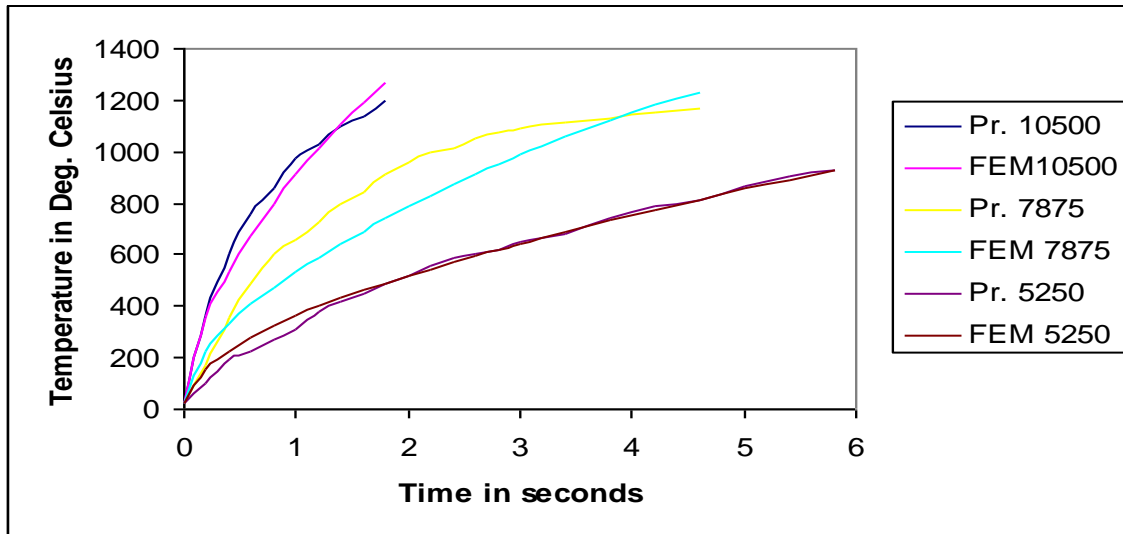

Fig. (13) The temperature response of the central node for three values of excitation current (10500A, 7875A, 5250A) as compared with practical measurements.

For 10500A case Fig.(14) shows the comparison between the practical measurements and the numerical calculation results.
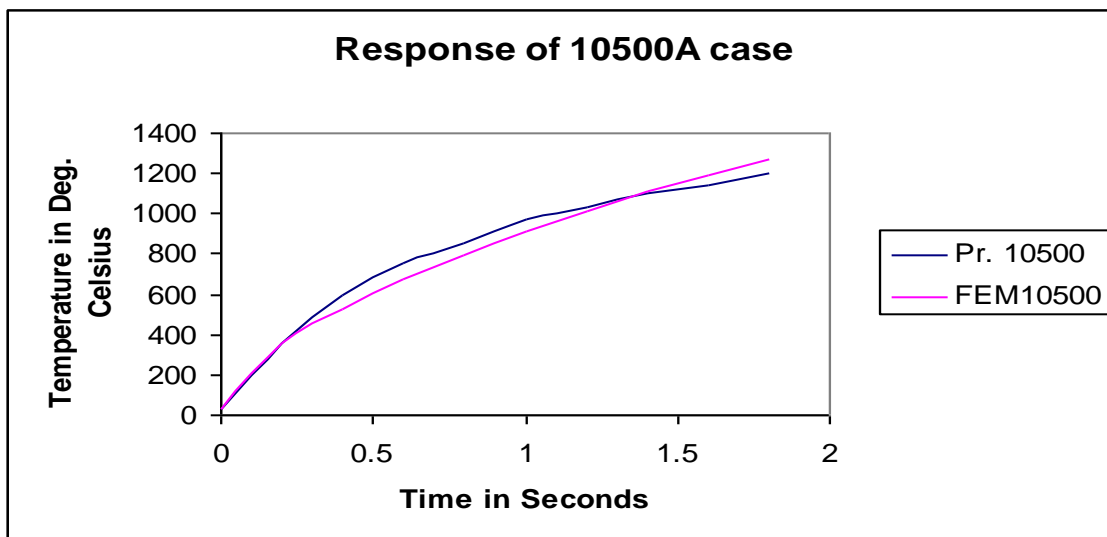
Fig. (14) The 10500A case results

The heat distribution inside the billet is shown in Fig. (15), the heat is concentrated in the central region near the inductor while that at the billet center is approximately not affected because the heating time is very short. Fig. (16) represents the case of 7875A.
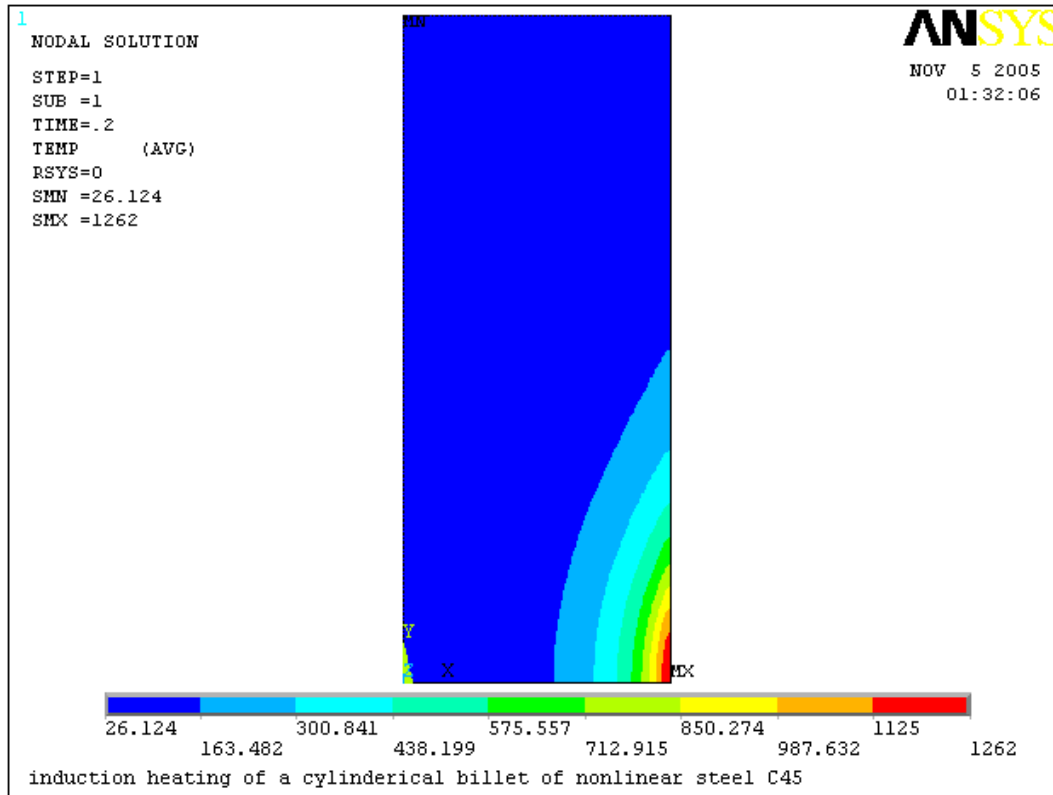
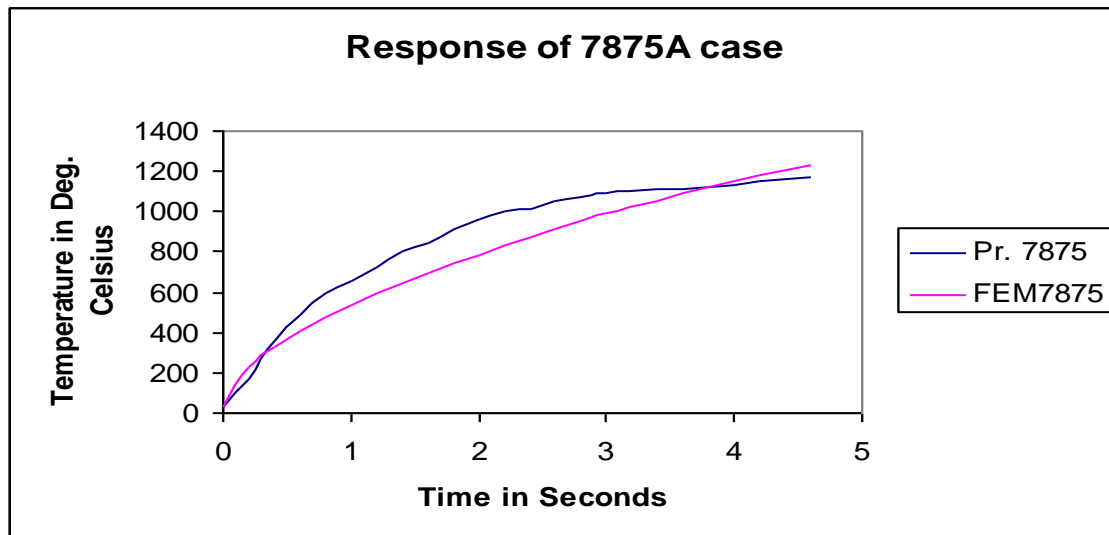**Fig. (15)** A contour plot of the nodal temperature for 10500A case

Fig (16) The 7875A case results

The heat distribution inside the billet in this case is shown in Fig. (17). The heat distribution shows more heat can reach the central region compared with the case of 10500A case, that is because the heating time of this case is 4.8 seconds, leads the heat to reach these regions by conduction.
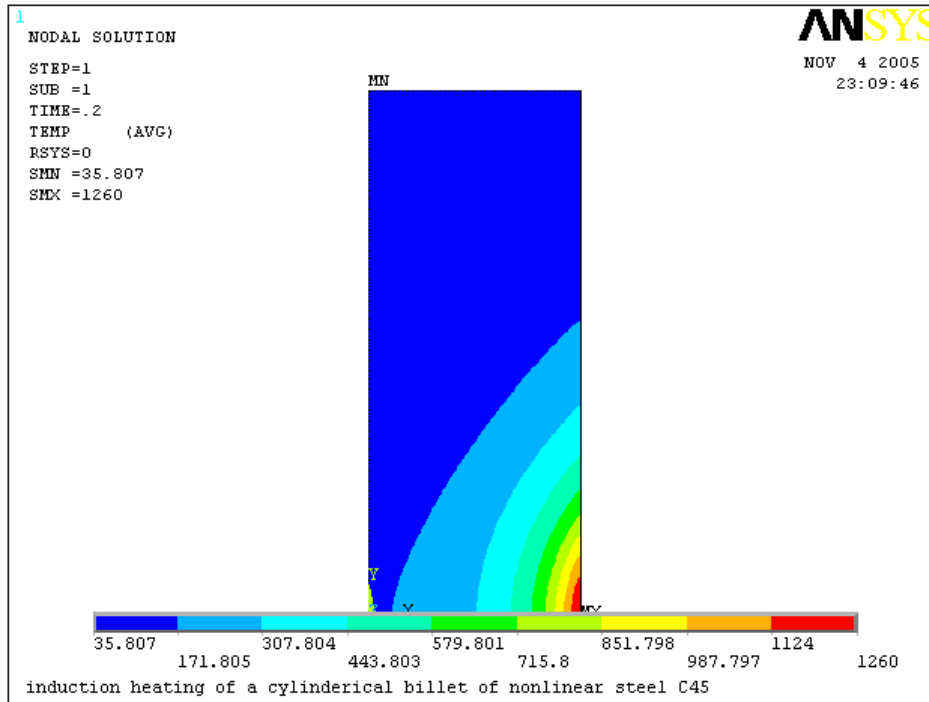
Fig. (17) A contour plot for the nodal temperature for the case of 7875A.

The third case is that of 5250A. It is the longest process among the three cases. The results in this case show a good agreement with the practical one. Fig.(18) shows the temperature-time response   of the highest temperature node as compared with the practical measurements.
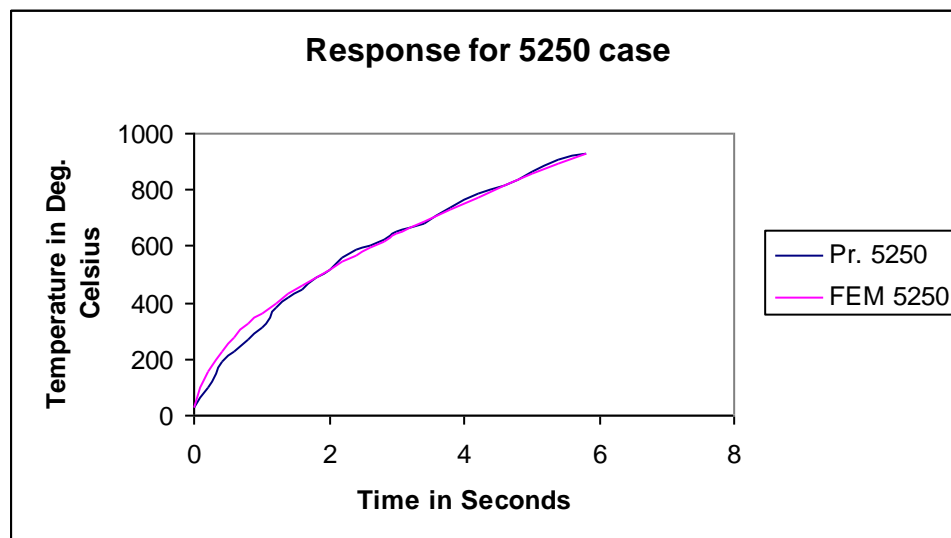

Fig. (18) The 5250A case results

4335

F.A. Abood
A. F. Batti
A.H. Ahmad
E. M. Abdul-Baki

Modeling of Induction Heating Process of
A Conducting Ferromagnetic Materials

The contour plot represents the heat distribution of this case. In spite of using half the current used in the first case, the heat reaches largest area inside the billet section, which happens due to the conduction inside the material along the heating time that elapses about six seconds. Fig. (19) shows the heat distribution inside the billet section for this case of exciting current.
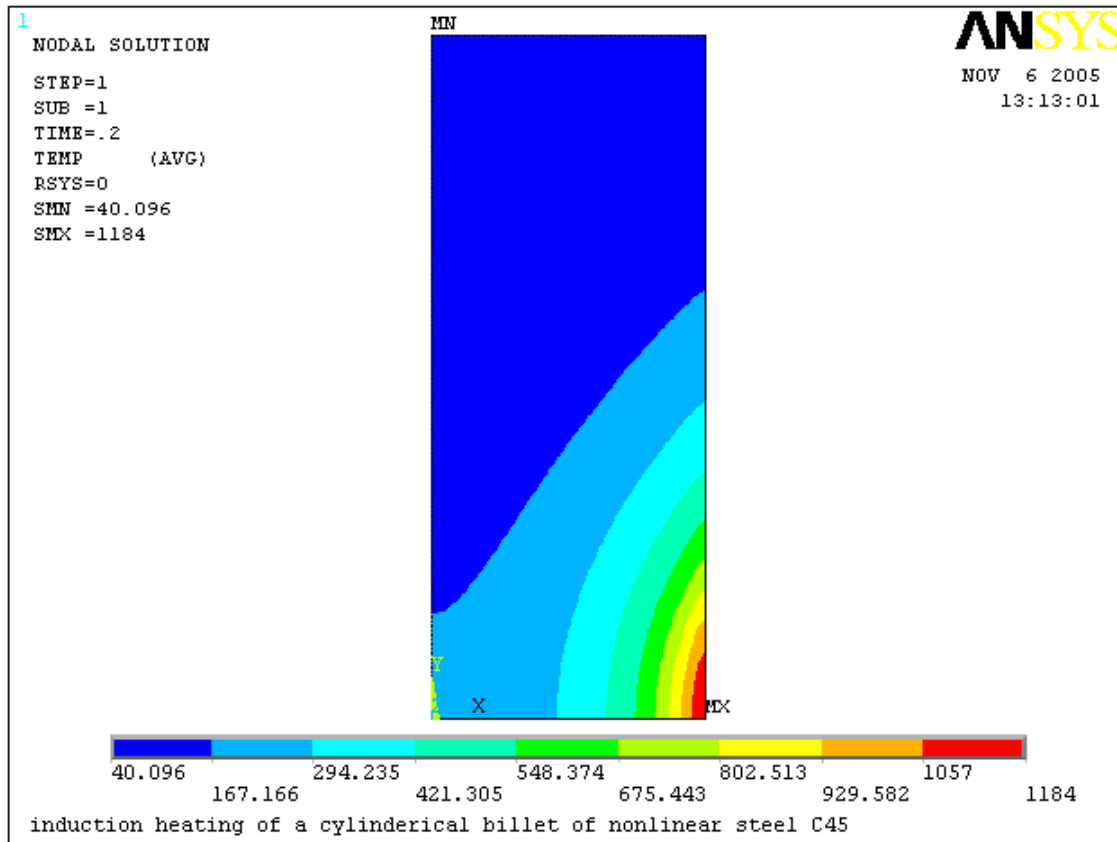

Fig. (19) A contour plot of the nodal temperature for 5250A case

Discussion and future work

The results obtained in this part of the research show many facts as follows:

a. The penetration of power inside the billet is not a function of material properties and the supply frequency and current only, but it is a function of the heating period also.

b. The algorithm used in this analysis gives an acceptable results for the three cases, which affirm the reliability of this type of numerical analysis, and assist the confidence to use it in future in industrial applications.

c. The prediction of induction furnace performance is not an easy problem especially in the case when its core (the work piece) is an alloy of a ferromagnetic material because the following information are needed :

- A precise description of the furnace geometry in details.
- The behavior of the physical properties (of the different materials used in furnace itself and for that of its work piece) with temperature, which is a

difficult task especially when the alloys are used. These properties are precisely (Electrical Conductivity, The Effective Relative Permeability, The Thermal Conductivity, and The Enthalpy of the core material).

- The constants considered in the heat transfer analysis like the Stefan-Boltzman constant, Form Factor, and the Emissivity Coefficient, for the purpose of determination of the energy losses from the external surfaces of the billet by Radiation, and the Film Coefficient used in determining the effect of energy losses due to Convection. The determination of these coefficients is very difficult task because they depend on the surface softness and the geometry of the work piece and the furnace, and they are function of temperature also, and cannot be determined accurately and they are often determined empirically. So they are sources of error in this type of analysis.

d. This algorithm proposed to be as a computer aided design method for the axi-symmetrical induction furnace. It can determine the required furnace geometrical shape and the excitation current and the frequency required to be supplied to its coil in order to do certain heat treatment for a work piece of a certain shape and manufactured from a certain material in the required period of time.

This study can be extended in future to determine the equivalent values of the inductance, resistance, and capacitance of the furnace and their variation with temperature during operation. If this analysis coupled to the circuit of the power supply will aid to study the whole system.

List of Symbols:

A	Magnetic vector potential	Wb.m^{-1}
B	Magnetic flux density	Tesla
C_p	Specific heat	kJ/kg.^{o}C
E	Induced electromotive force	Volt
$Enth$	Enthalpy	J/kg
H	Magnetic field intensity	Amp.m^{-1}
HGEN	Heat generation in each element	J.m^{-1}
I	Current	Amp
J	Current density	Amp.m^{-2}
k	Thermal conductivity	W/m.^{o}C
$Q_{induction}$	The Joule heat from the electromagnetic process	J.m^{-3}
T	Temperature	^{o}C
t	Time	Seconds
μ	Permeability	Henry.m^{-1}
α	Film coefficient	W.^{o}C^{-1}
ε	Permitivity	F.m^{-1}
ξ	Emissivity of the surface	
ρ_e	Electrical Resistivity	Ω.m
ρ_m	Density	kg.m^{-3}
σ_e	Electrical conductivity	$(\Omega.m)^{-1}$

σ_s Stefan-Boltzmann constant $W.m^{-2}.K^{-4}$

δ The Skin depth   m

ϖ The angular Frequency   Rad. Sec^{-1}

REFERENCES

• J. Davies, and P.Simpson, "Induction Heating Handbook", *McGraw-Hill Book Company (UK)*, 1979.

• A. Vasiliev, I. Pozniak, V. Greshnov, "Modeling and Investigation Hardening Process", *International Scientific Colloquium* "Modeling for Electromagnetic Processing", Hannover, March (24- 26), 2003.

• Razzaq A. Marsuq, "Analysis and Study of Design Criteria of Induction Furnaces", *M.Sc. Thesis, University of Baghdad*, *Iraq.*(1994).

• Fadhil A. Abood, "Direct Circuit Coupled Based Finite Element Analysis of Three Phase Induction Motor", *Ph.D. Thesis, University of Technology. Baghdad, Iraq*. 2002.

• Jorg Cstroeski, "Boundary Element Methods for Inductive Hardening", *Ph.D. Thesis, University of Topengen, Germany*, 2003.

WATER CONING IN ASMARY RESERVOIR-FAUQI FIELD

Ass. Prof. Dr. Talib A. Saleh
College of Engineering
Petroleum Engineering Department
University of Baghdad

Shaker M. Khalaf
Ministry of Oil- South
Oil Company

ABSTRACT

Water coning in oil wells is one of the most serious problem because when the water reach to perforated zone, it will be produced with oil. Water with oil will form other problems in refinery, such as corrosion, and it will affect the purity of different petroleum products.

The present work deals with fauqi field Asmari reservoir which is an active water drive reservoir.

An empirical equation has been proposed to calculate the critical production rate. This equation is obtained by regression of the data which are collected from Missan oil field. The proposed equation gives better results than Schools and Myer equations when compared with the actual production rate.

الخلاصة :

يعتبر تقمع الماء في آبار النفط واحداً من المشاكل الخطيرة لأنه عندما يصل الماء الى منطقة التثقيب ينتج مع النفط . الماء مع النفط يشكل مشاكل أخرى في المصافي مثل التآكل ويؤثر على نقاوة المشتقات النفطية . هذا البحث يتعامل مع حقل الفكه مكمن الاسمري والذي يخضع الى دفع مائي نشيط . لقد تم الحصول على معادلة تجريبية لحساب معدل الانتاج الحرج . هذه المعادلة تم الحصول عليها من تحليل البيانات التي جمعت من حقل ميسان، مكمن الاسمري . المعادلة المقترحة تعطي نتائج افضل من طريقة شول وماير وغاردنر عندما تقارن بمعدل الانتاج الحرج الحقيقي.

INTRODUCTION

Water and gas coning is considered as one of the serious problems that is faced in large number of oil fields.

Water coning depends on the properties of the porous medium, oil-water viscosity ratio, distance from the oil-water interface to the well, production rate, densities of the fluids and capillary effects. In oil recovery, water coning is highly unwanted. At high production rates, the water propagates upwards until the oil-water interface reaches the well. At this stage, the well begins to produce water and oil simultaneously, leading to lower oil production. At low production rates, the oil-water interface

assumes a stable shape, and the well performance is not impaired. The estimate of the optimal production rate is thus crucial and the subject of most work on water coning.

In general, in water drive reservoirs, vertical wells, are usually completed in the upper section of the pay zone in order to reduce water coning. In addition ,vertical wells in reservoirs which have gas cap, are usually perforated as low as possible to be as far as possible from the oil-gas contact.

If there are two states of drive, the vertical well is normally perforated near the center of the oil zone or nearer to the oil- water contact. This is because the tendencies of coning are inversely proportional with the density difference and are directly proportional with viscosity.

The density difference between gas and oil is normally higher than the difference between water and oil. Therefore, gas tendency is less in water. However ,since viscosity of the gas is less than viscosity of water, then for the same pressure draw down, the flow rate of the gas is higher than the flow rate of water. The difference of the density and viscosity between water and gas tend to balance one another.

Therefore in order to decrease the gas and water coning perforations should be made near the center of the oil zone. From practical experience most of the wells are perforated nearer to the oil water contact rather than oil gas contact.

The naturally fractured reservoirs, especially those with vertical fractures could have severe coning in spite of high reservoir permeability. This is because water and gas move rapidly through high permeability (vertical) fractures. This is especially true in fractured reservoirs with low matrix permeability, and large matrix blockes where water imbibition in the matrix is very slow. In several fractured limestone and reef reservoirs coning problems are severe due to vertical fracturing.

Coning can be minimized by reducing pressure draw down , this can be attained by reducing oil producing rate , and in many instances , it is operationally impractical.

When flowing pressure gradient near the well bore causes gas or water flowing in the vertical direction across bedding planes, coning phenomena will occur and it will be steady when producing rate & flowing pressure gradient are constant.

If flowing pressure gradient is higher than that enough to overcome the gravity forces, then, water and gas coning will be unsteady.

Coning problem had been studied by many authors. Farely (1959), Morris (1964), Szilos (1975) presented empirical equations for calculating critical flow rate above which coning may occur. Quinet (1992), Guinard (1993) used electrical models to simulate coning problem, Phillip and Hasson (1994) proposed laboratory Model to simulate this problem.

CRITICAL RATE

Since the early days, several experiments and mathematical analyses were conducted to solve coning problems. One of the basic analyses was if oil is produced at a sufficiently low rate or if pressure drawdown in a vertical well is reduced, coning of water and gas can be avoided, and only oil is produced. This low rate is called the critical rate. Thus, the critical rate is defined as the maximum rate at which oil is produced without production of gas or water.

Vertical Well Critical Rate Correlations

Several vertical well critical rate correlations are available in the literatures, some of which are summarized in equations 1 to 9. It is important to note that these correlations are valid for a continuous oil pay zone with oil water contact or gas-oil contact or both. These correlations show that the critical rate depends upon effective oil permeability, oil viscosity, density difference between oil and water or oil and gas, well penetration ratio hp/h, and vertical permeability kv .

Craft and Hawkins(1959) Method

$$q_o = \frac{0.00708 k_o h (P_{ws} - P_{wf})}{\mu_o B_o \ln(r_e / r_w)} PR \tag{1}$$

$$PR = b' \left[1 + 7 \sqrt{\frac{r_w}{2b'h}} \cos(b'90^o) \right] \tag{2}$$

Meyer and Gardner (1963) Method:

Gas Coning:

$$q_o = 0.001535 \frac{\rho_o - \rho_g}{\ln(r_e / r_w)} \left(\frac{k_o}{\mu_o B_o} \right) [h^2 - (h - h_p)^2] \tag{3}$$

Water Coning:

$$q_o = 0.001535 \frac{\rho_w - \rho_o}{\ln(r_e / r_w)} \frac{k_o}{\mu_o B_o} (h^2 - h_p^2) \tag{4}$$

Simultaneous Gas and Water Coning :

$$q_o = 0.001535 \frac{k_o}{\mu_o B_o} \frac{(h^2 - h_p^2)}{\ln(r_e / r_w)} \left[(\rho_w - \rho_o)\left(\frac{\rho_o - \rho_g}{\rho_w - \rho_g}\right)^2 + (\rho_o - \rho_g)\left(1 - \frac{\rho_o - \rho_g}{\rho_w - \rho_g}\right)^2 \right] \tag{5}$$

Chapron(1986) Method:

$$q_o = \frac{3.486 \times 10^{-5}}{B_o} \frac{k_h h^2}{\mu_o} [\Delta\rho] q_c^* \qquad (6)$$

In the U.S. oil field units, Equation (6) can be rewritten as:

$$q_o = \frac{4.888 \times 10^{-4}}{B_o} \frac{k_h h^2}{\mu_o} [\Delta\rho] q_c^* \qquad (7)$$

The value of q_c^* is given in the following table as a function of α:

α	q_c^*
4	1.2133
13	0.8962
40	0.7676

A correlation of tabulation is given in Equation (8):-

$$q_C^* = 0.7311 + (1.9434/\alpha) \qquad (8)$$

Where:

$$\alpha = (r_e/h) \sqrt{k_v/k_h}$$

Schols(1972) Method:

$$q_o = \frac{(\rho_w - \rho_o)k_o(h^2 - h_p^2)}{2049\mu_o B_o} \times \left[0.432 + \frac{\pi}{\ln(r_e/r_w)} \right][h/r_e]^{0.14} \qquad (9)$$

PROPOSED CORRELATION

Data collected were for ten oil wells from missan oil field. The published correlations have been applied for these wells, but non of them have concide with actual critical production rate. The wells which have been exceeded these rates, water coning have occurred after a period of time shown in tables below. Therefore a trail was done to find an empirical equation satisfying these values. By the method of trial and error, the following equation was suggested which gave a very good degree of accuracy. In this equation two parameters were introduced these are; the capillary

pressure and degree of heterogeneity of the reservoir which were not included in any other equation

$$q_0 \max = 0.00175 \left(\frac{\rho w - \rho_0}{\ln(r_e / r_w)} \right)^{1.075} \left(\frac{K_o}{\mu_o Bo} \right) (h^{2.15} - D^{1.995})(H.D) + 87.8 \ln P \quad (10)$$

Where

$q_{0\ max}$ = critical production rate   STB/D
ρ_W= water density   gm/cc
ρ_o= oil density   gm/cc
 r_e= drainage radius   ft
r_w = well radius   ft
K_o = oil permeability   md
μ_o = oil viscosity   cp
B_o= oil formation volume factor   bbl/STB
H= formation thickness in   ft
D= distance   ft
H.D= heterogeneity degree of reservoir   -
PC = capillary pressure   psia

The parameters involved in eq. (10) are measured in the laboratories of south oil company.

Table (1) qomax by proposed correlation

	FQ-1		FQ-2		FQ-7		FQ-8T		FQ-16	
year	h`(ft)	q_{omax}STB/D	h`(ft)	q_{omax}STB/D	h`(ft)	q_{omax}STB/D	h`(ft)	q_{omax}STB/D	h`(ft)	q_{omax}STB/D
1999	141.5	412.94	89.09	717	127.8	730.49	134.37	1648.9	101.5	396.26
2000	141.4	412.76	88.99	715.8	127.7	729.83	134.27	1646.69	101.4	396
2001	141.1	412.23	88.69	712.17	127.4	727.86	133.97	1640	101.1	395.31
2002	140.9	411.91	88.51	710	127.2	725.82	133.79	1636.14	100.9	394.88
2003	140.9	411.82	88.46	709.4	127.2	723.76	133.74	1635	100.9	394.76

Table (2) the critical production rate by Schols, myer and Gardener

FQ-10			FQ-11		FQ-23		FQ-21A		FQ-22A	
year	h`(ft)	q_{omax}STB/D	h`(ft)	q_{omax}STB/D	h`(ft)	q_{omax}STB/D	h`(ft)	q_{omax}STB/D	h`(ft)	q_{omax}STB/D
1999	177	554.5	183.6	706.2	170.5	7048.3	—	—	—	—
2000	176.9	554.1	183.5	706	170.4	7048	139.3	940.6	—	—
2001	176.6	553.8	183.2	705.95	170.1	7047.5	139	940	—	—
2002	176.5	553.4	183	705.83	169.9	7046	138.8	939.6	114.6	1569.7
2003	176.4	552.9	182.9	704.9	169.9	7045.5	138.7	938.9	114.6	1569.1

Now this equation gives results very close to the actual rates which are given below in table (3).

Table (3) the actual production rate by South Oil Company

year	FQ-1	FQ-2	FQ-7	FQ-8	FQ-16
	q_{omax}STB/D	q_{omax}STB/D	q_{omax}STB/D	q_{omax}STB/D	q_{omax}STB/D
1999	413	717.1	730.5	1649	396.3
2000	412.8	715.78	729.82	1646.7	396.1
2001	412.25	712.17	727.87	1640	395.31
2002	411.92	710	725.82	1636.15	394.88
2003	411.83	709.38	723.77	1635	394.78

year	FQ-10	FQ-11	FQ-23	FQ-21A	FQ-22A
	q_{omax}STB/D	q_{omax}STB/D	q_{omax}STB/D	q_{omax}STB/D	q_{omax}STB/D
1999	554.6	706.19	7048.3	—	—
2000	554.12	706	7048.1	940.5	—
2001	553.8	705.96	7047.49	940	—
2002	553.39	705.83	7046	939.6	1569
2003	552.91	704.9	7045.51	938.95	1569.2

CONCLUSIONS

- An Empirical equation was developed to calculate critical rate of (FAUQI field) and it gave accurate results compared with other methods.

- Trial and error method was used to find the empirical equation.

NOMENCLATURE

$q_{o\,max\,=}$ oil flow rate without water   STB/D

h' = elevation of water cone   ft

ϕ = porosity

q_L = liquid flow rate   STB/D

q_w = water flow rate   STB/D

p_c= capillary pressure   Psi

q_o = critical oil rate, m^3/hr

k_h = horizontal permeability   md

k_v = vertical permeability   md

h= oil column thickness   m

μ_o= viscosity,   cp

$\Delta\rho$= $\rho_w - \rho_o$ density difference   gm/cc

ρ_w = water density   gm/cc

ρ_o = oil density   gm/cc

B_o = formation volume factor   Res m^3/St m^3

r_e = radius of drainage area   in

r_w = radius of well   in

K_o= oil permeability   md

REFERENCES

- Chapron, " Theoretical Study of Coning Toward Horizontal and Vertical Wells in Anisotropic Formation , Sub critical and Critical Rates", Paper SPE 15377,Presented at the Annual Technical Conference and Exhibition, NewOrleans, Louisiana, Oct., 5-8, 1986.

- Craft,B,Cand Hawkins,M,F: "Applied petroleum Reservoir Engineering" ,Glewood Cliffs, New Jersey, Practice-Hall, 1959.

- FARELY F. J., "some aspects on the problems of oil wells",NEW-ZELAND , 1959.

- Guinard Mme,"Une circuit electrique", J.de (C.N.R.S) ,Oct.,28,1984.

- GUTTON C., "problem de formation de cone dleau dans le puits du petrol",rapport du universite du clermnt Ferrand,France 1978.

- Hel mut R.M, "something about the water cone formation in oil wells",S.P.E. NOV. 5-6 (1979).

- Jacque P. and Nadine, "Formation de cone dleau dane le puits du petrole",Universite descience et technologie,NANcy,France 1982.

- Jaune M. and A.Abass, "Cone dl eau arec la production du petrole",Seminare dl lmivers;du Marseille,france 15,NOV.,1986.

- MORRIS R. L., "Water coning in oil well is a great problem" ,A.I.M.E September 1964.

- Myer,H.L,and Gardener,A.O., "Mechanics of Two Immiscible Fluids in Porous Media", Journal of Applied Physics,vol.25,No.11 pp.1400, 1985.

- PHILLIP,O. and Hasson J., " Lab. Model to simulate the water coning in oil fields",J.P.T.,Nov. 1994.

- Quinet J., "Circuits electriques des amplificateurse", 1992.

- Schols,R,S., " An Empirical Formula for the Critical Oil Production Rates", Erdoel Erdgas,Z,vol.88,No.1,pp6-11,January 1972.

- Szilos,a.p., "production and transport of oil and gas development in petroleum science",elesevier scientific publishing company,Amesterdam,oxford,Newyork 1975.

NEW CORRELATION FOR OIL FORMATION VOLUME FACTOR AT AND BELOW BUBBLE POINT PRESSURE

Omar F. Hassn and Dhefaf J. Sadiq

Department of Petroleum Engineering, College of Engineering, University of Baghdad

ABSTRACT

The best source of oil properties data is the laboratory PVT analysis of a reservoir fluid sample. However, in the absence of experimentally measured properties of reservoir fluids, these physical properties must be estimated from correlations.

This paper employs more than thirty PVT reports that have been taken from different Iraqi fields. These reports contain about four hundred experimental points.

The paper suggests new correlation to calculate oil formation volume factor at and below bubble point pressure. All of the previous correlations did not take the pressure as a factor or independent variable because they calculate the oil formation volume factor at bubble point pressure only. The new correlation introduce the pressure while omit the solution gas-oil ratio which has been employed in all previous correlations.

The accuracy of the proposed correlation of the experimental data is assessed through various statistical tests and comparing them with those achieved for some published correlations. These tests show that the new correlation has the best fitting with the experimental data for Iraqi oils. Cross plot technique is also applied to check the performance of the correlation and it gave the same index of the statistical criteria method.

The new correlation reported absolute average error of 1.876%, sum of squared residuals of 0.395327, variance of 0.0093 and standard deviation error of 0.096337288.

KEY WORDS

Formation volume factor, bubble point, correlation, Iraqi oils,   Experimental data.

INTRODUCTION

The oil formation volume factor, Bo, is defined as the ratio of the volume of oil (plus the gas in solution) at the prevailing reservoir temperature and pressure to the volume of oil at standard conditions. Evidently, Bo always is greater than or equal to unity. (Ahmad 2007)

Many correlations for estimating oil formation volume factor have been published in the past seven decades. Most of these correlations yield reasonably accurate results when applied at the bubble-point pressure. But, for pressures below the bubble point, the calculated oil formation volume factor may yield considerable error.

Most of the published empirical Bo correlations employ the following generalized relationship:

$$B_o = f\left(R_s, \gamma_o, \gamma_g, T\right)$$

Some of the empirical correlations for predicting oil volume factor are presented in this paper:

Standing (1947) constructed correlation for calculating oil formation volume factor of oils using field data of reservoir temperature, solution gas oil ratio at bubble point and oil and gas gravities. Standing used more than one hundred experimental data points.

Vasquez and Beggs (1976) developed empirical correlation by using approximately six thousand data points- measured over wide ranges of pressure, temperature, specific gravity of oil and specific gravity of gas. They found that the specific gravity of gas was a strong correlating factor and, unfortunately, this is often one of the variables measured with the least degree of consistency. The specific gravity of gas depends on the pressure and temperature of the separators, which may not be available.

Glaso (1980) suggested a new approach that based on the concept that the paraffinicity of the oil influences the gas / liquid equilibrium of black oil mixtures containing methane. Glaso used the regression analysis to develop his correlation.

Al-Marhoun (1985) developed correlation for calculating oil formation volume factor for Middle East crude oils at the bubble point pressure. This correlation was developed from database of more than seventy bottom hole fluid samples and expressed as functions of reservoir temperature, gas gravity, solution gas – oil ratio at bubble point and stock tank oil gravity. Al-Marhoun employed nonlinear regression method to build the correlation.

Petrosky (1990) developed empirical correlation for Gulf of Mexico crude oils. His relationship correlated the oil formation volume factor versus solution gas-oil ratio at bubble point, specific gravity of gas, specific gravity of oil and reservoir temperature.

Omar and Todd (1993) suggested a correlation for calculating oil formation volume factor at bubble point using data from Malaysian offshore oil fields at South China Sea. They used linear and nonlinear regressions.

NEW OIL FORMATION VOLUME FACTOR CORRELATION

The correlation is developed through some sequential steps which can be summarized as follows:

- Detection of the objective of the study which is suggestion of new correlation to calculate oil formation volume factor at and below bubble point pressure.
- Identification of the important factors that affect the value of oil formation volume factor. The paper proposed that these factors are pressure, reservoir temperature, stock tank oil gravity and specific gravity of gas.
- Presentation of a statistical model to correlate the objective function (oil formation volume factor) versus the factors that illustrated in Step.2.
- Collecting the required experimental data for Iraqi oils to employ them in the correlating process.
- Refining the collected experimental data.
- Suggestion of many mathematical forms of the correlation to choose the best.

These steps lead to the suitable correlation. Nonlinear multiple regression has been done to form the new correlation.

The following form is selected to represent the new oil formation volume factor

$$B_o = a_1 P^{a_2} T^{a_3} API^{a_4} \gamma_g{}^{a_5} + a_6 \qquad (1)$$

Table (1) lists the values of the coefficients of equation (1)

Table (1)

Coefficient	The Value
a_1	0.000005
a_2	0.639887
a_3	0.604183
a_4	0.961566
a_5	1.041364
a_6	1.079483

This form has been chosen according to its statistical indices and the difference between its results and the measured data.

CHECKING THE VALIDITY OF THE NEW CORRELATION

Two checking methods were attained to evaluate the performance of the new correlation which are statistical criteria and cross plot:

- DATA BASE

In this section, all of experimental data that were employed to develop the new correlation was used for checking the validity of the correlation

A-STATISTICAL CRITERIA

Table (2) shows comparison between the statistical criteria for the new correlation and the published ones.

The indices explain that the new correlation is the best among them to correlate Iraqi oils.

Table (2) The Statistical Criteria

The Correlation	Average Absolute Error %	Sum of Squared Residuals	Variance	Standard Deviation Error
New	1.876	0.395	0.0093	0.096
Standing	2.881	0.788	0.0104	0.102
Vasquez and Beggs	8.179	4.833	0.0158	0.126
Glaso	5.125	2.011	0.0125	0.112
Al-Marhoun	4.439	1.688	0.0096	0.098
Petrosky	4.134	1.292	0.0115	0.107

B- CROSS PLOT METHOD

In this technique, the estimated oil formation volume factors are plotted versus the experimental values to create the cross plots . A 45° straight line is drawn on the cross plot which passes through the points of coincidence of experimental and calculated values. The closer the plotted data points are to this line, the better the correlation.

Figures (1) through (6) show that the current correlation is the best among the others used. Vasquez and Beggs correlation is the worst fitting correlation to the experimental data.

Therefore the new correlation gives improvement in the estimation of oil formation volume factor at and below bubble point pressure for Iraqi oils.

- EXTERNAL IRAQI OIL SAMPLE

In this section, external oil sample (sample which was not used to generate the correlation) used to evaluate the new correlation.

Table (3) includes the statistical criteria of the correlations with this sample. These criteria show the superiority of the new correlation for Iraqi oils and the others .

Table (3) The Statistical Criteria

The Correlation	Average Absolute Error %	Sum of Squared Residuals	Variance	Standard Deviation Error
New	2.116	0.013	0.016	0.128
Standing	3.545	0.029	0.019	0.138
Vasquez and Beggs	10.574	0.234	0.025	0.157
Glaso	6.123	0.081	0.019	0.137
Al-Marhoun	5.236	0.064	0.018	0.135
Petrosky	4.355	0.038	0.017	0.132

CONCLUSIONS

A new correlation presented in this work for oil formation volume factor at and below bubble point is proper for application in petroleum engineering, specially for Iraqi oils.

It is new approach that the pressure is introduced in development of the correlation for calculating oil formation volume factor at and below bubble point.

The new correlation has been done by nonlinear regression technique to correlate oil formation volume factor with four input variables which are pressure, reservoir temperature, oil gravity, and specific gravity of gas.

NOMENCLATURE

API : API gravity
B_o : Oil formation volume factor, bbl/STB
P : Pressure, psig
R_s : Solution gas-oil ratio, scf/STB
T : Reservoir Temperature, ^{o}F
γ_g : Specific gravity of gas
γ_o : Specific gravity of oil

REFERENCES

- Ahmad, T., "Equations of State and PVT Analysis ", Gulf Publishing Company, Houston, Texas, 2007.

- Al-Marhoun, M. A., "PVT Correlations for Middle East Crude Oils", JPT, May 1988.

- Glaso, O.," Generalized Pressure-Volume-Temperature Correlations", JPT, May 1980.

- Omar, M. and A. Todd, "Development of new modified black oil correlations for Malaysian crudes", SPE 25338, 1993.

- Petrosky, G., "PVT Correlations for Gulf of Mexico Crude Oils", MS Thesis, University of Southwestern Louisiana, Lafayette, 1990.

- Standing, M. B., "A Pressure-Volume-Temperature Correlation for Mixtures of California Oil and Gases", Drilling & Prod. Prac., API, 1947.

- Vasquez, M. E. and Beggs, H. D., "Correlations for Fluid Physical Property Prediction", JPT, June 1980.
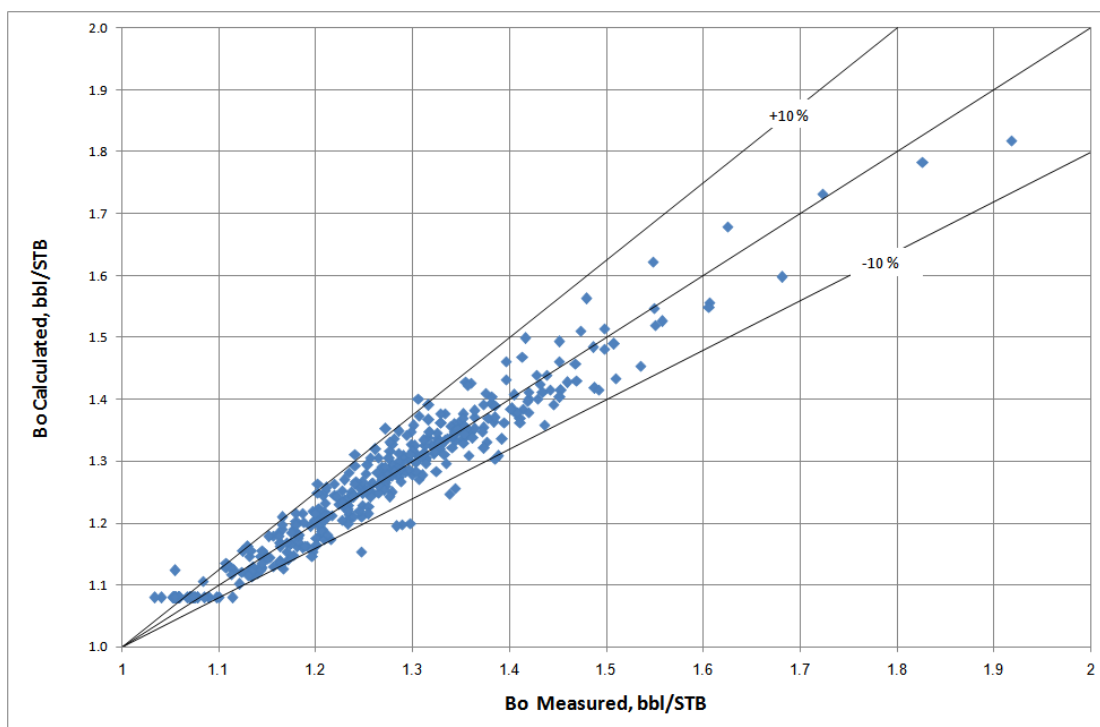
Figure (1) Cross Plot of the oil formation volume factor (Experimental data versus the values from new correlation)
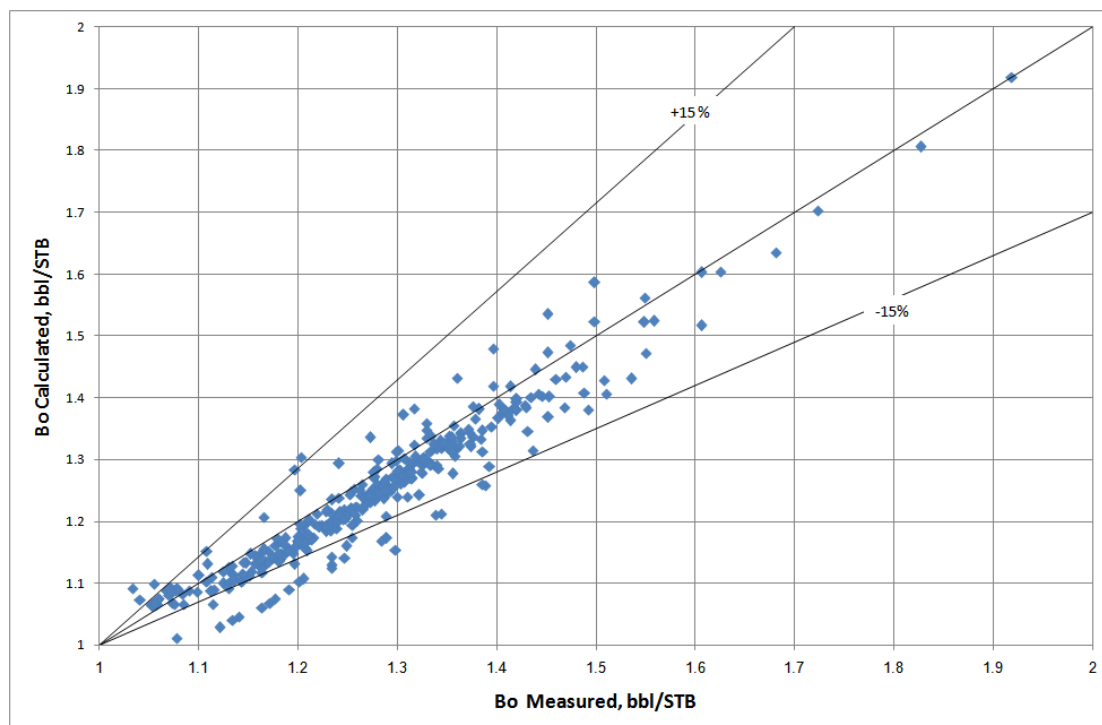
Figure (2) Cross Plot of the oil formation volume factor (Experimental data versus the values from Standing correlation)
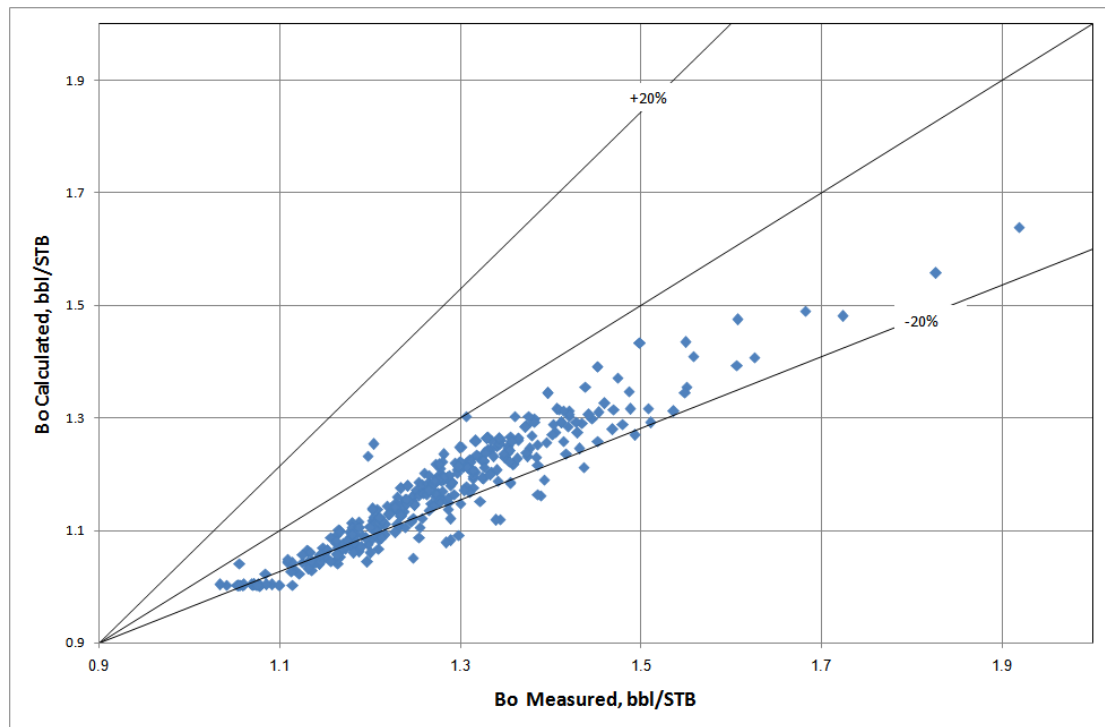
Figure (3) Cross Plot of the oil formation volume factor (Experimental data versus the values from Vasquez and Beggs correlation)
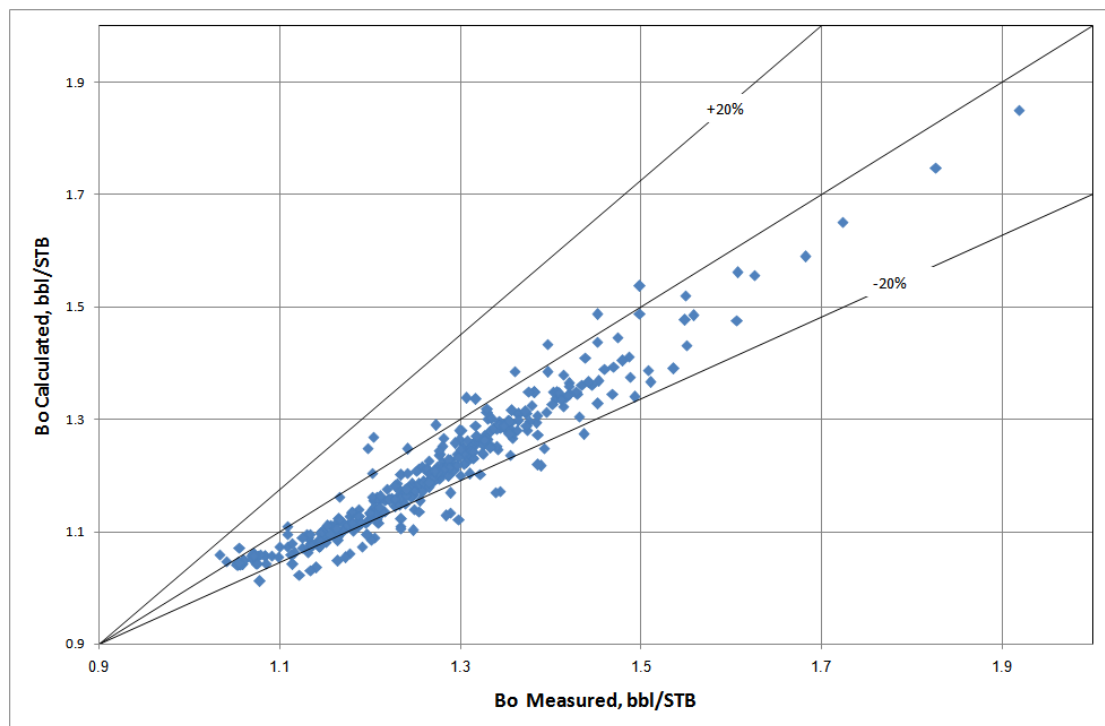
Figure (4) Cross Plot of the oil formation volume factor (Experimental data versus the values from Glaso correlation)
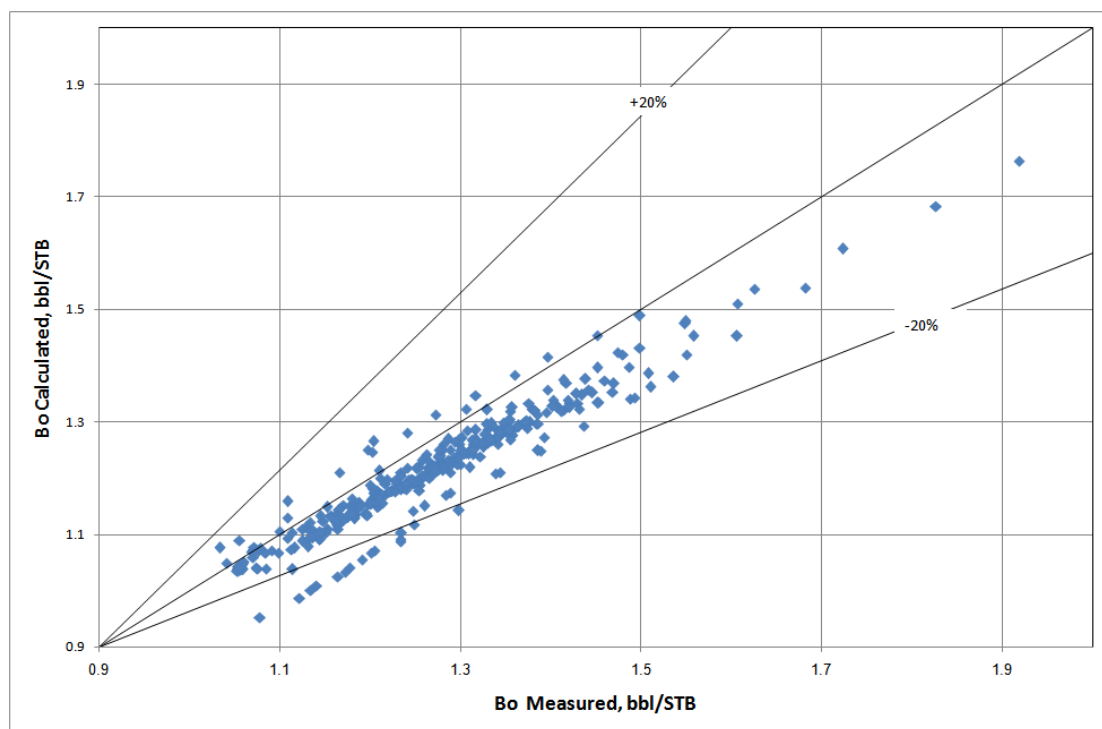
Figure (5) Cross Plot of the oil formation volume factor (Experimental data versus the values from Al-Marhoun correlation)
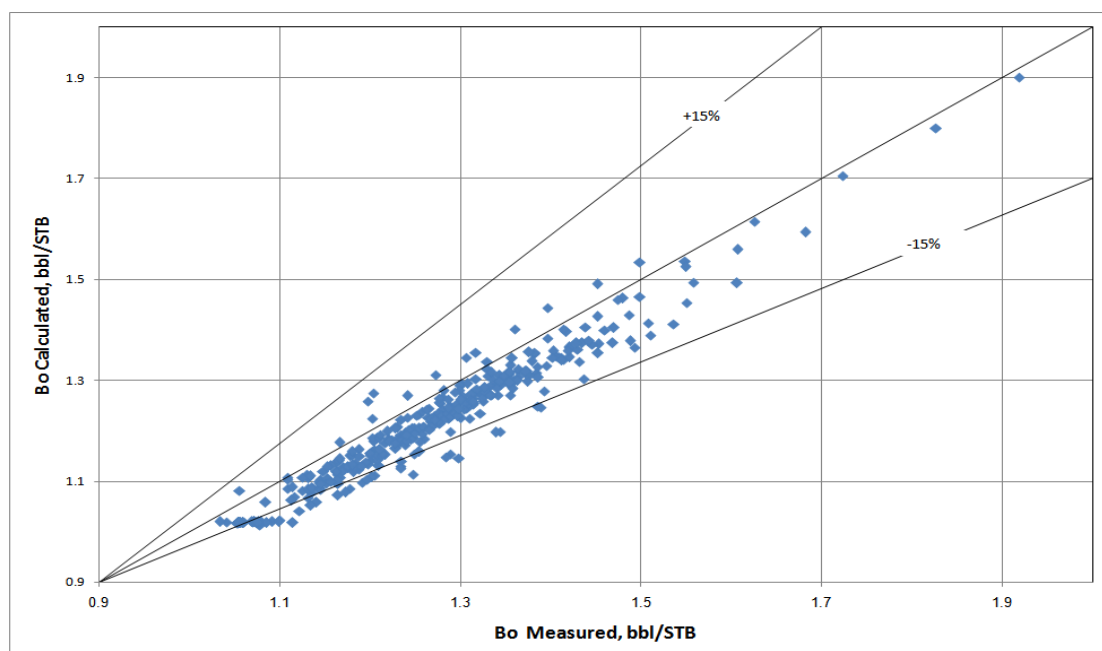
Figure (6) Cross Plot of the oil formation volume factor (Experimental data versus the values from Petrosky correlation)

TREATMENT OF INDUSTRIAL WASTE WATER USING REVERSE OSMOSIS TECHNIQUE

Nada S.Ahmedzeki, Sama M. Abdullah, Rasha H. Salman.
University of Baghdad, College of Engineering, Chem.Eng.Dep.

ABSTRACT

Reverse osmosis technique was used for the treatment of industrial waste water. Ions like calcium, magnesium, sodium, sulfate, and nitrate were found in the waste water of the General Company of Vegetable Oil with high concentrations which must be treated for reuse. Feed water containing the above mentioned ions was fed to the RO unit at feed flow rates (0.4 and 0.8 lit/min) and different operating pressure (2-4bar) .It is concluded that increasing operating pressure and feed flow rate improved the separation by a decrease in the concentration of ions in the product. High rejection was obtained for all ions present in feed water, ranging from (63.8-97.6%). Rejection of TDS was 87% when the concentration of TDS was reduced from 1192 to 154.94 ppm.

الخلاصة

تقنية التنافذ العكسي أستخدمت لمعاملة المياة الصناعية . أيونات الكالسيوم و المغنيسيوم و الصوديوم و االكبريتات و النترات توجد في المياه الصناعية المطروحة من الشركة العامة للزيوت النباتية وبتراكيز عالية يجب أن تعالج لغرض اعادة استعمالها. المياه الحاوية على الأيونات أعلاه تدخل الى وحدة المعالجة بالتناضح العكسي بمعدل جريان (0.4 و0.8 لتر/دقيقة) وتحت ضغط تشغيلي (2-4 بار).لقد استنتج ان زيادة الضغط ومعدل الجريان ادى الى تحسين عملية الفصل بتقليل تركيز الايونات في الماء الناتج. أزالة عالية لكل الأيونات الموجودة في المياه الداخلة تمت بمعدل (63.8-97.6 %). ومعدل أزالة لكمية المواد الصلبة الكلية الذائبة كان (87%) عندما أنخفضت هذه الكمية من 1192 الى 154.94جزء بالمليون.

INTRODUCTION

The use of reverse osmosis (RO) to remove salts and impurities from water had been a recognized technology to improve water quality therefore it had a valuable application in the reuse of waste water streams. The benefit includes; reduced discharge, reduced purchases and the conservation of water resources. In the reverse osmosis process, water passes through a semi-permeable membrane which removes inorganic minerals like radium, sulfate, calcium, magnesium, potassium, sodium, nitrate, fluoride and phosphorous. It also helps to remove some organic compounds including some pesticides (Zibrida et al., 2000). RO can be used for the removal of arsenic which occurs naturally and can contaminate drinking water through the erosion of rocks and minerals or through human activities such as fossil fuel burning, paper production, cement manufacturing, and mining. Natural contamination of groundwater by arsenic has become a crucial water quality problem in many parts of the world (Pawlak, 2006). Often, reverse osmosis units are used in combination with a mechanical filter and an activated carbon filter. The water passes through the mechanical filter first, where sand and large particles are removed, then through the reverse osmosis unit, and lastly through the activated carbon filter which removes organic compounds (Daniels, and Mesner, 2005).

Applications of membrane technologies for water and wastewater treatment is growing due to decreasing price of membranes and more stringent regulations for water quality. Membrane separation processes have following advantages in industrial applications:

- appreciable energy savings , - clean and easy to apply technology, -replaces several conventional processes like filtration, distillation, ion-exchange and chemical treatment with smaller and more efficient equipment - produces high quality products - allows greater flexibility in designing systems. During the last two decades significant advances have been made in the development and application of microfiltration (MF), ultrafiltration (UF), nanofiltration (NF) and reverse osmosis (RO) processes. MF membranes reject suspended particles only, UF membranes reject suspended particles and high molecular weight compounds, NF membranes also reject low molecular weight compounds, and RO membranes also reject ions (Kochany, 2007, and Amjad and Zibrida, 1998).

Over 100 different materials are used to make RO membranes, however the two most commonly used membranes are made from cellulose acetate (CA) and polyamide thin film composite (TFC). These may come in spiral, tubular hollow fiber, and plate and frame. Hollow fiber (HF) and flat sheet are the most commonly used RO membrane configurations. Although HF RO elements provide more surface area, they are more prone to fouling..

Most studies on industrial waste water using RO were limited on either feed containing NaCl salt (Ahmed, 2000, and Mohammed, 2008) or feed containing dye (Mahmood, 2001). In the present study, investigation of five different monovalent and divalent ions (Ca^{++}, Mg^{++}, Na^+, SO_4^{--}, NO_3^-) was the point of view in the treatment of industrial waste water. The important parameter to be compared is the rejection percentage.

EXPERIMENTAL WORK:

(i) Experimental apparatus:
The Experimental apparatus consists of the following parts:
1) QVF feed tank with capacity of 20 liter.
2) Centrifugal pump is used to pump the feed at a pressure of 4-6 bar.
3) Rotameter of (0.2-2 lit/ min.).
4) 5-stage reverse osmosis system supplied by So-Safe Water Technologies.
1. Wound Polypropylene Yarn (WPP) or Spun Polypropylene (SPP) is used for pre-filtration to remove the sediments.
2&3. Activated carbon (GAC) and dual purpose carbon (DPC) used for the purification for taste and odor.
4. Desalination and purification using reverse osmosis membrane. Thin film composites membrane (The spiral – wound module type TFC – 8822HR) is installed for best permeate water quality.
5. Water polishing and purification unit using In-line granular activated post carbon cartridge (ILGAC-10).
The schematic diagram of the experimental apparatus is shown in Fig. 1.

(ii) Experimental Procedure:
Industrial water from the factories of The General Company of Vegetable Oil was analyzed for the specified ions; Ca^{++}, Mg^{++}, Na^+, SO_4^{--}, NO_3^-. Feed solution to the RO unit, containing the aforementioned was prepared. Table 1 shows the analysis of the prepared feed water. Salts of analytical grades from Merck Company were used.

Feed solution containing the specified ions, with the appropriate concentrations, was added to the 20 liter feed tank. The outlet valve was opened to fill the pipes with water. The pump

was switched on and the feed rate of 0.4 and 0.8 lit/min was set. Operating pressure range was (2-4 bar) for each flow rate. Concentrations of the product solution were analyzed using Atomic absorption technique.

RESULTS AND DISCUSSIONS

Operating pressure affects the performance of RO units. Concentrations of the specified ions as a function of the operating pressure were drawn for both feed flow rates. The results are shown in Figs. (2-6).The effect of operating pressure and feed flow rate on the total TDS is shown in Fig 7. It is obvious that increasing the operating pressure or feed flow rate improves the degree of separation for each ion. However, the operating pressure has a pronounced effect compared with feed flow rate. Increasing operating pressure offers a pressure gradient across the membrane and the driving force will be higher, therefore water is forced to pass through the membrane and %rejection is increased. Considerably high pressures are necessary to overcome osmotic pressure which is mainly a function of concentration and molecular weight (Amjad and Zibrida, 1998 ;Singh and Heldman,1993).

When the feed rate was increased, concentration of ions in product solution and hence, TDS, were decreased and %Rejection was increased. This means that the degree of separation is increased by an increase of the throughput rate and increase of mass transfer coefficient between the membrane and feed flow.

% Rejection for 0.8 lit/min flow rate is also calculated in order to investigate the degree of separation for each ion as shown in Fig.8. 87% of TDS are rejected which is an acceptable value, and for individual ions, it can be seen from Fig.9, that SO_4^{--} and NO_3^- ions have the lower %Rejection while, NO_3^- has the lowest. Nitrate is so soluble and non-reactive; therefore it is very difficult to be removed from water. These results are in agreement with those obtained by Ellen, 2007. Therefore, it is possible to say that the best operating conditions are feed flow rate 0.8 lit/min and operating pressure 4 bars.

CONCLUSIONS:
1. The concentration of ions in the product solution decreases with increasing operating pressure. Increasing operating pressure are necessary to overcome the osmotic pressure and the driving force will be higher, therefore, TDS decreased.
2. The concentration of ions in the product solution decreases with increasing feed flow rate.
3. The percent of rejection for each ion differ from each other. Sulfate and nitrate were lower than other ions. Nitrate ions had the lowest % Rejection.
4. It is demonstrated that the RO process could effectively applied for the removal of calcium, magnesium, sodium, sulfate, and nitrate ions. The best operating conditions are feed flow rate of 0.8 lit /min and 4 bar operating pressure.

NOMENCLATURE
MF   Microfiltration
NF   Nanofiltration
ppm   Part per million
RO   Reverse osmosis
TDS Total dissolved solids
UF   Ultrafiltration

REFERENCES

- Ahmed F., 2000 "Study of factors affecting the efficiency of reverse osmosis process" MSc.Thesis, University of Baghdad.

- Amjad Z. and Zibrida J., 1998, Reverse Osmosis Technology: Fundamentals and Water Applications. Association Water Technologies, Inc. Annual Convention, Washington, DC.

- Barbara Daniels, and Nancy Mesner, 2005"Drinking Water Treatment Systems" Water Quality, Utah state University extension., NR/WQ/2005-24.

- Ellen R. Campbell 2007, "Removal is essential for excess nitrate" Water technology online.
- www.watertechonline.com.

- Kochany, J., 2007, "Wastewater Treatment by Membrane Technology" ONESTOGA-ROVERS & ASSOCIATES, vol.7 No.3.

- Mahmood M., 2001, MSc.Thesis, University of Baghdad.

- Mohammed B., 2008, "Membrane separation process for treatment and reuse of water" MSc.Thesis. University of Baghdad.

- Pawlak Z., Żak S., Zabłocki L.2006, "Removal of Hazardous Metals from Groundwater by Reverse Osmosis" Polish J. of Environ. Stud. Vol. 15, No. 4, , 579-583.

- Singh, R.P. and Heldman, D.R. 1993. "Introduction to Food Engineering," 2nd ed. Academic Press, Inc., Harcourt Brace & Company, San Diego, California.

- Zibrida J., Amjad Z., Zuhi R. and Lewis J. 2000, ""Advances In Reverse Osmosis; Application in water reuse" Corrosion, paper No.314.

Recycle valve

Rotameter

Reverse osmosis
unit

Pressure gauge

Feed Tank

Pump

Concentrated
solution

Product solution
(Permeate)
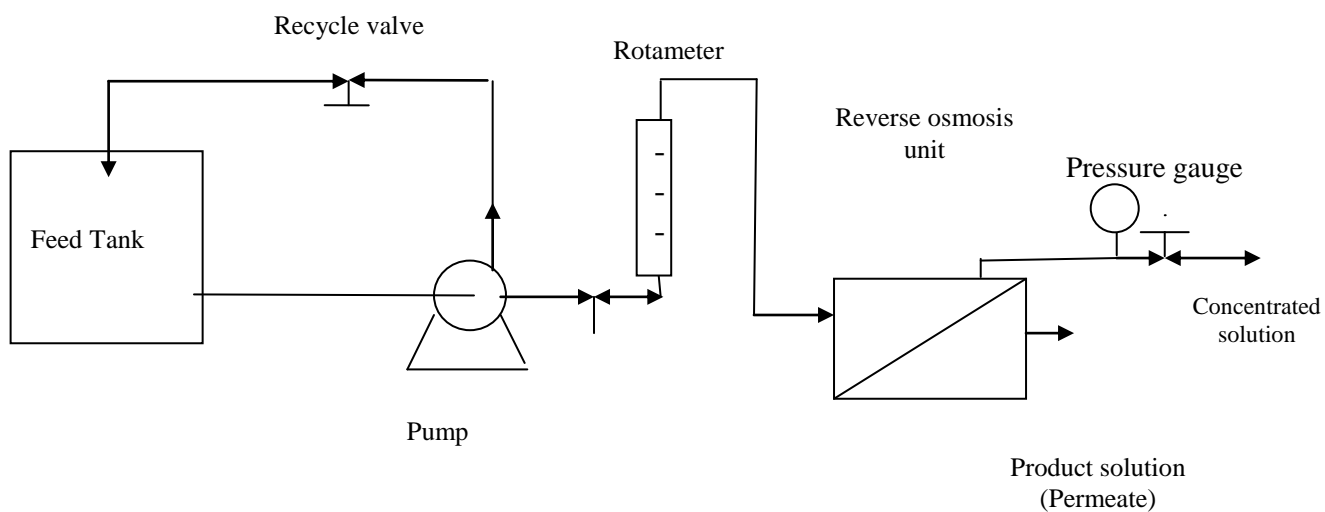
Fig. 1 Schematic diagram of reverse osmosis unit.
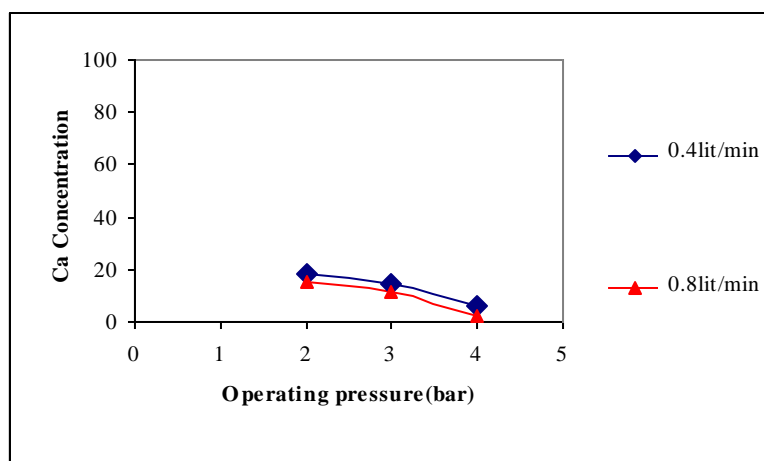
Fig. 2Concentration of Ca^{++} vs operating pressure.
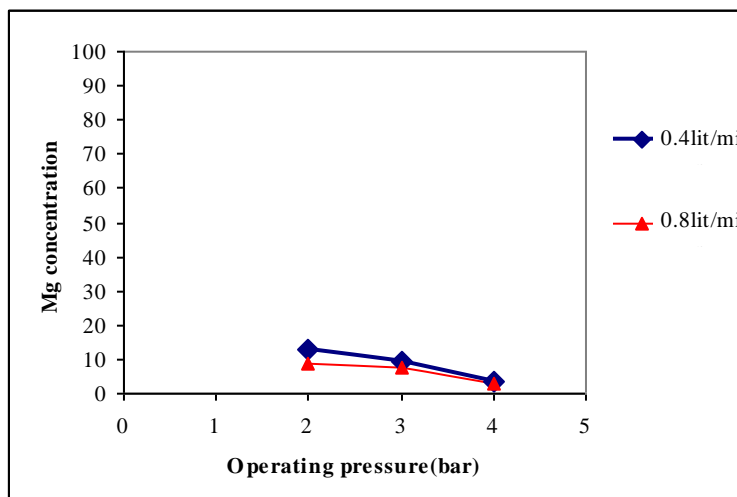
Fig. 3 Concentration of Mg $^{++}$ vs operating pressure.
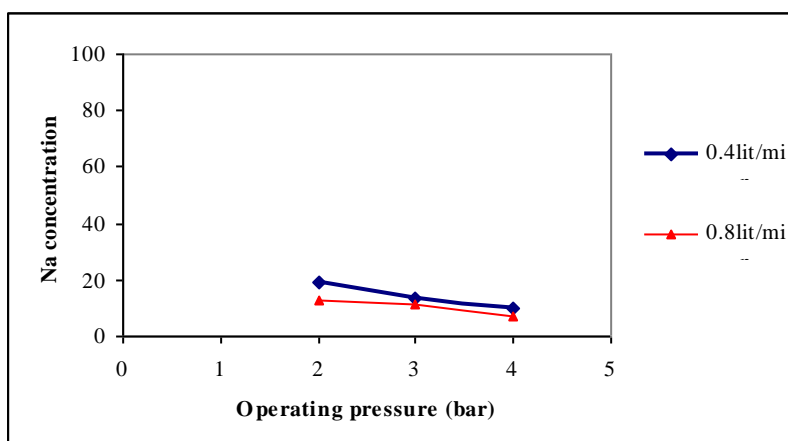
Fig. 4 Concentration of Na$^+$ vs operating pressure.
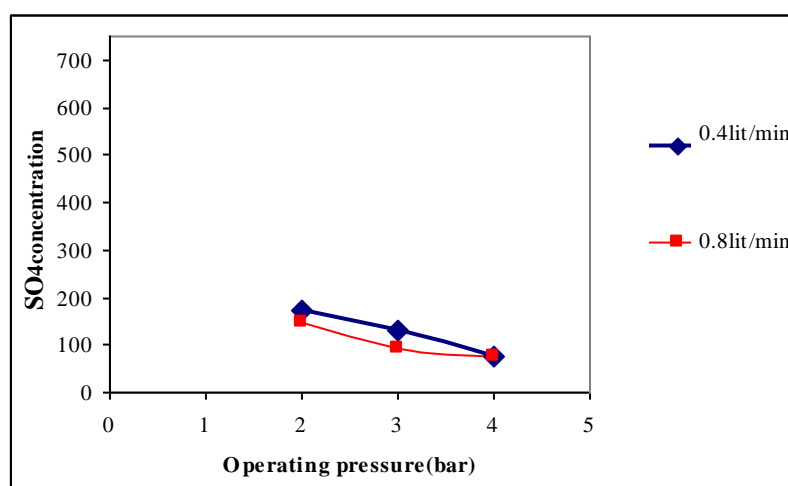
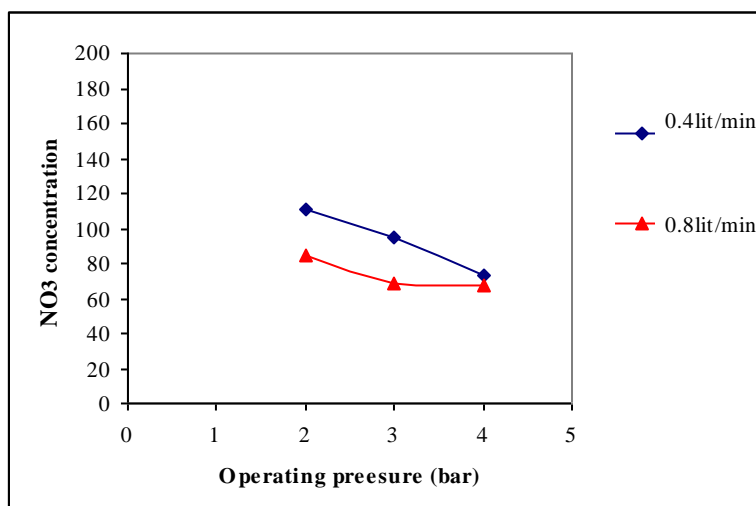**Fig. 5 Concentration of SO$_4$$^{--}$ vs operating pressure.**

Fig. 6 Concentration of NO$_3^-$ vs operating pressure.
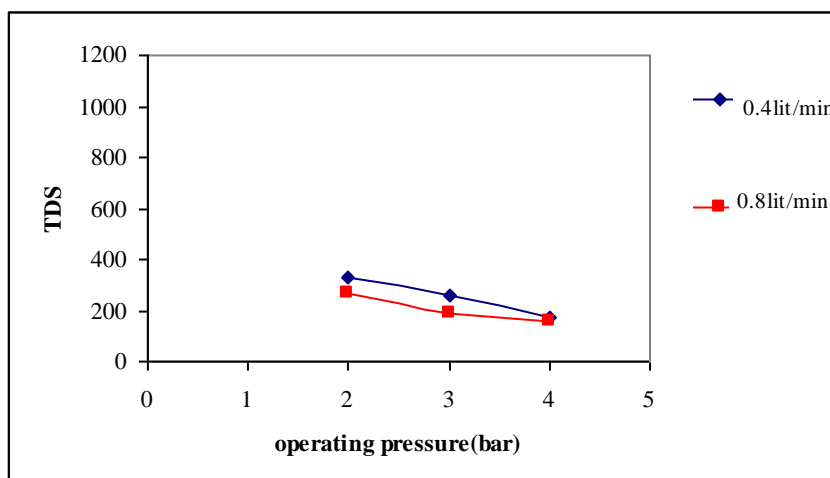
Fig. 7 Total dissolved solids vs operating pressure.
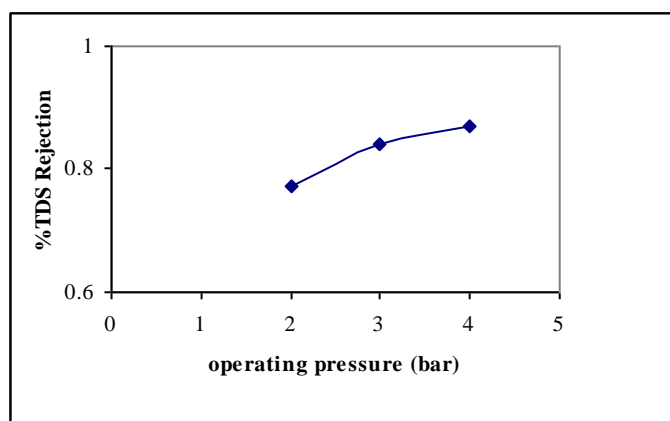
Fig. 8 % TDS Rejection vs operating pressure.
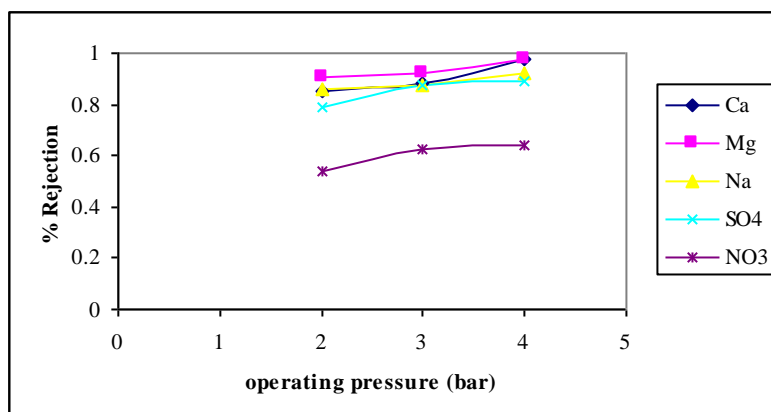
Fig. 9 % Rejection for different ions vs operating pressure.

Table 1. The initial concentrations of feed solution.

Feed water ion	Concentration (ppm)
Ca^{++}	100
Mg^{++}	100
Na^{+}	90
SO_4^{--}	717
NO_3^{-}	185
TDS	1192

DEVELOPMENT OF A LAN SIMULATION TOOL
BASED ON WINDOWS ENVIRONMENT

Hamid M. Ali, Nidhal Ezzat and Wisam F. Kadhim
University of Baghdad

ABSTRACT

The Internet's rapid growth has spurred the development of new protocols and algorithms to meet changing operational requirements such as security, multicast transport, mobile networking, policy management, and quality of service support. Development and evaluation of these operational tools requires answering many design questions. This work proposes a computer network simulation program, devoted for wired LAN systems. The simulator would be able to work under Microsoft Windows NT platforms, also it has the potential to provide an emulation environment which should be suitable for testing protocols above the TCP layer under the Windows NT platform supported network layers, and offering scalability by running the simulator under distributed network system.

KEYWORDS
Network Simulators, Modeling.

الخلاصة

أدى التنامي السريع للإنترنيت إلى تشابك عملية التطوير لبروتوكولات وخوارزميات جديدة لتحقق المتطلبات العملية المتغيرة، مثل أمن المعلومات (Security)، شبكات الأجهزة المتنقلة (Mobile Networks)، إدارة اسلوب العمل (Policy Management)، جودة الخدمة (Quality of Service). تطوير وتقييم هذه الأدوات التشغيلية تتطلب الإجابة عن العديد من التساؤلات التصميمية. هذا البحث يقترح نظام محاكاة لشبكات الحاسبات، مخصص لمنظومات الـ(LAN) السلكية. نظام المحاكاة المقترح يكون قادر على العمل ضمن نظام التشغيل (Microsoft Windows NT)، كذلك له القابلية على توفير محيط والذي يكون مناسباً لفحص البروتوكولات ما فوق (TCP layer) باستخدام طبقات الشبكات (network layers) التي توفرها أنظمة التشغيل (Windows NT platform)، و يوفر نظام المحاكاة المقترح المقياسية (Scalability) عن طريق تشغيل المحاكاة في أنظمة شبكات موزعة (Distributed Network System).

INTRODUCTION

The network simulators exist in many forms and work on different criterion of computer networks, some of these simulators can combine the simulation of more than one network system, and others can be specifically created to simulate a particular network protocol. This fact has brought into the surface some drawbacks in the simulation level of the current simulators, in reference to the concept of the common simulator [BEF00] that can work on most of the network systems and protocols.

The upside of this divergence in functionality is realistic marketing; some vendors' simulators are optimized for managing LANs (Local Area Networks) and others for WANs (Wide Area Networks), some merely provide network diagramming and limited simulation while others perform more sophisticated global network modeling. The downside is that no one simulator can perform all the required functionality, where if a particular network is needed to be modeled,

analyzed, and simulated, then multiple simulators are required, besides the notable differences between them that imply the same job [Jim98].

Most of the simulators can simulate all of the network elements, but some of the packages fall short. Where some can't simulate disks, chips or controllers, some can't mirror frame queuing performance or media speed, and others can't simulate device-level details such as hardware architectures. With the exception of some simulators, most of the simulators are not considered to be system-level simulation devices. That means they are limited in their ability to determine how the performance of the end stations will impact the performance of the network [Jim98].

Another important issue to consider is that most of the network simulators do not support the emulation feature; that is linking the simulated network to an actual real network, thus extending the study criterion on the performance and behavior.

- OBJECTIVE OF THE WORK
In this work, the modeling of the basic network components used (clients, servers, hubs, and routers) was accomplished using Windows NT resources and the proposed network simulator had a simulation engine capable of: adding and removing of network components during runtime, configuring network components' parameters, and performance results calculation. The proposed network simulator also has a timed events management to perform the required simulation scenarios, like: server crash, router failure, or link sudden disconnection, where these events are user generated according to specified time during the simulation run.

The work included a validation test to the proposed network simulator by running a file transfer application (as an example) on a simulated network from one hand and a similar real network on the other hand all under the same timed events, then comparing the simulation results.

- MODELING OF NETWORK ELEMENTS
The network resources of Windows NT Platform were used to model each network element, where they were based on some of the network architecture functionality of Windows. The network protocols of Windows (like TCP/IP) were used as the protocol layers in the simulation engine, instead of programming prototypes of these protocols (like other simulators do, especially those programmed under UNIX), this would make the protocol modeling approaches much more to reality, since the actual protocol would be used in the simulation process.

The modeling of end-systems, like clients and servers, were based on creating a network resource by adding virtual network adapters, so that Windows network architecture would assign a set of protocol layers on top of each virtual network adapter, which would lead to an accessible network resource representing either a client or a server.

The modeling of the intermediate-systems, like hubs and routers, were based on assigning connections' lists and routing tables that would be used in packet filters within the protocol layers in the Windows network architecture, so that each connection's list would represent a hub, and each routing table would represent a router.

- WINDOWS NT NETWORK ARCHITECTURE
Microsoft® Windows® 2000 and later operating systems use a network architecture based on the seven-layer networking model developed by the ISO (International Standards Organization). Introduced in 1978, the ISO OSI (Open Systems Interconnection) Reference model describes networking as: "a series of protocol layers with a specific set of functions allocated to each layer. Each layer offers specific services to higher layers while shielding these layers from the details of how the services are implemented. A well-defined interface between each pair of adjacent layers

defines the services offered by the lower layer to the higher one and how those services are accessed" [Mic01a]

Figure 1 represents a model of Windows 2000 network architecture. In the figure, components that are on the same horizontal level provide similar functionality. The top layer of the diagram is where user applications reside. In order to communicate with other networked computers, additional software and hardware support is needed. Each layer below the applications and services layer provides services that are necessary to create packets of data, arrange for their delivery, and send them across the physical media to another computer.
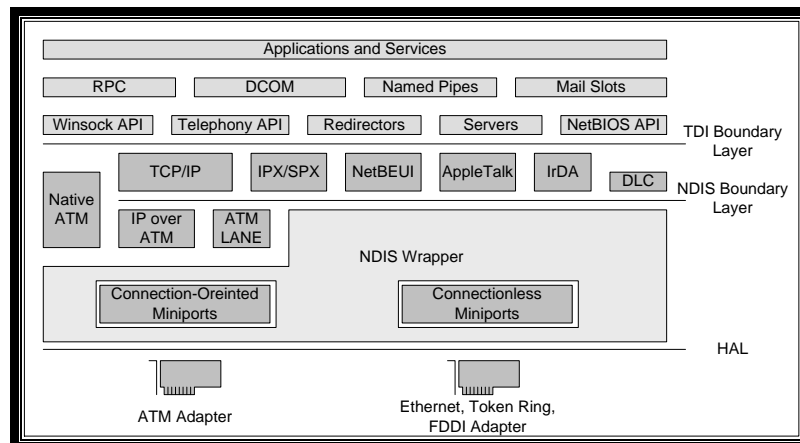
Figure 1: Windows 2000 Network Architecture Layers [Mic01a].

The Windows Network Architecture provides packet filtering techniques that can be used to filter and process inbound and outbound TCP/IP transport protocol data. There are two types of these techniques: user mode techniques and kernel mode techniques. Figure 2 shows some of these techniques.

User mode is the processor mode in which applications run. User mode processes have access only to their own address space and must use established interfaces to obtain other system services. This protects the operating system and improves its performance [Mic01b].

Kernel mode is the processor mode, in which operating system code (such as system services and device drivers) runs. It is a highly privileged mode of operation where the code has direct access to all memory, including the address spaces of all user-mode processes and applications, and to hardware. Processes running in kernel mode have access to advanced CPU features for I/O and memory management [Mic01b].
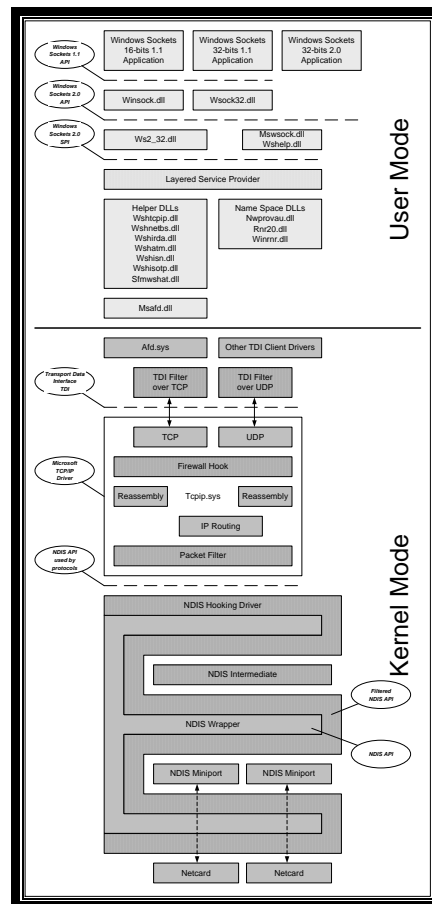
Figure 2: Some TCP/IP Traffic Processing Techniques[Mic01b].

- PROPOSED NETWORK SIMULATOR

In order to meet some of the intended simulation requirement of the network research [BHH99], this work focused on the design of a network simulator based on the following specification:

- Simulation criterion that focuses on the impact of changes in network behavior on the application layer and user mode applications.
- Use of Microsoft® Windows® NT Platform to model the network elements, where Windows network resources are used to model the targeted network elements, like clients, servers, hubs, and routers.
- The network simulator models and functions would be included as DLLs (Dynamic Linked Libraries), so it can be used under any supported platform and with wide variety of network applications, thus leading to increase in level of abstraction.
- Use of flexible graphical user interface that would improve the interaction with the network simulator, and make easy access to its functions.
- Applying a simulation scenario based on network components' failures and recovers on specified times by the user to simulated real world events on networks, like router failure or server crash.
- Provide the potential for supporting full emulation capabilities, where the simulated model can be accessed directly form an outside real network and vice versa, so that all the traffic can be monitored and data analyzed.
- Capability of simulating large scale networks depending on the full emulation potential support, using parallel operation of multiple simulators running on different machines connected via a real network, thus reducing both time and resources.

4367

Simulator Design
A. Clients & Servers Models

In order to model the clients and servers, it should be pointed out that each client and each server represents a system of applications running on a networking protocols stack that are on top of one NIC at minimum. Therefore, to create a model of a client (or a server), an NIC should be added to the system, so that the Windows device management would add the appropriate protocol layers and drivers to make this NIC functional and the applications to work on it.

Since it's not convenient to add physical NICs to the system to represent the clients and servers, another method can be applied instead, which is through the use of virtual NICs. These virtual NICs are merely driver entries at the miniport diver layer or intermediate miniport driver layer, where there is no actual NIC bound to it. Windows network architecture provides two types of these virtual NIC drivers: Microsoft Loopback Adapter, and NDIS MUX Intermediate driver.

There is no documentation about the Microsoft loopback adapter, except the installation method and the general use of it. Microsoft provided this loopback adapter as a dummy NIC that can be used for troubleshooting the network configurations and settings, another advantage of Microsoft loopback adapter is achieved through installing Active Directory on a Domain Controller that doesn't have a network adapter. Normally, this is not a possibility as active directory requires that a network adapter be installed first. If it is needed to install active directory on a computer without a network card, such as a test or a lab environment, Microsoft loopback adapter can be installed instead of physically installing a network adapter.

The MUX intermediate miniport driver is an NDIS 5 driver that demonstrates the operation of an N:1 or 1:N MUX driver, i.e. one which creates multiple virtual network devices on top of a single lower adapter. Protocols bind to these virtual adapters as if they are real adapters [Mic01a]. The number of virtual miniports exposed by a MUX intermediate driver can be different than the number of lower physical adapters that are bound to the driver. A MUX intermediate driver exposes virtual miniports in a 1:N, N:1, or even an M:N relationship with underlying adapters. This results in complicated internal bindings and data paths [Mic01a].

In an N:1 configuration, a MUX intermediate driver can expose many virtual miniports for a single physical adapter below. Overlying protocols bind to these virtual miniports of the MUX intermediate driver in the same way that they bind to non-virtual miniports. The MUX intermediate driver handles requests and sends that are submitted to the driver for specific connections at each virtual miniport. The driver repackages and transfers these requests and sends down to the NDIS miniport driver for the bound physical adapter. Figure 3 illustrates an N:1 MUX intermediate driver configuration [Mic01a].
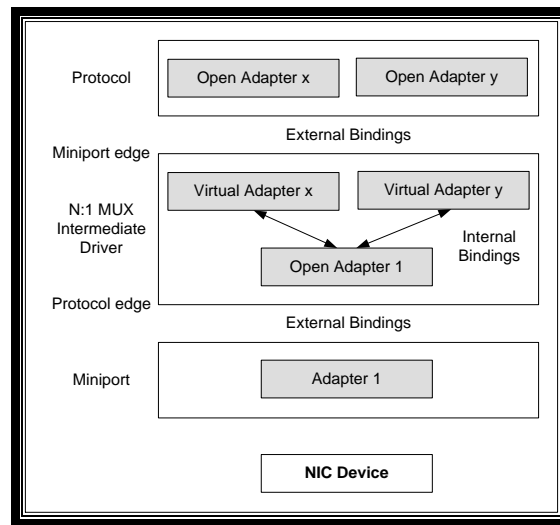
Figure 3: NDIS N:1 MUX intermediate driver configuration[Mic01a].

B. Hubs & Routers Models

Since there are no real NICs, there exist no actual physical connection between the simulated clients and servers; also it would mean there is no physical routing operation can be applied. So in order to model the physical connections, hubs and routing operation, it would be useful to use the packet filtering techniques provided by Windows network architecture.

The most useful technique to use for modeling the physical connections, hubs, and routers is the Firewall-Hook driver. This fact comes from the following aspects (refer to figure 2 for details):

- The Windows network architecture TCP/IP routes all the internal traffic at the protocol driver layer (TCP/IP driver), which means there no traffic is going down to the NDIS layers below.
- All the configured network adapters that exist in the system, whether they were actual or virtual, are treated as being all connected together, even if they have different IP addresses.
- The firewall-hook driver is located within the TCP/IP driver on top of the IP routing functions.
- It's a kernel mode packet filter that performs its operation on all the packets traffic of every application running on the system. Yet, it supports the interaction of the user on its operation, which makes it user mode configurable.

Therefore, the modeling of the physical connections, hubs, and routers can be made through modeling only the lists of connections and routing tables. And theses lists and tables are passed to the firewall-hook driver to perform the connections and routing operation, provided that the routing is only static.

The filter hook driver only allows one filter function installed in the system. If one application already uses this functionality, the targeted application doesn't work. With firewall-hook driver, this problem has no existence, all filter functions can be installed as required. Each filter function has a priority assigned, so the system will call one function after another (in priority order) until a function returns "DROP PACKET". If all functions return "ALLOW PACKET", the packet will be allowed. This can be thought as a chain of functions, this chain is broken when one of them returns "DROP PACKET", and the order of each function in the chain is given by its priority value [Jes04].

Figure 4 represents an example of the firewall-hook driver operation, with the following processes:

- A packet is received at the host, IP driver has the list of filter functions ordered by priority (the function with more priority is Filter Function 1).
- First, the IP driver passes the packet to the highest priority filter function and waits for the return value.
- Filter Function 1 returns "ALLOW PACKET".
- Because Filter Function 1 allows the packet, IP driver passes the packets to the next filter function: Filter Function 2.
- In this case, Filter Function 2 returns "DROP PACKET". So, IP driver drops the packet and does not continue calling next filter function.
-
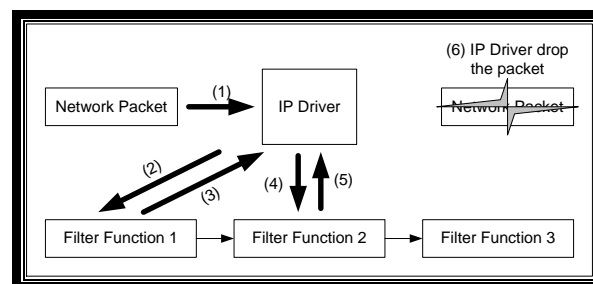
Figure 4: An Example of Firewall-hook Driver Operation[Jes04].

Another problem that can be found with filter hook drivers is that for sent packets, the user can't access packet content data. However, all data can be accessed with a firewall-hook driver. The structure of data received in a firewall-hook filter function is more complex that the one received in filter hook driver. It's more similar to the structure of packets that can be found in an NDIS driver, where the total packet is composed by a chain of buffers. As filter hook driver, firewall-hook driver is only a kernel mode driver used to install a callback function (but firewall-hook driver installs a callback in IP driver). In fact, the process to install a firewall-hook driver is similar to the one used to install a filter hook driver [Jes04].

C. Simulation Engine
The simulator engine consists of three major functions: adding the modeled network components (Clients, Servers, Hubs, and Routers) to the system during runtime, configuration of network parameters of each installed component, and calculating the performance results of the simulated network. The design of the simulator engine would also consider the support for full emulation, such that the simulator would be beneficial at all levels of usage.

After the modeled network components are added in the system as designed to form the simulated network, it's required to configure the network parameters of each added component, like IP address, subnet mask, default gateway, and DNS (Domain Name Service) server. Microsoft Windows provides a set of classes and functions that can be used for this purpose, these classes and functions are found in WMI (Windows Management Instrumentation).

WMI is a component of the Microsoft Windows operating system and is the Microsoft implementation if the WBEM (Web-Based Enterprise Management), which is an industry initiative to develop a standard technology for accessing management information in an enterprise environment. WMI uses the CIM (Common Information Model) industry standard

to represent systems, applications, networks, devices, and other managed components. WMI can be used to automate administrative tasks in an enterprise environment [Mic01a].

When activating the designed network in simulation mode, it's important to calculate the performance of the network, like bandwidth, percentage of sent and received packets, and each protocol status. The mechanism by which Windows collects performance data on various system resources is the *performance counter*. Windows contains a pre-defined set of performance counters with which the user can interact; some of these are found on all Windows 2000 systems and some are custom to specific applications and are found only on certain systems [Mic01a].

D. Events & Time Management

The events and time management in the proposed network simulator would include user generated scenarios that would run in a timed-event sequence. The user would specify the type of action to be taken and the corresponding time for the action to occur. These actions can take the form of servers' crashes, routers failures, and links sudden disconnections, so that the user can measure the degree of interaction between the network nodes and explore the vulnerable points in order to avoid them.

This type of management can be achieved through the use of a time ordered list or table that would be referenced on a time bases in respect to a simulation timer, where at every time tick the table would be referenced to check whether the current simulation time matches one of the events time. At that point, if a match found, the events and time manager would execute the event using WMI functions to disable a certain virtual adapter that models a client or a server, or remove a set of filtering rules that represent a hub or a router.

Each events table entry would contain the following information to represent an action:
- Time of the event, which is referenced to the simulator timer.
- Network node to be disabled, that indicates whether a client, server, hub, or a router to be crashed.
- Duration of the action, where it sets the time for which the action would take from failure to recovery.

System Architecture

The simulator system architecture is divided into two main sections (or layers): Simulation Platform (VNetSimPlatform), and Application Layer (VNetSimApplication). The reasons behind such architecture are:
- Provide transparency of the kernel mode used resources from the application layer that is used by the user.
- Make the simulation platform as stand alone set of resources, which makes it easier for future development to upgrade the functions within the platform or the application layer without affecting the other.

Figure 5, shows the general system architecture of the network simulator.
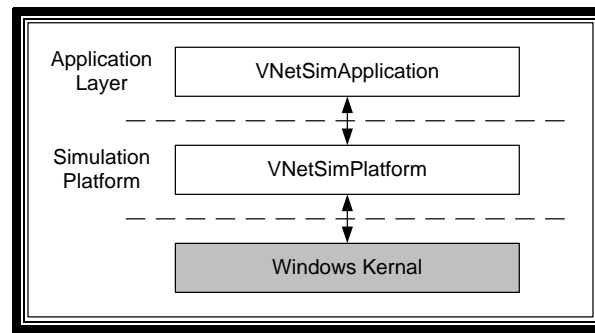
Figure 5: Simulator General System Architecture.

E. Simulation Platform (VNetSimPlatform)

This layer is considered as the kernel mode layer of the simulator, it provides the functions that use windows resources to perform the modeling of each network component (such as Clients, Servers, Routers, and Hubs) and manage these resources to appear as objects to the upper application layer. The simulation platform consists of a layered set of DLLs (Dynamic Linked Libraries); each one handles certain functions or models a set of network components. Figure 6 shows the components of the simulation platform.
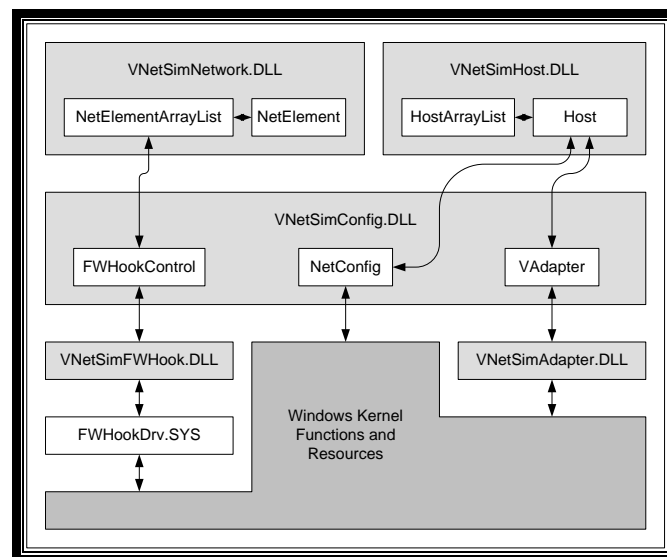
Figure 6: Components of Simulation Platform.

The simulation platform uses a collection of programming languages to perform its functions, where at the lower layers conventional C language was used with drivers (such as FWHookDrv.SYS), also the C++ language was used with the DLLs that operate with Windows system calls and functions (such as those used in VNetSimAdapter.DLL and VNetSimFWHook.DLL). At the upper layers, C# language was used with the DLLs that work as objects of the modeled network components (such as VNetSimHost.DLL and VNetSimNetwork.DLL), as well as the DLLs working as interfaces between the object DLLs and the kernel mode DLLs (such as VNetSimConfig.DLL).

The reason for such variety in programming languages is that at every level of the simulation platform there are certain needs that each programming language can provide better than the others. In the case of drives, commonly conventional C language can be used in order to compile and build the driver. As for the DLLs that operate on Windows resources and kernel functions, the C++ language is known to be a very efficient and strong tool to work with Windows resources and supports their requirements from pointers, complex data structures,

etc. Whereas C# language support for pointers and complex data structures is considered to be unsafe code by the complier.

The C# language is easier to deal with than C++ in regard to the reduce in complexity and the compilation features provided by the Dot Net environment, also in aspects of developing the graphical user interface, which makes the C# more convenient to use at upper layers that is used by the application layer as well as to hide the complexity of the underlying functions and resources [TWA02].

F. Application Layer (VNetSimApplication)

The application layer performs most of the management functions and operations performed by the network simulator, where it can be considered as the simulator kernel. The application layer consists of four main blocks of functions, as shown in figure 7, each block is responsible for certain set of functions.
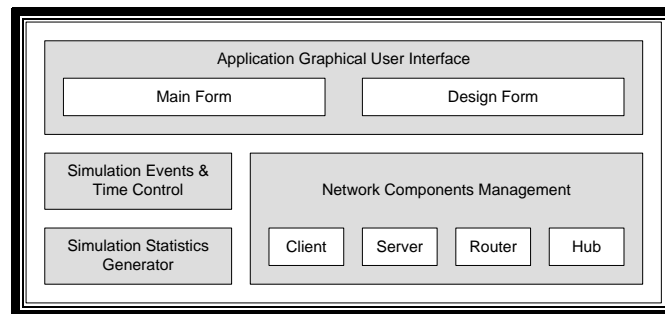

Figure 7: Block Diagram of the Application Layer.

• Application Graphical User Interface

This block represents the graphical user interface forms that would appear to the user. It handles the operations and calling functions associated with each graphical object, such as menus and toolbars, and pass the control to the corresponding block to perform the required functions. The application graphical user interface contains two classes: main form class, and design form class.

The main form class is a windows form class that represents the main window of the graphical user interface. It holds the main menu, the main toolbar and it works as a container for the design form. The design from class is also a windows form class that works as the document where the users draw the design of the network to be simulated by using network components icons found in the main form toolbar.

• Network Components Management

This block holds the graphical and functional classes that represent the network components, such as Clients, Servers, Hubs, and Routers. The main function of the network components management block is to provide a transformation between the application layer space objects into the simulation platform space objects so as to keep control over the array lists of objects at the two spaces.

For example, if the user adds a client to the design form, a client object is added to the application layer space; hence, it is added to the clients' array list along with its configuration parameters. On the other hand, the network components management block would make a transformation of the client object from the application layer space into the simulation platform space by adding a host object to it, so it is added also to the hosts' array list along with the client's configuration parameters. This step would add a loopback adapter to the

system to represent that client object and the adapter's configuration is set according to the network parameters of the client object.

• Simulation Events & Time Control

This block contains a single class which is called Simulation class. It contains a timer object to provide the necessary timing for the simulation runtime process. The class also contains an array list that works as a timed-events table, so it can hold the type of events to be activated during the simulation run in a timely manner.

• Simulation Statistics Generator

This block is responsible for generating the statistics report of the simulation run, where it contains instances of the performance counters built in the firewall hook driver, which would provide the data required by the user to analyze the performance of the simulated network under specific events.

* IMPLEMENTATION AND PERFORMANCE

The network simulator was implemented mostly in Microsoft .Net C# language, except for some parts of the simulation platform, where it can operate on Windows NT platforms (Windows 2000 Server, Windows 2000 Professional, Windows XP Home Edition, Windows XP Professional Edition, and Windows 2003 Server).

The network simulator was deployed under Pentium 4 with Windows XP SP2 and a validation test was implemented on the proposed network simulator by running a file transfer application (as an example) on a simulated network (shown in Figure 8) from one hand and a similar real network on the other hand all under the same timed events listed below:

- Client 1 performs a download operation from the file server at early start of the simulation process, during that operation the file server crashes for 2 seconds then recovers.
- After several seconds, Client 3 performs another download operation from the file server, during that operation the network hub experience a power failure for 5 seconds then recovers.
- Client 2 performs an upload operation to the file server to update some data, during that operation client 2 experiences a system halt for 5 seconds then recovers.
- Finally, client 3 performs a download operation from the file server, but this time client 3 experiences a system halt for 5 seconds then recovers.

By comparing the simulation results, the validation test results (Figure 9) showed an acceptable tolerance with slight difference that comes form the several factors like: the variable processing conditions of the operating systems where the application was running on, the tolerance of simulation and modeling of the proposed network, and accuracy of timed events when applied at both simulated and real networks.
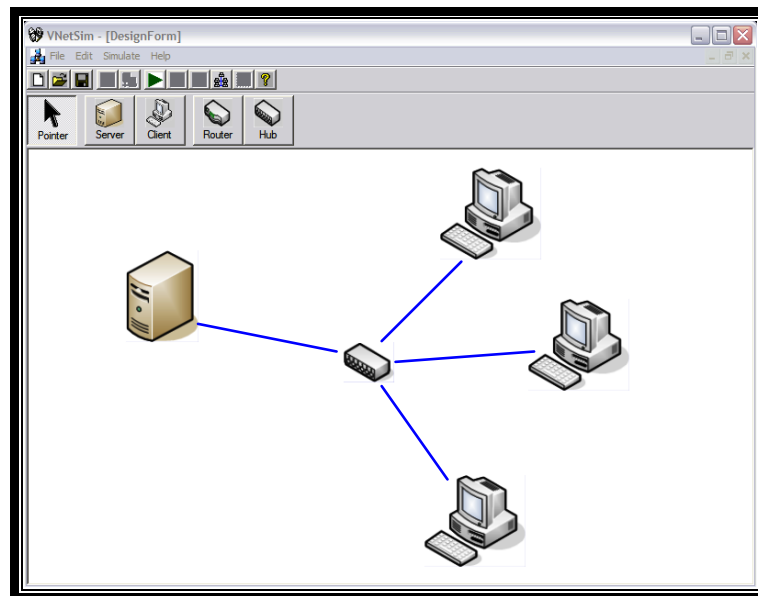
Figure 8: Network Topology that the Sample Application would be tested on.

From		To		Simulated Bytes/sec		Real Bytes/Sec	
Device	IP Address	Device	IP Address	Sent	Received	Sent	Received
Client 1	192.168.10.1	Server	192.168.10.10	302	1512	300	1550
Client 1	192.168.10.1	Server	192.168.10.10	231	1345	250	1350
Client 1	192.168.10.1	Server	192.168.10.10	133	0	150	3
Client 1	192.168.10.1	Server	192.168.10.10	213	342	225	350
Client 3	192.168.10.3	Server	192.168.10.10	312	383	315	300
Client 3	192.168.10.3	Server	192.168.10.10	462	1234	460	1300
Client 3	192.168.10.3	Server	192.168.10.10	12	0	15	7
Client 3	192.168.10.3	Server	192.168.10.10	21	23	30	30
Client 2	192.168.10.2	Server	192.168.10.10	123	462	130	475
Client 2	192.168.10.2	Server	192.168.10.10	1351	235	1400	235
Client 2	192.168.10.2	Server	192.168.10.10	0	125	5	130
Client 2	192.168.10.2	Server	192.168.10.10	12	152	15	155
Client 3	192.168.10.3	Server	192.168.10.10	342	351	350	350
Client 3	192.168.10.3	Server	192.168.10.10	43	1523	50	1550
Client 3	192.168.10.3	Server	192.168.10.10	9	231	10	235
Client 3	192.168.10.3	Server	192.168.10.10	12	521	15	525

Figure 9: Network Statistics resulted from running the Sample Application.

* CONCLUSION AND FUTURE WORK

The network resources of Windows NT platform can be used to model each network element, where they can be based on some of the network architecture functionality of Windows.

The modeling of end-systems, like clients and servers, can be based on creating a network resource by adding virtual network adapters, so that Windows network architecture would assign a set of protocol layers on top of each virtual network adapter, which would lead to an accessible network resource representing either a client or a server.

The modeling of intermediate-systems, like hubs and routers, can be based on assigning connections' lists and routing tables that would be used in packet filters within the protocol layers

in the Windows network architecture, so that each connection's list would represent a hub, and each routing table would represent a router.

It was found that using timed events table for events management is the best way to make user defined simulation events, where the user is free to set any type of events to occur at a specific time during simulation run, these types of events can take the form of: server crash, router failure, or link sudden disconnection. Those user-generated events would help in measuring the degree of interaction between network nodes, and explore the vulnerable points in network application development in order to avoid them.

The proposed network simulator has the potential to continue the research in the following topics of network simulation:

- Use of Mux intermediate driver to model the end-system network components instead of Microsoft loopback adapter, and modify the driver source code to support more user interaction in its operation, like embedding the routing and hub connections within the Mux driver.
- Develop new virtual drivers that would model wireless LANs, and ATM NICs, that could be used to expand the criterion of protocols the network simulator would support and simulate.
- Develop the application layer of the simulator to support more functionality regarding the scenario generation of events and time management functions, also to provide sniffing and more advanced performance counters and measures to be useful in the analysis of the simulated network.

REFERENCES
- [BEF00]   Lee Breslau, Deborah Estrin, Kevin Fall, and Sally Floyed, *"Advances in Network Simulation"*, IEEE Computer, Vol. 33, No. 5, p. 5967, http://citeseer.ist.psu.edu/bresl au00advances.htm, 2000.

- [BHH99]   Sandeep Bajaj, Padma Haldar, Mark Handley, and Ahmed Helmy, *"Improving Simulation for Network Research"*, Technical Report 99-702, University of Southern California, Los Angeles, http://citeseer.ist.psu.edu/bajaj99improving.html, March 1999.

- [Jes04] Jesús O., *"An Adventure: How to Implement a Firewall-Hook Driver"*, Code Project, Article available at: http://www.codeproject.com/internet/FwHookDrv.asp?df=100& forumid=121826&exp=0&select= 960283, 2004.

- [Jim98]   Duffy Jim, *"Simulation Tools are as Varied as LANS They Model"*, Article available   at: http://www.findarticles.com/p/articles/mi_qa3649/is_199802/ai_n8790436.html, 1998.

- [Mic01a]   Microsoft Corporation, Microsoft Windows XP Driver Development Kit, *"Network Drivers"*, 2001.

- [Mic01b]   Microsoft Corporation, Microsoft Development Network, Windows NT Workstation 4.0 Resource Kit, *"Kernel Mode and User Mode"*, April 2001.

- [TWA02]   Adrian Turtschi, Jason Werry, Joseph Albahari, and Greg Hack, *"C#.Net Web Developer's Guide"*, Syngress Publishing, Inc., 2002.

ABBREVIATIONS

ATM	Asynchronous Transfer Mode
CIM	Common Information Model
DLL	Dynamic Linked Library
DNS	Domain Name Service
ISO	International Standards Organization
LAN	Local Area Networks
NDIS	Network Driver Interface Specification
NIC	Network Interface Card
OSI	Open Systems Interconnection
TCP/IP	Transmission Control Protocol/Internetwork Protocol
WAN	Wide Area Networks
WBEM	Web-Based Enterprise Management
WMI	Windows Management Instrumentation

EFFECT OF ZRO$_2$, WO$_3$ ADDITIVES ON CATALYTIC PERFORMANCE OF PT/HY ZEOLITE COMPARED WITH PT/Γ-AL$_2$O$_3$ FOR IRAQI NAPHTHA TRANSFORMATION

Maha Al-Hassany
Asst. lecturer/ Chemical Engineering Department/
College of Engineering/ University of Baghdad

ABSTRACT

Light naphtha treatment was achieved over 0.3wt%Pt loaded-alumina, HY-zeolite and Zr/W/HY-zeolite catalysts at temperature rang of 240-370°C, hydrogen to hydrocarbon mole ratio of 1-4 0.75-3 wt/wt/hr, liquid hourly space velocity (LHSV) and at atmospheric pressure.

The hydroconversion of light naphtha over Pt loaded catalyst shows two main reactions; hydrocracking and hydroisomerization reactions. The catalytic conversion of a light naphtha is greatly influenced by reaction temperature, LHSV, and catalyst function. Naphtha transformation (hyroisomerization, cracking and aromatization) increases with decreasing LHSV and increasing temperature except hydroisomerization activity increases with increasing of temperature till 300°C then began to decrease due to the formation of hydrocracking reaction. The investigation of Pt containing catalysts under study shows a very high hydrogenlysis activity , due to presence of metal component (i.e. Zr, W) which enhances the rate of paraffin isomerization and cracking.The hyroisomerization and the hydrocraking activities can be arranged as follows,.

Pt/Zr/W/HY > Pt/HY > Pt/γ-Al$_2$O$_3$

The results showed that, Pt/γ-Al$_2$O$_3$ has higher activity for the direct dehydrogenation of C$_6$ and C$_7$ paraffin's present in naphtha to aromatics than Pt/HY and Pt/Zr/W/HY. This was due to pore volume catalyst ,the aromatics compounds increased as the pore volume increased.

الخلاصة

في هذا البحث تم دراسة تأثير إضافة الزركونيوم و التانكستن على حفاز البلاتين المحمل بالزيولايت و مقارنته بالالومينا للنفثا درس تحول النفثا على حفازات محتوية على بلاتين ،زركونيوم ،تانكستن محملة على زيولايت و بلاتين محمل على الالومينا بين درجات حرارة من 240-370 درجة مؤية و معدلات سرع فراغية 0.75 -3 و نسبة الهيدروجين الى النفثا من 1 -4 نسبة مولية . وجد ان هناك تفاعلين أساسيين لتحولات النفثا و هي التكسير و الأزمرة و التي بدورها تتاثر بدورها بدرجة الحرارة و السرع الفراغية . اظهرت النتائج ان تحول النفثا يزداد بقلة السرع الفراغية و زيادة درجة الحرارة وجد إن تحولات المركبات مثل البنتان الهكسان العاديان الى المتشابهات الاكثر تشبعا تزداد بزيادة درجة الحرارة لحد 300 درجة مؤية ثم تبدا هذه التحولات بالنقصان بسبب تاثير تحولات التكسير و قد وجدت برافينات الهكسان و الهبتان صعوبة في التحول الى مركبات عطرية بواسطة حفاز البلاتين ،زركونيوم ،تانكستن المحمل على زيولايت اذا ما قورن بالحفاز بلاتين محمل على الومينا و ذلك بسبب حجم المسام حيث ان المركبات الارماتية تزداد بزيادة حجم المسام.

INTRODUCTION

Octane number in gasoline is conventionally boosted by addition of aromatics and oxygenated compounds. However, as a result of increasingly stringent environmental legislation the content of these compounds in gasoline is to be reduced and thus industry has been forced to investigate alternative processes to reach the required octane levels (Rafael et al., 2008).

The gasoline pool composition affect it research octane number (RON). To increase the octane number of the light straight run naphtha, it must be isomerized and as a result RON increases. This increase is achieved by isomerizing n-pentane and n-hexane (the main component of (LSR) naphtha) to the corresponding isomers. (Srikant, 2003).

Isomerization reaction are commercially performed using bifunctional catalyst consisting of a metal support like alumina or HY zeolite. (Gauw et al., 2002). Bifunctional metal/acid zeolite catalysts are used in a various industrial process, viz., hydroisomerization of C_5-C_6 alkanes, hyrocracking, dewaxing etc. On these catalysts the alkanes transformation involves hydrogenation and dehydrogenation steps on the metallic sites, isomerization or cracking step on the acid sites and diffusion steps of the oleffinic intermediates from the acid to metallic sites and vice versa. That is why their activity, stability and selectivity depend on the characteristics of the acid and of the metallic sites, in particular on the balance between the acid and the hydrogenation functions, and on the characteristics of the zeolite pores (Alvarez, et al., 1996; Ward, 1999).

Many authours such as (Jeong et al., 1997 and Lawlor et al., 1998) show that, the maximum isomer yield is reached when the metal and acidic functions of the catalysts were balanced. Also show that Pt/HY has good activity and selectivity for naphtha isomerization at high reaction temperature. Therefore, tha main aim of the present work is to study the enhancement of catalytic performance by co-impregnation with Zr and W using 0.3wt%Pt/HY zeolite catalyst in order to obtain a maximum isomerization yield.

EXPERIMENTAL

- Catalyst preparation In this study three types of catalysts were used, and these catalysts are as follows:
- HY-zeolite (CBV 600) catalyst powder was supplied from zeolyst International Company and used as support for catalyst preparation.

- 100 gm of HY-zeolite powder was mixed with 30% montmorillonite clay as a binder. The resulting mixture was mixed with water to form a paste. An extrudates with 0.3cm×0.5cm were formulated and dried overnight at 100°C, then 0.3wt%Pt/HY zeolite was prepared by impregnation method with proper solution of hexachloropatinic acid containing of 0.1590 gm of hexachloropatinic acid and 8 ml deionized water for 20 gm catalyst . The impregnated extrudates were then dried at 110°C overnight then calcinated at 300°C for 3 hours in a furnace with dry air.

- WO_3/ZrO_2/Pt/HY catalyst was prepared by co-impregnation with proper solution of ammonium meta tungsten (Sigma Aldrich) and zirconium tetra chloride (BDH) and deionized water containing of 0.3880 gm zirconium tetra chloride and 0.8615 gm ammonium meta tungsten and deionized water till the volum of solution equal to pore volume of 40 gm (i.e.32 ml) of Pt/HY zeolite. The impregnated extrudates were then dried at 110°C overnight and calcinated at 700°C for 2 hours in a furnace with air.

- Pt/γ-Al$_2$O$_3$: commercial Pt/γ-Al$_2$O$_3$ supplied form Al- Dura refinery with surface area of 204 m^2/g, pore volume of 0.45 ml/g and density of 0.62 g/cm^3 was used as a support.

FEEDSTOCK

The feedstock used in hydroisomerization runs was light straight run (LSR) naphtha supplied from Dura rifinery and its properties listed in Table (1).

Table (1) Properties of LSR naphtha.

Composition	Wt%
i-C$_4$	1.5
n-C$_4$	3.8
i-C$_5$	4.9
n-C$_5$	4.7
i-C$_6$	8.5
n-C$_6$	41.6
Cyclo-C$_6$	5.7
i-C$_7$	4.9
n-C$_7$	5.8
Cyclo-C$_7$	8.7
n-C$_8$	3.2
Benzene	2.9
Toluene	3.8
API Sp. Gr. @ 60°/60°F	74.8

Some properties of prepared catalyst, and support are tabulated in Table (2).

Table (2): Properties of prepared catalysts.

Catalyst	0.3wt%Pt/γ-Al$_2$O$_3$	0.3wt%Pt/HY zeolite	0.3wt%Pt/Zr/W/HY zeolite
Surface are, m^2/g	207	435.6	415.8
Bulk density, g/cm^3	0.62	0.466	0.488
Pore volume, cm^3/g	0.45	0.374	0.308

CATALYTIC ACTIVITY TEST

The catalytic activity test was achieved in a continuous down flow fixed-bed reactor. The reactor was carbon steel tube with an outside diameter of 1.9 cm, 2mm thick and 80 cm long.Fig.1 shows the process flow diagram. The platinum containing catalysts were reduced with H$_2$ at 350°C for 3 hr (Masologites and George, 1987 and Jan-Ku, et al., 1988).

The catalytic reaction were carried out with LHSV of 1-4 h^{-1}, at temperature range of (240-370°C), hydrogen to feed mole ratio of 1-4 and at atmospheric pressure. Liquid products were trapped by condenser at -10°C. Sample were collected periodically and analyzed by gas chromatography. The gas chromatography model 438 Aa-VSA, supplied by Agilent Technologies Company. This devised equipped with capillary column of 0.25mm diameter, 100m length and packed with CP-SIL-SCB and FID detector.
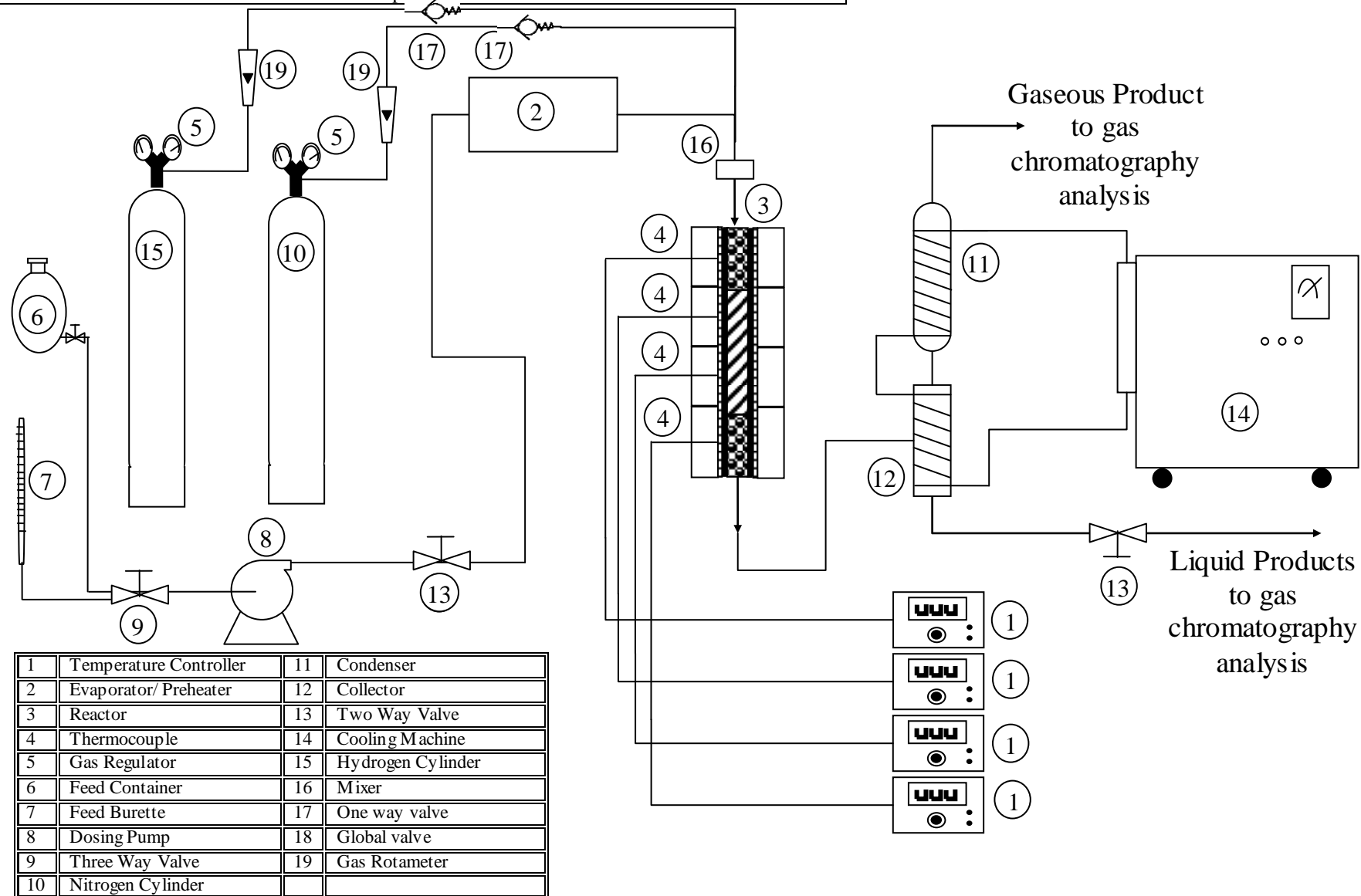
1	Temperature Controller	11	Condenser
2	Evaporator/ Preheater	12	Collector
3	Reactor	13	Two Way Valve
4	Thermocouple	14	Cooling Machine
5	Gas Regulator	15	Hydrogen Cylinder
6	Feed Container	16	Mixer
7	Feed Burette	17	One way valve
8	Dosing Pump	18	Global valve
9	Three Way Valve	19	Gas Rotameter
10	Nitrogen Cylinder		

Fig. 4.3, Flow diagram of the **continuous laboratory reaction unit**.

RESULTS AND DISCUSSION

In the present work ,the hydroconversion of light naphtha feedstock on the catalyst shows two essential reactions; hydrocracking and hydroisomerization. Other reactions, such as cyclization and aromatization were significantly different with all three catalysts.

Cracking activity

The results shown in Figs 2-5 that a certain amount of cracking products with the amount formation of C_1-C_4 were obtained between 240-350°C reaction temperature and LHSV of 0.75-3 h^{-1}. It can be clearly show that the amount formation of C_1-C_4 products are the lowest for Pt/γ-Al_2O_3 and highest for Zr/W/Pt/HY zeolite, throughout all experiments. The cracking yields are increased by increasing temperature and decreasing LHSV for all catalysts but are still the lower for Pt/γ-Al_2O_3 therefore; the cracking activity sequence can be arranged as follows:

Zr/W/Pt/HY > Pt/HY > Pt/γ-Al_2O_3

The increasing of transformation of naphtha on Zr/W/Pt/HY may be due to slightly enhancement of acid sites. According to Table 2, the pore volume of Zr/W/Pt/HY is lower than other catalysts. A decreases in a pore volume leads to increasing in ΔH_{ads}. An increase in ΔH_{ads} indicates of increasing of surface coverage, resulting in an increase in the number of molecules available for reation. Such explication are agree with Eder et al., 1997.

The results indicate that the low LHSV is favored for high conversion of naphtha, this means that increasing the residence time, which offer a plenty of contact time of feedstock to react on the catalyst (Jolly et al., 1999).

The change in the number and the strength of acid sites on Zr/W/Pt/HY is directly affects the state of the metal sites (Yan Liu et al., 2006). The combination of these two parameters influences the cracking activity due to the presence of metal component which enhance the rate of paraffin isomerization and cracking; paraffin can be dehydrogenated on a metal site and the resultant alkenes are much easier crack or isomerized depending on the acid strength of the catalysts.
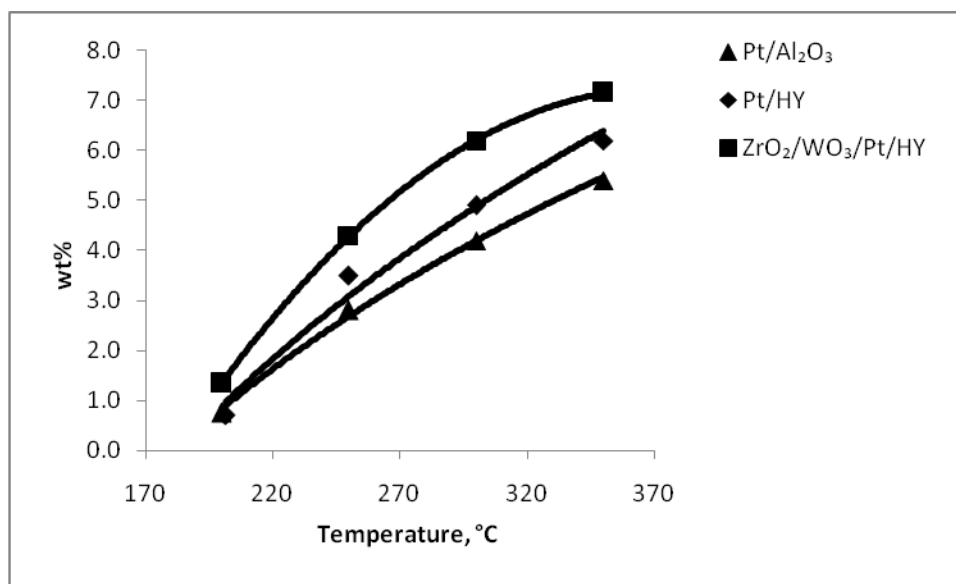

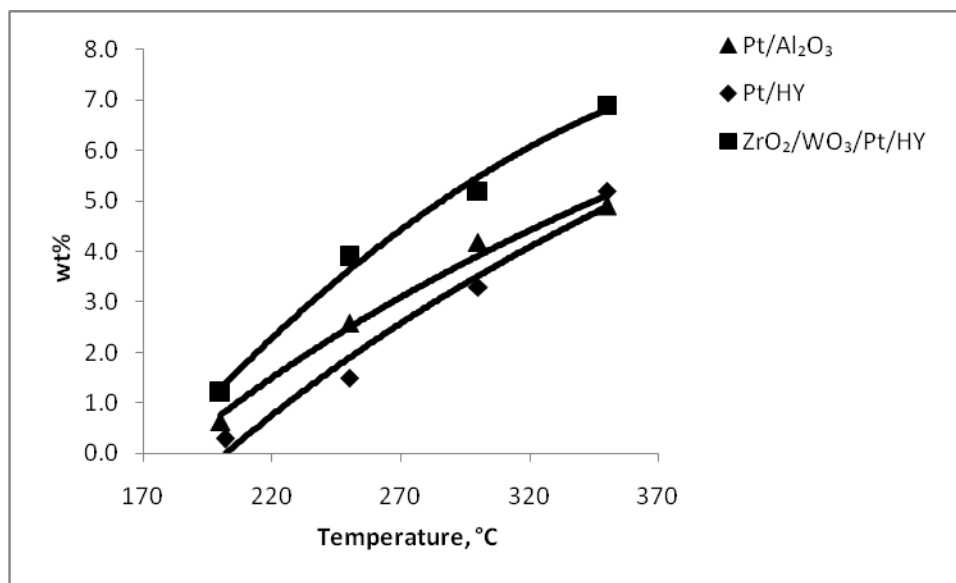**Fig.2,** The effect of temperature on hydrocracking product at LHSV=0.75 h^{-1}.

M.Al-Hassany

Effect of ZrO$_2$, WO$_3$ additives on catalytic performance
Of Pt/HY zeolite compared with Pt/γ-Al$_2$O$_3$ for Iraqi
Naphtha transformation

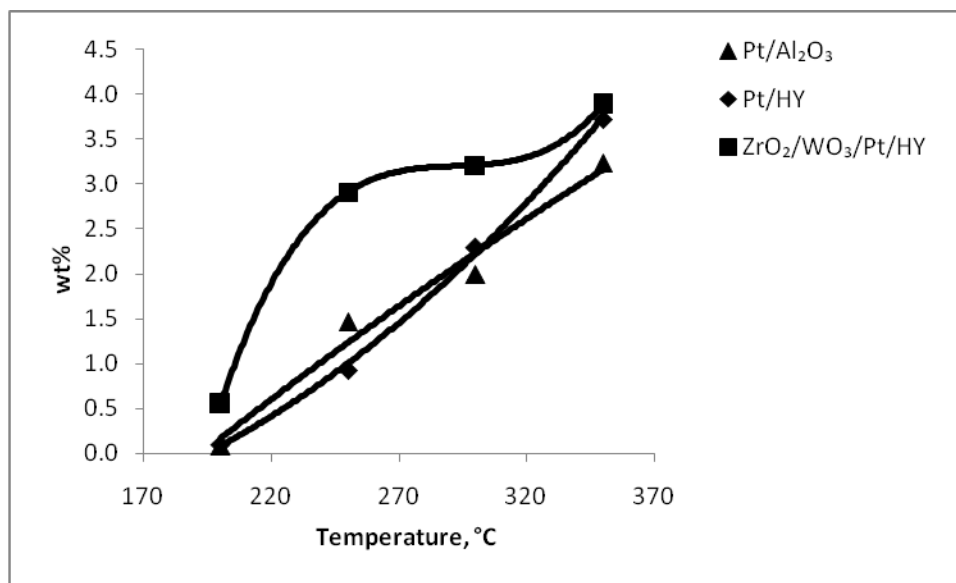**Fig.3,** The effect of temperature on hydrocracking product at LHSV=1 h^{-1}.

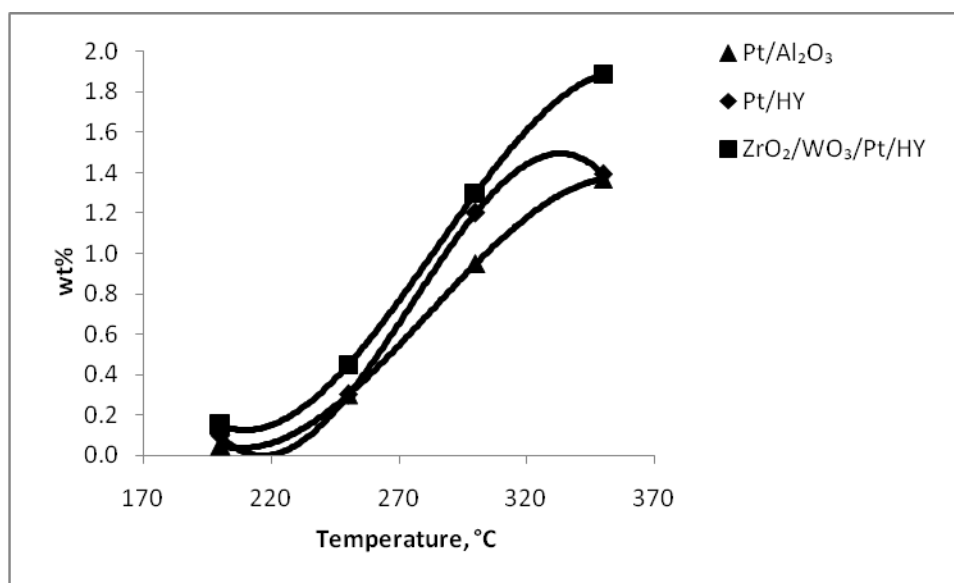**Fig.4**, The effect of temperature on hydrocracking product at LHSV=2 h^{-1}.

Fig.5, The effect of temperature on hydrocracking product at LHSV=3 h^{-1}.

HYDROISOMERIZATION ACTIVITY

The hydroisomerization of light naphtha over Pt loaded catalyst types is influenced by the LHSV, reaction temperature and the support base, as shown in Figs.6-9. All results indicate that, the low LHSV is favored for hydroisomerization of naphtha as discussed previously. Also the results show a remarkable rise in an isomerization activity, for all the tested catalyst and as the temperature raises till 300°C, and then isomerization activity began to decrease due to the cracking activity.

Since isomerization reaction is slightly exothermic, a low temperature favors the production of light naphtha isomers with high octane level. The data illustrated in a Table 2 and Figs. 6-9 indicate that Pt/ Zr/W/ HY zeolite produced the highest light naphtha isoparaffins through the temperature range 240-370°C as a compared to the other catalysts.

It is will known that HY zeolite has much stronger acidity than amorphous alumina, by the fact that the production of carbenium ion is energetically favored over that of carbonium ions. At higher temperature, i.e. above 300°C, the formation of carbonium is much faster than the carbenium ion and lead to the formation cracked product at the dehydrogenated site. That due to the fact of cracking reaction are endothermic, so a high temperature favors the production of cracked hydrocarbon (Gluseppe et al.,1986).

At a high temperature operation (>300°C) and from analogy to liquid phase, super acid chemistry, the monomolecular or protolytic cracking mechanism was originally proposed to proceed through a non-classical, penta-coordinated carbonium ion resulting from the proton attack of C-C or C-H bonds. Recent compulational and experimental of studies have suggested a distorted, strongly surface-coordinated transition state as opposed to a stable, carbonium ion intermediate. This perhaps explains why carbonium ions have not been directly observed in a zeolite. Monomolecular cracking become important under the limiting conditions of very low alkene coverage which implies high temperature, low partial pressure and low conversion of naphtha. (Hello et al., 2002) and (Willimas et al., 2000).
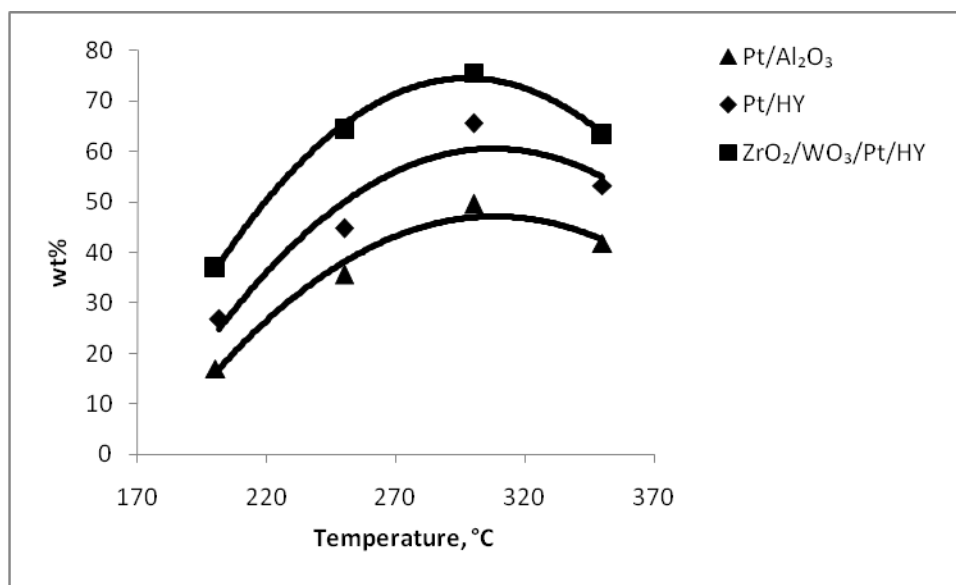
M.Al-Hassany
Effect of ZrO$_2$, WO$_3$ additives on catalytic performance
Of Pt/HY zeolite compared with Pt/γ-Al$_2$O$_3$ for Iraqi
Naphtha transformation

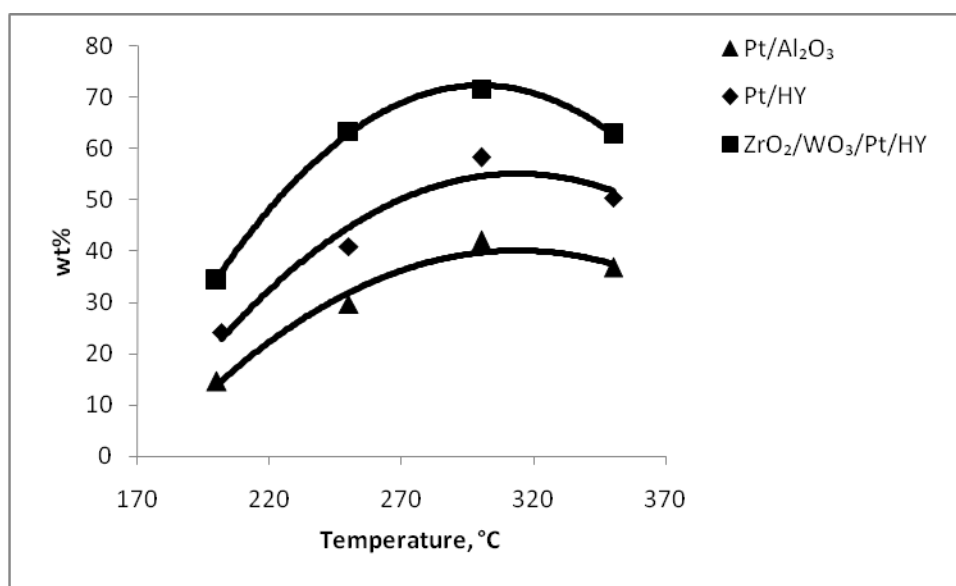**Fig.6,** Isomers yield versus reaction temperature at LHSV=0.75 h^{-1}.

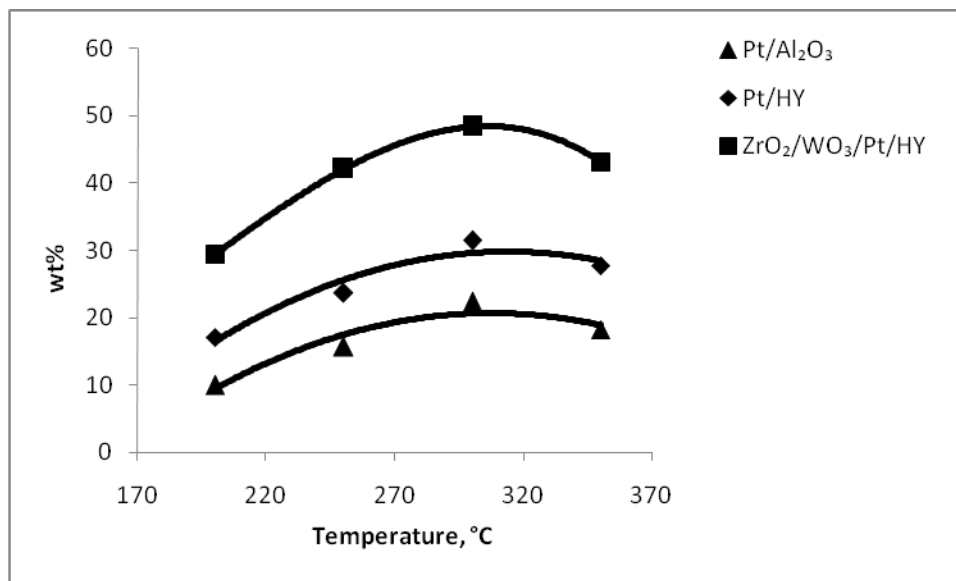**Fig.7,** Isomers yield versus reaction temperature at LHSV=1 h^{-1}.

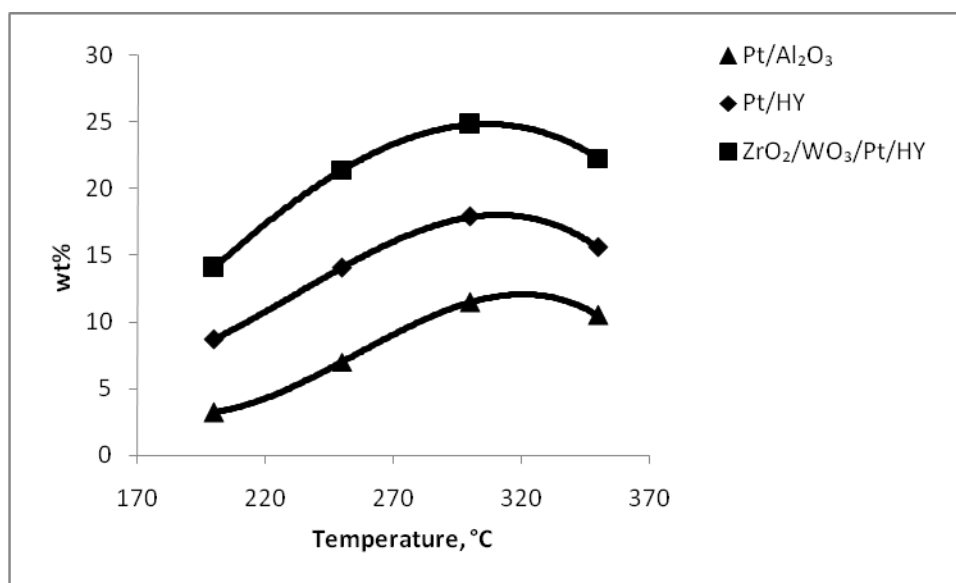**Fig.8**, Isomers yield versus reaction temperature at LHSV=2 h^{-1}.

Fig.9, Isomers yield versus reaction temperature at LHSV=3 h^{-1}.

HYDROCYCLIZATION AND AROMATIZATION ACTIVITIES

It is well known that Pt/γ-Al$_2$O$_3$ has higher activity for the direct dehydrogenation of naphthenes to benzene than Pt/HY catalyst as shown in the figs 10-17. The production of benzene by the enlargement of C$_5$ cyclic ring to a C$_6$ cyclic ring.

The kinetic diameter of hexane is 4.8 Å, with an increase of about 0.7 Å for every additional increase in branch length, the kinetic diameters of benzene and cyclohexane are 6.75 and 6.9 Å respectively (Jan Ku et al., 1988). The fact that the hydrocarbons have a kinetic diameter greater than half the effective pore diameter of Zr/W/Pt/HY and Pt/HY as shown in Table 2 implies that any strongly adsorbed C$_6$ would create a barrier to diffusion of other C$_6$ .Thus strongly adsorbed C$_6$ cyclic can induce resistance to the mass transfer of

M.Al-Hassany   Effect of ZrO_2 , WO_3 additives on catalytic performance
Of Pt/HY zeolite compared with Pt/γ-Al_2O_3 for Iraqi
Naphtha transformation

a n-hexane to the pore interior, resulting in an induced pore blockage. With the Zr/W/Pt/HY and Pt/HY zeolite catalysts, an initial increase in a catalyst activity can be observed after 3 hours reaction, the activity is very stable (are practically identical before and after the various changes in operating conditions). While the Pt/γ-Al_2O_3 bed appears white at the inlet and increasingly dark colored, indicating coke formations, toward the reactor exit.

      It was found that Zr/W/Pt/HY and Pt/HY stimulate to a much higher extent than Pt/γ-Al_2O_3, the skeletal isomerization reaction of C_5/C_6 and in a lower extent the production of benzene by enlargement of C_5 cyclic ring to a C_6 cyclic ring. In contrast, Pt/γ-Al_2O_3 enhances to a greater extent the direct dehydrogenation of C_6 to benzene than the other catalysts (Mohamed and Ahmed, 2004),
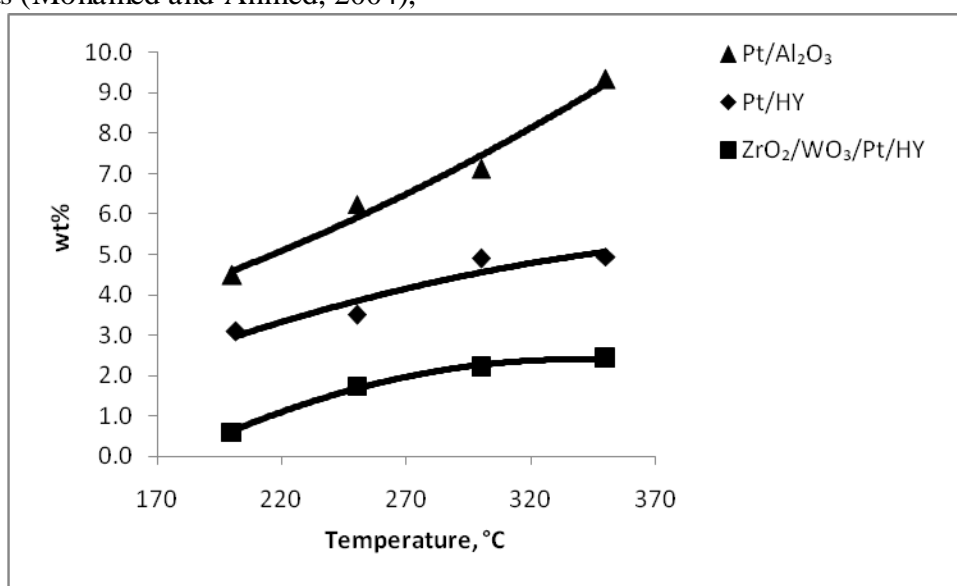
Fig.10, Percent of hydrocyclization products versus reaction temperature at LHSV=0.75 h^{-1}.

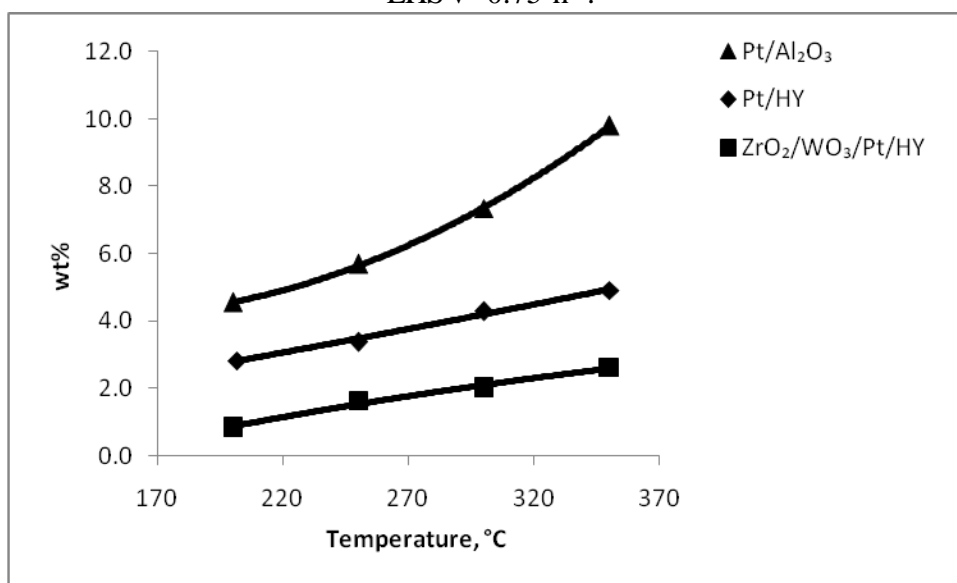**Fig.11**, Percent of hydrocyclization products versus reaction temperature at LHSV=1 h^{-1}.
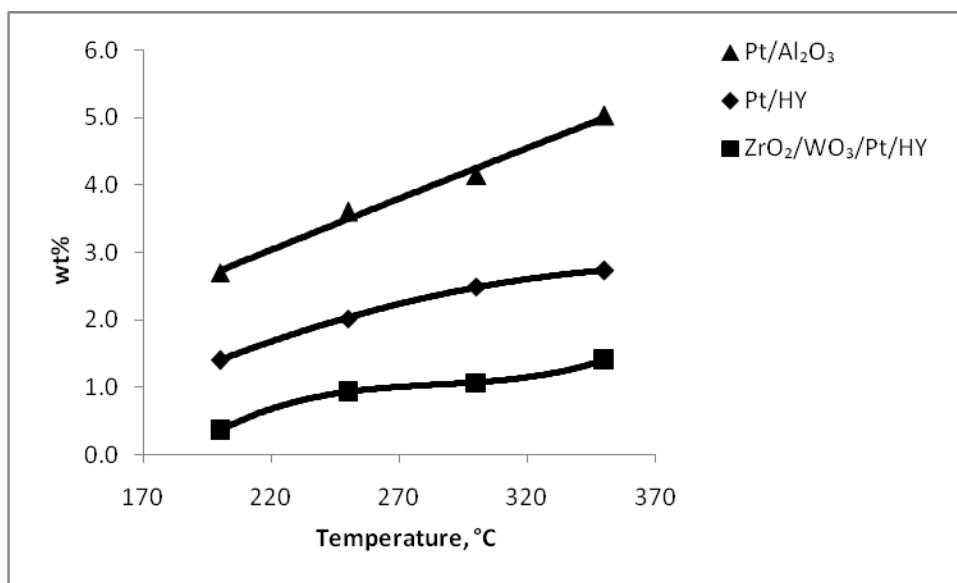
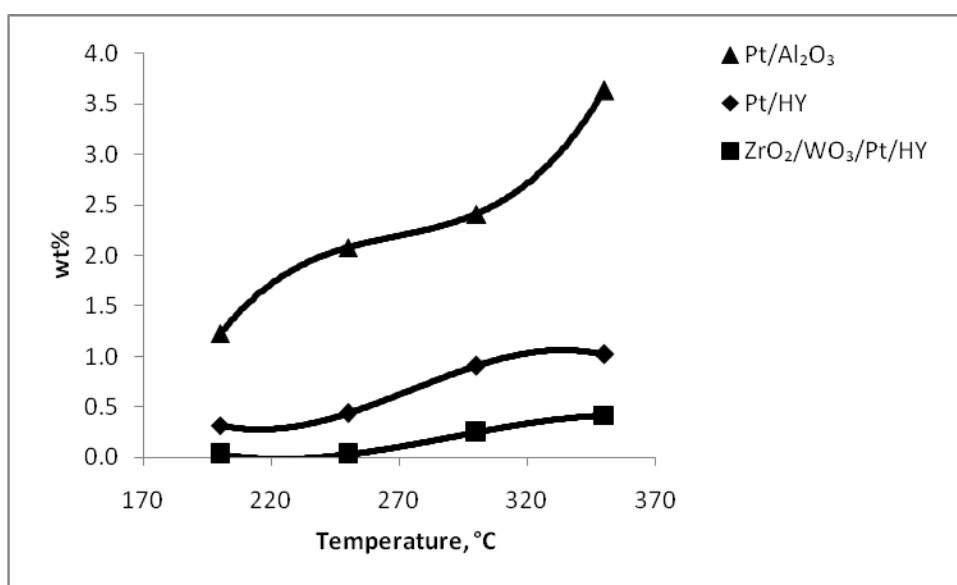**Fig.12,** Percent of hydrocyclization products versus reaction temperature at LHSV=2 h^{-1}.

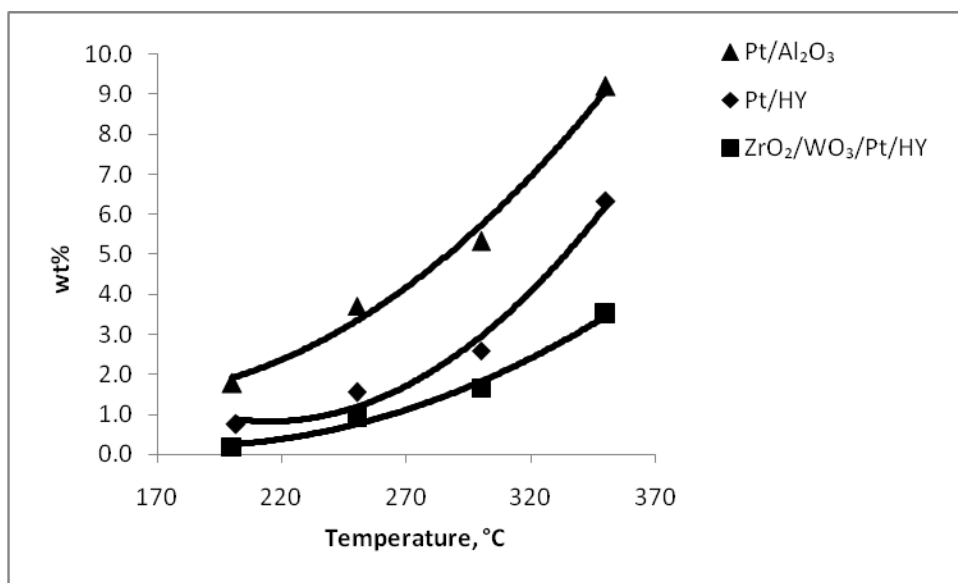**Fig.13,** Percent of hydrocyclization products versus reaction temperature at LHSV=3 h^{-1}.

M.Al-Hassany   Effect of ZrO_2 , WO_3 additives on catalytic performance
Of Pt/HY zeolite compared with Pt/γ-Al_2O_3 for Iraqi
Naphtha transformation

Fig.14, Percent of aromatics versus reaction temperature at LHSV=0.75 h^{-1}.
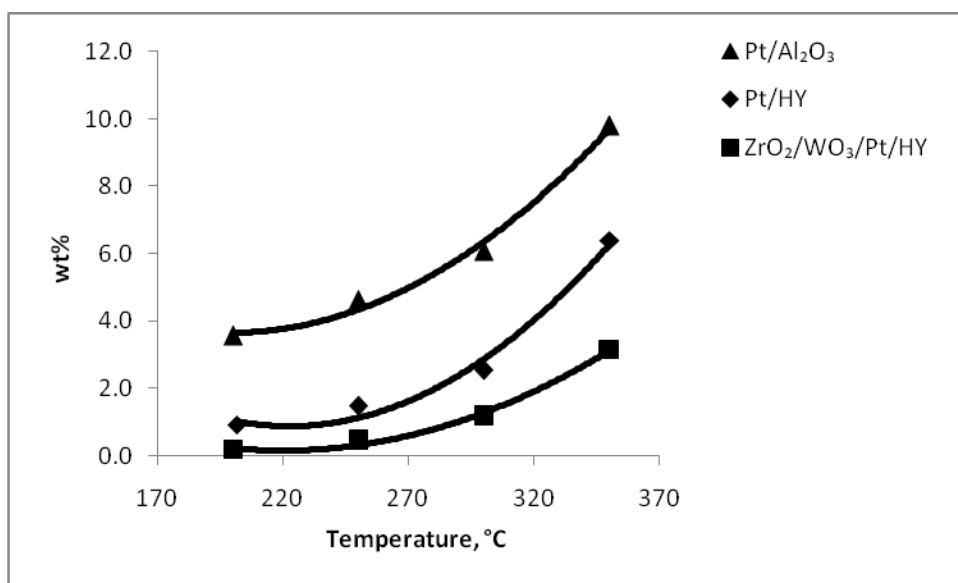
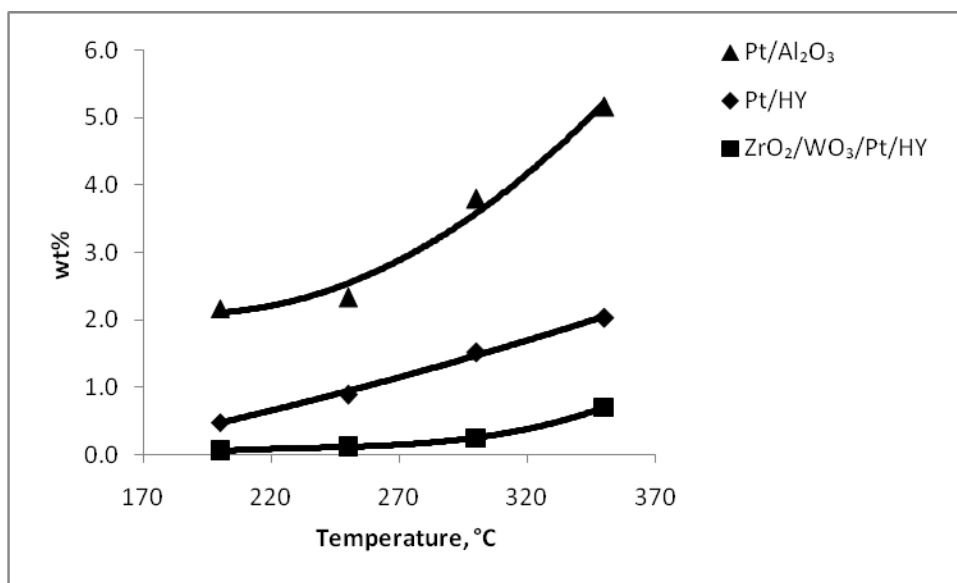**Fig.15,** Percent of aromatics products versus reaction temperature at LHSV=1 h^{-1}.

Fig.16, Percent of aromatics products versus reaction temperature at LHSV=2 h^{-1}.
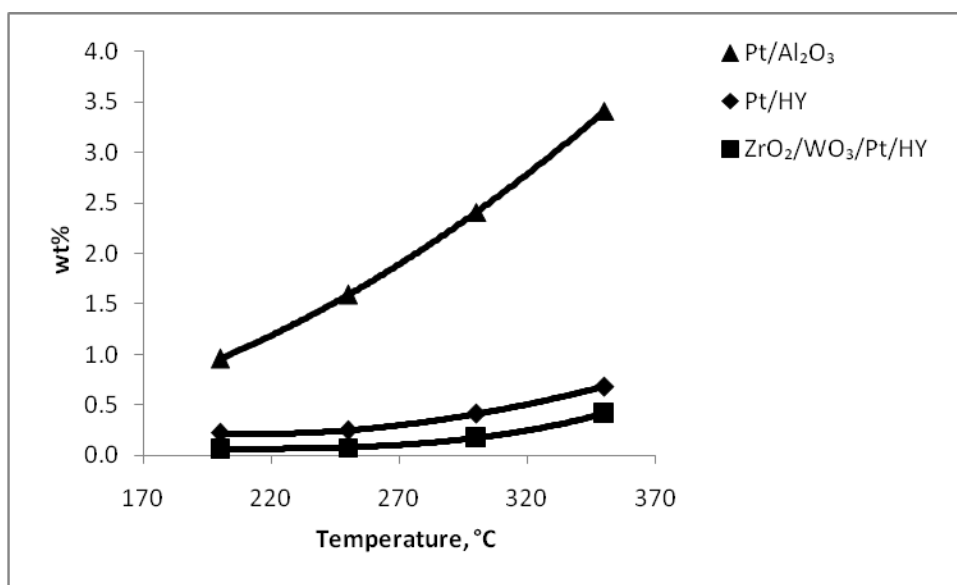

Fig.17, Percent of aromatics products versus reaction temperature at LHSV=3 h^{-1}.

CONCLUSION

It is found that Pt/Zr/W/HY is the best catalyst for producing isoparffines due to its higher acidity compared with Pt/HY and Pt/ γ-Al$_2$O$_3$ .The Pt/Zr/W/HY catalyst showed lower activity for aromatization of naphtha to cyclopareffins and benzene selectivity than Pt/HY and Pt/ γ-Al$_2$O$_3$ due to their pore volume.

A smaller pore volume leads to lower aromatization activity and higher isomerization and cracking activity.

The maximum isoparaffins extent was achieved and reached 78% at 300°C and LHSV of 0.75 hr^{-1} on Pt/Zr/HY and aromatics extent was reached 10% at 370°C and LHSV of 0.75 hr^{-1} on Pt/ γ-Al$_2$O$_3$.

M.Al-Hassany   Effect of ZrO_2 , WO_3 additives on catalytic performance
Of Pt/HY zeolite compared with Pt/γ-Al_2O_3 for Iraqi
Naphtha transformation

REFERENCES

- Alvarez F., F.R.Ribeiro, G.Perot, Thomazeau, and M.Guisnet, 1996, "Hydroisomerization and hydrocracking of alkanes" , J.cat., 162, 174-180.

- Eder F., Stockenhuber M., Lercher J.A.,1997 , "On the role of pore size and tortuosity for sorption of alkanes in molecular sieves ", J. Phys. Chem. B: 101, 5411-5419 .

- Gauw F.J.M., Grandell J., Santen R.A., 2002, "The intrinsic kinetics of n-hexane isomerization catalyzed by Pt loaded solid acid catalyst", J. Cat. 206, 295-304.

- Gluseppe E. Glannetto, Guy R. Perot, and Michel R. Gulenet, 1986, "Hydroisomerization and hydrocracking of n-alkanes.1. Ideal hydroisomerization PtHY catalysts", Ind. Eng. Chem. Prod. Res. Dev., 25, 481-490.

- Hollo, J. Hancsok, D. Kallo, 2002, "Kinetics of hydroisomerizaion of C_5-C_7 alkanes and their mixture over platinum containing mordenite" A Applied Cat. A: General, 229, 93-102.

- Jan-Ku, Chen, A.M. Martin, Young Gull Kim and Vijay T. John, 1988, *"Mechanical study of isomerization of n-hexane", Ind. Eng.* 27, 401-409.

- Jeong Kyu Lee, Hyun-ku Rhee, 1997, "Characteristics of Pt/HY-beta and Pt/H-mordenite catalyst for the isomerization of n-alkane", Catalyst Today, 38, 235-242.

- Jolly, J.Saussey, M. Bettahar, J.C. Lavalley, 1997, "Reaction mechanisms and kinetics in n-hexane cracking", 156, 71-96.

- Lawlor, Lawrence J., Marphy, William J., 1988, "Naphtha isomerization using a medium", US patent, 4734539.

- Masologites., George,1987, "Method of treating a used Pt group alumina catalyst with a metal promoter", US patent, 4070306.

- Mohamed L, Kh. and Ahmed H.S., 2004, "Isomerization of light over Pt containing support", Egypt J. chem. 47, 3, 293-303.

- Rafael Roldan, Anderew M. Beale, Manuel S. S., Francisco., Romero, Cesar, Juan P., Gopinathan,2008, "Effect of the impreantion order on the nature of the metal particles", J. Cat., 254 ,12-26.

- Srikant Gopal, 2003, "Synthesis, Modification, Characterization and catalytic study of zeolite" Ph.D. Thesis, university of cininnati.

- Ward, J.W.,1993,"Fuel Process Technol",35,55.

- Williams B.A, W. Ji, Miller, Snurr, 2000, "Evidence of a different reaction mechanisms during the cracking of n-hexane" Applied Cat. A: General, 203,179-190.

- Yan Liu,Yejun Guan,Can Li, Juan L.,Geok J., Eng Chew, Fethi K.,2006,"Effect of ZnO additives and acid treatment on catalytic performance of Pt/W/Zr for heptane isomerization,"J. of cat.244,17-23.

THE EFFECT OF SELF-EQUILIBRATING STRESSES DUE TO MULTI-LINE SPOT WELDED STIFFENERS ON THE NATURAL FREQUENCIES OF PLATE

Dr. Faiz F. Mustafa
University of Baghdad
AL-Khwarizmi college of Eng.

Dr. Kareem N. Salloomi
University of Baghdad
AL-Khwarizmi college of Eng.

Sahar M. Saliman
University of Baghdad
College of Engineering

ABSTRACT

In this paper an investigation has been made into the effect of residual stresses on the vibration characteristics of a thin rectangular stainless steel plate with multi-line spot welded stiffeners. A new general frequency equation with and without the effect of residual stresses due to multi-line spot welding along the length and width of the plate for different boundary conditions were obtained. The results give that the free ends tries to increase the natural frequencies while the clamped edges try to decrease the natural frequencies; also the central position weld line has the great influence on the natural frequencies.

الخلاصة

تم في هذا البحث دراسة تأثير الاجهادات المتبقية نتيجة اللحام النقطي لعدة خطوط عموديه وافقية على خصائص الاهتزازات بالنسبة الى الصفائح الرقيقة المقواة والمقاومة للصدأ. تم اشتقاق معادلات جديدة للترددات الطبيعية بوجود وعدم وجود تأثير الاجهادات المتبقية لعدد من خطوط اللحام النقطي بالأتجاه الطولي والعرضي للصفائح الرقيقة المقواة لبعض الحالات ذات حدود التثبيت المختلفة. حيث أظهرت النتائج ان النهايات الحرة تعمل على زيادة الترددات الطبيعيةعلى العكس من النهايات المقيدة والتي تعمل على التقليل من الترددات الطبيعية، أضـافةً" ان قيمة الاجهادات المتبقية وموقع خط اللحام له التأثير الكبير على الترددات الطبيعية.

KEYWORDS

Spot welding, Residual stresses, Vibration, Stiffened plate, Rectangular plate

INTRODUCTION.

The wide use of stiffened structural element in engineering began mainly with the application of steel plates for hulls of ships, steel bridges and aircraft structures. The stiffening usually has a small part of the total weight of the structure, substantially influence their strength and performance under different load conditions. Recently, Guo 2002, Jung 2002, and Nacy, 2002, studied the free vibration analysis of stiffened plates and shells, it was found that the stiffeners shape its distributions have a great effect on the natural frequencies and mode shapes of the plate.

F. F. Mustafa	The Effect of Self-Equilibrating Stresses Due to
K. N. Salloomi	Multi-Line Spot Welded Stiffeners on the
S.M. Saliman	Natural Frequencies of Plate

On the other hand, residual stresses are induced at each stage of the life cycle in most engineering component, from original material production to final disposal. Residual stresses are created by welding, forging, casting, rolling, machining, surface treatment, heat treatment etc.

Resistance spot welding is a process used for joining faying surfaces. Major advantages of resistance spot welding are high speed and suitability for automation. Many researches have been published regarding joining strength and residual stresses of spot welds, Berglund 2002, Bae 2003, and Xin 2005. Faiz 2006, studied the effect of spot distributions and residual stresses induced from spot welding, on the vibration characteristics of plates with one array of spot welded stiffeners on the longitudinal centerline of thin rectangular plate. Theoretical method based on the theory of bending of thin plate was used to obtain the governing differential equation; expressions of the exact frequency equation were derived. Finite element modeling was adopted to predict the tendom force produced due spot welding, finding the natural frequencies and mode shapes.

- VIBRATION ANALYSIS OF THE ORTHOTROPIC PLATES.

Due to the existence of stiffeners, the fundamental equation for small deflection theory of bending of thin plates is used to give the details of the theoretical analysis of residual stresses that result from welding and its effect on the natural frequencies and mode shapes. The governing differential equation of deflection for an orthotropic plates, subjected to a force (N_x per unite length) acting on the edges of the orthotropic plate, Timoshenko 1961, can be written as

$$D_x \frac{\partial^4 w}{\partial x^4} + 2H \frac{\partial^4 w}{\partial x^2 \partial y^2} + D_y \frac{\partial^4 w}{\partial y^4} = N_x \frac{\partial^2 w}{\partial x^2} \tag{1}$$

Where $H = D_{xy} + 2G_{xy}$ and D_x, D_y, D_{xy}, G_{xy} represents the flexural and torsional rigidities of an orthotropic plate respectively.

The strain energy stored in a plate element, Golf 1976, **Fig. 1**. is the sum of the work done by the bending moments, $M_x dy$ and $M_y dx$ and by the twisting moment $M_{xy} dy$ and $M_{xy} dx$, neglecting the work done by the shearing forces and by any stretching of the middle plane of the plate.

The work done by the bending moments is

½ * moment * angle between the sides of the element after bending.

In the xz plane the angle is: $-\left(\frac{\partial^2 w}{\partial x^2}\right) dx$, and in the yz plane : $-\left(\frac{\partial^2 w}{\partial y^2}\right) dy$

The negative singe occurs because a sagging downwards curvature (positive) has a decreasing slope as x increases. The energy stored due to bending (dU_b) is therefore given by:

$$dU_b = \frac{1}{2}\left(M_x \frac{\partial^2 w}{\partial x^2} + M_y \frac{\partial^2 w}{\partial y^2}\right) dxdy \tag{2}$$

The relative rotation of the element faces due to twist are $\dfrac{\partial^2 w}{\partial x \partial y} dx$ and $\dfrac{\partial^2 w}{\partial x \partial y} dy$

since $M_{xy} dy$ and $M_{yx} dx$ are the twisting moments, and $M_{xy} = M_{yx}$ the same amount of energy is stored by both couples. Then, total energy due to twisting (dU_t) is given by:

$$dU_t = M_{xy} \frac{\partial^2 w}{\partial x \partial y} dxdy \tag{3}$$

Substituting the expressions for the moments and adding (dU_b) and (dU_t) to produce the total energy stored in an element (dU), we get:

$$dU = \frac{1}{2}\left\{ D_x (\frac{\partial^2 w}{\partial x^2})^2 + 2D_{xy}(\frac{\partial^2 w}{\partial x^2}\frac{\partial^2 w}{\partial y^2}) + 4G_{xy}(\frac{\partial^2 w}{\partial x \partial y})^2 + D_y(\frac{\partial^2 w}{\partial y^2})^2 \right\} \tag{4}$$

This function is composed of the following elements:

½*(x-direction bending moments*rotation); $\dfrac{1}{2}\left\{ D_x (\dfrac{\partial^2 w}{\partial x^2})^2 + D_{xy}(\dfrac{\partial^2 w}{\partial x^2}\dfrac{\partial^2 w}{\partial y^2}) \right\}$

½*(y- direction bending moments*rotation); $\dfrac{1}{2}\left\{ D_y (\dfrac{\partial^2 w}{\partial y^2})^2 + D_{xy}(\dfrac{\partial^2 w}{\partial x^2}\dfrac{\partial^2 w}{\partial y^2}) \right\}$

½*(twisting moments*rotation); $\dfrac{1}{2}\left\{ G_{xy} (\dfrac{\partial^2 w}{\partial x \partial y})^2 \right\}$

The strain energy stored in a complete plate is obtained by integration eq. (4) over the surface.

$$U = \frac{1}{2}\iint \left\{ D_x (\frac{\partial^2 w}{\partial x^2})^2 + 2D_{xy}(\frac{\partial^2 w}{\partial x^2}\frac{\partial^2 w}{\partial y^2}) + 4G_{xy}(\frac{\partial^2 w}{\partial x \partial y})^2 + D_y(\frac{\partial^2 w}{\partial y^2})^2 \right\}dxdy \tag{5}$$

The maximum kinetic energy of the element, Len 1989, is:

$$\partial T = \frac{1}{2}\rho h \omega^\circ w^2 \partial x \partial y \tag{6}$$

ω° of the plate my be deduced from the energy balance. Than the angular frequency, Golf 1976:

$$\int dU = \int dT \tag{7}$$

F. F. Mustafa	The Effect of Self-Equilibrating Stresses Due to
K. N. Salloomi	Multi-Line Spot Welded Stiffeners on the
S.M. Saliman	Natural Frequencies of Plate

- RESIDUAL STRESS ANALYSIS.

It is assumed in the following analysis that any cross-section (x and y = constant), the plate is under longitudinal compression distribution uniformly a cross the breadth of the plate, with the equilibrating tension concentrated on the line of spot welding at $(y = r_{yi})$, for each line of welding across the length of the plate.

Also, the plate under longitudinal compression distributed uniformly a cross the width of the plate, with the equilibrating tension concentrated on the line of welding at and deflection $(x = r_{xi})$, for each line of spot welding across the width of the plate **Fig. 2**.

The component of maximum strain energy of the element due to the mid-plane forces, Timoshenko 1961, **Fig. 1**, is:

$$\partial U_r = \frac{1}{2} N_x (\frac{\partial w}{\partial x})^2 \partial x \partial y + \frac{1}{2} N_y (\frac{\partial w}{\partial y})^2 \partial x \partial y \tag{8}$$

The strain energy due to the mid-plane forces may therefore be written, by eq. (8) as

$$U_r = \frac{1}{2} N_x \left\{ \int_{-a}^{a}\int_{-b}^{b} (\frac{\partial w}{\partial x})^2 dxdy - b \int_{-a}^{a} (\frac{\partial w}{\partial x})^2 \Big|_{y=r_{yi}} dx \right\} + \frac{1}{2} N_y \left\{ \int_{-a0}^{a}\int_{-b}^{b} (\frac{\partial w}{\partial y})^2 dxdy - a \int_{-b}^{b} (\frac{\partial w}{\partial y})^2 \Big|_{x=r_{xi}} dy \right\} \tag{9}$$

In this case N_{xi} and N_{yi} is a negative constant, Golf, 1976. In the case of the mechanical system shown in **Fig. 3**. The total strain energy and kinetic energy are:

$$U = \frac{1}{2} \int_{-a}^{a}\int_{-b}^{b} \left\{ D_x (\frac{\partial^2 w}{\partial x^2})^2 + 2D_{xy} (\frac{\partial^2 w}{\partial x^2}\frac{\partial^2 w}{\partial y^2}) + 4G_{xy} (\frac{\partial^2 w}{\partial x \partial y})^2 + D_y (\frac{\partial^2 w}{\partial y^2})^2 \right\} dxdy +$$

$$\sum_{i=1}^{n} \left\{ \frac{1}{2} N_{xi} \left[\int_{-a}^{a}\int_{-b}^{b} (\frac{\partial w}{\partial x})^2 dxdy - b \int_{-a}^{a} (\frac{\partial w}{\partial x})^2 \Big|_{y=r_{yi}} dx \right] \right\} + \sum_{i=1}^{n} \left\{ \frac{1}{2} N_{yi} \left[\int_{-a}^{a}\int_{-b}^{b} (\frac{\partial w}{\partial y})^2 dxdy - a \int_{-b}^{b} (\frac{\partial w}{\partial y})^2 \Big|_{x=r_{xi}} dy \right] \right\} \tag{10}$$

$$T = \frac{1}{2} \rho h \omega^{\circ} \int_{-a}^{a}\int_{-b}^{b} w^2 dxdy \tag{11}$$

Then eq. (7) can be written as:

$$\int_{-a}^{a}\int_{-b}^{b} \frac{1}{2} \left\{ D_x (\frac{\partial^2 w}{\partial x^2})^2 + 2D_{xy} (\frac{\partial^2 w}{\partial x^2}\frac{\partial^2 w}{\partial y^2})^2 + 4G_{xy} (\frac{\partial^2 w}{\partial x \partial y})^2 + D_y (\frac{\partial^2 w}{\partial y^2})^2 \right\} dxdy +$$

$$\sum_{i=1}^{n} \left\{ \frac{1}{2} N_{xi} \left[\int_{-a}^{a}\int_{-b}^{b} (\frac{\partial w}{\partial x})^2 dxdy - b \int_{-a}^{a} (\frac{\partial w}{\partial x})^2 \Big|_{y=r_{yi}} dx \right] \right\} +$$

$$\sum_{i=1}^{n} \left\{ \frac{1}{2} N_{yi} \left[\int_{-a}^{a}\int_{-b}^{b} (\frac{\partial w}{\partial y})^2 dxdy - a \int_{-b}^{b} (\frac{\partial w}{\partial y})^2 \Big|_{x=r_{xi}} dy \right] \right\} = \frac{1}{2} \rho h \omega^{\circ} \int_{-a}^{a}\int_{-b}^{b} w^2 dxdy \tag{12}$$

In general the form of w is not know. However, if assumed form, normally chosen to satisfy the boundary conditions, is substituted in eq. (10). The displacement function $w(x, y, t)$ is approximated by means of the expansion, Kaldas 1981:

$$w(x, y, t) \cong w(x, y)\sin \omega t = \sin \omega t \sum_{ij} C_{ij} X_i(x) Y_j(y) \qquad (13)$$

Let the plate be placed in a coordinate system with the origin at its center and the edge (a) is parallel to X-axis and the edge (b) is parallel to Y-axis.

Table. 1. shows expressions of the displacement functions for different boundary conditions having one free edge. Substituting each expression separately in eq. (12), integrating over the given domains, applying boundary conditions and rearranging terms to obtain the final form of the frequency equation as listed below,

$$C_1 \frac{D_x}{a^4} + C_2 \frac{(D_{xy} + 2G_{xy})}{a^2 b^2} + C_3 \frac{D_y}{b^4} + \sum_{i=1}^{n} \frac{N_{xi}}{a^2} \{ A_1 + A_2 (\frac{r_{yi}}{b}) + A_3 (\frac{r_{yi}}{b})^2 + A_4 (\frac{r_{yi}}{b})^3 + A_5 (\frac{r_{yi}}{b})^4$$

$$+ A_6 (\frac{r_{yi}}{b})^5 + A_7 (\frac{r_{yi}}{b})^6 + A_8 (\frac{r_{yi}}{b})^7 + A_9 (\frac{r_{yi}}{b})^8 \} + \sum_{i=1}^{n} \frac{N_{yi}}{b^2} \{ B_1 + B_2 (\frac{r_{xi}}{a}) + B_3 (\frac{r_{xi}}{a})^2 + B_4 (\frac{r_{xi}}{b})^3$$

$$+ B_5 (\frac{r_{xi}}{a})^4 + B_6 (\frac{r_{xi}}{a})^5 + B_7 (\frac{r_{xi}}{a})^6 + B_8 (\frac{r_{xi}}{a})^7 + B_9 (\frac{r_{xi}}{a})^8 \} = K\rho h \omega_s^{\circ}$$

$$(14)$$

where $C_1, C_2, C_3, A_1, A_2, A_3, A_4, A_5, A_6, A_7, A_8, A_9, B_1, B_2, B_3, B_4, B_5, B_6, B_7, B_8, B_9$ and K are constants depending on the boundary conditions as tabulated in **Table. 2**.

For the stress free condition (no residual stresses $N_{xi} = N_{yi} = 0$), then eq. (14) reduced to:

$$C_1 \frac{D_x}{a^4} + C_2 \frac{(D_{xy} + 2G_{xy})}{a^2 b^2} + C_3 \frac{D_y}{b^4} = K\rho h \omega_s^{\circ} \qquad (15)$$

If $i = 1, r_{xi} = r_{yi} = 0$, this meaning the lines of welding along the length and width of the plate are at the center, and all constant in **Table. 2,** will be zero excepts $C_1, C_2, C_3, A_1, B_1,$ and k.

- RESULTS AND DISCUSSIONS.

An easy procedure was used in this paper to predict the effect of residual stresses due to multi-line of welding along the length and width of a spot welded stiffened plate on the natural frequency. A stainless steel plate of dimensions (120*100*0.6 mm) and a stiffener of (120*20*0.6 mm) were connected by spot welding. The plate and stiffener were assumed of the material with (E=207*10³ N/mm^2 , G=80*10³ N/mm^2 and $\upsilon = 0.3$) . In this study three different boundary conditions with one edge is free were discussed (C.C.C.F., C.C.S.F. and S.C.S.F.).

Fig. 4,5 and 6. shows the variation of the fundamental frequencies with welds self-equilibrating stresses on the longitudinal and perpendicular center lines in a thin stiffened rectangular plate with edges C.C.C.F. . As shown in **Fig. 3**, the mid-plane forces N_X exist at any position along the width of the stiffener will decrease the natural frequency by a percent of (21.5% max.) beyond that of free-stress. The frequency change may be

F. F. Mustafa	The Effect of Self-Equilibrating Stresses Due to
K. N. Salloomi	Multi-Line Spot Welded Stiffeners on the
S.M. Saliman	Natural Frequencies of Plate

understood in terms of energy. For given amplitude of vibration the variation of strain energy in a cycle, largely due to the basic flexural and torsional stiffness of the plate is modified through the work done by the in-plane stresses under mid-plane extension. In the present case the in-plane stresses reduce the total exchange between potential and kinetic energy, and a reduction in frequency therefore follows. On the other, hand the mid-plane forces N_y exist along the length of the plate will increase the natural frequency by a percent of (33.3% max) beyond that of free stress except at the edges in which the natural frequency will decrease beyond that of free stress case. This discussion may be valid also to other cases of boundaries (i.e C.C.S.F. and S.C.S.F.) as shown in **Fig. 7,8,9,10,,11 and 12**, these results gives a good agreement with the analytical results obtained by Dickinson, 1978, without including the residual stress and Golf, 1976, Al-Ammir, 2004, with including the residual stresses.

Fig. 5,8 and 11, shows that the position of spot weld line have a great influence on the natural frequencies when it lays parallel to the clamped edge and it have a little influence a long the free edge parallel to the length of the plate. The changing of residual stress have a significant effect on the magnitude of natural frequency, It is clear that the natural frequency decreased with increasing the magnitude of residual stress spatially near the clamped edge and less pronounced near the free edge as shown in **Fig. 13,15 and 17**. On the other hand **Fig. 6,9 and 12**, indicate that the central position spot weld line increased the natural frequency while the natural frequency decreased when it lays near the edges along the width of the plate.

Fig. 14,16 and 18, gives the effect of magnitude of residual stresses on the natural frequency along the width of the plate, it clear that the natural frequency increased with increasing the magnitude of residual stresses when the spot weld line lays at the middle of plate and decreased with increasing of residual stresses at the two edges of the plate with a little different for case 2 as shown in **Fig. 16**, which have an identical edges along the width of the plate.

CONCLUSIONS

An important conclusion is that the boundary condition and amount of residual stresses have important factors and significant influence on the natural frequency, the free ends tries to increase the natural frequency while the clamped edges try to decrease the natural frequency, this is so clear in **Fig. 5,8 and 11,** therefore in case of C.C.C.F. spot welded plate the free end increased the natural frequency by a percent of 48.39% max., while in case of C.C.S.F. spot welded plate by a percent of 29.05% max., and in case of S.C.S.F. spot welded plate by a percent of 24.28% max.. Also the results give an indication that the central position weld line has the great influence on the natural frequency and this is shown well in **Fig. 6,9 and 12,** so, in case of C.C.C.F. spot welded plate the increase was 48.91% max., while in case of C.C.S.F. spot welded plate by a percent of 35.94% max., and in case of S.C.S.F. spot welded plate by a percent of 26.37% max .

REFERENCES

- Al-Ammri, "A Comparative Study between the (VSR) and Post-Weld Heat Treatment on the Fatigue Life Characteristic of Steel," Ph.D. Thesis, University of Baghdad, College of Engineering, Mechanical Department, 2004.

- Bae D. H., Sohn I. S., and Hong J. K., "Assessing the Effects of Residual Stresses on the Fatigue Strength of Spot Welds", Welding Journal, 18-23, (2003).

- Berglund D., and Runnemalm H., "Comparison of Deformation Pattern and Residual Stresses in Finite Element Models of a TIG-Welded Stainless Steel Plate", Volvo Aero Corporation, Manufacturing Process Development, Sweden, (2002).

- Dickinson, S. M., "The Buckling and Frequency of Flexural Vibration of Rectangular, Isotropic and Orthotropic Plate Using Rayleigh's Method," Journal of Sound and Vibration, 61, pp. 1-8, 1978.

- Faiz et al, "Static and Dynamic Analysis of Plates with Spot Welded Stiffeners" Ph.D. Thesis, Mechanical Engineering, Baghdad University, October 2006.

- Golf, P., "The Effect of Self-Equilibrating Stresses on the Natural Frequencies of a Free-Free Rectangular Plate," Journal of Sound and Vibration, 47, pp. 85-94, 1976.

- Guo M., Harik I. E., and Ren W. X., "Free Vibration Analysis of Stiffened Laminated Plates Using Layered Finite Element Method", Structural Engineering and Mechanics, 14, 245-262, (2002).

- Jung J. Y., and Kim J. H., "Vibration Control of Stiffened Plates With Integrated Piezoelectrics", School of Mechanical and Aerospace Engineering. Coll. of Engineering, Seoul, Korea, (2002).

- Kaldas M. M. and Dickinson S. M., "The Flexural Vibration of Welded Rectangular Plate", Journal of sound and vibration, 75(2), pp. 163-178, 1981.

- Len Groud, "The Welding" , Hodder and Straughton, 1989.
- Nacy S. M., Abdullah M. Q., and Ali M. M., "Free Vibration Analysis of Stiffened Conical Shell", Journal of Engineering, Coll. of Engineering, Baghdad University, 8, 263-275, (2002).

- Timoshenko S. P. and Gere J. M., "Theory of Elastic Stability of Plate", McGraw-Hill, New York, 1961.

- Xin Long, "Finite Element Analysis of Residual Stress Generation During Spot Welding and its Affect on Fatigue Behavior of Welded Joint", Ph.D. Thesis, University of Missouri-Columbia, December, (2005).

F. F. Mustafa	The Effect of Self-Equilibrating Stresses Due to
K. N. Salloomi	Multi-Line Spot Welded Stiffeners on the
S.M. Saliman	Natural Frequencies of Plate

SYMBOLS:

a, b	Plate side length (mm)
D	Flexural rigidity of an isotropic plate (N.mm)
Dx,Dy	Flexural rigidity of an orthotropic plate in x and y directions
Dxy	Torsional rigidity of an isotropic plate
G	Shear modulus of isotropic material (N/mm^2)
Gxy	Shear modulus of orthotrpic material
H	Enthalpy of material (W.S.C/mm^3)
h	Plate thickness (mm)
Mx,My	Bending moment in x,y direction (N.mm)
Mxy	Twisting moment (N.mm)
Nx, Ny	Edge forces per unit distance (N/mm)
r_{xi}, r_{yi}	Welding position along the x and y-axis (mm)
T	Kinetic energy of the element (W)
t	Time (sec)
U	Strain energy stored in complete plate (W)
Ub	Strain energy stored due to bending (W)
Ut	Strain energy stored due to twisting (W)
Ur	Strain energy stored due to concentrated force (W)
u, v, w	Displacement components in x,y,z directions
x, y, z	Cartesian coordinates
C-C-C-F	Clamped-Clamped-Clamped- Free
C-C-S-F	Clamped-Clamped-Simply- Free
S-C-S-F	Simply-Clamped-Simply-Free
ρ	Mass density (Kg/mm^3)
ω°	Angular frequency (rad/S)
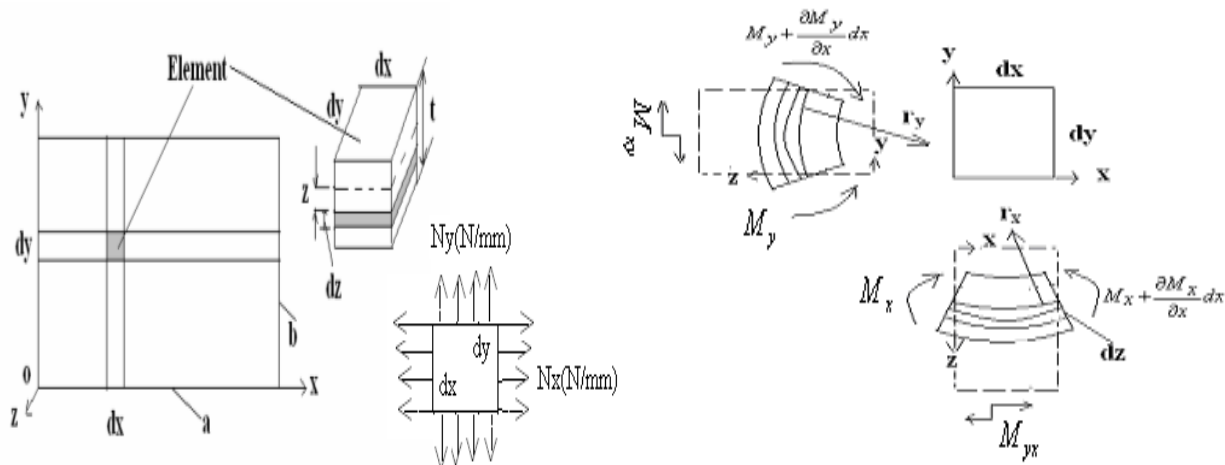
Fig. (1) Thin plate in Bending

Spot welding

Residual stress distribution on section A-A

A

Compression

Tension
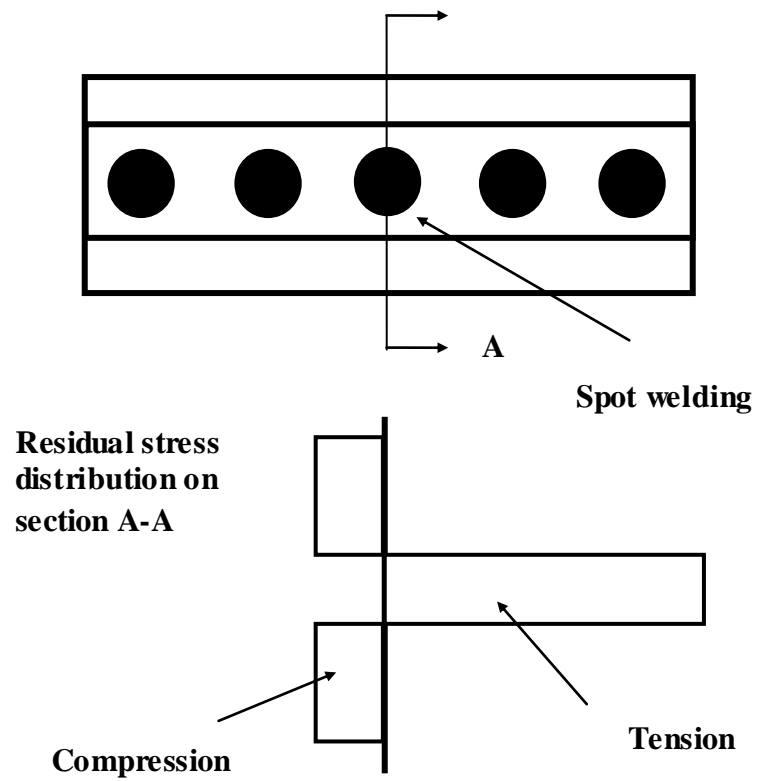
Fig.(2) Plane Loading of a Stiffened Plate.

F. F. Mustafa	The Effect of Self-Equilibrating Stresses Due to
K. N. Salloomi	Multi-Line Spot Welded Stiffeners on the
S.M. Saliman	Natural Frequencies of Plate

Lines of Welding
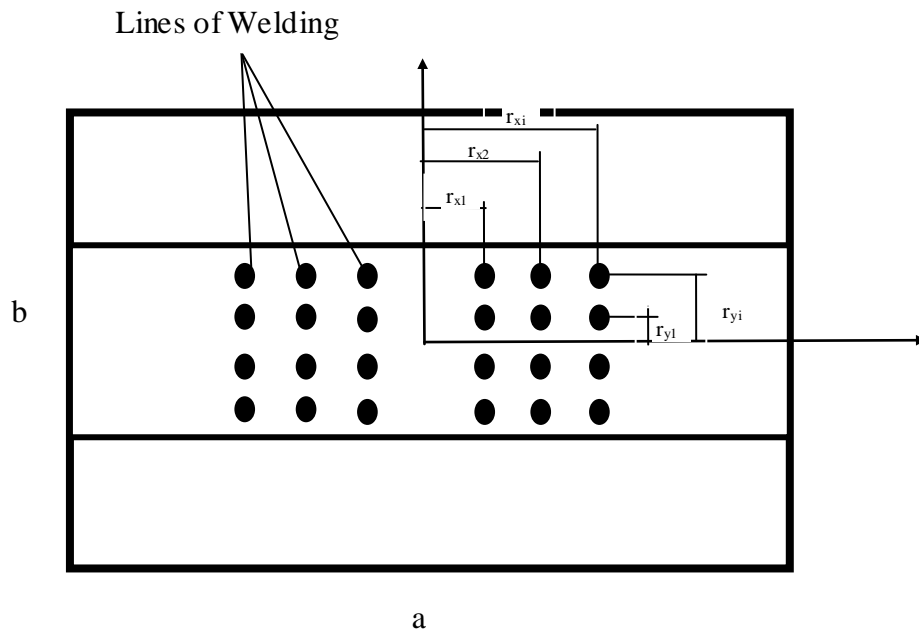
Fig.(3) Plane Loading of a Plate

Table 1 Displacement functions

Boundary Conditions	Displacement Functions
C-C-C-F	$w = C[(\frac{2x}{a})^2 - 1]^2[1 + \frac{56}{17}(\frac{y}{b}) + \frac{24}{17}(\frac{y}{b})^2 - \frac{32}{17}(\frac{y}{b})^3 + \frac{16}{17}(\frac{y}{b})^4]\sin\omega t$
C-C-S-F	$w = C[1 + \frac{x}{a} - 6(\frac{x}{a})^2 - 4(\frac{x}{a})^3 + 8(\frac{x}{a})^4][1 + \frac{56}{17}(\frac{y}{b}) + \frac{24}{17}(\frac{y}{b})^2 - \frac{32}{17}(\frac{y}{b})^3 + \frac{16}{17}(\frac{y}{b})^4]\sin\omega t$
S-C-S-F	$w = C[1 - \frac{6}{5}(\frac{2x}{a})^2 + \frac{1}{5}(\frac{2x}{a})^4][1 + \frac{56}{17}(\frac{y}{b}) + \frac{24}{17}(\frac{y}{b})^2 - \frac{32}{17}(\frac{y}{b})^3 + \frac{16}{17}(\frac{y}{b})^4]\sin\omega t$

Table 2 Values of the constants C$_1$, C$_2$, ……,K

Constant	C-C-C-F	C-C-S-F	S-C-S-F
C1	1	1	1
C2	69.312/504	64.77/238.73	56.24/97.54
C3	32.358/504	32.358/238.73	32.358/97.54
A1	163428/10253	2941704/194807	4167414/317843
A2	-1028160/10253	-18506880/194807	-26218080/317843
A3	-2134080/10253	-2021760/10253	-54419040/317843
A4	-864000/10253	-15552000/194807	-22032000/317843
A5	1330560/10253	23950080/194807	33929280/317843
A6	-138240/10253	-2488320/194807	-3525120/317843
A7	-967680/10253	-17418240/194807	-24675840/317843
A8	552960/10253	9953280/194807	14100480/317843
A9	-138240/10253	-2488320/194807	-3525120/317843
B1	-1211760/71771	-16899840/1363649	-25317360/2224901
B2	0	-9331200/194807	0
B3	4665600/10253	51321600/194807	69984000/317843
B4	0	9331200/194807	0
B5	-27993600/10253	-205286400/194807	-214617600/317843
B6	0	-298598400/194807	0
B7	74649600/10253	373248000/194807	223948800/317843
B8	0	298598400/194807	0
B9	-74649600/10253	-298598400/194807	-74649600/317843
K	1/504	1/238.73	1/97.54

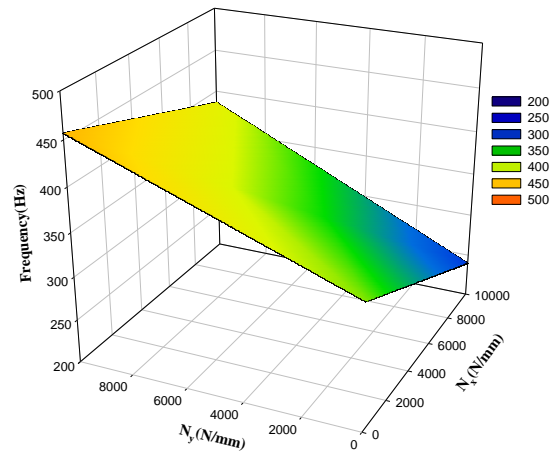| F. F. Mustafa | The Effect of Self-Equilibrating Stresses Due to |
| K. N. Salloomi | Multi-Line Spot Welded Stiffeners on the |
| S.M. Saliman | Natural Frequencies of Plate |

Case one: C.C.C.F.

Fig.(4) Fundamental Frequency due to the Self-Equilibrating Stresses at the Longitudinal and Perpendicular Centerlines of a C.C.C.F.
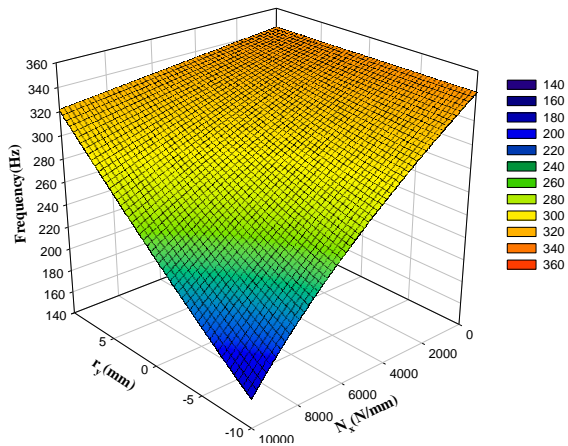**Stiffened Plate**

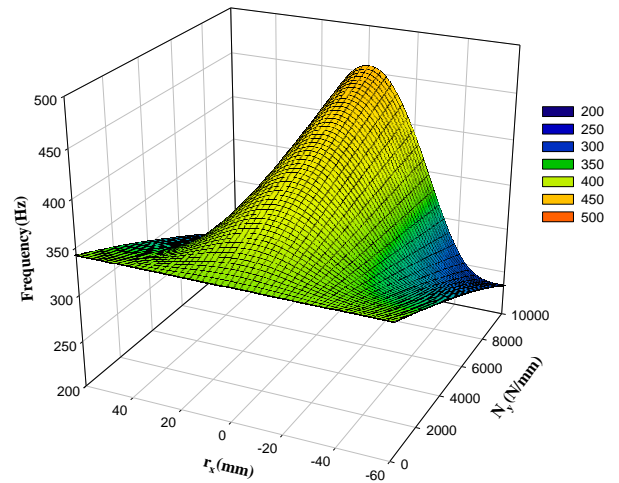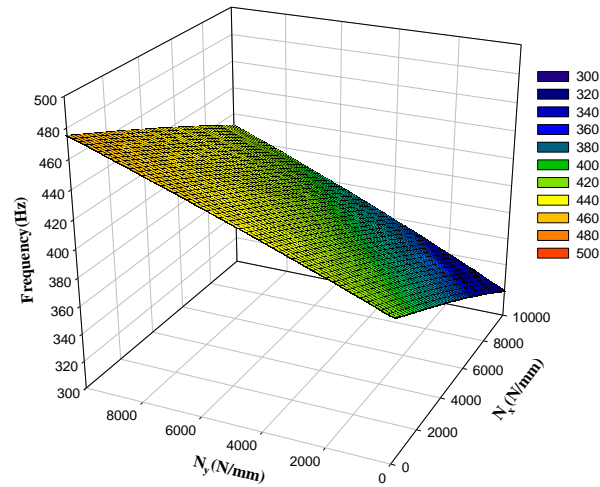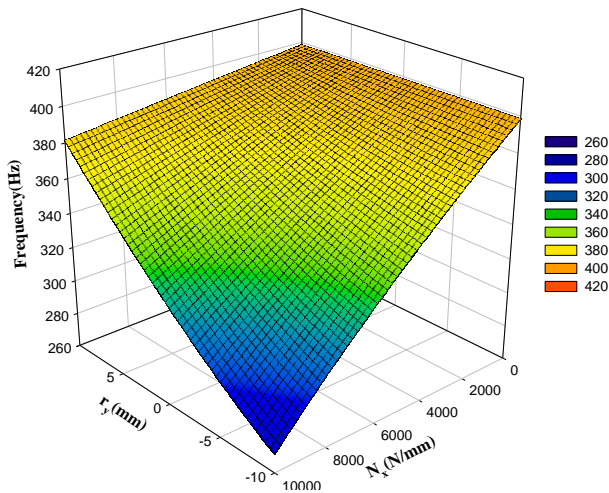**Fig.(5) Fundamental Frequencies of C.C.C.F. Stiffened plate due to the Longitudinal Self-Equilibrating Stresses**

Fig.(6) Fundamental Frequencies of C.C.C.F. Stiffened plate due to the Perpendicular Self-Equilibrating Stresses

Case two: C.C.S.F.

**Fig.(7) Fundamental Frequency due to the Self-Equilibrating Stresses at the Longitudinal and Perpendicular Centerlines of a C.C.S.F.
Stiffened Plate**

**Fig.(8) Fundamental Frequencies of C.C.S.F. Stiffened
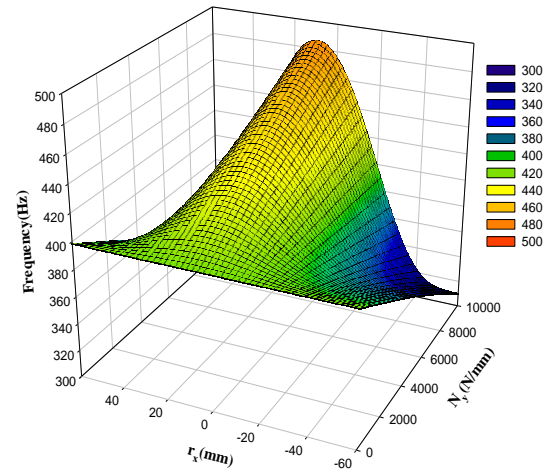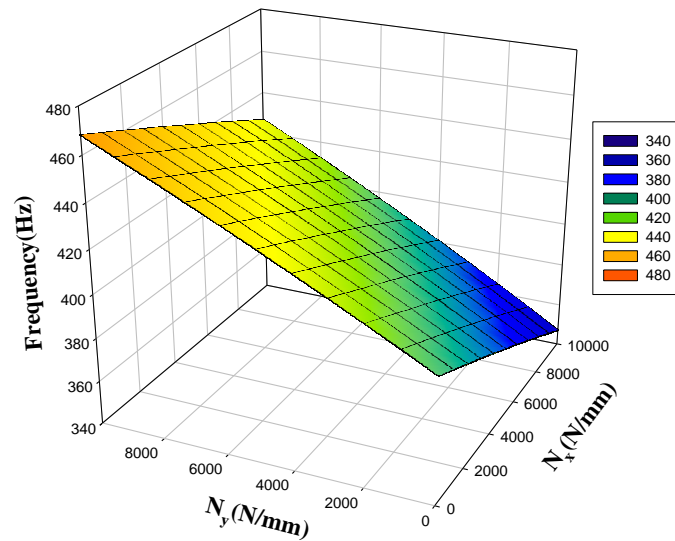plate due to the Longitudinal Self-Equilibrating Stresses**

**Fig.(9) Fundamental Frequencies of C.C.S.F. Stiffened
plate due to the Perpendicular Self-Equilibrating Stresses**

F. F. Mustafa	The Effect of Self-Equilibrating Stresses Due to
K. N. Salloomi	Multi-Line Spot Welded Stiffeners on the
S.M. Saliman	Natural Frequencies of Plate

__Case three: S.C.S.F.__

**Fig.(10) Fundamental Frequency due to the Self-Equilibrating Stresses at the Longitudinal and Perpendicular Centerlines of a S.C.S.F.
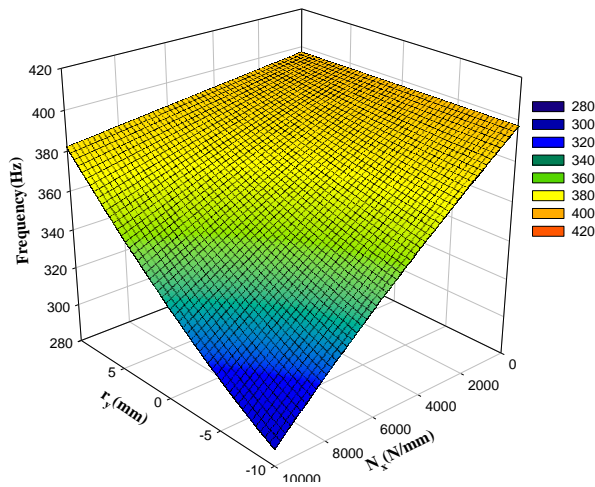Stiffened Plate**

**Fig.(11) Fundamental Frequencies of S.C.S.F. Stiffened
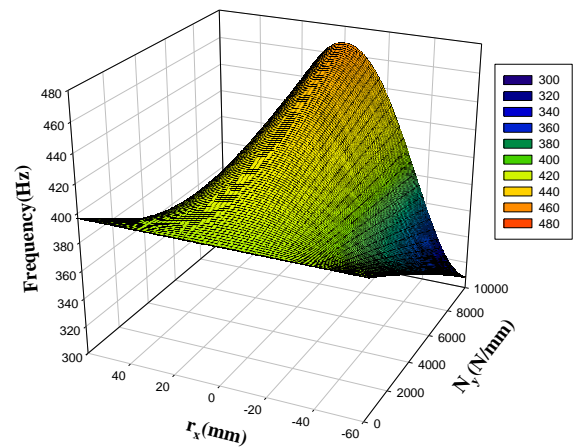plate due to the Longitudinal Self-Equilibrating Stresses**

**Fig.(12) Fundamental Frequencies of S.C.S.F. Stiffened
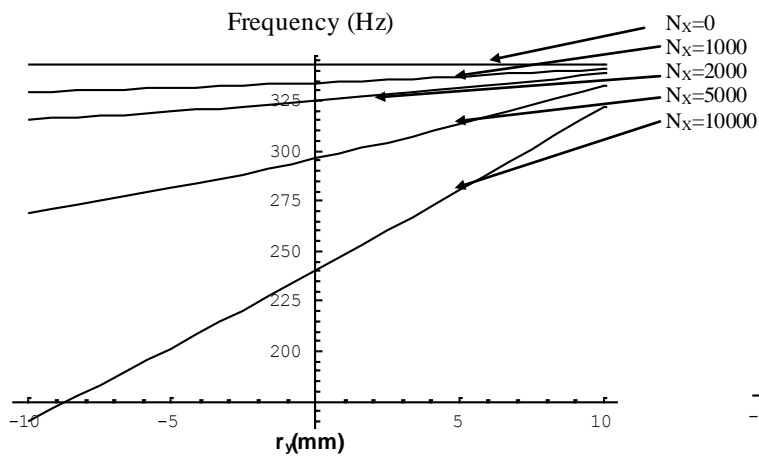plate due to the Perpendicular Self-Equilibrating Stresses**

Frequency (Hz)

Fig.(13) Fundamental Frequencies of C.C.C.F. Stiffened plate due to the Longitudinal Self-Equilibrating Stresses
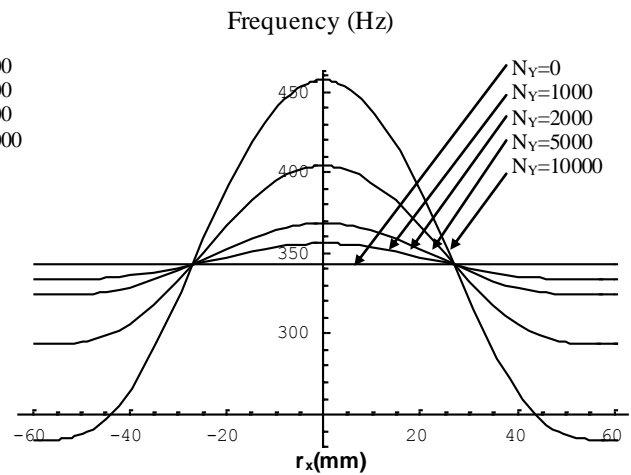
Frequency (Hz)

Fig.(14) Fundamental Frequencies of C.C.C.F. Stiffened plate due to the Longitudinal Self-Equilibrating Stresses

Frequency (Hz)

Fig.(15) Fundamental Frequencies of C.C.S.F. Stiffened plate due to the Longitudinal Self-Equilibrating Stresses

Frequency (Hz)

Fig.(16) Fundamental Frequencies of C.C.S.F. Stiffened plate due to the Longitudinal Self-Equilibrating Stresses

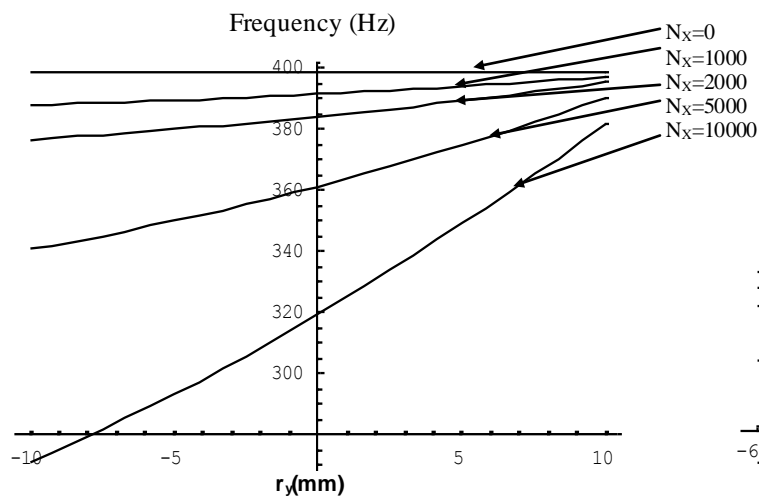| F. F. Mustafa | The Effect of Self-Equilibrating Stresses Due to |
| K. N. Salloomi | Multi-Line Spot Welded Stiffeners on the |
| S.M. Saliman | Natural Frequencies of Plate |

Fig.(17) Fundamental Frequencies of S.C.S.F. Stiffened plate due to the Longitudinal Self-Equilibrating Stresses

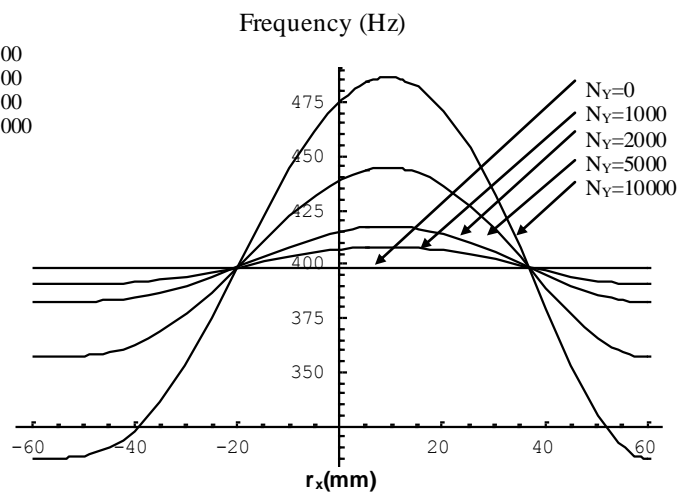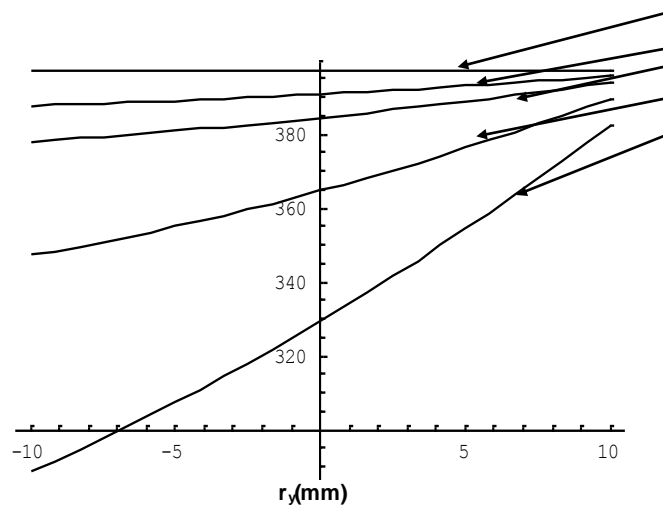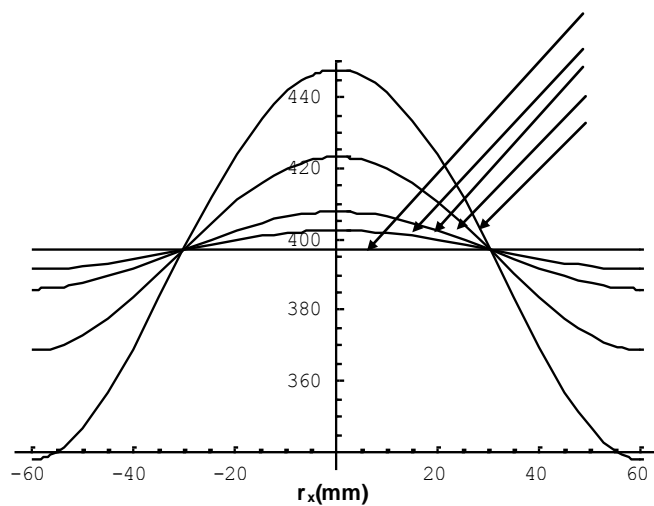**Fig.(18) Fundamental Frequencies of S.C.S.F. Stiffened plate due to the Longitudinal Self-Equilibrating Stresses**

SOME PROPERTIES OF HIGH PERFORMANCE CARBON FIBRES CEMENT COMPOSITES

Assist. Prof.Nada. Al – Jalawi
Eng. College/ Baghdad university

ABSTRACT

The paper presents properties of high performance concrete reinforced with relatively high percentage of choped carbon fibers vol. fraction ranging from (1 to 5) %. The great advantage of such composites is their relatively high flexural strength. A low water to cement ratio of 0.3 with super plasticizer was used in order to keep the cement mix easily workable. To improve the properties, a locally existing pozzolan based on reactive meta- kaolin was used in the mixture together with silica sand. A high modulus carbon fibers (450 KN/mm^2) were also used. In addition to the flexural strength, dynamic modulus of elastisity were found using dynamic methods.

The results showed that the specimen failed in flexureal by a single crack although the ultimate tensile strength and the stiffness of the composite were increased as the fibers content was increased.

Keywords: carbon fibers, reactive meta- kaolin, silica sand, super plasticizer, flexural strength, dynamic modulus of elastisity

بعض خواص الخرسانة عالية الأداء المسلحة بألياف الكاربون

الخلاصة

يقدم البحث خواص الخرسانة العالية الأداء المسلحة بألياف الكاربون بنسب حجمية عالية نسبياً تتراوح من (1 – 5) % . إن الفائدة الكبيرة لهذا النوع من الخرسانة هي مقاومتها العالية للشد في الانحناء.تم استخدام نسبة واطئة من المـاء/السمنت تسـاوي (0.3) مع استخدام ملدن متفوق للحصول على قابليـة تشغيل مقبولـة كمـا تم استخدام بوزلان محلي متكون من دقيق الكاؤولين النشط واستخدام رمل ذو أساس سيليكي وكانت ألياف الكـاربون من نـوع ذات معامل المرونـة العاليـة (450 كيلونـت/ملـم^2)، بالإضــافة إلـى الخـواص الانحنائيـة فقـد تـم بحـث الخـواص الديناميكية باستخدام طـرق ديناميكية، وبينت النتـائج بـأن نـوع فشـل النمـاذج كانت بشـق منفرد (single crack) وأن كلاً من مقاومة الانثناء القصوى ومعامل المرونة تزداد بزيادة نسبة الألياف.

INTRODUCTION

During the last few decades, fiber reinforced cement composites have attracted much interest, because of their high strength enhanced ductility and toughness (Hannant 1977,R.N.Swamy1989). This paper is concerned with a new type of fiber cement composite with comparatively a high volume fraction of high modulus carbon fibers (Raouf 1976) ranging from 1 to 5 % by volume. In order to reduce porosity a low w/c ratio (0.3) has been used together with a super plasticizer to provide a suitable workability.

In order to improve the strength and durability fine and sintered Kaolin at 750 ^{o}C has been used as an active pozolan having an activity index of 115 (Mohammad 2005) using 20 % Kaolin/cement ratio.

Very few is published on properties of carbon fiber cement composite, it was therefore decided to carry out further work for obtaining further information.The great advantages of carbon fibers are their high tensile strength and high stiffness, it was therefore thought necessary to find out how these properties affect that of composite.

The main features of this work as compared with others can be summarized as follows :

a – A relatively high carbon fiber volume fractions have been used ranging from 1 to 5 %.

b – A fine sintered local pozolan have been used as partial replacement of cement in order to obtain a high performance cement matrix (Edward 2001).

c – Electro dynamic and ultrasonic tests in addition to flexural test have been used to find dynamic and flexural properties

MATERIALS AND METHODS

- The cement

The cement used in casting all specimens was ordinary portland cement supplied by Kubaisa factory the chemical analysis and physical properties are shows in table (1) and table (2) which conforms to IQS-5.

Pozalan

The pozalan used consisted of meta kaolin sintered at 750°c and crushed into fine powder in a ball mill into a very fine powder (7213 cm^2/gm) all passing seive 325 as shown in tables 3 and 4.

carbon fibers

These fibers have much higher specific strength and stiffness than steel fibers, and for this reason their use for stregthening and stiffening building materials such as wood, plastics, and concrete, is attractive.

Carbon fibers are manufactured by heat treatment of certain types of acrylic fibers which are stretched whilst at high temperatures(Walter 1972). This operation increases the tensile strength and stiffness of the graphite, and provides a certain desired molecular orientation.

At present the fibers are commercially produced by several firms. Those used in this work were supplied by sika.The fibers were cut from carbon fiber woven cloth into short lengths.The fiber properties are shown in table (5)

The cement matrix

An ordinary Portland cement paste with water to cement ratio of 0.3. The low water – cement ratio was selected on the basis of experience, and in order to minimize the tendency of the fibers to segregate during compaction.

Moulds

Moulds of formica-lined wood, each holding three specimens. Each specimen measured 250×50×50 mm.

Testing

The specimen were first tested nondestructively to find modulus of elasticity according to BS 1881 then they were tested in flexure (4-point loading method)

Table (1) Chemical analysis and compound composition of cement

Oxides	Content %	Iraqi specification limitation IQS 5/1984
CaO	62.2	
SiO_2	21.8	
Al_2O_3	5.1	
MgO	3.4	5% max.
Fe_2O_3	3.3	
SO_3	2.33	2.8% max.
L.O.I	0.9	4% max
I.Res.	0.7	1.5% max.
L.S.F.	0.87	0.66-1.02
Compound Composition (Bogue's equations)		
C_3S	41.84	
C_2S	31.02	
C_3A	7.92	
C_4AF	10.03	

Table (2) Physical properties of cement

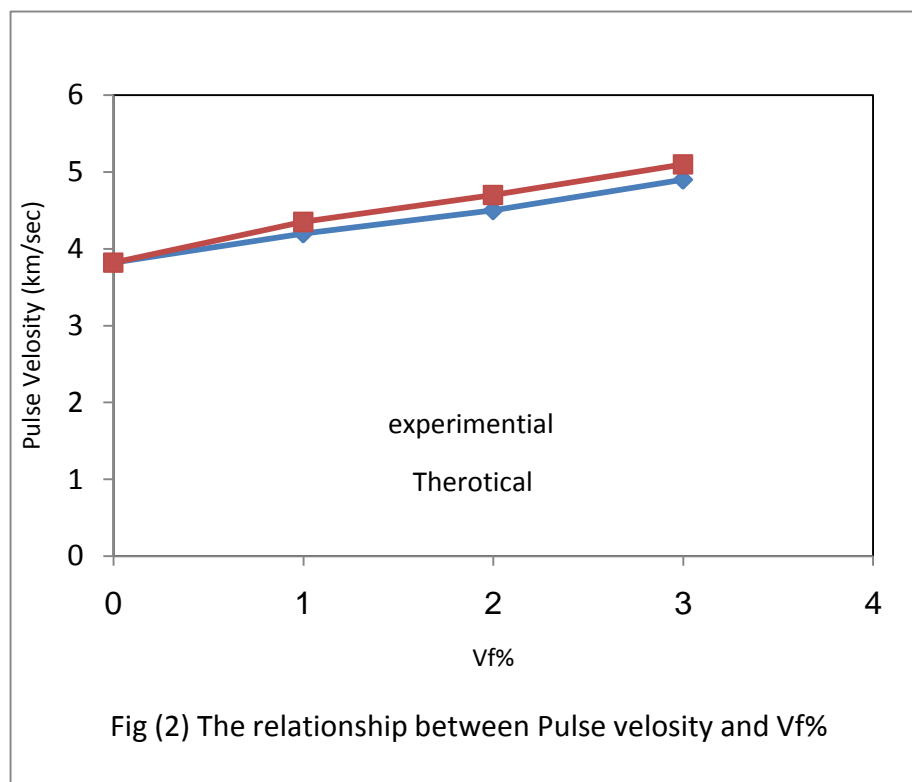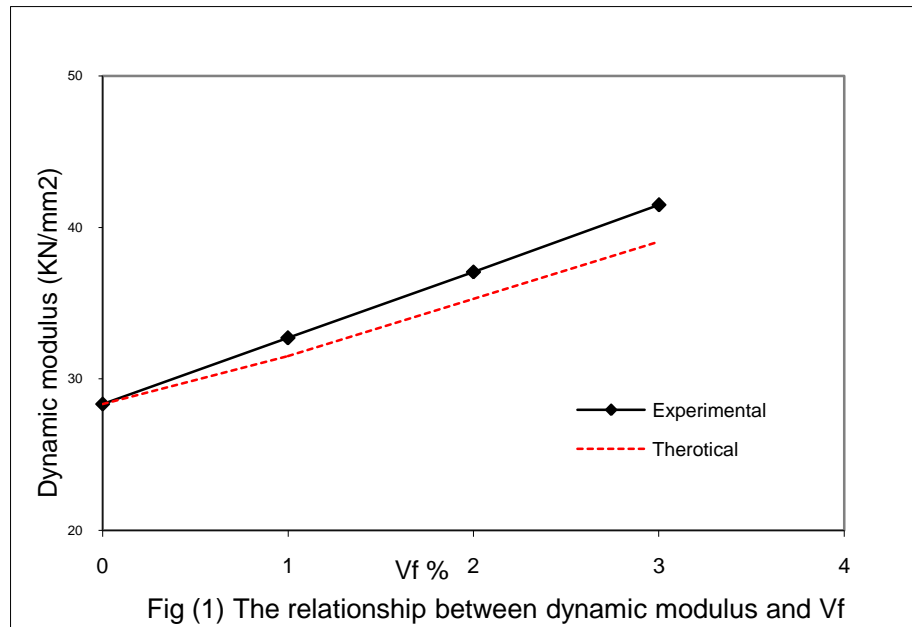| Property	Result	Iraqi specification limitation IQS 5/1984
Fineness by air permeability method (Blaine)	3780 cm^2/gm	Not Less than 2300 cm^2/gm
Initial Setting time	97 min	Not Less than 45 min
Final Setting time	4 hrs.	Not more than 10 hrs.
Soundness (Autoclave method)	0.4%	Not more than 0.8%
Compressive strength 3-day 7-day	20.6 Mpa 27.8 MPa	Not Less than 15 Mpa Not Less than 23 MPa

Table (3) Physical properties of Metakoalin

No.	Property	Result
1	Fineness	7213 cm^2/gm(all passing seive 325)
2	Specific weight	2.6 gm/cm^3
3	PH	6
4	Colour	Redish-White

Table (4) Chemical properties of koalin clay

No.	Oxides	Content %	specification limitation ASTM C-618
1	SiO_2	47.35	Not Less than 70%
2	Al_2O_3	35.13	
3	Fe_2O_3	1.4	
4	CaO	0.6	Not more than 1.5%
5	MgO	0.4	
6	SO_3	0.2	
7	K_2O	0.2	
8	H_2O	0.34	Not more than 3%
9	L.O.I	8	Not more than 10%

Table (5) Properties of Carbon Fiber(Hannant 1977)

Properties	Value
Diameter(um)	9 um
Density (kg/m^3 10^3)	1.9 (kg/m^3) 10^3
Young modulus (GN/m^2)	400 GN/m^2
Tensile strength(MN/m^2)	2600 MN/m^2

Fig (1) The relationship between dynamic modulus and Vf

Fig (2) The relationship between Pulse velosity and Vf%
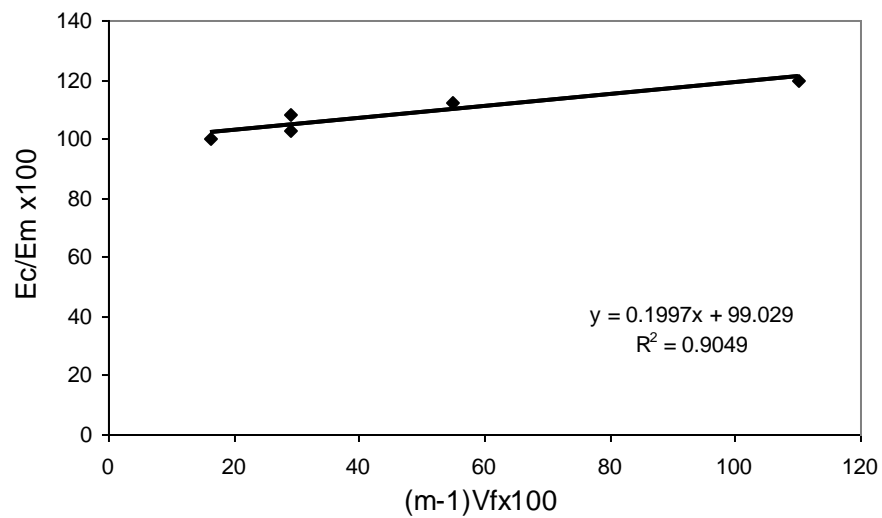
Fig (3) Variation of Ec/Em with (m-1)Vf for randomly distributed fiber, cement composite

$y = 0.1997x + 99.029$
$R^2 = 0.9049$

Fig (4) The relationship between flexural strength and Vf

$y = -1.0651x^2 + 12.816x + 2.3922$
$R^2 = 0.9888$
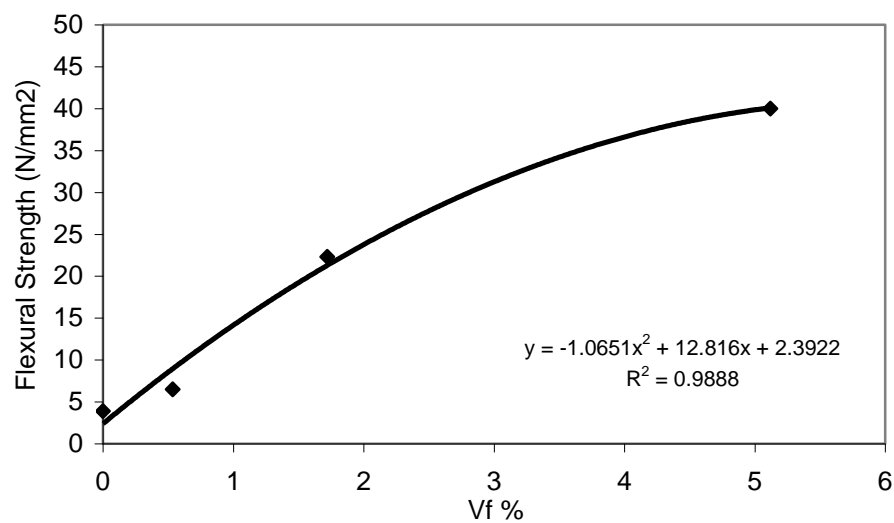
DISCUSION OF THE RESULTS

Only 28 days test results are analysed. Each result is an average of 3 tests, all specimens were dried cured inside plastic bags to avoid the adverse effects of unclean water curing on the fibers.

1-Fig (1) shows that the dynamic modulus (E_d) of unidirectionaly aligned carbon fibers cement composite increases linearly with volume fraction (V_f). The full line (1) indicates the least square fit given by

$E_c = 28.34 + 436\ V_f$ ....(1)

Correlation coefficient = 0.98

Where :

E_c is the composite dynamic modulus (KN/mm^2).

V_f is the volume fraction.

The broken line shows the predicted line given by the theory of two phases on the assumption that E_f of carbon fibers equals 455 KN/mm^2.

It can be seen that the therotical values of E_c under estimate those obtained experimentally, this may be for several reasons not included in the theoritical equation for example refect in shrinkage namely the precense of the fibers offers restraint to the shrinkage.

2-Fig (2) shows the relationship of pulse velocity with V_f. It can be seen that the varation is similar to that of E_d because of the close relationship between pulse velocity and E_d.

3-Fig (3) shows the variation of dynamic (E) in case of randamly oriented carbon fibers. It can be seen that it varies linearly. In order to find a therotical equation the ratio of E_c and E_m where plotted aganist $(m-1)V_f$ as in equation (2)

$E_c/E_m = 0.2(m-1)V_f +1$ ....(2)

Where m denotes modular ratio between carbon fiber and the cement matrix.

4-Reference to fig (4) shows relationship between flexural strength and V_f.

It can be seen that increase in flexural strength is high and exponantial V_f. The failure mode of all specimen was by single cracking.

CONCLUSIONS

- The following conclusions can be drawn from the experimental results of this work. The main findings may be summarised as follows:

- The effect of carbon fibers on dynamic modulus of unidirectionally aligned carbon fiber varies linearly with V_f it was shown that the rule of mixture under estimate the dynamic modulus because of the reduction in matrix shrinkage also the pulse velocity vary in smpathy of E- modulus.

- In case of randamly distributed carbon fibers the relationship between Ec and Em vary according to the equation (2) .

- The relationship of the flexural strength and V_f was found to be exponatial with a good correlation factor as shown in fig (4)

-REFERENCES

* Edward. D, Nawy.G, "Fundamentals of high –performance concrete",Second Edition, printed in the USA ,2001.

* Hannant.D.J "fiber cement and fiber concrete"New York 1977

* Raouf Z.A., Al. Hassani S.T.S. and Simpson J.W. "Explosive testing of fiber reinforced cement composites" Concrete, April 1976 London.

* Walter J.A, "Carbon fiber cement composites" Civil Eng. London, April 1972

المصادر العربية

* آر ـإن ـسوامي "خرسانة مسلحة جديدة " ترجمة د. محمد الآوسيوباسل طه ناجي، وزارة التعليم العالي والبحث العلمي – الجامعة المستنصرية ـكلية الهندسة 1989.

* محمد حمودي صالح ،"الخواص الانحنائية لالواح الفيروسمنت عالي الاداء" أطروحة ماجستير ـكلية الهندسة ـالقسم المدني – جامعة بغداد 2005.

BEARING CAPACITY OF SHALLOW FOOTING ON SOFT CLAY IMPROVED BY COMPACTED CEMENT DUST

Dr. Bushra S. Albusoda   **Azhar S. Yaseen**
Dr. Mosa J. Aziz Al-Mosawe   **Lecturer, Civil Eng.Departement**   **B.Sc.,Civil Eng. Department.**
Professor, Civil Eng. Department   **University of Baghdad**   **University of   Baghdad**
Head of Baghdad University   **E−Mail:albusoda@yahoo.com**   **E-Mail: azharealhilo@yahoo.com**

ABSTRACT

Low bearing capacity of weak soil under shallow footings represents one of construction problems. Kaolin with water content converges to liquid limit used to represent the weak soil under shallow footing prototype. On the other hand, cement dust, which can be defined as undesirable industrial waste material come from cement industry, was used to improve the bearing capacity of the soft soil considered in this research. The soft soil was prepared in steel box $(36 \times 36 \times 25)$ cm and shallow square footing prototype (6×6) cm were used .Group of physical and chemical tests were conducted on kaolin and cement dust. The improvement were performed by making trench under the footing filled with compacted cement dust (at its optimum moisture content) at three depths (D=B, D=2B, D=3B), the trench had the same footing Dimensions, note that (B) represent the footing width. Pressure-settlement curves were used to predict the ultimate bearing capacity. The improvement ratio in bearing capacity was calculated by comparing the ultimate bearing capacity value when testing the kaolin alone with its value of kaolin improved with compacted cement dust at the same value of eccentricity. It is important to note that eccentricity values were chosen according to the rule of middle third of footing base(i.e.,e≤B/6). The improvement ratio was about (197%) in average value, that represent a good ratio of improvement.

الخلاصة

تمثل قابلية التحمل الواطئة للترب الضعيفة اسفل الاسس الضحلة من أهم مشاكل الانشاء. استخدمت تربة الكاؤولين بمحتوى رطوبة يقترب من حد السيولة لتمثيل التربة الضعيفة اسفل نموذج الاساس الضحل كما تم استعمال مادة غبار السمنت وهي من مواد المخلفات الصناعية التي تنتج من عملية صناعة الاسمنت وبكميات كبيرة تم استعمالها في تحسين قابلية تحمل التربة الضعيفة الممثلة بمادة الكاؤولين التجاري في هذا البحث.تم تحظير التربة داخل صندوق من الحديد بأبعاد(36×36×25)سم مع نموذج لاساس مربع ضحل(6×6)سم . أجريت مجموعة من الفحوص الفيزيائية والكيميائية لمادة الكاؤولين ومادة غبار السمنت وتمت عملية التحسين من خلال عمل شق اسفل انموذج أألساس الضحل وبنفس طول وعرض ألأساس وتم حدل مادة غبار السمنت فيه (عند محتوى الرطوبة ألأمثل) ولثلاثة اعماق مختلفة (D=B,D=2B,D=3B)، علما ان B تمثل عرض ألأساس.أ جريت مجموعة من فحوص التحميل

على التربة قبل وبعد التحسين وبتحميل مركزي ولامركزي مع الأخذ بنظر الأعتبار قاعدة منتصف ثلث قاعدة الأساس اي (e≤B/6)في التحميل اللامركزي.

أستخدمت العلاقة بين الضغط المسلط على الأساس مع الهبوط الحاصل في الأساس لإيجاد مقاومة التحمل القصوى للتربة تحت تأثير الاحمال المسلطة ولكل انواع الفحوص. تم احتساب نسبة التحسين في مقاومة التحمل من خلال مقارنة مقاومة التحمل القصوىلتربة الكاؤولين بمفردها مع مقاومة التحمل القصوى لتربة الكاؤولين مع مادة غبار السمنت ولنفس مسافة التحميل اللامركزي. اعتمد البحث على عدة معادلات خطية تقريبية لتفسير النتائج العملية للفحوص، وصل معدل نسبة التحسين الى (197%) وهو ما يعتبر نسبة تحسين جيدة بالنسبة الى مقاومة التحمل.

KEYWARDS: bearing capacity, improvement of soft clay, cement dust, shallow footing, eccentric loading

INTRODUCTION

Many researchers studied the improvement and stabilization of soft soil using different methods and procedures.

Khdhair (1997) used one type of stabilization which was carried out on Nasriyia sand dunes by cement dust, he made an experimental set up consisting of a wind tunnel that was designed and manufactured, and tests were performed to check the suitability of this material. Three different suspensions were prepared at a constant concentration with different mix ratios of cement dust and Portland cement.

The satisfactory results were obtained from using cement in a ratio of (90% cement dust + 10% portland cement) suspended in water in concentration of 0.33kg of this material for each liter of water applied to sand at $10\ell/m^2$ rate

Chakrabrti and Bhandri (2004) worked on improvement of settlement behavior and vertical stress dispersion of soft clay using compacted pulverized fuel Ash. They showed in most of cases the ground improvement becomes expensive, increasing the total project cost. Pulverized fuel Ash (PFA) is waste material from thermal power plants and creates problems during its disposal. The research was conducted using normally consolidated commercial kaolin (soft clay) in a test tank and the transfer of load to the soft clay was arranged through a model footing. It was revealed from the results that the improvement of load carrying capacity could be remarkably increased, using compacted PFA layer on soft clay. The percentage of improvement of bearing capacity has been revealed in two ways. The first by increase of diameter wells with the depth of compacted PFA, though the improvement is more in case of increment of depth (Z) of PFA bed, rather than increment of diameter (D'). The percentage of improvement of bearing capacity, for different depths and diameter of compacted PFA varies from 12 to 390. The stress dispersion was also improved for different depths and diameters of compacted PFA bed.

Deschamps (1998) used FBC and stoker Ashes as roadway fill. It was noticed that approximately 100,000 m^3 of atmospheric fluidized bed combustion (FBC) ash and stoker ash were used as structural fill in the construction of a large roadway embankment. The embankment is ~ 200 m long and 10m high, and it supports an extension of a street across a gravel quarry in waste Lafayette, Ind. An over view of the project and construction operation is described, and the results of geotechnical laboratory tests and field monitoring presented. Instruments used in the monitoring of fill behavior include settlement plates, vertical and horizontal inclinometers, seismic cross-hole tests, and preconstruction standard penetration tests.

Consequently, the cement dust material was used in stabilization but not used in improvement of soft clay, therefore; an idea was started to use this material in improving the bearing capacity of shallow footing on soft clay.

MATERIAL PROPERTIES

Kaolin

The kaolin clay used in this research was of commercial grade. It was from North of Hussainiat, AL-Anbar Governorate, Iraq.

Physical properties of kaolin, shear strength and compressibility parameters could be shown in **Table 1**

Table 1 Physical properties, shear strength and compressibility parameters of kaolin

Property	Value	Type of test	Standard
LL%	44%	Atterberge limits	ASTM 4318
PI	25%		
G_s	2.77	Specific gravity of solids	ASTM D854
e_o	0.819	Standard Consolidation test	ASTM D2435
n	0.45		
Cc	0.34		
ϕ_u	0	Unconfined compression test	ASTM 2166
C_u	13 kPa		
C_v	$5.608*10^{-8}$ m^2/s	Standard Consolidation test	ASTM D2435

It was obvious from results shown in **Table 1** that the clay was classified as low plasticity clay (CL) according to the Unified soil classification system.

Chemical tests were carried out on kaolin with assistance of the state of geologic surveying and mining and the chemical composition of kaolin can be shown in **Table 2**

Table 2 Chemical composition of kaolin

Chemical composition				
L.O.I.*	TiO_2	Fe_2O_3	SiO_3	Al_2O_3
13.4-15.1%	1.4-2.96%	0.5-1.96%	38-45%	35.5-41.4%

*L.O.I: Loss of Ignition

White kaolin which selected was provided by (The state of geologic surveying and mining) from Dewielca lies in the west of Iraq.

Cement Dust

The cement dust provided from cement factory of Al-Kuffa, Najaf Governorate, Iraq. Specific gravity test, standard Proctor and direct shear test were conducted on cement dust. The results are shown in **Table 3**

Table 3 Results of physical, standard Proctor and direct shear test for cement dust

Material Properties	Value	Type of test	standard
LL	28%	Atterberge limits	ASTM 4318
PL	NP		
G_s	2.66	Specific gravity	ASTM D854
$\gamma_{d\ max}$	18.5 kN/m^3	Standard Procter test	ASTM D698
$\omega_{opt.}$	25%		
C_u at $\omega_{opt.}$	50kPa	Direct shear test	ASTM D3080
ϕ_u at $\omega_{opt.}$	29°		

Chemical tests were conducted for cement dust with the assistance of NCCLR. The results could be shown in **Table 4**

Table 4 Results of chemical tests for cement dust

SO_3 %	4.11
Organic matter %	0.22
$CaCo_3$ %	49
Cl %	0.04
pH	7.22

EXPERIMENTAL WORK

In order to simulate the behavior of shallow footing on weak soil, special techniques were used to achieve this purpose. These techniques include the manufacturing of steel box having the dimensions (36×36×25) cm.This box was filled with kaolin prepared at water content near its liquid limit. Also,a steel plate of (6×6 × 0.5)cm was used to simulate the shallow footing. A trench was made under the

footing that resting on soft kaolin. The trench had the same dimensions of footing and excavated at different depths (D=B, D=2B, D=3B), where B represents footing width. Then, the trench filled with compacted cement dust (at its optimum moisture content) to the desired depth. **Fig. 1** shows a simple section in model loading test and the detail of footing and cement dust column which support it.
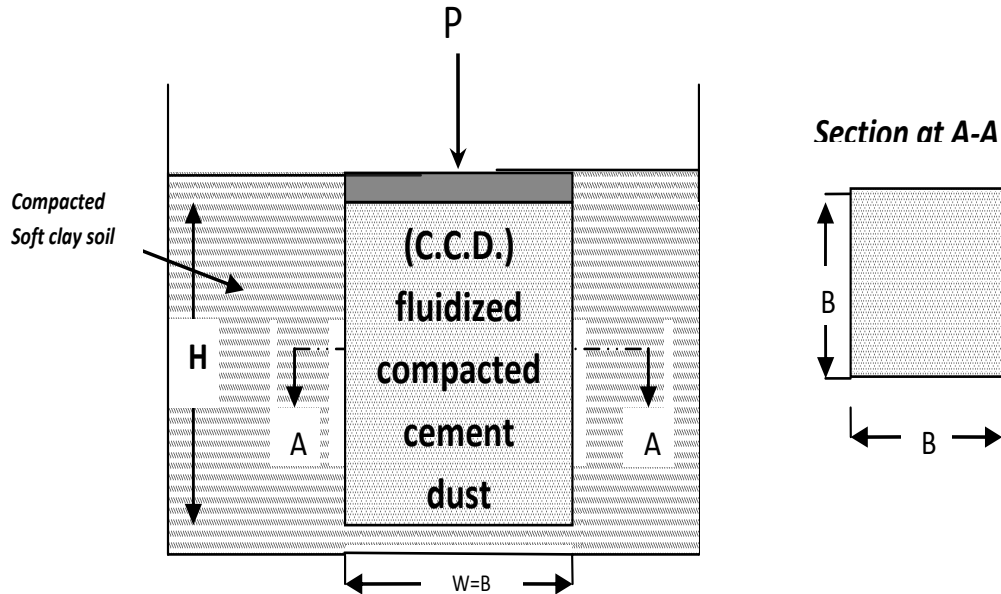

Fig.1 Rectangular footing on **C.C.D.,** note that: width of compacted cement column **C.C.D.** =W, width of footing = B, W=B

Then, the footing is loaded at the beginning of the test until failure is reached. The settlement at centre and edge of the footing is recorded with the use of video camera.

Compacted cement dust (C.C.D.)

The cement dust was prepared at optimum moisture content ($\omega_{opt..}$=25%) three depths of C.C.D. (H=6,H=12,H=18cm) were used. The sample of soft soil was prepared by putting the first layer of kaolin .Then; scaled steel mold was put and centered in length and width of steel box at the desirable depth which worked on. Then the trench under the footing was filled with compacted cement dust at its maximum dry density and optimum water content. It is compacted to the desired depth.

Results of load –settlement tests

Typical load (kN) vs. foundation settlements at edge and centre of foundation diagrams were obtained from loading tests as shown in **Fig.2** to **Fig.4**. The ultimate bearing capacity is defined as the point where a maximum value of q_u is clearly arrived, or where slope $\Delta s/\Delta q$ becomes maximum and the load vs. settlement not remains practically linear thereafter Vesic (1973).
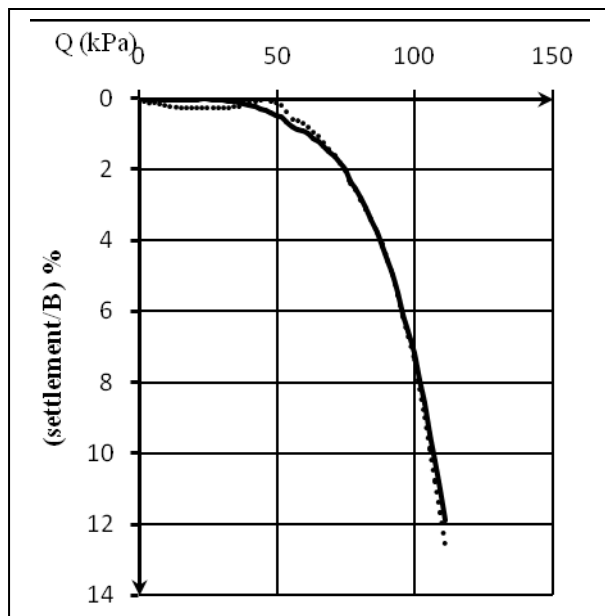
4421

Fig.2 Pressure-settlement ratio curve for kaolin with cement dust (H/B=1), concentric loading
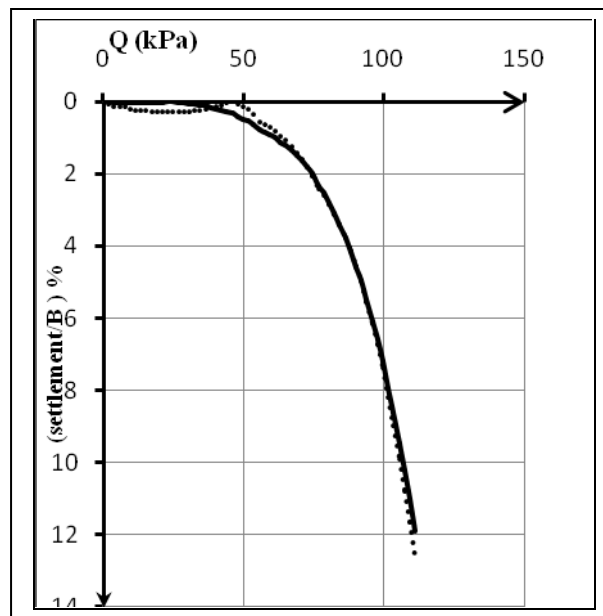

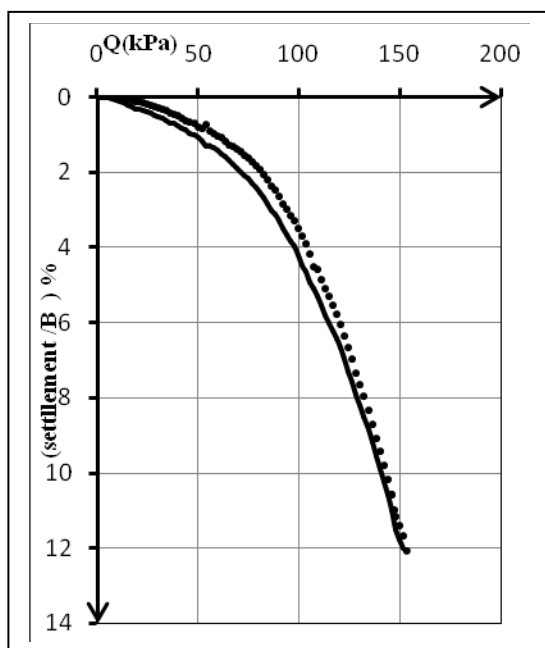**Fig.3** Pressure-settlement ratio curve for kaolin with cement dust (H/B=2), concentric loading

Fig.4 Pressure-settlement ratio curve for kaolin with cement dust (H/B=3), concentric loading

Effect of (H/B) ratio on Bearing Capacity

In general, the ultimate bearing capacity incrased as H/B ratio increased. This behavoir was expected due to the increase in strength of soil under the footing as the (H/B) ratio, of the cement dust used for improvement, increased . In addtion, the ratio of improvement increased as the (H/B) ratio increased . The largset ratio of improvement getten for soil improved by cemnent dust at H/B=3,see **Fig.5** and **Table 4** . This behavoir may be explained accoring to the shear strength prameters, where the cohesion and angle of internal friction of cement dust were (50 kPa, 29^0) respectively.
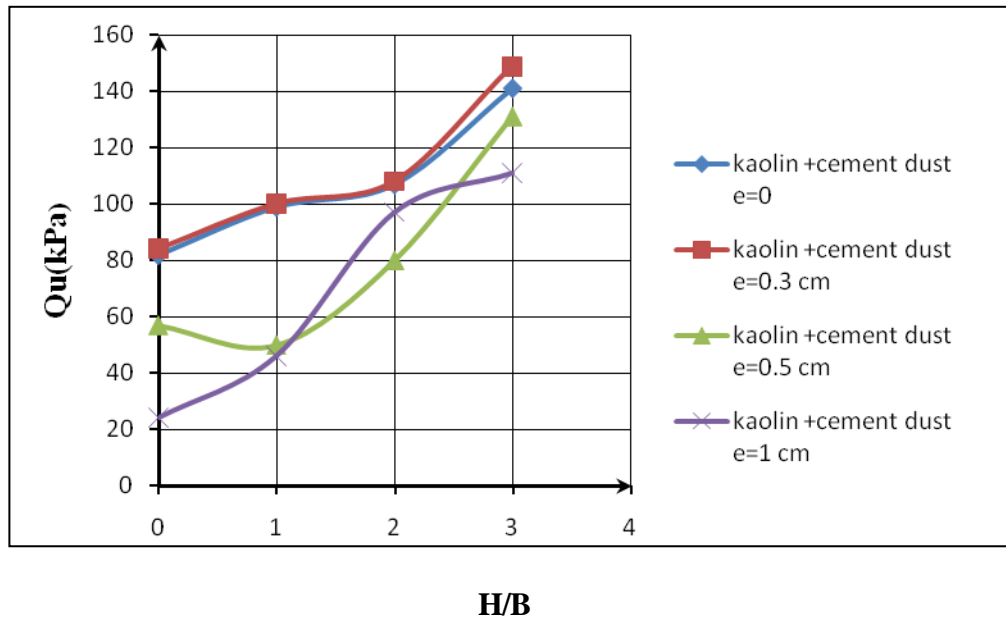

H/B
Fig.5 Ultimate bearing capacity – H/B ratio relation

M.J. Aziz Al-Mosawe   Bearing Capacity Of Shallow Footing On Soft
 B.S. Albusoda   Clay Improved By Compacted Cement Dust
 A. S. Yaseen

Table 4 Type of the tests and the ultimate bearing capacity values

Type of material used	Qu(kPa)	H/B	e(cm)	percent of improvement ratio%	Test No.
kaolin	82	0	0	0	1
kaolin +cement dust	99	1	0	21	2
kaolin +cement dust	107	2	0	30	3
kaolin +cement dust	142	3	0	73	4
kaolin	84	0	0.3	0	5
kaolin +cement dust	100	1	0.3	19	6
kaolin +cement dust	108	2	0.3	29	7
kaolin +cement dust	149	3	0.3	77	8
kaolin	57	0	0.5	0	9
kaolin +cement dust	50	1	0.5	-12	10
kaolin +cement dust	80	2	0.5	40	11
kaolin +cement dust	131	3	0.5	130	12
kaolin	24	0	1	0	13
kaolin +cement dust	46	1	1	92	14
kaolin +cement dust	98	2	1	308	15
kaolin +cement dust	111	3	1	363	16

Effect of Eccentricity on Bearing Capacity
The eccentricity has large effect on ultimate bearing capacity. Generaly the ultimate bearing capacity decreased as the eccenricity increased as shown in figure **Fig.5** .This behavior may be attributed to the reduction in effictive area as eccentrisity increased.

Improvement ratio in the ultimate bearing capacity
Foundation was reaching to failure if the settlement would be greater than (10%) from footing width, ASTM (D1194-94) so the bearing capacity at this ratio was equal to the ultimate bearing capacity. **Fig.6** shows the variation of improvement ratio with eccentricity at different (H/B) ratios. It is important to know that the improvement ratio is defined as:-

$$\text{Ratio of improvement (r) } \% = \frac{Q_{improved} - Q_{without\ improvement}}{Q_{without\ improvement}} *100 \%$$
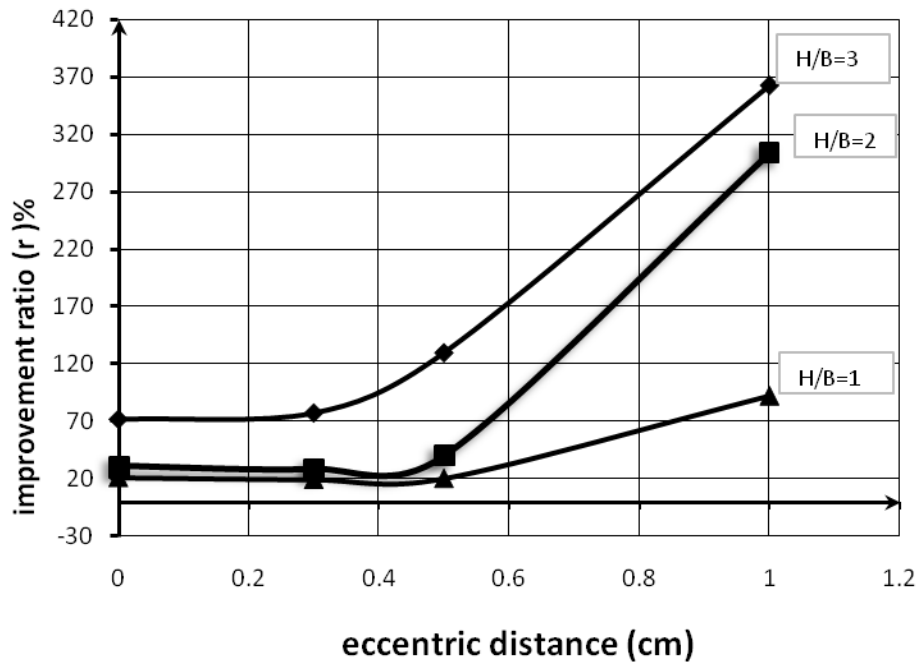
Fig.6 Ratio of improvement and eccentricity relationship at different values of H/B, "kaolin-cement dust"

Fig.7 gave the clear effect of (C.C.D.) depth on the ultimate bearing capacity. The maximum improvement ratios were appeared at (H/B) ratio equal to (3).
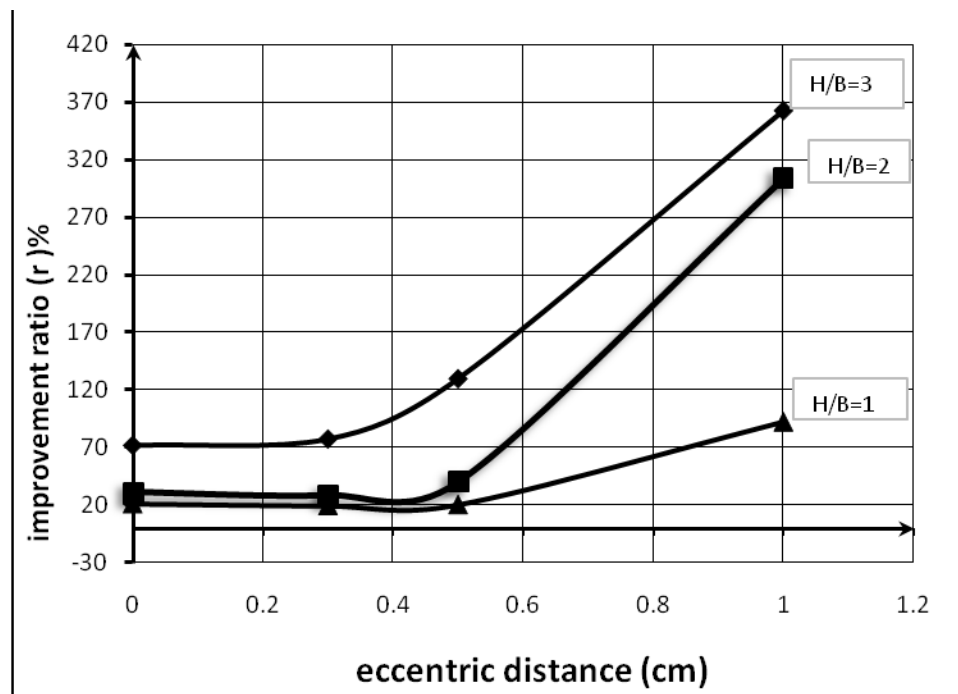

Fig.7 Ratio of improvement and eccentricity relationship at different values of H/B ratio, "kaolin improved by cement dust"

4425

Equations obtained from experimental results

Ratio of improvement in bearing capacity for cement dust used in improvement at different values of eccentricity were varied with the change in H/B ratio ,see **Fig.8**. In general, acceptable equations were obtained that simulate the incrase in r % with incrase of the H/B ratio for different values of eccentricity.
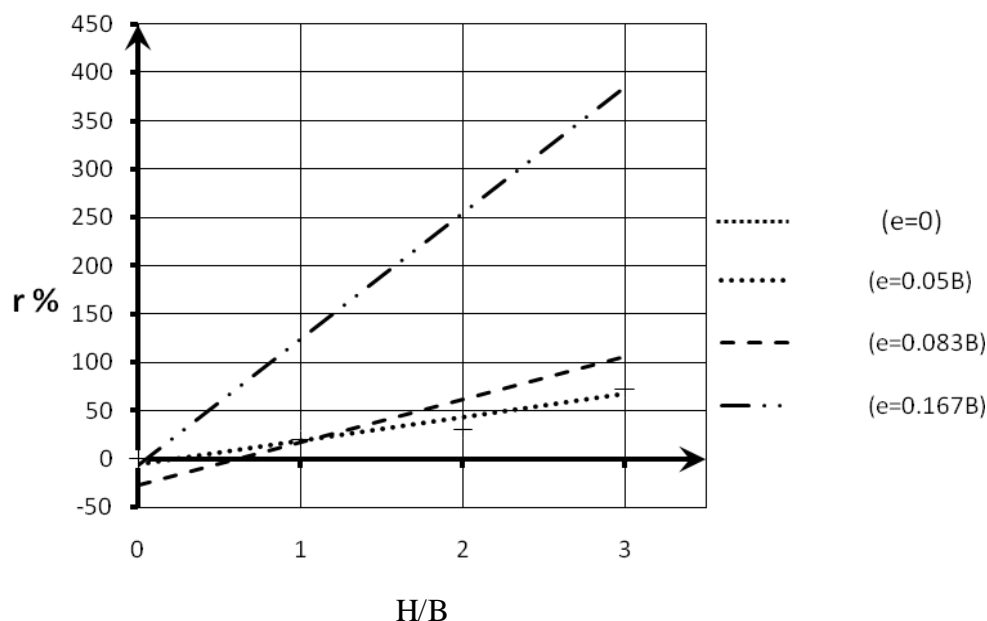

Fig.8 Ratio of improvement and H/B relationship at different values of eccentricity, "kaolin improved by cement dust

Table 5 shows the all equations can be use to predict the improvement ratio for any (H/B) ratio given, all equations was linear and have acceptable values of (R^2) (difference between the experimental results and the fitting equation results).

Table 5 Predicted equations for estimating improvement ratio from depth ratio

Type of material and test	Equations	R^2
Kaolin+ cement dust , e=0	r %= 24(H/B) -5	0.895
Kaolin+ cement dust, e=0.05B	r %= 24(H/B) -5	0.895
Kaolin+ cement dust, e=0.85B	r %= 44(H/B) -27	0.788
Kaolin+ cement dust, e=0.167B	r %= 130(H/B) -5	0.954

CONCLUSIONS

 Number of laboratory loading tests of shallow square footing supported by **(C.C.D.)** columns made in soft clay have been presented, based on the these results the following conclusions can be drawn:-

- There are acceptable improvement ratios for square footing prototype can be obtained (370%) in maximum value and (119%) in minimum value of improvement ratio(r %).
- Bearing capacity of soft soils under the shallow footing can be increased by making square trench under the footing with the same dimensions of it and for different depths. This trench is filled with compacted cement dust at optimum water content.
- The maximum improvement ratios in ultimate bearing capacity was appeared at maximum values of the (H/B) ratio which equal to (3).
- More acceptable ratios can be used for (H/B) ratios less than (3).
- Many fitting equations were obtained to estimate the improvement ratio from H/B ratio,all equation are linear and have acceptable values of (R^2).

REFERENCES

- ASTM D854-02 Standard Test Methods for Specific Gravity of Soil Solids by Water Pycnometer.

- ASTM D698-00 a Standard Test Methods for Laboratory Compaction Characteristics of Soil Using Standard Effort (12,400 ft-lbf/ft3 (600 kN-m/m3)).

- ASTM D1194-94 Standard Test Method for Bearing Capacity of Soil for Static Load and Spread footings.

- ASTM D2166-80 Standard Test Method for Unconfined compression Test of Soils.

- ASTM D2435-80 Standard Test Method for Standard Consolidation Test of Soils.

- ASTM D3080-98 Standard Test Method for Direct Shear Test of Soils under Consolidated Drained Conditions.

- ASTM D4318-00 Standard Test Methods for Liquid Limit, Plastic Limit, and Plasticity Index of soils.

- Chakrabrti and Bhandri,(2004), "Improvement of Settlement Behavoir and Vertical Dispersion of Soft Clay Using Compacted Pulverised Fuel Ash", Department of Civil engineering , Both at Jadavpur University, Kolkata 700 032. IE(I) Journal- CV, Vol 84, February

- Das B.M. and Hanna A.M,(1988),"Model tests for shallow strip foundation on granular trench" (GSP 16), ED BM Das, ASCE, New York,.110-124.

- Deschamps, R.J. (1998), " Using FBC and Stoker Ashes as Roadway Fill: A Case Study". Journal of Geotechnical and Geoenviromental Engineering. Vol.124, No.11 /November.

- Khadhair, A.A. (1997), "Stabilization of Nasriyia Sand Dunes by Cement Dust", M.SC. Thesis, Buildings and Construction Department, College of Engineering, University of Technology, Baghdad.

- Vesic A.S., (1973),"Analysis of Ultimate loads of Shallow Foundations", J. soil Mech. Found. Div. (ASCE), 99(1), 45-73.

NOTATIONS

Symbol	Meaning
C.C.D.	Compacted cement dust
C_u	Undrained shear strength
H/B	Ratio between the depth of cement dust column to the footing width
L.O.I	Loss Of Ignition
NCCLR	National Centre of Construction Laboratories
PFA	Pulverized fuel Ash
Q_u	Ultimate bearing capacity
R^2	difference between the experimental data and fitting equation
r %	Improvement ratio in ultimate bearing capacity

ASSESSMENT OF PHENOL DERIVATIVES IN COOLING TOWER SYSTEM AS BIOCIDES

Muslet Sh.Hussain *   Shaimaa.A.Ahmed Reshan*   Samar K. Dhaidan*
* Chemical Engineering Department – College of Engineering – University of Baghdad –Iraq.

ABSTRACT:

  One of the major problems facing the industrial utilities especially cooling towers is biofouling. Many techniques and measures have been taken and still continuing researches are under way. Biocides and water qualities were the main area of research for evaluation. Friendly biocides are preferable for controlling viable count and fungi, but many harmful still in use.

  The main objective of this research work is to predict a relationship covering the concentration of Cl and Br – containing compounds as biocide and the performance.

  It was concluded that the chlorophenol is the major effective biocide used (reduce it for about 80%, while bromophenol to about 65%) and that material although they are highly approved, but suffer pitting corrosion.

الخلاصه:

يعتبر الفشل البايلوجي أحد أهم المشاكل الرئيسيه التي تواجهها ابراج التبريد في المرافق الصناعية. فبالرغم من استخدام و توظيف عدة تقنيات و اساليب سيطرة و تحكم إلا أن المشاكل مازالت تستثير أهتمام الابحاث و استمراريتها في هذا المجال. في الوقت ذاته تلعب المياه و نوعيتها و مصادرها دوراً رئيسياً في تحديد استخدام المضادات الحيوية(بايوسايد) خاصة تلك التي تعتبر من اعداء البيئة و منها مشتقات الفينول التي لازالت تستخدم الى وقتنا الحاضر ، لكن التفتيش عن عن مضادات حيوية صديقة للبيئة لازالت قيد الاهتمام و التفتيش.

البحث يهدف الى ايجاد علاقه بين استخدام مشتقات الفينول الحاوية على الكلورين و البرومين و تحديد كفائتها كقاتل احيائي ،النتائج المستحصلة من البحث تظهر تفوق الكلوروفينول كقاتل احيائي على البروموفينول(حيث اظهر الاول انخفاضاً بنسبه 80% في العدد الحي بينما الثاني بنسبة 65%) ،مع الاخذ بنظر الاعتبار كمية المواد العضوية المترسبة و التي تسببت بأحداث بعض التنقر لبعض السبائك الفائقة.

KEY WORD: Biocide, chlorohenol, cooling tower, pitting corrosion.

INTRODUCTION:

  From a water cycle shown in Fig. (1) For a factory, it can be concluded that a cooling tower system is the main part in single train process.

  Such waters scheme although subjected to a pretreatment before using, but still dangerous to materials being used in the process such as heat exchangers and main piping systems. Some containing floating materials being mainly organic carbon widely differed in their content

depending on operating parameters and the quality of the make-up water but will always support microbial growth [Cloete TE, Brozel VS, and Van Holy A, 1992].

As heat exchanger experienced a large surface area already, they provide favorable conditions for bacterial attachment [Characklis WG (1990)]. Leading to form a tangled mass of fiber termed a biofilm [Characklis WG and Cooksey KE (1983)]. Formatting of a biofilm begins with attachment of free floating microorganisms to a surface, these are first colonists. Although biofilm are beneficial for removing undesirable substance from rivers and waste – water treatment systems they are responsible for biofouling. The industrial problems associated with biofouling are essentially those that accrue to all fouling mechanisms – namely, increased back pressure, for a given flow rate and, in heat exchangers reduced heat transfer for a given temperature difference [Fletcher M. (1992)].the major economic impact caused by biofilm in cooling water system is because of energy losses due to an increase in the fluid fractional resistance and increase in heat transfer resistance [Michael L., 2003].
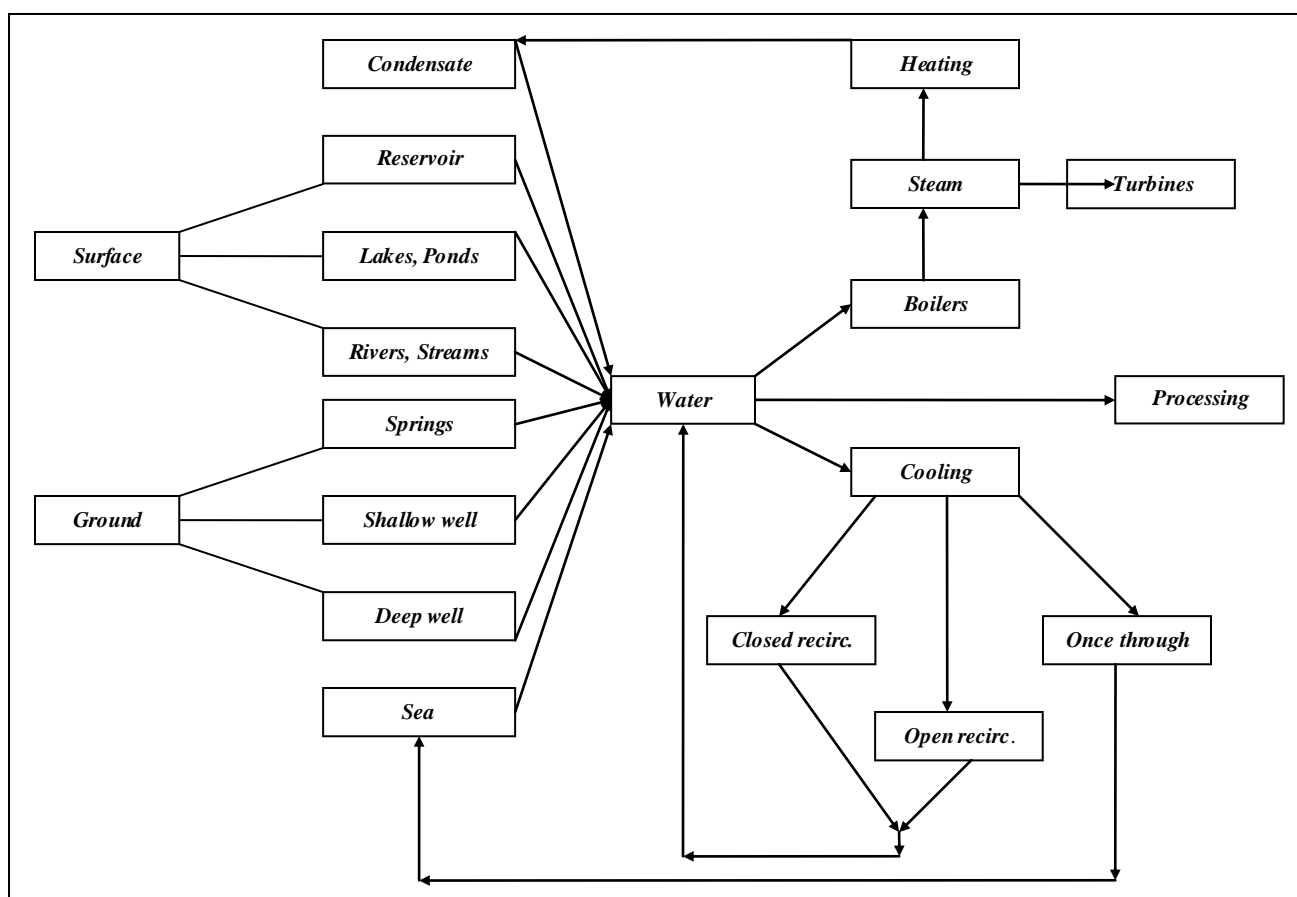

Fig. 1: The water cycle in a factory.

Also the presence of microorganisms that adhere to different surface can damage the metal surface by bio-corrosion [Michael L.2004].

One of the most effective tools to minimize their biofilm in industrial water system is by chemical treatment using biocides, to reduce the vial content or synthetic dispersant or

enzymes for removal of such biofilm formed. It is of great desire that the biocide should meet the following criteria [Favstritsky et al (1992)]:

1- Wide kill spectrum – the agent should be effective against a wide variety of microorganisms, such as, for example, algae, bacteria, fungi, mold, and other aquatic organisms.
2- Fast rate of kill.
3- Low cost.
4- Useful in wide range of PH.
5- Non- corrosive to metal.
6- Compatible with commonly used cooling tower treatment chemicals such as scale inhibitor and corrosion inhibitor.
7- Unaffected by organic contaminants or nitrogen compound in the water recirculation system.
8- Ease of handling and application.

Biocide can be grouped into two general categories, oxidizing and non –oxidizing depending on the mechanism used to kill target organisms [John A.Viel, et al, (1997)].

In general the non-oxidizing biocides function primarily by altering the permeability of the cell walls of the microorganisms and interfering with their biological process. Numerous non-oxidizing chemicals have been used as their primary biocide or as supplement to oxidizing biocide application. One product that is widely used in electrical power industry is quaternary ammonium salts (quits). Some other non-oxidizing biocide used includes organo-sulfer compound, chlorinated phenolics, and glutaraldehyde, isothiozoline, triazine, di-bromonitriloproionamide (DBNPA), and heavy metals compounds [Tanji Y., et al, (2002)].

Oxidizing biocide cause irreversible oxidation /hydrolysis of protein group in the microorganisms and of the surface to the cooling tower equipment. The result of this process is loss of normal enzymes activity and cell death. Most oxidizing biocide are chlorine or bromine compounds. Chlorine is generally an excellent algaecide and bactericide although some strains of bacteria can develop chemicals resistance to chlorine. Liquid bromine has also been used in the treatment of biofouled cooling towers. Chlorine and bromine when they added to water, they form hypochlorous acid (HOCl) and hypobromous acid (HOBr), which acts as the active ingredient. Historically chlorine gas was widely used because of it is low cost. However in recent years many users have switched to other form of chlorine because of the health and safety risk associated with handling chlorine gas. Bleach (sodium hypochlorite) is now widely used as source of HOCl. Sources of HOBr are becoming increasingly popular in place or in addition to sources of HOCl. Sodium bromide is often added along with bleach. The sodium bromide reacts with the HOCl to form HOBr, which is an effective micro biocide over a wider PH range than is HOCl. Another biocide, 1-bromo, 3-chloro, 5, 5-dimethylhydanation (BCDMH) serve as chlorine and bromine donor and can generate HOBr.

Several phenols are used for disinfectant or preservation purposes [McDonnel,G. and Russell, D.1999].Phenol induces progressive loss of intracellular constituents from treated bacteria and produces generalized membrane damage with intracellular coagulation occurring at higher concentration [Hugo,W.B.1999,Russell,A.D.2003]. The plasma membrane of fungi is also damaged [Russell, A.D. and Furr, J.R. 1996]. Although A.niger and C.albcans are less susceptible than bacteria [Goddard, P.A. and McCue, K.A. 2001]. Low concentrations are claimed to lyes growing culture of E.Coli, staphylococci and streptococci, but this effect has not been examined in detail. Fentichlore, a chlorinated phenol, acts as an uncoupling agent against susceptible bacteria.

Bacterial spores are very resistant even to high concentration of phenol, but germination is inhibited by low phenol concentrations [Russell A.D. 1990]. Mycobacteria may be inactivated by phenolics, the damage being presumably membrane-orientated.

This paper describe the result of laboratory studies comparing the efficiency of two non-oxidizing biocide , chlorophenol and bromophenol and a mixture of them , for control of biofilm development in laboratory cooling tower and the effect of these biocide on the 904L and 316 SS was noticed.
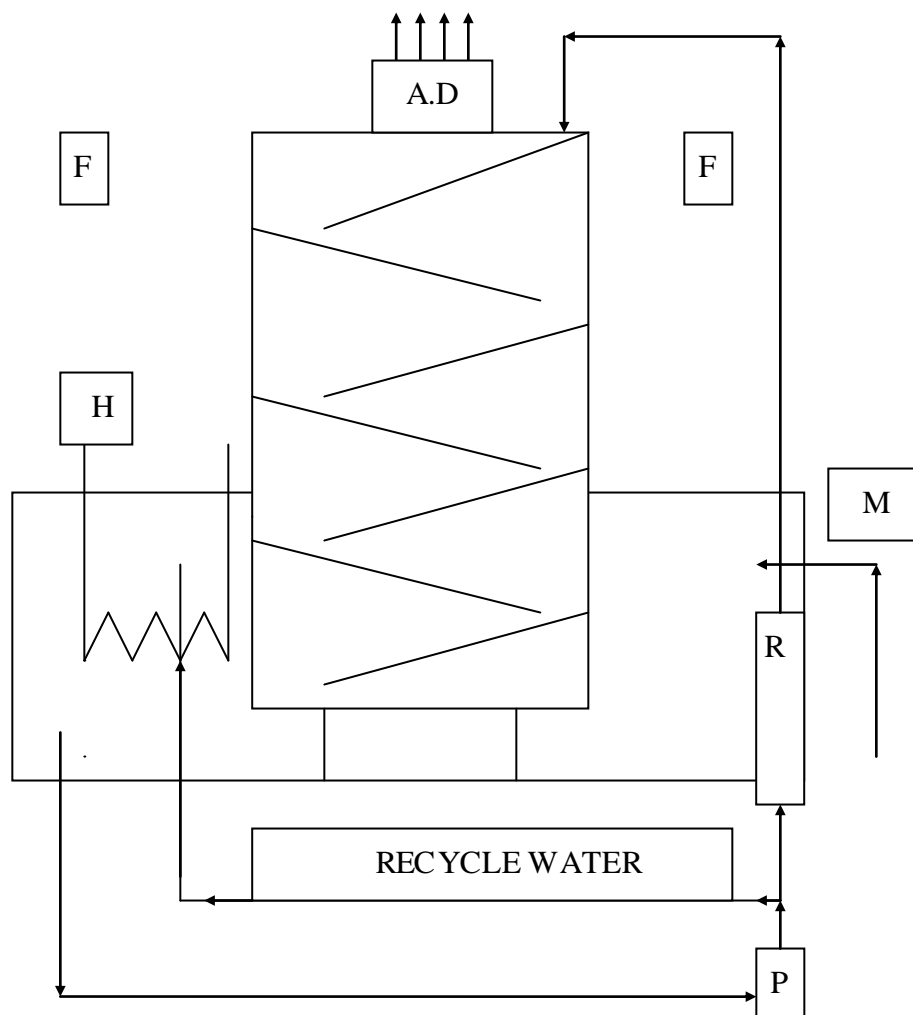
EXPERIMENTAL SETUP:

An assimilation of cooling tower has been designed and fabricated by the research group advised and approved by the scientific group of the department. The main constituent of such is shown in figure (2).

The system consists of pyrexpex tower (30*30*60 cm) contained within (50*50*40 cm) basin. The basin contains an over flow port positioned to provide a constant 40L working volume in the system , the tower contained water flow distribution box at the top and a series of slates (covered by sponge) which were positioned to provide a uniform cascade of recirculation water. The system has a recirculation water flow regulator and a make-up water supply. A portion of the recirculation water flow was diverted at the bottom of the basin to supply mixing within the system, the remainder where returned to the distribution box. An air draft fan has been positioned in the top of the tower to pull air out side the tower from the top with a temperature of about 43°C (the air in to the tower from holes in the bottom with a temperature of 35°C). The tower received a daily supplement of sodium nitrate (23mg/l) and sodium phosphate (20 mg/l) and once per week (50 mg/l) of kaolin to support microbial growth these condition has showed the maximum growth of microbial [Melo L.F., Bott T.R. 1997]. The cooling tower received a daily inoculation of (10 ml) of mixed population of algae and bacteria which was obtained from surface scraping from industrial cooling tower. The pH of the recirculated water was maintained at 8.5 using NaOH and H_2So_4 . The slats which served as the sampling sits were pre-fouled prior to each experiment to provide an initial biofilm. At the start of each experiment, the slats where brushed to remove the majority of the adherent biofilm and placed in the tower directly beneath the distribution box.

In the first run the tower served as the no treatment control, the other runs received two per week sludge doses of biocide to the water in the basin which where as follow; (25 ppm chlorophenol, 12.5/12.5 ppm mixture of chlorophenol and bromophenol, 25 ppm bromophenol) after two weeks of operation to each of the biocide the biofilm developed where assayed.

The total solid content was determined by drying (5 ml) of samples at 103°C over night, the samples then weighed and then ignited at 550°C for one hour in furnace to calculate the volatile solid content. Total viable hyperopic bacteria were determined by preparing special media for bacteria and fungi, the media for bacteria was a nutrient agar antisepticises by the auto clave, and the media for fungi was saboured agar or potato dextrose agar (PDA). A serial of dilution were prepared and 1 ml of the medias were raised in dishes, the bacteria were incubate at 37°C for 1 to 2 days and the fungi at 20-30°C for 5 to 7 days. Then we count the cells according to the following low: CFU (cell/ml) =colony number * dilution inverse (Department of Biology, college of Science, Baghdad University).

For the investigation of the corrosion of 904 and 316 SS, coupons of 10*30*1 of them were prepared, they were wet polished with polishing paper and then cleaned with acetone and dried and weighed.

M	make up water	P	Pump
R	rotameter	H	Heater
F	Fluorescents	A.D	air draft fan

Fig. 2: Experimental set-up cooling water system.

RESULTS AND DISSCUTION:

For more than a century, phenol, and phenol derivatives are known to be the most available antiseptic agents, and also as antibacterial of microbial organisms. One of their major drawbacks that these are hazardous and not as friendly as naturally occurring chemicals to the environment. Their action as a biocide is located within the intucellur penetration of the cytoplasm of the living cells. Such a penetration will act to precipitate the proteins. Further more phenol derivatives are membrane dissolving action agents. They penetrate into the liquid phase of the cytoplasm membrane causing a leakage of its constituents. It is advisable to recall some important problems encountered in cooling water systems before discussing the results obtained. Such problems are interrelated as corrosion proceeds , an electrochemical reaction will take place which involve the dissolution of metal ions into circulated water , as water is slightly alkaline, the recirculation water in this study was of pH = 8.5 , scaling of sparingly soluble carbonate films will develop on surfaces of the pipes and heat exchangers components.

In meantime fouling due to attachment of inert debris of organic and inorganic, organic usually very loosely bounds to the metal surfaces affecting heat transfer and fluid flow. At the end microbiological growth were cells of bacteria , fungi and algae multiply to such proportions that they forms deposit easily visible to the eye which cause fouling. The principle area of this study was the performance of two non-oxidizing biocides (chlorophenol and bromophenol) against the growth and development of microorganisms in biofilm. Such results shown in the histogram chart(fig. 3) reveal clearly that under these circumstances of using one biocide i.e. chlorophenol at 25 ppm concentration, for 2 weeks time, greatly reduced the vial count(about 80%) but the fungi did not show the same decrease(65%) , while total solids (fig.4) mainly related to algae growth , still much higher than expected, the volatile solids parameters is a reflection to the total biomass present and is an important consideration in maintaining optimum performance of heat exchangers. The use of bromophenol with chlorophenol as a ratio of 1:1 and bromophenol alone at 25 ppm also show a decrease in vial count but it was not like the use of chlorophenol alone(about 65% for the vial count and 50% for the fungi). The same behavior for total solid, while the volatile solid show more decreases than the total solid.

The reasons for the variations in non-susceptibility arising between types of microorganisms can then be ascribed to: (I) the considerable difference in adsorption by and the uptake into cells resulting from the dissimilarities in composition and architecture of the outer cell layers;(ii) possible slight marked difference in actual target sites so that the affinity of sites for biocide is modified ;(iii) possible differences in the amount of available target sites; (iv) the presence within some type of cells of protective chemicals such as the spore-specific that protect against DNA damage ;(v) stress responses , i.e. the manner in which cells respond to harmful agent; and (vi) the presence of biofilm .

One can conclude that unless a multi-systems inhibiting formulation is used, still some other constituent will grow faster on the expenses of other parameters. So biocides, together with anti-scaling , anti-fouling with continues dosing is the only way of treating heat exchanger cooling systems to be trouble –free in service.

Biocide of chlorophenol as stated earlier are intercellular penetrate , causing a destruction of living cells of microorganisms and note algae controlling systems , as already seem from the green deposit formulating on metal surfaces of the two alloys 316 and 904L , which are superior in microbiological corrosion situation(they did not show a notified weight loss).
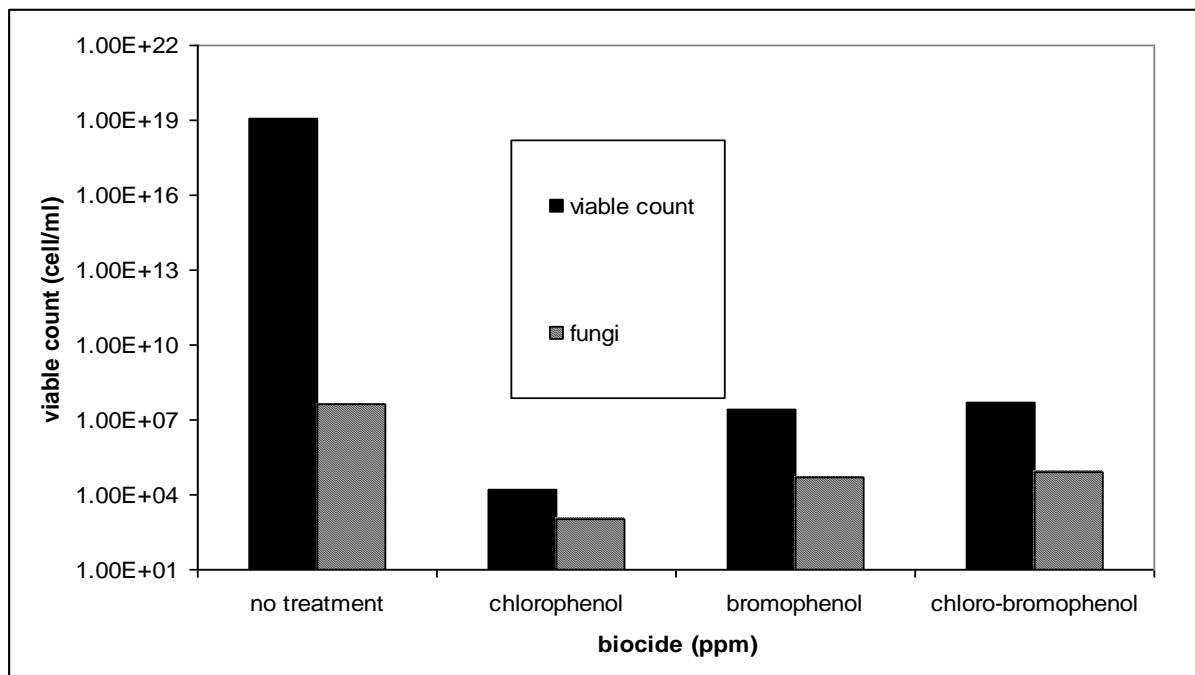
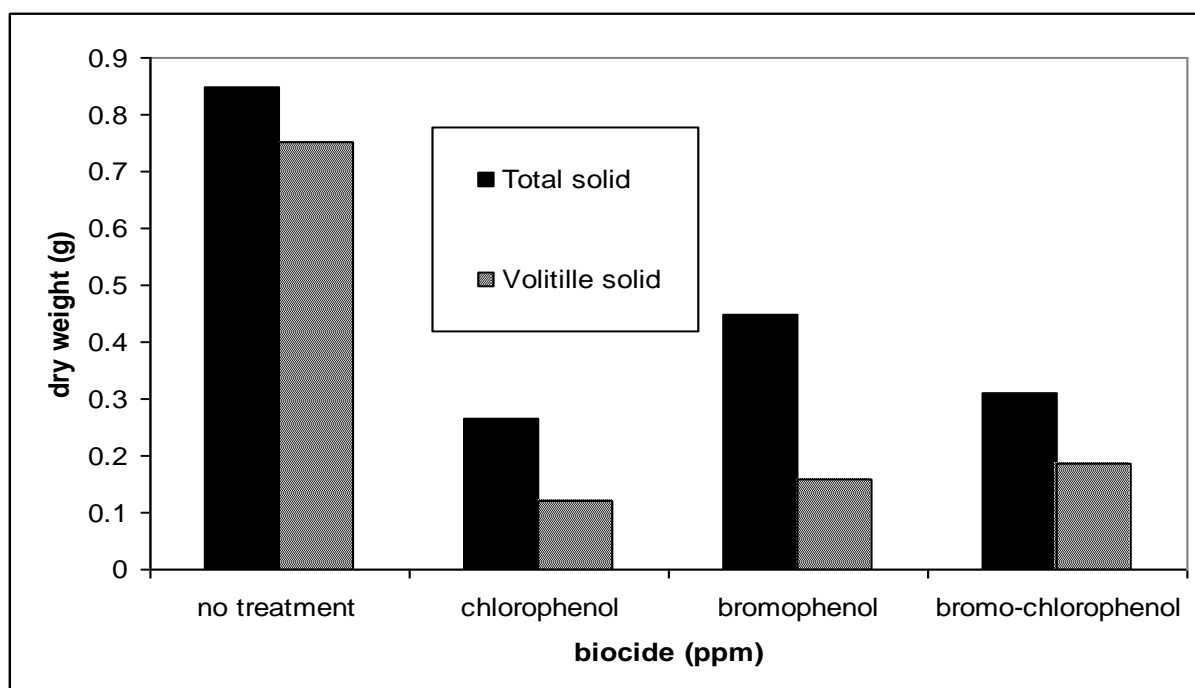**Fig. 3: Microbial Populations of cooling tower biofilms treated with biocides**.

Fig. 4: Dry Weight content of cooling tower biofilms treated with biocides

Theoretically speaking, as water flow through the system, corrosion products sometimes are protective as oxides try to expel, and spill away revealing new surfaces to corrode, unless a corrosion inhibiter to stifle the process should be added. While biocides are more effective in killing suspended cells and preventing any growth of the microorganisms and scaling agents were performed into the system, hence no crystal growth modification observed. On the other hand, algae growth was at appreciable amount as already obvious from the histogram chart.

Conclusion:
1. In order to get a trouble-free cooling water system in service, the design criteria, water quality, size of equipment, temperature, make-up water and evaporation rate should be taken into consideration when a treatment procedure is suggested.
2. Chlorophenols and derivatives are cell killer but algae growth promoters.
3. An integrated system of complete formulation of corrosion inhibitors, biocides, anti-scaling, and anti-fouling agents are preferable.

REFRENCES:

- Characklis WG (1990) "*Microbial biofouling control*". In: characklis WG and Marshall KC (Eds) Biofilms (pp 585-633). John Wiley and Sons, New York.

- Characklis WG and Cooksey KE (1983) "*Biofilm and microbial fouling*". Adv.Appl. Microbial.

- Cloete TE, Brozel VS, and Van Holy A (1992) "*Practical aspects of biofouling control in industrial water system*". Int. Biodeterioration and Biodegradation 29:299-341.

- Favstritsky et al (1992). "*Method for the control of biofouling in recirculation water system*". United state patent, patent number 4,935,153.

- Fletcher M. (1992), "*Bacterial Metabolism in biofilm, Science and technology*" (pp 113-124).

- Goddard, P.A. and McCue, K.A. (2001), "*Phenolic compound. In Disinfection, Sterilization and Preservation*", 5th edn, (Block, S.S, Ed) pp255-281. Lippincott Williams and Wilkins, Philadelphia, PA, USA.

- Hugo, W.B. (1999), "*Disinfection mechanisms. In principle and practice of disinfection, Preservation and Sterilization*", 3rd edn (pp258-283), Blackwell science, Oxford, UK.

- John Aviles , James K. Rice, Mary E.S.Raivel (1997), "Biocides usage in cooling tower in the electric power plant and petroleum refining industries", US department of energy.

- McDonnell, G. and Russell, A.D. (1999), "*Antiseptics and disinfectants: activity, action and resistance* ", Clinical Microbiology Reviews. 12, 147-79.

- Melo, L.F. and Bott, T.R., (1997), "*biofouling in water system*", Experimental Thermal and fluid science; 14:375-381.

- Michael, L., (2003), "*control and monitoring of biofilm in industrial application*", Int. Biodeterioration and Biodegradation 51:255-363.

- Michael, L. (2004), "*Biocorrosion towards understanding interaction between biofilms and metal*". Curr. Opin. Biotechn. 15,181-186.

- Russell, A.D. (1990),"*The bacterial spore and chemical sporicidal agents*", Clinical Microbiology Reviews, 3, 99-119.

- Russell, A.D. and Furr, J.R. (1996), "Biocides: mechanisms of antifungal action and fungal resistance ", Science progress, 79, 27-48.

- Russell, A.D, (2003), "Similarities and differences in the response of microorganisms to biocides", Journal of Antimicrobial Chemotherapy, 6:750-763.

- Tanji Y., Nakano T., Hori K., Miganaga K., Unno H., (2002) ,"*anti bacterial activity of biocide on biofilm*". Corrosion Eng.51:777-785.

STUDY ON ABSORPTION OF OZONE IN WATER USING PERFORATED SIEVE TRAY COLUMN

Sarmad Foad Jaber

sarmadfoad@yahoo.com

Chemical Engineering Department-Collage of Engineering-Baghdad University

ABSTRACT

The aim of this work is concerned with detailed study of transfer of ozone into water.. Since ozone cannot be stored or conveniently purchased by the gram, pound, gallon or ton, it must be produced on site as needed, (where needed and when needed). The process will carried out with two important assumptions; first that ozone is the only active species that physically dissolves in water. And second that there is no chemical reaction .the process carried out in a perforated sieve tray column with 1 m long and 33 cm diameter. The effects of process variables such as (Water flow rate, pH and air flow rate which is refer to the concentration of free ozone in the gas phase in the absorption column). The result show that the absorption rate increases with increasing the water flow rate and decreasing the air flow rate in a pH range (7-8).

<div dir="rtl">

دراسة امتصاص الاوزون بالماء في برج امتصاص ذو صواني مثقبة

الخلاصة

الهدف من هذا البحث كان اجراء دراسة تفصيلية لعملية امتصاص الاوزون من قبل الماء. وحيث ان الاوزون لايمكن خزنه او نقله فان البحث تطلب انتاجه موقعيا بشكل مباشر مصاحب لعملية الامتصاص (الاوزون ينتج اينما وحيثما يتم استخدامه). والبحث اجري بشكل كامل على اساس فرضيتين، الاولى هي ان الاوزون هو الجزيئة الفعالة الوحيدة التي تذوب في الماء خلال الدراسة والثانية هو عدم وجود تفاعل كمياوي. وتم دراسة عدة متغيرات هي الدالة الحامضية، معدل جريان ماء الامتصاص ومعدل الجريان للهواء الداخل الى برج الامتصاص والذي يحدد نسبة الاوزون في الطور الغازي داخل برج الامتصاص. وقد استخدم برج امتصاص ذو صينية مثقبة وصينية منخل لتوفير وسط التماس بين الاوزون والطور السائل بطول متر واحد وعرض 33 سم.

وقد دلت النتائج المستحصلة على ان معدل الامتصاص يزداد بزيادة معدل جريان الماء وخفض معدل جريان الهواء في مدى للدالة الحامضية يتراوح بين (7-8).

</div>

INTRODUCTION

Today it is possible to produce ozone in high concentration from the feed gas oxygen under economical conditions and introduce it to water. Producing ozone from air you will have a solution of ozone, oxygen and nitrogen in to water. Producing ozone from oxygen you will only have solution of ozone and oxygen in to water. [1]

Ozone has greater disinfection effectiveness against bacteria and viruses compared to chlorination. In addition, the oxidizing properties can also reduce the concentration of iron, manganese, sulfur and reduce or eliminate taste and odor problems. Ozone is a colorless gas that has an odor similar to smell of the air after a major thunderstorm. Solubility in Water by weight at 20ºC: 0.003 g/l (3 ppm) [2]

In 1785, Van Marum noticed that air near his electrostatic machine acquired a characteristic odor when electric sparks were passed. In 1801, Cruickshank observed the same odor at the anode during the electrolysis of water. In 1840 Shonbein named the substance, which gave off this odor, "ozone", from the Greek word "ozein" - to smell. In 1857 Siemens designed an ozone generator that has since evolved into the present day, cylindrical dielectric type that makes up most of the commercially available ozone generators in use, and which has sometimes been called the "Siemens Type" ozone generator. The first drinking water plant to use ozone was built at Oudshoom, Holland in 1893. Another, drinking water plant began operations at Nice, France, in 1906. Since Nice has been using ozone since that time, it is generally referred to as the "birthplace of ozonation for drinking water treatment."[3]

Abbas H. Sulaymon carried out an absorption process for ozone with water in a packed bed column and give a good results for the rate of absorption and show that the optimum absorption rate for ozone with water could be obtained in the pH (7-8) and also show that the temperature of the ozone generator will increase and that will accelerate the decomposition of ozone after approximately 20 minutes. [4]

Some application of ozone to potable – water treatment is sterilization of all forms of bacteria and viruses; increased settling; removal of tastes, odors, and colors; oxidation of sulfides, cyanides, and algae; removal of trihalomethan precursors; and oxidation of organic materials. Excessive dose of ozone will lead to the formation of per manganate, which gives water a pinkish color. This soluble form of manganese (Mn) correspond to a theoretical stoichiometry 2.20 mgO_3/mg Mn. Stoichiometry is the determination of the proportions in which chemical elements combineor are produced and the weight relation in a chemical reaction.[5]

Ozone exists as a gas at room temperature. The gas has a pungent odor readily detectable at concentration as low as 0.02 to 0.05 ppm (by volume), which is below concentration of health toxic concern. Ozone gas is highly corrosive and toxic [6]

Perforated sieve trays are cheapest and satisfactory for most applications. This kind of trays has been used for many years for liquid gas contacting in commercial absorption columns. The perforated sieve tray have lower coast in comparison with bubble cup trays. The relative cost will depend on the material of construction used. [10]

This kind of trays may be divided according to their operating principles in to two categories, first one are trays with downcomer, in which the gas rises through holes in the tray floor, bubbles through the liquid in fairly uniform manner and liquid flows across the tray floor over an outlet wire through a downcomer to the tray below. These tray are also classified according to the number of liquid passes on the tray: a single pass tray for normal liquid flow rates $(11 - 110 \text{ m}^3/\text{hr})$; reverses flow tray(inlet and outlet downcomers are on the same side of the tray) for low liquid rates (up to $11\text{m}^3/\text{hr}$); multiple pass tray(the liquid stream is sub-divided by using several downcomers) for high liquid rates(exceeding $110\text{m}^3/\text{hr}$) and large diameter columns [11.14].

The other kind of this trays are that trays without downcomer, in which gas rises through holes in the tray floor and at the same time liquid counter currently through these holes onto the tray below. Liquid flow forms random patterns in draining and does not form continuous streamlets from each hole. These trays have a narrower range of efficient operable loadings, but they are used when a low pressure drop is required. [12, 13]

The aim of this study was to discover the suitability of the perforated sieve tray as a contact media between water and ozone and finding the optimum hydrodynamics for the absorption process of ozone in water

Experimental work

Experimental Apparatus

The experimental laboratory apparatus used consist of the following:
Glass column, Liquid storage tank, Blower, Centrifugal pump, Connecting pipes, Measuring instruments and Ozone generator as shown in figure 1.
The column employed was a cylindrical glass pipe, 1m long, 0.3m diameter. The inside of the column was fitted with one perforated tray and one chimney tray. The perforated tray made of aluminum. 5 mm thick and 0.3 m diameter. The chimney tray (some times called weepage collection tray) was made of aluminum, 5mm thick and 0.3m diameter. This tray is located below the perforated tray, in order to collect liquid weeping from the perforated tray, on the one hand, as well as ensuring uniform gas flow distribution at the region beneath the perforated tray, on the other hand, in order to prevent possible localized preferential weeping from the test tray caused by gas flow misdistribution.
A spherical glass tank was used with 50 liters volume was used to collect liquid overflowing the outlet serrated weir on the one hand as well as acting as reservoir for all the liquid employed in the rig on the other hand. This tank connected to the supply recirculation pump which fed the liquid to the rig.
A suitable centrifugal blower was used to introduce air at ambient conditions to the rig below the chimney tray via suitable piping arrangements.
A locally fabricated orifice plate was employed as air flow measuring device, following insertion in a suitably located position to ensure absence of flow disturbance. Also a suitable proprietary area flow meter was used to measure the liquid flow rate. Although the meter was originally calibrated for water flow.

The pH value of water before and after treating was measured by means of digital pH-held with range from 0-14.

The duration time for all experiment will be 20 minutes. Because after that time its known from previous work that the temperature of the ozone generator will increase and that will accelerate the decomposition of ozone and in the final results mean decreasing the amount of ozone that being absorbed.
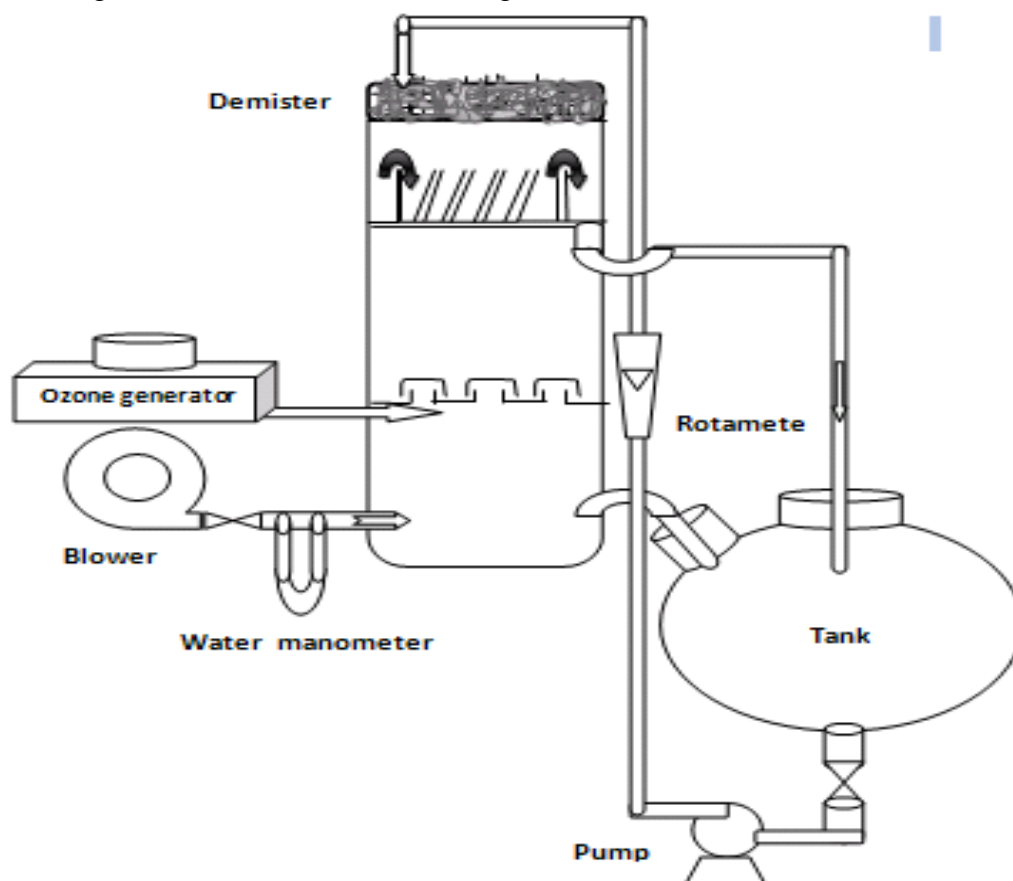

Fig. 1 Schematic flow diagram of the absorption unit

Experimental procedure

The raw water was bringing up from Tigris River at Aljaderiah town in the middle of Baghdad to the laboratory and left for ten days to settling.

- Initially, a sufficient quantity of the water to be used was prepared and introduce to the liquid tank. This liquid quantity amount to be about 50 liters.
- The air blower was operated and the air flow was adjusted to a value of 200 m^3/hr by a manual gate value utilizing the installed calibrated orifice meter for this purpose. This value of air flow corresponded to the minimum required to avoid dumping of the liquid from the perforated test tray at its minimum adopted inlet flow rate of 250 lit/hr.
- The supply recirculation liquid pump was then operated and the liquid flow was adjusted at 250 lit/hr by the globe valve upstream of the area flow meter which is utilized for this purpose. This value of liquid flow was practically the minimum

stable rate of flow achievable in the rig due to the variation in the reservoir tank liquid level over the duration of an experimental run.

- The glass column was then observed to ensure that some liquid overflowed the outlet serrated weir. If that was not the case, the air flow rate was very gradually increased to achieve this overflow and subsequently fixed and recorded at this over flow occurrence. This procedure was necessary to keep away from the dump point.

- Ozonized oxygen gas produced from the ozone generator passes in countercurrent to water at the bottom of the column, at the end of the duration time for the experiment, the ozone concentration in water was determined using pH meter.

- The next step was to increase the air flow by increments to value corresponding approximately to 215, 277, 310, 340, 393 and 412 m^3/hr while maintaining the liquid flow rate at 250 lit/hr; and again after the end of the operation duration time was determined the concentration of the ozone in water.

- The procedure pointed out in points (2) to (6) above was repeated for increments in the liquid flow rate to the perforated tray; namely 300, 350, 400, 450 and 500 lit/hr.

RESULTS AND DISCUSSION

At the time that ozone species and water molecules come in to contact, the absorption process will take place. Where the gases come in to contact with water, and all the theories of mass transfer between liquid and gas can explain this process with two important assumptions, first is that ozone is the only species that physically dissolved in water, and second that there is no chemical reactions.[4]

Figure 2 shows the relations between ozone concentrations (which are referring to the amount of ozone being absorbed) with the air flow rate at different water flow rates. It's clear that the amount of ozone absorbed with water decreases with increasing air flow rate at low water flow rates. But at high water flow rate such as 450 and 500 lit./hr the absorption rate will increase especially in the air flow rate range between 275 and 350 m^3/hr. decreasing the flow rate of air that which carry the ozone gas species in the perforated sieve tray column will increase the contact time of ozone species with water molecules and give this species more chance to meet with water molecules. Also at high water flow rate the amount of ozone being absorbed increase even with increasing air flow rate because the huge amount of water that will be available at that high rates will increase the chance even for high velocity ozone species to come in to contact with water molecules but not for air flow more that 350 m3/hr because this will again decrease the chance for the ozone species to come in to contact with water molecules even at high water flow rates and that is relates to the increasing the velocity of air which carry the ozone gas and as a result decreasing the contact time for the ozone and water. it's clear from the figure that the for high liquid flow rates (400 lit/hr) and above, the optimum air flow rate will be between (300 to 350) m^3/hr.
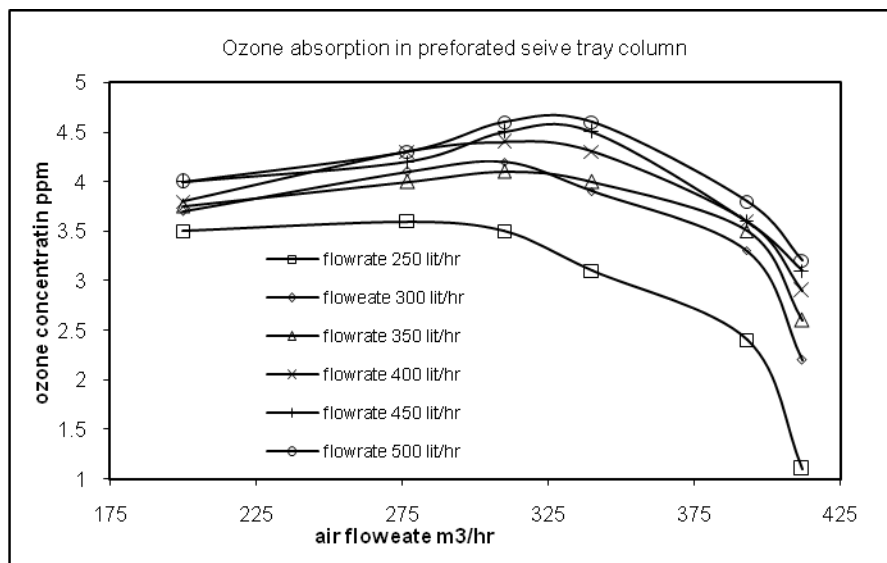
Fig.2 Ozone concentration vs. air flow rate at different water flow rate

Figure 3 shows the relation between ozone concentration and air flow rate at different Hydrogen number (pH) and similarly to figure 2 the ozone concentration decrease with increasing air flow rate for all range of pH being studies and of course for the same reasons of the above figure.
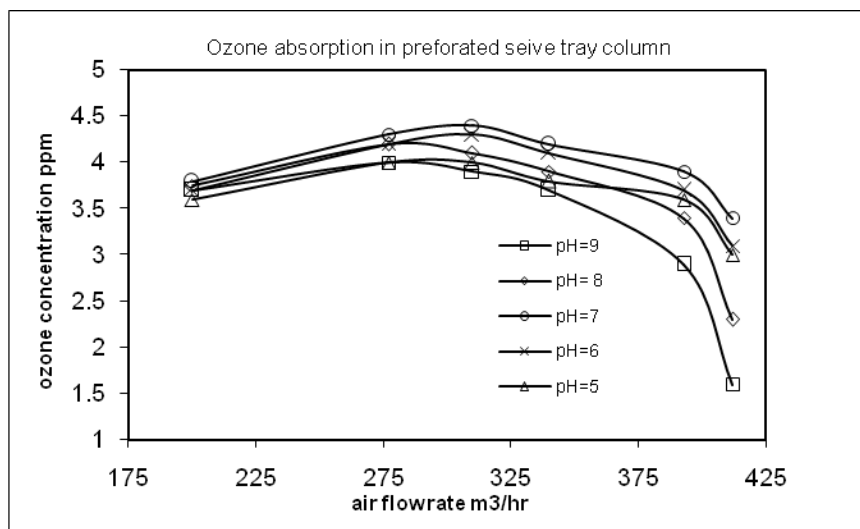

Fig. 3 Ozone concentration vs. air flow rate at different pH

Also figure 3 shows that the maximum absorption rate obtained in the pH range from (7-8) and this clearly observed in the figure 4.
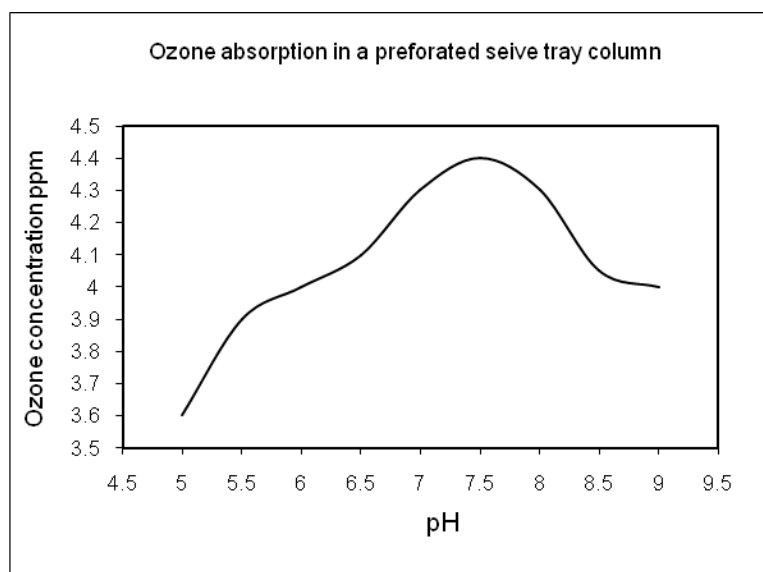
Fig 4 Ozone concentration vs. pH

It's clear that increasing pH will increase the concentration of ozone in water until pH reaches the range between approximately (7-8) then the concentration will decrease again. The hydrogen number of water is an important factor affecting the absorption of ozone in water and this is related to the hydroxide ions initiate ozone decomposition, which involves the following reactions
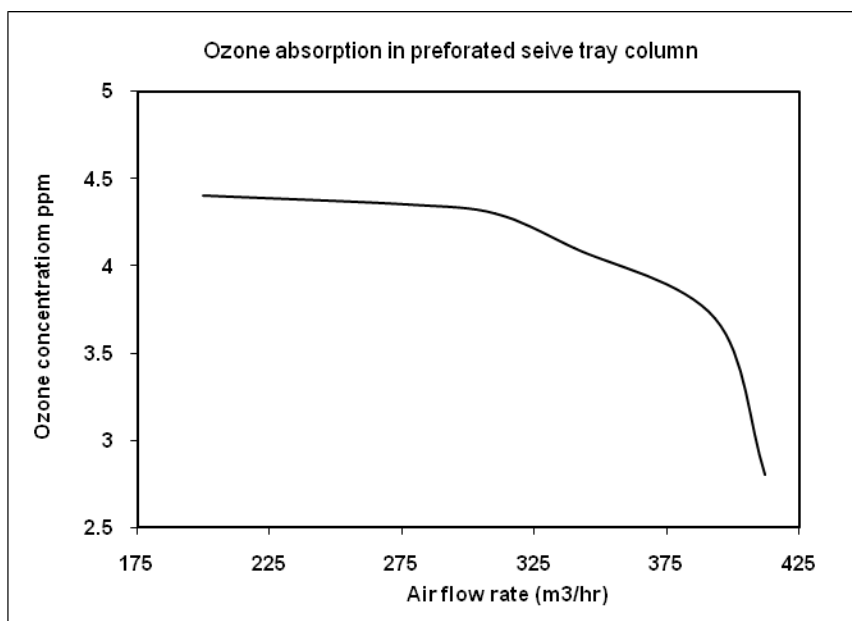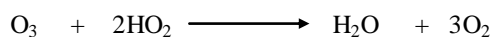
$$O_3 \ + \ OH \longrightarrow HO_2 \ + \ O_2$$

$$O_3 \ + \ 2HO_2 \longrightarrow H_2O \ + \ 3O_2$$

Fig. 5 Ozone concentration vs. air flow rate

Figure 5 shows that the absorption rate of ozone decreasing with increasing air flow rate and this related to the decreasing of contact time between ozone species and water molecules.
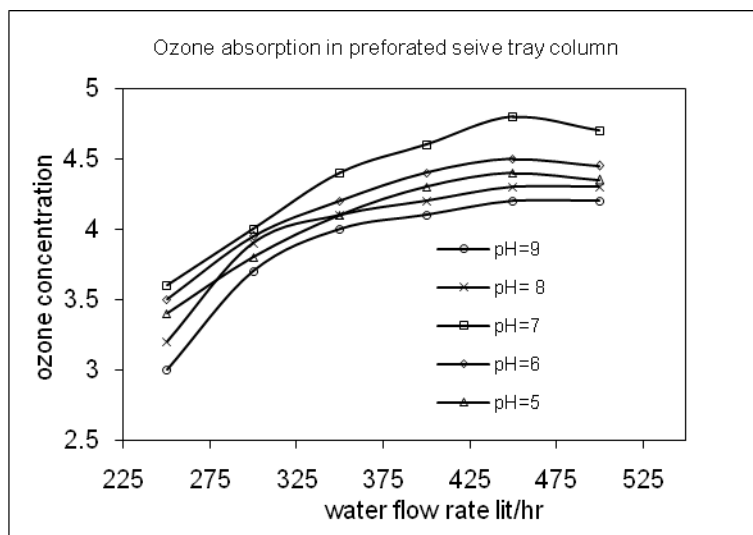

Fig.6 Ozone concentration vs. water flow rate at different pH

Figure 6 shows that the absorption rate of ozone increases with increasing water flow rate for all hydrogen numbers range tested in this work, and this related to the increasing of water molecules that might come in to contact with ozone. also this figure shows that at high water flow rate range between 400 – 500 lit/hr the absorption rate does not increase as much that happened in the lower range because most of ozone species already be recovered for the same limited amount of ozone supplied to the absorption unit.

CONCLUSIONS

o   The amount of ozone absorbed in the sieve perforated tray column increase with increasing water flow rate and decreasing air flow rate and keeping the pH range between (7-8).

o   Increasing the air flow rate in this kind of absorbers is an important factor for increasing the performance of absorption, but that will effect negatively on the ability for ozone to dissolve in water , and that lead to think twice before choosing this kind of absorber as a contact medium between ozone and water.

REFERENCES

- International conference on ozonation and related oxidation processes in water and liquid waste treatment : (Berlin, April 21-23, 1997)

- Wilkes University Center for Environmental Quality Environmental Engineering and Earth Sciences PO Box (111)- 84 West South Street - Wilkes-Barre, PA 18766(Internet).

- Stopping the Invasion - Eliminating Aquatic Nuisance Species Using Ozone-2008 Nutech O3, Inc (Internet)

- Abbas H. Sulaymon, "IJCPE"Iraqi journal of Chemical and Petroleum Engineering Vol.10 No.1 (March 2009) P. 29-34

- Rip G.Rice & M.E.Browning, "Ozone Treatment of Industrial Waste Water", Pollution Technology Review, No.84, (1981).

- Rip G.Rice & Paul K.Overbeck, "Ozone and The Safe   Drinking Water Act", GDT Corporation, (1998), "By Internet".

- "Tech brief" National drinking water clearing house 'Tech brief Twelve. December 1999'

- American water works association 1993. Controlling Disinfection by-products.

- Environmental Technology Initiative (ETI). Project funded by the U.S. Environmental Protection Agency under Assistance Agreement NO.CX824652.

- Coulson, J.M. and Richardson, J. F.,"Chemical Engineering" Vol.2,3rd ed. P.552,Pergamon(1978).

- Coulson, J.M. and Richardson, J. F.,"Chemical Engineering"Vol.6, 1st ed.,P.453,Pergamon(1978).

- Backhurst, J.R. and Harker,J.H., "Process plant design", P.169, Heineman Educational Books Ltd (1973).

- US. Patent, No. 5 843 307, Des. (1998).

- Treybal R.E, "Mass – Transfer Operation", Mc Graw- Hill, 3rd ed., (1980).

THE EFFECT OF COARSE AGGREGATE RATIO ON THE PROPERTIES OF NO FINE LIGHT WEIGHT CONCRETE

Hind.H.HAMAD. Assist.Lecturer, Researcher, Engineering affair department, University of Baghdad, Iraq
Luma Abdul. Ghani. Zghair Assist. Lecturer, Eng. College,, Al-Mustansyria University, Baghdad/Iraq

ABSTRACT

The main object of this work is to study the effect of coarse aggregate/cement ratio (A/C) on the property of no fine concrete. In this work, three ratio of A/C were used (6, 9 and 12 by weight).The cement content is maintained constant ($125kg/m^3$) while the w/c ratio ranges from (0.39 to 0.55 by weight). Tests are carried out on hardened concrete to investigate the effect of coarse aggregate/cement ratio on the compressive strength, absorption%, density, porosity%, ultrasonic pulse velocity, acoustic impedance of mixes.

The results showed that increasing the percentage of A/C ratio by weight from 6 to 12 for the used mixes reduces the compressive strength, ultrasonic pulse velocity and acoustic impedance, on the other hand the porosity and the absorption percentage, increase with increasing ratio of A/C for all studied mixes.

At 28 days the compressive strength , ultrasonic pulse velocity and acoustic impedance tests with A/C ratio of (12) are (2.8.MPa), (2km/sec) and (3×10^6 Kg/(sec.m^2)) respectively while decreasing the ratio to (6) improves these properties to (9.3MPa), (3km/sec) and (5.7×10^6 Kg/(sec.m^2)) respectively On the other hand the porosity and the absorption % decrease with decreasing the ratio of A/C for all studied mixes . At 28 days the porosity and the absorption % with A/C ratio of (12) are (40%) and (2.7%) respectively with decreasing the ratio to 6 decrease these properties to (19%) and (1%) respectively.

The densities of the mixes were tested. At 28 days the density with A/C ratio of (12) are (1512 kg/m^3)with decreasing the ratio to 6 increase the density to(1907 kg/m^3)

Based on the analysis of experimental results, several graphs and tables have been prepared to study the properties of no fine concrete.

تاثير نسبة الركام الخشن على خواص الخرسانة
الخالية من الركام الناعم

الخلاصة

الهدف الأساسي لهذا العمل هو دراسة تاثيرنسبة الركام الخشن/ السمنت (A/C) على خواص
الخرسانة الخالية من الركام الناعم . تم استخدام ثلاثة نسب وزنية من (A/C) ، (6 ، 9 و 12) . محتوى
السمنت ثابتاً(125 كغم/م^3) بينما نسبة الماء / السمنت تتراوح بين (0.39 الى 0.55) . اختير اجراءالفحوصات
على الخرسانة المتصلبة لدراسة تاثيرنسبة الركام الخشن/ السمنت على مقاومة الانضغاط ، نسبة الامتصاص ،
الكثافة ، المسامية ، فحص الموجات الصوتية و فحص المعاوقة الصوتية .
النتائج اظهرت ان زيادة نسبة (A/C) من 6 الى 12اوزنيا" ادى الى نقصان في مقاومة الانضغاط ،
فحص الموجات الصوتية و فحص المعاوقة الصوتية من الناحية الاخرى المسامية و نسبة الامتصاص قد
ازدادت عند زيادة نسبة (A/C) للخلطات الخرسانية.
في عمر 28 يوم مقاومة الانضغاط ، فحص الموجات الصوتية و فحص المعاوقة الصوتية عند نسبة
(A/C) (12) كانت (2.8 ميكاباسكال)،(2كم\ثا) و (10^6× 3 كغم\(ثا . م^2)) على التوالي بينما نقصان
النسبة الى(6) ادى الى تحسين الخواص السابقة (9.3 ميكاباسكال)، (3 كم\ثا) و (10^6× 5.7 كغم\(ثا . م^2)
) على التوالي و من الجانب الاخر المسامية و نسبة الامتصاص قلت مع تقليل نسبة (A/C) للخلطات
الخرسانية.
في عمر 28 يوم المسامية و نسبة الامتصاص عند نسبة (A/C) (12) كانت (40%) و (2.7%)على
التوالي بينما نقصان النسبة الى(6) ادى الى تقليل تلك الخواص الى   (19%)   و(1%) .
تم فحص الكثافة للخلطات الخرسانية في عمر 28 يوم عند نسبة (A/C) (12) وكانت (1512كغم\م^3) بينما
نقصان النسبة الى(6) ادى الى زيادة في الكثافة الى (1907كغم\م^3)،
اعتمادا على تحليل النتائج مختبريا ، بضع رسومات و جداول اعدت لدراسة خواص الخرسانة الخالية من الركام
الناعم.

KEYWORDS

No fine concrete , coarse aggregate/cement ratio (A/C), compressive strength, absorption% ,density**,** porosity % **,** ultrasonic pulse velocity and acoustic impedance.

INTRODUCTION

No-Fines concrete is a mixture of cement, water and a single sized coarse aggregate combined to produce a porous structural material. It has a high volume of voids, which is the factor responsible for the lower strength and its lightweight nature . No-fines concrete has many different names including zero-fines concrete , pervious concrete and porous concrete[1].

Neville[2] defined No-fine concrete as a form of lightweight concrete obtained when fine aggregate is omitted i.e. consisting of cement, water and coarse aggregate only. No- fines concrete is thus an agglomeration of coarse aggregate particles , each surrounded by a coating of cement paste up to about 1.3 mm thick.

The ACI 213R - 87 [3] uses densities to categorize concrete according to its application :-

- Low density concrete has a density between 300 and 800 kg/m^3
- Structural concrete has a density between 1350 and 1900 kg/m^3 and has a minimum strength of 17 MPa .
- Moderate strength concrete its compressive strength is between 7and17 MPa

Meininger [4] reported that , in no fine concrete the water – cement ratio in the range of 0.35 to 0.45 does a better job of coating the coarse aggregate without causing too much balling in the mixer or , at the opposite extreme, being so wet that paste tends to run off the aggregate . He also reported that the properties of no –

fines concrete depend not only on its proportion but also on its compaction , too much compaction can reduce the air voids and plug the flow channels , too little compaction will leave the structure with very high air voids resulting in low strength and a raveling surface.

Abadjieva et al [5] determined that the compressive strength of on – fine concrete increases with age at a similar rate to conventional concrete. The no –fines concrete specimens tested had aggregate-cement ratios varying from 6:1 to 10:1. The 28 day compressive strength obtained by these mixes ranged from 1.1 and 8.2 MPa , with the aggregate-cement ratio of 6:1 being the strongest . He concluded that the most plausible explanation for the reduced strength was caused by the increased porosity of the concrete.

Harber[1]   reported that , the density of no-fine concrete is dependent upon the void content in the concrete. Due to the high air content it is a lightweight concrete with a density of about two third of conventional concrete. The density of no-fine concrete normally ranges between 1600 and 1900 kg/m^3. This is dependent upon the shape, size and density of aggregate, the aggregate-cement-water ratio and the compaction exerted on the concrete.

AL-Rubayie [6]   reported that , the aggregate-cement ratios effect the property of No-fines concrete , he concluded that decreasing the ratio from 1:10 to1:6 lead to increasing the density and the compressive strength and decrease the absorption percentage.

Research Significance

In this study, an experimental work has been carried out to achieve the following:-
- Producing No Fine concrete according to the requirement for the mechanical properties of no fine light weight concrete with density ranges between 1600 and 1900 kg/m^3 by using different coarse aggregate-cement ratio (6:1, 9:1 and 12:1) .
- Evaluating the effect of aggregate-cement ratio on the mechanical properties of the concrete in its hardened state properties.

Materials
- Cement

Ordinary Portland cement (type I) is used in this study. The cement is (*Al-Qassim*) from Saudi Arabia origin was used in all mixes throughout this study. Its chemical and physical properties are given in Tables (1 and 2). Test results indicated that the adopted cement conformed to the Iraqi specification No.5 /1984 [7].

Table 1: Chemical composition properties of cement *

Oxides	%	IOS 5:1984 requirements
CaO	62.20	-
SiO$_2$	22.10	-
Al$_2$O$_3$	4.55	-
Fe$_2$O$_3$	3.34	-
MgO	2.32	≤5.0%
SO$_3$	1.85	≤2.8%
Na$_2$O	0.31	-

K$_2$O	0.43	-
L. O. I.	1.54	≤4.0%
Main compounds (Bogue's equation)		
C3S	44.64	-
C2S	29.68	-
C3A	6.41	-
C4AF	10.16	-

Table 2: Physical composition and properties of cement *

Properties	Cement	IOS 5:1984 requirements
Fineness Blaine method (m^2/kg)	310	≥ 225
Vicat set times(hr:min) Initial Final	2:10 3:40	≥45 min ≤10 hours
Compressive Strength (N/mm^2) at 3 days 7 days	18.6 27.5	>15 >23
Soundness: autoclave %	0.24	<0.8

* Chemical and Physical tests were made by the National Center Laboratories for Construction and Research (NCCLR)

- Coarse Aggregate

The aggregate generally used in no-fines concrete application usually ranges from 10 mm to 20mm.Five percent oversized and ten percent undersized materials are acceptable for use but there should be no particles smaller than 5 mm (Neville) [2]. If there are too many small particles it will tend to fill the voids , affecting the porosity of the concrete and associated properties.

Crushed gravel obtained from AL-Nebai area was used. The maximum coarse aggregate size was chosen to be 10mm. Table (3) shows the grading of coarse aggregate which conforms to the Iraqi specification No. 45/1984[8]. Table (4) illustrates the specific gravity, sulfate content and absorption of coarse aggregate.

Table 3: Grading of coarse aggregate of maximum size 10 mm

Sieve Size (mm)	Passing%	Limits of Iraqi specification No.45/1984
14	100	100
10	93.3	85-100
5	12.5	0-25
2.36	0	0-5

Table 4: properties of coarse aggregate*

Physical Properties	Test Results	Limit of the Iraqi Specification No.45/1984
Specific gravity	2.61	-
Sulfate content %	0.06	$\leq 0.1 \%$
Absorption%	0.59	-
S.S.D	1650	-

* Physical tests were made by the National Center Laboratories for Construction and Research (NCCLR)

-Mixing Water
Ordinary tap water was used for mixing and curing for all concrete mixes of this study

Mix Proportions
The mix proportions for no – fines concrete depends predominantly on the final application. In building applications, the aggregate-cement ratio used is leaner, usually ranging from 6:1 to 10:1. This leaner mix ensures that the void ratio is high and prevents capillary transport of water. However, in pavement applications the concrete strength is more critical and aggregate-cement mixes as low as 4:1 is used. This lower ratio ensures an adequate amount of bonding between the aggregate and cement to withstand the higher loads. [1].In this search three aggregate –cement ratio by weight are used (6, 9 and 12) to study the effect of coarse aggregate ratio on the properties of no fine concrete.

Concrete Mixes
The weight method were carried out in design the concrete mixes . Three concrete mixes are used . These concrete mixes differed by water/cement ratio and the amount of coarse aggregate. After many trials, the details of the mixes used throughout this investigation are given in Table (5).

Table 5: Concrete mixes

Mix	Cement Kg/m^3	Water Kg/m^3	Aggregate Kg/m^3	w/c by weight	Aggregate-cement Ratio by weight
M$_1$	125	48.8	750	0.39	6
M$_2$	125	56.3	1125	0.45	9
M$_3$	125	68.8	1500	0.55	12

OPERATIONAL PROCEDURE

The following operating procedure was undertaken when using the pan mixer: [1] [2]

- The inside surface of the mixer was moistened.
- The aggregate should be dampened before mixing in order to facilitate uniform coating by the cement paste.
- The aggregate and the half of the required water was added.
- The mixing was started and the cement and remaining water was added slowly.
- The mixing continued until the aggregate was sufficiently covered with cement paste.
- The mix was discharged into the wheelbarrow by fully opening the trap.
- The motor was turned off.
- The power at wall was isolated.
- The inside of the pan mixer was cleaned with water.

No- fines concrete must be placed very rapidly because the thin layer of cement paste can dry out ; this would result in a reduced strength.

HARDENED CONCRETE PROPERTIES

Five tests were carried out on no fine concrete mixes compressive strength, density, absorption , porosity , ultrasonic pulse velocity, and acoustic impedance tests .

RESULTS AND DISCUSSION

- Compressive strength of hardened concrete

The compressive strength test was determined according to BS1881: part 116:1989 [9]. This test was measured on 150 mm cubes using an electrical testing machine with a capacity of 2000 kN, at loading rate of 15 MPa per minute.

According to BS 1881 :part 113 :1983 [10] the specimens for the compression test have been compacted . The average of three cubes was adopted for each test. The test was conducted at ages of 7, 28, and 90 days { tests made in Laboratories of Baghdad University}.The compressive strength results of the different studied concrete mixes are shown in Table (6) . These results indicate that: the compressive strength decreases with increases percentage of coarse aggregate/cement ratio .The recorded compressive strength results range from (9.3 - 2.8) MPa for all mixes at 28 days age.

Table 6: Compressive strength results of concrete mixes

Mix	Aggregate-cement ratio	w/c	Compressive Strength test MPa for ages		
			7 day	28 day	90 day
M1	6	0.39	5.0	9.3	11.4
M2	9	0.45	4.4	7.3	9
M3	12	0.55	1.8	2.8	3.4

Fig. (1) shows the increase in compressive strength with time, with decrease in the ratio of coarse aggregate, this can be related to the development of the interface bonds

between the bulk hydrated cement paste and the aggregate, this agrees with many study [5] [6] .

Effect of water-cement ratio on compressive strength

The w/c ratio as such is not the main controlling factor and , in fact , there is a narrow optimum w/c ratio for any given aggregate. A w/c ratio higher than the optimum would make the cement paste drain away from the aggregate particles whereas , with too low w/c ratio , the cement could not be achieved[2]

Fig. (2) shows the increase in compressive strength with decrease in w/c ratio, this agrees with many study [5] [6] .

Fig. 1: Relation between compressive strength and age	**Fig. 2: Relation between compressive and w/c ratio**

- Density and Absorption of Hardened Concrete
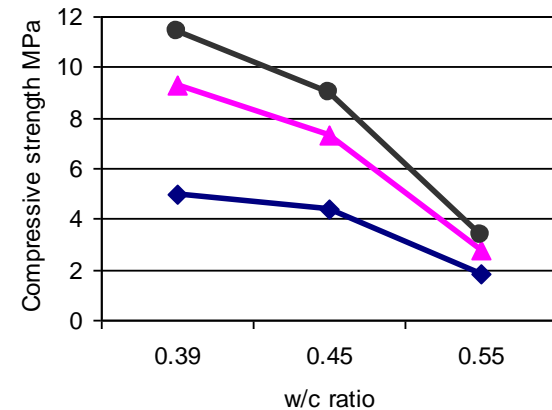
The absorption test was performed according to ASTM C642-82 [11] . This test was carried out on (150) mm cube specimens. At each test age the specimens weighted and dried in oven at temperature of (100-110) ^{o}C for 24 hours { tests made in Laboratories of Baghdad University, civil eng. Department}. After removing each specimen from the oven, it allowed to cool in dry air to temperature of 20-25 ^{o}C, then weighted. The specimens returned to oven for additional 20 hours drying period, and the procedure repeated until the difference between any respectively two successive weights is less than 0.5%, then the last weight considered to be the oven dry weight. After this, the specimens immersed in water at approximately 21 ^{o}C for not less than 48 hours and until two successive weights of the surface dried sample at intervals of 24 hours showed an increase in weight of less than 0.5% of the heavier weight. The specimen surface dried by removing surface moisture with a towel, and then weight. The heavier weight is considered saturated surface dry weight. The density and absorption results of the different studied concrete mixes are shown in Table (7) .The test conducted at age 28days. The average of three specimens adopted at each test. According to the ACI 213R - 87 [1] test result indicate that the concrete mixes with A/C ratio (9 and 12) were conform to moderate concrete .

Table 7: Density and Absorption results of the different studied concrete mixes

Mix	Aggregate-cement Ratio by weight	w/c	Density kg/m³	Absorption %
			28 day	28 day
M1	6	0.39	1907	1
M2	9	0.45	1555	1.5
M3	12	0.55	1512	2.7

Figs. (3) and (4) show the effect of coarse aggregate ratio on both absorption and densities of all mixes respectively, decreasing the ratio of aggregate and the w/c ratio leads to decrease the absorption percentage and increase the densities of the mixes. This behavior may be ascribed to significant w/c reduction which improves the uniformity of the microstructure and reduces the capillary porosity leading to better packing and increase in the density and reduces the absorption percentage. This agree with study [6] [12] . Fig. (5) shows relationship between density and absorption percentage ,

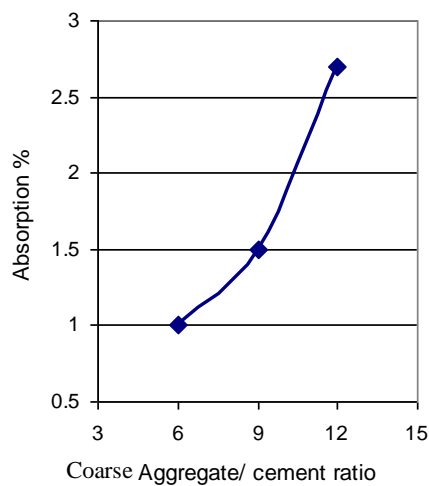**Fig. (3) Relation between absorption % with A/C ratio**

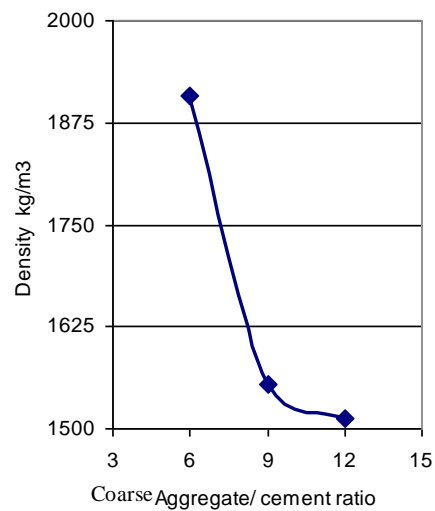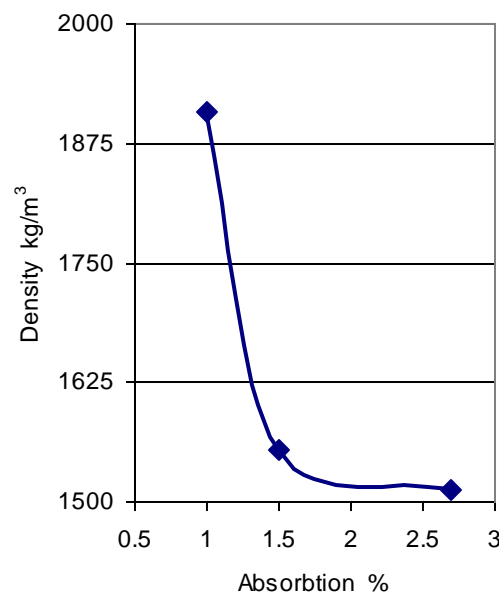**Fig. (4) Relationship between densities with A/C ratio**

Fig.(5) Relation between absorption % and densities

- Porosity of concrete mixes

Neville[2] defined porosity as the total volume of the overall volume of pores larger than gel pores , expressed as a percentage of the overall volume of the hydrated cement paste , is a primary factor influencing the strength of the cement paste .

The porosity test was carried out at 28 days by using standard cubes measuring $(150 \times 150 \times 150)$ mm .The average value of three cubes was calculated by the following equation [12]

Porosity= Density $\times$ Absorption

Table (8) showed the average result of this test

Table 8: Porosity results of concrete mixes

Mix	Aggregate-cement Ratio by weight	w/c	Density kg/m³	Absorption %	Porosity %
			28 day	**28 day**	**28 day**
M1	6	0.39	1907	1	19
M2	9	0.45	1555	1.5	23
M3	12	0.55	1512	2.7	40

Fig. (6)   Shows the effect of coarse aggregate ratio on porosity of all mixes respectively, decreasing the ratio of aggregate and the w/c ratio leads to decrease the porosity, percentage. Figs. (7) And (8) show relationship between porosity with both

of compressive strength and density respectively. It was clear that increasing % porosity lead to an decreasing in both of compressive strength and density This behavior may be ascribed to significant increasing the porosity lead to increase the voids witch lead to decreasing compressive strength and density this agrees with study done by AL - Zangy [12] .
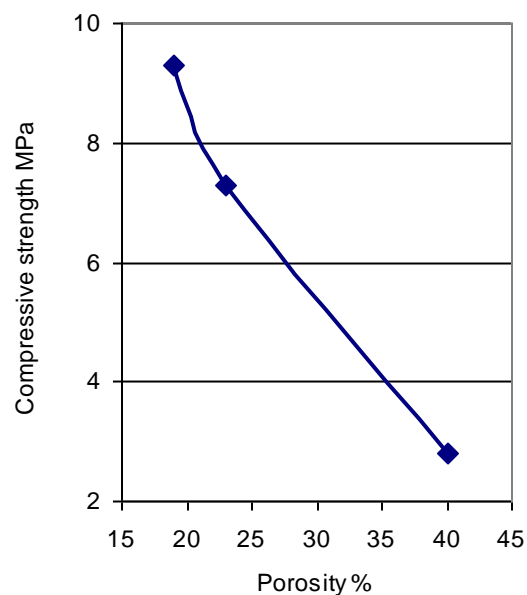
**Fig. (6) Relation between porosity percent
With A/C ratio**
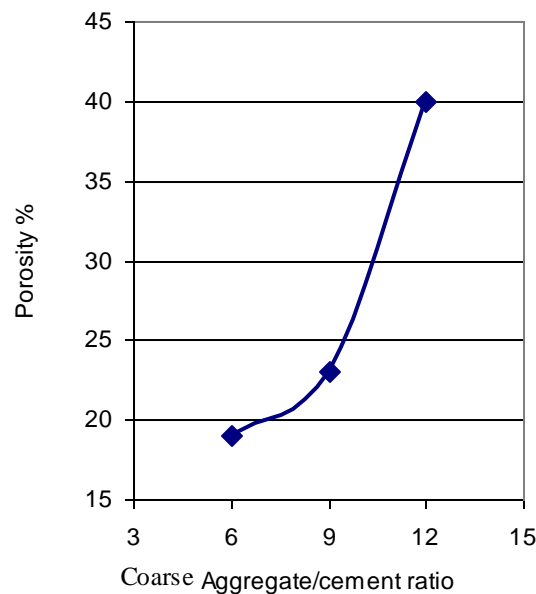
**Fig. (7) Relationship between porosity

and density**
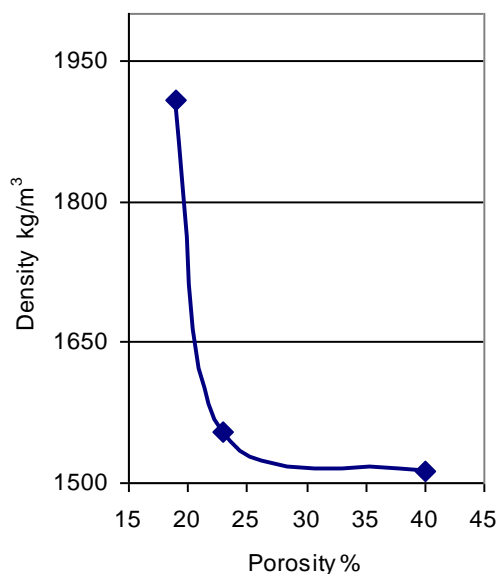
**Fig. (8) Relationship between

porosity and compressive strength**

 * Ultrasonic Pulse Velocity Test (UPV)

The ultrasonic test is a useful tool for assessing the uniformity of concrete and detecting cracks and voids. It gives useful information about size of micro-cracks zone, crack growth and the interior structure of the concrete element. [13]

According to ASTM C597-02 [14], the Portable Ultrasonic Non – Destructive Digital Indicating Tester (PUNDIT) is used. Standard cubes measuring (100 ×100) mm were demoulded one day after casting. { tests were made in Laboratories of Baghdad}

The time of travel between initial onset and the reception of the pulse was measured electronically . The path length between transducers, divided by the time of travel, gives the velocity of wave propagation:

V = L / T ………………………………………… (2)
where
V = Ultrasonic Pulse Velocity, km/sec
L = path length, mm
T = transit time, μ sec

Results of the ultrasonic pulse velocity test for all mixes, cured in tap water at 28, day, are listed in Table (9) .
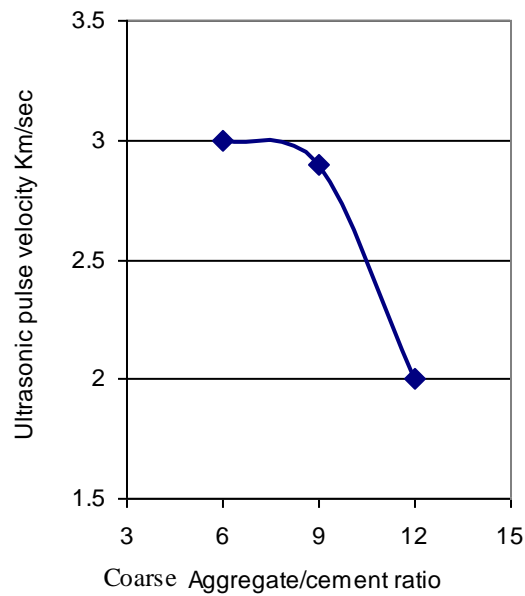
Table 9: Ultrasonic Pulse Velocity results of concrete mixes

Mix	Aggregate-cement Ratio by wieght	w/c	Ultra-pulse velocity Km/sec	
			28 day	
M1	6	0.39	3	
M2	9	0.45	2.9	
M3	12	0.55	2	

Fig.(9) shows the effect of coarse aggregate/cement ratio on ultrasonic pulse velocity of all mixes, decrease in this ratio and the w/c ratio leads to increase the ultrasonic pulse velocity .Figs. (10) and (11) show relationship between ultrasonic pulse velocity test with both of compressive strength and density respectively

It appears from these figures that as the compressive strength and density increase the ultrasonic pulse velocity increase at a different rate. This behavior may be ascribed to significant increasing the density lead to decrease the voids witch lead to decrease the spend time of velocity of the waves throw concrete, This agrees with many studies [13] [15].

**Fig. (9) Relation between Ultrasonic Pulse Velocity
With A/C ratio**

**Fig.(10)
Relationship**

Ultrasonic pulse velocity Km/sec

Coarse Aggregate/cement ratio

Ultrasonic pulse velocity Km/sec
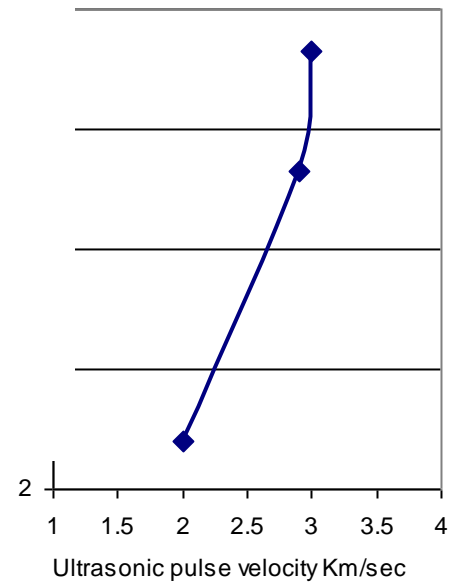
**between ultrasonic
density**

**Fig.(11) Relation between ultrasonic pulse
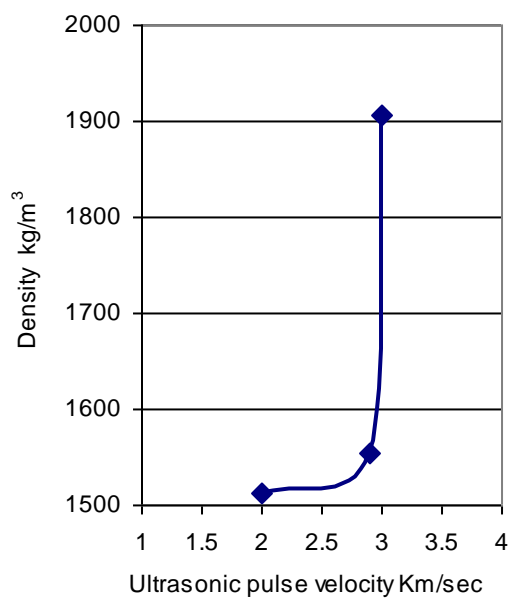velocity and compressive strength**

pulse velocity and

Density kg/m^3

Ultrasonic pulse velocity Km/sec

- Acoustic Impedance test

The acoustic impedance is a characteristic which use to make comparison between Loudness in different environment such like Loudness in air and concrete.[16] Table (10) showed The acoustic impedance for various materials

Table (10) The acoustic impedance for various materials[16]

Name of material	Density (kg/m^3)	Ultrasonic Pulse Velocity m/sec	Acoustic Impedance Rayls $\times 10^6$ Kg/(sec.m^2)
Normal concrete	2300 — 2500	4000 — 4500	9.2 — 11.3
Light weight concrete with Light weight aggregate	1200 — 1600	3000 — 3500	3.6 — 5.6
Iron	7700 — 7800	5900 — 6000	45 — 47
Aluminum	2700	6300	17
Copper	8900	4760	42
Water	1000	1480	1.48
Air	1.21	343	415×10^{-6}

The acoustic impedance was determined in this study using the pulse velocity method, in compliance with ASTM C 597-02[14] . In the present work, standard cube measuring (150 ×150) mm were demoulded one day after casting testing were cured in water and tested at 28 days .The Acoustic Impedance is calculated, as follows [16]

Acoustic Impedance = ρ V

V = ultrasonic Pulse Velocity, km/sec

ρ = concrete density (kg/m^3)

Table (11) showed the average result of this test

Table 11: Acoustic Impedance results of concrete mixes

Mix	Aggregate-cement Ratio by weight	w/c	ultrasonic Pulse Velocity km/sec	concrete density (kg/m^3)	Acoustic Impedance Rayls $\times 10^6$ Kg/(sec.m^2) 28 day
M1	6	0.39	3	1907	5.7
M2	9	0.45	2.7	1555	4.1
M3	12	0.55	2	1512	3

Fig. (12) shows the effect of coarse aggregate/cement ratio on the acoustic impedance of all mixes, increasing the ratio of coarse aggregate/cement ratio and the w/c ratio leads to decrease acoustic impedance. This agrees with studies done by AL-Jeelawi[6]

Figs. (13) (14) and (15) show relationship between acoustic impedance test with compressive strength , porosity % and density respectively

Fig. (12) Relationship between Acoustic Impedance and coarse aggregate/cement
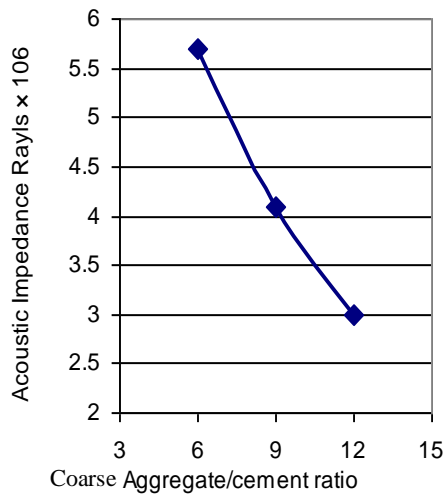
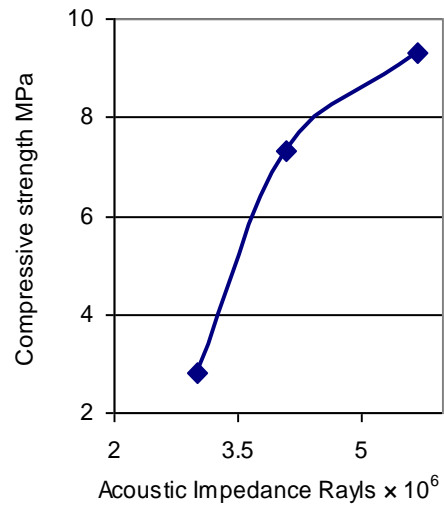**Fig. (13) Relationship between Acoustic Impedance and Compressive strength**

Fig. (14) Relationship between Acoustic Impedance and porosity
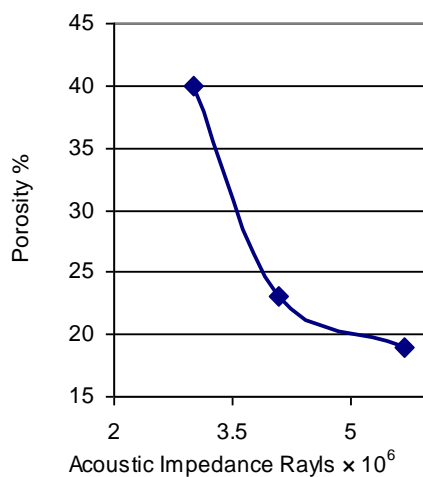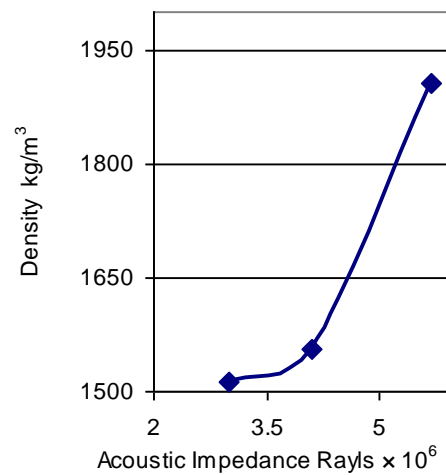
Fig. (15) Relationship between Acoustic Impedance and density

It appears from these figures that as the porosity increases, the acoustic impedance is decreases On the other hand the acoustic impedance increase with increasing the compressive strength and density at a different rate. This behavior may be ascribed to significant increasing the compressive strength lead to decrease the voids witch lead to increase in density and Acoustic Impedance and decrease in porosity This agrees with many studies [12] [16].

CONCLUSIONS

- These results indicate that, the compressive strength increases   with time .The recorded compressive strength results range from about (9.3 to 2.9) MPa for all mixes at 28 days age.
- The aggregate-cement ratios effect the property of No-fines concrete , decreasing the ratio from 12 to 6 lead to increasing the density , ultrasonic pulse velocity , compressive strength and the acoustic impedance tests and decrease the absorption percentage and the porosity %.
- The analysis of results detected that there is an inverse relation between compressive strength, density ultrasonic pulse velocity and acoustic impedance with the A/C ratio. On the other hand the absorption % and porosity % is related directly with A/C ratio.
- It was clear that the compressive strength and density increases by decreasing the porosity %.
- The UPV increases directly with compressive strength and density.
- The tests clarified that the acoustic impedance increases directly with compressive strength and density on the other hand there is an inverse relation between Acoustic Impedance and the porosity %.

REFERENCES

- Harber, P., J.,   " Applicability of No-Fines Concrete as a Road Pavement " University of Southern Queensland Faculty of Engineering and Surveying , October 2005.
- Neville, A.M., "Properties of Concrete", Longman Group, Ltd., Fourth Edition, 2002, PP.412-423.
- ACI 213R – 87 , Guide for structural lightweight aggregate concrete , ACI Manual of concrete practice, part 1: Materals and General properties of concrete 1994, 27 pp.
- Meininger , R,. C,. " No-Fines Pervious Concrete for Paving " Concrete International : Design and Construction. Vol. 10. No. 8 August pp 20-27 .
- Abadjieva , T and Sephiri , P., " Investigation on Some Properties of No-Fines Concrete " Department of Civil Engineering University of Botswana.
- Al-Rubayi, I. ,T.,K., "Using of local materials to produce light weight paving units for Baghdad municipality projects ", M.Sc. Thesis, University of Technology, May 2007, pp.169-171.
- IOS NO. 5 : 1984 , Iraqi cement standard for Portland cement.
- IOS NO. 45: 1984 , Iraqi standard for aggregate.
- B.S.1881, Part 116, 1989, "Method for Determination of Compressive Strength of Concrete Cubes", British Standards Institution, P.3.

- B.S.1881, Part 113, 1983, "Method for making and curing no- fines test cubes ", British Standards.
- ASTM C642-97,"Standard Test method for Density, Absorption, and Voids in Hardened Concrete" , ASTM Standards, .04.02,2003,PP.1-3.
- Al-Zangy, R. , A., "Properties Of Low Density Concrete ", M.Sc. Thesis, University of Technology, May 2003, p.115.
- Naik , T. R., Malhorta , V. M. , and Popvics , J. S. , **"The Ultrasonic Pulse Velocity Method "**,CRC Press LLC 2004 P. 7.
- ASTM C597-02 "Standard Test Method for Pulse Velocity Through Concrete", Annual Book of ASTM Standard, Vol. 04-02, 2002.
- Lin , Y. , Kuo , S. F. , Hsiaio , C. , and Chao , P. L. ,**"Investigation of Pulse Velocity – Strength Relationship of Hardened Concrete" ,** ACI Materials Journal , V. 104, No. 4, July – August 2007, PP.344-350.
- AL- Jeelawi , N., M., F., " properties of light weight concrete with a view to thermal insulation and acoustic impedance " M.Sc. Thesis, University of Baghdad, August 1997, pp.78 - 79.

التحولات العمرانية في مراكز المدن المقدسة
(مدينة النجف الاشرف إنموذجاً)

بهجت رشاد شاهين   حسن حيدر عبد الرزاق كمونة

جامعة بغداد ــ كلية الهندسة   ماجستير هندسة معمارية ــ بيئة وتكنولوجيا

المستخلص

تعد التحولات العمرانية من القضايا المهمة التي شغلت العاملين في حقل العمارة وتصميم المدن . وان مراكز المدن المقدسة الاسلامية قد تأثرت وبشكل واضح وكبير بالتحولات الناتجة عن ازدياد الحاجات الانسانية والتقدم الحضاري والتكنولوجي (الغير مدروس) .

وتظهر مشكلة البحث بصورة جلية في عملية التطور والتوسع للمدن المقدسة التي تمر في مرحلة صعبة بالنسبة لنسيجها التقليدي من جراء ما اصابها من تمزق في نسيجها وتحولها الى نسيج مفكك بعيداً عن نمط العمارة العربية الاسلامية التقليدية وذلك من خلال ادخال عناصر غريبة من الطرز والتفاصيل المعمارية غير الملائمة مع النسيج العمراني التقليدي .

ان عدم وجود وعي عام للمحافظة على الابنية والمدن التاريخية المقدسة سواء عند الافراد او المجتمع او دوائر الدولة هو أساس المشكلة ، وتوصل البحث الى ان الحل يأتي من خلال مواجهة هذا التيار الجارف لعملية التحضر المفرط والتحول السريع الذي رافقه نبذ للاشكال والصيغ العمرانية التقليدية والتوجه نحو اقتباس المفاهيم الغربية دون تحسس لطبيعة الموروث الحضاري والمعماري للمدن المقدسة وامكانية ترابط هذه المفاهيم مع الواقع القائم .

وانطلاقاً من ذلك جاءت اهمية القيام بدراسة المركز التاريخي لمدينة النجف الأشرف حتى نتمكن من المحافظة على هويتها وشخصيتها التاريخية ذات الطابع الديني المميز للاجيال القادمة كنموذج للمدن المقدسة ذات طابع العمارة الأسلامية التقليدية .

وقد قسم البحث الى محورين رئيسيين المحور الاول يدرس مفهوم التحولات عموماً والمحور الثاني يدرس التحولات في المركز التاريخي لمدينة النجف الاشرف القديمة .

Architectural Transformations in Holy Cities Center
" The holy city of Najaf as model "

ABSTRACT

The Architectural transformations is one of important issues that have held thought the workers in the field of architecture and design of cities, The Center of Holy Islamic Cities are affected clearly & changes caused by Increased humanitarian needs and the progress of civilization and from technology inputs.

The research shows the problem very clearly in the process of development and expansion of the holy cities undergoing a difficult period for the traditional fabric as a result of the hit torn fabric and turn them into the fabric of disassembled away from the pattern of the traditional Arab-Islamic architecture, through the introduction of Extraneous elements of style and architectural details compatible with third-traditional urban fabric.

The absence of a public awareness to preserve the historic buildings and the holy cities both at the individual or society or government departments are the basis of the problem,

The search find a solution that comes through the face of this overwhelming power over the process of urbanization and the rapid transformation of non-accompanied versions of the forms of traditional physical and the trend towards western concepts without quotation sensitivity to the nature of cultural and architectural heritage of the holy cities and the possibility of the interdependence of these concepts with reality.

Based on this study was the importance of the historical center of the city of Najaf so that we can preserve the historical identity and personality of a religious nature as a unique model for future generations holy cities of a traditional Islamic architecture.

The research is divided into two main parts , the first part studied the transformations , the second part studied the transformations in the historical center of the old city of Holy Najaf.

الكلمات الرئيسية :

التحولات العمرانية ، المدن المقدسة ، النسيج التقليدي ، مرحلة صعبة ، نموذج الاجيال القادمة .

المحور الاول :

التحولات في المدينة

* التحولات كمفهوم : (Transformation)

تعتبر التحولات من القضايا المهمة التي شغلت اغلب العاملين في مجال العمارة حيث يصف الكاتب (Anthony) في كتابه بـان التحـولات هـي عمليـة تغيير فـي العمـارة كنتيجـة ديناميكيـة داخليـة وخارجيـة . فالتحولات تعبر عن عملية تغيير بشكل تجعله يصل الى اعلى حالات الاستجابة لتأثير تلك الديناميكيـة . (Anthony , 1996 , P.66)

ويعرف (د. حيدر كمونة) التحول على انه التغير الى حالة مختلفة نتيجة فعل ما يقتضي تغيير عنصر (او اكثر) موجود ضـمن تكوين مـا أو ازالتـه ، او اضـافة عنصـر جديد او اكثر اليـه . ممـا يـؤدي الـى خلق علاقات جديدة بين العناصر الموجودة اصلاً من جهة ، وبينها وبين العنصر او العناصر التي تسبب التحول من جهة اخرى ، سواء اكانت هذه العناصر ذات طبيعة مادية ام معنوية ... الحالة الجديدة شأنها شأن الحالة القديمة قد تتصف بالاستقرار وقد لا تتصف . ويمكن لهذا التحول ان يكون تدريجياً بحيث يمثل جزءاً من التطور الطبيعي للحالة القائمة ، او يكون مفاجئاً فيتخذ طابع المواجهة العنيفة التي قد يصعب تقبلها ... في البداية على الاقل . (حيدر ، 2007 ، ص174-175)

وعليه يمكن تعريف التحول بعامة على أنه التغير الى حالة مختلفة نتيجة فعل ما يقضي تغيراً او ازالـة عنصر او اكثر ضمن تكوين ما او اضافة عنصر جديد او اكثر اليه ، مما يؤدي الى خلق علاقات

جديدة بين العناصر الموجودة اصلاً من جهة والعناصر التي تسبب التحول من جهة اخرى .

* التحولات في المدن التقليدية :

خلال ثلاثة او اربعة عقود مضت كان مقياس سرعة التحول العمراني في معظم المدن العربية مذهلاً ، فلقد اثر الرفاه المادي والتكنولوجي المتقدم بعمق في المشهد العمراني للمدن مؤثراً بذلك في معظم الخصائص المادية والقيم الاجتماعية والتوسع الحضري للمدن العربية الاسلامية .

ان معظم التحولات الحالية للعديد من المدن التقليدية ومدينة النجف واحد منها كان يتركز على المرور والشوارع المستقيمة التي تدمر في اغلب الاحيان نسيج المدينة التقليدية فضلاً عن فتح ساحات عامة كبيرة وهندسية في النسيج التقليدي نقلاً لفكرة الساحات الغربية التي تتلاءم مع متطلباتهم الوظيفية والاجتماعية والبيئية وغير الملائمة للمدينة التقليدية .

ان حصول ذلك نتيجة ان الكثير من عمليات التصميم الحالية في المدن التقليدية قد حدثت على اساس المنفعة والافادة قصيرة الامد بدلاً من نظرية الفائدة طويلة الامد ، وبذلك فقدت المدينة التواصل مع هويتها وشخصيتها المميزة التي كانت تتميز بها ، وفقدت المدينة التقليدية الحالية التوافق والترابط العضوي بين اجزائها المختلفة ، وهذا ايضاً انعكس على الحياة الاجتماعية في المدينة واصبحت المدينة اليوم جميلة بمبانيها المنفردة الذاتية على امتداد نسيجها التقليدي الذي اسهم في تأكيد تمزيق النسيج التقليدي في حين ان جمال المدينة التقليدي يأتي من تفاعلها مع الناس وترابط مبانيها والكثافة البصرية العالية والتماسك العالي بين مكوناتها على مستوى المخطط وعلى مستوى الكتل البنائية بعضها مع البعض ، ويلعب المبنى الواحد في خلق شخصية الجزء والكل في آن واحد ، وهكذا غاب عن المدن العربية التقليدية اليوم الانسجام والتكامل بين ذاتية المبنى الواحد وتشكيل المدينة العمراني كله . (خالد ، 1985 ، ص43)

من هذا كله فان تحولات المدينة العربية التقليدية اليوم اتجهت من التحول العضوي المنسجم مع طبيعتها وجوهرها التخطيطي الى التخطيط الشبكي عن طريق تكوينها الفضائي وشوارعها وتوزيع المباني فيها مما سبب افتقار المناطق الى التدرج في خصوصية فضاءاتها وضعف القدرة على ايجاد فضاءات مميزة .

* الاسباب التي دعت الى التحولات :

هناك ثلاثة عوامل أدت إلى ظهور المدينة المعاصرة والتحول من الانموذج التقليدي الى المعاصر وهي على وفق الآتي :-

‐ المفاهيم والأفكار لدى المعمار :‐

هناك موقفان في العالم العربي يقودان اعادة تكوين البيئة العمرانية الجديدة أولهما (موقف التقليديين) الذين يقرون بشرعية الماضي وبأنه الدليل الوحيد الذي يمكن الأخذ به لتشكيل الحاضر وموقف كهذا لا يمكن أن يؤدي إلا إلى عزلة المجتمع عن واقعه المعاصر ، وبذلك يصبح الموقف العام من الماضي تقليد (محاكاة) له

ليس إلا ، ولا يرفض دعاة هذا الاتجاه وانصاره استعمال التقنية الحديثة (المستوردة) فذلك ضرورة للمجتمع شريطة إفراغ وتجريد تلك التقنية من مضامينها الثقافية كافة التي نشأت فيها .

أما الموقف الثاني فهو (موقف الرافضين) فلا يقفون عند إنكارهم شرعية التقاليد فحسب بل انهم لا يقرون بأصالتها ومصداقيتها بوصفها مصدراً للحاضر ، فهم ينظرون إلى التقاليد على انها عنصر يعيق التقدم فهم يعتقدون أن النهج الوحيد لصحوة المجتمع وتقدمه هو عن طريق محو كل شيء تقليدي وتجاهله والبدء من نقطة الصفر وبناء على ذلك يضطر المجتمع الى اللجوء الى استيراد ما أمكن من الأفكار والتقنيات من الثقافات الاخرى . (صالح ، 1994 ، ص241)

فالموقفان يتفقان على نقطة واحدة الا وهي رغبتهما في استعمال التقنية الحديثة في مجتمعاتهم وكلاهما متطرف في طرحه ومرفوض في فكرته .

أن محاولة الدمج بين الموقفين هو الاصح على أن يكون التقليد بشكل تحليل واستلهام من الماضي بدلاً من الاستنساخ والمحاكاة المباشرة وتستعمل التقنية الحديثة بشكل لا يسئ إلى الموروث (أي اتخاذ صفة الوسطية العقلانية والرصانة) .

– التقنية والتكنولوجيا :–

ويتمثل العامل الثاني الذي سهل الانسياق وراء البيئة العمرانية المعاصرة وهجر البيئة التقليدية في التغيرات التي طرأت على طبيعة التقنية وحجم التنمية العمرانية . إذ أن التقنية الحديثة وفرت الإمكانات و الخيارات المختلفة لتصبح تحت إمكانية المهندس المعماري وتصرفه وان طريقة التعامل مع هذه الإمكانات هي التي حددت مقدار الإفادة منها ، أو مقدار الآثار السلبية التي خلفتها ، فاستعمال تقنيات البناء و المواد الحديثة قد فتح آفاقاً جديدة في البناء فظهرت المباني ذات الارتفاعات العالية ولكن من دون مراعاة المقياس الإنساني ومقدار تقبل نسيج المدينة العمراني لهذا النوع من المباني ، ودراسة علاقتها مع الفضاءات المحيطة. (لمياء ، 2000 ، ص53)

فادى ذلك الى اختلال في توازن البيئة التقليدية للمدينة المحلية باستيراد قيم ومبادئ جديدة غريبة عن المجتمع العربي فضلاً عن ظهور وظائف جديدة واختلاف في استعمالات الأرض وتعدد في الحرف وطرق الإنشاء ومواد الإنشاء القديمة والجديدة . والمصمم العقلاني هو الذي يعمل على ادخال التقنية الجديدة ضمن نفس اصول القيم الراهنة للنسيج القديم .

– قضايا العمارة والتحضر :–

ان هذا العامل قد شجع وعمل بشكل أو بآخر على تعزيز استمرار وتوطد نمو البيئة العمرانية المعاصرة التي تتعلق بالعمارة والتحضر على المستويين الفكري والتطبيقي فمجال الدراسات العمرانية جاء نتيجة تطور العلوم الإنسانية المعاصرة التي تأسست ونمت على مبادئ التحضر في الغرب إذ نرى أن في أية دراسة للمدن الإسلامية أو أية مدينة من مدن العالم الثالث لا تزال تأخذ أنموذج نشوء المدينة الغربية وتطورها منطلقاً لها إلا ما ندر .

كما أن الانتقال التام الى الدراسات التحليلية للمدينة العربية الإسلامية ساعد على توطيد ذلك الاتجاه فضلاً عن التقنية الحديثة والأفكار والتوجهات السياسية . (صالح ، 1994 ، 243-244)

ان الاسفادة من التجارب الغربية في العمارة والتخطيط ، وكذلك التجارب العربية السابقة بما يلائم المفاهيم الاسلامية (اعتماد الدين الاسلامي مصدراً للفكر) والبيئة الطبيعية للخروج بعمارة ذات روح متواصلة مع الماضي والحاضر .

ومن ذلك كله فان التحولات هي تغيرات ضمن تكوين معين يخلق علاقات جديدة بين عناصر التكوين (الموجود اصلاً) ، ويعد التحول التقليدي او التحول بالاستعارة من الاستراتيجيات المهمة التي يمكن اتباعها عند التحول . وان التحولات التي حصلت في المدينة العربية ادت الى فقدان وضوح التوجيه للتكوين الفضائي وفقدان خصائص المدينة التقليدية .

خلاصة المحور الاول

ان القوى المشكلة للخصائص المتغيرة في المراحل التعاقبية للمدن المقدسة تركت اثراً واضحاً في تشكيلة البنية العمرانية ، وهي كمثل (المحرك) الدائمي الذي يتقدم بالبنية وينقلها من مرحلة إلى أخرى ، فكل تكامل في البنية العمرانية يتبعه تداعياً وانحلالاً فيها ، وفي كل الحالات لابد من وجود تحول وتغير في تركيبة البنية مع (الزمن) تمثل هذه المتغيرات آلية هذا التحول وهذه المتغيرات هي:

أ– القوى الخارجية : وهي:

* القوى السياسية : فنلاحظ ان هذه القوى قد شكلت عاملاً حساساً في تشكيل بنية المدينة ، وكانت العامل المهيمن في المراحل التي مرت بها المدن التقليدية العراقية ، فتوالي السلطات والقوى السياسية المتنوعة الأجناس والأصول على حكم المدينة ولكل من هذه القوى تأثيرها في تركيبها وبنيتها ، منها ايجابي ساهم في أعمارها ومنها ما هو سلبي ساهم في تخريبها .

* القوى التقنية : لقد كان لدخول التقنيات الحديثة في المدينة أثرها الواضح في تغيرها وفي كافة المراحل التي مرت بها فدخول (المركبة) داخل المدينة غير الكثير من المعالم العمرانية والعلاقات الشكلية ، كما ان دخول مواد البناء الجديدة قد ساهم في تغير تقنيات البناء وبالتالي البنية العمرانية التي انعكست على المدينة عموماً ، فضلاً عن متطلبات العيش المعاصر .

ب–**القوى الداخلية** : وهي قوى (اجتماعية–اقتصادية): فكل مجتمع له خصوصيته وان المجتمع المشكل لمدينة النجف في المرحلة الأولى ليس هو في المرحلة المعاصرة حيث شهدت تغيرات كثيرة في التقاليد ، مع ثبات (الدين الإسلامي وقيمه وتقاليده) .

المحور الثاني :

المركز التاريخي لمدينة النجف الاشرف

* الموقع النشأة الاولى :

تقع مدينة النجف على الحدود الجنوبية للصحراء الغربية في العراق وعلى بعد (10كم) الى الغرب من نهر الفرات ، وتبتعد (160كم) الى الجنوب الغربي من مدينة بغداد و (78كم) شرق مدينة كربلاء.

فهي تقع بين خطي عرض (31-32) وخطي طول (44-45) وموضعها الجغرافي يتمثل بربوة مرتفعة تطل من الجنوب الغربي على منخفض بحر النجف وتطل من جهتي الشمال الشرقي على فضاء فسيح تشغله مقبرة وادي السلام اما من جهة الغرب فالصحراء الغربية في حين تمتد الى الشرق من المدينة اراضٍ زراعية باتجاه الكوفة . (احمد سوسة ، 1945 ، ص265)

هذا الموقع الجغرافي أكسب المدينة مناخاً قارياً صحراوياً قاسياً انعكس لاحقاً على نمط تخطيط المدينة وعمارتها فضلاً عن ان موقعها هذا جعلها مفتوحة على الصحراء بعيدة عن الحواجز ومعرضة للهجمات مما اضطر سكانها الى تسويرها عبر مراحلها المختلفة . (الشكل 1)
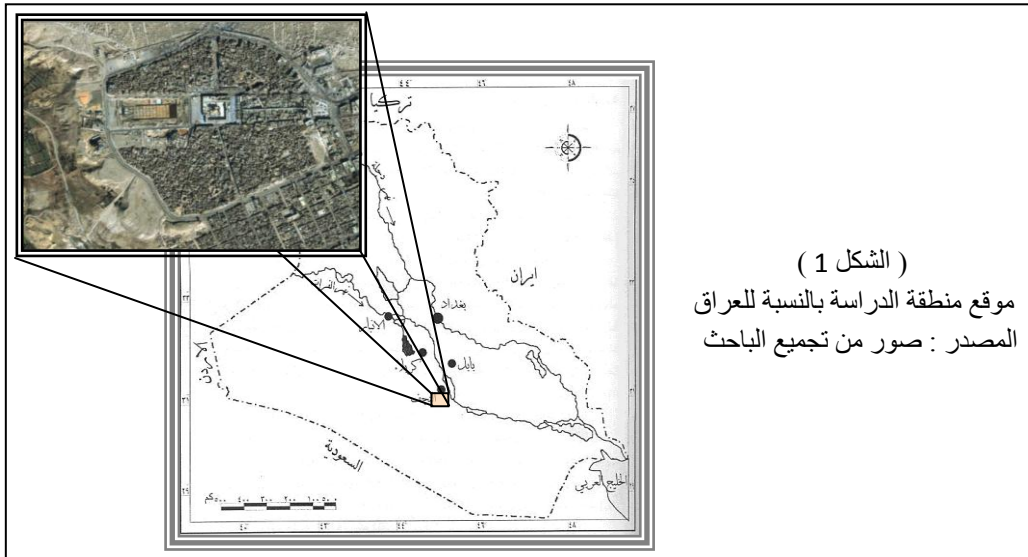
(الشكل 1)
موقع منطقة الدراسة بالنسبة للعراق
المصدر : صور من تجميع الباحث

* اثر عوامل البيئة في تكوين النسيج الحضري لمدينة النجف :

تختلف طبيعة تشكيل هذا النسيج وصياغة اشكال المباني والفضاءات الحضرية باختلاف البيئة الحضرية التي تنمو فيها المدينة ، وتنقسم هذه البيئة قسمين :

• البيئة الطبيعية : وهي ثابتة على مر الزمن المعاصر للمدينة .

• البيئة الثقافية : وهي متغيرة على مر العصور بسبب عوامل هي :

- تأثير العقيدة الدين الاسلامي .

- تأثير الجوانب الاجتماعية .

- العادات والتقاليد .

- العامل الاقتصادي .

- العامل السياسي .

769

- التكنولوجيا ومواد البناء .

فالتكون الشكلي والفضائي للنسيج الحضري لمدينة النجف لم يكن نتيجة تخطيط مسبق ولا عفوية بل جاء نتيجة طبيعية لتفاعل الانسان مع بيئته الثقافية والطبيعية ، وهذه النتيجة هي عصارة تجارب وممارسات كان للزمان والمكان أثر اساسي في بلورتها ، مما اعطى للنسيج الحضري خصوصياته ومميزاته ، ويمثل الدين الاسلامي العامل (من بين العوامل البيئة الثقافية) في التأثير والتفاعل مع العوامل البيئة الطبيعية لتشكيل النسيج الحضري والتكوين الفضائي لمدينة النجف ، بينما بقية العوامل تؤثر بدرجات متفاوتة لتعزيز العامل الاساسي .

ان الهيكل الحضري في مدينة النجف القديمة يتحدد اساساً بتأثير القيم الدينية والمبادئ والقيم الاخلاقية والروحية التي انبثقت مباشرة من الايمان بالاسلام ، ويمكن ملاحظة ذلك عن طريق اقامة المؤسسات والمدارس الدينية التي يحتاجها الدين الاسلامي التي تعُد محور الحياة اليومية وفعاليتها الروحية والاجتماعية والاقتصادية بشكل انعكس على اسلوب تخطيط مدينة النجف الاشرف وتوزيع استعمالات الارض ونظام الحركة فيها وهي التي تتنظم بنمط يؤكد على اهمية موقع هذه المؤسسات . (حيدر ، 2005)

فعلى مستوى النسيج الحضري لمدينة النجف القديمة ينعكس اثر عوامل البيئة الطبيعية على شكل هذا النسيج الذي يظهر على شكل نسيج متداخل كثيف متلاحم وذلك بتكاثف وتجميع الابنية وتراصها بحيث لايتعرض لاشعة الشمس المباشرة الا اقل مساحة ممكنة من الواجهات والسطوح . وهكذا نجد ان نسيج مدينة النجف القديمة يتميز بتداخل الكتل الصلبة ذات السطوح المستوية والفتحات القليلة والصغيرة الى الخارج .

ومن المعالجات المناخية التي ميزت مدينة النجف هو اللجوء الى الانخفاض الى المستويات دون مستوى الارض ببناء السراديب التي تقلل من اكتساب الحرارة وزيادة نسبة الرطوبة ، مما ادى الى تغيير في التنظيم الشكلي والتداخل الفضائي للابنية المكونة لنسيج المدينة . كما ان استعمال المعالجات المعمارية الاخرى كملاقف الهواء (البادكيرات) التي اتخذت اشكالاً جمالية وايقاعية وبكتل هندسية بارزة ، ميزت خط سماء مدينة النجف وساعدت في تلطيف المناخ داخل المسكن عن طريق جلب الهواء وتلطيفه وادخاله الى السرداب . وفي النجف توجد انواع من السراديب وهي كالآتي :- (الحاج ، 1948)

1- السراديب الارضية الموجودة في اغلب الدور ، معدل عمقها ستة امتار تقريباً .

2- سراديب السن (الهصهاص) ومعدل عمقها عشرة امتار .

3- سراديب سن (القرض) ومعدل عمقها خمسة عشر متراً .

4- سراديب رأس الطار ومعدل عمقها خمسة وعشرون متراً ، وهذا النوع قليل جداً وبارد جداً .

لقد امتاز النسيج العمراني المحيط بالمرقد بنسيج عضوي مترابط ترابطاً دقيقاً إذ ينتقل الانسان ضمن هذا النسيج في الازقة الضيقة التي تعطي المقياس الانساني المطلوب ، فان هذا الانتقال يحقق مبدأ الشد والجذب بين الزائر والمرقد ، إذ يشاهد القباب والمنائر بين تارة واخرى داخل الزقاق ، وعندما يصل الى المرقد فانه يدخل

الفضاء الواسع (الصحن) للمرقد ليتفاجئ بهذا الفضاء الواسع ، وهنا يشعر الانسان بالخشوع والتقوى اللازمة والضرورية للاماكن المقدسة . *

ومن ذلك كله نستخلص الآتي :-

○ لقد تعرضت الفضاءات المحيطة بالمرقد المقدس الى ممارسات تصميمية وتخطيطية احدثت تغييرات جوهرية في تكوينها الحضري تمثلت في ازالة المناطق المحيطة بالمرقد (التي تمثل مركز التكوين) وعزلها عن محيطها الحضري بما يتناقض والمبدأ الذي صممت على اساسه . فضلاً عن ماسببته هذه الممارسات من خسارة فادحة للنسيج التراثي وخصائصه الحضرية والعديد من الابنية ذات القيم التاريخية ، فانها خلقت مشاكل جديدة تمثلت في توليد المزيد من حركة السيارات حول المرقد ، فاحدثت تلوثاً بصرياً وبيئياً يتنافى مع المكانة الدينية والروحية لهذا المرقد . كما ان قرار الازالة هذا ادى الى التقليل من هيمنة فضاء الصحن على تكوين المدينة الفضائي العام وغياب عنصر المفاجأة من الصحن . ولم يقتصر الضرر على ذلك فحسب ، اذ ان واجهات اسوار المرقد كشفت الى الخارج مما دعا التعامل معها بوصفها ابنية نصبية وهو اقتباس للمفهوم الغربي ، مما استدعى المزيد من الهدم وخلق فضاءات واسعة لاستيعاب الواجهات الجديدة بشكل اوضح . ان ازالة هذه المناطق المحيطة بالمرقد تعدّ خسارة كبيرة للمدينة القديمة كما ان عزل هذا المرقد عن اطاره الحضري المتميز وجعله شاخصاً منفرداً في الفضاء يمكن رؤيته من الجهات جميعها مما افقده خصائصه التقليدية والمبادئ الاساسية التي صمم لها اصلاً .

○ ان احدى مشاكل بيئة المدينة تنبع من الحالة الرديئة للابنية المحيطة بالمرقد ذات الطرز المعمارية الغريبة التي لا تتعاطف مع خصائص المنطقة وهويتها المحلية ولا تأخذ بالحسبان القيمة المعمارية المتفردة للروضة الحيدرية الشريفة ، مما اضعف من هيمنة المرقد على تكوين المدينة الفضائي . (الشكل 2)

(الشكل2)
صور توضح الابنية المحيطة بالمرقد الشريف المتمثلة بالفنادق ذوات الطرز المعمارية الهجينة عن هوية المدينة
المصدر : الباحث

---

* لغرض الاستزادة بالمعلومات في هذا المجال راجع المصدر حيدر ، 1971 .

ذ

* مشاريع التطوير والدراسات التي طرأت على مدينة النجف القديمة :

منذ ان بدأت المدينة تتعرض لضغوط التغير لم تجر ايه محاولة جدية ومتكاملة لتطوير المدينة . فقد ادى شق الشوارع في جسم المدينة عام (1954 م) وقبله هدم السور من قبل السلطات البلدية عام (1938 م) ادى كل ذلك الى حدوث اضرار في التكوين الفضائي الحضري للمدينة واعطى فرصة لتغيير المناطق التاريخية على جانبي هذه الطرق الى استعمالات تجارية اكثر ربحاً .

وكذلك ازالة النسيج المحيط بالمرقد ومعاملته كبناء منفصل والتعاطي مع جدرانه الخارجية كواجهة ، وبعد ذلك جاءت المقترحات التطويرية المتمثلة بمشاريع مدينة الزائرين ومركز الخدمات السياحية التي تم تخصيص موقعاً لها ضمن النسيج التقليدي للمدينة ، مما استدعى ازالة مساحات واسعة من هذا النسيج لتوفير المتطلبات المكانية للمشروعين في كل من محلة العمارة ومحلة الحويش .

وكذلك الانتهاء من المراحل التمهيدية للتصميم المعماري المقترح في مركز مدينة النجف التقليدية والذي يقترح تحويل منطقة مدينة الزائرين الى صحون تابعة الى المرقد الشريف وكذلك ايجاد صحن يحيط بالروضة الحيدرية على مسافة (60م) من كل جهاته ، وكذلك ازالة المنطقة الواقعة بين ساحة الامام علي (ع) (ساحة الميدان) والروضة الحيدرية (المتمثلة بمنطقة السوق الكبير) والمقترح انشاء صحن واسع مفتوح من جهة ساحة الامام علي (ع) يحده سوقان كبيران موازيان للصحن الجديد .

ويلاحظ من كل ذلك عدم وجود سياسة حفاظ وتطوير شاملة لعموم المركز التأريخي لمدينة النجف فلم تجري اي محاولة جدية ومتكاملة لتطوير المدينة .

اما اهم المحاولات في هذا الاتجاه هي :

– الدراسات العمرانية والتخطيطية التي جرت على مدينة النجف :

جرت للمدينة عدة دراسات تطويرية وهذه الدراسات هي :

○ **دراسة مؤسسة دوكسيادس 1956 :**

ان التقرير الذي خرجت به هذه الدراسة لاينم عن ادراك لطبيعة التخطيط التقليدي ولأهمية التأريخية والتراثية لمركز مدينة النجف التأريخي او لطبيعة النسيج الحضري المتضام . اذ يذكر ان الاحوال البيئية السيئة الناتجة عن الكثافات العالية للسكان والازدحام ونقص الخدمات والفعاليات الاجتماعية لايمكن تحسينها الا باجراءات جذرية (Radical) ويتضمن ذلك ازالة مالايقل عن (50%) من مساكنها وتحسين الباقي . (IRAQ , 1958 , P.76-83)

لقد خلا التقرير من اي اشارة الى ضرورة وضع سياسة حفاظ على الابنية ذات القيمة المعمارية والتأريخية الكبيرة او الحفاظ على الشخصية الحضرية للمدينة وهويتها المحلية كما اقترح شق المزيد من الطرق لحل مشاكل المرور وتدفق الزوار .

دراسة هيئة التخطيط العمراني عام 1979 :

في عام (1979 م) تم اعداد التصميم الاساسي الثاني لمدينة النجف الكبرى من قبل هيئة التخطيط العمراني حيث جرى تحويل مقترحات التصميم الاول المعد من قبل شركة (Doxiadis) . وقد وقع هذا التقرير في نفس اخطاء التقرير السابق إذ لم يتعرض التصميم الى حل مشاكل نسيج المدينة الحضري التقليدي ولم يؤكد على الحفاظ على خصائصها الحضرية المميزة . الا انه اقترح عدة مشاريع لاعادة التطوير لقطاعات من المدينة القديمة وهذه المشاريع هي : المركز التجاري ومدينة الزائرين ، ومركز الخدمات السياحية ، مشروع توسعة دورة الصحن باربعة اتجاهات وبمسافة (60م) والمدينة السياحية في منخفض بحر النجف . (جمهورية العراق ، 1987 ، ص12-13)

ان دراسة مؤسسة دوكسيادس في عام (1956 م) وكذلك الدراسة التكميلية لها من قبل هيئة التخطيط لعام (1979 م) تدل على عدم امتلاك هذه الجهات روح الفهم للقيم الراهنة التي حملتها هذه المدينة العريقة....واستناداً الى ذلك اتجهت نحو ابسط الطرق في حل مشكلة تحرك الزائرين وزيادة اعدادهم ومشاكل تردي الحالة الانشائية للمعالم الآثارية ، فاعطت الحق لنفسها بهدم المعالم الآثارية وتوسيع الشوارع وشق الشوارع الجديدة واستخدام كل مفردة تعمل على ازالة تاريخ امتنا الاسلامية عموماً والتاريخ العظيم لعمارتنا العراقية خصوصاً .

○ **دراسة المديرية العامة للتخطيط العمراني عام 1986 :**

حيث قامت المديرية باعداد دراسة لتطوير مدينة النجف يشمل المركز التأريخي ومحلاته الجديدة (الاولى والثانية والثلمة والشوافع) والمقبرة الكبرى . وقد تضمنت هذه الدراسة عدة جوانب حيث تطرقت الى الخصائص المميزة للمدينة وعناصرها الحضرية الواجب الحفاظ عليها وابرازها هيمنة المرقد الشريف على تكوين المدينة الفضائي ، والحفاظ على الابنية ذات القيمة المعمارية والتأريخية واهمية الحركة والوصول في المدينة ، والنقص في اعداد مواقف المركبات فضلاً عن مقترحات لتحويل بعض الطرق الى ممرات سابلة ومنع مرور المركبات فيها كما تطرقت الدراسة الى ضرورة تعديل التصميم الاساسي للمدينة ليتلائم مع مشاريع التطوير المقترحة للمدينة والتي ينبغي ان تكون مترابطة مع بعضها البعض ومع هيكلية المدينة بصورة عامة .

غير ان ذلك لم يمنع الدراسة من الوقوع في بعض الاخطاء والتناقضات كان اهمها توسيع دورة الصحن لمسافة (60م) والذي يؤدي الى ازالة (40م) تقريباً من طول محور السوق الكبير فضلاً عن المزيد من عمليات الازالة والتهديم للنسيج التقليدي ، وخلق فضاءات حضرية تنافس فضاء الصحن وتؤدي الى اضعاف تأثيره وهيمنته . (جمهوية العراق ، 1987 ، ص14)

وبذلك تكون الدراسة قد ناقضت توجهها الاول الذي كان ينصب على التأكيد على خصائص المدينة التقليدية المميزة والحرص على المحافظة على هوية المدينة العربية الاسلامية .

– **مشاريع التطوير المنفذة والمطروحة773حالياً وآثارها السلبية على المدينة :**

مرت المدينة بعدة تحولات تطويرية في الآونة الاخيرة بعضها منفذ والبعض الآخر قيد الدراسة والبحث وهذه المشاريع هي :

أ- نبذة عن مشاريع التطوير :
أ-1. مشروع مدينة الزائرين

اعتمدت التصاميم التي أقرت في هذه المرحلة على خلق فضاء وسطي واسع (على امتداد المساحة المخصصة لانشاء مدينة الزائرين) خالقة بذلك محور بصري يربط المرقد الشريف بمنخفض بحر النجف حيث الموقع المخصص لمشروع المدينة السياحية .

وان المشروع عبارة عن شريطين من الابنية على شكل صناديق مثقبة تتوسطها مسقفات تعمل كاواوين موحدة باعمدة وبشكل محوري متوجه نحو المرقد الشريف ، وهي اشكال مجردة ليس لها اي انتمائية الى التراث وقيم مدينة النجف القديمة . اما ما ذكر عن الجهة المصممة حول تقسيم القواعد المربعة للسقيفة الوسطية الى ثلاثة اقسام ترتفع مكونة اشكال تحمل ايحاء لاشكال الخيم تجسيداً للماضي ... .   (الشكل 3)

نؤكد ان لاعلاقة لاشكال الخيم بمقومات واصول العمائر في مدينة النجف التاريخية والحضرة الحيدرية الشريفة .

ان التناقض الكبير مع طبيعة النسيج التقليدي للمدينة يعطي للمرقد مسحة تصميمية غريبة مشابهة لاسلوب التعامل مع النصب والكنائس في اوربا .

فضلاً عن ذلك فان هذا الفضاء الواسع سوف يعمد الى تقليل واضعاف هيمنة فضاء الصحن على الهيكلية الفضائية للمدينة .
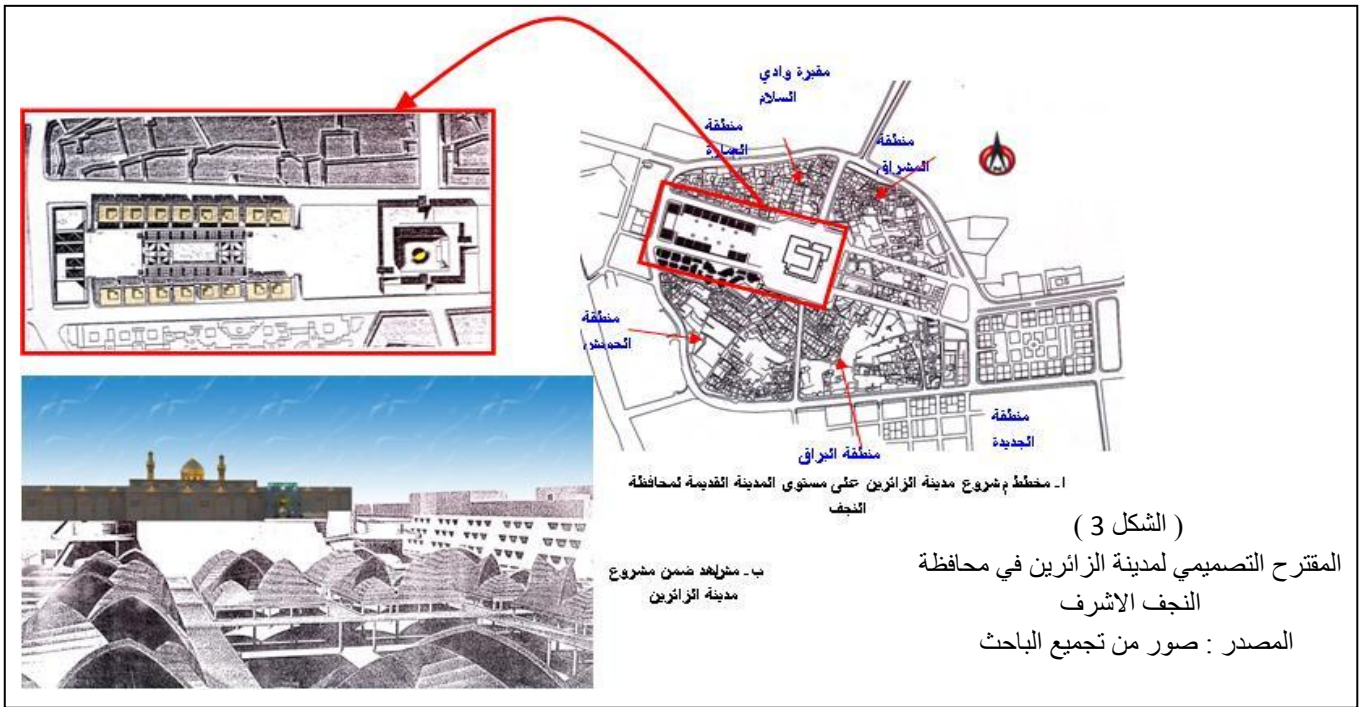
كما ان الفنادق غريبة في تصميمها مقحمة في اشكالها ومفرداتها ، كما ان ارتفاعات الكتل البنائية للمشروع عالية الارتفاع سوف تشوه خط سماء المدينة التقليدية وتسهم في اضعاف هيمنة قبة ومآذن المرقد على خط السماء ، فضلاً عن هدفها الاقتصادي الصرف والذي سيحول مدينة النجف القديمة الى ساحة للاكتساب المادي والصراع التجاري .. (وتحذر اللجنة التخصصية) من استكمال هذه المشاريع التي ستؤدي الى موت مدينة النجف القديمة وانهاء صلتها بالماضي .* (تقرير 2005 ، ص11)

جاء هذا المشروع على حساب ازاحة جزء من النسيج التقليدي وعدد من البيوت واماكن التراثية فضلاً عن عدم وجود ربط بين النسيج التقليدي للمدينة وبين التصميم اذ يظهر المشروع وكأنه كتل بنائية فرضت في داخل المدينة القديمة .

ان قرارات الازالة سابقة الذكر (هدم المنطقة المحاذية للمرقد من جهة محلة العمارة والجهة المقابلة لمحلة الحويش) ترتب عليها الطعنة القاتلة لهذه المدينة التاريخية لاغراض التطوير ، وفتح متنفس كبير داخل المدينة

---

* لجنة متخصصة من اساتذة معماريين ومخططين من جامعة بغداد والجامعة التكنولوجية وجامعة النهرين ، قدمت تقريراً حول الوضع الراهن لمدينة النجف (غير منشور) 2005 .

القديمة الذي بدأ ينافس صحن المرقد الشريف الذي كان يمثل مركز التكوين العمراني للمدينة القديمة . وهكذا عزل المرقد الشريف عن محيطه العمراني . وفصله عن النسيج التقليدي وفقد قيمته التاريخية والاثارية والانسانية ، فضلاً عن هذا وذاك ان ازالة محلة العمارة لوحدها لغرض بناء مدينة الزائرين قد هدمت ما يقارب خمسين مدرسة ومسجد وحسينية ومقبرة ومعلم تراثي (نذكر منها دار الملا ، ودار الموسوي ، ومدرسة الخليلي ... الخ من المعالم الآثارية) .

(الشكل 3)
المقترح التصميمي لمدينة الزائرين في محافظة النجف الاشرف
المصدر : صور من تجميع الباحث

١-2. مقترح مشروع (رؤوف الانصاري ، 2007) تطوير مركز مدينة النجف الاشرف وتوسعة الروضة الحيدرية :

تطرح الدراسة المقدمة عن المشروع نبذة عن واقع المدينة التي يوضح فيها المهندس الاستشاري بان النظام البائد قد ألحق ضرراً كبيراً ببنية مدينة النجف معمارياً وتخطيطياً (من خلال تهديمه لمساحات واسعة في مركز المدينة ، ثم تطرق الى اهمية المرقد بالنسبة الى المدينة وكذلك الى عدد الزوار الذين يؤمونها يومياً (المقدر حوالي (3-4) ملايين زائر في المناسبات الدينية) ، وكذلك انتقدت الدراسة التهديم الذي اصاب المدينة من جهة منطقة العمارة والحويش بحجة توسيع هذه المنطقة وتطويرها من دون وضع دراسة علمية لاعادة تصميمها .

وكذلك اكدت الدراسة على النسيج العمراني للمدينة والتشويه الذي الحق بالمناطق المحيطة بالروضة الحيدرية وان غياب الحلول والمعالجات الصحيحة ادى الى فقدان هذه المدينة المقدسة للعديد من معالمها الاسلامية المميزة . ويبين من هذا الطرح ان الاستشاري ضد مسألة تهديم مساحات حول مرقد الامام بسبب تمزيقه للنسيج الحضري .

وفي نهاية المقدمة (المعطاة في الدراسة) تؤكد الدراسة على اهمية الحفاظ على هذه المعالم المعمارية والنسيج العمراني للمدينة بسبب كونه يعطي للمدينة هويتها المحافظة . ويؤكد الاستشاري في حديثه عن المدينة باهمية السوق القديم (السوق الكبير) من الناحية الاقتصادية بالمدينة واعتباره محوراً لحركة المشاة الرئيسية المؤدية الى الروضة الحيدرية المطهرة ويعتبره علامة مميزة لمدينة النجف الاشرف.

بعد ان بدات الدراسة بايراد نبذة بسيطة عن الاعمال التي حصلت في المدينة خلال مراحل تاريخية مختلفة منوهة بذلك ضمناً عن امكانية لتغيير ملامح المدينة كلما دعت الحاجة لذلك ، ما دامت وراءه نوايا حسنة من شأنها تطوير الطاقة الاستيعابية للمدينة من الزوار (التي تمثل المشكلة الاساس في نظر الاستشاري) ... ومن هنا جاء تأكيد المشرف على المشروع باعادة تخطيط مركز مدينة النجف الاشرف لاعادة احياء الشخصية العمرانية التاريخية لمركز المدينة التراثي من خلال الاهداف الآتية :

- الحفاظ قدر الامكان على المعالم التاريخية والدينية للمدينة القديمة .
- التأكيد على تكامل وترابط الابنية الجديدة المقترحة مع الروضة الحيدرية .
- ضمان استمرارية حركة المشاة باتجاه الروضة بكل سهولة ويسر .
- التأكيد على الهوية الثقافية والدينية للمدينة واحياء رصيدها التراثي الاصيل .

وبعدها تنتقل الدراسة الى الخطوط المقترحة للتطوير العمراني لمركز المدينة والتي تقسم حسب الدراسة الى : (الشكل 4)

(أ) المنطقة المحيطة بالروضة الحيدرية الشريفة .

(ب) المنطقة المحصورة بين شارعي الامام الصادق والامام زين العابدين (ع) والممتدة من ساحة الامام علي (ع) او (ساحة الميدان) الى الروضة الحيدرية والتي تشمل ايضاً السوق الكبير .

(ج) المنطقة الممتدة من الروضة الحيدرية الى الجهة المطلة على بحر النجف والتي تسمى حالياً بمدينة الزائرين او منطقة العمارة سابقاً .

ونظراً للكم الهائل من الزوار المتوافدين يومياً الى هذه المدينة ترتئي الدراسة ايجاد سوقين كبيرين على جانبي الصحن المقترح الممتد من ساحة الامام علي (ع) الى الروضة الحيدرية ويكون السوقين ملاصقين للصحن . ان الهدف من بناء هذين السوقين (حسب قول الاستشاري) هو احياء وتكريم السوق الكبير الذي سيتم هدمه بسبب التشويه العمراني الذي اصابه في نهايات القرن العشرين بالبلوك الاسمنتي وصفائح الجينكو والذي يغلق المشهد البصري عن مرقد الامام علي (ع) الذي يجب ان يكون العنصر المهيمن والاهم في مدينة النجف الاشرف .
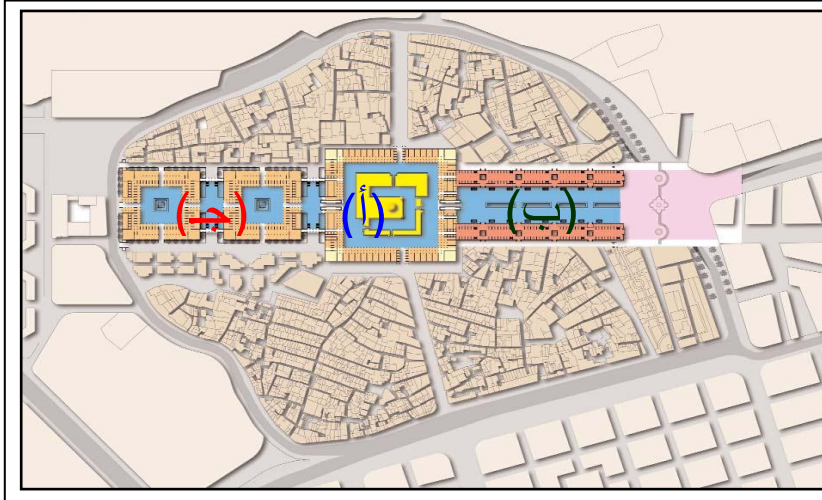
(الشكل 4)
المقترح التصميمي لمدينة النجف القديمة الذي أعدهُ الدكتور رؤوف الانصاري
المصدر : د. رؤوف محمد علي الانصاري ، 2007 ، ص20

وتعد دراسة التطوير هذه انها قد احيت السوق الكبير بانشاء سوقين جديدين تكريماً لذلك السوق الذي سيتم هدمه والاشارة اليه عن طريق هذين السوقين الجديدين !!!

* المشاكل التصميمية والتخطيطية التي ظهرت من خلال مشاريع التطوير المقترحة :

كان الموروث الحضري لمدينة النجف والى حد قريب اكبر واغنى تراث في المدن التقليدية في العراق الا انه تعرض وبشكل مستمر الى الفقدان بشكل سريع ولازال الخطر قائماً من فقدان اكبر . ومن اهم العوامل التي ادت الى تمزق النسيج الحضري في المدينة هي :

– شق الشوارع المستقيمة وبشكل متعسف ودون دراسة للخصائص الفضائية التركيبية لنظام الحركة السابق والذي يمكن تطويره دون هذه العمليات وقد ادى ذلك الى تهشيم الكيان وتجزئته الى اجزاء متفرقة تفتقر الى الوحدة والترابط الاجتماعي والعمراني .

– ازالة المناطق المحيطة بالصحن الشريف والتي كانت تمتد حتى جدار الصحن من جهاته الاربع . (الشكل 5)

– ازالة اجزاء كبيرة من النسيج الحضري وخاصة في محلة العمارة ذات التراث الغني لاغراض مشروع مدينة الزائرين ومن محلة الحويش لاغراض مشروع مركز الخدمات السياحية .

– استكمال المراحل التمهيدية لمشروع التصميم الاساسي الجديد لمدينة النجف القديمة الذي سيزبل واحد من اهم معالمها الاثرية القائمة وهو السوق الكبير المسقف الذي يتجاوز عمره المئتي عام ، فضلاً عن الدور والمنازل القريبة من الصحن والتي تمتاز بعمارة نجفية خاصة لايعرفها الا من عاش بين جدرانها . (رؤوف ، 2007)

– كما ساهمت عوامل اخرى في هذا التمزق من بينها انعدام الصيانة داخل ازقة المدينة ومبانيها .

ويعتبر تمزق النسيج الحضري من اخطر المشاكل التي تعاني منها المدينة واكثرها تهديداً لشخصية المدينة الحضرية لانه ادى :–

(1) فصل المرقد عن اطاره الحضري (Urban context) .

(2) فقدان خصائص التنظيم الفضائي الشمولي والموضعي المميز للمدينة .

(3) تمزق النسيج الاجتماعي المرادف للنسيج العمراني .

(4) فقدان العديد من الابنية ذات القيمة المعمارية والتاريخية .

(5) التلوث البيئي والبصري الناتج عن دخول المركبات وعلى نطاق واسع الى قلب المركز التاريخي.

ولذلك ينبغي ترميم النسيج الكلي ومعالجة التمزقات وملئ الفجوات وصولاً الى استعادة كيان المدينـة الاصلي .

(الشكل 5)
شكل يوضح اثر شق الشوارع حول مرقد الامام الامر الذي احدث تحولات في بنية المدينة التقليدية
المصدر : الباحث

مرقد الأمام علي (عليه السلام) بعد شق الشوارع يلاحظ تفكك النسيج مبتعدا عن المرقد الشريف بشكل غير متعارف عليه في المدن الإسلامية
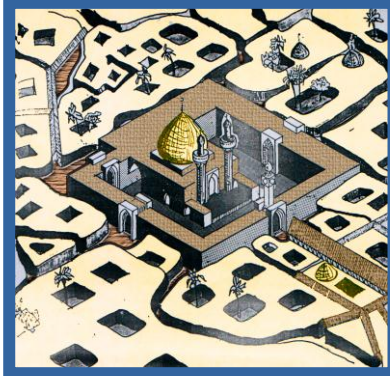
مرقد الأمام علي (عليه السلام) قبل شق الشوارع يلاحظ تضام النسيج و احتضانه للمرقد الشريف و يلاحظ بوضوح هيمنة المرقد بهيئته الروحية و المادية على المدينة

* الموقف من مقترح مشروع تطوير مركز مدينة النجف الاشرف المقدم عام 2007 :

ان الغاية الكبرى من مناقشة هذا المشروع هو كيفية الحفاظ على ما تبقى من الموروث وعدم التفريط به ، نحن ليس بيدنا القرار ، ولكن باستطاعتنا ان نوجه المشروع نحو المسلك الصحيح واعطاء الايجابيات والسلبيات قبل ان يتحول من الورق الى الواقع .

ان المبررات التي قدمتها الجهات المعنية بالمشروع ضعيفة جداً مقابل جسامة العمل المقترف بحق هذا الصرح التاريخي . حيث ان استيعاب عدد الزائرين المتزايد وكون المنطقة تعاني من اهمال بسبب ضعف الخدمات المقدمة اليها ..... ، وان الغاية من توفير اسواق حديثة ومكان للزائرين غاية نبيلة ولكن لاتكون على حساب هذا التراث الحضاري .

ان العمل ضمن نسيج حضري تاريخي له من التميز والقدسية يتطلب الحذر والانتباه الى نقاط عديدة اهمها هيمنة الشواخص التاريخية في المنطقة ، والحفاظ على الهوية المتميزة لمدينة النجف الاشرف ، فضلاً عن ابراز البعد الزماني والمكاني للمبنى الجديد الذي بصدد الانشاء بدون المساس بتلك الهوية .

وان دراسة مشروع المقترح التطويري تثير عدة نقاط تستوجب الوقوف عندها ومناقشتها . والتي سيتم ايرادها هنا حسب تسلسل ورودها في الدراسة التي نحن بصددها :

اولاً : فيما يخص الروضة الحيدرية :-

ان مقترح ايجاد صحن واسع يحيط بالروضة الحيدرية من جهاتها الاربعة (وعلى مسافة (60م) من كل جهة) قد عولج باسلوب حجب ملامح الصحن الاساسي بالكامل مما يحتاج الى اعادة نظر في الربط بين هذا الصحن الاساسي دون ان يحجب رؤية الاخير من محاور الحركة الرئيسية المؤدية اليه . (الشكل 6)

ان عملية استنساخ الواجهات الرئيسة للصحن وتعميمها على كافة الابنية الجديدة المقامة من توسعة الصحن الى الاسواق ، قد تؤثر بشكل سلبي على هيمنة الروضة الحيدرية من خلال طرازها المعماري المتفرد في المنطقة فضلاً ان هذا الاستنساخ المباشر يعد تزويراً ساذجاً للقيم التراثية فهو لايحترم الفرق الزماني بين الاصل والتحديث ، وبهذا يفقد المبنى شيئاً كبيراً من اصالته ومصداقيته التاريخية . (الشكل 7)
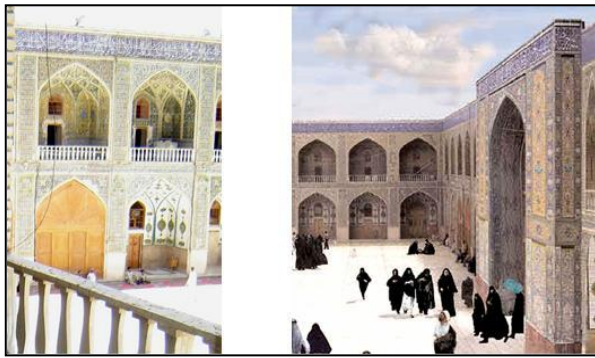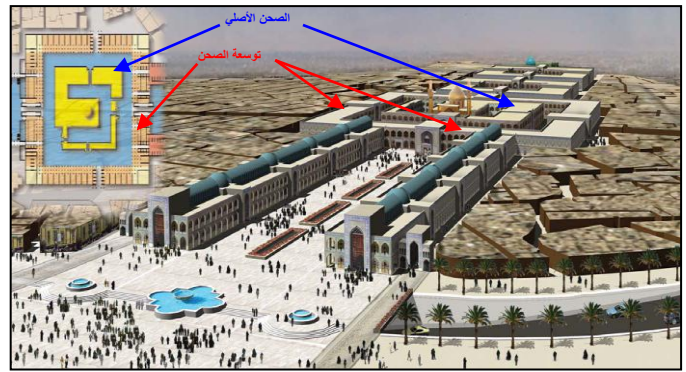

تفاصيل الاواوين في الحرم الحيدري الشريف تفاصيل الاواوين في جميع فضاءات المشروع الجديد

(الشكل 7)
استنساخ واجهات الصحن الحيدري الشريف وتعميمها على ابنية المشروع الجديد كافة
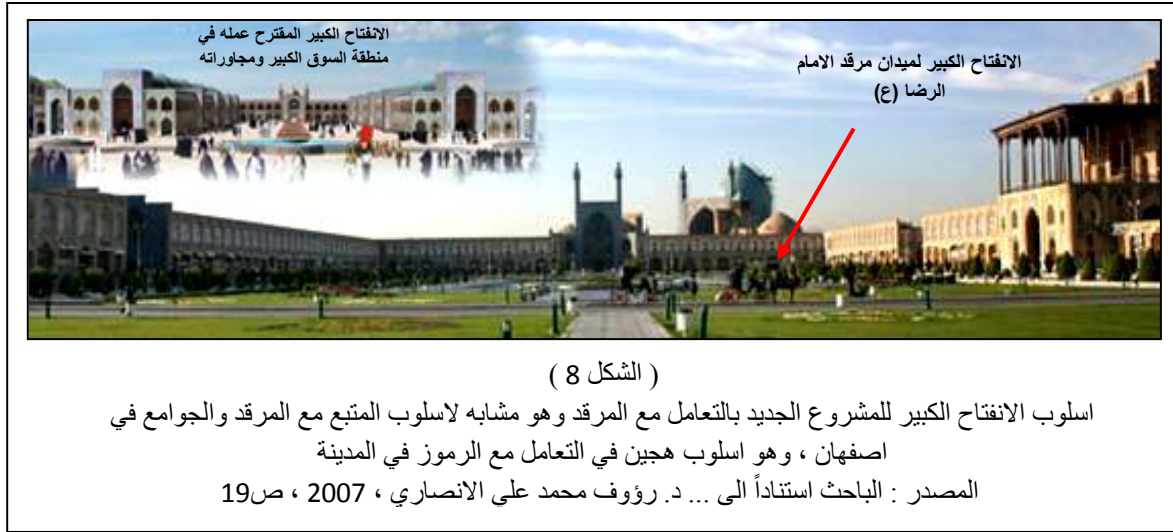المصدر : صور من تجميع الباحث الباحث

(الشكل 6)
يوضح حجب الصحن المقترح لملامح الصحن الحيدري الشريف بالكامل
المصدر : الباحث استناداً الى ... د. رؤوف محمد علي الانصاري ، 2007 ، ص20

كما ان الصحن المقترح الممتد من ساحة الامام علي (ع) الى الروضة المطهرة واقتراح تسقيف جزء منه برواق عريض يحمي الزوار في الشتاء والصيف ويوفر الخدمات للزوار حسب ما جاءت به الدراسة ، في الحقيقة ان هذه المساحة لاتفي حاجة (3-4 ملايين زائر في المستقبل) من الخدمات والمتطلبات التي يجب ان توفر اليهم وان عملية حماية الزائرين من الشمس بهذه الطريقة بالنسبة لهذه المساحة المحددة غير مجدية وهي لاترتبط بهوية مدينة النجف (اي عمارة دخيلة على المدينة) . وان خلق هذا الصحن الكبير في وسط المدينة القديمة (وهو نفس الخطأ الذي وقع فيه مشروع مدينة الزائرين) . كما ان الانفتاح الكبير جداً المقترح عمله في منطقة السوق ومجاوراته ، مزق ما تبقى من النسيج الحضري للمدينة وهو اسلوب غريب على المدن العربية التقليدية ، مما جعل اسلوب التعامل مع المرقد مشابه لاسلوب التعامل مع مرقد (الامام الرضا (ع)) في مدينة اصفهان في ايران ، مما افقد المدينة هويتها كمدينة عربية عراقية نجفية .(الشكل 8)

يوضح الشكل (4) الفصل الواضح في النسيج وكأنه قسم المدينة القديمة الى نصفين ، وعلى الرغم من محاولة المشروع الجديد في ربط الابنية الجديدة مع الروضة الحيدرية ولكن بالمقابل زادت من عزلتها عن

779

المناطق المحيطة بها (التقليدية) ، وكأنه اقام جدار عازل بين الضريح والمدينة القديمة .

(الشكل 8)
اسلوب الانفتاح الكبير للمشروع الجديد بالتعامل مع المرقد وهو مشابه لاسلوب المتبع مع المرقد والجوامع في اصفهان ، وهو اسلوب هجين في التعامل مع الرموز في المدينة
المصدر : الباحث استناداً الى ... د. رؤوف محمد علي الانصاري ، 2007 ، ص19

ان هذا الاسلوب سيؤدي الى طمس هوية المدينة وهو بازالة اكبر معلم (Land mark) في المدينة بعد المرقد الشريف المتمثل بالسوق الكبير .

ثانياً : فيما يخص الاسواق الجديدة المقترحة في مركز المدينة :–

تشير الجهة المصممة كما اشرنا سابقاً الى تكريم واحياء السوق الكبير المقترح ازالته ! من خلال ايجاد سوقين كبيرين على جانبي الصحن المقترح ، فاذا كان المصمم يعتقد باهمية هذا السوق وبانه يستحق التكريم والاحياء فلماذا يتخذ قراراً بهدمه ؟ ، واذا لم يكن هذا السوق بتلك الاهمية فما الحاجة الى تكريمه على نحو يُفرض على التصميم الجديد ؟ فهو هنا يهدم ويبني نصباً تذكارياً للعنصر المهدم ، ما العبرة من التهديم والتكريم بعدها ؟!

اشارة الدراسة المقدمة ان احدى الاسباب المهمة لازالة السوق الكبير هو التشويه الذي اصابه في العقدين الاخيرة من القرن الماضي . ان السبب الذي طرحته الدراسة لتهديم السوق الكبير والمنطقة المحيطة به ليس سبباً مقنعاً لإزالة هذا المعلم النجفي . لان التشويه الذي اصابه في مرحلة معينة يعبر عن مرحلة ما مر بها السوق ولكن اثره ومعالمه وتاريخه باقٍ الى حد الآن . وان وجود السوق في هذا المكان ليس وليد مرحلة قريبة وانما وجد مع وجود المدينة ونشؤها اي قبل مائتي سنة . وان ازالته بهذا الشكل يعتبر تخريب بحق المدينة المقدسة . وان تكريمه بهذان السوقان يعتبر تشويه لهوية المدينة النجفية ولعمارتها المتميزة . أليس من الافضل ان يتم اعادة بناء السوق الكبير كما كان في سابق عهده ، من ان يتم هدمه نهائياً .

ان عملية التطوير المذكورة تستهدف ازالة المنطقة باكملها التي من شأنها تغيير الطبيعة العمرانية للمدينة فضلاً عن تغيير نمط الحركة داخلها . وهذا تجاوز سافر على المدينة القديمة تضاف الى التجاوزات التي حصلت للمدينة منذ تهديم سور المدينة وشق الشوارع الاسفلتية داخلها .

فضلاً عن ان الاسواق الحديثة المقترح انشاؤها تؤثر على هيمنة الروضة الحيدرية والبعد التاريخي لها وهويتها المحلية وذلك من عدة نواحي :

- الانفتاح الكبير غير المدروس لمنطقة السوق الكبير والذي مزق النسيج الحضري وغير قوى التوازن للنسيج .
- ارتفاع نسب الكتل المستعملة وخاصة المداخل .
- استنساخ بوابة الصحن واستعمالها بشكل مبالغ فيه (في المباني المخصصة لتوسعة الصحن والاسواق) مما افقدها تميزها .

ان الاستخدام المبالغ لمثل هذه التفاصيل يفقدها قيمتها الجمالية وقدرتها على جذب انتباه الزائر ويكون مبعثاً للملل .

وفي هذه المرحلة يطرح الاستشاري رأيه عن السوق الكبير بانه يغلق المشهد البصري عن مرقد الامام (ع) وهو بطابقين ، فهو يعود ويبني سوقاً يثلاث طوابق ولن يحجب الرؤيا ؟

ومن خلال ملاحظة المنظور الخاص بمداخل الاسوق الحديثة نجد ان ارتفاعها مقارب لارتفاع القبة الحيدرية المطهرة وبارتفاع سور الصحن الحيدري الحالي ، وبهذا يظهر لنا انه فقط من منطقة المحور الطولي يستطيع الزائر ان يرى قبة الامام ومنارته ، اما اذا كان في جانبي المحور الطولي فانه لن يستطيع رؤية أي شي. (الشكل 9)

بعد ازالة المعالم العمرانية للمنطقة (المتمثلة بالسوق الكبير) والذي تعترف الدراسة ذاتها باهميته التاريخية ، هل يكفي هذان السوقان للتعريف بتاريخ السوق الكبير وهل سيفي هذا الحل بمتطلبات الاجيال اللاحقة التي لها الحق في التعرف وامتلاك هذا الموروث الحضاري والتاريخي ؟!؟
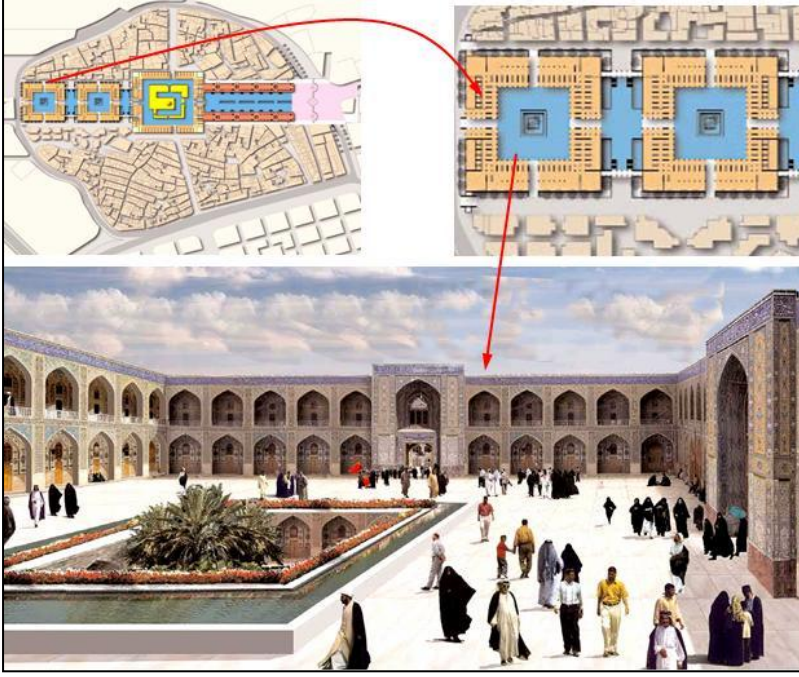

(الشكل 9)
شكل يوضح ارتفاع الابنية المقترحة بالنسبة الى المرقد وسور المرقد الشريف
المصدر : الباحث استناداً الى ... د. رؤوف محمد علي الانصاري ، 2007 ، ص19

ثالثاً : فيما يخص تطوير الجهة الغربية من المرقد (مدينة الزائرين) :-
تقترح الجهة المصممة ايجاد صحنين واسعين يكونان امتداداً طبيعياً لصحن الروضة الحيدرية .
ان ادخال هذا المقترح ضمن مشروع التطوير 781

(الشكل 10)

الصحون المقترحة في المشروع الجديد الواقعة في منطقة العمارة بدل مشروع
مدينة الزائرين

المصدر : الباحث استناداً الى ... د. رؤوف محمد علي الانصاري ، 2007 ، ص19

صفة ايجابية لاستعادة جزءاً من لمحة النسيج التقليدي الذي بدأ يتفكك بسبب مشاريع التطوير التي مرت على المدينة وكذلك التأكيد على روحية المدينة الديني الانساني .

ولكن جاء تصميم هذين الصحنين واسعين اشبه ما يكون بالكتل المزروعة وسط النسيج العضوي والتي صممت على اساس انها امتداد للصحن الحيدري الشريف ، فهي مبالغ في حجمها ، وشكلها وبالتالي ستضيع هيمنة الصحن الحيدري على مستوى المدينة القديمة . (الشكل 10)

خلاصة المحور الثاني

ان حالة التدهور والتداعي الذي بلغته مدينة النجف القديمة أدت الى تهديد الرصيد الهائل من الموروث الحضاري والخصائص المتفردة بالأندثار والزوال والذي يعود جانب منه في العديد من الحالات الى أقتباس المفاهيم الأساسية الغربية (إذ أصبحت الغربية مرادفة للتطور) وأقحامها بشكل قسري ومتعسف دون تحسس وادراك لطبيعة النسيج الحضري وخصائص التكوين الفضائي لتلك المدينة والتي تبلورت عبر قرون عدة من الزمن ، كما كان للممارسات الخاطئة من قبل الجهات والهيئات التصميمية و التخطيطية دور كبير في التأثير السلبي على النسيج الحضري وتمزيق وحدته واضمحلال خصائصه ولقد أدت عملية أزالة مساحات واسعة من النسيج الحضري لمدينة النجف القديمة تحت ذرائع وتبريرات مختلفة الى فقدان العديد من الشواخص والرموز المعمارية ذات القيم التاريخية والمعالم التراثية او عزلها عن محيطها وفقدان ترابطها بأطارها الحضري الذي أرتبطت به عبر حقب طويلة ففقدت بذلك الكثير من دلالاتها ومعانيها وجعلتها في وضع لم تكن مصممه له أساساً على الأطلاق ، وحلت محلها خلال زمن قصير أنماطاً غربية لا تنسجم مع الواقع شكلاً ومضموناً (يمكن ان تناسب أي مدينة في العالم) وتهدد بتحول المدينة القديمة الى نسخ مشوهة من المدن الغربية . الا انه يمكن القول بأن الفرصة لم تفت بعد للحفاظ على أصالة تكوينها وخصائصها المميزة واستمرارها في الحياة والتواصل الحضاري ، وذلك لأنها تعد تراثاً وكنزاً حضارياً لكونها جزءاً من الماضي الذي نعتز به . وإن الأعتزاز بالأصالة والرغبة بالحفاظ على الأرث الحضاري العريق ليس كافياً بل يتطلب الأمر تظافر كل الجهود كما يتطلب اتخاذ الإجراءات الفعالة من خلال وضع ضوابط و محددات عمرانية وتخطيطية قانونية للسيطرة

على ما يحدث في المدينة القديمة من تحول ، إن السيطرة المطلوبة في هذه المدينة لا يعني بأي حال من الأحوال منع وإخماد التطوير ، إذ إن أبقاء هذه المدينة على واقع حالها سيؤدي إلى اضمحلالها وإخلائها حتى من سكانها .

* الاستنتاجات

– يجب ان لاتكون التحولات العمرانية في سياساتها المختلفة استنساخاً للماضي لان هذا هو الجمود الحضاري ، وان لايكون تقليداً للغرب ينقصه الشخصية العربية الاسلامية والطابع المحلي ، وانما يكون توظيفاً للتكنولوجيا الحديثة والاستفادة من التراث لتكوين شخصية جديدة تحكي قصة هذا الجيل وللاجيال القادمة .

- لقد ادت التحولات الكبيرة في التكوين العمراني لمدينة النجف القديمة الى تقليل التفاعل بين السكان والبيئة العمرانية وبالتالي تشتت المجتمع ، حيث لاتوجد في المدينة فضاءات مليئة بالحياة العامة ، فقد فقدت فضاءاتها كل معانيها ودلالاتها ومقياسها الانساني ، واصبحت الطرق المخصصة لحركة المركبات هي المظهر الطاغي على تكوين المدينة فافقدتها شخصيتها واصالتها للقيم المادية على القيم الانسانية والمعنوية والروابط الاجتماعية ، وشملت هذه التحولات الانسان المعاصر الذي بدت نظرته سطحية باهتة لمنظر المدينة. واصبحت المدينة الجميلة في نظره تتكون من مجموعة مباني متفردة وجميلة ولكنها بعيدة عن تكامل التكوين العمراني لعموم المدينة .

– ان التعامل مع الشواخص الدينية الموجودة كابنية نصبية هو اقتباس للمفهوم الغربي في التعامل مع النصب ، مما سيفقدها وظيفتها الروحية ويفكك النسيج المتضام ويبعدها عن اعطاء مشاعر روح السماء وتجسيد افكار الاسلام فيها . خصوصاً وان الهيكل العمراني لمدينة النجف القديمة يتحدد اساساً بتأثير القيم الدينية والمبادئ والقيم الاخلاقية والروحية التي انبثقت مباشرة من الايمان بالاسلام ووجهاء النجف الاشرف وعلمائها التي تذكر الازقة الموجودة لحد الآن تحركاتهم ووقع خطواتهم .

– ان الخصائص المتفردة من النسيج التقليدي لمدينة النجف القديمة وعناصر التكوين الاساسية لهيكلها العمراني هي استجابة لتفاعل عوامل عديدة (عوامل البيئة الثقافية ، وعوامل البيئة الطبيعية) التي لازالت معظمها قائمة ومؤثرة لحد الآن ، وليس هناك مبرر لاقحام انظمة عمرانية غريبة تؤدي الى الاخلال بالتوازن القائم بين محتوى البيئة العمرانية ومكوناتها المتفردة .

لاسيما وان الأنماط العمرانية التقليدية ليست عاجزة عن أستيعاب التطور المعاصر اذا تهيأت لها أسباب التخطيط العلمي الدقيق لكي تحافظ المدينة على رونقها وهويتها النجفية .

– على المشاريع التطويرية ان تعمل على زيادة اللحمة في نسيج المدينة المتمزق وان يكون هدفها هو ان يزور الزائر الحياة التقليدية ثم المدارس الدينية وصولاً الى المرقد حيث يعمل على تحويل زيارة

– النسيج الى جزء من الزيارة الاساسية للمرقد مما يعمق من تقدير التراث وارتباطه بالاصالة . وعلى ان ينظر للمدينة على انها محمية عالمية لايحق لأحد ان يتلاعب بقيمها ودلالاتها التراثية .

المصادر

- المصادر الاجنبية

- Anthony , C. Antoniades , **" Poetics of Architecture – theory of design "** , Professional . Reference , and Trade Group 605 , Third Avenue , New York , 1996 .
- Iraq , Ministry of Planning , Development Board , Doxiadis Associates Consulting Engineer's **, " The Future of Najaf &Kufa "** , 1958 .

- المصادر العربية

- احمد سوسة ، " **وادي الفرات ومشروع سدة الهندية** " ، مطبعة المعارف ، بغداد ، 1945 .

- الحاج عبد الحسن شلاش ، " **ابار النجف ومجاريها** " ، النجف الاشرف ، مطبعة النجف ، نشر عام 1948 .

- تقرير اللجنة التخصصية " **حول مشروع توسعة الحرم الحيدري الشريف في النجف الاشرف** " ، تقرير غير منشور ، عام 2005 .

- جمهورية العراق ، وزارة الحكم المحلي ، المديرية العامة للتخطيط العمراني ، قسم المناطق الوسطى ، " **مشروع تطوير مدينة النجف القديمة** " ، بغداد ، 1987 .

- حيدر عبد الرزاق كمونة ، " **المدينة وآثارها المعمارية** " ، مجلة سومر ، الهيئة العامة للاثار والتراث ، العدد 27 ، 1971 .

- حيدر عبد الرزاق كمونة ، " **سبل الحفاظ والتجديد الحضري لمدينة النجف القديمة** " ، المؤتمر العلمي الرابع للمعهد العالي للتخطيط الحضري والاقليمي ، جامعة بغداد ، بغداد ، 2005 .

- حيدر عبد الرزاق كمونة ، " **التغير في خصوصية المدينة بين التراث والمعاصرة** " ، بيت الحكمة ، مجلة الحكمة ، العدد 44 ، بغداد ، تموز ، 2007 .

- خالد السلطاني ، " **واقع العمارة المعاصرة في العراق** " ، وزارة الثقافة ، دار الشؤون الثقافية العامة ، مجلة افاق عربية ، العدد9 ، بغداد ، 1985 .

- رؤوف محمد علي الانصاري ، " **مقترح مشروع تطوير مركز مدينة النجف الاشرف وتوسعة الروضة الحيدرية** " ، مجلة المهجر ، صادرة عن جمعية رعاية العراقيين ، المملكة المتحدة ، العدد 48 ، لندن ، حزيران ، 2007 .

1. صالح بن علي الهذلول ، " **المدينة العربية الاسلامية واثر التشريع في تكوين البيئة العمرانية** " ، الطبعة الاولى ، دار السهن للطباعة والنشر ، المملكة العربية السعودية ، الرياض ، 1994 .

- لمياء سليم الداهري ، " **الحد من اثر الفكر الغربي في تخطيط المدينة العربية الإسلامية** " ، رسالة ماجستير غير منشورة ، جامعة بغداد ، مركز التخطيط الحضري و الإقليمي للدراسات العليا ، بغداد ، 2000 .

أدارة وتخطيط الكلفة في مشاريع التشيد

مرفت رزاق ولي الطائي   زهير ميخائيل ساكو

جامعة بغداد – كلية الهندسة – قسم المدني

COST MANAGEMENT AND PLANNING IN CONSTRUCTION PROJECTS

ABSTRACT

This research aims at emphasizing the significance of sound management and cost planning from the beginning of the project undertaking in order to facilitate the proper establishment for conducting and systemizing the project costs. Also, to determine the major obstacles that affect the management and scheduling of construction costs and to suggest solutions through demonstrating the roles of the parties involved in the project. According to the preliminary information, data, and exploratory readings collected about this matter, the research hypothesis is formulated as follows:-

" In fact, there is a critical need to determine the proper fundamentals of cost conduct and planning according to a sound clear system, taking into account what is currently applied and followed in order to assess these procedures and improve them as mach as possible."

In order to meet the aims of this research, a scientific methodology is pursued in :-

- the presentation and review of most the local and international references that are directly relevant to the research, and aided by reports and articles from the internet from websites of engineering facilities of relevancy.

- the case study for five projects. which are currently under construction in Iraq, analyzing them thoroughly in order to point out about their positive and negative aspects.

- the open questionnaire and the regular closed questionnaire forms based on the data and information collected through the theoretical review and the open questionnaire to conclude and examine some concepts concerning the actual management status of cost planning.

The research hypothesis has proved to be workable. Thus, it was possible to define the major obstacles that affect the process of construction cost management and planning; also, to suggest an appropriate plan for cost management and planning using a formula that facilitates the process of establishing and conducting all the details of construction cost to handle the weakness points on time, and to be able to propagate for cost management and planning and to inform the relevant parties or beneficiaries about how to take the proper decisions according to modern methods.

KEYWORD
(Cost, Contracts, Management, Planning, Project, Estimation, Monitoring, control, budget, Resources).

الخلاصة

يهدف البحث الى تأكيد أهمية إتباع الإدارة السليمة والتخطيط المحكم للكلفة منذ بداية إقرار المشروع الإنشائي لتسهيل مهمة وضع الاسس الصحيحة لمتابعة وضبط كلفة المشروع.بالإضافة الى تحديد المعوقات الأساسية التي تؤثر على عملية ادارة وتخطيط الكلفة الإنشائية ومحاولة تقديم مقترحات حلول لها من خلال توضيح دور الأطراف المشاركة في العملية الإنشائية . واستنادا الى المعلومات الأولية والقراءات الاستطلاعية والبيانات التي تم جمعها والتي كانت عن هذا الموضوع،فقد تم صياغة فرضية البحث كما يأتي:-

"ان واقع الحال يؤشر الحاجة الملحة لتحديد الاسس الصحيحة في ادارة وتخطيط الكلفة في تنفيذ المشاريع ضمن منهاج واضح وسليم والاخذ بنظر الاعتبار ماهو معمول به حاليا من اجل تقييم هذه الاسس وتطويرها قدر الامكان".

من اجل تحقيق أهداف البحث،فقد تم إتباع منهجية علمية للبحث تضمنت مايلي:-

1- استعراض معظم المصادر المحلية والعالمية ذات الصلة المباشرة بموضوع البحث لغرض الوقوف على احدث التقنيات الادارية والتخطيطية الخاصة بكلف التشييد ومتابعتها والسيطرة عليها،كما تمت الاستعانة بتقارير ومواضيع منشورة عبر الانترنيت لمواقع بعض الجهات الهندسية ذات العلاقة بموضوع البحث.

2- دراسة حالة لخمس من مشاريع التشييد قيد الانشاء حاليا في العراق.تم تحليل تلك المشاريع من اجل الوقوف على الجوانب السلبية والايجابية المتعلقة بموضوع البحث.

3- القيام باستبيان مفتوح وتحليله ثم تصميم استمارة الاستبيان المغلق النظامية بالاعتماد على ما جمع من بيانات ومعلومات من خلال الدراسة النظرية والاستبيان المفتوح ،للتعرف والتحقق من بعض الامور المتعلقة بواقع ادارة وتخطيط الكلفة في مشاريع الشييد في ظل المتغيرات الكثيرة التي اثرت عليها.

كنتيجة للخطوات المتبعة في تطبيق هذه المنهجية فقد تم التوصل الى اثبات فرضية البحث.وانطلاقا من هذه الفرضية فقد تم اقتراح خطة علمية مناسبة لادارة وتخطيط الكلفة بصيغة تسهل من عملية متابعة وضبط الكلفة الإنشائية لكافة تفاصيل المشروع الانشائي من اجل معالجة نقاط الضعف في وقتها المناسب. يهدف البحث ايضا الى نشر ثقافة ادارة وتخطيط الكلفة واتخاذ القرارات المناسبة وفقا للاساليب الحديثة في اوساط الاطراف ذات العلاقة بذلك.

(كلفة، عقود، إدارة، تخطيط، مشروع، تخمين، متابعة، ضبط ، ميزانية، موارد)

– المقدمة:

لا يخفى الدور الرئيس الذي تلعبه الكلفة كعنصر هام في مشاريع التشييد،لذلك يفترض ان تنال الاهتمام والتركيز في مشاريع التشييد،اذ قد تتعرض الجهة المنفذة لمشروع إنشائي ما إلى خسائر مالية كبيرة او انخفاض في الربح المتوقع أثناء تنفيذها والذي قد يكون ناتجا عن سوء التخطيط لكلف فقرات العمل او ضعف السيطرة على إدارة الكلفة وعدم القدرة على توفير البيانات والمعلومات التي تعطي صورا واضحة عن توزيع كلف العمل اثناء التنفيذ.لا ينطبق هذا الكلام على منفذي المشاريع الإنشائية(المقاول) فقط بل انه يشمل صاحب العمل أيضا لكون عملية إدارة الكلفة وتخطيطها بالتحديد تبدأ مع بداية نشوء فكرة المشروع ،وما دراسات الجدوى والدراسات الاقتصادية الا دليل اكيد لأهميتهما في أغراض السيطرة على الكلفة أثناء التنفيذ.

– إدارة الكلفة في مشاريع التشييد:–

تُعرف الادارة الانشائية بانها تطبيق المعرفة والقدرات باستخدام التقنيات والادوات المختلفة في الفعاليات المخطط لتنفيذها للحصول على المنشأ المطلوب انجازه وبما يتلائم مع متطلبات صاحب العمل ،عرفها الجلالي في دراسته بانها(فن توجيه وتنسيق الموارد البشرية والمادية خلال حياة المشروع عبر استخدام التقنيات الحديثة لتحقيق الاهداف المحددة مسبقا)(الجلالي:2005).

لارتباط الإدارة بعملية تخطيط الأعمال بصورة عامة أهمية كبيرة ،حتى لو لم تبرز أهميتها بصورة جلية بإعطاء نتائج ملموسة فهي بالتأكيد تؤثر على جوهر عملية التخطيط وخاصة في المشاريع الإنشائية(Sue:1997).ففي مجال البناء بالوطن العربي؛ نشأت خلال الفترة الماضية عدة شركات ومؤسسات خاصة تعمل بمجال ادارة المشاريع الانشائية ،يمكن ايجاز دورها بعمل الدراسات الاتية:–

– دراسة المخططات والمواصفات وتطبيق مفاهيم الهندسة القيمية عليها ومن ثم وضع التوصيات اللازمة لتحسين اداء المشروع وإمكانية تخفيض التكلفة العمومية له.

– وضع التكلفة الاجمالية للمشروع.

– وضع جداول البرامج الزمنية للتنفيذ.

– ربط جداول التنفيذ بالتدفقات النقدية اللازمة–وتوفير التمويل اللازم حسب مراحل التنفيذ.

– تفتيت المشروع وطرحه لمناقصة عامة او خاصة وترسيه أجزاء المشروع على مقاولين الباطن.

– متابعة التنفيذ من خلال جهاز إداري هندسي متخصص.

– تقديم تقارير دورية لصاحب المشروع لتقدم التنفيذ–مع تقديم دراسة مقارنة لخطط المشروع مع التنفيذ.

– الحرص على الشفافية بنقل المعلومات لصاحب المشروع–وتوضيح مسببات المشاكل بموقع المشروع.

ان اعتماد الأسس الإدارية والأساليب التخطيطية الصحيحة لكلف تنفيذ مشاريع التشييد وفق المتغيرات الكثيرة التي تحدث في الواقع الانشائي،يعمل على تجنب الانحراف عن الأهداف المطلوبة ويضمن الاستخدام الصحيح للإمكانيات والموارد المتوفرة ضمن ادارة هندسية خبيرة تسعى لتحقيق اهداف المشروع. **الشكل (1)** يبين الوظائف الاساسية لعملية ادارة المشروع الانشائي (التخطيط ،التنفيذ والمراقبة) وتاثيرها المباشر على جميع مفردات المشروع (الجلالي:2005) .
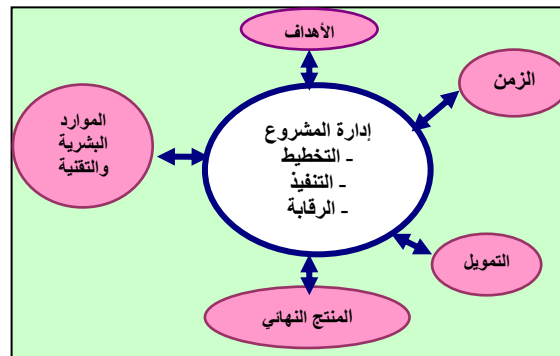
شكل(1) ادارة المشروع الهندسي(الجلالي:2005)

- أساسيات إدارة الكلفة في مشاريع التشييد :

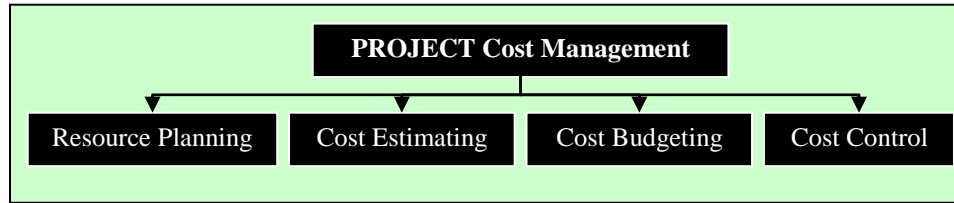ان ادارة كلفة المشاريع تشتمل على مجموعة من العمليات وئالاجراءات المهمة التي لها العلاقة بانجاز المشروع واتمامه ضمن الميزانية المالية المقررة له،الشكل (2) يبين العمليات الاساسية لادارة الكلفة في مشاريع التشييد وهي كالاتي(Pmbok:2003):-

شكل(2) اساسيات إدارة كلّف المشروع نظرة عامّة (Pmbok:2003)

* تخطيط الموارد (Resources Planning).

يعتبر تخطيط الموارد ضروريا لإحداث التوافق بين مطالب الموارد للمشروع وبين وجود تلك الموارد من جهة اخرى، وذلك بتحديد تفاصيل الموارد المطلوبة لتنفيذ العمل والتي يمكن توفيرها والبدائل لهذه الموارد في حالة عدم توفرها وحسب مراحل المشروع.كما يجب تعريف الفعاليات وتخمين مدة كل فعالية كذلك الاطلاع على معلومات سابقة تشمل أنواع الموارد وكمياتها المستخدمة لتنفيذ إعمال مشابهة لمشاريع سابقة.

* تخمين الكلفة (Cost Estimating).

يعد تخمين الكلفة عملية اساسية لكل مشروع ويمكن تعريفه بانه عملية احتساب كميات المواد والعمالة والمعدات المتوقع استخدامها لانجاز أعمال المشروع الإنشائي ضمن مواصفات محددة واحتساب كلفة المشروع بناء على ذلك(الحديثي:2006).التخمين عبارة عن وضع نطاق او مجال محدد يتوقع ان تكون الكلف والكميات في اطاره،وقد يكون حسابات تفصيلية ودقيقة للمشاركة بتقديم العطاءات من قبل المقاولين الراغبين في المساهمة بالمناقصات.فبالنسبة لصاحب العمل فانه يستخدم التخمين لايجاد كلف توظيف راس المال ،لتحديد الجدوى الاقتصادية من المشروع ولتقدير مبلغ الضريبة.اما الاستشاري فيستخدم التخمين للوقوف على الكلف التقريبية للمشروع،للمساعدة في اختيار الموقع الاقل كلفة او الاختيار بين التصاميم بعد مقارنة كلفها.اما المقاول فيعتمد على تخمين الكلفة لتقديم عطاء تنافسي بربح معقول.

* وضع ميزانية الكلفة (Cost Budgeting).

تشمل الإدارة الكلفوية تنفيذ الإجراءات المالية التي ينص عليها عقد التشييد كذلك تعيين الموارد المالية المخمنة من اجل القيام بانجاز فعاليات المشروع.وكذلك ارساء اجراءات نقدية مناسبة تتفق مع الممارسات القياسية المعروفة في مجال التشييد.

* ضبط الكلفة (Cost Control).

يقصد بها السيطرة على التغييرات الحاصلة في ميزانية المشروع.ولكنها تعتبر العملية الاهم لكونها تزامن المشروع منذ اقرار انشائه حتى اكمال انجازه.

وبقدرتعلق الامر فان ادارة الكلف تصف تاثير قرارات المشروع الخاصة بجميع الكلف المستخدمة لانجاز

المشروع في أي مرحلة من مراحله لضمان تنفيذه ضمن الكلفة المقررة له (Pmbok:2003).ان هذا المفهوم الواسع لادارة كلف المشاريع لطالما يتعلق بمصطلح الكلفة الحياتية(Life-Cost Cycle) التي تعرف بانها(طريقة لحساب الكلفة الحقيقية للمرافق،وهذه تتطلب تحديد تكاليف التشغيل في مرحلة ماقبل التخطيط بالاضافة إلى تكاليف نشاطات التصميم والإنشاء والصيانة)،ان الكلفة الحياتية مع أساليب هندسة القيمة Value Engineering (فرع هندسي يختص في تحليل التصاميم الهندسية او المعدات وذلك لمحاولة تعديل التصميم او المعدات بهدف تسهيل انشائها او استبدال قطع ارخص منها وذلك لتخفيض الكلفة الكلية من دون التاثير السلبي على الأداء العام للتصميم او المعدات)(كولد هابرواخرون:1984)، يستخدمان معا لتقليل الكلفة والوقت،زيادة الجودة والاداء والمساعدة في اتخاذ القرارات المثلى (Pmbok:2003)،الشكل(3) يبين اهمية التداخل بين عمليتي تخطيط وضبط الكلفة خلال مراحل تحقيق المشروع المختلفة.
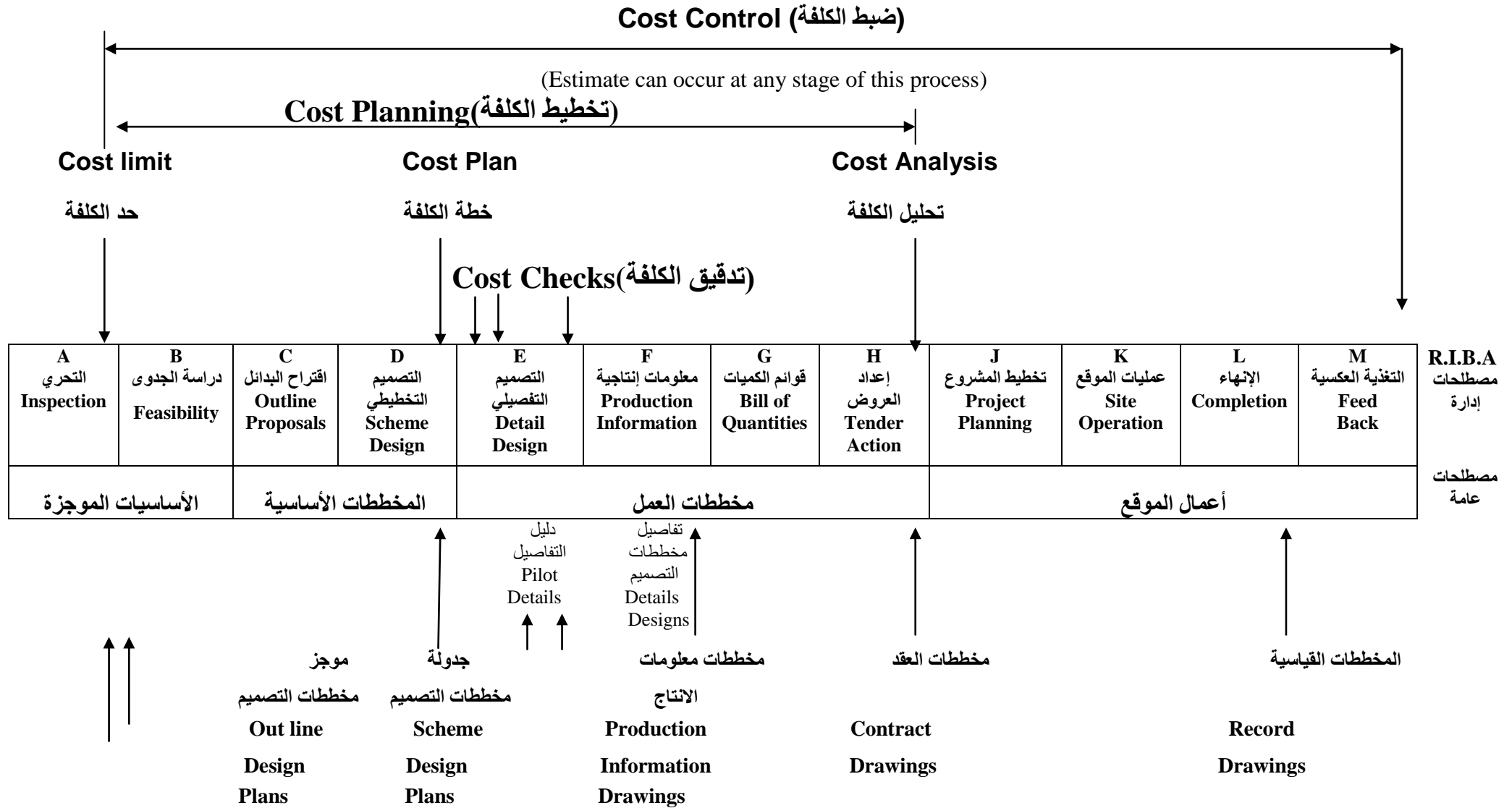
– تخطيط الكلفة في مشاريع التشييد:–

تهتم هذه الوظيفة الإدارية بتوقع المستقبل وتحديد أفضل السبل لإنجاز الأهداف التنظيمية.يعتبر التخطيط من الوظائف الرئيسية للادارة وهو يسبق الوظائف الاخرى،حيث يجري التفكير اولا بالهدف والتخطيط لتحقيقه. وهذه العملية ترتبط بعاملين اولهما هو التنبؤ بالمتغييرات التي تحدث في البيئة سواء اكانت تكنولوجية ام اقتصادية ام في طبيعة المنافسة ام في السياسات الحكومية وثانيهما معرفة الموارد المتاحة سواء اكانت بشرية ام مادية(سالم:1998).التخطيط يساعد الادارة المسؤولة عن المشروع في تحديد اهدافه وربطها بالوسائل المتاحة لتحقيق تلك الاهداف.اضافة الى ذلك ان خطة المشروع توفر قاعدة لمراقبة وقياس تقدم العمل وفق جدول معين لتحديد الانحرافات واسبابها لغرض معالجتها بما يكفل تلافي التاخير في انجاز العمل او زيادة كلفته (Hendrickson:2003).والشكل(4)يمثل برمجة بسيطة لمتطلبات التخطيط الانشائي.
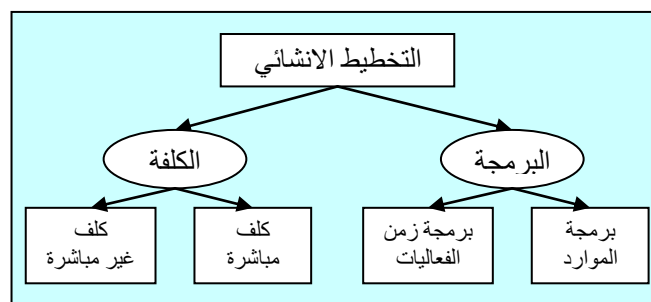
شكل (4) متطلبات التخطيط الإنشائي (Hendrickson:2003)

– اسلوب إجراء تخطيط الكلفة في مشاريع التشييد:–

لقد تباينت الكثير من الدراسات حول الاجراءات الواجب اتباعها من قبل مدير المشروع لانجاز المهمات الادارية التخطيطية الموكلة اليه بشكل كفوء للمشروع بشكل عام.حاولت هذه الدراسات تصنيف المفردات المتعلقة باسلوب اجراء التخطيط وايجاد نمط للخطوات المتبعة لاعداد البرامج للمشاريع.لذلك وبضوء هذا التباين ولاجل تحديد إطار متكامل لإجراءات التخطيط بصورة عامة فلقد تم تصنيف مفردات الإطار وتبويبها إلى ثلاثة مراحل رئيسية(يتضمن كل منها عدة مراحل ثانوية)وهي:–

Cost Control (ضبط الكلفة)

(Estimate can occur at any stage of this process)

Cost Planning(تخطيط الكلفة)

Cost limit　　　　　　　**Cost Plan**　　　　　　　**Cost Analysis**

حد الكلفة　　　　　　　خطة الكلفة　　　　　　　تحليل الكلفة

Cost Checks(تدقيق الكلفة)

A	B	C	D	E	F	G	H	J	K	L	M	R.I.B.A
التحري	دراسة الجدوى	اقتراح البدائل	التصميم التخطيطي	التصميم التفصيلي	معلومات إنتاجية	قوائم الكميات	إعداد العروض	تخطيط المشروع	عمليات الموقع	الإنهاء	التغذية العكسية	مصطلحات إدارة
Inspection	Feasibility	Outline Proposals	Scheme Design	Detail Design	Production Information	Bill of Quantities	Tender Action	Project Planning	Site Operation	Completion	Feed Back	

مصطلحات عامة
الأساسيات الموجزة	المخططات الأساسية	مخططات العمل	أعمال الموقع

دليل التفاصيل
Pilot Details

تفاصيل مخططات التصميم
Details Designs

موجز	جدولة	مخططات معلومات	مخططات العقد	المخططات القياسية
مخططات التصميم	مخططات التصميم	الانتاج		
Out line	Scheme	Production	Contract	Record
Design	Design	Information	Drawings	Drawings
Plans	Plans	Drawings		

شكل(3) يبين أهمية تداخل عمليتي تخطيط وضبط الكلفة اثناء مراحل المشروع المختلفة(R.I.B)

أ- الإجراءات التحضيرية.

ب- استحداث برنامج للعمل.

ج- المتابعة والسيطرة على البرنامج.

ولكون تخطيط الكلفة هو الجزء المهم والاصعب من عملية التخطيط العامة للمشروع، فان هذه المفردات العامة تنطبق ايضا على عملية تخطيط الكلفة ولو بشكل مستفيض من الخصوصية بقدر تعلق هذه المفردات وتأثيرها على الكلفة سلبا وايجابا.الشكل(5)يمثل خطة اقترحتها الباحثة لتخطيط الكلفة بصيغة من عملية متابعة وضبط الكلفة الانشائية لكافة تفاصيل المشروع الانشائية.

* الاجراءات التحضيرية :-

أكدت الكثير من الدراسات على ان استحداث برنامج للعمل وتطويره يجب ان يبدأ منذ المراحل الاولية للمشروع ومنذ تخويل صـلاحيات السلطة والمسؤولية لمشروع مـا من المستويات الاداريـة العليا في المنظمـة إلى مدير مشروع ما.وبعد عملية التخويل تبدأ سلسلة من الاجراءات المتناغمة للعمل قبل اعداد البرنامج والمتعلقة بتنظيم المسؤولية والتسهيلات الممكنة لعمل المشروع وانجازه.

* وضع المعايير (انواعها،طرق تخمينها)

تعد خطوة وضع المعايير المرحلة الاولى من عملية التخطيط ،والمعيار هو مستوى الاداء المرغوب تحقيقه لقياس الاداء الفعلي ويطلق عليه ايضا (معدلات قياسية)،وبدون توافر المعايير التي بضوئها يقاس الأداء يضل المدير طريقه إلى الحكم السليم على كفاءة الأداء لذا يضطر إلى التخمين او استخدام طرق الحساب التقريبي(Role of Thumb)التي قد لايعول على نتائجها.تكون المعايير على نوعين(التكريتي:2002)(سمير:1987):-
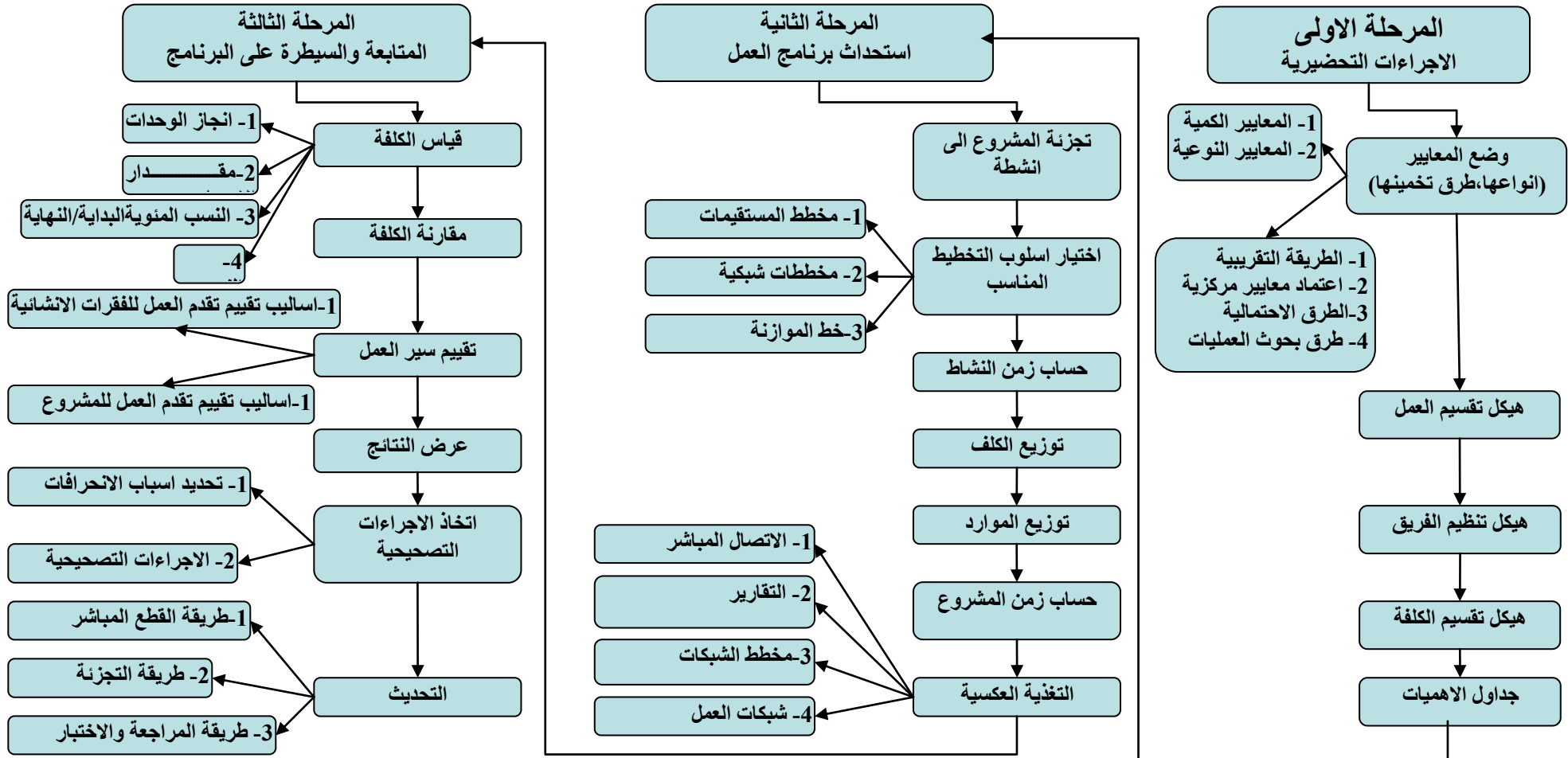
1- المعايير الكمية Quantitative Standard:-هي المعايير المادية التي يمكن التعبير عنها بصورة رقمية مثل(الزمن،الكلفة،عدد العاملين..وغيرها) تتميزيانها محددة بصورة مقبولة ويمكن قياسها وفهمها بسهولة.

2- المعايير النوعية Qualitative Standard:- هي معايير شخصية يعبر عنها بنواحي يصعب قياس كميتها كجودة الانتاج،تقييم سلوك العاملين وغيرها.

* هيكل تقسيم العمل Work Breakdown Structure(WBS)

لكي يكون بالامكان تخطيط الكلفة للمشروع من الضروري تخطيط ومتابعة كافة اجزائه،حيث من الضروري استحداث نظام هيكل تقسيم العمل(WBS)الذي يستخدم من بداية المشروع الى نهايته.يعتبر هذا الهيكل القاعدة لتخطيط المشروع لانه يعتبر الاساس لكل من مخطط توزيع المسؤوليات وتنسيق الاهداف وتوزيع الكلفة على اجزاء العمل وعلى برنامج المتابعة والسيطرة (اسماعيل:1996).يحدد هيكل تقسيم العمل الاطار (Curtis:2005) لـ:-

1. تعريف العمل الواجب انجازه.

2. بناء خطة لتحديد الاسلوب التخطيطي والسيطرة.

3. تلخيص حالة الجدولة الزمنية والكلفة للبرنامج لاعدادها للمستويات العليا للتعرف على مستويات الانجاز.

وبالاعتماد على هيكل تقسيم العمل (WBS) يمكن استحداث الهيكلين المكملين الاتيين.

اسلوب اجراء تخطيط الكلفة في مشاريع التشييد

المرحلة الاولى
الاجراءات التحضيرية

المرحلة الثانية
استحداث برنامج العمل

المرحلة الثالثة
المتابعة والسيطرة على البرنامج

1- المعايير الكمية
2- المعايير النوعية

وضع المعايير
(انواعها،طرق تخمينها)

1- الطريقة التقريبية
2- اعتماد معايير مركزية
3-الطرق الاحتمالية
4- طرق بحوث العمليات

هيكل تقسيم العمل

هيكل تنظيم الفريق

هيكل تقسيم الكلفة

جداول الاهميات

تجزئة المشروع الى انشطة

1- مخطط المستقيمات
2- مخططات شبكية
3-خط الموازنة

اختيار اسلوب التخطيط المناسب

حساب زمن النشاط

توزيع الكلف

توزيع الموارد

حساب زمن المشروع

1- الاتصال المباشر
2- التقارير
3-مخطط الشبكات
4- شبكات العمل

التغذية العكسية

قياس الكلفة

1- انجاز الوحدات
2-مقـــــدار
3- النسب المئويةالبداية/النهاية
4-

مقارنة الكلفة

1-اساليب تقييم تقدم العمل للفقرات الانشائية

تقييم سير العمل

1-اساليب تقييم تقدم العمل للمشروع

عرض النتائج

اتخاذ الاجراءات التصحيحية

1- تحديد اسباب الانحرافات
2- الاجراءات التصحيحية

التحديث

1طريقة القطع المباشر
2- طريقة التجزئة
3- طريقة المراجعة والاختبار

شكل (5) يبين الخطة المقترحة لتخطيط الكلفة بصيغة تسهل من عملية متابعة وضبط الكلفة الانشائية(اعداد الباحثة)

* هيكل تنظيم فريق العمل (OBS) Organization Breakdown Strucure

بعد مراجعة اوليات المشروع ومتطلبات رب العمل ووضع المعايير وبعد استحداث هيكل تقسيم العمل الاولي الذي يعرض العمليات الاساسية للانجاز ،تتكون لمدير المشروع مؤشرات كافية تساعده على اختيار وتنظيم كادر العمل الذي يضم مختلف الاختصاصات الهندسية وغيرها المطلوبة لاداء العمل (Oberlender:2000).

* هيكل تقسيم الكلفة Cost Breakdown Structure(CBS)

يتم من خلال(CBS) تحديد الكلف لفقرات المشروع كافة من الاعلى إلى الادنى والتي يطلق عليها تسمية فقرات العمل،فيحدد كلف فقرات العمل لايجاد كلفة الوحدة والتي تقارن لاحقا مع كلفة الوحدة الفعلية في عملية السيطرة،لذا يكون لكل جزء من اجزاء هيكل تقسيم العمل مركز كلفة خاص به((Cost Center(CC)).

* جداول الاهميات (Milestone Chart)

الخطوة التالية في أسلوب اجراء التخطيط هي انشاء جداول للاحداث الرئيسية،لإنها تؤشر البداية و النهاية لسلسلة مترابطة من الفعاليات التي يمكن من خلالها قياس سير العمل في المشروع دون الدخول في التفاصيل. اذ تحدد هذه الجداول بعد المناقشة مع المستويات الادارية المختلفة والمختصين في وقت مبكر من المشروع. يمكن ادخال معلومات هائلة إلى هذه الجداول من وصف الفعاليات،المسؤوليات,مدة انجاز العمل،تاريخ بدء المهمة وانتهاءها،فترات المرونة للفعالية وغيرها من البيانات التي تهم العاملين والمتابعين للعمل (التكريتي:2002). -

استحداث برنامج للعمل

* تجزئة المشروع إلى أنشطة

من المعروف ان كل نشاط يستهلك قدرا معينا من الوقت والموارد ولكي يكون بامكان الجهة المخططة من معرفة المشروع بشكله الواقعي وادراك العلاقات المرتبطة بين الخطوات والمراحل المتبعة لابد من تجزئة المشروع إلى مجموعة من الانشطة المختلفة.حيث يتم التقسيم للانشطة المختلفة على اساس تقسيم العمل (WBS)او على اساس الاحتياجات البشرية واختصاصاتهم(OBS)او على اساس توزيع الموارد المالية(CBS).بصورة عامة يمكن تصنيف الانشطة الى انشطة مستقلة واخرى اعتمادية إلى(الطائي:1971).

* اختيار اسلوب التخطيط المناسب

يختلف اختيار اسلوب التخطيط المناسب من مشروع لاخر،بالاعتماد على حجم وطبيعة المشروع ودرجة تعقيده والمدة اللازمة لاكمال العمل بالاضافة الى متطلبات صاحب العمل. او يلجا البعض إلى استخدام عدة اساليب في آن واحد كما هو الحال في البرنامج الحاسوبي ((Primavera Project Planner(P3) حيث يستخدم مخطط المستقيمات(Bar Chart) مع مخطط الشبكية(PERT) (التميمي:2004).

* حساب زمن النشاط

عند انشاء نظام معين تركب الاجزاء المختلفة مع بعضها بطرق متعددة لتشكيل البدائل،ويتطور مخطط العمل من خلال البحث عن الحلول المختلفة للزمن المطلوب لانجاز النشاط والتي توفر في نفس الوقت المتطلبات الثلاثة معا زمن وكلفة ونوعية.بذلك يسمح لاحتمالات الانشطة المفردة ان تربط على طول مع الفترات

الزمنية بحيث يصل في النهاية إلى التخمين الناتج للزمن الكلي لاكمال المشروع.

* توزيع وتسجيل الكلف

عملية توزيع الكلف ضرورية لتوزيع بيانات الكلفة الى عنوان محدد ضمن تصنيف محدد او نظام ترميز معين،كما تتضمن تسجيل الكلف لإظهار كافة المصروفات التي تعود لفقرات محددة من العمل وهي عملية ضرورية لتجهيز بيانات تتم معالجتها فيما بعد حيث تستخدم المعلومات الناتجة عنها في الحصول على كلفة المواد،الاجور،المعدات والكلف غير المباشرة لفقرة ما مع تقسيماتها .وبسبب محدودية الموارد قد يعتمد المدراء على بيانات الكلفة في اقرار اي الاجراءات التي تحقق العائد المثالي للشركة حيث يقوم محلل الكلفة بجمع وتصنيف ثم تلخيص البيانات المالية الخاصة بكلف الانتاج وتهيئة التقارير الدقيقة في اوقاتها المناسبة لإغراض التقييم والسيطرة على العمليات التي يقام بتنفيذها .

* توزيع الموارد

تبدأ عملية توزيع الموارد البشرية والمادية،كالمعدات والمواد لكل نشاط بعد تقدير الوقت اللازم لانجازه حيث يتم تحديد النوعية والكمية ومعدلات الاحتياجات لانجاز النشاط (جاراش:1984).فكلما كبر حجم المشروع وتعقدت طبيعته كلما ازدادت الحاجة إلى الاهتمام بتوزيع الموارد نظرا لمردوده الاقتصادي والاداري.

* حساب زمن المشروع

بعد عملية وضع وحساب زمن الانشطة المختلفة للمشروع وتوزيع الكلفة والموارد يقوم مدير المشروع بحساب زمن المشروع ومدة انجازه.هناك ثلاثة انواع من المدد الزمنية والواجب تحديدها،هي(كريم:1988):-

- مدة انجاز اعتيادية: تعتمد عادة في انجاز المشاريع التي تكون فيها الامكانيات البشرية متوازية.
- مدة انجاز بطيئة: تحتاج إلى اقل كلفة مباشرة(استخدام اقل عدد من القوى العاملة لتنفيذ انشطة المشروع).
- مدة انجاز سريعة:تعتمد على استخدام امكانيات بشرية كبيرة وهو أسلوب مكلف عادة.

* التغذية العكسية

ان عملية القياس تقع على عاتق المراقبين والعاملين في المشروع وكذلك تكون من ضمن مسؤوليات الاجهزة الثانوية الداعمة لمدير المشروع ،ولكي تتم عملية تنفيذ سير العمل لابد من نقل البيانات إلى الادارة بالتغذية العكسية حيث تصل هذه البيانات والمعلومات لمدير المشروع بعدة وسائل منها الاتصال المباشر، التقارير, مخطط المستقيمات و شبكات العمل.(كولدهابروواخرون:1984)

* مرحلة المتابعة و السيطرة :-

هي عملية مستمرة لمقارنة الانجازات الفعلية بالعمليات المخططة.واتخاذ الاجراءات التصحيحية لمعالجة الانحرافات .تعتبر هذه المرحلة محور عملية التخطيط ،اذ يتم من خلالها القيام بعدة اجراءات من اعمال المتابعة ،القياس ،المقارنة ،التحليل والتفسير من اجل تحديد وضع سير العمل في المشروع:-

* قياس الكلفة   Cost Measurement

يعد قياس كلفة العمل احد المرتكزات الاساسية التي يعتمد عليها مدير المشروع لاجراء العمل بشكل ثابت ليتسنى له القيام بالمراحل اللاحقة،وعادة ماتجري عملية القياس لكمية الاعمال التي تنفذ دوريا ليتم مقارنتها مع الكميات الكلية للعمل الواجب انجازه بموجب البرنامج التخطيطي(اسماعيل:1996).

ولكون عملية قياس سير العمل من الانشطة المتغيرة باستمرار فان هذا يتطلب تاشير نسب الانجاز المتحقق على برنامج المشروع بحيث يمكن ان يراه كافة الاشخاص المتتبعين لسير العمل وعندما يراد تحديد المقدار الكمي لنسبة الانجاز المتحققة للمشروع فالعلاقة البسيطة التي تحدد ذلك هي(الالوسي:1999):

* مقارنات الكلفة   Cost Comparisons

بعد الانتهاء من جمع المعلومات والبيانات اللازمة عن الأداء الفعلي،تاتي الخطوة المهمة في تقييم سير العمل بمقارنته بالمعايير الموضوعة مسبقا التي تحدد مستوى معينا من العمل،وتحتاج عملية المقارنة هذه إلى تحليل المعلومات والبيانات المجمعة وتفسيرها. ان عملية تحليل الكلفة هي عبارة عن مجموعة الاساليب والطرق المستخدمة في تحديد الوحدة المنتجة او عملية من العمليات او احد المشاريع او التعاقدات والتي من خلالها تزود الادارة بالكلف الكلية والتفصيلية للخدمات والإعمال التي تقوم بتنفيذها لإغراض التخطيط ، الرقابة،السيطرة وتقييم الموارد لتمكن الادارة من اتخاذ القرارات.هناك عنصرين اساسيين في عملية التقييم يجب على مدير المشروع او المسؤولين عن عملية التقييم ملاحظتها عند مراقبة عمليات الانتاج وتحليل الكلفة،حيث تتم مقارنة النتائج الفعلية مع مقادير الموازنة وتعريف مساحات التباين،وذلك من خلال مقارنة الكلفة ومقارنة مدة التنفيذ ودرجة سير العمل.وتجدر الاشارة إلى وجود عمليات مقارنة اضافية يمكن اجراؤها لغرض السيطرة على اداء كلفة المشروع(Ahuja:1976):-

أ– مقارنة النسب المئوية للنفقات المخططة مع النسب المئوية المتحققة ومقارنة المقدار المتبقي من الميزانية المرصودة للعمل مع كلفة المتطلبات اللازمة لتحقق الانجاز.

ب– مقارنة معدل الانتاجية المخططة مع الانتاجية المتحققة.

* تقييم تقدم سير العمل:– Work Evaluation Manners

على ضوء ماسبق يمكن ان تصنف الاساليب المستخدمة في تقييم تقدم العمل إلى ما يلي:

اولا: اساليب تقييم تقدم العمل للفقرات الانشائية.

يعد مستوى الدقة والجهد والكلفة والوقت هي المتغييرات التي تتحكم في اختيار الاسلوب المستخدم لمتابعة تقدم العمل لان لكل اسلوب نقاط قوة وضعف تستخدم للمفاضلة بين الاساليب بعضها على بعض،ان امكانيات

المشروع المتوفرة ومحدودية الموارد قد تكون سببا اساسيا في تفضيل اسلوب على اخر.ويعد القرار المتخذ في ضوء تقييم تقدم العمل هو اول اختبار حقيقي للصيغة الصحيحية المختارة للتخطيط (Twort &Rees:1995).

فيما يلي اهم الاساليب المستخدمة في تقييم تقدم العمل للفقرات الانشائية:-

- اسلوب قياس وحدات العمل المنجز للفقرات الانشائية.
- اسلوب قياس النسبة المنقضية من الفترة الزمنية المخصصة لتنفيذ الفقرة.
- اسلوب استخدام حجم الموارد المستخدمة في تنفيذ الفقرة.
- اسلوب استخدام الخبرة في تقدير نسبة انجاز الفقرة.
- اسلوب مراقبة الميزانية والجدولة المتكاملة

ثانيا: اساليب تقييم تقدم العمل للمشروع.

تعد طرق تقويم تقدم العمل للفقرات الانشائية التي سبق عرضها ضرورية للاسباب الاتية(العجيلي:1996):-

- معرفة الكفاءة في التنفيذ.
- معرفة مدى توافق اوقات التنفيذ الخاصة بالفقرات الانشائية للبرنامج الزمني المعد للمشروع.
- تحديد المعوقات التي قد تؤدي إلى تاخر الانجاز للفقرات الانشائية.

اساليب تقويم تقدم العمل للفقرات لاتعطي صورة واضحة عن مستوى الأداء وتقدم العمل للمشروع باكمله ولاتظهر الانحرافات المالية والزمنية التي قد تحدث في برنامج تقدم العمل للمشروع وبالتالي سيتاخر تشخيص ومعالجة هذه الانحرافات،لذلك يلجأ إلى استخدام اساليب تقويم تقدم العمل للمشروع والتي تقسم إلى نوعين:-

النوع الاول: يعبر عن تقدم العمل في المشروع على شكل نسب مئوية للانجاز.

النوع الثاني: يعبر عن تقدم العمل في المشروع من خلال تحديد الانحرافات الحاصلة في المواقف المالية والزمنية والمواردية احيانا وهو اقرب إلى اسلوب عرض معلومات التقويم.

وبصورة عامة يمكن اعتماد اساليب تقييم تقدم العمل للمشروع وكما يلي:-

- اسلوب منحني الكلفة (S- Curve).
- اسلوب مؤشرات تقدم العمل والكلفة.
- اسلوب النسبة المئوية للانجاز.
- اسلوب الاوزان المعيارية.
- اسلوب استخدام التمثيل البياني.

* نتائج التقييم:(عرض النتائج):-

تاخذ اساليب عرض النتائج اشكال مختلفة يفضل في كثير من الاحيان ان تتسم بالسهولة والبساطة في نقل المعلومة وتترجم وضع المشروع بشكل واضح ومدروس.ففي حالة استخدام مؤشرات العمل فانه يترجم إلى منحنيات التباين حيث يسهل مهمة فهم المشروع والانحراف الحاصل فيه(Oberlender:2000)،أو يستخدم اسلوب المستقيمات او منحني سير العمل لتوضيح حالة المشروع من دون الحاجة إلى الاستعانة بالكتابة أو الشرح.

* اتخاذ الإجراءات التصحيحية Correcting Action

الخطوة الأخيرة في عملية الرقابة هي قيام الادارة ببعض التصرفات التي تؤدي الى تصحيح الانحرافات المؤثرة بين الأداء الفعلي والمعايير الموضوعة اذ يتم تغيير بعض المعايير أو تعديل الاستراتيجيات بمرحلتين:

أ) تحديد أسباب الانحرافات: بيان ماذا كانت هذه الأسباب تتعلق بأخطاء في تنفيذ الاستراتيجية أم أمور طارئة وغير متوقعة في البيئة الخارجية؟ وينبغي لتحديد هذه الأسباب الاجابة عن سلسلة من الأسئلة لعل أهمها، الاستيضاح عن مدى ملائمة الاستراتيجية في ظل قيام الانحرافات.

ب) اتخاذ الاجراءات التصحيحية وذلك من خلال: اما تعديل الاستراتيجية التي لاتحقق المعايير المطلوبة أو تعديل المعايير بعد اجراء تقييم العلاقة بين المعايير المستخدمة والنظام الرقابي المستخدم(محمد السيد:1993).

* التحديث Updating

لاكمال متطلبات عملية متابعة سير العمل في المشروع لابد من القيام بتحديث كامل لبرنامج التنفيذ،فهذه العملية تهدف إلى تعديل خطة المشروع في سبيل تحقيق الاهداف المحددة للمشروع(الكلفة المحددة،زمن الانجاز)،وهي عبارة عن اعادة جدولة الجزء المتبقي من فعاليات المشروع وتتم بعد ان يتم تجميع المعلومات وتبويبها وتقييمها من قبل ادارة المشروع(الادارة العليا)حيث تاتي كناتج طبيعي للخطوات التي تسبقها(Ahuja:1980).كما ان قرار التحديث هو قرار الادارة العليا للتنفيذ ويجب ان لايؤخذ بطريقة متسرعة اواعتباطية(Harris:1982).هناك عدة طرق يمكن استخدامها لاجراء عملية التحديث لبرنامج التنفيذ(البندنيجي:2000):

أ- طريقة القطع المباشر Separating Method:- تتضمن هذه الطريقة اعادة تقويم جميع فعاليات المشروع وتحديد مدة تنفيذ كل منها من جديد .

ب- طريقة التجزئة Partitioning Method:- يتم تقسيم المشروع إلى فصائل مرتبطة مع بعضها البعض وتتم عملية التحديث للفصيلة التي تاثرت بعملية التحديث فقط.

ج- طريقة المراجعة والاختبار Review & Test Method:- يقوم المبرمج باستعراض لبرنامج المشروع كما يمثله مخطط المستقيمات او المخطط الشبكي ويؤشر على الفعاليات التي ستتاثر بعملية التحديث باشارة مميزة ثم يقوم بالتعديل الجزئي دون المساس بالفعاليات الاخرى التي لاتتاثر بعملية التحديث.

– التحري الميداني عن واقع إدارة وتخطيط الكلفة في بعض مشاريع التشييد المحلية:-

يعرف التحري الميداني بانه عملية جمع المعلومات والاحصائيات والحقائق المطلوبة من اجل تسجيل الموقف الحالي للنظام (المشروع).جُزِءَ التحري الميداني الى قسمين وكما يلي:

* دراسة حالة لواقع ادارة وتخطيط الكلفة في بعض مشاريع التشييد المحلية:

تم تسجيل الوضع السائد في مجال ادارة الكلف وتخطيطها لخمس من المشاريع الانشائية المحلية التي تنفذ حاليا(مشروع كلية الاعلام والبناية الملحقة به، عمادة العلوم ،قسم الفلك– كلية العلوم،قسم التقنيات الإحيائية – كلية العلوم وبناية القاعات– كلية العلوم) معتبرين هذه المشاريع نماذج ممثلة لأغلب مشاريع الدولة من حيث ضوابطها وأساليب إدارتها للحصول على معلومات وبيانات كافية لتشخيص واقع الحال ومقارنتها مع الاساليب

787

والتقنيات التي جرى عرضها خلال الدراسة النظرية الخاصة بمفاهيم الادارة الحديثة في عمليات تخطيط وضبط الكلف في مشاريع التشييد وتاشير نقاط الضعف والقوة في هذه المفاهيم والعمليات المعتمدة في اسلوب عملية ادارة الكلف لهذه المشاريع الإنشائية. تم في هذه الدراسة توضيح مراحل انجاز هذه المشاريع منذ بداية اقرارها حتى تنفيذها،تسجيل وتبويب البيانات الكلفوية المتعلقة بالأنشطة المالية ليتم تحليلها الى عناصر الكلف الموقعية والتي شملت المواد، المكائن،الايدي العاملة والمقاولات الثانوية ومن بعدها اجراء قياس ومقارنة لبيانات الكلف الموقعية.ان نتائج تحليل الكلفة تم توضيحها في جداول خاصة تبين الكلفة المباشرة لكل فقرة من فقرات العمل والكلف غير المباشرة مع حصتها من كلف التحميلات الادارية الموقعية وكلف التحميلات الادارية للمقر الرئيسي والدائرة الالية والتي ظهرت خلال فترة التنفيذ.ولتسهيل اجراء عملية المقارنات بين الكلف الفعلية المتحققة واسعار المقاولة ومعرفة مقدارالربح اوالخسارة لابد من معرفة القيم الحقيقية لما يلي:-

- كلفة العمل المنفذ :التي تتمثل بكلف فقرات العمل التراكمية في المدة التي تم تنفيذ كل فقرة خلالها ، أي المصروفات الكلية التراكمية في زمن المقاولة.

- قيمة العمل المنفذ: وهي عبارة عن قيمة فقرات العمل التراكمية في المدة التي نفذت كل فقرة خلالها.

- مستحقات المقاول الفعلية: المبالغ الصافية المستلمة التراكمية عن قيمة الاعمال المنفذة عند تاريخ استلامها وهو يمثل المبلغ المستحق للمقاول وفقا لاسعار جدول الكميات.
  مستحقات المقاول الفعلية = كمية العمل المنجز فعلا × سعر الوحدة (المسعرة حسب العقد)

- مصروفات المقاول الفعلية: عبارة عن انواع الكلف التراكمية المتحققة عن تسديد مبالغ الاعمال المنفذة فعلا والتي تستمر لما بعد انتهاء مدة تنفيذ المقاولة.
  مصروفات المقاول الفعلية = كمية العمل المنجز × كلفة انجاز وحدة العمل(المصروفة فعلا)

تم مقارنة كلف العمل المنفذ لكل فقرة مع قيمته(المقارنة التي تهم المقاول الرئيس) مع توضيح البيانات اللازمة لاغراض مقارنة كلف التنفيذ الموقعية الحقيقية لكل فقرة او عنصر مع الكلفة التخمينية.والاشكال ادناه تمثل المنحنيات الخاصة بالتدفق النقدي الخاصة بهذه المشاريع بعد توضيح القيم الكلفوية لجميع الموارد المطلوبة.
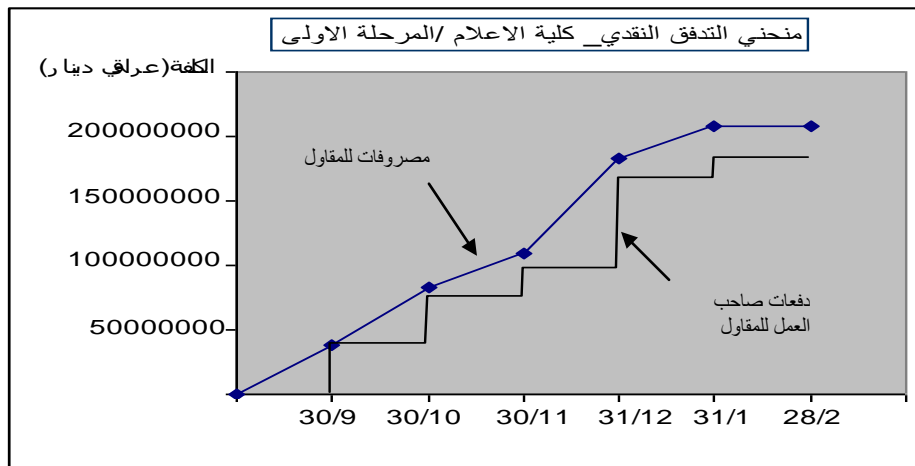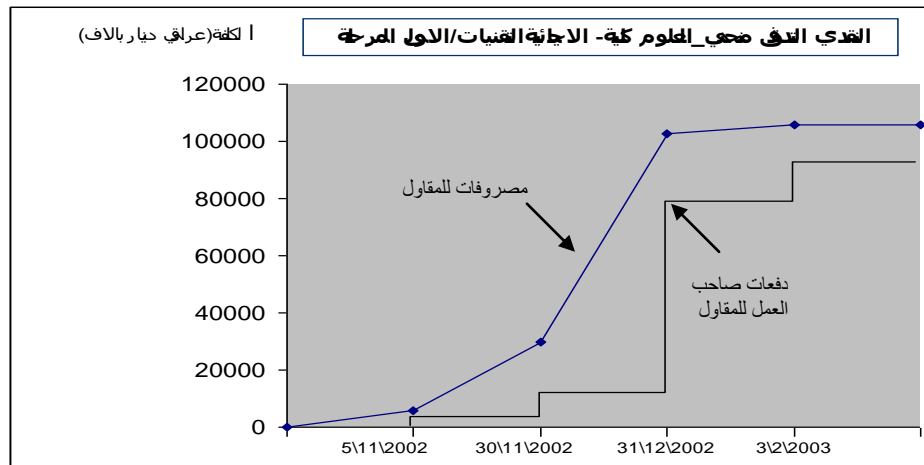
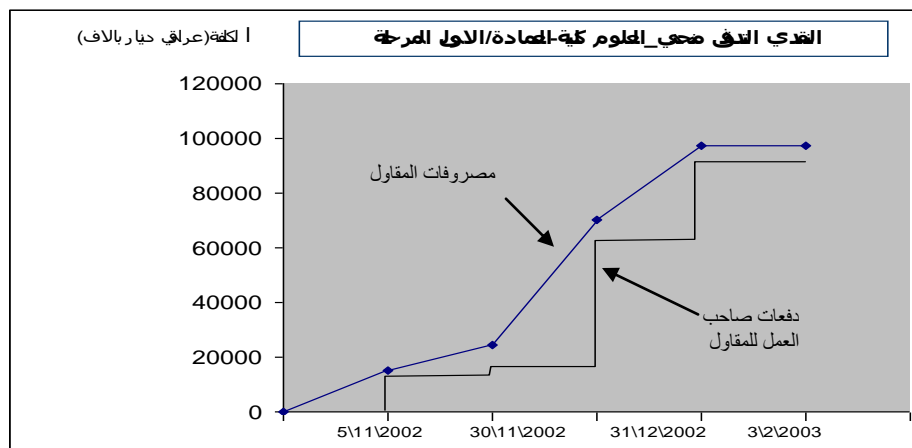**شكل رقم(6) يبين دفعات صاحب العمل ومصروفات المقاول(كلية الاعلام-المرحلة الاولى)**
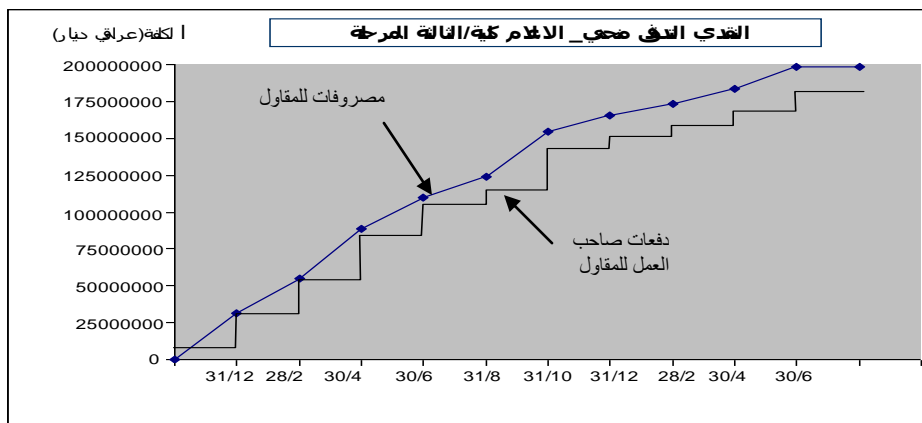
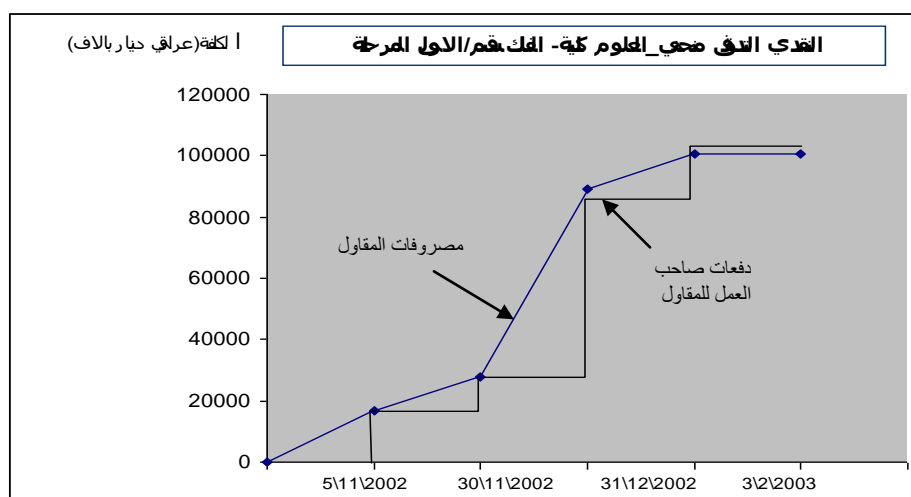**شكل رقم(7) يبين دفعات صاحب العمل ومصروفات المقاول(كلية الاعلام-المرحلة الثالثة)**
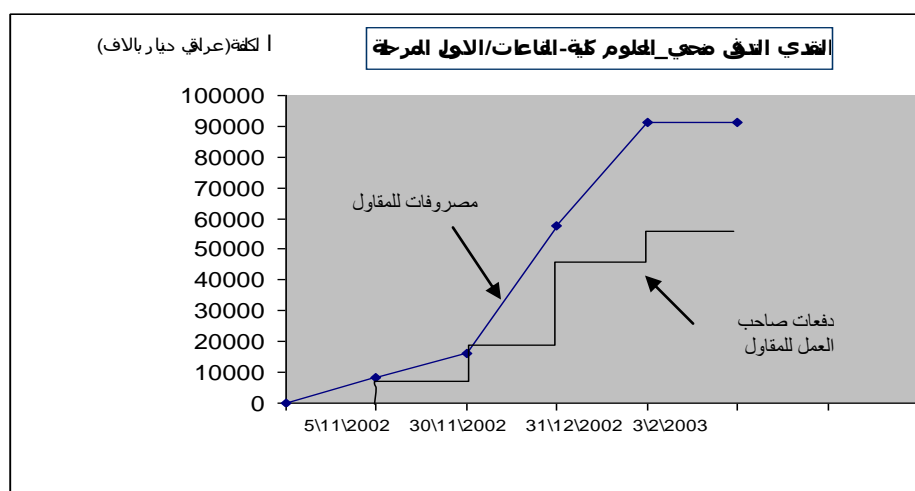
شكل (8) يبين دفعات صاحب العمل ومصروفات المقاول ـ كلية العلوم _ القاعات- المرحلة الاولى
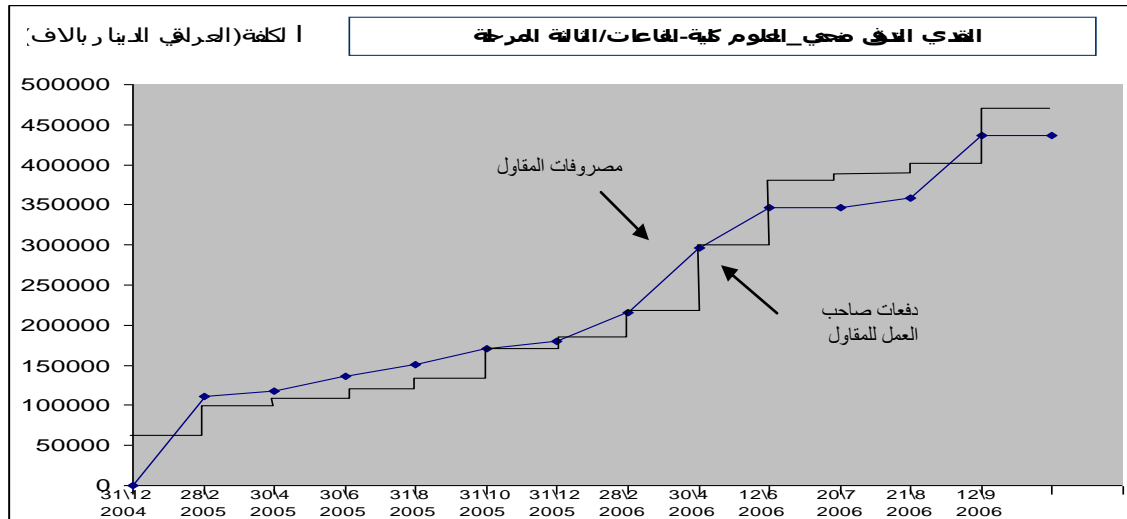
شكل (9) يبين دفعات صاحب العمل ومصروفات المقاول ـ كلية العلوم _ التقنيات الاحيائيةـ المرحلة الاولى
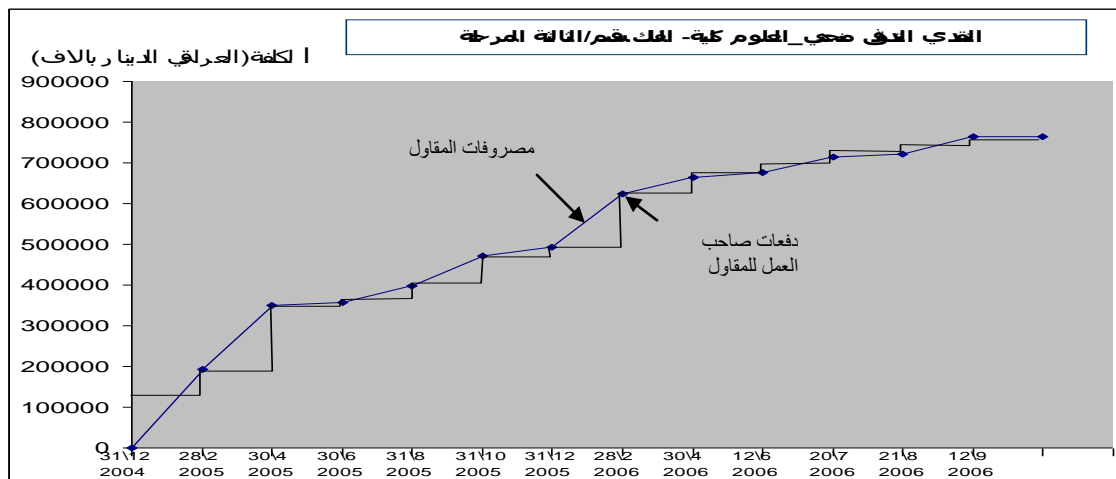

شكل (10) يبين دفعات صاحب العمل ومصروفات المقاول ـ كلية العلوم _ العمادةـ المرحلة الاولى
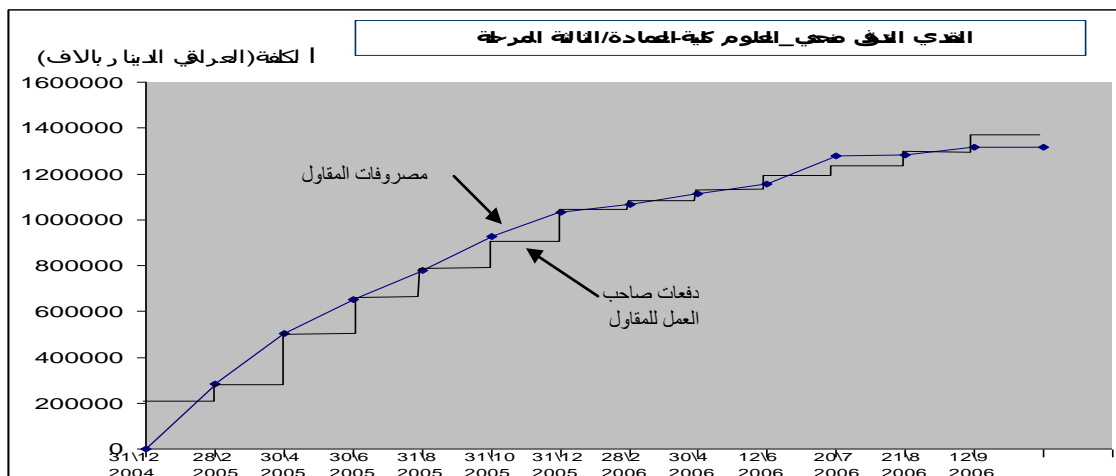

شكل (11) يبين دفعات صاحب العمل ومصروفات المقاول ـ كلية العلوم _ قسم الفلكـ المرحلة الاولى
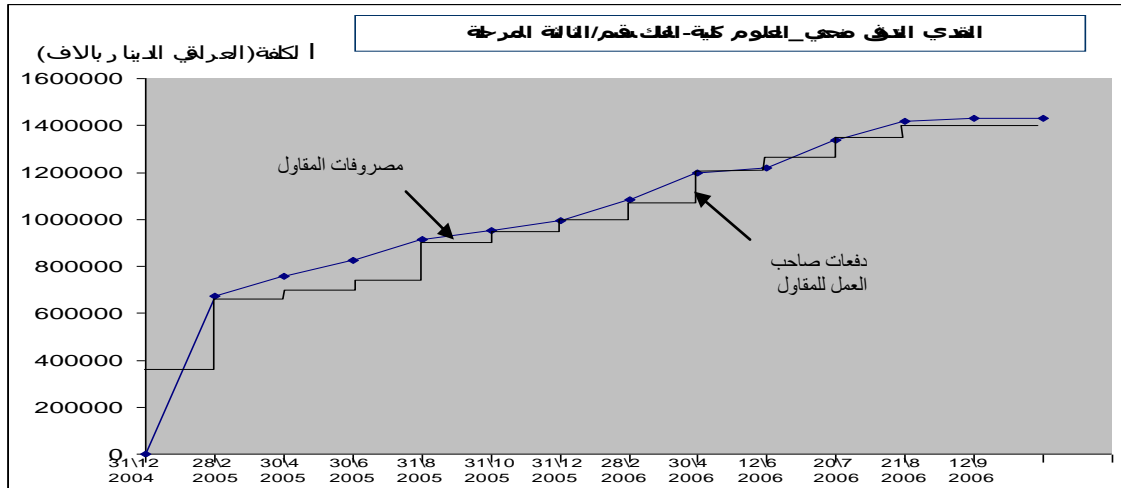
شكل (12) يبين دفعات صاحب العمل ومصروفات المقاول ـ كلية العلوم _القاعاتـ المرحلة الثالثة

شكل (13) يبين دفعات صاحب العمل ومصروفات المقاول ـ كلية العلوم _التقنيات الاحيائيةـ المرحلة الثالثة

شكل (14) يبين دفعات صاحب العمل ومصروفات المقاول ـ كلية العلوم _العمادةـ المرحلة الثالثة

شكل (15) يبين دفعات صاحب العمل والمقاول ـ كلية العلوم ـ قسم الفلك ـ المرحلة الثالثة

* الاستبيان الميداني:ـ

الاستبيان هو وسيلة من وسائل الاتصال مع المجتمع ومنهم الخبراء وذوي المهارات للاستفادة من قاعدة المعلومات المتوفرة لديهم والبناء عليها عند تقييم او تنفيذ المشاريع الجديدة.

* الاستبيان المفتوح:ـ

تمثل الاستبيان المفتوح بالمقابلات الشخصية مع عدد من المسؤولين في الدولة من الملاكات القيادية الادارية والهندسية وعدد من المقاولين اصحاب شركات القطاع الخاص من العاملين في مجال ادارة وتنفيذ مشاريع التشييد في مختلف المجالات والمستويات الادارية ذات العلاقة بإدارة وتخطيط الكلفة،بالإضافة إلى اراء اصحاب العمل في مجال الكلفة وكيفية مراعاة مصالحه المادية وانجاز العمل ضمن الميزانية المحددة وخلال الزمن المحدد وفي الوقت نفسه يجب ان تكون مستوفية كافة الشروط. تم تحديد الاسئلة الخاصة باستمارة الاستبيان المفتوح كما موضحة بالملحق رقم (1) بالمحاور الاساسية التالية :ـ

المحور الاول:ـ ادارة وتخطيط المشروع الانشائي .

المحور الثاني:ـ ادارة وتخطيط الكلف الانشائية(المواد،المكائن والمعدات،الايدي العاملة،المقاولات الثانوية وكلف التحميلات الادارية).

المحور الثالث:ـ تفاصيل عمليات المتابعة,الرقابة والسيطرة على الكلفة الانشائية.

* الاستبيان المغلق:ـ

بالاعتماد على ما جمع من بيانات ومعلومات من خلال الاستبيان المفتوح وما امكن استخلاصه من الدراسة النظريـة،للتعرف والتحقق مـن بعض الامـور المتعلقـة بواقـع ادارة تخطيط الكلفـة فـي مشاريع التشييد،في ظل المتغيرات الكثيرة التي اثرت على هذه العملية ،وبالاستناد على ما ورد في المواصفات القياسية Work study BSI3138 من ان تقنيات الاستجواب Questioning technique وعصف الافكار Brain storming هما من اساليب جمع المعلومات وإيجاد الحلول من خلال تحليل الاراء المختلفة للمشاركين في الاستبيان. ولكون مفهوم الكلفة عند صـاحب العمل يختلف عمـا هـو لـدى المقاول فقد تـم اختيـار نموذجين،يتكـون النمـوذج الاول

من(44)عينة لمدراء المشاريع والمهندسين التابعين لصاحب العمل كجهة تصميم واشراف.اما النموذج الثاني
فيتألف من(38)عينة لمدراء المشاريع والمهندسين التابعين للشركات المنفذة (المقاول) مع الحرص ان تكون
الجهات المشمولة بالاستبيان تضم اغلب أنواع مشاريع التشييد.تناولت الأسئلة الاستبيانية سواء كانت موجهة إلى
صاحب العمل او المقاول المحاور المحددة الآتية كما موضحة بالملحق رقم(2)ولكن مع اختلاف في مضمون
الأسئلة اعتمادا على دور كل طرف في هذه المحاور الرئيسية على عملية انجاز المشروع:

المحور الاول:– المعلومات التعريفية والمهنية للافراد المستبينين.

المحور الثاني:– إدارة وتخطيط الكلفة في مشاريع التشييد

المحور الثالث:– التعاقدات واساليب التنفيذ في مشاريع التشييد

المحور الرابع:– مراحل تطور المشروع الإنشائي

المحور الخامس:– الأسباب المؤدية إلى ضعف ادارة وتخطيط الكلفة في مشاريع التشييد

* الاختبار الإحصائي لنتائج الاستبيان المغلق:

الاستدلال الاحصائي واحد من اكثر جوانب عملية اتخاذ القرارات اهمية وحيوية في الاقتصاد والاعمال والعلوم
كافة،ويتعلق بالتقدير واختبار الفروض.التقدير هو عملية استنتاج او تقدير احد معالم المجتمع(مثل وسطه μ
وتباينه σ^2) من الاحصاء المناظر والخاص بعينة مسحوبة من المجتمع. تم القيام بتحليل نتائج الاجوبة بالطرق
الاحصائية لغرض استخلاص النتائج على ضوء هذه الاجوبة،وهذا ماتم اجراءه على نتائج اجوبة نموذجي
البحث المشمولة بالاستبيان الميداني المغلق،لان استخدام الاحصاء كأداة للبحث يتعدى جمع البيانات الى
تحليلها للتعبير عن مدلولاتها الظاهرية تعبيرا علميا يستفاد منه في كافة مجالات اتخاذ القرار .

* إجراء اختبار الفرضيات (Hypothesis Test).

اختبار الفروض عن نتائج المجتمع(مثل وسطه μ وتباينه σ^2) هو جانب اساسي من جوانب الاستدلال والتحليل
الإحصائي ،ففي مواقف اتخاذ قرارات كثيرة،يكون من المهم تحديد مااذا كان وسطان او نسبتان لمجتمعين
يتساويان او يختلفان،فاذا امكننا ان نعزو الفرق بين وسطي او نسبتي العينتين الى الصدفة, اذا كان المجتمعان
يتبعان التوزيع الطبيعي,او اذا كان كل من($n1,n2>30$) فان توزيع المعاينة للفرق بين الوسطين (او
النسبتين) في العينة يتبع ايضا التوزيع الطبيعي،او يتبع التوزيع الطبيعي تقريبا بخطأ معياري معطى بالمعادلة
التالية(سالفاتور:1997):

لاختبار اذا كانت $\mu1= \mu2$ $\sigma_{x1-x2}=((\sigma1^2/n1)+(\sigma2^2/n2))$ ½   ......   (2-1)

الفروض التي يجري اختبارها:–

Ho: $\mu1 =\mu2$	or	Ho: $\mu1-\mu2 = 0$
H1: $\mu1\neq \mu2$	or	H1: $\mu1-\mu2 \neq 0$

وهذا اختبار ذو ذيلين وتقع منطقة القبول للفرض H0 في حدود ±1.96تحت المنحني الطبيعي القياسي.

ارتأت الباحثة اجراء هذا الاختبار على محور البيانات التوضيحية لافراد عينتي المجتمعين(صـاحب العمـل والمقاول)لمعرفة مـدى تناسـق مسـتوى افـراد المجتمعين وظيفيـا ومهنيـا وعلميـا وخـدميا (بمعنـى سـنوات الخدمـة والتخصص) ومدى التوافق بينهما للحصول على اجابات تؤخذ بنظر الاعتبار في الدراسة اللاحقة من البحث.وكانت نتيجة الاختبار تشير الى ان قيمة σx1-x2 = 0,7023 وقيمة Z= 0,7023 وبما ان Z تقع داخل منطقة القبول،فإننا نقبل(H0)،أي μ1= μ2،عند مستوى معنوية 5%.وهذا يعني انه لايوجد دليل إحصائي يشير الى ان مستوى المستبينين للعينات مختلف للنموذجين،مما يؤكد ان المستبينين كانوا بنفس درجة التأهيل للاجابة على اسئلة الاستبيان من الناحية العلمية والعملية.

* اجراء **تحليل التباين** (Analysis of Variance).

يستخدم تحليل التباين لاختبار فرض ان متوسطات مجتمعين او اكثر متساوية او مختلفة عندما تكون المجتمعات موزعة توزيعا طبيعيا مع تساوي التباين .حيث يمكن استخدام هذا الفحص لتحديد ما إذا كان هناك درجات اختلاف بين مجموعتين من البيانات. على سبيل المثال، يمكن فحص نقاط الاختبار للفتيان والفتيات المتقدمين لمدرسة ثانوية وتحديـد إذا كانـت درجـة التغيـر فـي الاجابـات بـين الفتيـات مختلفـة عـن تلـك الموجـودة بـين الفتيان(سالفاتور:1997)(Richard:1994)،الخطوات كالاتي:-

خطوة (1) تقدير تباين المجتمع من التباين بين متوسطات العينات (MSA) .

خطوة (2) تقدير تباين المجتمع من التباين داخل العينات(MSE) .

خطوة (3) حساب النسبة F=(MSA/MSE) .

خطوة (4) اذا كانت F المحسوبة اكبر من قيمة F الجدولية عند مستوى المعنوية ودرجات الحرية المعينـة،فان الفرض العـدميH0 عـن تسـاوي متوسـطات المجتمعـات،يرفض لصـالح الفـرض البـديل،H1. الخطـوات السـابقة موضحة بالجدول رقم (1).

جدول(1) جدول تحليل التباين ANOVA(سالفاتور:1997)

مصدر التغيير	مجموع المربعات	درجات الحرية	متوسطات المربعات	النسبة F
بين الاوساط يفسره العامل(A)	SSA=r∑(xj-x)²	c-1	MSA=SSA/(c-1)	MSA/MSE
داخل العينات (الخطأ او غير المفسر)	SSE= ∑∑ (xij-xj)²	(r-1)c	MSE=SSE(r-1)c	-
الاجمالي	SST= ∑∑ (xij-x)²=SSA+SSE	rc-1	-	-

عندما :-

Xj = متوسط العينة j المكونة من r مشاهدة= (∑i x ij)/r		............(2-3)
Xj = متوسط العينة j المكونة من r مشاهدة= (∑i x ij)/r		............(2-4)
X= المتوسط الكبير لكل العينات = (∑i∑j x ij)/rc		.........(2-5)
SSA = مجموع المربعات التي يفسرها العامل (xj- x) ² = r ∑		.........(2-6)
SSE = مجموع مربعات الخطا والتي لايفسرها العامل =²(xij- xj) ∑ ∑		.........(2-7)
SST = مجموع المربعات الاجمالي=SSA+ SSE =²(xij- x) ∑ ∑		........(2-8)
درجات حرية البسط = c-1		.........................(2-9)

حيث C = عدد العينات

درجات حرية المقام = c(r-1) ....(2-10)

حيث r = عدد المشاهدات في كل عينة

ولكون نموذجي صاحب العمل والمقاول يخضعان للتوزيع الطبيعي من نتائج الفحص السابق الا ان نتائج فحص التباين اوجدت ان هناك درجة اختلاف بين نتائج الاجابات الخاصة لكل منهما وذلك بعد ايجاد قيمة F المحسوبة لغرض مقارنتها مع قيم F الجدولية.ويبدو ذلك منطقيا لان لكل منهما(صاحب العمل أو المقاول)له وجهة نظره الخاصة فيما يخص مفهوم إدارة وتخطيط الكلفة بما يحقق مطالبه ويؤمن التزاماته المالية بحيث يؤدي الى انجاز المشروع ضمن المدة المقررة والميزانية المحددة من وجهة نظر صاحب العمل ويحقق الربح المعقول من وجهة المقاول من جهة اخرى.الملحق رقم(3)يبين نتائج تحليل التباين.

– الاستنتاجات

خرج البحث بمجموعة من الاستنتاجات كان اهمها مايلي:–

- ان العمل الذي تم القيام به قد عزز من الفرضية والتي تم اعتمادها في منهجية البحث والتي تنص على(هناك ضعف في كفاءة ادارة وتخطيط الكلفة في مشاريع التشييد ناتج عن غياب الوعي في استخدام الأساليب العلمية في ادارة وتخطيط الكلفة خلال المراحل الكلية لانجاز المشروع).

- بصورة عامة ،هناك ضعف في عملية أدارة وتخطيط مشاريع التشييد ،والتي ظهر بانها تتاثر بالعوامل التالية وبنسب متفاوتة :

أ – عدم وضوح الرؤيا عند وضع البرمجة و الخطط.

ب – عدم ايلاء التخطيط الأهمية المطلوبة.

ج – نقص البيانات والمعلومات الكلفوية المطلوبة.

د – ضعف في كفاءة الاداء للكادر الخاص بالبرمجة والتخطيط.

- وجود ضعف واضح في مجال التخطيط لمختلف التشكيلات والقطاعات المحلية سببه عدم الاهتمام بالاستخدام الامثل للمستويات الثلاثة لعملية التخطيط والبرمجة في المشاريع،والاعتماد على نوع واحد من انواع التخطيط الروتيني، والتركيز على الوقت فقط وإهمال مجالات التخطيط الاخرى،مثل استخدام البدائل وهندسة القيمة وتحسن النوعية.

- هناك تلكؤ في تطبيق المفاهيم الخاصة بإدارة وتخطيط الكلفة في مشاريع الخطة الاستثمارية بسبب صدور التخصيصات المالية لكل سنة بصورة منفردة وهذا غير ملائم للمشاريع الإنشائية التي مدتها اكثر من سنة للأسباب التالية:–

أ–صدور الخطة الاستثمارية متأخرة عن بداية السنة .

ب– عدم ورود التخصص المالي بصورة مطابقة لبرمجة العمل الاصلية مما يضطر القائمين على التخطيط والبرمجة الى الالتزام بالمبلغ المخصص وليس بالمبلغ المطلوب ومحاولة إنهائه مع نهاية السنة، الأمر الذي عرض المشاريع الى انحرافات في الكلفة المخمنة مما يؤدي ايضا الى التأخير في التنفيذ.

• لقد بين البحث وجود مشاكل في عملية جمع وتسجيل البيانات بدقة والخاصة بنسب تقدم العمل والكلف المصروفة في المشاريع بالإضافة الى ضعف الاسلوب المستخدم حاليا في تسجيل البيانات الكلفوية (النظام المحاسبي الموحد) حيث يستخدم لإغراض المقارنات والتي لا تمثل بيانات دقيقة عن الكلفة ومصروفات وقيمة العمل المنفذ لغاية تاريخ معين.اضافة الى عدم وجود نظام موحد لتبويب المعلومات وحفظها مما يؤدي الى انعدام التعاون المعلوماتي بين ادارات المشاريع .

• زيادة ملحوظة في كلف المشاريع بعد احداث عام 2003 مقارنة بالسنوات السابقة،بسبب ما يلي:

أ – زيادة في اسعار المواد الداخلة في عملية البناء والأيدي العاملة لتوقف المعامل الانشائية عن العمل خلال الفترة التي اعقبت توقف الحرب مع زيادة في اجورالمعدات والأيدي العاملة.

ب – زيادة اجور النقل وكلف المخاطر نتيجة الضعف الامني.

ج – ضعف تخطيط وإدارة موارد المشروع المختلفة .

د – عدم اعتماد مبادئ تقليص الكلفة كهندسة القيمة او التقويم الانشائي .

ضعف دور الاقسام الادارية كالتخطيط والمتابعة والدراسات والتصاميم في متابعة تقدم العمل في المشاريع والكلفة الفعلية المصروفة،إضافة الى مايتعلق بدور هذه الاقسام في اعمال تخطيط وتخمين المشاريع.

• لا يوجد دور حقيقي لمدير الانشاء في اغلب مشاريع التشييد في العراق الامر الذي يؤدي الى افتقار المشروع للخدمات التي تقدمها ادارة الانشاء ومن بينها متابعة فعاليات المشروع وتنسيق ادوار اطراف عملية

• تحقيق المشروع وتنظيم علاقاتهم مع بعضهم البعض.

• تراكم الخبرة يتكون لدى المنتسبين المستمرين بالخدمة فقط،لذلك فان تسرب وابتعاد هذه النخبة عن العمل يسبب ضياع جهود وخبرات متراكمة للقائمين على المشاريع ومنفذيها.كذلك انعدام التوثيق لمختلف البيانات والتحليلات والنتائج للأعمال المنفذة منهم لاسيما سجل الوقائع اليومية والمتعلقة بالكلفة والوقت والظروف المحيطة الاخرى.

• وجود خلل كبير في الاستخدام الامثل للتطبيقات الحاسوبية في ادارة وتخطيط كلف مشاريع التشييد،وإهمال الطاقات الكبيرة التي يمتلكها هذا الجهاز في تسهيل اعمال التوثيق والمتابعة والتحليل للبيانات الخاصة بكلف المشاريع او نسب تقدم العمل فيها فضلا عن عدم استخدام البرامجيات الخاصة بأعمال التخطيط في المشاريع.

- التوصيات :

- توجيه مشاريع بناء القدرات البشرية في عموم المؤسسات بما يخدم تحقيق اهداف تقوية هذه المؤسسات من خلال اعداد دورات تطويرية في مجال ادارة وتخطيط الكلفة واشراك المهندسين والمحاسبين بتلك الدورات لتطويرهم ورفع مستواهم العلمي والفني بما يتلائم مع التطور الحاصل في العلوم الهندسية والمالية وخاصة في مجال التخطيط والبرمجة والسيطرة باشكالها.

- تطوير العمليات التخطيطية وتفعيل فريق العمل فيها،بالاضافة الى استخدام اساليب التحفيز المختلفة لحث الافراد على العمل ضمن الخطط الموضوعة.

- تطوير دور الاقسام الادارية كالتخطيط والمتابعة والدراسات والتصاميم في متابعة تقدم العمل في المشاريع والكلفة الفعلية المصروفة بالاضافة الى مايتعلق بدور هذه الاقسام في اعمال التخطيط والتخمين للمشاريع لتسجيل وتقدير الالتزامات المالية والمصروفات ومقارنة التكاليف الناتجة مع الزيادات في تقديرات الكلفة وضبط التكاليف الفعلية مقابل الميزانية المخمنة والقيام بتقديم البدائل الفنية المقبولة في حالة انحراف مسارات الكلف الحقيقية عن التخمينية.

- الاهتمام بعملية توثيق البيانات الكلفوية في المشاريع الانشائية المختلفة وتحقيق تغذية عكسية للمعلومات فعالة ومؤثرة في تحديث وتصحيح الكثير من الاجراءات المالية والمحاسبية.

- ضرورة التعريف باساليب التخطيط للمشاريع ومنها اسلوب المسار الحرج لاعتماده في اعداد منحنيات الكلفة المبكرة والكلفة المتاخرة والمقارنة معها.

- استخدام منحني الكلفة كوسيلة من وسائل المراقبة والسيطرة للحصول على مؤشرات سير العمل والتدفقات المالية للصرفيات وربطها بالميزانية المحددة للمشروع للتاكد من تحقيق الاهداف المطلوبة.

- تطبيق مبدأ هندسة القيمة في المشاريع للاختيار بين البدائل المتاحة.

- دراسة امكانية اشاعة استخدام اسلوب الادارة الانشائية في تنفيذ مشاريع التشييد الضخمة ذات المواصفات الفنية الخاصة.

- اعادة بناء الهيكل التنظيمي لهيئات التشييد سواء في القطاع العام او الخاص لتشمل ضمن هيكليتها اقسام لادارة وتخطيط الكلفة في مشاريع التشييد مهمتها الاشراف على المهام التالية(تخطيط الموارد,تخمين الكلفة،ميزانية المشروع وضبط الكلفة) وهي جهة تعمل لصالح صاحب العمل ولها صلاحية الاشراف على كلف التنفيذ.

- اعتماد صيغة جديدة لاصدار اوامر التغيير تعتمد على مبدأ السرعة للتفاوض مع المقاول واعتماد الية جديدة لتسعير الفقرات غير المدرجة في جدول الكميات التي تظهر اثناء تنفيذ المشروع من خلال الاتفاق مسبقا على صيغة احتساب الاجور التي يتم اضافتها الى الكلفة الحقيقية للعمل من خلال قوائم مصادقة او من خلال لجنة مشتركة اشبه بلجان التنفيذ امانة لغرض تسعير تلك الاعمال.

– المقترحات والدراسات المستقبلية :

لغرض التوسع بموضوع البحث تقترح الدراسات المستقبلية الاتية:

- تطوير قاعدة للبيانات والمعلومات الكلفوية والانتاجية واعتبارها اساسية لاعداد نظام هندسي لتقييم السيطرة على ادارة وتخطيط كلف مشاريع التشييد.

- بناء نظام اداري متطور لادارة وتخطيط الكلفة في مشاريع التشييد،و ادخال بعض المؤثرات الخارجية على عمله مثل(ارتفاع اسعار المواد الانشائية،اسعار تاجير المكائن والمعدات،اجور الايدي العاملة وعوامل اخرى والتي من شانها ان تؤثر على كلفة العمل حيث يمكن من خلالها التوسع في مجال تحديد الاسباب المؤثرة في حصول التباين بين كلف العمل المنجز والكلفة المخمنة.

- دراسة القوانين والانظمة والتعليمات الرسمية المؤثرة في عملية السيطرة على ادارة وتخطيط كلفة مشاريع التشييد.بهدف اعادة النظر فيها من جهة والتقليل من المعوقات الحالية من جهة اخرى.

- اجراء دراسة لتقييم عملية استخدام التطبيقات الحاسوبية ذات العلاقة والتي من شانها مساعدة صاحب العمل في اتخاذ القرارات المناسبة خلال عملية تحقيق المشروع الانشائي مثل اقرار الحاجة لتحقيق المشروع خلال مرحلة دراسة الجدوى وغيرها،اضافة الى مساعدة المقاول في اتخاذ القرارات المناسبة عند تقديم اسعاره عند العطاء،ومن جهة اخرى يساعده على المحافظة على هذه الكلفة خلال عملية تنفيذ المشروع الانشائي .واعطاءه مؤشرات الانحراف والتباين في الوقت المناسب لاتخاذ القرار المناسب.

– المصادر :

- إسماعيل،نازنين علي،"التخطيط للمشروع الهندسي–دراسة تطبيقية في المنظمات الاستشارية في العراق"، رسالة ماجستير مقدمة إلى قسم الهندسة المعمارية، الجامعة التكنولوجية،1996.

- البندنيجي ،بشار سعد ظاهر،"تصميم نظام ادارة معلومات للسيطرة ومتابعة كلف التنفيذ لمشاريع وزارة الري"، رسالة ماجستير،جامعة بغداد ، قسم الهندسة المدنية ،2000.

- التكريتي،ندى صبحي عبد المجيد،" السيطرة على تخطيط المشروع الهندسي"، رسالة ماجستير مقدمة إلى قسم الهندسة المعمارية، الجامعة التكنولوجية،2002.

- التميمي ،سميعة "تطوير برنامج لضمان جودة التخطيط الانشائي لمشاريع الطرف" رسالة ماجستير ،الجامعة

- التكنلوجيا،قسم البناء والانشاءات،2004.

- الجلالي،محمد "دورة حياة المشروع الهندسي" ،تجميع عارف سمان،موقع المدينة للعلوم والهندسة،2005.

- الحديثي،احمد عبد الفتاح نعمة،"التطبيقات الحاسوبية في ادارة مشاريع التشييد"،رسالة ماجستير ،جامعة بغداد، قسم الهندسة المدنية ،2005.

- الطائي،اسماعيل،محمد علي،"المهندس والمسار الحرج"،المركز القومي للاستشارات والتطوير الادار ،بغداد 1971.

- العجيلي،حاتم خليفة،"نظام تقويم تقدم العمل في المشاريع الانشائية باستخدام نظام الاوزان المعيارية للفقرات الانشائية"،رسالة ماجستير،جامعة بغداد، قسم الهندسة المدنية ،1996.

- جاراللـه،محمـد ابـراهيم ونوارة،جمـال محمـد،"ادارة المشـاريع الهندسـية"،دار جـون وايلـي وابنائـه للطباعة،انكلترا،1984.

- سالفاتور،دومينيك،"سلسلة ملخصات شوم_نظريات ومسائل في الاحصـاء والاقتصاد القياسي"،الدار الدولية للنشر والتوزيع،القاهرة ،مصر،ترجمة الدكتورة سعدية حافظ منتصر،1997،الطبعة الرابعة.

- سـالم،فؤاد الشيخ ،زيـاد رمضـان،اميمة الـدهان ومحسـن مخامرة،"المفـاهيم الاداريـة الحديثة"،الطبعـة السادسة،شركة الشرق الاوسط ،الاردن، 1998.

- سمير ،احمد عسكر،"المدخل إلى ادارة الاعمال"،دار النهضة العربية،1987.

- كريم،عزيز نوري،"ادارة الاعمال الانشائية– السيطرة على الكلفة"،دراسة مقدمة إلى اتحاد المقاولين العراقيين،مجلة المقاول، العدد الاول،1988.

- كولـدهابر واخرون،ستانلي،جها،شاندراك،ماسـيدو مـانويلي،"النظم الاداريـة لهندسـة التشـييد"،ترجمة د.أنيس التتير،محمد عمر جمجوم،دار وايلي،نيويورك،1982.

- محمـد السـيد،إسـماعيل،" الإدارة الإسـتراتيجية (مفـاهيم وحـالات تطبيقية)"،الناشـر المكتب العربـي الحديث ، 1993.

- Ahuja. H.N."Construction Performance Control by Network ".John Wiley &sons ,Inc, U.S.A,1976.

- Ahuja, Hira N., "Project Management Techniques in Planning And Controlling Construction Project", John Wiley and Sons), 1980.

- Curtis R. Cook , "Just Enough Project Management: The Indispensable Four-Step Process for Managing Any Project Better, Faster, Cheaper", McGraw-Hill ,Inc. ,USA ,

- 2005.

- Harris, F.C & McCoffer, R., (Construction Plant: Management and Investment Decisions), Richard Clay Ltd., Great Britain, 1982.

- Handrickson C. "Project Management for Construction Planning". 2nd Ed. Prepared for WWW Publication, Ce .Cmn.edu, Version 2.1 prepared Summer, 2003.

- Oberlender , Garold ," Project Management For Engineering and Construction", McGraw-Hill,2000.

- Pmbok Guide," A Guide to the Project Management Body of Knowledge" 2000 Edition, Project management Institute Newtown Square, Pennsylvania USA, Library of Congress Cataloging-in-Publication Data,2003.

- Sue Nugus," Financial planning &Budgeting Techniques ",Using Spread Sheets,Kogan Page Limited,1997.

- Twort, A.G. & Rees .J. Gorder, "Civil Engineering: Supervision and Management", 3rd edition, Edward Arnold, Ltd, G.B.London.1995.